The Rhodium-Catalyzed Dynamic Kinetic Asymmetric Pauson−Khand Reaction of Allenyl Carboxy Esters

by

Lauren Claire Burrows

Bachelor of Arts in Chemistry, Colgate University, 2012

Submitted to the Graduate Faculty of the

Kenneth P. Dietrich School of Arts and Sciences

in partial fulfillment of the requirements for the degree of

Doctor of Philosophy

University of Pittsburgh

2018

UNIVERSITY OF PITTSBURGH

Kenneth P. Dietrich School of Arts and Sciences

This dissertation was presented

by

Lauren Claire Burrows

It was defended on

May 18, 2018

and approved by

Scott G. Nelson, Professor, Department of Chemistry

Peng Liu, Assistant Professor, Department of Chemistry

Kevin Noonan, Associate Professor, Department of Chemistry, Carnegie Mellon University

Dissertation Advisor: Kay M. Brummond, Professor, Department of Chemistry

The Rhodium-Catalyzed Dynamic Kinetic Asymmetric Pauson−Khand Reaction of Allenyl Carboxy Esters

Lauren Claire Burrows, PhD

University of Pittsburgh, 2018

The Rh(I)-catalyzed allenic Pauson−Khand reaction (APKR) is an efficient, redox-neutral method of synthesizing α-acyloxy cyclopentenones. An enantioselective APKR would provide access to chiral, nonracemic α-acyloxy and α-hydroxy cyclopentenones and their corresponding redox derivatives. Rapid scrambling of axial chirality of allenyl acetates in the presence of Rh(I) catalysts enables the conversion of racemic allene to enantiopure cyclopentenone product in a Type I dynamic kinetic asymmetric transformation (DyKAT). A combined experimental and computational approach was taken to develop an effective catalytic system to achieve the asymmetric transformation. The optimization of the denticity, and steric and electronic properties of the ancillary ligand (initially (*S*)-MonoPhos, 16% ee), afforded a hemilabile bidentate (*S*)-MonoPhos-alkene-Rh(I) catalyst that provided α-acyloxy cyclopentenone product in up to 72% ee. Upon discovery of the reactive and enantioselective (*S*)-MonoPhos-alkene catalyst, the remaining reaction conditions were optimized using a statistical design of experiments (DOE) strategy. Reaction temperature, CO atmosphere, catalyst counteranion, concentration, solvent identity, additive equivalents, and ligand/Rh stoichiometry were evaluated simultaneously in two iterations of DOE experimentation. Discovery of optimal conditions enabled an increase in enantioselectivities and an expansion of the APKR scope to include methyl-substituted alkynes and a three-carbon-tethered allene-yne.

The good yields and enantioselectivities effected by the phosphoramidite class of ligands in the APKR inspired an exploration of electron-deficient phosphoramidite ligands in the

enantioselective Pauson−Khand reaction (PKR) of 1,6-enynes. Lowest-energy reaction profiles of the cationic Rh(I)-(*R*)-BINAP, Rh(I)-(*S*)-MonoPhos, and Rh(I)-"CO-only" catalysts were calculated, and agreement between experimental reaction rates and the activation energies of the oxidative cyclization step was found. We observed that the PKR of cationic Rh(I)-catalyst is accelerated 3000-fold in the presence of (*R*)-BINAP, and 180-fold in the presence of either one or two (*S*)-MonoPhos ligands (ligand to Rh ratio of 1.1 or 2.2). The absolute configuration of the PKR product was confirmed by VCD spectroscopy and matches that predicted by calculations. We anticipate that these mechanistic studies will enable the application of phosphoramidite ligands in the PKR of new enyne substrates.

TABLE OF CONTENTS

LIST OF TABLES

LIST OF FIGURES

LIST OF SCHEMES

ACKNOWLEDGEMENTS

I have been incredibly fortunate in my time here at Pitt to be surrounded by many role models and friends. First, my advisor, Professor Kay Brummond, who from the start has pushed me to do my best work. Whenever I felt frustrated in my research, I always felt motivated and encouraged after talking with Kay. I admire her ability to focus the broader impacts of our work, and her positive outlook. I am grateful to have spent my time here learning from her. I have also had the pleasure of working closely with Professor Peng Liu for the past several years. His kindness and patience throughout both of our collaborative projects has made the process very enjoyable. I also thank Professor Tara Meyer for her guidance while I wrote my original research proposal. I will carry much of her advice with me as I move forward in my career. I also thank Professor Scott Nelson for his encouragement over the years, especially during my first year as a graduate student. Thank you to all of my lab mates, past and present, who helped train me and passed on their wisdom. Thank you to Ashley Bober, Sarah Wells and Laura Kocsis for your friendship throughout my time as a graduate student. Thank you to current Brummond Group members Joe Burchick, Humair Omer, Tuğçe Erbay, Dan Dempe, Joe Winklebauer, and Eric Deihl for making working in the lab fun every day. I also want to acknowledge Luke Jesikiewicz and Gang Lu for providing the calculations described in this dissertation, and for their flexibility and enthusiasm in all of our discussions.

I want to thank my parents, John and Linda Parrette for supporting me in all these years of my education. From both of my parents I have learned the value in challenging myself. Thank you to my brothers, Daniel Parrette and Nathan Parrette, whose passions and hard work in their own respective careers are an inspiration to me. I am grateful to my friends here in Pittsburgh and afar

who have been a constant source of support and perspective: Jane Huang, Kirsten Lunn, and Ramsey Hanna and Emily Sackmann. Thank you to Margaret Proviano, Tina Burrows, Jake Burrows, and Michael Vranesevich for making Pittsburgh my home. Finally, of all of the chemistry knowledge I've gained and the friends I've made in graduate school, nothing has changed my life and made me as happy as my husband, Jim Burrows. Thank you for being by my side every day. I know that God has guided my steps and blessed my life here. I am grateful to have had the opportunity to spend my time learning and growing in the field of chemistry alongside so many wonderful people.

1.0 CYCLOPENTENONES IN NATURAL PRODUCT SYNTHESIS.

Cyclopentenones are valuable synthetic building blocks and appear often in complex molecule syntheses. Their utility arises from the wide array of known transformations of the enone functionality.[1-2] As evidenced by the examples in Figure 1, a number of modifications can be made to the cyclic enone, with each carbon of the cyclopentenone having unique reactivity. For example, the carbonyl can undergo 1,2-addition under regioselective Luche reduction conditions. Electrophilic alkylation can be carried out α to the carbonyl, and the allylic 3-position can be selectively brominated using *N*-bromosuccinimide.[3] The enone functionality can react via 1,4-addition with a variety of nucleophiles to afford substitutions at the 4-position, often with a high degree of enantioselectivity.[4] The electron deficient alkene can undergo epoxidation, [2+2], [4+2], and [3+2] cycloadditions, cyclopropanation, hydrogenation, and dihydroxylation reactions. The 5-position can react with carbon electrophiles in Baylis-Hillman-type reactions to afford functionalized products.

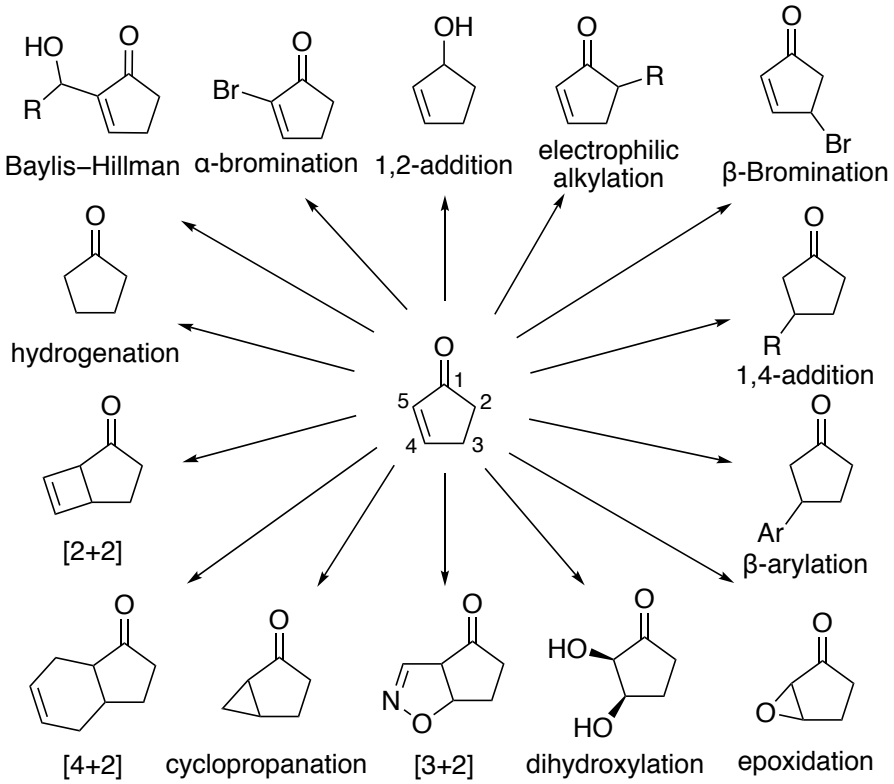

Figure 1. Functionalization of cyclopentenones.

Because of their utility as building blocks in organic synthesis, a variety of methods have been developed to access cyclopentenones from acyclic precursors.[1, 5] Several disconnection strategies can be realized using either ring-closing reactions of linear precursors, multicomponent cycloadditions, or ring expansion reactions (Figure 2). Classical cyclization routes using linear precursors include acid-catalyzed Nazarov cyclization, and intramolecular Wittig and aldol reactions. Transition metal-catalyzed ring-closing reactions include Ru-catalyzed Grubbs metathesis, Rh-catalyzed intramolecular hydroacylation and Au-catalyzed Rautenstrauch rearrangement.[5] Multicomponent reactions can be effected through [4+1], [3+2] and [2+2+1] reactions. Finally, a ring-expansion of cyclobutanol, or ring-contraction of cyclohexa-2,5-dienones can also afford the desired cyclopentenone product.

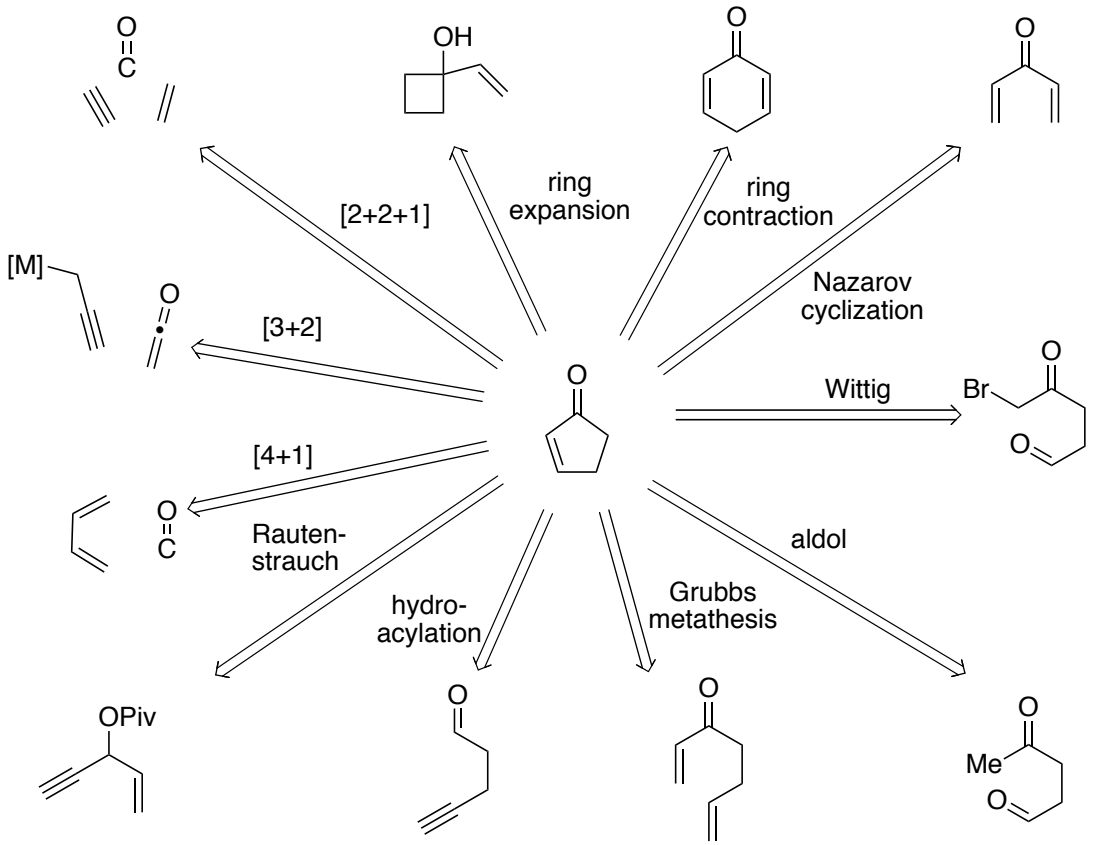

Figure 2. Methods to access cyclopentenones.

Although many methods exist to access cyclopentenones, the synthesis of chiral cyclopentenones remains a challenge. Rather than enantioselective synthesis, the introduction of chirality in cyclopentenone synthesis is most often achieved using available chiral synthons such as chiral carbohydrates, carbonyl-based compounds (such as (*R*)-camphor,[6-7] (*R*)-pulegone[8-9], and α-santonin[10]), and chiral unsaturated hydrocarbons (such as (*R*)-limonene[11]) as starting materials. Catalytic enantioselective syntheses of cyclopentenones is rare, and is predominantly effected using Nazarov cyclization or Pauson−Khand reactions.[4] Reliance on the chiral pool limits the testing of alternate enantiomers of synthesized molecules.[12] Therefore, further development in the enantioselective synthesis of chiral cyclopentenones would enable access to unexplored chemical space.

1.1 NATURAL PRODUCTS CONTAINING ALPHA-OXYGENATED CYCLOPENTENONES.

1.1.1 Natural products containing α-carboxy and α-hydroxy cyclopentenones and various redox derivatives.

Many of the biologically-relevant cyclopentenone-containing natural products, and redox derivatives, also contain acetoxy or hydroxy groups in the α-position. Representative examples of these natural products and drug candidates are shown in Figure 3. Guanacastepene A (**1.1**) is a diterpene isolated from fungi in the *Daphnopsis Americana* tree in Costa Rica, and exhibits potent activity against strains of *Staphylococcus aureus* and *Enterococcus faecalis.*[13] Stemonamine (**1.2**) contains a challenging spirocyclic architecture and has been used as both a drug for respiratory disease and as an insecticide.[14-15] Caribenol B (**1.3**) features an α-hydroxy cyclopentenone and has shown activity against *Mycobacterium tuberculosis* and *Plasmodium* parasites.[16-17] Resiniferatoxin (**1.4**) is isolated from the *Euphorbia resinifera* plant in Morocco, and has been investigated as a starting point for a new class of analgesics because of its ability to activate sensory neurons.[18] The compound possesses a complex and densely functionalized tetracyclic core containing a α-hydroxy cyclopentenone.[19-20] Phorbol (**1.5**) is isolated from the *Croton tiglium* plant, and shows both antiviral and anticancer activity.[21-22] A total synthesis of phorbol (**1.5**) was completed in in 2015.[23] Ryanodine (**1.6**) is a regulator of calcium ion channels and was isolated from *Ryania speciosa,* a Central American shrub. The highly oxygenated tetracyclic ring system was synthesized in 18 steps via a cyclopentenone intermediate.[24-26] Kedarcidin (**1.7**) is the cytotoxic chromophore component of a protein-chromophore complex and demonstrates antibiotic and antitumor activity.[27-28] Valtrate (**1.8**) is an anti-HIV compound isolated from the roots of the

valerianae officinalis plant. Thapsigargin (**1.9**) is an inhibitor of the sarco-endoplasmic reticulum calcium $^{2+}$ ATPase (SERCA) and is used in biomedical studies of calcium transport channels. Inhibition of the SERCA pumps leads to accumulation of calcium ions and cell apoptosis. Mipsagargin (**1.10**) is a derivative of Thapsigargin, which induces apoptosis in prostate cancer cells.

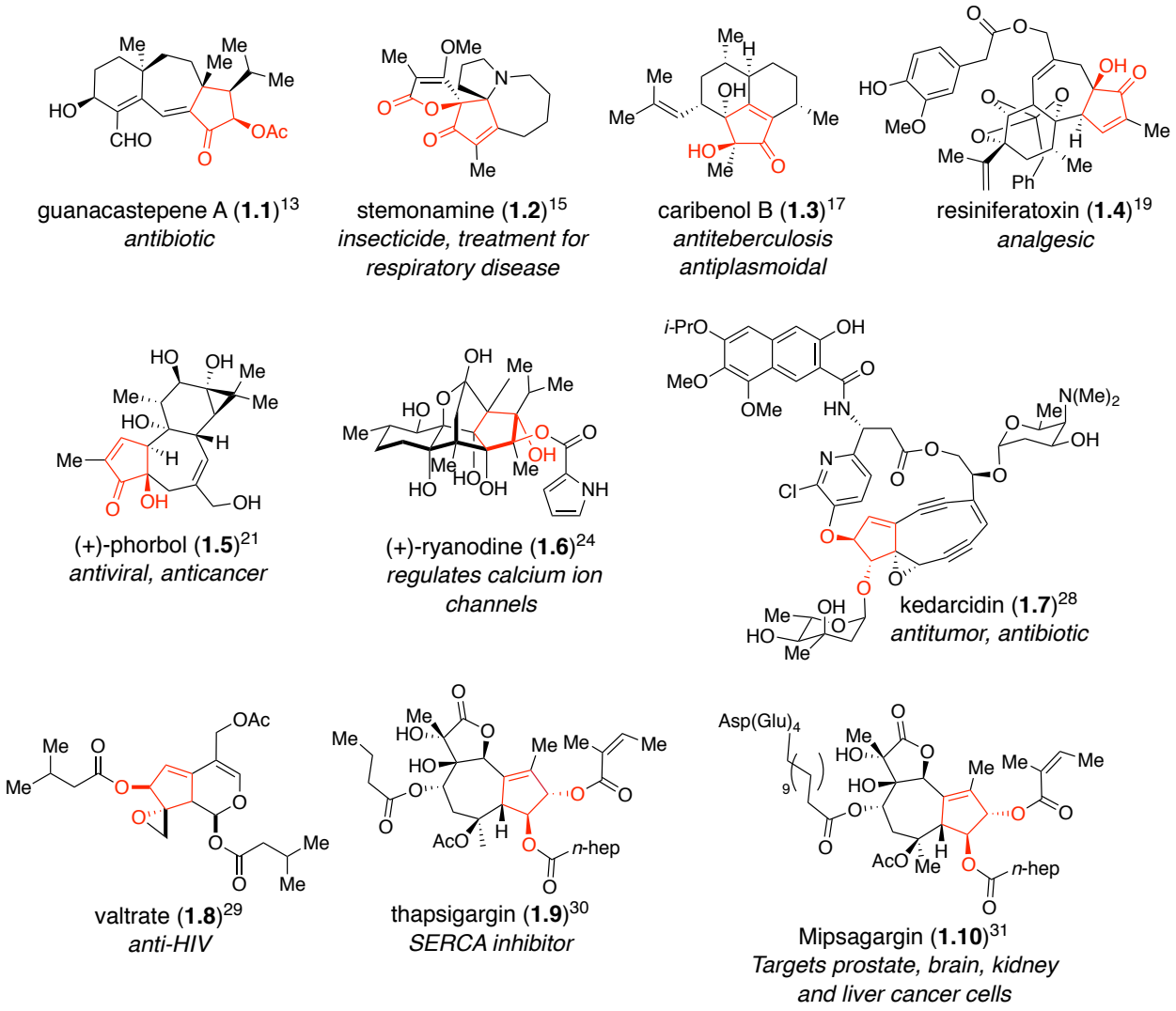

Figure 3. Natural products with α-oxygenated cyclopentenones and redox derivatives.

All of the chiral α-oxygenated natural products shown in Figure 3 also contain complex fused ring systems. An enantioselective method of preparing these polycyclic α-oxygenated compounds would have applications in natural product synthesis and the study of their analogs. We are particularly interested in Thapsigargin (**1.9**) because of its potential as a therapeutic. The synthesis of analogs of Thapsigargin (**1.9**) is expected to lead to more effective drug candidates.[29-31]

1.1.2 Thapsigargin prodrug development.

Thapsigargin (Tg, **1.9**) is isolated from *thapsia gargainca* and has been recognized as a histamine liberator since 300-400 BC, when it was observed to cause blistering on skin.[31] More recently, Tg (**1.9**) is valued for its ability to disrupt calcium ion channels in cells. The compound is a subnanomolar inhibitor of the SERCA pump, and upon exposure to Tg (**1.9**), calcium builds up in the cell and ultimately induces apoptosis.[31] Tg (**1.9**) has gained recent attention due to the clinical success of Mipsagargin (**1.10**), a derivative of Tg (**1.9**).[32] Mipsagargin (**1.10**) was developed as a drug for prostate cancer, and has been successfully used to treat liver, brain and kidney cancer as well. A central challenge of developing treatments for prostate cancer is the slow proliferation of prostate cancer cells, which makes them difficult to distinguish from healthy cells. However, prostate cancer cells can be distinguished by their expression of the prostate-specific membrane antigen (PSMA). Mipsagargin (**1.10**) consists of the highly toxic Tg (**1.9**), with a linker containing a peptide which is cleaved upon exposure to PMSA.[33] Therefore, Mipsagargin (**1.10**) targets prostate cancer cells independent of cell proliferation. Mipsagargin (**1.10**) is in the final stages of Phase II clinical trials. After treatment with Mipsagargin (**1.10**), many patients with previously aggressive tumors are now in remission.[34]

1.1.3 Thapsigargin structure-activity relationships.

Investigation of analogs of Tg (**1.9**) is an important part of the drug discovery process. Thus, the effect of changing various side chains of Tg (**1.9**) on SERCA inhibition activity has been studied.[29, 35] A Tg analog, dOTg (**1.11**) lacking a C-2 ester showed between 10-25 times lower SERCA inhibition activity than Tg (**1.9**) (Figure 4).[35] Removal of other side chains at the C-3 (dATg, **1.12**), C-8 (dBTg, **1.13**) and C-10 (dCTg, **1.14**) positions resulted in greater decreases in activity. Thapsivillosin F (**1.15**) and thapsigarcin (**1.16**) are natural products related to Tg (**1.9**) which are also isolated from *Thapsia garganica*. Thapsivillosin F (**1.15**) has an unsaturated C-8 side chain and lacks a C-2 carboxy octanoate group. This compound afforded a 6.5-fold decrease in SERCA inhibition activity compared to Tg (**1.9**). Thapsigarcin (**1.16**), which contains a carboxy hexanoyl group at C-2 rather than an octanoyl group, showed a 2.2-fold decrease in activity.[29] This change in activity for such a minor structural variation supports the importance of the C-2 side chain. The C-2 benzoate analog **1.17** demonstrated 8 times lower activity than Tg.[36] In addition to these tested analogs, at least five different C-2 analogs have been observed in related natural products isolated from *Thapsia garganica*, which have not been tested for SERCA inhibition activity.[37] The existence of these naturally occurring analogs could support the biological significance of the C-2 side chain.

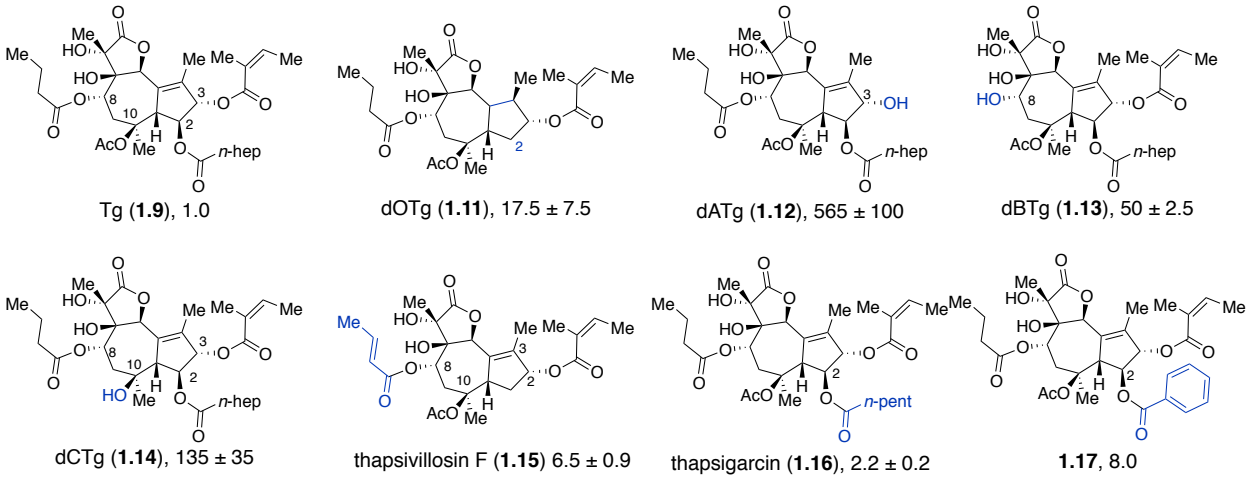

Figure 4. Relative concentration of 50% SERCA inhibition activity compared to Tg.

The role of the C-2 side chain is an underexplored area in structure-activity relationship studies of Tg (**1.9**) analogs as drug candidates. Substitutions at this position are well-tolerated, and even small changes, such as substituting octanoate for hexanoate, lead to changes in activity. The opposite stereochemistry at the C-2 position has not been tested. Development of synthetic methods and strategies to access alternate substitutions and stereochemistry at the C-2 position could reveal advantageous biological activity.

1.1.4 Recent syntheses of Thapsigargin.

Currently, Tg (**1.9**) is supplied by extraction from the fruit and roots of *thapsia garganica.*[38] However, because of the success of Mipsagargin in clinical trials, some expect that the demand for Tg(**1.9**) could reach up to one ton/year in the near future.[31] The limited supply and localized growth of *Thapsia garganica* has inspired several chemical synthesis of this valuable compound. The first total synthesis of Thapsigargin was completed in 42 steps by Ley and coworkers in

2003.[39] Two total syntheses have been reported in recent years, which improve upon this first total synthesis.

Baran and coworkers reported an 11-step synthesis of Thapsigargin from (*R*)-dihydrocarvone (Scheme 1).[40] The stereoselective synthesis of the [5, 7] cyclopentenone ring system was achieved by Hg-lamp irradiation of dieneone **1.18** in glacial acetic acid. The octanoate group was furnished through α-oxidation using potassium permanganate, octanoic acid and octanoic anhydride. Four subsequent transformations provided Tg (**1.9**) in 0.14% overall yield.

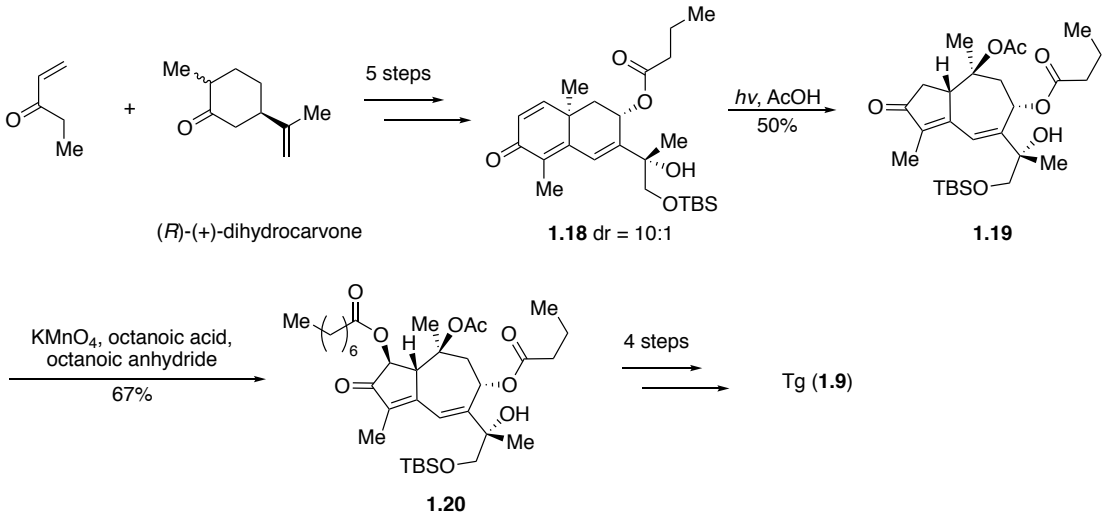

Scheme 1. Baran's 11-step total synthesis of Thapsigargin.

Evans and coworkers reported a 12-step total synthesis of Tg (**1.9**) from (*R*)-carvone (Scheme 2).[41] The cyclopentene ring was installed via an ozonolysis and intramolecular aldol condensation using piperidinium acetate. The seven-membered ring and the lactone were accessed by a vanadium-mediated pinacol coupling/lactonization cascade reaction. Diastereoselective introduction of the C-2 carboxy group was achieved using manganese acetate and octanoic acid. This synthesis provides Tg (**1.9**) in 5.8% overall yield.

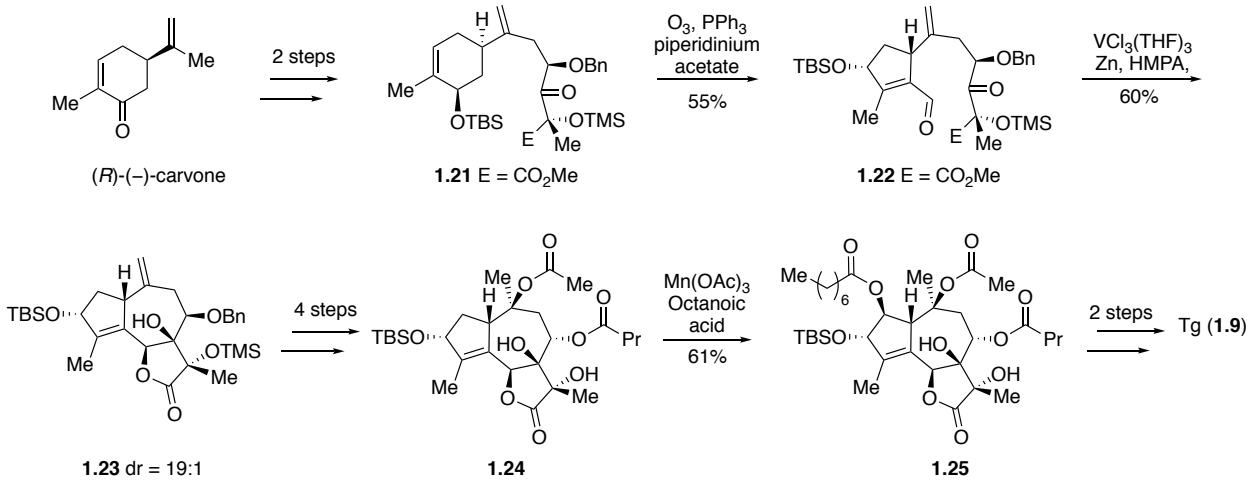

Scheme 2. Evans' 12-step total syntheses of Thapsigargin.

Both recent syntheses of Tg (**1.9**) rely on the manganese acetate-mediated acetylation strategy. Notwithstanding the advantages of this approach for the introduction of various carboxy groups, the diastereoselectivity is substrate-controlled, and thus, the alternate stereochemistry cannot be accessed using this method. A catalyst-controlled method of synthesizing α-oxygenated ketones would enable access to new Tg (**1.9**) analogs.

1.2 METHODS OF PREPARING ALPHA-OXYGENATED KETONES.

The most common method of synthesizing α-oxygenated ketones is by the oxidation of enolates or silyl enol ethers.[42] For example, the Rubottom oxidation involves oxidation of silyl enol ether **1.26** with mCPBA (Scheme 3).[43] A siloxy epoxide intermediate **1.27** is opened under acidic conditions, providing stable oxocarbenium **1.28**. A 1,4 silyl migration followed by hydrolysis of the silyl ether **1.28** affords the TMS-protected α-hydroxy ketone **1.29**.[44] The synthesis of guanacastepene A (**1.1**) includes a Rubottom oxidation of silyl enol ether of **1.30** to install the α-

hydroxy group (Scheme 4, a).[45] The diastereoselectivity in this reaction results from equilibration of the hydroxyl group and its thermodynamic preference to adopt the equatorial conformation. A Rubottom oxidation was also employed in the first total synthesis of Tg (**1.9**).[39] Diastereoselective oxidation of **1.32** affords α-hydroxy product **1.3** in 87% yield over two steps (Scheme 4, b).

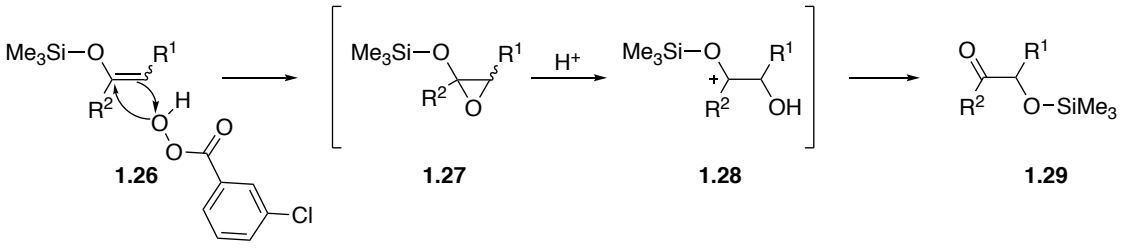

Scheme 3. Mechanism of the Rubottom oxidation.

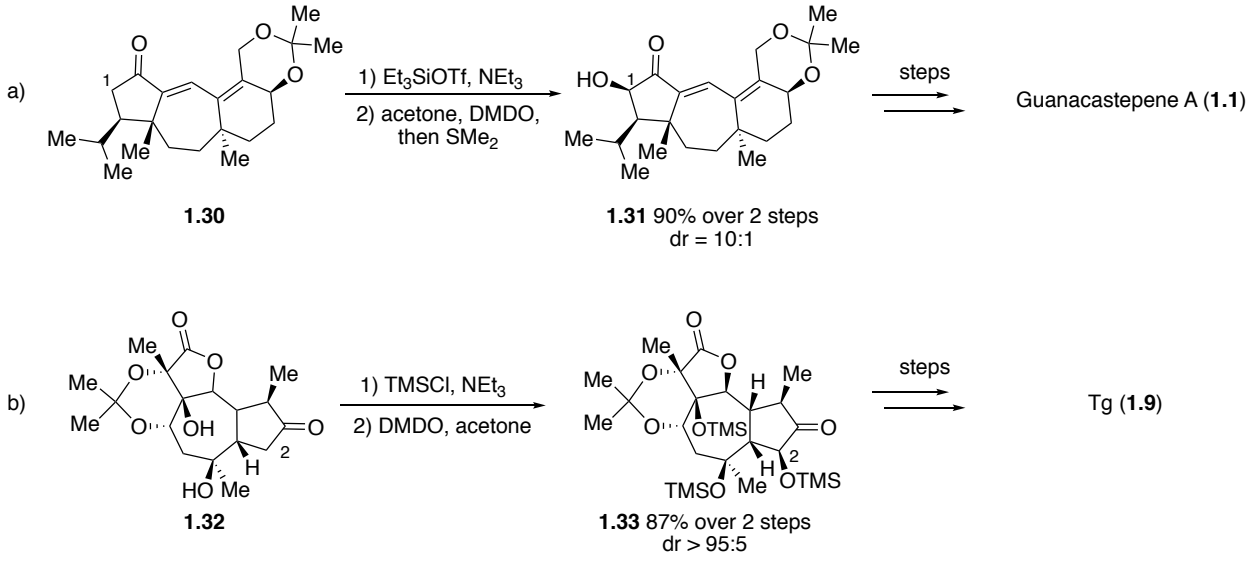

Scheme 4. Synthetic applications of the Rubottom oxidation.

An additional method of synthesizing α-hydroxy ketones is via the Davis oxaziridine oxidation.[46] This reaction involves oxidation of an enolate or silyl enol ether by an electrophilic oxaziridine. Chiral oxaziridines have been used to effect the oxidation enantio- and

diastereoselectively.[47] The reaction proceeds via nucleophilic attack by an enolate **1.34** on oxaziridine **1.35** (Scheme 5). Hemiaminal intermediate **1.36** collapses to afford the α-oxygenated ketone **1.37** and imine **1.38**. Acidic workup provides the corresponding α-hydroxy ketone. Despite the synthetic utility of these protocols to prepare α-oxygenated ketones, the need for strong bases limits the scope of both the Rubottom oxidation (Scheme 3) and the Davis oxaziridine oxidation (Scheme 5).

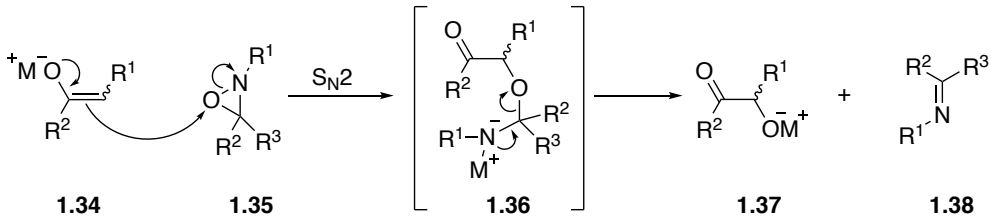

Scheme 5. Mechanism of the Davis oxaziridine oxidation.

As previously discussed, the oxidation of cyclic enones can be achieved in a one-step procedure by C(sp^3)-H activation using $KMnO_4$ and carboxylic acid.[48] This methodology was applied in the two recent total syntheses of Tg (**1.9**) (Scheme 1 and Scheme 2). Mild conditions allow for the installation of a variety of carboxy groups via a radical mechanism with a Mn(III)-carboxylate intermediate **1.40** (Scheme 6).[49] Direct incorporation of the carboxy group increases the step economy of the synthesis and represents an improved approach toward the synthesis of Tg(**1.9**); however, diastereoselectivity is substrate controlled. A method of synthesizing α-carboxy cyclopentenones whereby reagent control is used would offer a complementary approach to stereoisomeric Tg (**1.9**) analogs with enhanced therapeutic potential.

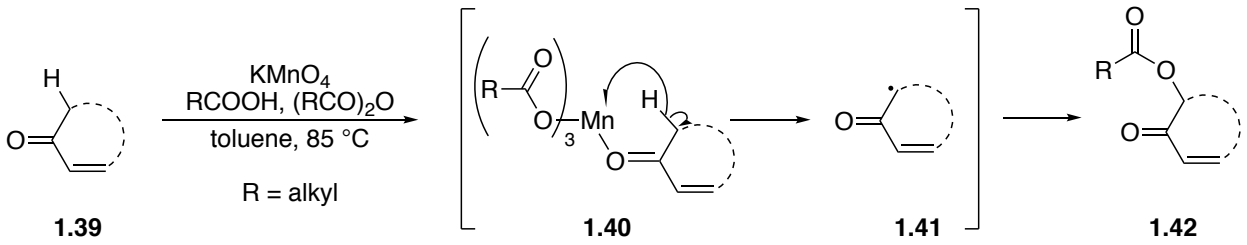

Scheme 6. Mechanism of α-carboxylation of cyclic enones.

1.3 SYNTHESIS OF CYCLOPENTENONES VIA THE RHODIUM(I)-CATALYZED PAUSON-KHAND REACTION.

1.3.1 Limitations of the Co-mediated PKR in synthesizing α-carboxy cyclopentenones.

The Pauson−Khand reaction (PKR) is a transition metal-mediated formal [2+2+1] cycloaddition between an alkene, an alkyne and a carbon monoxide.[50] When it was first introduced in 1971, dicobalt octacarbonyl dimer, $Co_2(CO)_8$, was used to mediate the intermolecular reaction between Co-complexed ethyne **1.43** and strained alkenes such as norbornene **1.44** (Scheme 7, a).[51] Despite the utility of the Co-mediated PKR in recent syntheses of complex natural products,[52-56] the synthesis of α-oxygenated cyclopentenones using the Co-catalyzed PKR is not feasible. For example, reaction of alkynehexacarbonyldicobalt complex **1.46** with vinyl carboxy benzoate **1.47** affords the reduced cyclopentenone product **1.48** exclusively (Scheme 7, b).[57] Upon formation of product **1.49**, the α-carboxy group is cleaved via a Co-mediated single electron transfer reaction where α-carboxy cyclopentenone **1.49** undergoes a one-electron reduction followed by elimination of the carboxy group. Thus, the Co-mediated PKR is not an efficient method of accessing chiral α-oxygenated cyclopentenones.

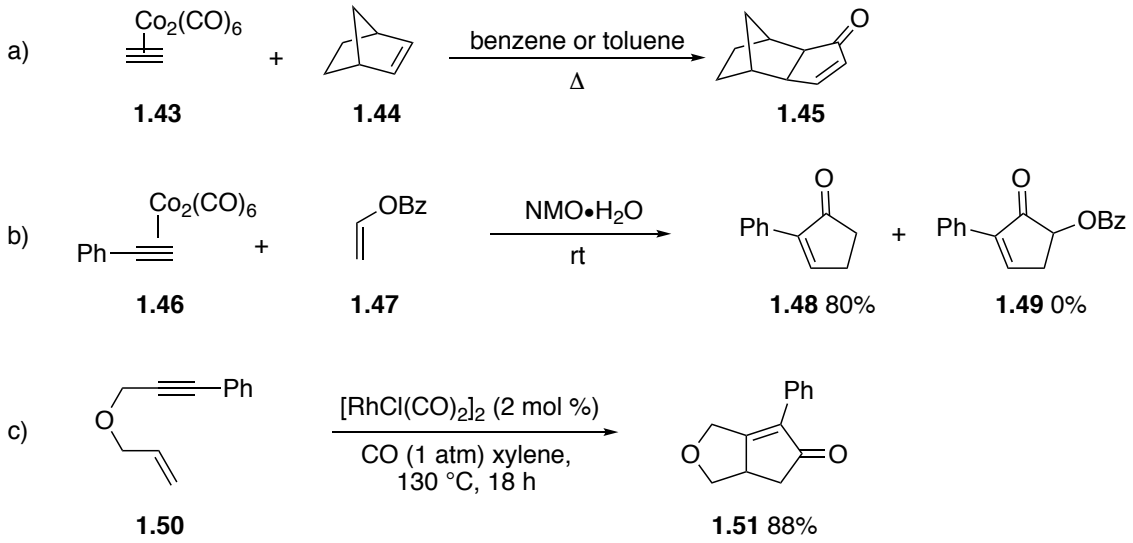

Scheme 7. Early examples of Co-mediated and Rh-catalyzed PKRs.

Catalytic Rh(I)-conditions have been developed as an alternative to stoichiometric Co conditions. In 1998, Narasaka reported the first Rh(I)–catalyzed PKR of tethered enynes.[58] These Rh conditions afford cyclopentenone products in high yields and with low catalyst loadings (Scheme 7, c). The Rh(I)-catalyzed PKR is a versatile reaction and often proceeds with high diastereoselectivity. For this reason, the Rh(I)-catalyzed PKR has been used to install cyclopentenones in numerous syntheses of natural products and other complex molecules.

1.3.2 Recent applications of the Rh(I)-catalyzed PKR in organic synthesis.

An advantage of the Rh-catalyzed PKR is its ability to afford high yields and diastereoselectivity in densely functionalized systems. For example, the Rh(I)-catalyzed PKR was recently employed to complete the tetracyclic ring system in the total synthesis of Ryanodine (**1.6**).[25-26] Several different PKR conditions were tested, including stoichiometric cobalt and molybdenum

conditions. Catalytic Rh(I) afforded the cyclopentenone product in highest yield and diastereoselectivity (Scheme 8, **1.52** to **1.53**). The authors report significant difficulty in the subsequent oxidation at the C-3 and C-4 positions. Fortunately, reacting cyclopentenone **1.53** with anhydrous selenium dioxide afforded the desired oxidation pattern at C-3, C-4 and C-12. A synthetic route involving installation of the C-3 oxygen during the PKR step could have provided an alternative solution to this problem.

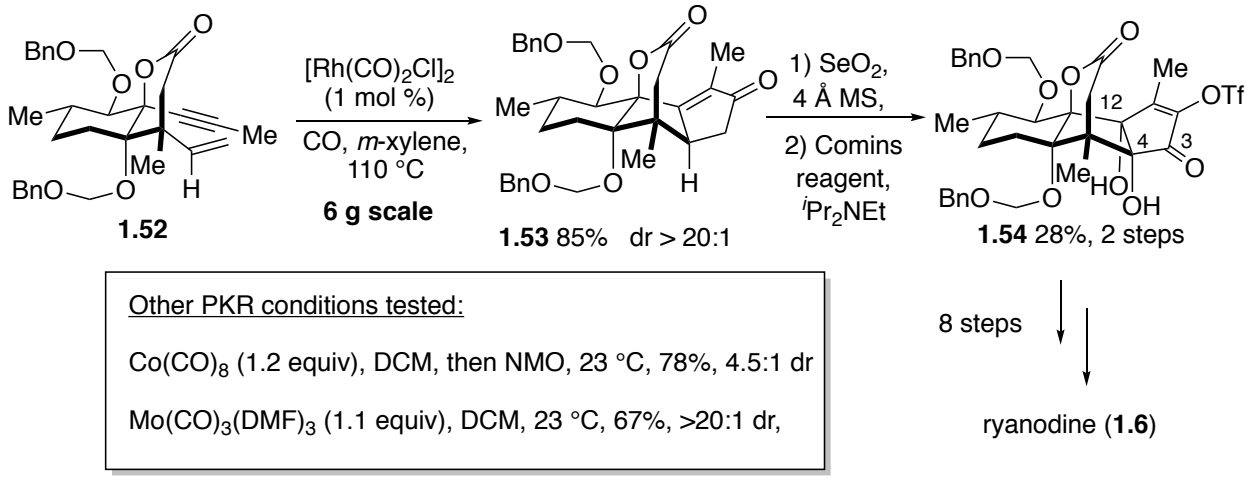

Scheme 8. Reisman's total synthesis of (+)-ryanodol via a Rh(I)-catalyzed PKR.

The Rh(I)-catalyzed PKR can also be coupled with other cycloaddition reactions to afford complex polycyclic rings. For example, a tandem PKR-Diels−Alder reaction of chiral propargyl 2,4-hexadienyl ether **1.55** occurs under carbon monoxide atmosphere in the presence of $[Rh(CO)_2Cl]_2$ catalyst (Scheme 9).[59] This reaction proceeds with high yield and diastereoselectivity to afford a single diastereomer of the tetracyclic compound **1.56**, which contains four new stereocenters and a quaternary carbon core. This domino reaction illustrates the utility of the PKR in the step-efficient syntheses of complex molecules.

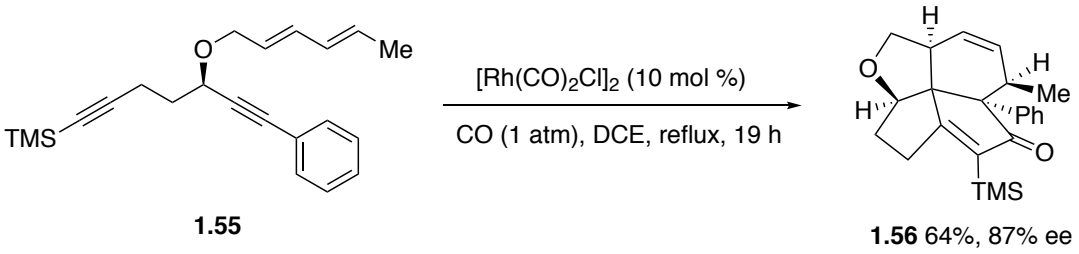

1.55

1.56 64%, 87% ee

Scheme 9. Domino PKR-Diels-Alder reaction to afford tetracyclic product 1.56.

1.3.3 Introduction to the allenic Pauson−Khand reaction (APKR).

Brummond and coworkers demonstrated that the Rh(I)-catalyzed PKR can also be extended to allene-ynes. The reaction of $[Rh(CO)_2Cl]_2$ with tethered allene-ynes **1.57** selectively affords 4-alkylidenecyclopentenones **1.58** (Scheme 10).[60] Alternatively, the allenic PKR (APKR) using stoichiometric $Mo(CO)_6$ provides α-alkylidenecyclopentenones **1.59**.[61] Predictable and selective reaction of one double bond of an allene over the other to form bicyclic ring systems makes the APKR a useful tool in complex molecule synthesis. Its utility can be extended by incorporation of additional rings on the carbon tether. As demonstrated by Brummond and coworkers, the APKR can be used to construct a variety of cyclopentenone-containing [6,7,5] fused ring systems, a scaffold that is present in numerous natural products (Scheme 11).[62] For example, tricyclic compounds **1.61** and **1.63** were accessed via the allenic Pauson−Khand Reaction (APKR) and closely correspond to the structures of Guanacastepene A (**1.1**) and Resiniferatoxin (**1.4**), respectively.

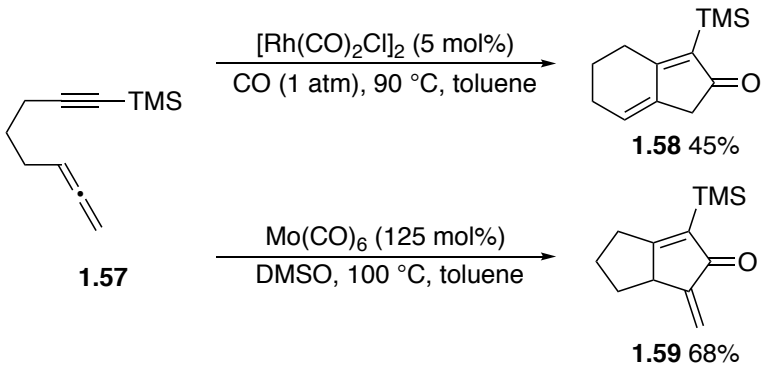

Scheme 10. Metal-dependent bond selectivity in the APKR.

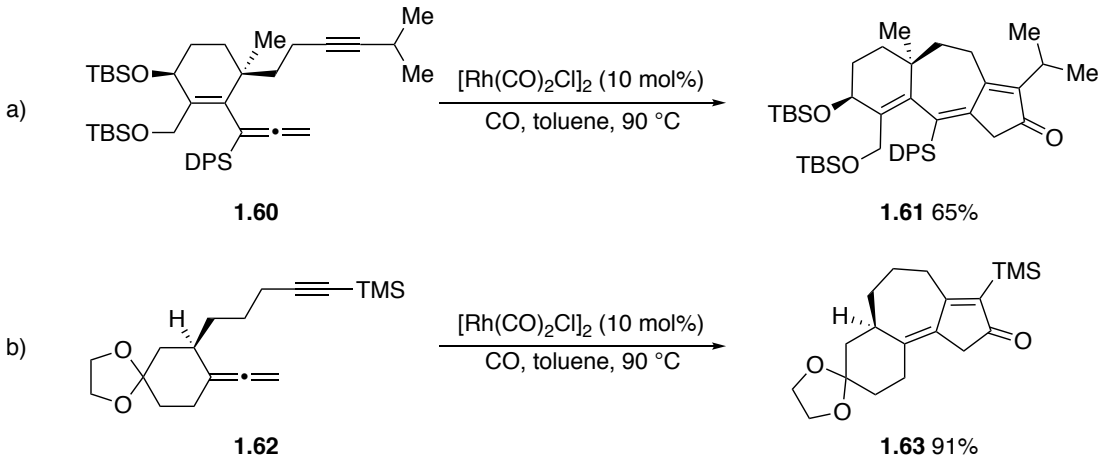

Scheme 11. Access to [6,7,5] fused ring systems via the APKR.

1.3.4 Applications of the APKR in the synthesis of natural products.

The allenic PKR was employed in the 14-step synthesis of (+)-ingenol (**1.66**) a terpene which exhibits anti-cancer activity (Scheme 12).[63] (+)-Ingenol (**1.66**) is approved as a topical medication for actinic keratosis, a precancerous skin condition.[64] The synthesis was developed in collaboration with LEO Pharma, who desired a short and scalable synthesis of this compound, amenable to the

synthesis of analogs. The Rh-catalyzed APKR of allene-yne **1.64** was used to establish the [6,7,5] ring scaffold in dieneone **1.65**.

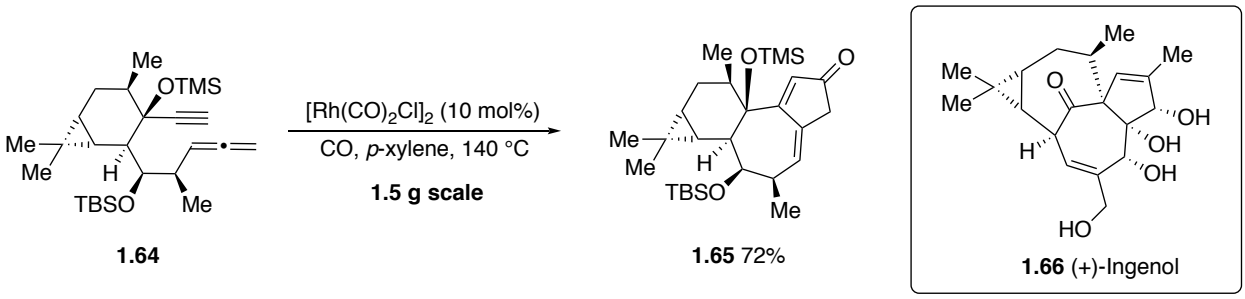

Scheme 12. Baran's synthesis of (+)-Ingenol.

The APKR also is an ideal strategy for accessing [5,7,5] fused ring systems of the guaianolide family of natural products (Scheme 13).[65] Guaianolides display interesting biological activity resulting from selective covalent modification of the α-methylene butyrolactone functionality.[66] Because of the electrophilic reactivity of the exocyclic methylene group, the α-methylene butyrolactone moiety is typically installed in the final steps of guaianolide synthesis and requires several steps.[67-69] Construction of the ring system via the APKR allows for early incorporation of the α-methylene butyrolactone moiety. APKR of allene-yne **1.67** proceeded in only 20 min in 92% yield (Scheme 13, a). This methodology was applied in the synthesis of **1.70**, a highly oxygenated analog of cumambarin A **1.71** (Scheme 13, b).[70] These examples illustrate how the high functional group tolerance of the Rh(I)-catalyzed APKR can be leveraged in step-economical syntheses.

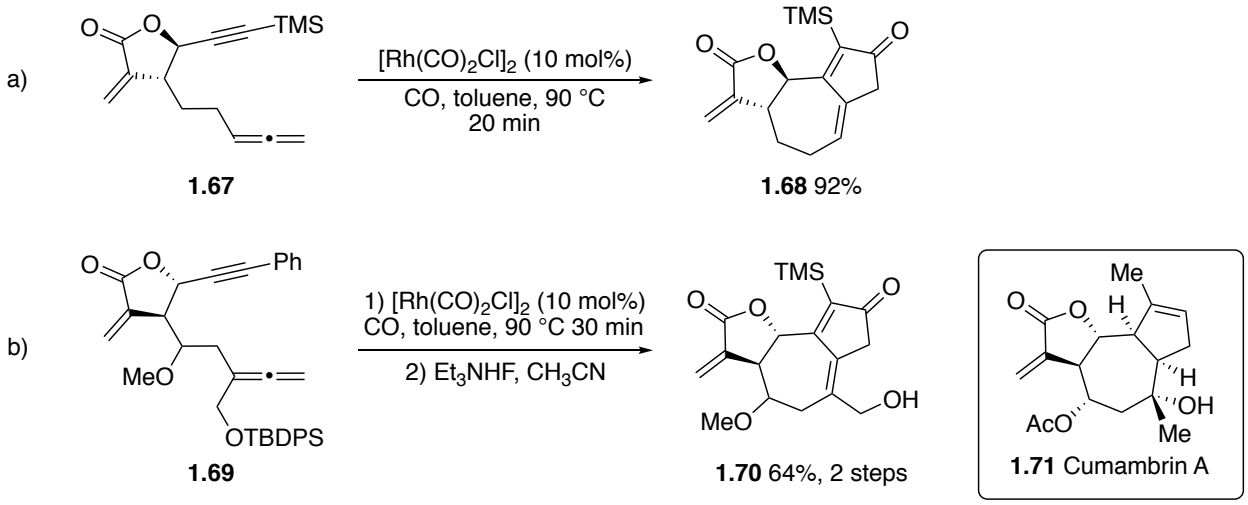

Scheme 13. APKR to access α-methylene butyrolactone-containing compounds.

1.3.5 The Rh(I)-catalyzed Pauson−Khand reaction of allenyl acetates.

Because of the mild conditions of the reaction, Matthew Davis, a former member of the Brummond research group, explored the feasibility of the APKR of allenyl acetates as a way of introducing the α-carboxy cyclopentenone functionality.[71] Both linear and cyclohexane-derived allene-ynes **1.72** and **1.74** were submitted to cyclocarbonylation conditions and the resulting bicyclic **1.73** and tricyclic **1.75** ring systems were obtained in good yields (Scheme 14). Rh(I) complexes do not readily undergo single electron transfer processes, so unlike similar PKRs using cobalt carbonyl complexes,[72] the carboxy groups of the cyclopentenone products **1.73** and **1.75** were not reductively removed. The Rh(I)-catalyzed APKR offers a redox economical way in which an oxygen-containing group can be installed on the position adjacent to a carbonyl of a cyclopentenone.

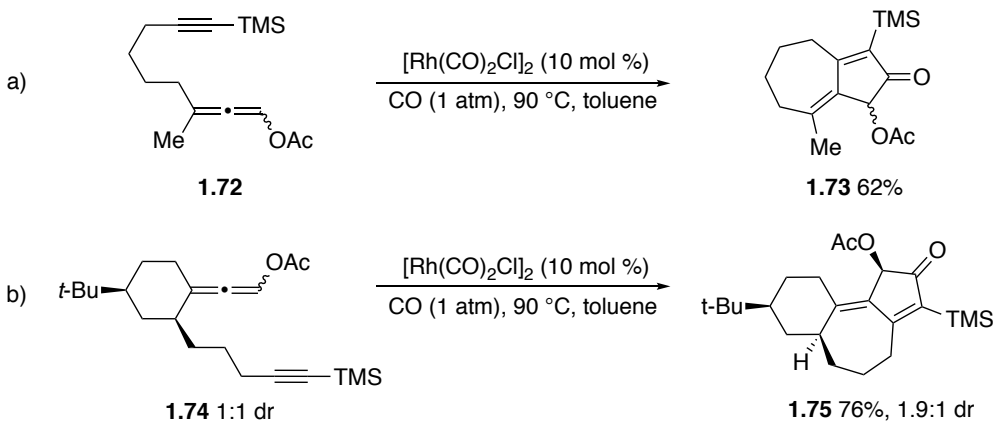

Scheme 14. APKR of allenyl acetates.

1.3.6 Determining the origin of the observed increase in dr.

Interestingly, the APKR product **1.75** was obtained in a nearly 2:1 dr, even though the allene-yne **1.74** was reacted as a 1:1 diastereomer ratio (Scheme 14, b). Several experiments were performed to determine the origin of this effect. First, a 3:1 diastereomeric mixture of allene **1.74** was subjected to the APKR conditions in toluene-d_8 and monitored by ^{1}H NMR spectroscopy (Scheme 15, a). After 40 min at 90 °C, complete scrambling of the allenyl acetate **1.74** axial chirality was observed, affording a 1:1 mixture of diastereomers with no evidence of APKR product **1.74**. When the reaction was performed at rt, scrambling occurred within 7 h, again with no evidence of APKR product. These results demonstrate that under the APKR conditions, the scrambling of allenyl acetate **1.74** axial chirality occurs at a faster rate than the cyclocarbonylation reaction. No scrambling of allenyl acetate axial chirality occurred in the absence of the Rh catalyst (Scheme 15, b). Therefore, it was concluded that the scrambling process was catalyzed by Rh. A proposed mechanism for the Rh(I)-catalyzed scrambling of allenyl acetate axial chirality involves η^2 coordination of the allene to give **1.77**, followed by nucleophilic attack of the central carbon of the

allene by the acetate, followed by rotation about the resulting sigma bond of **1.78** (Scheme 16). [73]

Based upon these results, it was hypothesized that the 2:1 dr of cyclopentenone **1.75** is either due to a kinetic preference for the reaction of one allenyl acetate isomer or alternatively, isomerization of the α-acyloxy ketone to the thermodynamically more stable product. Therefore, a third experiment was conducted in which a 5:1 dr of cyclopentenone product **1.75** was submitted to the APKR conditions to determine whether isomerization of the product could occur. No change of the diastereomeric ratio of the product was observed after 17 h at 90 °C (Scheme 15, c). This result eliminates the possibility that the observed diastereoselectivity was due to a thermodynamic preference for one α-carboxy cyclopentenone product. Taken together, these three ^{1}H NMR experiments suggest that the 2:1 diastereomeric ratio of product **1.75** is due to an energetic preference for one allenyl acetate diastereomer in the APKR transition state. This diastereoselective reaction led us to consider the potential application of this transformation in an enantioselective APKR.

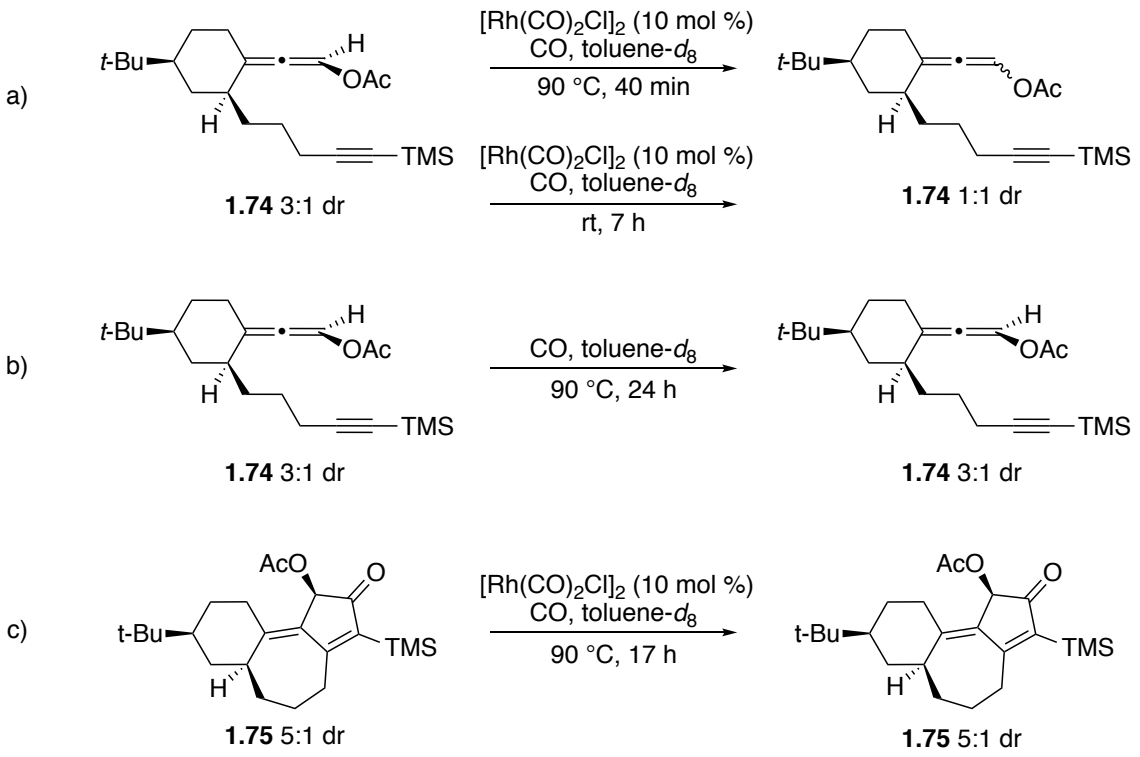

Scheme 15. Experiments probing the origin of APKR diastereoselectivity.

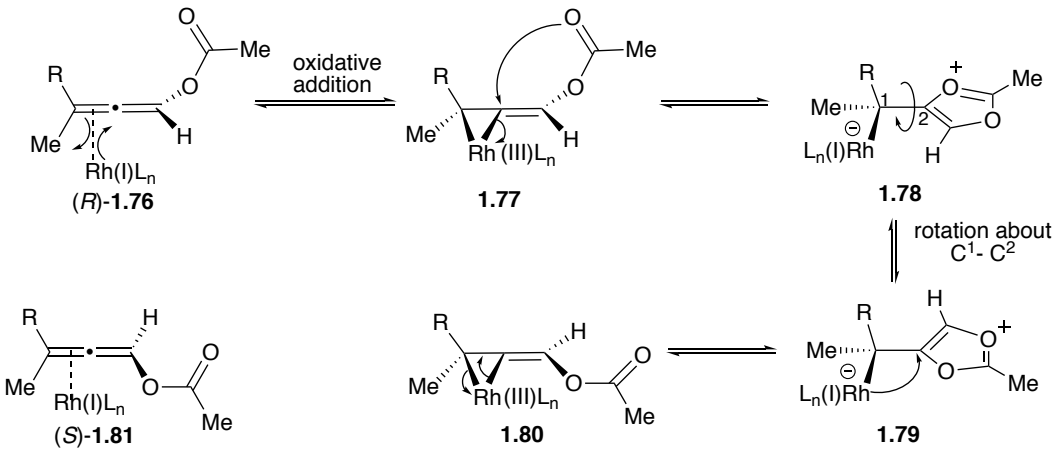

Scheme 16. Mechanism of Rh(I)-catalyzed scrambling of allenyl acetate axial chirality.

1.3.7 Introduction to the enantioselective Pauson-Khand reaction.

The first enantioselective PKR was effected with titanocene complex (*S,S*)-(EBTHI)Ti(CO)$_2$ **1.83** (Scheme 17).[74] Although the transformation was achieved with high yields and enantioselectivities, the complex **1.83** is extremely air and moisture sensitive, which limits the utility of this method.

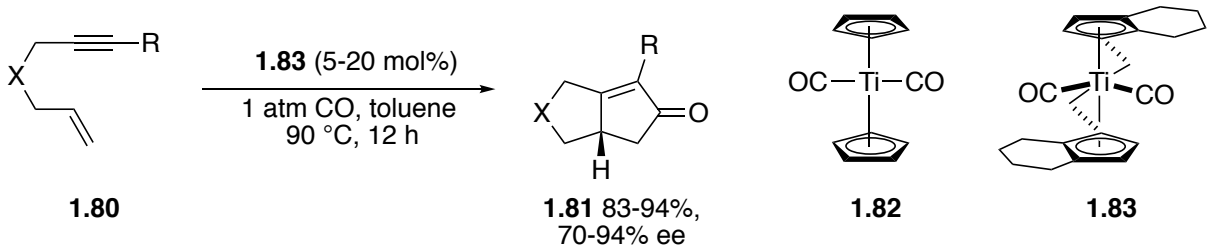

Scheme 17. Asymmetric PKR with a chiral titanocene complex.

Rhodium carbonyl complexes offer enhanced stability over titanium complexes. In 1998, rhodium(I) biscarbonyl chloride dimer, $[Rh(CO)_2Cl]_2$ was first used under atmospheric pressure of CO in the intramolecular PKR of tethered enyne **1.50** (Scheme 7, c). Unlike $Ti(Cp)_2CO_2$ (**1.82**), $[Rh(CO)_2Cl]_2$ only possesses nontunable ligands. This presented a challenge in the development of an asymmetric Rh(I)-catalyzed PKR. Incorporation of phosphine or cyclopentadienyl ligands on Rh(I) carbonyl complexes is made difficult by the high affinity of CO for the more electron rich late transition metal. The π-accepting CO ligands of $[Rh(CO)_2Cl]_2$ bind more tightly than those of $Ti(Cp)_2CO_2$ **1.82**. Under PK reaction conditions which include CO atmosphere, chiral ligands of rhodium complexes can be easily displaced by CO.[75]

Jeong and coworkers discovered that dinuclear rhodium catalyst *trans*-[RhCl(CO)(dppp)]$_2$ (dppp = 1,3-bis(diphenylphosphino)propane) furnished the cyclocarbonylation product **1.85** in 96% yield (Scheme 18, a).[76] These findings represent the first example of tunable phosphine ligands in the Rh-catalyzed PKR. While rate data was not supplied, Jeong and coworkers reported that the phosphine-ligated catalyst *trans*-[RhCl(CO)(dppp)]$_2$ significantly decelerated the PKR of malonate-tethered enyne **1.84** compared to [Rh(CO)$_2$Cl]$_2$. This result is unsurprising because phosphine ligands were also known to reduce reactivity of cobalt carbonyl complexes in the PKR.[77] Replacement of a π-accepting CO ligand with a σ-donating phosphine reduces the electrophilicity of the catalyst, making it less reactive toward enyne substrates. This reaction deceleration associated with phosphine incorporation, coupled with the difficulty of ensuring phosphine coordination because of competition with CO, means that the background reaction of the racemic phosphine-free Rh catalyst is likely to predominate over the reaction of the phosphine-bound catalyst in the PKR. Therefore, maintaining a chiral environment on the catalyst when asymmetric phosphine ligands are used is a significant challenge.

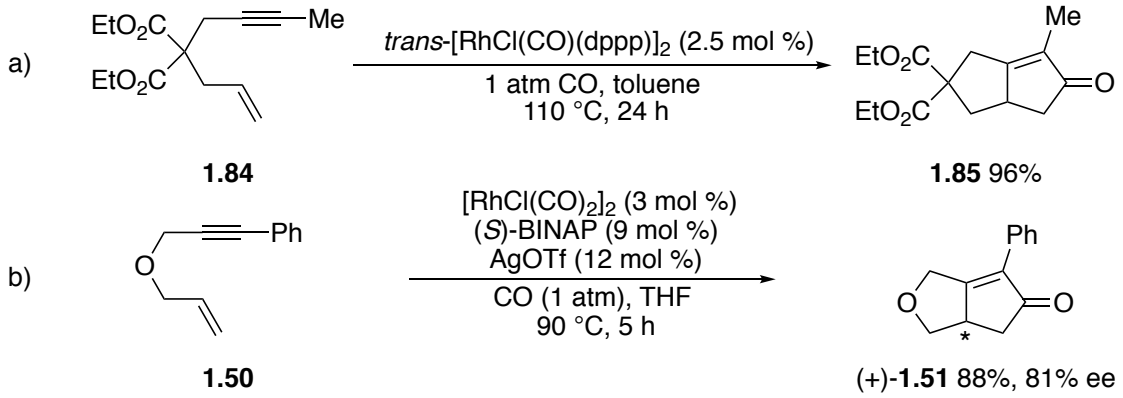

Scheme 18. Intramolecular rhodium(I)-catalyzed PKRs of 1,6- enynes.

The first enantioselective Rh(I)-catalyzed PKR of enynes was carried out using $[Rh(CO)_2Cl]_2$ with bidentate phosphine ligand (*S*)-BINAP (2,2'-bis(diphenylphosphino)-1,1'-binaphthyl) (Scheme 18, b).[75] The PKR of enyne **1.50** was effected in 88% yield and 81% ee under mild conditions of refluxing THF under 1 atm of CO. The low reactivity of Rh-bisphosphine complexes in the PKR was overcome by addition of silver triflate as an activator. Abstraction of the chloride ligand from the catalyst affords the cationic Rh(I)-(*S*)-BINAP complex with a triflate counteranion. This dramatically increases the reactivity of the otherwise inactive phosphine-ligated complex. The scope of the enantioselective Rh-catalyzed PKR is discussed in more detail in Chapter 4.

1.4 DYNAMIC KINETIC ASYMMETRIC PAUSON-KHAND REACTION OF ALLENYL ACETATES.

1.4.1 Introduction to stereoconvergent reactions.

The preparation of chiral molecules is of utmost importance in modern drug development. Different enantiomers of the same compound can often elicit different, and sometimes harmful, biological responses. Therefore, strategies used to effect asymmetric synthesis are an important area of development. The majority of enantioselective reactions involve the creation of a stereocenter from a prochiral starting material. Another strategy for effecting an enantioselective synthesis is by preferentially reacting a single enantiomer of a chiral racemic compound in a process known as kinetic resolution. A major drawback of this strategy is that the maximum product yield is 50%. If a mechanism exists for the interconversion of the two enantiomers of

starting material, then this drawback can be overcome. Through this dynamic interconversion process, racemic starting material can be converted to enantiopure product in 100% yield.[78]

Dynamic kinetic asymmetric reactions are classified according to the mechanism of interconversion of the enantiomers and the involvement of the catalyst.[78] In a dynamic kinetic resolution (DKR, Figure 5, a), interconversion of the enantiomers of the starting material is faster than the transformation of interest, and is independent of the reaction catalyst. An example of a DKR is the Pd-catalyzed Heck reaction of aryl iodides. The starting amide atropisomers **1.86** can interconvert by a rotation about the designated C-C bond.[79] A Type I Dynamic Kinetic Asymmetric Transformation (DyKAT) involves a rapid interconversion of the starting material enantiomers in a process which is catalyzed by the reaction catalyst (Figure 5, b). An example of a Type I DyKAT reaction is the asymmetric allylic alkylation of 2-alkylpyridines **1.88**. The chiral racemic allylic pivalate is deprotonated and the enantiomers interconverted via a Pd-π-allyl intermediate. The chiral Pd catalyst reacts selectively with one pivalate enantiomer in the subsequent alkylation reaction.[80] Alternatively, in a Type II DyKAT, the substrate interconversion is enabled on the catalyst, as it is being transformed into product. For example, propargyl pivalate **1.90** undergoes a formal [3,3]-sigmatropic rearrangement to afford a gold-bound allene.[81] One enantiomer of this gold-bound allene complex reacts faster with the chiral gold catalyst to afford the cyclized product **1.91**.

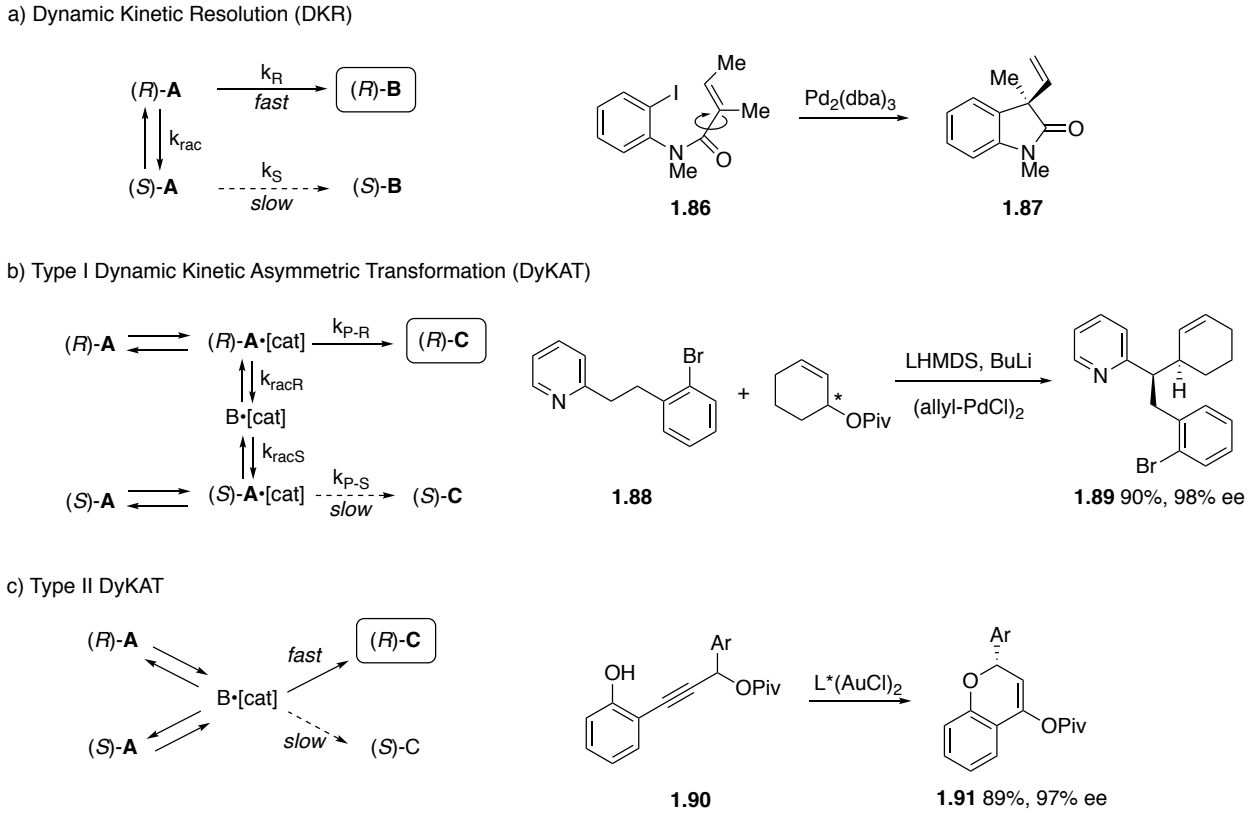

Figure 5. Mechanisms of stereoconvergent asymmetric reactions.

1.4.2 DYKAT approach to the enantioselective PKR of allenyl acetates.

Davis' experiments led us to believe that an enantiopure α-acetoxy cyclopentenone product is possible using a Type I DyKAT strategy.[82] In this type of reaction, a racemic substrate is converted to an enantiopure product because rapid substrate isomerization of the substrate and preferential product formation from one diastereomeric complex. Because allene isomerization occurs at a much faster rate (k_2 and k_{-2}, Scheme 19) than the APKR (k_1 and k_3), incorporation of a chiral Rh catalyst capable of accelerating k_1 over k_3 (or k_3 over k_1) could provide enantiopure APKR product **1.94** from a racemic mixture of allenyl acetates **1.92**.

A DyKAT of allenyl acetates would provide catalyst-controlled enantioselectivity in the synthesis of α-oxygenated polycyclic cyclopentenones. This reaction could be applied in the synthesis of analogs of Tg (**1.9**) further probe the structure-activity relationships of this important drug candidate. This work represents a rare example of a DyKAT reaction of an allene,[83-88] the first example of DyKAT in a cyclocarbonylation reaction, and the first catalyst-controlled enantioselective APKR. Thus, we set out to test the feasibility of the asymmetric APKR to prepare enantioenriched α-carboxy cyclopentenones.

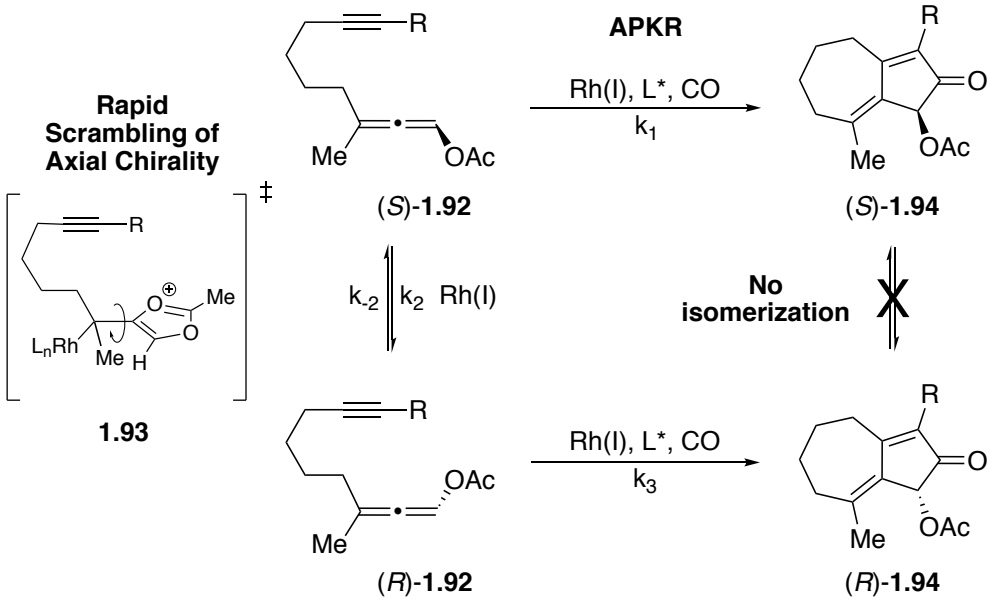

Scheme 19. Proposed Type I DyKAT of allenyl acetates.

2.0 COMPUTATIONALLY-GUIDED CATALYST DESIGN IN THE ASYMMETRIC PAUSON-KHAND REACTION OF ALLENYL ACETATES.

Currently, computational chemistry is most often used to *rationalize* experimental results rather than to *predict* them. However, computational tools are transforming our ability to predict enantioselectivity in transition metal catalyzed reactions and to guide the design of ligands *in silico*.[89] In turn, these predictive tools are mitigating experimental ligand screening, which is a resource intensive process. Transition metal catalyzed reactions are difficult to predict because of the large number of mechanistic possibilities and transition states by which the catalyst could react, and the small magnitude of relative energy differences.[90] Thus, *in silico* design of catalysts is considered by some to be a "holy grail" of computational chemistry.[91,92] In order to achieve this goal, experimental and computational chemists must work closely together to understand, and overcome, the shortcomings of computational methods for the prediction of experimental results. We set out to design a chiral Rh-catalyst for the asymmetric APKR via a three-step process: (1) Identifying an effective chiral ligand class in terms of reactivity and enantioselectivity, (2) Establishing the rate- and stereo-determining step of the APKR using DFT calculations and (3) varying the ligand-space on the metal to increase enantioselectivity. This last step was an iterative process where experiment served to benchmark calculated enantioselectivity, a process that required expanding the model to include mechanistic steps not previously considered. This three-

step, iterative process is illustrated in Figure 6. By using this approach, we identified an optimal ligand by experimentally testing a minimal number of ligands.

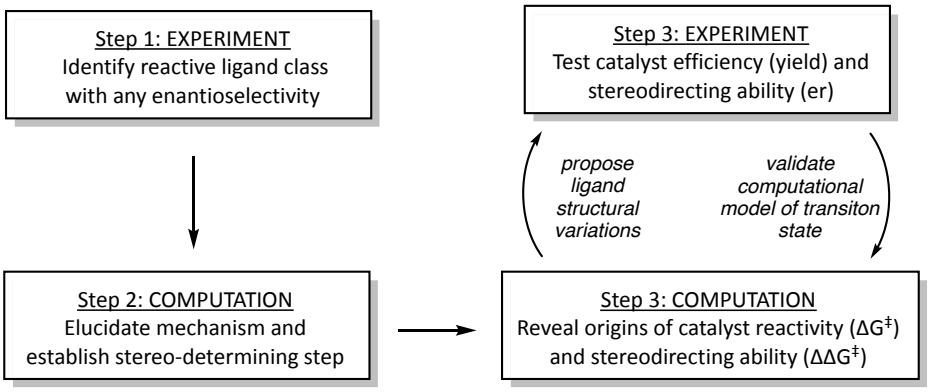

Figure 6. Iterative computational and experimental approach to catalyst design.

2.1 PREPARATION OF ALLENYL ACETATE APKR PRECURSORS.

To test the feasibility of the Rh(I)-catalyzed asymmetric APKR of allenyl acetates, it was envisioned that a number of allenes could be readily accessed from the alkynone **2.1** via the intermediate **2.2** (Scheme 20). Using this approach, the terminus of the alkyne (R^1) can be modified to incorporate alkyl, aryl and silyl groups. Additionally, the carbonyl group can be modified to include a variety of carboxy esters (R^2). Allenyl acetates **2.1** are prepared by a formal [3,3]-sigmatropic rearrangement of propargyl acetates **2.2**. The alkyne is incorporated via a Grignard addition of ethynylmagnesium bromide to methyl ketone **2.3**. Allene-yne **2.1** with a four-carbon tether was preferred, as it gave the highest yield in previous APKRs of linear allenyl acetates.[71]

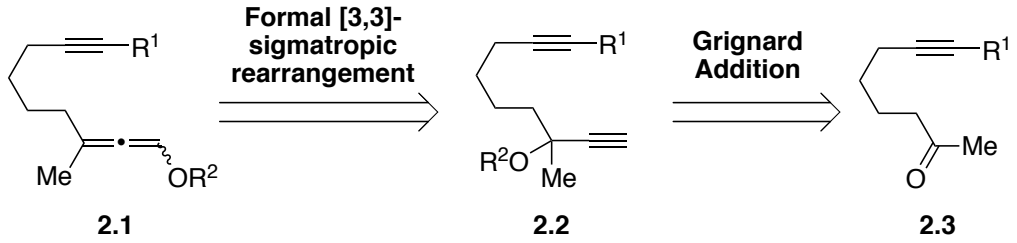

Scheme 20. Synthetic strategy to access allenyl acetates.

2.1.1 Synthesis of methyl ketones.

Methyl ketones were prepared via two routes. The first route was employed in the synthesis of phenyl (Ph) and triisipropylsilyl (TIPS)-substituted alkynes (Scheme 21). 5-Hexen-1-ol was tosylated using toluenesulfonyl chloride, dimethylaminopyridine and triethylamine to afford **2.4** in 98% yield. Next, tosylate **2.4** was reacted with the corresponding lithium salt of phenylacetylene and triisopropylacetylene, to give **2.5a** in 91% yield and **2.5b** in 39% yield. Terminal alkenes were submitted to palladium(II) chloride (0.25 equiv) and copper(I) chloride conditions, providing methyl ketones **2.6a** and **2.6b** in 45% and 64% yield, respectively.

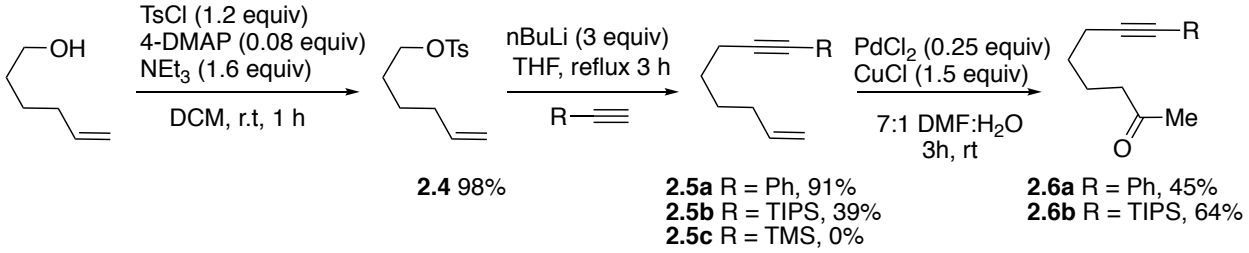

Scheme 21. Synthesis of methyl ketones 2.6a-b.

The synthesis of trimethylsilyl (TMS)-substituted alkyne substrates required an alternative route because of the volatility of the TMS alkene synthetic intermediate **2.5c**. Therefore, a synthetic route was employed for the synthesis of the TMS-allene where the hydroxyl group of alcohol **2.7** was converted to an iodide via a modified Appel reaction to afford 5-iodo-1-trimethylsilyl-1-pentyne (**2.8**) (Scheme 22). [93] Addition of the sodium salt of methyl acetoacetate to iodide **2.8** provided the β-ketoester **2.9** in quantitative yield. The β-ketoester **2.9** was reacted with lithium chloride (2.6 equiv), H_2O (1.0 equiv) in DMSO and heated to 130 °C for 14 h to afford the decarboxylated methyl ketone **2.6c** in 62% yield.

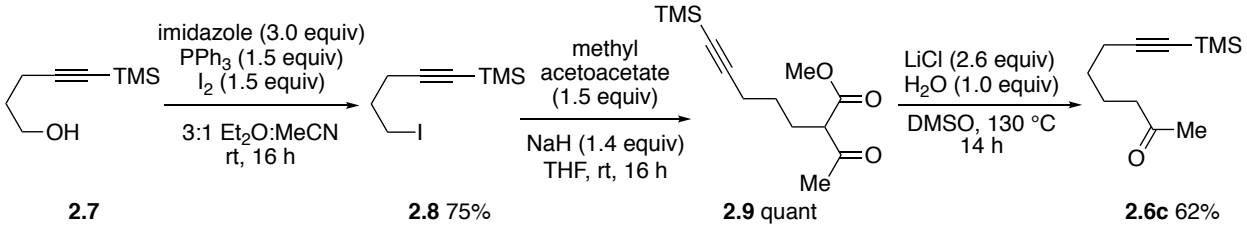

2.7 **2.8** 75% **2.9** quant **2.6c** 62%

Scheme 22. Synthesis of 8-trimethylsilyl-oct-7-yne-2-one (2.6c).

2.1.2 Synthesis of propargylic carboxy esters.

Conversion of the carbonyl of **2.6a-c** to the propargylic alcohols was accomplished by addition of ethynylmagnesium bromide. For the case where R^2 = Ac, addition of acetyl chloride directly to the resulting magnesium alkoxide affords the propargylic acetates **2.10a**, **2.10b** and **2.10c** in 65%, 62% and 71% yields (Scheme 23, a). In addition to the acetate-containing substrates **2.10a-c,** a series of four other carboxy-containing substrates were chosen to represent a range of electronic and steric effects. Synthesis of these carboxy esters required isolation of the tertiary propargylic

alcohol **2.11** (Scheme 23, b). Formation of the sterically-demanding pivalate **2.10d** was accomplished by the addition of pivalic anhydride (1.5 equiv) and scandium(III) triflate (5 mol %) to alcohol **2.11** in acetonitrile in 86% yield. Propargyl octanoate **2.10e** was accessed in 45% yield by addition of octanoic acid, *N*,*N*-dicyclohexylcarbodiimide (DCC) and 4-dimethyl aminopyridine (DMAP) to propargyl alcohol **2.11**. Propargyl benzoate **2.10f** was prepared in 55% yield by reacting propargyl alcohol **2.11** with benzoic anhydride, triethylamine, and DMAP. The electron-withdrawing *p*-nitrobenzoate (PNB) group was installed by reacting propargyl alcohol **2.11** with *p*-nitrobenzoyl chloride, and DMAP to afford **2.10g** in 84% yield. Reaction of TIPS-alkyne substrate **2.11b** with scandium(III) triflate gave **2.10h** in 71% yield. These carboxyl esters were then advanced to the final step of the allene-yne substrate synthesis.

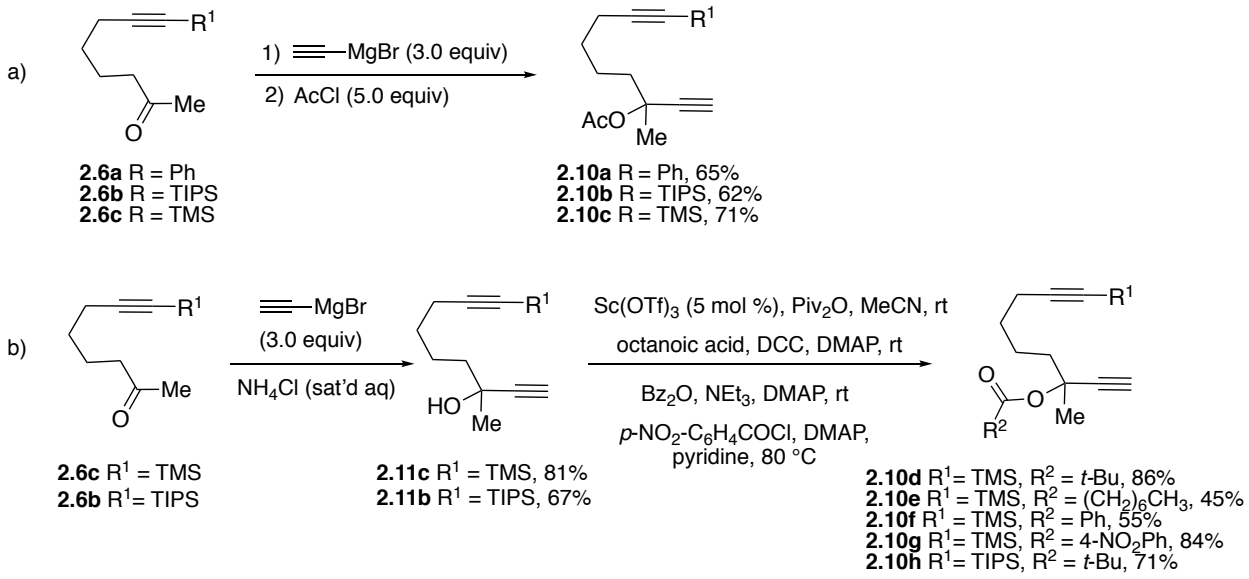

Scheme 23. Synthesis of propargyl carboxy esters 2.10a-g.

2.1.3 Synthesis of allenyl acetates.

Allenyl esters were prepared via a transition metal catalyzed formal [3,3] sigmatropic rearrangement of propargyl carboxy esters.[71] A variety of metal complexes can electrophilically activate the alkyne of propargyl carboxy ester toward addition of the ester (Scheme 24, a). For example, platinum(II) chloride catalyzes the rearrangement of acetate **2.15** to afford the allene **2.16** (Scheme 24, b).[94] Propargyl carboxy esters with bulky substituents such as indole **2.17** can also undergo this transformation when gold(III) chloride is used as a catalyst (Scheme 24, c).[95] Rhodium(II) bistrifluoroaceate dimer, $[Rh(OCOCF_3)_2]_2$, can catalyze the rearrangement of terminal propargylic carboxy esters to afford trisubstituted allenyl acetates in high yields (Scheme 24, d).[96] Because our targeted substrates also contain terminal allenyl carboxy esters, we hypothesized that these conditions would be effective in the synthesis of linear allene-ynes **2.21a-h**.

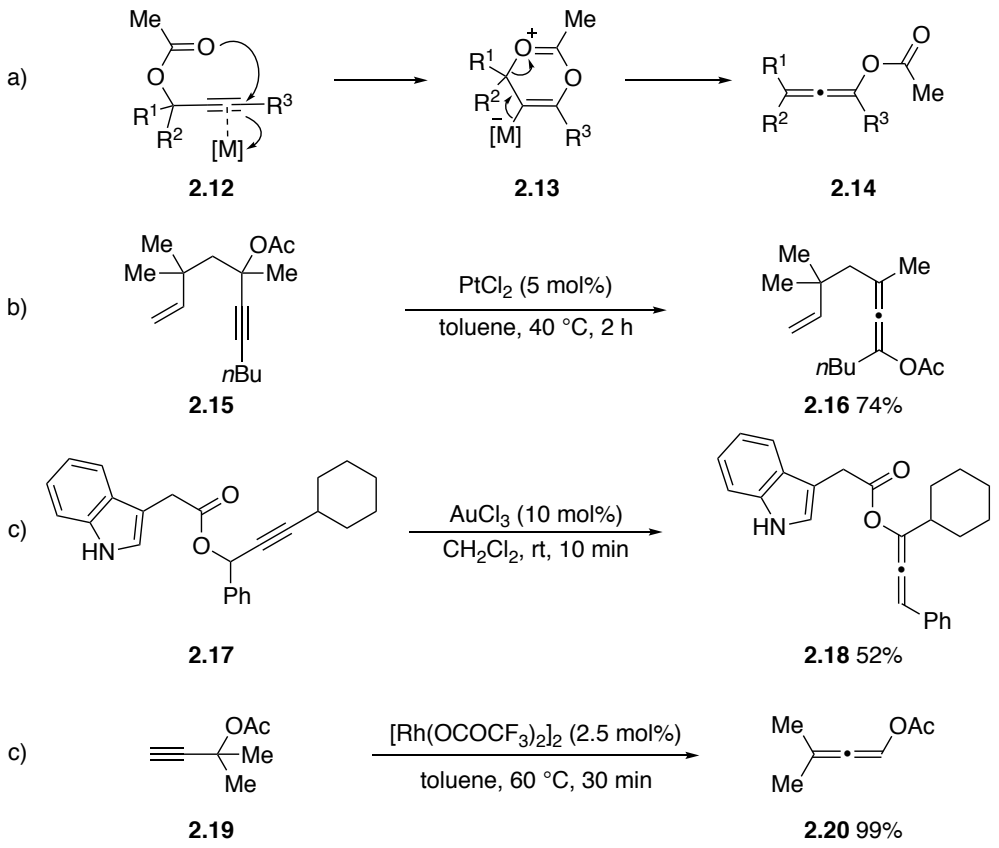

Scheme 24. Formal [3,3]-rearrangements of propargylic carboxy esters.

Propargyl carboxy esters **2.10a-g** were reacted with $[Rh(OCOCF_3)_2]_2$ in toluene at 50 °C. Formation of the allenyl acetate functionality was evident by the appearance of the allenic proton peak by ^1H NMR spectroscopy (~7.3 ppm), the allenic carbon in the by ^{13}C NMR spectroscopy (190 ppm), and the characteristic stretching frequency of the allene group by IR spectroscopy (~1955 cm^{-1}). Propargylic acetate **2.10a** was added to a solution of $[Rh(OCOCF_3)_2]_2$ in toluene and heated 75 min to afford allenyl acetate product **2.22a** in 91% yield (Table 1, entry 1). TIPS-substituted alkyne **2.10b** reacted in 60 min to provide allenyl acetate **2.22b** in 94% yield (entry 2), while TMS-substituted **2.10c** reacted with the Rh(II) catalyst to give allenyl acetates **2.21c** in 93% yield (entry 3). Propargyl pivalate **2.10d** reacted in only 35 min to give allenyl pivalate **2.21d** in 89% yield (entry 4). The lowest-yielding substrate was propargyl carboxy octanoate **2.10e**, which

reacted in 77% yield. Rearrangement of propargyl carboxy benzoate **2.10f** provided allenyl benzoate **2.21f** in 87% yield (entry 6). Propargyl *p*-nitrobenzoate **2.10g** was converted to allenyl *p*-nitrobenzoate **2.21g** in 89% yield (entry 7). Finally, reaction of propargyl pivalate **2.10h** with $[Rh(OCOCF_3)_2]_2$ afforded allenyl pivalate **2.21h** in 85% yield (entry 8). All propargylic carboxy esters tested underwent the Rh(II)-catalyzed rearrangement in high yields. The resulting allenyl carboxy esters were employed in studies of the asymmetric APKR.

Table 1. Rh(II)-catalyzed formal [3,3]-sigmatropic rearrangements of propargyl acetates.

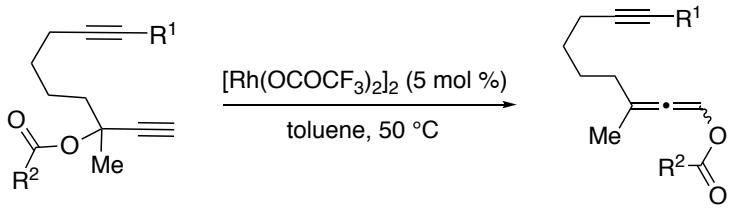

entry	R^1	R^2		time (min)	yield (%)
1	Ph	Me	**2.10a**	75	**2.21a**, 91
2	TIPS	Me	**2.10b**	60	**2.21b**, 94
3	TMS	Me	**2.10c**	90	**2.21c**, 93
4	TMS	*t*-Bu	**2.10d**	35	**2.21d**, 89
5	TMS	$(CH_2)_6CH_3$	**2.10e**	50	**2.21e**, 77
6	TMS	Ph	**2.10f**	60	**2.21f**, 87
7	TMS	4-NO_2Ph	**2.10g**	60	**2.21g**, 89
8	TIPS	*t*-Bu	**2.10h**	30	**2.21h** 85

2.2 IDENTIFICATION OF CATALYST, MODEL SUBSTRATE AND LIGAND CLASS FOR ENANTIOSELECTIVE APKR.

2.2.1 Identification of catalyst and model substrate for APKR studies.

To identify a preliminary reaction model system for DyKAT optimization, three allene-ynes **2.21a-c**, with different substituents at the alkyne terminus were reacted under neutral and cationic Rh(I) conditions (Conditions A and B, respectively, Table 2). The reaction of phenyl-substituted alkyne **2.21a** gave cyclopentenone **2.22a** in 30% and 61% yield (Table 2, entry 1), the triisopropylsilyl (TIPS)-alkyne **2.21b** afforded **2.22b** in 50 and 16% yield (entry 2), and the trimethylsilyl (TMS)-substituted alkyne **2.21c** afforded **2.22c** in 47 and 70% yield (entry 3), respectively. Because allene-yne **2.21c** gave the highest yield under the cationic rhodium(I) conditions in the presence of a phosphine ligand at lower temperature (50 versus 110 °C), we focused on the APKR of **2.21c** using cationic rhodium catalysts in the development of the asymmetric catalytic system.

Table 2. Identification of substrate and catalyst for model system.

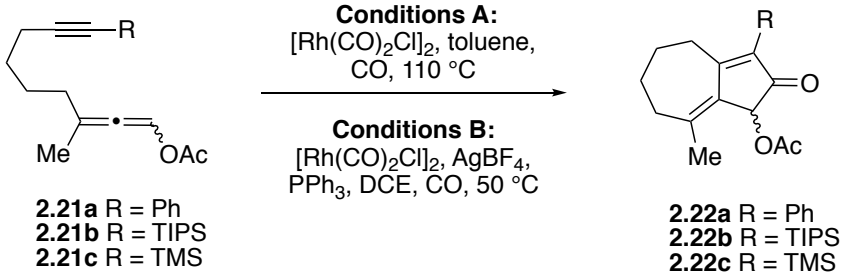

2.21a R = Ph
2.21b R = TIPS
2.21c R = TMS

2.22a R = Ph
2.22b R = TIPS
2.22c R = TMS

Entry	R		Conditions A	Conditions B
1	Ph	**2.21a**	30	61
2	TIPS	**2.21b**	50	16
3	TMS	**2.21c**	47	70

2.2.2 Identification of an effective ligand class for the asymmetric APKR.

Several different ligand classes were tested in order to identify a ligand which would afford APKR product in good yield and some enantioselectivity. First, two ligands were tested which have previously proven effective in the PKR of enynes. Bidentate phosphines (*R*)-BINAP (**2.24**) and (*R*)-MeOBIPHEP (**2.25**) both rendered the Rh catalyst unreactive, affording low yields of the desired cyclopentenone product **2.22c** and allenyl acetate degradation product, aldehyde **2.23c** as the major product**.** Most importantly, the products obtained from these bidentate phosphine catalysts were racemic (Table 3, entries 1 and 2). We hypothesized that either the Rh-ligand complexes were unselective, or the ligand was not effectively binding to the catalyst, resulting in predominance of the racemic background reaction. Therefore, *N*-heterocyclic carbene ligand 1,3-dimesitylimidazol-2-ylidene (IMes) was tested because of the strong metal-ligand binding ability of this ligand class. Catalyst Rh(IMes **2.26**)(cod)(Cl) was synthesized,[97] and tested in the APKR. No product was observed and only starting material was recovered (Table 3, entry 3). We expected that the strong σ-donating character of the NHC ligand played a role in deactivating the catalyst. Therefore, a more π-accepting, and less sterically-demanding phosphoramidite ligand (*S*)-MonoPhos (**2.27**) was tested. This ligand afforded cyclopentenone product **2.22c** in 76% yield and 16% ee (Table 3, entry 4). With a ligand in hand that afforded the APKR product with some enantioselectivity in good yield, we next set out to improve the enantioselectivity of the APKR by introducing modifications on the phosphoramidite ligand.

Table 3. Experimental screening of ligand classes in the APKR of 2.21c.

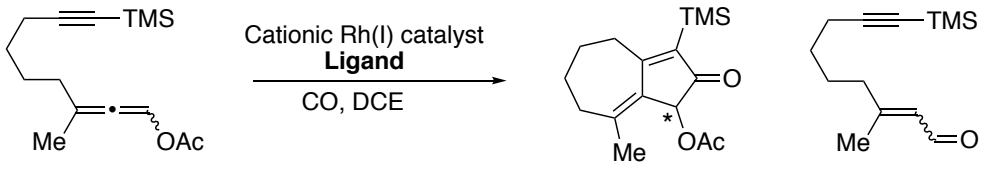

2.21c **2.22c** **2.23c**

Entry	Ligand	T	Time	Yield (%)		ee (%)[a]
		(°C)	(h)	**2.22c**	**2.23c**	
1[b]	(*R*)-BINAP (**2.24**)	90	16	13	18	0
2[c]	(*R*)-MeOBIPHEP (**2.25**)	80	5	21	28	2
3[d]	IMes (**2.26**)	50	15	0[e]	0	-
4[f]	(*S*)-MonoPhos (**2.27**)	50	5	76	5	16

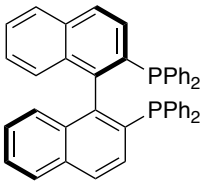

(*R*)-BINAP (**2.24**)

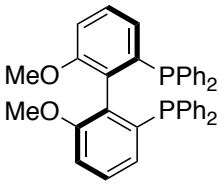

(*R*)-MeO-BIPHEP (**2.25**)

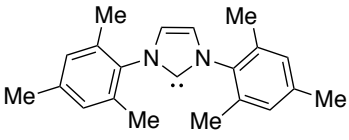

IMes (**2.26**)

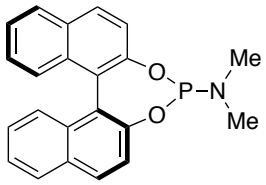

(*S*)-MonoPhos (**2.27**)

[a] Enantiomeric ratios were determined by HPLC using a chiral stationary phase. [b] $[Rh(CO)_2Cl]_2$ (10 mol %), **2.24** (22 mol %), $AgBF_4$ (20 mol %), DCE, CO (1 atm). [c] $[Rh(CO)_2Cl]_2$ (10 mol %), **2.25** (22 mol %), $AgBF_4$ (20 mol %), DCE, CO (1 atm) [d] [Rh(IMes **2.26**)(cod)(Cl)] (10 mol %), $AgBF_4$ (10 mol%) DCE, CO (1 atm). [e] Recovered starting material. [f] $Rh(cod)_2BF_4$ (10 mol %), **2.27** (15 mol %), DCE, CO (1 atm).

2.3 APKR WITH (*S*)-MONOPHOS LIGAND.

2.3.1 DFT-calculated mechanism of the APKR with (*S*)-MonoPhos.

Once monodentate phosphoramidites were identified as a reactive ligand class in the APKR, the mechanism of the reaction was elucidated using DFT calculations to determine the enantioselectivity-determining step (Scheme 25). The resting state of the catalyst is square-planar complex **2.28.** Coordination of allene-yne **2.21c** affords square-planar complex **2.29** as a low-

energy pathway (ΔG = +5.5 kcal/mol). Oxidative addition into 16-electron, two-CO, square pyramidal complex **2.29** requires an overall activation energy of 21.9 kcal/mol via **2.30-TS**. Alternatively, coordination of allene-yne **2.21c** to afford square-pyramidal complex **2.31**, followed by oxidative cyclization proceeds with an overall energy barrier of 17.6 kcal/mol. Thus, although the coordination of allene-yne **2.21c** to afford square planar complex **2.29** is more favorable, the rate-determining oxidative-addition step is more facile via square pyramidal transition state **2.32-TS**. Formation of Rh(III) metallacycle **2.33** is exothermic (ΔG = −13.1 kcal/mol). Therefore, the oxidative addition step is irreversible and thus, the rate-determining step. Subsequent CO insertion provides acyl complex **2.35**. Reductive elimination provides Rh-coordinated product **2.37**. All transition states are significantly lower in energy than the oxidative addition, and therefore, oxidative addition is the rate-and stereo-determining step.

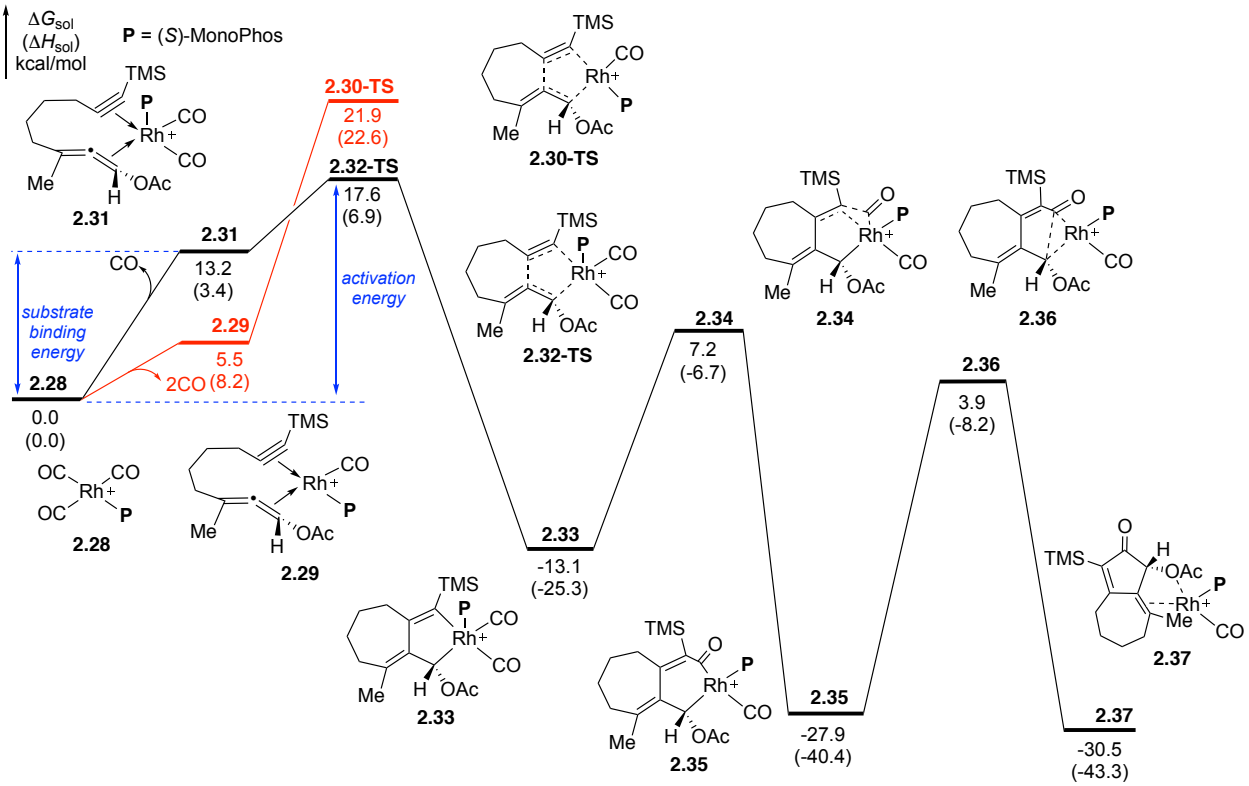

Scheme 25. Reaction energy profile of the Rh(I)-catalyzed APKR.

Reproduced with permission from Burrows, L. C.; Jesikiewicz, L. T.; Lu, G.; Geib, S. J.; Liu, P.; Brummond, K. M., *J. Am. Chem. Soc.* **2017**, *139* (42), 15022-15032. Copyright 2017 American Chemical Society. Geometry optimization was performed using B3LYP/6-31G(d)−LANL2DZ (Rh) and single point energy performed using M06/6-311+G(d,p)−SDD(Rh) /SMD(DCE).

2.3.2 Calculated Rh-(*S*)-MonoPhos transition state structures.

The reaction can proceed to afford either (*R*) or (*S*) cyclopentenone product **2.23**. Twelve different transition states were examined to determine the origin of enantioselectivity (16% ee, Table 3, entry 4). The phosphoramidite ligand can occupy three different positions on the catalyst relative to the substrate: *cis* to the acetate (**2.37-TS** and **2.39-TS**), *cis* to the silyl group (**2.38-TS** and **2.40-TS**), or in the apical position (**2.32-TS** and **2.41-TS**). For each geometric isomer, one rotational

isomer with a 180-degree rotation of the ligand about the Rh-P bond was included (**2.37-TS-rot**, **2.38-TS-rot**, and **2.32 TS-rot**). Thus, six unique transition states leading to both the (*R*)-and (*S*)-product **2.23** were considered. The lowest-energy complex is structure **2.32-TS**, leading to the (*R*) product **2.23**. However, structures **2.38-TS**, **2.37-TS**, **2.37-TS-rot**, and **2.40-TS-rot**, are all within 2.0 kcal/mol of the lowest-energy structure, indicating that the lowest-energy transition state is not possible to predict accurately. Due to the small range of transition state energies, it is expected that the (*S*)-Monophos (**2.27**) can easily rearrange to give another transition state isomer.

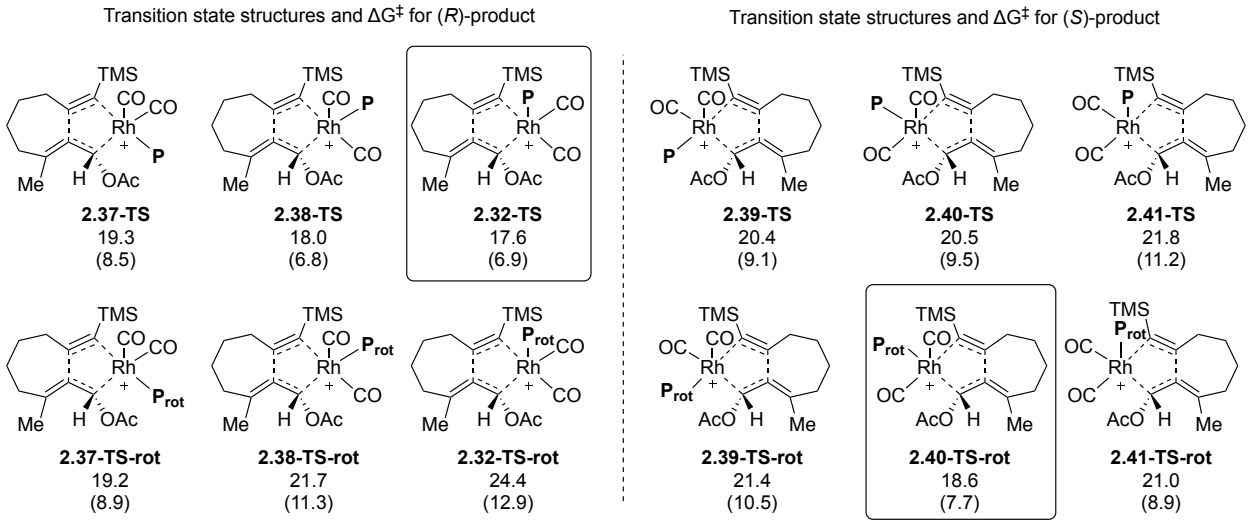

Figure 7. Transition state energies of Rh-(*S*)-MonoPhos APKR.

P_{rot} designates a different ligand conformation by rotation about the Rh–P bond. Tetrafluoroborate counteranion is omitted in the calculations. Reproduced with permission from Burrows, L. C.; Jesikiewicz, L. T.; Lu, G.; Geib, S. J.; Liu, P.; Brummond, K. M., *J. Am. Chem. Soc.* **2017**, *139* (42), 15022-15032. Copyright 2017 American Chemical Society.

The lowest-energy transition state structure (**2.32-TS**) shows the (*S*)-MonoPhos (**2.27**) ligand in the apical positon with steric interaction between the ligand and the acetate group of the substrate (Figure 8). We hypothesized that enhancing this interaction using a ligand with a wider

cone angle could lead to improved enantioselectivity while maintaining the good reactivity observed using the monodentate phosphoramidite (*S*)-MonoPhos (**2.27**).

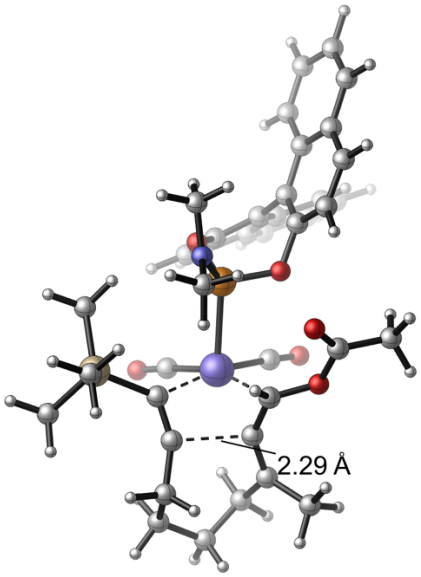

Figure 8. Lowest-energy transition state structure of Rh-(*S*)-MonoPhos-catalyzed APKR.

2.4 APKR WITH (*S*)-SIPHOS LIGAND.

2.4.1 Advantages of spirocyclic ligand framework.

Based on the transition states depicted in Figure 7, we postulated that an increase in steric interaction between the ligand and the substrate could be achieved using spirocyclic ligand (*S*)-SIPHOS (**2.42**). This ligand was chosen because of its fan shape, which provides an increased steric environment close to the metal center.[98] An additional advantage of the spirocyclic ligand (*S*)-SIPHOS (**2.42**) is its rigid chiral framework. The tetrahedral carbon provides central chirality

which cannot rotate, as opposed to a 1,1'-binaphthyl framework which can rotate to some degree about the C-C bond.

(*S*)-SIPHOS (**2.42**) was previously applied in the PKR of enyne **1.50** affording product **1.51** in 56% yield and 84% ee (Scheme 26).[99] The authors note that the reaction proceeds in higher yields and enantioselectivity with two equivalents of ligand to rhodium (56% yield, 84% ee versus 26% yield, 24% ee). Reaction of ligand (*R*,*S*,*S*)-SIPHOS-PE (**2.43**), which contains additional chiral centers on the amine, gave only trace product, which suggests that a sterically demanding amine hinders PKR reactivity. Compared to the PKR of **1.50** using (*S*)-BINAP (**2.24**), the PKR using monodentate ligand (*R*)-SIPHOS (**2.42**) proceeds in lower yield (56 versus 88%), and slightly higher enantioselectivity (84 versus 81% ee).[75] These results demonstrate that a monodentate ligand is capable of effecting a high level of enantioselectivity in the PKR. Based on the transition state structure **2.32-TS**, we hypothesized that the *ortho* hydrogens of (*S*)-SIPHOS (**2.42**) (colored red) would interact with the carboxy group of the substrate and afford higher enantioselectivity in the APKR than (*S*)-MonoPhos (**2.27**).

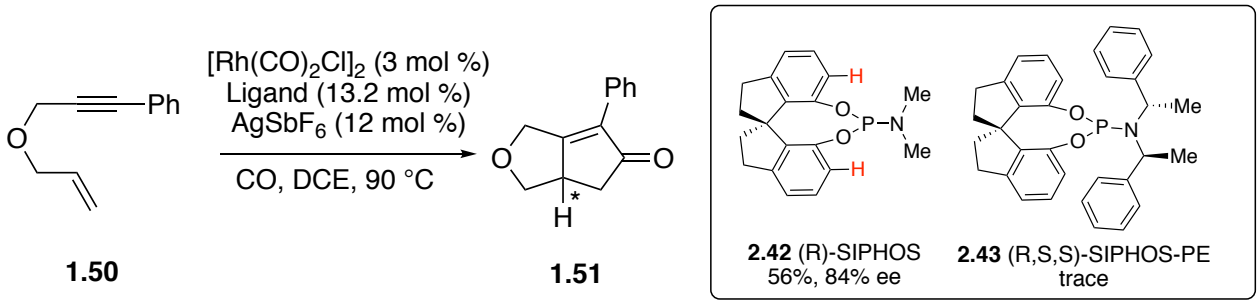

Scheme 26. Spirocyclic ligands in the asymmetric PKR.

2.4.2 APKR using (*S*)-SIPHOS ligand.

To test this hypothesis, allenyl acetate **2.21c** was reacted with $Rh(cod)_2BF_4$ (10 mol %) and (*S*)-SIPHOS (**2.42**) (11 mol %) to afford **2.22c** in 75% yield and 26% ee (Table 4, entry 1), representing a slight improvement over the 16% ee afforded by (*S*)-MonoPhos (**2.27**) ligand. Because the ee was so low, it was reasoned that a background reaction might be occurring. Therefore, the ligand to catalyst ratio was increased from 1.1:1 to 2.2:1, which resulted in an increase in enantioselectivity to 42% ee (entry 2). An increase in temperature from 50 to 90 °C was required to achieve reactivity. Further increases in ligand/catalyst ratio further reduced the reactivity of the catalyst. For example, when 30 mol % of (*S*)-SIPHOS (**2.42**) was used, only trace product was obtained after 40 h at 90 °C (entry 3), and when 40 mol % was used, no reaction occurred (entry 4). Based upon the higher temperatures necessary (entries 2-4) and poor conversion (entries 3-4) with higher ligand equivalents, we concluded that the phosphoramidite ligand decreases reactivity of the catalyst.

Table 4. Increasing (*S*)-SIPHOS equivalents in the APKR of allenyl acetate 2.21c.

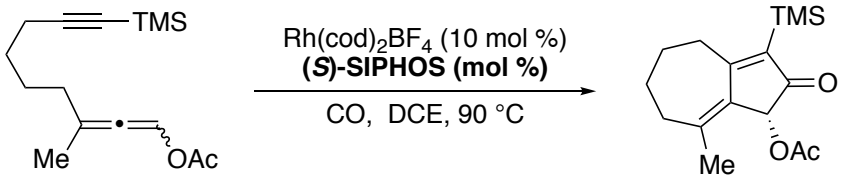

2.21c **2.22c**

Entry	(*S*)-SIPHOS (**2.42**) (mol %)	T (°C)	Time	yield (%)	ee (%)
1	11	50	18 h	75	26
2	22	90	9 h	67 [a]	42
3	30	90	40 h	Trace product [b,c]	-
4	40	90	40 h	No reaction	-

[a] The reaction was stirred 3 h at 50 °C, 3 h, at 70 °C, and 9 h at 90 °C. The reaction was not monitored closely during 9 h at 90 °C. [b] Approximately 75% allenyl acetate remaining. [c] Trace product observed by TLC was not isolated.

2.4.3 Substrates tested in the APKR using (*S*)-SIPHOS ligand.

(*S*)-SIPHOS (**2.42**) was tested in the APKR because of the postulated improved interaction between the substrate and the *ortho* hydrogens in the ligand (Scheme 26, colored red). In order to enhance this hypothesized interaction, several substrates were tested which differed in the steric demands of the substituents. For example, TIPS-substituted alkyne **2.21b** afforded APKR product in lower yield than the TMS-alkyne **2.21c**, suggesting that the silyl group has a detrimental interaction with the ligand during the APKR (Table 5, compare entries 1 and 2). Incorporation of a bulky allenyl carboxy pivalate group was expected to enhance interaction between the ligand and the carboxy group and improve enantioselectivity. Surprisingly, the enantioselectivity decreased to 27% ee (compare entries 1 and 3). Because of the propensity of monodentate ligands to rearrange (Figure 7), we hypothesize that the ligand moved to a new position on the metal to reduce steric interaction with the substrate. Increasing the steric bulk at both the alkyne and the

ester using TIPS-pivalate substrate **2.21h** gave no reaction. No product was observed after 24 h at 90 °C (entry 4). In an effort to improve reactivity, the substrate **2.21h** was subjected to microwave irradiation (entry 5) at 190 °C. The substrate, Rh catalyst and ligand were added to a microwave vial under nitrogen. The vial was evacuated and refilled with carbon monoxide gas and heated to 190 °C. Only starting material was recovered. These results show that the APKR using (*S*)-SIPHOS (**2.42**) is tolerant of steric bulk on the carboxy group, but is deactivated in the presence of a bulky alkyne group.

Table 5. APKR of Rh-(*S*)-SIPHOS catalyst.

entry	R^1	R^2		T (°C)	time (h)	yield (%)	ee (%)
1	TMS	Me	**2.21c**	90	9 h	**2.22c** 67	42
2	TIPS	Me	**2.21b**	90	16 h	**2.22b** 19	33
3	TMS	*t*-Bu	**2.21d**	90	8 h	**2.22d** 50	27
4	TIPS	*t*-Bu	**2.21h**	90	24 h	No reaction	-
5	TIPS	*t*-Bu	**2.21h**	190	MWI	No reaction	-

2.4.4 Study of reaction time of cationic Rh catalyst with no ligand.

A challenge in the development of an enantioselective reactions is the suppression of racemic background reaction pathways. A monodentate ligand such as (*S*)-SIPHOS **(2.42**) has a relatively weak ligand-metal binding energy compared to a bidentate ligand and is prone to displacement

from the active catalyst. Because increasing the equivalents of (*S*)-SIPHOS (**2.42**) ligand to Rh ratio to 2.2 equiv required higher reaction temperatures for PKR activity, and increasing to 3.0 and 4.0 equiv shut down the reaction (Table 4), we reasoned that the phosphoramidite ligand was decelerating the cationic Rh catalyst. A series of experiments were performed to better understand the magnitude of catalyst deceleration by the ligand. The time to reaction completion at four different temperatures was tested. The reaction of allenyl pivalate **2.21d** in DCE with $Rh(cod)_2BF_4$ catalyst was monitored closely by TLC, and yields were determined by ^1H NMR integration versus *o*-dichlorobenzene internal standard. At 90 and 70 °C, the racemic reaction was complete was only 15 and 20 minutes, respectively (Table 6, entries 1 and 2). At 50 °C, the reaction time slowed to 45 min (entry 3). At rt, the background reaction was complete after 18 h and afforded a low yield of product **2.22d** (35%, entry 4). The APKR of substrate **2.21d** with 22 mol % (*S*)-SIPHOS (**2.42**) proceeds in 8 h at 90 °C (Table 5, entry 3). Thus, the ligand-free catalyst reacts *approximately* 30 times faster than the (*S*)-SIPHOS (**2.42**)-bound catalyst in the APKR of allenyl pivalate **2.21d** (compare Table 5, entry 3 and Table 6, entry 1). These results indicate that the racemic background is rapid and must be suppressed in order to achieve high enantioselectivity.

Table 6. Rate of cationic Rh-catalyzed racemic APKR of allenyl pivalate 2.21d.

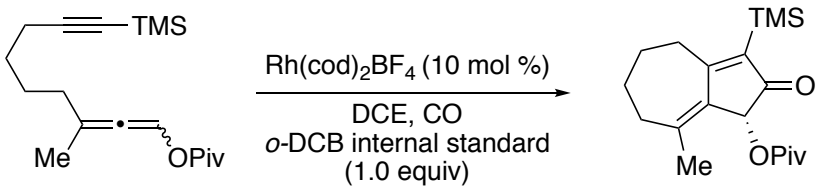

2.21d **2.22d**

entry	T (°C)	time	yield (%) [a]
1	90	15 min	55
2	70	20 min	70
3	50	45 min	61
4	rt	18 h[b]	35

[a] Yield was determined by integral comparison of the product resonance (5.8 ppm) to the *o*-DCB resonance (7.2 ppm). [b] The reaction was not closely monitored between 6 and 18 h.

2.4.5 Testing the stereochemical integrity of APKR product.

The low enantioselectivity of the Rh-(*S*)-SIPHOS (**2.42**) catalyst inspired an investigation to determine whether the APKR product maintained its stereochemical integrity over the course of the reaction. Therefore, several aliquots were taken throughout the APKR reaction time and subjected to analysis by HPLC (Table 7). The first aliquot after 1 h displayed the highest ee (entry 1, 28% ee), and the second and third aliquots showed that the ee of the product was relatively stable, with 26% ee observed after 6 and 18 h (entries 2 and 3). This experiment demonstrates that the product is not conformationally labile under the reaction conditions and eliminates this possibility as an explanation for the low enantioselectivity observed with (*S*)-SIPHOS (**2.42**).

Table 7. Enantioselectivity over reaction time.

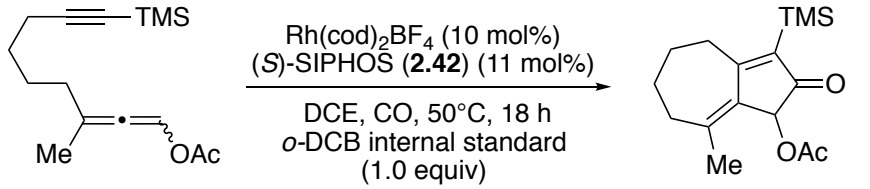

2.21c **2.22c** 75%, 25% ee

entry	time (h)	yield	ee (%)
1	1	9	28
2	6	53	26
3	18	77	26

[a] Yield was determined by integral comparison of the product resonance (5.8 ppm) to the *o*-DCB resonance (7.2 ppm).

2.4.6 Conclusions from the APKR studies using monodentate ligands.

Monodentate phosphoramidite ligands (*S*)-MonoPhos (**2.27**) and (*S*)-SIPHOS (**2.42**) provide APKR products in high yields, but low enantioselectivities. Both poor enantio-directing ability of the ligands ($\Delta\Delta G^{\ddagger}$ of only 1.0 kcal/mol for (*S*)-MonoPhos (**2.27**) catalyst), and propensity for rearrangement (Figure 7) contribute to the low enantioselectivity observed. The spirocyclic ligand (*S*)-SIPHOS (**2.42**) with enhanced rigidity and a wider cone angle afforded an incremental increase in enantioselectivity (26% ee versus 16% ee), which was enhanced further to 42% ee upon increasing the equivalents of ligand to Rh from 1.1 to 2.2. In APKR studies of both monodentate ligands, a rapid racemic background reaction was also likely contributing to the low enantioselectivity. Based upon these conclusions, we hypothesized that a chelating bidentate ligand could prevent rearrangement of the catalyst and prevent ligand dissociation from the rhodium center to enable improved enantioselectivity.

2.5 APKR WITH (*S*)-MEANILAPHOS LIGAND.

2.5.1 Introduction to phosphine-phosphoramidite ligands.

Given the high yields observed in the APKR using phosphoramidite ligands, we hypothesized that a bidentate ligand containing a phosphoramidite group would be a reactive and enantioselective catalyst in the APKR. We chose to test a hybrid, bidentate phosphine-phosphoramidite ligand because these ligands have demonstrated success in enantioselective hydroformylation, an analogous Rh(I)-catalyzed carbonylation reaction. Hydroformylation is one of the largest homogeneously catalyzed reactions in the chemical industry, and is therefore a well-studied reaction.[100] Careful tuning of ligand parameters in the Rh(I)-catalyzed reaction of syngas with alkenes has proven successful in achieving high regio- and enantioselectivity of the chiral branched product isomers.[101, 102] Hybrid phosphorous donor ligands contain two electronically and sterically distinct phosphorous donors, and offer improved catalyst definition over traditional bisphosphine ligands.[103] For example, (*R, S*)-Yanphos (**2.47**) affords chiral branched aldehyde in up to 98% ee in the hydroformylation of styrene (Scheme 27).[104]

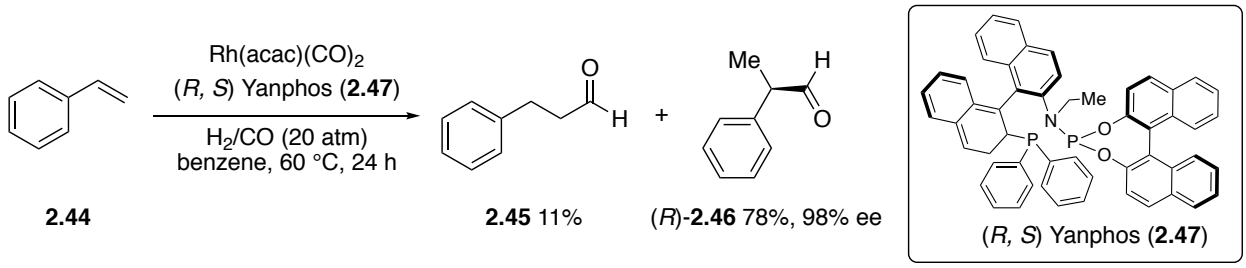

Scheme 27. Hydroformylation of terminal alkenes.

Because sterically demanding bidentate phosphine ligands (*R*)-BINAP (**2.23**) and (*R*)-MeOBIPHEP (**2.24**) demonstrated poor reactivity in the APKR, we desired a phosphine-

phosphoramidite ligand with as minimal steric demand as possible. As a model hybrid phosphine-phosphoramidite ligand we chose (*S*)-MeAnilaphos (**2.50**). a ligand which was first employed in the hydrogenation of (*Z*)-α-acetamidocinnamate (**2.48**) (Scheme 28).[105] Synthesis of phosphine-phosphoramidite ligand (*S*)-MeAnilaPhos (**2.50**) requires only two steps, and the ligand can form a stable cationic Rh complex (**2.51a**), which served as an initial indicator of its high binding affinity for rhodium.

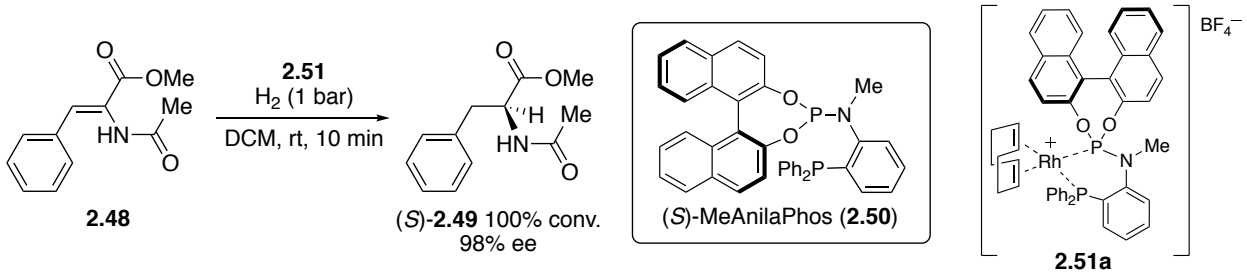

Scheme 28. Hybrid phosphine-phosphoramidite ligand (*S*)-MeAnilaPhos.

2.5.2 Ligand displacement energies of (*S*)-MonoPhos and (*S*)-MeAnilaPhos.

We expected that a bidentate ligand such as (*S*)-MeAnilaPhos (**2.50**) would be less likely than a monodentate ligand such as (*S*)-MonoPhos (**2.27**) to be displaced by carbon monoxide during the APKR. In order to test this hypothesis, the energy required to displace (*S*)-MonoPhos (**2.27**) and (*S*)-MeAnilaPhos (**2.50**) in the APKR transition state were calculated. The ligand displacement energy of (*S*)-MonoPhos (**2.27**) from **2.32-TS** is only 5.0 kcal/mol (Scheme 29, a), while the ligand displacement energy of (*S*)-MeAnilaPhos (**2.50**) from **2.52-TS** is 14.1 kcal/mol (Scheme 29, b). These calculations confirmed our expectation that a hybrid bidentate ligand would be less easily displaced during the APKR.

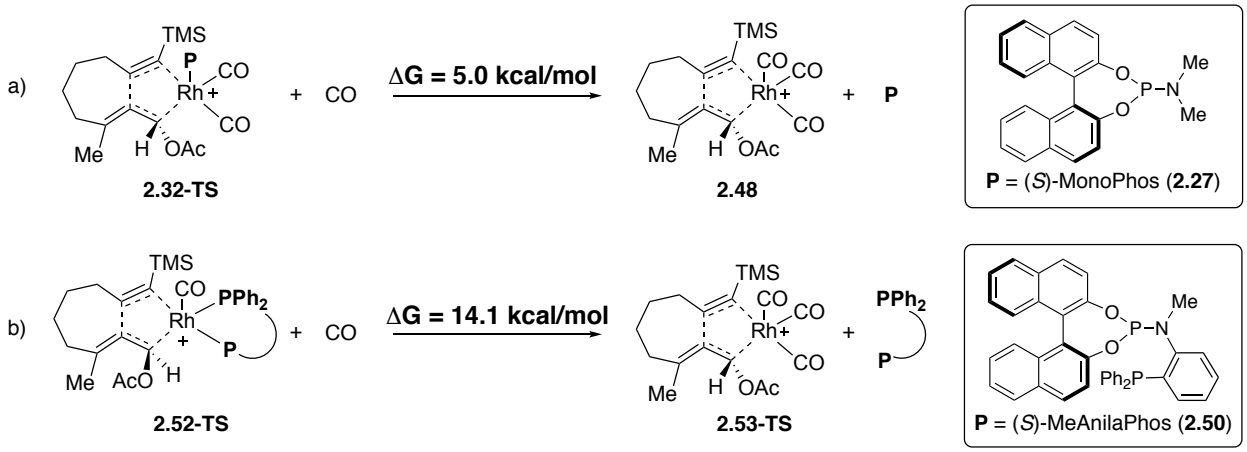

Scheme 29. Ligand displacement energies of (*S*)-MonoPhos and (*S*)-MeAnilaPhos.

2.5.3 DFT-calculated mechanism of the APKR with (*S*)-MeAnilaPhos.

In order to evaluate the potential of (*S*)-MeAnilaPhos (**2.50**) as an enantioselective ligand in the APKR, the lowest-energy reaction profile was calculated. Coordination of allene-yne **2.21c** to resting catalyst **2.54** to afford the four-coordinate square planar complex **2.55** proceeds with 20.3 kcal/mol (Scheme 30, red). Oxidative addition into complex **2.55** requires an additional 15.7 kcal/mol, with an overall activation energy of 36.0 kcal/mol. Alternatively, coordination of allene-yne **2.21** to afford the square-pyramidal complex **2.57** requires 22.4 kcal/mol. Oxidative cyclization from complex **2.57** requires only 6.0 kcal/mol. These calculations confirm that oxidative cyclization through the square-planar, five-coordinated complex **2.52-TS** is still the rate- and stereo-determining step.

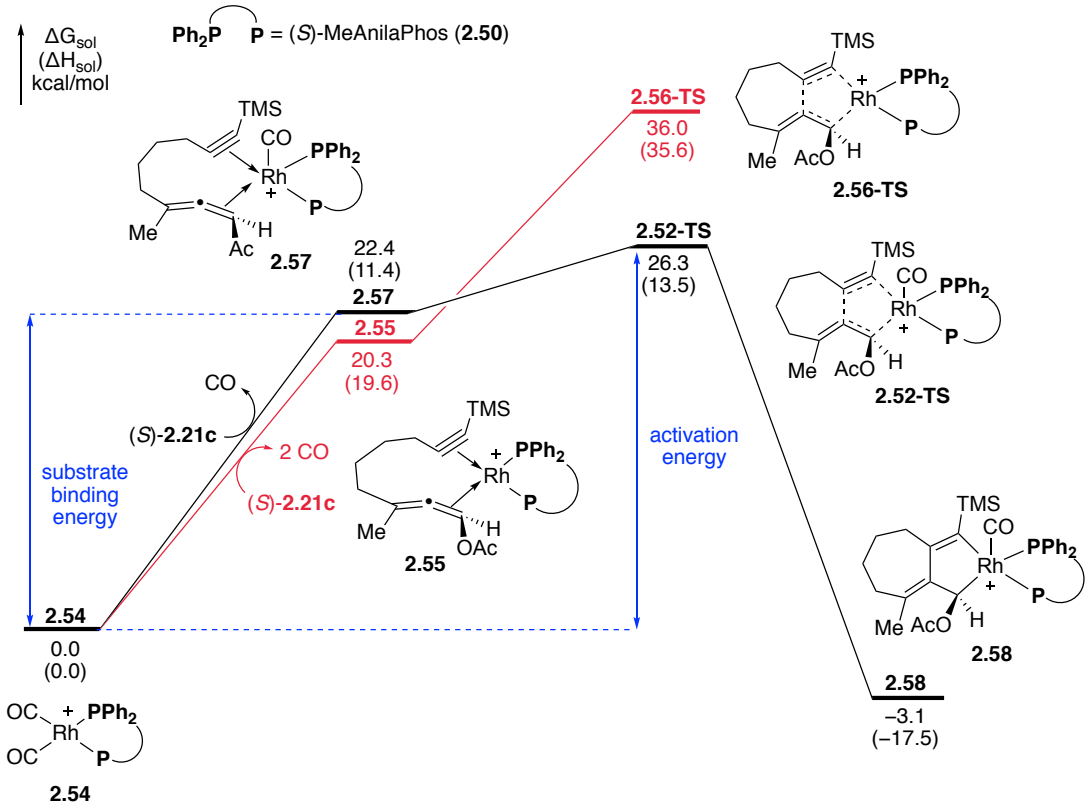

Scheme 30. Reaction energy profile of the APKR with (*S*)-MeAnilaPhos.

Reproduced with permission from Burrows, L. C.; Jesikiewicz, L. T.; Lu, G.; Geib, S. J.; Liu, P.; Brummond, K. M., *J. Am. Chem. Soc.* **2017**, *139* (42), 15022-15032. Copyright 2017 American Chemical Society.

The predicted enantioselectivity was evaluated by examination of the structures of the two lowest-energy transition state complexes leading to the (*R*)- and (*S*) complexes (Figure 9). In both transition state structures, the (*S*)-MeAnilaPhos (**2.50**) ligand is coordinated in the equatorial position with a molecule of CO in the apical position. The phosphine group of the ligand is located *cis* to the silyl group, while the chiral phosphoramidite group is located *cis* to the acetoxy group (Figure 9). The major transition state structure **2.52-TS** shows an earlier transition state, as demonstrated by the longer C-C bond which is forming (2.24 versus 2.18 Å). The large difference in energy between **2.52-TS** and **2.52TS'** ($\Delta\Delta G^{\ddagger}$ = +4.4 kcal/mol) indicates a high stereo-directing ability for this hybrid bidentate ligand.

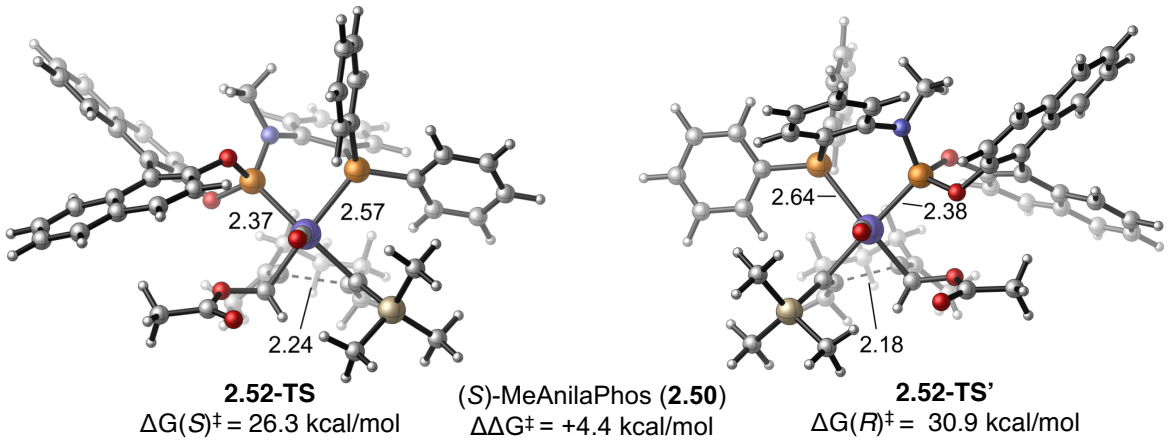

Figure 9. Lowest-energy transition state structures in the APKR with (*S*)-MeAnilaPhos.

2.5.4 Synthesis of (*S*)-MeAnilaPhos ligand.

This hybrid bidentate ligand (**2.50**) was synthesized in two steps starting from *N*-methylaniline. Ortho-lithiation of *N*-methylaniline was achieved by addition of *n*-butyllithium and carbon dioxide, followed by *t*-butyllithium. Chlorodiphenylphosphine was added dropwise at −70 °C and the was reaction allowed to warm to rt. After recrystallization in 10% MeOH in THF, 2-(diphenylphosphaneyl)-*N*-methylaniline (**2.59**) was isolated in 46% yield.[106] Sequential addition of *N*,*N*,-diisopropylethylamine (DIPEA), freshly distilled phosphorous trichloride, and (*S*)-BINOL to aniline **2.59** in DCM afforded (*S*)-MeAnilaPhos (**2.50**) in 76% yield. The ligand was isolated in 97% purity, with trace unreacted aniline **2.59** apparent by ^{31}P NMR. To avoid any interference of this impurity with the APKR catalyst, the ligand was recrystallized in hexanes, which provided (*S*)-MeAnilaPhos (**2.50**) in >99% purity in 26% yield (Scheme 31).

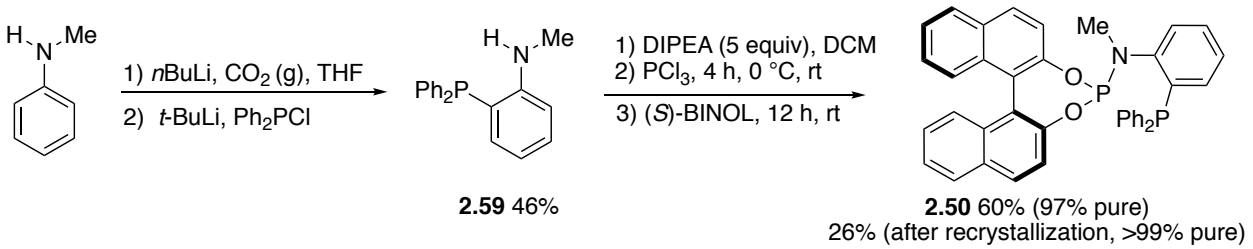

Scheme 31. Synthesis of (*S*)-MeAnilaPhos (2.50).

2.5.5 Synthesis and characterization of [Rh(cod)[(*S*)-MeAnilaphos)]BF_4].

In our APKR studies with monodentate phosphoramidite ligands such as (*S*)-MonoPhos (**2.27**) and (*S*)-SIPHOS (**2.42**), confirmation that the ligand was bound the Rh catalyst was difficult. An advantage of the (*S*)-MeAnilaPhos (**2.50**) ligand was its ability to form a stable cationic Rh complex which we expected would maintain its structural integrity throughout the reaction. In order to test this hypothesis, the cationic Rh-(*S*)-MeAnilaPhos complex (**2.51a**) was synthesized. A solution of (*S*)-MeAnilaPhos (**2.50**) in DCM was added dropwise to a solution of $Rh(cod)_2BF_4$ in DCM at −50 °C. The solution was allowed to warm to rt over 2 h and the resulting orange solution was concentrated, washed twice with diethyl ether, and dried under vacuum. The ^{31}P NMR spectrum of this complex **2.51a** shows two doublet of doublets, each split by ^{103}Rh and ^{31}P (Figure 10). The resonance occurring at δ = 134 ppm and with a $J_{Rh\text{-}P}$ of 256 Hz corresponds to the phosphoramidite group, while the resonance at δ = 24 ppm with a $J_{Rh\text{-}P}$ of 139 Hz corresponds to the phosphine group. This ^{31}P NMR spectrum matches that reported in the original synthesis of this complex.[105] The larger Rh-P coupling constant ($J_{Rh\text{-}P}$ = 256 Hz) of the phosphoramidite group indicates that Rh-$P_{phosphoramidite}$ bond is shorter than the Rh-$P_{phosphine}$ bond ($J_{Rh\text{-}P}$ = 139 Hz).[107]

Structures obtained by DFT calculations are in agreement with this experimental observation (Figure 9).

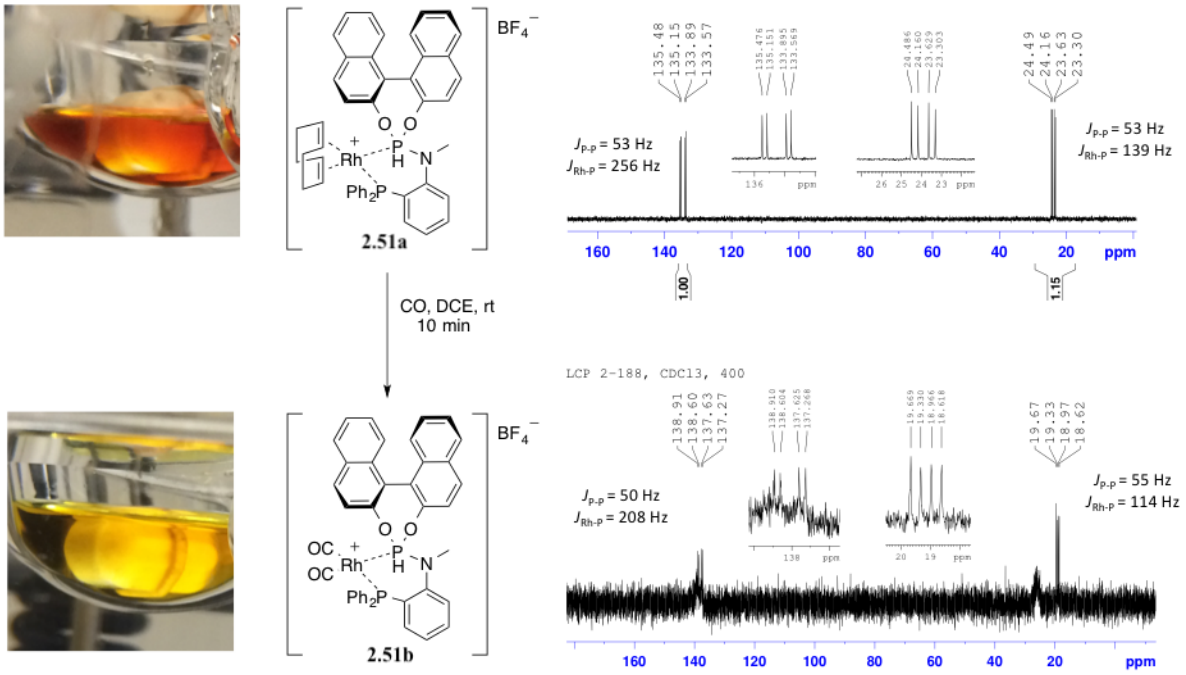

Figure 10. ^{31}P NMR spectra of Rh-(*S*)-MeAnilaPhos complexes.

Upon exposure of this complex to CO atmosphere in DCE, the solution turned from orange to yellow. We propose that the cod ligand was replaced by CO ligands, to afford complex **2.51b**. The resonances corresponding to the phosphoramidite group shifted slightly downfield (from 135 to 138 ppm) and phosphine groups shifts upfield (from 24 to 19 ppm). The Rh-phosphoramidite coupling decreases from 256 Hz to 208 Hz, and the Rh-phosphine coupling decreases from 139 to 114 Hz. This decrease in Rh-P coupling indicates that the lengths of both Rh-P bonds in the complex increase when the cod ligand is replaced with CO.[107] This change is expected based on the stronger trans influence of CO compared to cyclooctadiene. With both of these complexes

synthesized and characterized, we planned to use this information to ensure Rh-ligand binding during the APKR.

2.5.6 APKR using (*S*)-MeAnilaPhos ligand.

The reactivity of the prepared Rh-(*S*)-MeAnilaPhos (**2.50**) catalyst was tested in an APKR of allenyl acetate **2.21c**, in DCE solvent with 1 atm CO. Cyclopentenone product **2.22c** was obtained in 14 % yield and 0% ee (Table 8, entry 1). The racemic product suggested that the background reaction of free cationic Rh was predominating. The major product of this reaction was aldehyde **2.23c**, which was isolated in 46% yield. To avoid formation of the ligand-free catalyst, in subsequent reactions, the catalyst was generated *in situ* using a slight excess of (*S*)-MeAnilaPhos ligand (**2.50**). For example, the reaction of $Rh(cod)_2BF_4$ (10 mol %) with (*S*)-MeAnilaPhos (11 mol %) in DCE afforded 18% yield of product **2.22c**, with a small improvement to 12% ee (entry 2). Again, the major product isolated was aldehyde **2.23c**.

Table 8. Conditions tested in APKR using (*S*)-MeAnilaPhos (2.50).

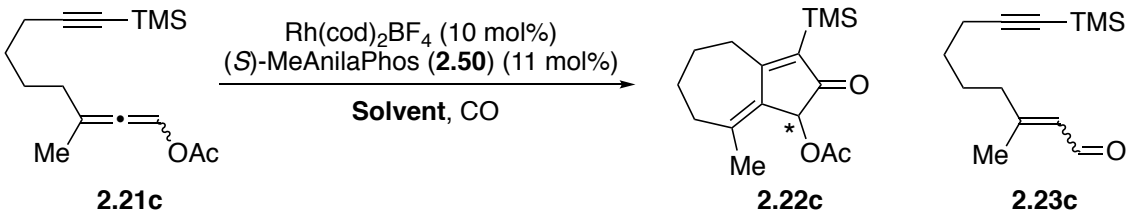

2.21c **2.22c** **2.23c**

entry	solvent	T (°C)	time (h)	**2.22c** (%)	ee (%)	**2.23c** (%)
1[a]	DCE	70	2	14	0	46
2[b]	DCE	50	15	18	12	31
3[c]	TFE	70	48	20	29	[d]
4	MeCN	70	48	10	6	[d]
5	chlorobenzene	90	72	10	2	[d]

[a] Pre-formed [Rh((*S*)-MeAnilaPhos (**2.50**)(cod)]BF_4 was employed as a catalyst. [b] In entry 2, and all subsequent entries in Table 8, the catalyst was generated *in situ* prior to the APKR. [c] Other solvents tested which gave no product or only trace product include: benzene, xylenes, 1,2-dichlorobenzene, nitrobenzene, dioxane, *t*-butyl methyl ether, *t*-butanol, carbon tetrachloride, chloroform, and dichloromethane. [d] Percentage yield of aldehyde **2.23c** was not determined, however, TLC evidence shows that aldehyde **2.23c** is the major product.

An extensive solvent screen was carried out to determine whether a different solvent could improve reactivity of the Rh-(*S*)-MeAnilaPhos (**2.50**) catalyst. Thirteen different solvents of varying polarity and coordinating ability were chosen and tested in the APKR. These reactions were performed simultaneously using an InnovaSyn parallel reactor. Only three solvents afforded APKR product: 1,1,1-trifluoroethanol (TFE), acetonitrile (MeCN) and chlorobenzene (Table 8, entries 3-5). The highest yield and enantioselectivity were observed when TFE was used as a solvent (20% yield, 29% ee, entry 3). Both acetonitrile and chlorobenzene afforded product in low yield and close to zero enantioselectivity (entries 4 and 5). Reactions with all thirteen solvents tested afforded aldehyde **2.23c** as the major product. Therefore, the origin of this undesired formation of aldehyde **2.23c** was investigated.

2.5.7 Mechanism of formation of APKR byproduct aldehyde 2.23c.

The APKR of bidentate ligands such as (*R*)-BINAP and (*S*)-MeAnilaPhos (**2.50**) afford aldehyde **2.23c** as the major product. Two different mechanisms are known for the hydrolysis of allenyl acetates to give aldehydes.[108] First, protonation of the central carbon of the allene generates a carbocation **2.60**. Water can then attack the acyl group, breaking the C-O bond to afford aldehyde **2.23c**. Alternatively, an ester hydrolysis to generate the corresponding allenol alcohol, followed by tautomerization can give aldehyde **2.23c** (not shown). Both of these mechanisms involve water.

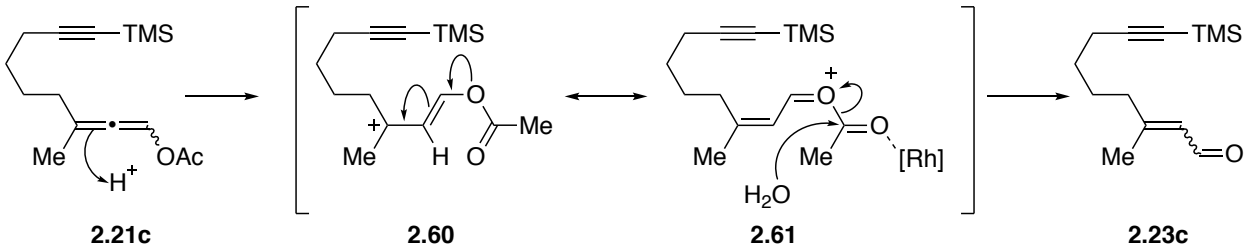

Scheme 32. Proposed mechanism of aldehyde formation.

Based on these known mechanisms, we hypothesized that residual water in the reaction mixture was causing the formation of aldehyde **2.23c**. To test this hypothesis, a solution of allene **2.21c**, $Rh(cod)_2BF_4$ (5 mol %), and water (20 μL, 40 equiv) in DCE were reacted under CO atmosphere (Table 9, entry 2). The cationic ligand-free conditions were chosen for this experiment because it was known that these conditions would typically (without added water) react quickly and in good yield (see Table 6). After 3 h, the reaction was proceeding cleanly (~25% conversion) with only trace aldehyde observed by TLC, indicating that the added water was not causing aldehyde formation.

Table 9. Experiments testing role of water in aldehyde byproduct formation.

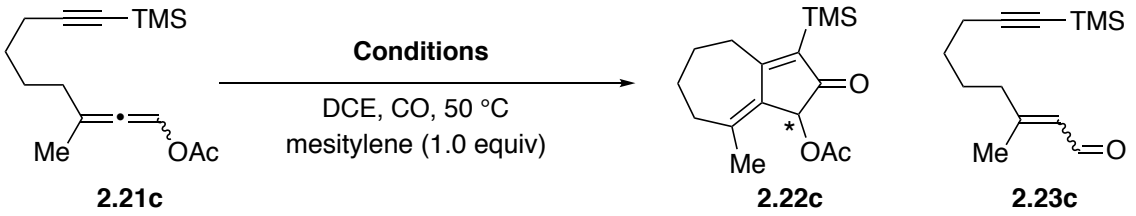

2.21c **2.22c** **2.23c**

entry	$Rh(cod)_2BF_4$ (mol %)	(*S*)-**2.50** (mol %)	H_2O (equiv)	**2.22c** (%)[a]	ee (%)	**2.23c** (%)[a]
1	5	6	0	18	12	31
2	5	0	40 [c]	26, -	-	7
3	0	6	0	0[b]	-	0

[a] Yields were determined by ^{1}H NMR integral comparison to mesitylene internal standard. [b] Quantitative recovery of starting allene **2.21c** was observed by ^{1}H NMR. [c]The reaction mixture was exposed to air after 3 h.

At this point in the reaction, we tested whether atmospheric oxygen would cause aldehyde formation. To this end, the CO balloon was removed from the vial, and replaced with a needle open to the air (entry 2). After reacting 12 h open to the air, product was formed in 26% yield, with only 7% aldehyde formation. No starting allene was recovered. A poor yield is expected because the majority of the reaction was carried out in the absence of CO atmosphere. However, the observation of only 7% aldehyde after the reaction was exposed to both water and oxygen for 12 h indicates that neither of these factors alone are the cause of aldehyde formation, and that the bidentate ligand must be present.

Because aldehyde formation occurred in reactions containing (*S*)-MeAnilaPhos (**2.50**) and not in reactions with other ligands such as (*S*)-MonoPhos (**2.27**) and (*S*)-SIPHOS (**2.42**), we tested whether that the ligand itself, or another impurity within the material, was facilitating the conversion to the aldehyde byproduct. A solution containing allene **2.21c,** (*S*)-MeAnilaPhos (**2.50**) (6 mol %), DCE and was heated at 50 °C under CO atmosphere (Table 9, entry 3). After 15 h, quantitative recovery of the starting allene was observed, with no aldehyde present. This result

indicates that Rh is involved in the conversion of allene-yne **2.21c** to aldehyde **2.23c**. Based on these two experiments, it is clear that both the $Rh(cod)_2BF_4$ catalyst and the bidentate ligand must be present for aldehyde formation. It is possible that the bulky cationic Rh complex is incapable of catalyzing the PKR, and instead coordinates the acyl group, activating it towards hydrolysis by trace water or acid.

2.5.8 Conclusions from the APKR studies using hybrid bidentate ligand.

Although a high enantioselectivity was predicted for the Rh-(*S*)-MeAnilaPhos (**2.50**) catalyst ($\Delta\Delta G^{\ddagger}$= +4.4 kcal/mol, Figure 9), low reactivity was observed experimentally. We postulate that this poor reactivity resulted from the high-energy barrier required for the substrate **2.21c** to coordinate to the sterically hindered complex. The high substrate binding energy of 22.4 kcal/mol indicates that the sterically demanding bidentate ligand prohibits the allene-yne from binding to Rh in a bidentate fashion to undergo the oxidative cyclization step. Isolation of aldehyde **2.23c** as a major product of this reaction suggests that only the allenyl acetate is coordinating to the Rh catalyst. Taken together, the above experimental and computational investigations illustrate the important role of the denticity of the phosphoramidite ligands on APKR reactivity.

2.6 APKR WITH (*S*)-MONOPHOS-ALKENE LIGAND.

After several experiments which suggested that the Rh-(*S*)-MeAnilaPhos (**2.50**) complex was formed but was not active in the APKR, an alternative approach was taken to maintain the high reactivity of monodentate phosphoramidite ligands such as (*S*)-MonoPhos (**2.27**) and (*S*)-SIPHOS

(**2.42**), while improving ligand to Rh binding and preventing rearrangement of the complex. Hybrid phosphoramidite-alkene ligands offer improved ligand-metal binding over monodentate ligands without hindering catalyst reactivity.[109] Unlike bidentate phosphine or phosphoramidite ligands, the hemilabile alkene group can easily dissociate during the catalytic cycle. Phosphoramidite-alkene ligand **2.62** was first introduced by Carreira *et al.* in the Ir-catalyzed asymmetric conversion of an allylic alcohol into an allylic amine.[110] Soon thereafter, Dorta *et al.* applied the same ligand in the Rh-catalyzed asymmetric 1,4-addition of arylboronic acids to enones.[111]

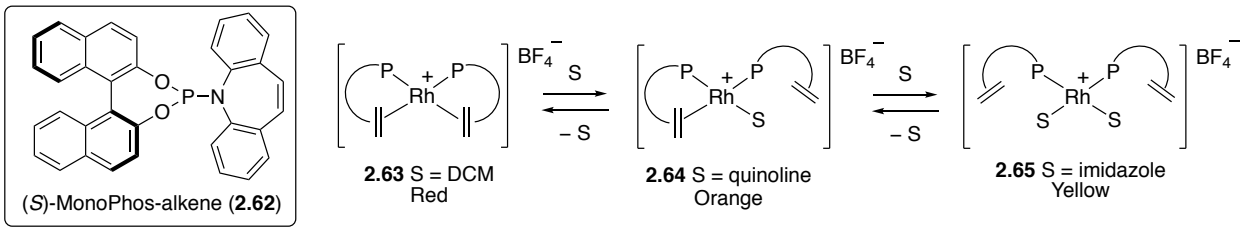

Scheme 33. Hemilability of (*S*)-MonoPhos-alkene ligand in Rh complexes.

Dorta and coworkers performed mechanistic studies which demonstrated the hemilability of the alkene moiety towards cationic Rh complexes. For example, in solution with noncoordinating solvent DCM with a 2:1 ratio of ligand **2.62** to Rh, both alkene groups coordinated to the metal (**2.63**, Scheme 33).[109] In quinolone, a bulky, moderately coordinating solvent, the solvent was mono-coordinated, replacing one alkene group (**2.64**). In the coordinating solvent imidazole, the solvent displaced both alkene groups on the metal (**2.65**). Each of these complexes were isolated as solids and characterized by ^{31}P NMR and X-ray crystallography. Based on these experiments described in the literature, we hypothesized that incorporation of a hemilabile alkene group on the APKR catalyst could help maintain ligand coordination to Rh (thus improving

enantioselectivity) and easily dissociate to enable substrate coordination (thus improving yield). Therefore, to test these hypotheses, (*S*)-MonoPhos-alkene (**2.62**) was synthesized and applied ligand in the APKR of allenyl acetates.

2.6.1 Synthesis of (*S*)-MonoPhos-alkene (2.62).

The optimized, large-scale synthesis of phosphoramidite-alkene ligand **2.62** in only two steps from dibenzazepine and (*S*)-BINOL was reported by Dorta and coworkers (Scheme 34, a).[112] In the reported procedure, dibenzazepine was deprotonated using triethylamine and reacted with phosphorous trichloride to provide dichloride **2.66** in 96% yield (89 g, Scheme 34, a). Dichloride **2.66** was subsequently added to (*S*)-BINOL to afford ligand **2.62**, also in 96% yield, after purification by recrystallization. Our efforts to replicate these results on a much smaller scale (300 mg) proved unsuccessful. For example, dichloride **2.66** was obtained in 19% yield, and (*S*)-MonoPhos-alkene (**2.62**) in 11% yield (Scheme 34, a, red). Although the ligand **2.62** is somewhat unstable to silica gel, we expected that on a small scale, we could recover more product after purification by column chromatography than by recrystallization. We attributed the low yield of the air-sensitive intermediate **2.66** oxidation by air, which was negligible on the large scale reported. Ultimately, we achieved optimal yield of **2.62** using a modified version of this synthesis, in which the dichloride **2.66** was not isolated, and the final product, **2.62**, was purified by column chromatography rather than recrystallization (Scheme 34, b). Using this modified route, the synthesis was shortened to one step, and the yield of **2.62** was improved to 78%.

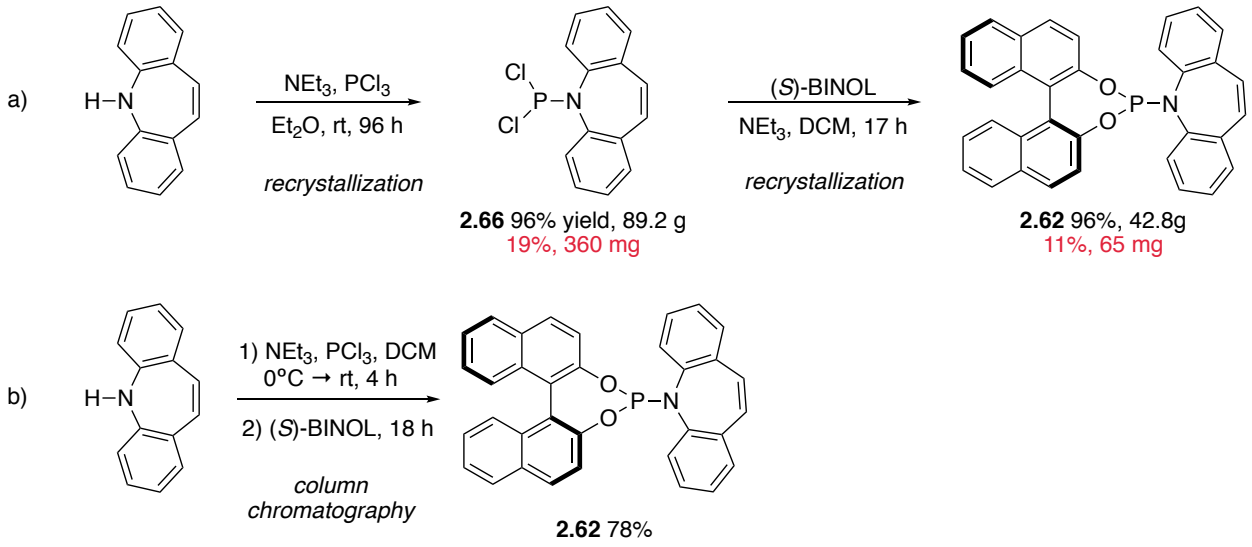

Scheme 34. Synthesis of phosphoramidite-alkene ligand 2.62.

2.6.2 APKR with (*S*)-MonoPhos-alkene ligand.

In order to test the hypothesis that the hemilabile alkene coordinating group would improve enantioselectivity of the phosphoramidite ligand, (*S*)-MonoPhos-alkene **2.62** was applied in the APKR of allenyl acetate **2.21c**. Product **2.22c** was obtained in 76% yield and 54% ee, the highest ee observed at that point (Table 10, entry 1). Moving forward, mesitylene was incorporated as an internal standard for yield determination by ^{1}H NMR spectroscopy. Gratifyingly, we observed that incorporation of this the aromatic additive improved the *isolated* yield of the reaction from 49 to 76% (compare entries 1 and 2). This enhancement in yield is attributed to the ability of mesitylene to stabilize the cationic Rh catalyst.[113] This high yield (76%) combined with good enantioselectivity (54%) inspired further reaction optimization. We anticipated that a lower concentration of CO would reduce displacement of the ligand by CO. Therefore, the CO concentration was lowered to 0.1 atm (balloon of 10% gas mixture of CO/Ar), the selectivity

improved to 64% ee (entry 3). When the steric bulk of the acetate group was increased to a carboxy pivalate group, the enantioselectivity was further increased to 71% ee (entry 4). The octanoyl group, which is present in Thapsigargin (**1.9**) is also well-tolerated, demonstrating the potential application of this reaction in the synthesis natural and unnatural enantiomers of Tg (**1.9**). Benzoate product **2.22f** was obtained as a white solid in 77% yield and 70% ee (entry 6). These results demonstrate that the APKR using (*S*)-MonoPhos-alkene (**2.62**) ligand proceeds in good yield and ee, and can be applied to allene-ynes with various carboxy ester groups.

Table 10. APKR of allenyl acetates using (*S*)-MonoPhos-alkene ligand.

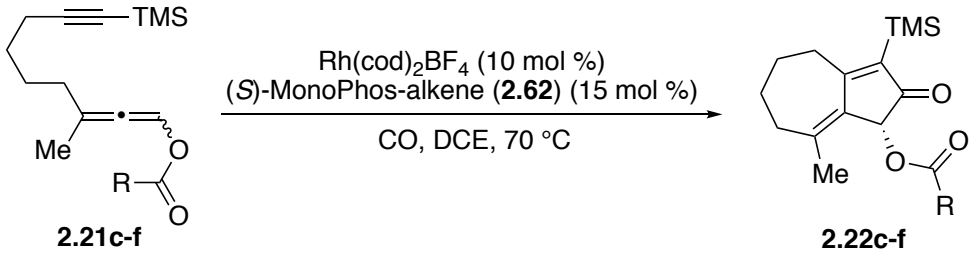

2.21c-f **2.22c-f**

entry	R^2		CO/Ar (%)	Mesitylene (equiv)	time (h)	yield (%)[b]	ee (%)
1	Me	**2.21c**	100	0	16	**2.22c** 49	54
2	Me	**2.21c**	100	1.0	15	**2.22c** 76	54
3	Me	**2.21c**	10	1.0	15	**2.22c** 71	64
4	*t*-Bu	**2.21d**	10	1.0	15	**2.22d** 50	71
5	$(CH_2)_6CH_3$	**2.21e**	10	1.0	17	**2.22e** 70	61
6	Ph	**2.21f**	10	1.0	20	**2.22f** 77	70

[a] Reactions were performed on 0.05 mmol (13-16 mg) scale. [b] Yields were determined by integral comparison of product resonance (5.8 ppm) with mesitylene resonance (6.8 ppm).

2.6.3 Experiments supporting Type I DyKAT mechanism.

Based on previous experiments of allenyl acetate diastereomers, a Type I DyKAT mechanism was postulated, with scrambling of allene axial chirality being both rapid, and catalyzed by Rh (Chapter 1, Scheme 15). Several experiments were performed to explore the validity of this hypothesis using enantiomers of allenyl acetate **2.21a**. Ph-substituted alkyne substrate was chosen as a substrate for this experiment because enantiomers of **2.21a** were readily resolved by HPLC using a chiral stationary phase. In a first experiment, enantiopure allenes (+)-**2.21a** and (−)-**2.21b** were submitted to APKR conditions (Scheme 35, a and b), and complete scrambling of axial chirality of both allenes (+)-**2.21a** and (−)-**2.21b** was observed after 30 minutes. At this point in the reaction, no product formation was observed by TLC, which rules out a Type II DyKAT in which the starting material is racemized by the catalyst at the same rate as the reaction of interest. Both reactions were complete after 20 h, and afforded APKR product in 60% ee. Regardless of which enantiomer of starting material was used, (+)-**2.21a** or (−)-**2.21a**, the same product, (*R*)-**2.22a,** was formed, Therefore, enantioselectivity in the APKR is catalyst-controlled, and is established during the APKR. The low yields of these reactions were attributed to the small scale of the experiments (3.5 mg each).

In a second experiment, enantiopure allene (−)-**2.21a** was submitted to the reaction conditions in the absence of the Rh catalyst. The allene proved configurationally stable after 20 h at rt. This demonstrates that the racemization of allenyl acetates is catalyzed by Rh, and rules out a dynamic kinetic resolution mechanism. Taken together, the results of these mechanistic studies support catalyst-controlled enantioselectivity enabled by rapid, Rh-catalyzed allenyl acetate isomerization. Therefore, the enantioselective APKR of allenyl acetates is classified as Type I DyKAT.

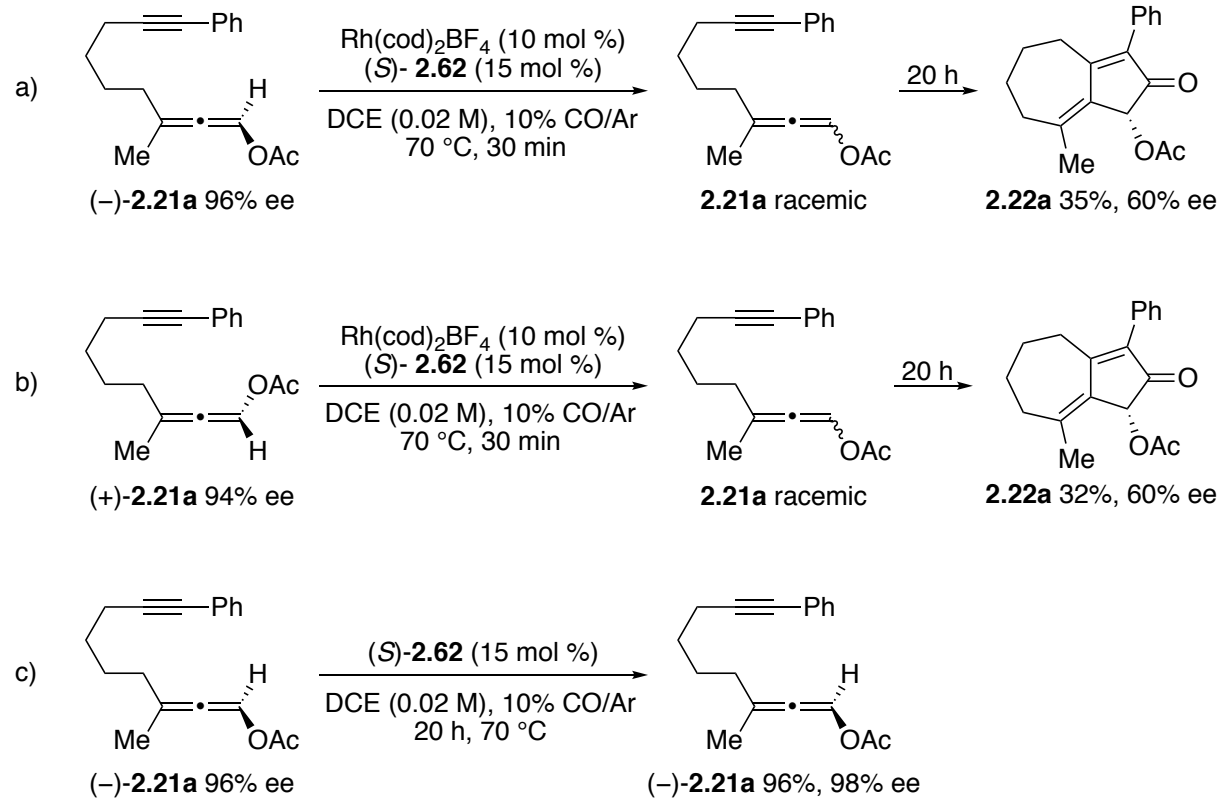

Scheme 35. Experiments confirming Type I DyKAT mechanism in the APKR.

Reproduced with permission from Burrows, L. C.; Jesikiewicz, L. T.; Lu, G.; Geib, S. J.; Liu, P.; Brummond, K. M., *J. Am. Chem. Soc.* **2017**, *139* (42), 15022-15032. Copyright 2017 American Chemical Society.

2.6.4 DFT-calculated mechanism of the APKR with (*S*)-MonoPhos-alkene.

Because the alkene group of phosphoramidite-alkene ligand **2.62** can be either bound or unbound during the APKR, the lowest-energy mechanisms of both pathways were calculated to determine the transition states of the enantio-determining step (Scheme 36). In the presence of CO, the *alkene unbound* resting catalyst **2.69** is favored over the *alkene bound* resting catalyst **2.68** by 8.7 kcal/mol. The reaction pathway with the *alkene unbound* is on the left, and the reaction pathway with the *alkene bound* is on the right (Scheme 36). In the *alkene-unbound* pathway (left),

coordination of the allene-yne substrate to replace one CO ligand proceeds in 18.4 (*S*) and 12.0 (*R*) kcal/mol. Oxidative addition occurs via (*R*)-**2.71-TS** with a transition state energy difference ($\Delta\Delta G^{\ddagger}$) of 4.4 kcal/mol, favoring the (*R*) product enantiomer. In the *alkene-bound* pathway (right), the five-coordinated, substrate-bound complex with the alkene bound was not located. The oxidative addition transition states with the alkene bound were located. Thus, the oxidative addition step can occur with a concerted coordination of the alkene via (*S*)-**2.74-TS**. The oxidative addition transition states with the ligand alkene moiety bound differ by only 1.1 kcal/mol, favoring the (*S*)-product **2.22c**.

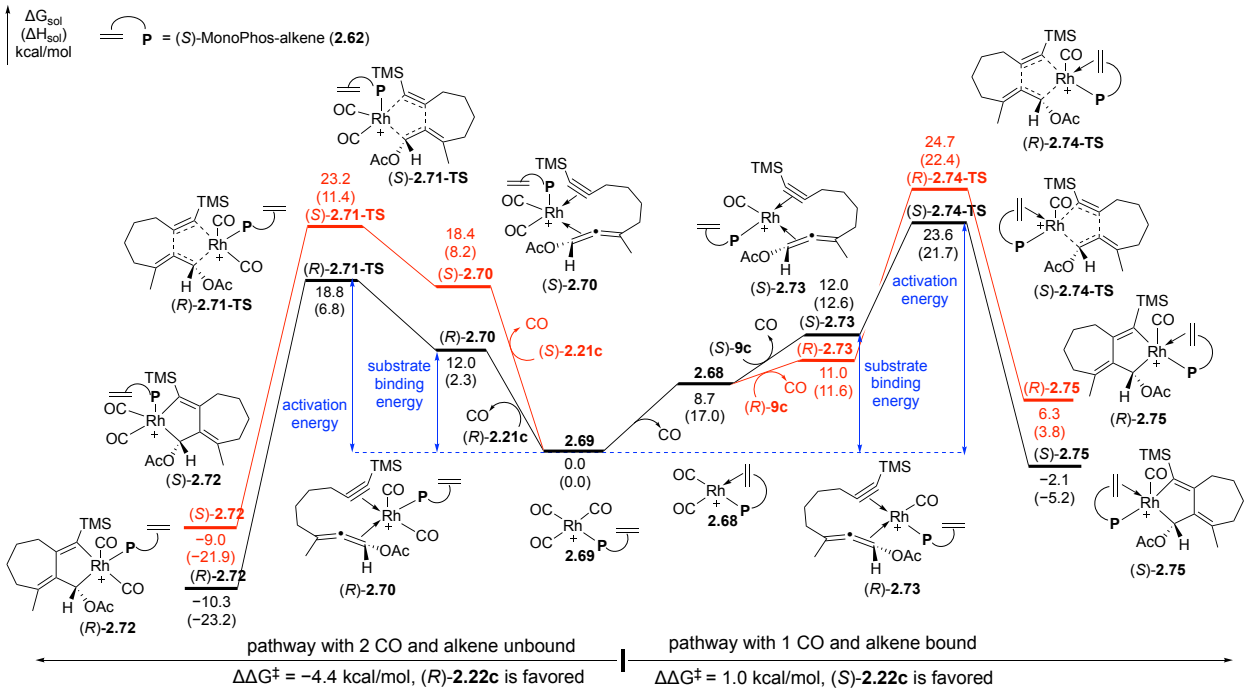

Scheme 36. Calculated energy profile of the Rh-(*S*)-MonoPhos-alkene-catalyzed APKR.

In the favorable *alkene unbound* APKR pathway, six different oxidative cyclization transition state isomers are possible in the reaction with each enantiomer of allene-yne **2.21c**. The activation energies of all twelve transition state isomers using the (*S*)-MonoPhos-alkene (**2.62**) ligand were calculated to determine the origin of enantioselectivity. The two lowest-energy transition states in the reaction with each enantiomer are shown in Figure 11. The lowest-energy transition state in the reaction with (*R*)-**2.21c** that lead to (*R*)-**2.22c** ($\Delta G^{\ddagger}$ = 18.8 kcal/mol) is much more stable than the lowest-energy transition states in the reaction with (*S*)-**2.21c** that forms (*S*)-**2.22c** ($\Delta G^{\ddagger}$ = 23.2 kcal/mol).

Unfavorable steric repulsions between the substrate and ligand result in a high barrier for the pathway to form the minor enantiomer (*S*)-**2.22c**. In (*S*)-**2.71-TS**, one steric interaction that is easily identified is between the binaphthyl backbone of the ligand and the TMS group of the substrate, which is evidenced by the short H···H distance (2.17 Å) between the TMS and the binaphthyl group. In comparison, in the lowest-energy transition state leading to (*R*)-**10c** (Figure 11), the distance between these two groups is much longer (2.34 Å).

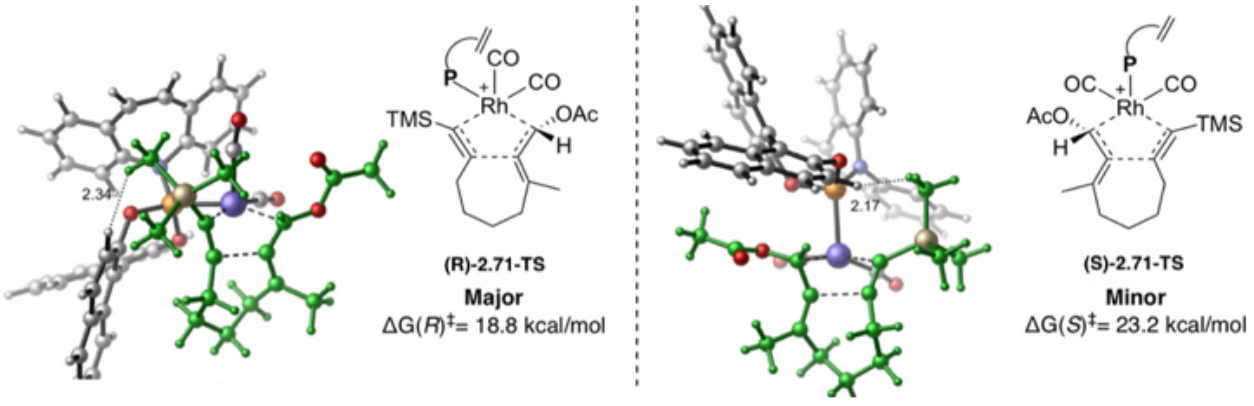

Figure 11. Lowest-energy transition state isomers of APKR with (*S*)-MonoPhos-alkene.

Reproduced with permission from Burrows, L. C.; Jesikiewicz, L. T.; Lu, G.; Geib, S. J.; Liu, P.; Brummond, K. M., *J. Am. Chem. Soc.* **2017**, *139* (42), 15022-15032. Copyright 2017 American Chemical Society.

2.6.5 Crystal structure verifying absolute configuration of APKR product.

Calculations with (*S*)-MonoPhos-alkene (**2.62**) predict that the (*R*) absolute configuration of APKR product **2.22c** is preferred (Scheme 36). To test this computational prediction experimentally, the APKR was performed on allene-yne **2.21f** to give benzoate **2.22f** as an amorphous white solid (77% yield, 70% ee, Table 10, entry 6). After recrystallization in pentane (30 mg/mL), product **2.22f** was obtained in 82% ee. After a second recrystallization in pentane, product **2.22f** was obtained in 97% ee. An X-ray quality crystal was grown by slow cooling in hexanes. The absolute configuration of benzoate **2.22f** was unambiguously assigned as (*R*) by X-ray crystallography (Figure 12). Therefore, we assign the absolute configuration of acetate product **2.22c** as (*R*), based on analogous HPLC retention times of the major and minor enantiomers. This stereochemical assignment of (*R*)-**2.22c** matches that predicted by computation (Scheme 36).

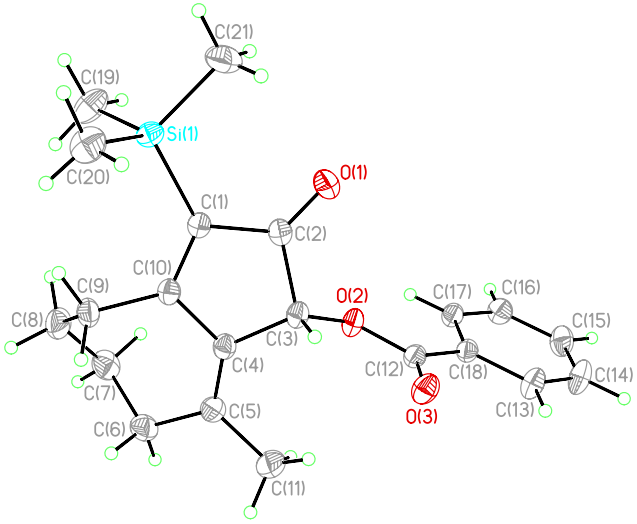

Figure 12. X-ray crystal structure of benzoate (*R*)-2.22f.

Reproduced with permission from Burrows, L. C.; Jesikiewicz, L. T.; Lu, G.; Geib, S. J.; Liu, P.; Brummond, K. M., *J. Am. Chem. Soc.* **2017**, *139* (42), 15022-15032. Copyright 2017 American Chemical Society.

2.6.6 Experimental validation of alkene unbound pathway.

To experimentally test whether the reaction proceeds via the *alkene unbound* pathway, saturated ligand **2.76** was applied in the APKR. (*S*)-MonoPhos-sat'd (**2.76**) was synthesized from dihydro-5H-dibenzo[b,f]azepine and (*S*)-BINOL. The reaction of **2.21c** using (*S*)-MonoPhos-sat'd (**2.76**) ligand provided **2.22c** in 90% yield and 34% ee, with the same major enantiomeric product as that obtained with **2.62** (Table 11, entry 2). This result suggests that the alkene in **2.62** is unbound in the oxidative cyclization transition state, as predicted by DFT calculations, which show that the *alkene unbound* pathway is lower energy (Scheme 36). The higher enantioselectivity with phosphoramidite-alkene ligand **2.62** confirms our hypothesis that the hemilability of the ligand plays a crucial role in achieving a high level of enantiocontrol by preventing rearrangement or dissociation of the ligand. The APKR of **2.21c** using (*S*)-MonoPhos-sat'd (**2.76**) ligand represents the highest yielding APKR of an allenyl acetate to date (90%, Table 11, entry 2)

Table 11. Comparison of (*S*)-MonoPhos-alkene and (*S*)-MonoPhos-sat'd in APKR.

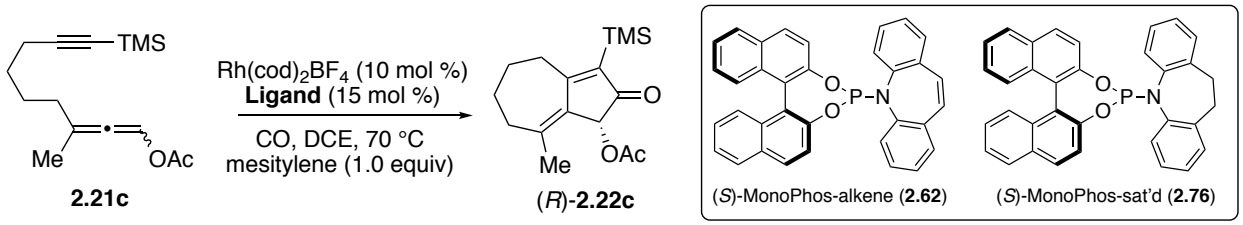

entry	ligand	time (h)	yield (%)	ee (%)
1	(*S*)-MonoPhos-alkene (**2.62**)	15	71	64 (*R*)
2	(*S*)-MonoPhos-sat'd (**2.76**)	15	90	34 (*R*)

2.6.7 Conclusions of the computationally-guided catalyst design.

The computed activation free energies in the enantioselectivity-determining oxidative cyclization step of the APKR of **2.21c** with three different ligands (*S*)-MonoPhos (**2.27**), (*S*)-MeAnilaPhos (**2.42**), and (*S*)-MonoPhos-alkene (**2.62**) are summarized in Figure 13. The DFT calculations revealed significant effects of the phosphoramidite ligands on both reactivity and selectivity. Most of the transition state isomers with (*S*)-MonoPhos (**2.27**) have low activation free energies, enabling high reactivity, however, very similar activation free energies in the (*R*)- and (*S*)-selective pathways, results in poor enantioselectivity. In the case of the bidentate (*S*)-MeAnilaPhos (**2.50**) ligand, both the (*R*)- and (*S*)-selective pathways with ligand require high activation energy, indicating the low APKR reactivity of this class of ligand. Finally, the (*R*)-selective transition state isomers with the (*S*)-MonoPhos-alkene (**2.62**) ligand are noticeably more stable than the (*S*)-selective transition states, and have relatively low barriers, enabling good reactivity.

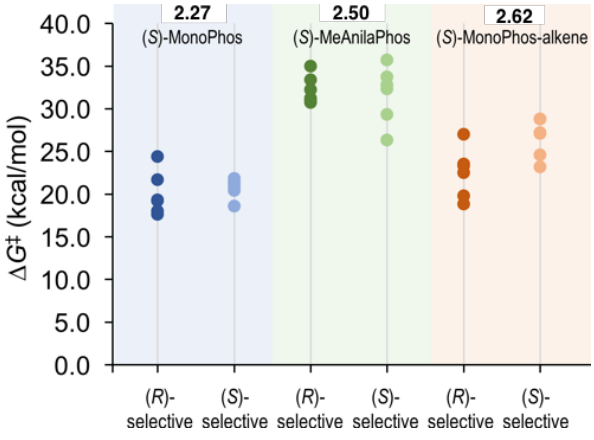

Figure 13. Summary of computed activation energies of the oxidative cyclization transition state isomers in the Rh-catalyzed APKR of allene-yne 2.21c with different ligands.

Reproduced with permission from Burrows, L. C.; Jesikiewicz, L. T.; Lu, G.; Geib, S. J.; Liu, P.; Brummond, K. M., *J. Am. Chem. Soc.* **2017**, *139* (42), 15022-15032. Copyright 2017 American Chemical Society.

The asymmetric APKR of allenyl acetates represents the first example of a DyKAT carbonylation reaction, the first catalyst-controlled enantioselective PKR of an allene, and a rare example of a DyKAT of an allene. A reactive and enantioselective catalyst was designed through a unique combination of DFT studies and laboratory experiments. Once phosphoramidites were identified as a reactive ligand class with low enantioselectivity ((*S*)-MonoPhos (**2.27**), 16% ee), mechanistic information provided by computation enabled us to achieve good enantioselectivity ((*S*)-MonoPhos-alkene (**2.62**), 64% ee) after experimentation with only four different phosphoramidite ligands, demonstrating the power of computation in streamlining the selection of chiral ligands.

2.7 APKR WITH (*S*)-SIPHOS-ALKENE.

Once the phosphoramidite-alkene moiety was identified using computation and experiments, we set out to improve the ligand scaffold to further enhance enantioselectivity. During investigations of monodentate phosphoramidite ligands, a change from (*S*)-MonoPhos (**2.27**) to (*S*)-SIPHOS (**2.42**) afforded an increase in enantioselectivity from 16 to 26% ee. We hypothesized that a similar enhancement could be achieved by incorporating an (*S*)-SIPHOS-alkene (**2.78**) ligand in the asymmetric APKR. To this end, (*S*)-SIPHOS-alkene (**2.78**) was synthesized in a manner similar to that of (*S*)-MonoPhos-alkene (**2.62**). To dibenzazepine was added triethylamine and phosphorous trichloride (Scheme 37). After stirring 3 h at rt, (*S*)-SPINOL (**2.77**) was added, and the mixture reacted 16 h. (*S*)-SIPHOS-alkene (**2.78)** was isolated in 40% yield. This ligand was then applied in the APKR of allenyl acetates.

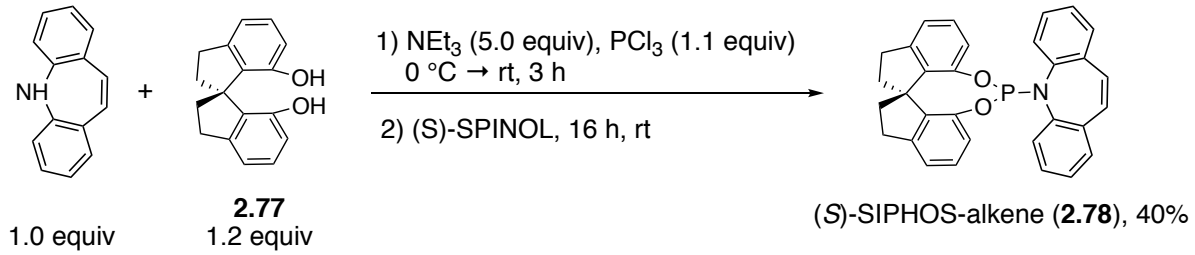

Scheme 37. Synthesis of (*S*)-SIPHOS-alkene.

Reaction of allenyl acetate **2.21c** using (*S*)-SIPHOS-alkene (**2.78**) ligand afforded product (*S*)-**2.22** in 77% yield and 42% ee (Table 12, entry 1). The yield of the reaction was slightly higher than that of (*S*)-MonoPhos-alkene (**2.62** 77% versus 71%), and the enantiomeric ratio was significantly decreased using the spirocyclic ligand (42% versus 64%). Similarly, allenyl benzoate **2.21f**, and octanoate **2.21e** reacted with lower enantioselectivity than with the (*S*)-MonoPhos-alkene (**2.62**) ligand. Increasing the CO atmosphere to 100% reduced enantioselectivity to 16% (entry 4). (*S*)-SIPHOS-alkene (**2.78**) ligand afforded (*S*)-cyclopentenones as the major products, the opposite absolute configuration as products afforded by (*S*)-MonoPhos-alkene ligand (**2.62**).

Table 12. APKR using (*S*)-SIPHOS-alkene ligand.

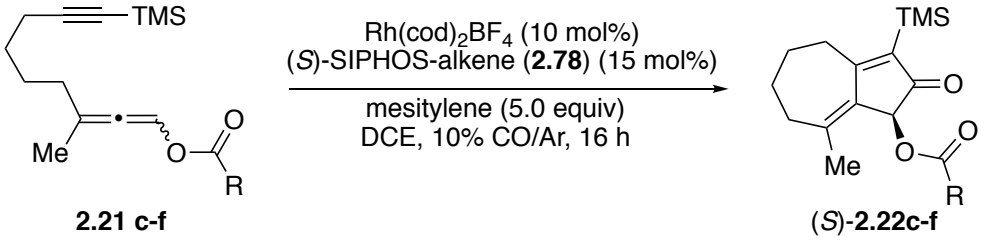

2.21 c-f (*S*)-**2.22c-f**

entry	R		CO/Ar (%)	yield (%)[a]	ee (%)
1	Me	**2.21c**	10	**2.22c** 77	42 (*S*)
2	Ph	**2.21f**	10	**2.22f** 66	32[b] (*S*)
3	$(CH_2)_6CH_3$	**2.21e**	10	**2.22e** 68	48 (*S*)
4	Me	**2.21c**	100	**2.22c** 74	16 (*S*)

[a] Yield was determined by integral comparison of the product resonance (5.8 ppm) to the internal standard mesitylene (6.8 pm). [b] Baseline separation of enantiomers was not achieved, and therefore, the reported ee value may be inaccurate.

SUPPORTING INFORMATION

CHAPTER 2

General Methods

Unless otherwise indicated, all reactions were performed in flame-dried glassware under an inert atmosphere of dry nitrogen and stirred with Teflon-coated magnetic stir bars. All commercially available compounds were purchased and used as received unless otherwise specified. The solvents tetrahydrofuran (THF) and dichloromethane (DCM) were purified by passing through alumina using the Sol-Tek ST-002 solvent purification system. Toluene, 1,2-dichloroethane (DCE), acetonitrile (MeCN), and triethylamine (Et_3N) were distilled from calcium hydride prior to use. *N,N*-Dimethylformamide (DMF) was stirred overnight with magnesium sulfate and distilled from barium oxide. Deuterated chloroform ($CDCl_3$) was dried over 3 Å molecular sieves. Gasses N_2, O_2, 100% CO, and 10% CO/Ar, were purchased from Matheson Tri Gas. Ligands (*S*)-MonoPhos and (*S*)-SIPHOS were purchased from Strem Chemicals and used as received. All ligands were stored and weighed in a nitrogen-filled glovebox. Purification of compounds by flash column chromatography was performed using silica gel (40-63 μm particle size, 60 Å pore size). TLC analyses were performed on silica gel F_{254} glass-backed plates (250 μm thickness). Preparatory TLC separations were performed on silica gel glass-backed plates with UV254 (1000 μm thickness, Sorbent catalog number 1617124). ^{1}H NMR, ^{13}C NMR and ^{31}P NMR spectra were recorded on Bruker Avance 400, or 500 MHz spectrometers. Spectra were referenced to residual chloroform (7.26 ppm, ^{1}H; 77.16 ppm, ^{13}C). Chemical shifts (δ) are reported in ppm and multiplicities are indicated by s (singlet), d (doublet), t (triplet), q (quartet), quint (quintet), and m (multiplet). Coupling constants, *J*, are reported in hertz (Hz). All NMR spectra were obtained at

room temperature. IR spectra were obtained using a Nicolet Avatar E.S.P. 360 FT-IR. EI mass spectroscopy was performed on a Waters Micromass GCT high resolution mass spectrometer, while ES mass spectroscopy was performed on a Waters Q-TOF Ultima API, Micromass UK Limited high resolution mass spectrometer. HPLCs were performed using a Waters 600 series solvent delivery module with a photodiode array with an injection volume of 50 μL and a flow rate of 1.0 mL/min. Optical rotations (reported in 10 $deg^{-1}cm^2\ g^{-1}$) were measured at 589 nm (sodium D line) using a Perkin Elmer 241 spectropolarimeter.

Experimental conditions, physical characterization, spectral data and HPLC traces (if applicable) for the following compounds, including syntheses and characterization of all precursors and spectral data, were recently published and can be found in the Supporting Information of: Burrows, L. C.; Jesikiewicz, L. T.; Lu, G.; Geib, S. J.; Liu, P.; Brummond, K. M., *J. Am. Chem. Soc.* **2017**, *139* (42), 15022-15032. Additionally, data and calculations pertaining to the computational aspect of this chapter are also detailed in the Supporting Information of the aforementioned publication.

Synthesis of methyl ketone 2.6c

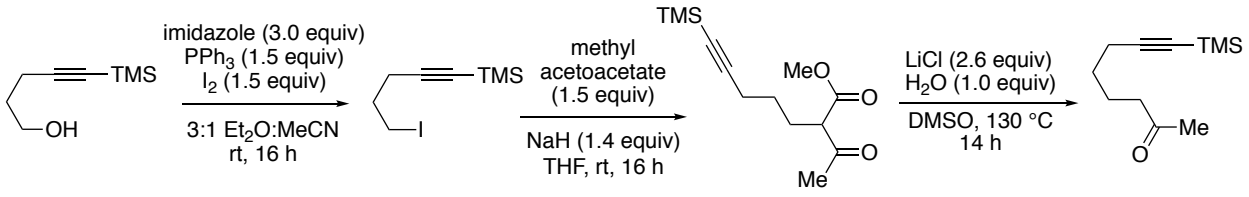

2.7 **2.8** 75% **2.9** quant **2.6c** 62%

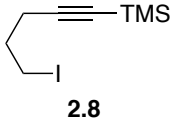

2.8

(5-Iodopent-1-yn-1-yl)trimethylsilane (2.8). The synthesis of **2.8** was performed in a manner analogous to that previously reported.[71] To a 500-mL, 2-necked round-bottomed flask was added alcohol **2.7** (7.2 g, 46 mol, 1.0 equiv) dissolved in 3:1

ether:MeCN (180 mL, 0.25 M). The flask was cooled to 0 °C using an ice/water bath. The septum was temporarily removed and imidazole (9.4 g, 138 mmol, 3.0 equiv), triphenylphosphine (18 g, 69 mmol, 1.5 equiv), and iodine (18 g, 69 mmol, 1.5 equiv) were added as solids. The reaction mixture was stirred vigorously and allowed to warm to rt. After 16 h at rt, complete consumption of the starting alcohol was observed by TLC. The reaction mixture was filtered through a plug of silica gel and concentrated by rotary evaporation. The crude product was purified by silica gel flash column chromatography (1% ethyl acetate/hexanes) to yield the title compound as a yellow oil (9.18 g, 75%) LCB 4-129

^{1}H NMR (500 MHz, $CDCl_3$)

3.29 (t, J = 7.0 Hz, 2 H), 2.36 (t, J = 7.0 Hz, 2 H), 2.00 (quint, J = 7.0 Hz, 2 H), 0.15 (s, 9 H) ppm

^{13}C NMR (125 MHz, $CDCl_3$)

205.0, 86.0, 32.2, 21.0, 5.3, 0.2 (3 C) ppm

IR (thin film)

2889, 2821, 5152, 1700, 1607, 1445, 1235, 1131, 834, 751 cm^{-1}

TLC R_f = 0.9 (20% ethyl acetate/hexanes) [silica gel, $KMnO_4$ stain]

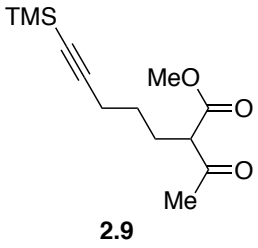

2.9

8-(Trimethylsilyl)oct-7-yn-2-one (2.9). The synthesis of **2.9** was performed in a manner analogous to that previously reported.[71] To a 250-mL, two-necked, round-bottomed flask equipped with a nitrogen inlet adaptor and septum was added sodium hydride (60% dispersion in mineral oil, 1.93 g, 48.2 mmol, 1.4 equiv) followed by THF (35 mL, 1.4 M). The flask was evacuated and refilled with nitrogen, and placed in an ice/water bath. Methyl acetoacetate (5.6 mL, 6.01 g, 51.8

mmol) was added via syringe, dropwise over five minutes. The ice/water bath was removed, and the reaction mixture stirred 10 min. TMS-iodopentyne **2.8** (9.18 g, 34.5 mmol, 1.0 equiv) was dissolved in DMF (35 mL, 1.0 M) and added via syringe, dropwise over 10 min. After 16 h at rt, the reaction was complete, as evidenced by TLC. The reaction mixture was diluted with ether (100 mL) and transferred to a 500-mL separatory funnel, and washed with water (100 mL). The organic layer was extracted with ether (3 x 100 mL). The combined organic layers were backwashed with brine (100 mL), dried over magnesium sulfate, filtered and concentrated by rotary evaporation, yielding the title compound as a light-yellow oil (8.8 g, quant). LCB 4-130

^{1}H NMR (500 MHz, $CDCl_3$)

3.74 (s, 3 H), 3.47 (t, J = 7.5 Hz, 1 H), 2.27-2.21 (m, 5 H), 1.95 (q, J = 7.5 Hz, 2 H), 1.53-1.48 (m, 2 H), 0.14 (s, 9 H) ppm

IR (thin film)

2923, 2868, 2149, 1695, 1419, 1344, 1235, 1136, 834, 751, 632 cm^{-1}

HRMS (FTMS + p ESI)

[M+H] calcd for $C_{13}H_{23}O_3Si$, 255.1411; found, 255.1420

TLC R_f = 0.5 (10% ethyl acetate/hexanes) [silica gel, $KMnO_4$ stain]

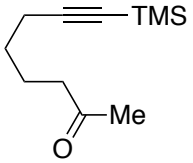

2.6c

8-(Trimethylsilyl)oct-7-yn-2-one (2.6c). To a 100-mL, two-necked, round-bottomed flask equipped with reflux condenser, and nitrogen inlet adaptor was added β-ketoester **2.9** (2.95 g, 11.6 mmol, 1.0 equiv) dissolved in DMSO (46 mL, 0.25 M), followed by lithium chloride (1.28 g, 30.2 mmol, 2.6 equiv). The flask was evacuated and refilled with nitrogen, and water (0.21 mL, 11.6 mmol, 1.0 equiv) was added via syringe. The flask was lowered into a preheated oil bath (130 °C). After 14 h, complete consumption of the

starting β-ketoester was observed by TLC. The flask was removed from the oil bath and allowed to cool to rt. The reaction mixture was diluted with ether (100 mL) transferred to a 500-mL separatory funnel, and washed with water (100 mL). The organic layer was extracted with ether (2 × 100 mL). The combined organic layers were backwashed with brine (100 mL), dried over magnesium sulfate, filtered and concentrated by rotary evaporation. The crude product was purified by silica gel flash column chromatography (10% ethyl acetate/hexanes) to yield the title compound as a light-yellow oil (1.42 g, 62%) LCB 4-007

^{1}H NMR (500 MHz, $CDCl_3$)

2.45 (t, J = 7.5 Hz, 2 H), 2.24 (t, J = 7.0 Hz, 2 H), 2.14 (s, 3 H), 1.68 (quint, J = 7.0 Hz, 2 H), 1.53 (J = 7.0 Hz, 2 H), 0.14 (s, 9 H) ppm

^{13}C NMR (125 MHz, $CDCl_3$)

208.9, 107.0, 84.9, 43.3, 30.0, 28.1, 23.1, 19.8, 0.2 (3 C) ppm

IR (thin film)

2956, 2867, 2174, 1716, 1431, 1359, 1249, 1149, 843, 760, 699, 640 cm^{-1}

HRMS (FTMS + p ESI)

[M+H] calcd for $C_{13}H_{19}O_2$, 197.1356; found, 197.1355

TLC R_f = 0.6 (10% ethyl acetate/hexanes) [silica gel, $KMnO_4$ stain]

Synthesis of propargyl alcohols 2.11c and 2.11b.

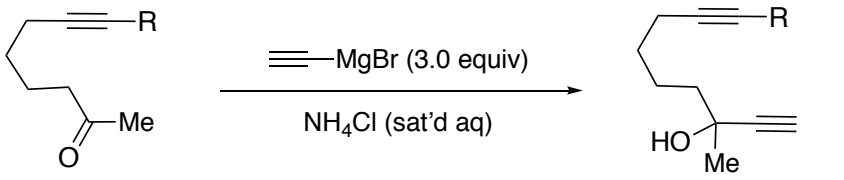

2.6c R = TMS
2.6b R = TIPS

2.11c R = TMS, 81%
2.11b R = TIPS, 67%

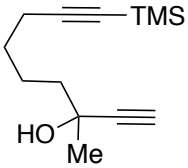

2.11c

3-Methyl-9-(trimethylsilyl)nona-1,8-diyn-3-ol. The synthesis of **2.11c** was performed in a manner analogous to that previously reported.[71] To a 250-mL, two-necked, round-bottomed flask equipped with a nitrogen inlet adaptor and septum was added methyl ketone **2.6c** (1.2 g, 6.1 mmol, 1.0 equiv) in THF (61 mL, 0.1 M). The solution was cooled to 0 °C using an ice/water bath. Ethynylmagnesium bromide (37 mL, 0.5 M in THF, 18 mmol, 3.0 equiv) was added dropwise via syringe, in two portions, over 10 min. After 1 h at 0 °C and 20 min at rt, complete consumption of methyl ketone **2.6c** was observed by TLC. Sat'd aq. ammonium chloride (100 mL) was added to the flask and the mixture was transferred to a 500-mL separatory funnel and the aqueous layer extracted with ether (3 × 100 mL). The combined organic layers were washed with brine (200 mL), dried over magnesium sulfate, collected by vacuum filtration, and concentrated by rotary evaporation. The crude product was purified by silica gel flash column chromatography (5-10% ethyl acetate/hexanes) to yield the title compound **2.11c** as a yellow oil (1.1 g, 81%). 4-008

^{1}H NMR (500 MHz, $CDCl_3$)

2.43 (s, 1 H), 2.53 (t, J = 7.0 Hz, 2 H), 1.96 (br. s, 1 H), 1.70-1.56 (m, 6 H), 1.50 (s, 3 H), 0.14 (s, 9 H) ppm

^{13}C NMR (125 MHz, $CDCl_3$)

107.4, 87.7, 84.9, 71.5, 68.2, 43.0, 29.9, 28.7, 23.9, 19.9, 0.3 (3 C) ppm

IR (thin film)

3412, 3310, 2951, 2866, 2174, 1641, 1250, 1110, 843, 760 cm^{-1}

HRMS (FTMS + p ESI)

$[M + H]^+$ calcd for $C_{13}H_{23}OSi$: 223.1513, found 223.1508

TLC R_f = 0.3 (15% ethyl acetate/hexanes)[silica gel, $KMnO_4$ stain]

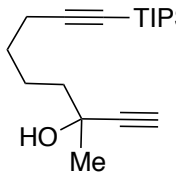

2.11b

3-Methyl-9-(triisopropylsilyl)nona-1,8-diyn-3-ol (2.6b). The synthesis of **2.11b** was performed in a manner analogous to that previously reported.[71] To a 50-mL, two-necked, round-bottomed flask equipped with a nitrogen inlet adaptor and septum was added methyl ketone **2.6b** (0.50 g, 1.78 mmol, 1.0 equiv) in THF (8.9 mL, 0.2 M). The solution was cooled to 0 °C using an ice/water bath. Ethynylmagnesium bromide (11 mL, 0.5 M in THF, 5.4 mmol, 3.0 equiv) was added dropwise via syringe over 10 min. After 90 min at 0 °C and 20 min at rt, complete consumption of methyl ketone **2.6b** was observed by TLC. The septum was removed and sat'd aq. ammonium chloride (5 mL) was added to the flask. The mixture was transferred to a 125-mL separatory funnel and diluted with ether (40 mL) and water (40 mL). The aqueous layer was extracted with diethyl ether (3 × 100 mL). The combined organic layers were washed with brine (50 mL), dried over magnesium sulfate, collected by vacuum filtration, and concentrated by rotary evaporation. The crude product was purified by silica gel flash column chromatography (5-10% ethyl acetate/hexanes) to yield the title compound **2.11b** as a clear oil (0.37 g, 67%). LCP 3-038

^{1}H NMR (500 MHz, $CDCl_3$)

2.42 (s, 1 H), 2.29 (t, J = 6.5 Hz, 2 H), 1.90 (s, 1 H), 1.70-1.64 (m, 4 H), 1.61-1.55 (m, 2 H), 1.49 (s, 3 H), 1.43-1.03 (m, 21 H) ppm

^{13}C NMR (125 MHz, $CDCl_3$)

109.0, 87.8, 80.6, 71.5, 68.2, 43.2, 29.8, 29.1, 23.9, 20.0, 18.8 (6 C), 11.5 (3 C) ppm

IR (thin film)

3389, 3310, 2942, 2893, 2171, 1463, 1368, 1109, 995, 883, 660 cm^{-1}

HRMS (FTMS + p ESI)

$[M + H]^+$ calcd for $C_{19}H_{35}OSi$: 307.2457, found 307.2479

TLC R_f = 0.3 (10% ethyl acetate/hexanes) [silica gel, *p*-anisaldehyde stain]

Synthesis of TIPS-pivalate 2.21h.

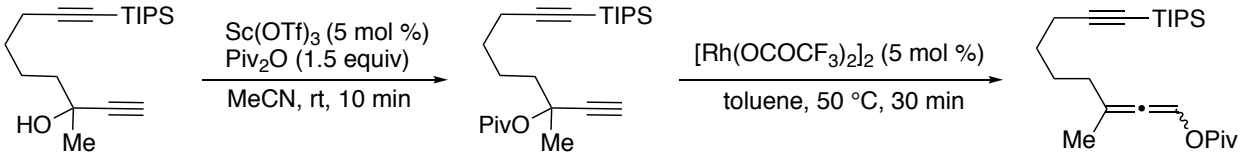

2.11b **2.10h** 71% **2.21h** 85%

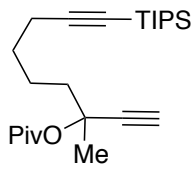

2.10h

3-Methyl-9-(triisopropylsilyl)nona-1,8-diyn-3-yl pivalate (2.10h). The synthesis of **2.10h** was performed in a manner analogous to that previously reported.[71] To a two-necked, 15-mL round-bottomed flask equipped with a septum and nitrogen inlet adaptor was added propargyl alcohol **2.11b** (0.30 g, 0.98 mmol, 1.0 equiv) in MeCN (4.9 mL, 0.20 M) via cannula. Pivalic anhydride (0.30 mL, 1.47 mmol, 1.5 equiv) was added via syringe at rt. Scandium(III) trifluoromethanesulfonate (24 mg, 0.049 mmol, 0.05 equiv) was dissolved in MeCN (1.0 mL, 0.05 M) was added slowly via syringe. After 10 min at rt, complete consumption of starting alcohol was observed by TLC. Sat'd aq $NaHCO_3$ (10 mL) was added slowly and stirred for an additional 10 min. The solution was transferred to a 250-mL separatory funnel and diluted with diethyl ether (50 mL) and water (50

mL). The aqueous layer was extracted with diethyl ether (2 x 50 mL), dried over magnesium sulfate, gravity filtered, and concentrated under reduced pressure. The crude product was purified by silica gel flash column chromatography (5% ethyl acetate/hexanes) to yield the title compound **2.10h** as a clear oil (0.27 g, 71%) LCP 3-050

^{1}H NMR (400MHz, $CDCl_3$)

2.49 (s, 1 H), 2.29 (t, J = 6.4 Hz, 2 H), 1.97-1.92 (m, 1 H), 1.86-1.79 (m, 1 H), 1.68-1.53 (m, 4 H), 1.65 (s, 3 H), 1.18 (s, 9 H), 1.08-0.99 (m, 21 H) ppm

Contains impurity (pivalic anhydride) at 1.26 (s) ppm

^{13}C NMR (100 MHz, $CDCl_3$)

176.8, 108.9, 84.1, 80.5, 74.3, 73.0, 41.4, 39.3, 29.0, 27.2, 26.7 (3 C), 23.5, 20.0, 18.8 (6 C), 11.4 (3 C) ppm

Contains impurity (pivalic anhydride) at 26.4 ppm

IR (thin film)

3313, 2942, 2866, 2171, 1741, 1463, 1285, 1144, 1098, 883, 661, 623 cm^{-1}

HRMS (FTMS + p ESI)

$[M + H]^+$ calcd for $C_{24}H_{43}O_2Si$: 391.3032, found 391.3052

TLC R_f = 0.3 (5% ethyl acetate/hexanes) [silica gel, *p*-anisaldehyde stain]

General procedure A. [3,3] sigmatropic rearrangement of propargyl esters to afford allenyl carboxy esters. Allenyl carboxy esters were synthesized in a manner analogous to that previously reported.[114] To a single-necked, round-bottomed flask was added rhodium(II) trifluoroacetate dimer (5 mol %) in a nitrogen-filled glovebox. The flask was sealed with a rubber septum, removed from the glovebox, and placed under nitrogen with an inlet needle. Propargyl carboxy ester (1.0

equiv) was weighed into a separate 15-mL conical flask in open atmosphere, sealed with a rubber septum, and the flask evacuated and refilled with nitrogen (3x). Toluene was added to the flask containing progargyl carboxy ester via syringe (0.2 M) and the solution transferred via cannula all at once to the catalyst-containing round-bottomed reaction flask. The flask was lowered into a preheated oil bath (50 °C) and after 35 to 90 min, consumption of propargyl acetate was observed by TLC. The reaction was allowed to cool to rt and the stir bar removed. The reaction mixture was concentrated by rotary evaporation and immediately purified by silica gel flash column chromatography.

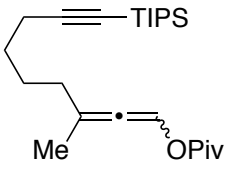

2.21h

3-Methyl-9-(triisopropylsilyl)nona-1,2-dien-8-yn-1-yl pivalate (2.21h). Follows general procedure A. rhodium(II) trifluoroacetate dimer (21 mg, 0.032 mmol, 0.05 equiv), propargyl pivalate **2.10h** (0.25 g, 0.64 mmol), toluene (3.2 mL, 0.2 M). After 30 min, complete consumption of propargyl pivalate was observed by TLC. The crude product was purified by silica gel flash column chromatography (2% ethyl acetate/hexanes) to yield the title compound **2.21h** as a yellow oil (0.21 g, 85%). LCP 3-051

^{1}H NMR (400 MHz, $CDCl_3$)

7.25 (sextet, J = 2.0 Hz, 1 H), 2.26 (t, J = 6.4 Hz, 2 H), 2.12-2.08 (m, 2 H), 1.82 (d, J = 2.0 Hz, 3 H), 1.63-1.53 (m, 4 H), 1.24 (s, 9 H), 1.06-1.02 (m, 21 H) ppm

^{13}C NMR (100 MHz, $CDCl_3$)

189.8, 176.6, 115.2, 109.9, 109.0, 80.43, 39.1, 34.8, 28.3, 27.2 (3 C), 26.3, 20.6, 19.8, 18.8 (6 C), 11.4 (3 C) ppm

IR (thin film)

2942, 2865, 2171, 1978, 1742, 1462, 1281, 1134, 1036, 1003, 883, 676 cm^{-1}

HRMS (FTMS + p ESI)

$[M + H]^+$ calcd for $C_{24}H_{43}O_2Si$: 391.3027, found 391.3034

TLC R_f = 0.4 (5% ethyl acetate/hexanes) [silica gel, *p*-anisaldehyde stain]

General Procedure B: APKR of allenyl carboxy esters using (*S*)-SIPHOS-alkene (2.62). In a nitrogen-filled glovebox, rhodium(I) bis(1,5-cyclooctadiene) tetrafluoroborate (8.9 mg) and (*S*)-SIPHOS-alkene (**2.62**) (12.7 mg), were weighed into separate 15-mL round-bottomed flasks and sealed with rubber septa. The flasks were removed from the glovebox and placed in a fume hood. Rhodium bis(1,5-cyclooctadiene) tetrafluoroborate was dissolved in DCE (2.4 mL, 0.0091 M) and a portion of this solution (0.55 mL, containing 2.0 mg Rh, 0.10 equiv) was added to each reaction test tube. (*S*)-SIPHOS-alkene (**2.62**) was dissolved in DCE (2.0 mL, 0.0014 M), and a portion of this solution (0.55 mL containing 3.6 mg (*S*)-SIPHOS-alkene, 0.15 equiv) was added to each test tube. The catalyst-ligand solution was stirred under nitrogen for 30 min at rt. The Teflon cap of the test tube was pierced with a needle attached to a balloon containing CO (10% CO/Ar or 100% CO), and the reaction was stirred under CO for 1 h at rt. Mesitylene (35 μL, 5.0 equiv) was added via syringe. Allenyl carboxy esters (0.05 mmol, 1.0 equiv) were weighed in separate flasks and sealed with septa. The flasks were evacuated and refilled with nitrogen, and DCE (0.55 mL) was added. Allenyl carboxy esters in DCE (0.55 mL, containing 0.05 mmol allene, 1.0 equiv) was added to the reaction test tube. The test tube was lowered into a preheated oil bath (70 °C) and the reaction mixture stirred under CO for 16 h. When complete, aliquots of the reaction mixture (0.3 mL) were taken via syringe, added to an NMR tube, and diluted with $CDCl_3$ (0.3 mL).[115] The samples were submitted for yield determination by ^1H NMR via integral comparison of the

mesitylene internal standard to the α-keto hydrogen peak of the product. Silica gel (0.2 g) was added to the reaction test tube, DCE removed by rotary evaporation, and the resulting mixture was loaded onto a silica gel column (0.7 cm diameter × 5 cm height). The product **2.22c** was isolated by flash column chromatography (10 × 1 mL fractions, eluting with 5-20% ethyl acetate/hexanes). Fractions containing product **2.22c** were combined, the solvent removed by rotary evaporation, and re-dissolved in HPLC-grade *i*PrOH/hexanes. Enantioselectivity was determined by HPLC using a Chiralpak IA-3 column and eluting with 0.5% *i*PrOH/hexanes at a flow rate of 1.0 mL/min. Enantiomers of **2.22c** eluted at 11 min (minor) and 14 min (major).

APKR of allenyl acetate 2.21c using (*S*)-SIPHOS-alkene ligand (2.78).

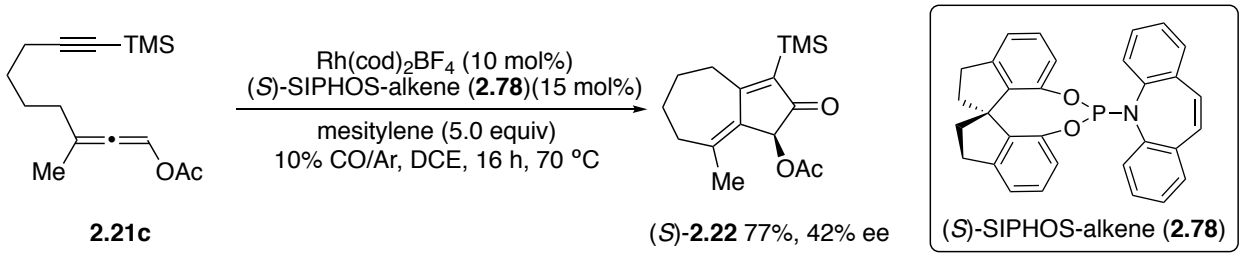

2.21c (*S*)-**2.22** 77%, 42% ee

Follows general procedure B: allenyl acetate **2.21c** (13 mg, 0.05 mmol, 1.0 equiv), rhodium(I) bis(1,5-cyclooctadiene) tetrafluoroborate (2.0 mg, 0.005 mmol, 0.10 equiv), (*S*)-SIPHOS-alkene (**2.78**) (3.6 mg, 0.0075 mmol, 0.15 equiv), mesitylene (35 μL 0.25 mmol, 5.0 equiv), DCE (0.03 M, 1.7 mL). The test tube was placed in a preheated oil bath (70 °C) under a balloon of 10% CO/Ar, and the solution stirred for 16 h. Yield was determined by integral comparison to the internal standard mesitylene (77%). LCP 4-143

Waters 600 HPLC, UV/PDA detector, 298 nm
Daicel CHIRALPAK-IA3, 25 cm column
0.5% *i*PrOH/hexanes, Flow rate: 1 mL/min

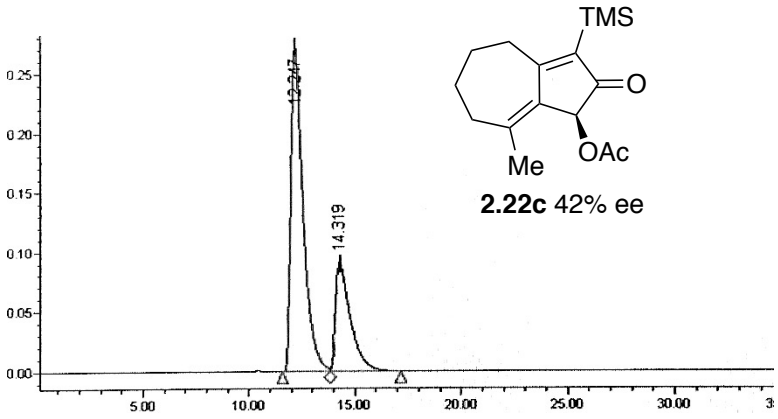

2.22c 42% ee

	Ret. Time (min)	Area (%)
Peak 1	12.247	71.15
Peak 2	14.319	28.85

APKR of allenyl benzoate 2.21f using (*S*)-SIPHOS-alkene ligand (2.78).

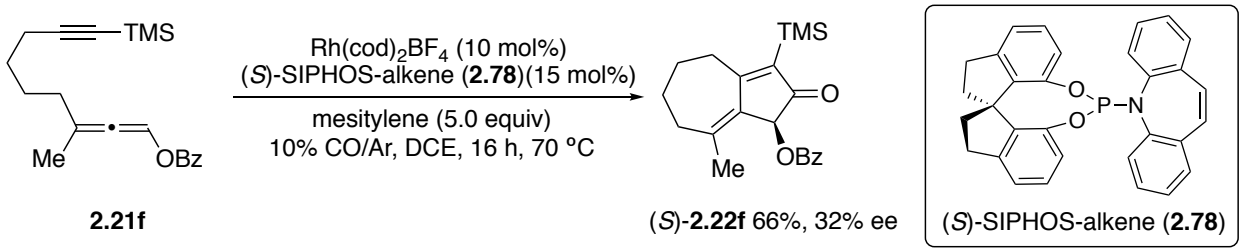

2.21f (*S*)-**2.22f** 66%, 32% ee (*S*)-SIPHOS-alkene (**2.78**)

Follows general procedure B: allenyl benzoate **2.21f** (16 mg, 0.05 mmol, 1.0 equiv), rhodium(I) bis(1,5-cyclooctadiene) tetrafluoroborate (2.0 mg, 0.005 mmol, 0.10 equiv), (*S*)-SIPHOS-alkene (**2.78**) (3.6 mg, 0.0075 mmol, 0.15 equiv), mesitylene (35 µL 0.25 mmol, 5.0 equiv), DCE (0.03 M, 1.7 mL). The test tube was placed in a preheated oil bath (70 °C) under a balloon of 10% CO/Ar, and the solution stirred for 16 h. Yield was determined by integral comparison to the internal standard mesitylene (66%). LCP 4-144

Waters 600 HPLC, UV/PDA detector, 298 nm
Daicel CHIRALPAK-IA3, 25 cm column
0.5% *i*PrOH/hexanes, Flow rate: 1 mL/min

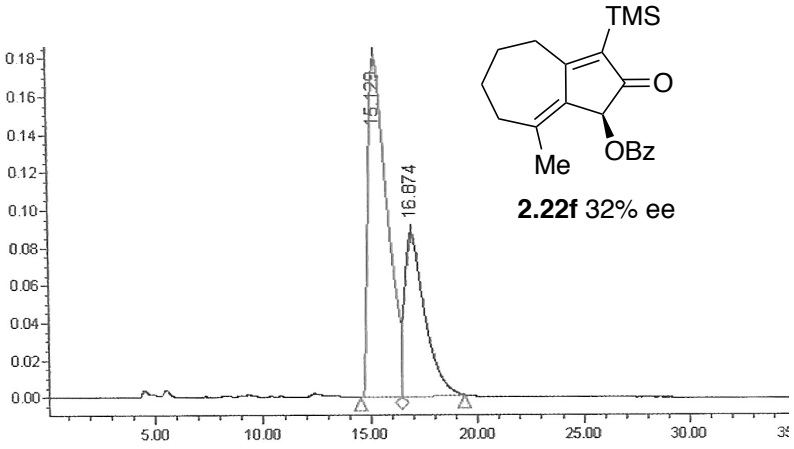

2.22f 32% ee

	Ret. Time (min)	Area (%)
Peak 1	15.129	66.15
Peak 2	16.874	33.85

APKR of allenyl octanoate 2.21e using (*S*)-SIPHOS-alkene ligand (2.78).

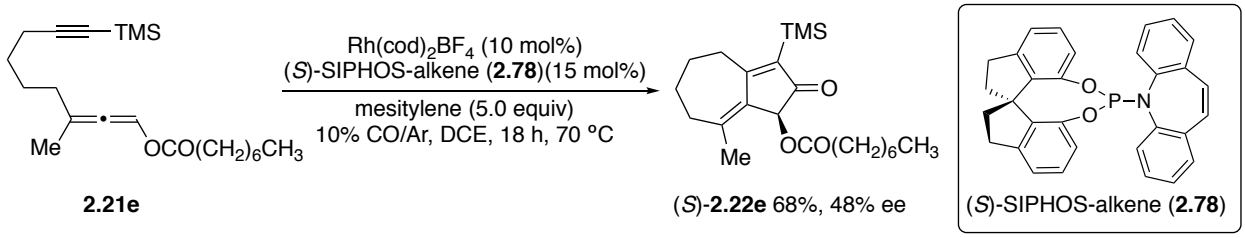

2.21e (*S*)-**2.22e** 68%, 48% ee (*S*)-SIPHOS-alkene (**2.78**)

Follows general procedure B: allenyl octanoate **2.21e** (17 mg, 0.05 mmol, 1.0 equiv), rhodium(I) bis(1,5-cyclooctadiene) tetrafluoroborate (2.0 mg, 0.005 mmol, 0.10 equiv), (*S*)-SIPHOS-alkene (**2.78**) (3.6 mg, 0.0075 mmol, 0.15 equiv), mesitylene (35 μL 0.25 mmol, 5.0 equiv), DCE (0.03 M, 1.7 mL). The test tube was placed in a preheated oil bath (70 °C) under a balloon of 10% CO/Ar, and the solution stirred for 18 h. Yield was determined by integral comparison to the internal standard mesitylene (68%). LCP 4-145

Waters 600 HPLC, UV/PDA detector, 298 nm
Daicel CHIRALPAK-IA3, 25 cm column
0.5% *i*PrOH/hexanes, Flow rate: 1 mL/min

	Ret. Time (min)	Area (%)
Peak 1	10.167	74.03
Peak 2	14.778	25.97

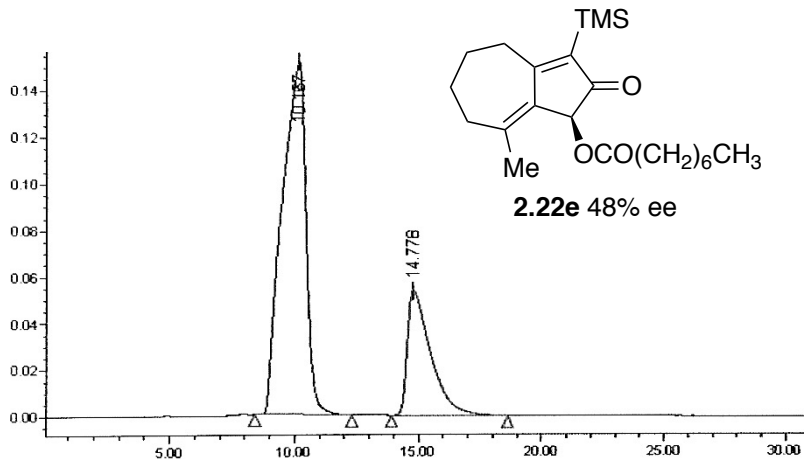

2.22e 48% ee

APKR of allenyl acetate 2.21c using (*S*)-SIPHOS-alkene ligand (2.78).

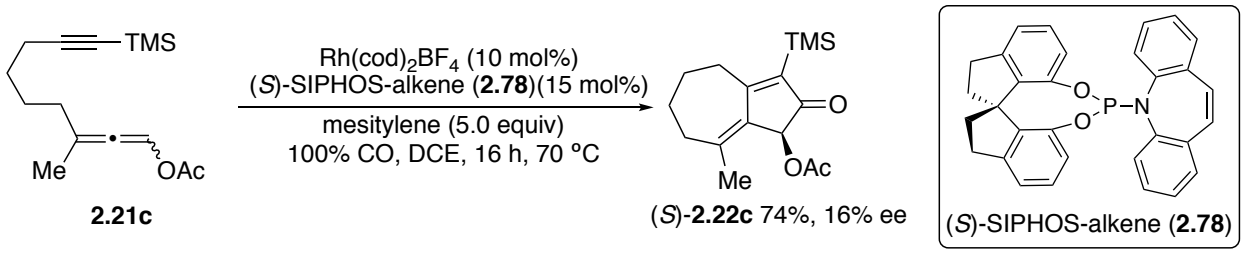

Follows general procedure B: allenyl acetate **2.21c** (17 mg, 0.05 mmol, 1.0 equiv), rhodium(I) bis(1,5-cyclooctadiene) tetrafluoroborate (2.0 mg, 0.005 mmol, 0.10 equiv), (*S*)-SIPHOS-alkene (**2.78**) (3.6 mg, 0.0075 mmol, 0.15 equiv), mesitylene (35 μL 0.25 mmol, 5.0 equiv), DCE (0.03 M, 1.7 mL). The test tube was placed in a preheated oil bath (70 °C) under a balloon of 10% CO/Ar, and the solution stirred for 16 h. Yield was determined by integral comparison to the internal standard mesitylene (74%). LCP 4-146

Waters 600 HPLC, UV/PDA detector, 298 nm
Daicel CHIRALPAK-IA3, 25 cm column
0.5% *i*PrOH/hexanes, Flow rate: 1 mL/min

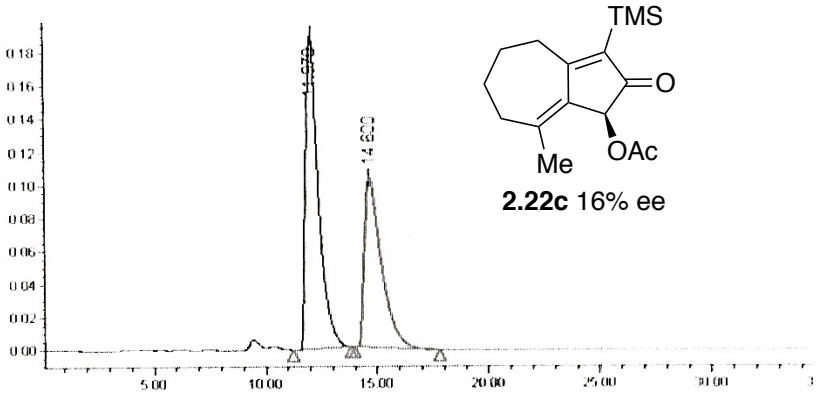

	Ret. Time (min)	Area (%)
Peak 1	11.970	57.95
Peak 2	14.600	42.06

3.0 OPTIMIZATION AND SCOPE OF THE ASYMMETRIC APKR WITH (*S*)-MONOPHOS-ALKENE LIGAND.

3.1 APKR EXPERIMENTAL PROCEDURE AND OBSERVATIONS.

The good yields combined with the good enantioselectivities of the APKR using the (*S*)-MonoPhos-alkene (**2.62)** ligand inspired further studies to identify the reaction conditions impacting the yield and ee, so that these responses could be improved further. Several reaction conditions were examined including scale, solvent, temperature, CO atmosphere, catalyst counteranion, additive identity and additive equivalents. Once these influential reaction conditions were identified, a strategy employing statistical design of experiments was used as a way of effecting an efficient optimization of yield and ee.

3.1.1 General procedure for the APKR of allenyl acetates.

*Preparation of Rh catalyst, (S)-MonoPhos-alkene ligand (**2.62**), and mesitylene solutions.* Cationic rhodium catalyst, $Rh(cod)_2BF_4$, and (*S*)-MonoPhos-alkene (**2.62**) ligand were each weighed in a nitrogen-filled glovebox into individual 10-mL round-bottomed flasks and sealed with septa. The flasks were removed from the glovebox and $Rh(cod)_2BF_4$ was dissolved in DCE (0.0091 M), and (*S*)-MonoPhos-alkene (**2.62**) was dissolved in DCE (0.014 M). Mesitylene was weighed into a

round-bottomed flask, placed under nitrogen, and dissolved in DCE (0.20 M). Allenyl acetate **2.21c** was weighed into a round-bottomed flask, placed under nitrogen, and dissolved in DCE (0.17 M).

APKR. Unless otherwise indicated, APKRs were performed on a 0.05 mmol (13 mg) scale in 8-mL test tubes, sealed with Teflon caps using an InnovaSyn reflux condenser (Figure 14, A and B). The red-orange solution of $Rh(cod)_2BF_4$ in DCE (2.03 mg 0.005 mmol, in 0.55 mL DCE, 0.10 equiv) was transferred to the reaction test tube via syringe, under nitrogen atmosphere. (*S*)-MonoPhos-alkene (**2.62**) in DCE (3.81 mg, 0.0075 mmol in 0.55 mL DCE, 0.15 equiv) was transferred to the test tube via syringe. The color of the homogeneous reaction mixture changed from red-orange to deep red gradually over 5 min. After 30 min at rt, the test tube was evacuated and refilled three times with 10% CO/Ar (g), alternating between an inlet needle attached to a vacuum and an inlet needle attached to a balloon of 10% CO/Ar. The color of the reaction mixture changed from deep red to yellow gradually over 5 minutes. After 1 h at rt under a balloon of 10% CO/Ar (Figure 14, C), mesitylene (6.0 mg, 0.05 mmol in 0.25 mL DCE, 1.0 equiv), then allenyl acetate **2.21c** (13 mg, 0.05 mmol in 0.30 mL DCE, 1.0 equiv) were transferred to the test tube, via syringe. The test tube was lowered into a preheated oil bath (70 °C) and the color of the homogenous reaction mixture changed from yellow to light orange, a color which remained consistent throughout the reaction. After 15 h, the reaction was complete, as observed by TLC. The reaction was cooled to rt, and an aliquot (100 μL) was taken using a syringe, transferred to an NMR tube, and diluted with $CDCl_3$ (500 μL).[115] Yields of product **2.22c** (5.8 ppm, 1 H) and aldehyde byproduct **2.23c** (9.9 ppm, 1 H) were determined by comparing ^1H NMR integrations with the internal standard, mesitylene (6.8 ppm, 3 H). Silica gel (0.2 g) was added to the reaction

test tube, DCE removed by rotary evaporation, and the resulting mixture was loaded onto a silica gel column (0.7 cm diameter × 5 cm height). The product **2.22c** was isolated by flash column chromatography (10 × 1 mL fractions, eluting with 5-20% ethyl acetate/hexanes). Fractions containing product **2.22c** were combined, the solvent removed by rotary evaporation, and re-dissolved in HPLC-grade *i*PrOH/hexanes. Enantioselectivity was determined by HPLC using a Chiralpak IA-3 column and eluting with 0.5% *i*PrOH/hexanes at a flow rate of 1.0 mL/min. Enantiomers of **2.22c** eluted at 11 min (minor) and 14 min (major).

A) 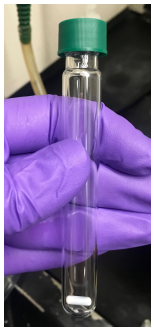 B) 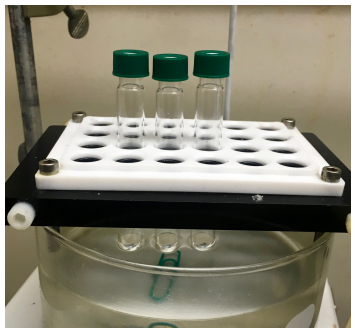 C) 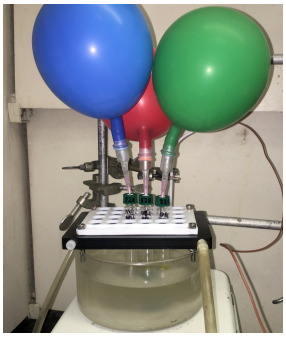

Figure 14. Test tubes in oil bath, secured with InnovaSyn reactor, stirring under CO balloons.

3.1.2 Proposed mechanism for the catalyst formation and allene-yne complexation steps.

Based upon the color changes observed during the reaction, and insights gained from DFT calculations, the following mechanism of catalyst formation is proposed (Scheme 38). The solution of cationic Rh complex, $Rh(cod)_2BF_4$ (**3.1**) in DCE solvent is red-orange in color. Addition of 1.5 equiv (relative to Rh) of hemilabile phosphoramidite-alkene ligand **2.62** provides a deep red mixture, which we propose contains one- and two-(*S*)-**2.62** coordinated complexes **3.2** and **3.3**

with the alkenyl group of the ligand *bound* to Rh. These "alkene-*bound*" complexes are proposed because the alkene-*bound* complex *cis*-**3.3**, has been characterized by X-ray crystallography and is known to be dark red in color.[109] When the inert nitrogen atmosphere was replaced with carbon monoxide (10% CO/Ar), a distinct color change was observed wherein the deep red reaction mixture turned light yellow, which likely corresponds to a change in the catalyst structure. We hypothesize that the coordinated 1,5-cyclooctadiene (cod) and alkene groups of **3.2** and **3.3** were replaced by CO ligands, affording a mixture of one- and two-(*S*)-**2.62**-coordinated complexes **3.4** and **3.5**, with the alkene groups of the ligand **2.62** not bound to Rh metal, a state that we will refer to as *unbound*. This proposed facile replacement of the alkene ligands by CO is supported by our calculations, which show that the alkene *unbound* complex **3.4** is ΔG = 8.7 kcal/mol lower in energy than the corresponding alkene-*bound* complex **3.6** (Chapter 2, Scheme 36). Upon addition of allene **2.21c** and heating from rt to 70 °C, the reaction mixture changed color from yellow to orange. Because CO becomes less soluble as temperature increases, we propose that this change in the solution color could indicate an increase in the red *alkene-bound* Rh species, such as **3.6** and **3.7** in solution.[116] Based upon our calculated lowest-energy reaction mechanism, coordination of the allene **2.21c** to complex **3.4** occurs to afford **3.8** with loss of one CO ligand (Scheme 38).[114] After reacting 15 h under 10% CO/Ar at 70 °C, the product **2.22c** is obtained.

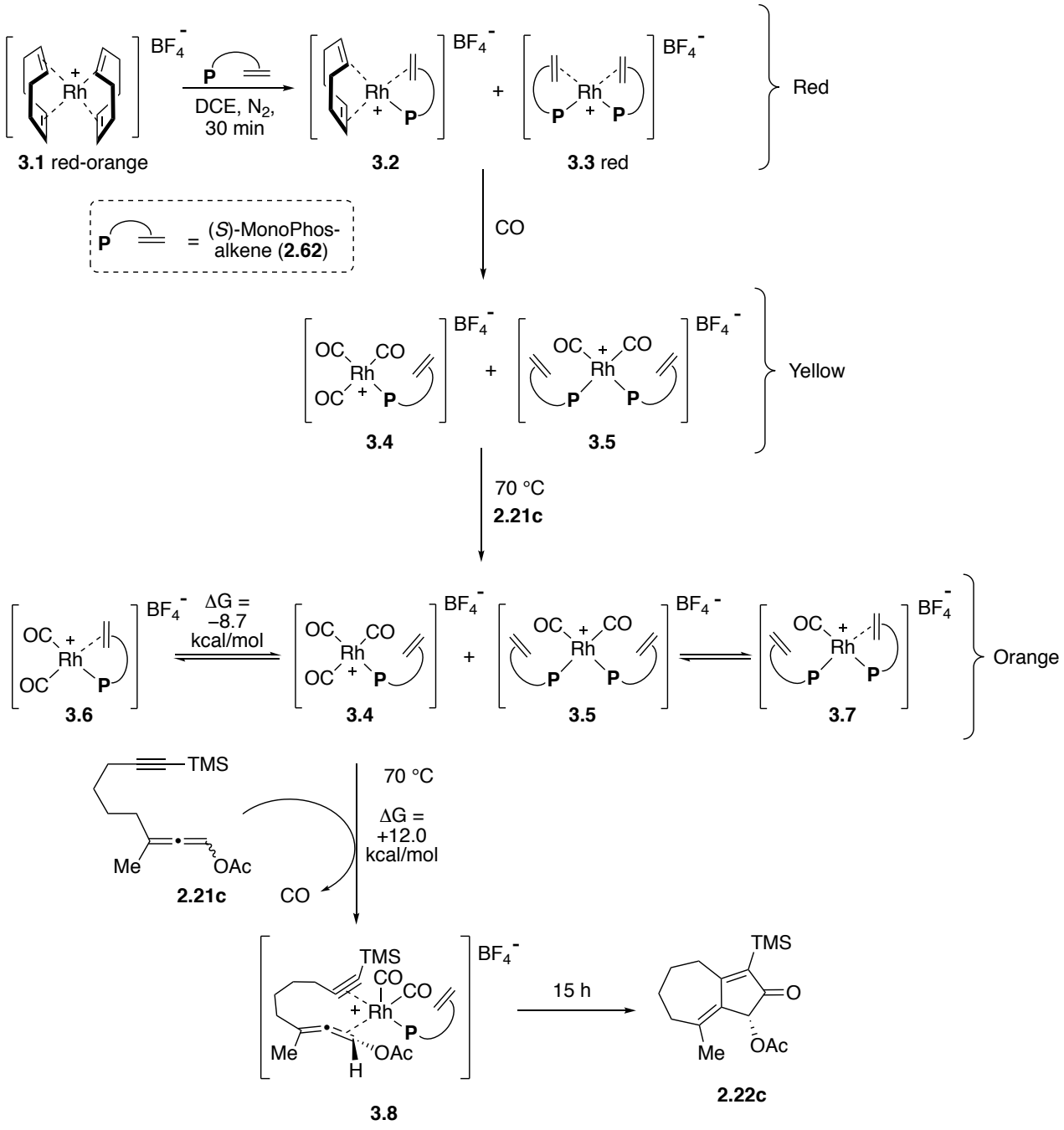

Scheme 38. Proposed mechanism for the Rh-(*S*)-MonoPhos-alkene catalyst formation and allene-yne complexation steps.

3.2 INITIAL OPTIMIZATION OF THE APKR YIELD AND EE WITH (*S*)-MONOPHOS-ALKENE LIGAND.

3.2.1 Effect of CO concentration on APKR yield and ee.

Our previous studies have demonstrated that the yield and enantioselectivity of the APKR is sensitive to CO concentration (see Chapter 2, Table 10, compare entries 2 and 3). Further, DFT calculations suggested that the two-CO, *alkene unbound* pathway has a higher $\Delta\Delta G^{\ddagger}$ and proceeds with enhanced enantioselectivity when compared to the one-CO, *alkene bound* pathway (Scheme 36). Based on these findings, we hypothesized that the concentration of CO in the reaction mixture was an influential variable in the APKR. However, the concentration of CO (or any gas) in solution is difficult to determine because it depends upon both atmospheric gas pressure, and the solution temperature.[116] Therefore, we set out to explore the role of CO concentration on APKR yield and enantioselectivity by modulating both CO atmosphere and reaction temperature.

A series of reactions were performed to test the effect of both CO atmosphere and temperature in the APKR (Table 13). These reactions were performed exactly as described in Section 3.1.1, changing only the composition of the CO atmosphere (2-100% CO) and the oil bath temperature (50 to 90 °C). Performing the APKR at 70 °C and 100% CO atmosphere afforded product **2.22c** in 76% yield and 54% ee (Table 13, entry 1). The reaction at lower temperature (50 °C) and lower CO atmosphere (10% CO/Ar) proceeded slowly (not complete after 96 h) with few byproducts (0% aldehyde **2.23**) and afforded product **2.22c** in higher ee (62%, entry 2) and higher yield (100% yield based upon recovered starting material). Both of these reactions (100% CO or low temperature) were yellow in color throughout, an observation that suggests a higher concentration of CO-bound complexes **3.4** and **3.5** (Scheme 38). Performing the APKR at 70 °C

with 10% CO/Ar afforded product **2.22c** in 16 h in 71% yield and 64% ee (entry 3). Lowering the CO atmosphere of the reaction further to 5% CO/Ar at 50 °C led to decreased product yield (23%), and an increase in the amount of aldehyde **2.23c (**15%, entry 4). For both entries 3 and 4, the reaction mixture was orange in color. Performing the APKR at high temperature (90 °C) afforded product **2.22c** in 25% yield, with many unidentified byproducts resulting from decomposition, as evidenced by TLC and ^{1}H NMR (entry 5). Performing the reaction with 2% CO/Ar gave a low yield of **2.22c** (7%) and a large amount of aldehyde **2.23c** (17%, entry 6). Reactions at high temperature (90 °C) or with very low CO atmosphere (2% CO/Ar) were red in color and afforded low yields.

We hypothesize that the yellow reaction mixtures correspond to a higher CO concentration (high CO atmosphere or low temperature) and red reaction mixtures correspond to a lower CO concentration (low CO atmosphere or high temperature). In turn, higher yields were observed in reactions with high CO concentration (yellow, entries 1 and 2), while lower yields were observed in reactions with low CO concentration (red, entries 5-6). The reactions giving the best yields and enantioselectivities were orange (entry 3). These results indicate that both temperature and CO have a significant impact on reaction yield, and that higher yields and fewer byproducts are provided in reactions with higher CO atmosphere (100% CO, entry 1) and lower temperature (50 °C, entry 2). In summary, the CO concentration impacted the yield greatly with a range of 7% to 75%. The CO concentration was less impactful on the enantioselectivity, with the ee range being 54 to 64% for the entries in Table 13, with no apparent trend observed.

Table 13. Effect of CO concentration on APKR yield and ee.

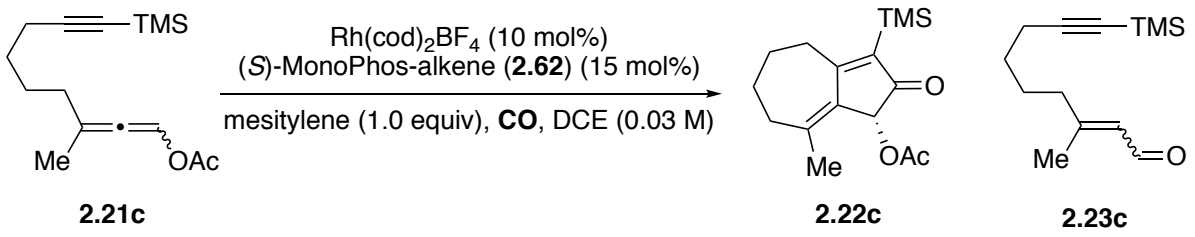

2.21c **2.22c** **2.23c**

entry	T (°C)	CO/Ar (%)	time (h)	yield (%)[a]	Aldehyde	ee (%)	color [b]
1	70	100	16	76	6	54	yellow
2	50	10	96	40 (100)[c]	0	62	yellow
3	70	10	16	71	9	64	orange
4	50	5[d]	28	23	15	60	orange [e]
5	90	10	3	25	2	54	red
6	50	2[f]	16	7	17	60	red

[a] Yields were determined by integral ratios for product resonance (5.8 ppm) and aldehyde resonance at 9.9 ppm, relative to mesitylene (6.8 ppm). [b] Color of the reaction mixture upon heating to the temperature indicated. Colors remained consistent for the entirety of the reactions unless otherwise indicated. [c] 60% unreacted starting material was observed in crude ^{1}H NMR, 100% yield based upon recovered starting material. [d] Atmosphere of 5% CO/Ar was generated by evacuating the reaction vial using an inlet needle and adding 4 mL Ar (g) and 4 mL 10% CO/Ar (g) via syringe. [e] The reaction slowly turned red over the course of the reaction. [f] Atmosphere of 2% CO/Ar was generated by evacuating the reaction vial using an inlet needle and adding 6.4 mL Ar (g) and 1.6 mL 10% CO/Ar (g) via syringe. Reproduced with permission from Burrows, L. C.; Jesikiewicz, L. T.; Lu, G.; Geib, S. J.; Liu, P.; Brummond, K. M., *J. Am. Chem. Soc.* **2017**, *139* (42), 15022-15032. © 2017 American Chemical Society.

3.2.2 Effect of internal standard on the APKR yield and ee.

Mesitylene was initially incorporated into the APKR reaction mixture as an "innocent" internal standard for yield calculations by ^{1}H NMR. However, it was soon discovered that incorporation of mesitylene positively affected the yields of the APKR. For example, addition of 1.0 equiv of mesitylene, relative to the allene-yne, improved the isolated yield of the APKR of allenyl acetate **2.21c** from 49 to 76% yield (see Chapter 2, Table 10, compare entries 1 and 2). Because the enantioselectivity was not affected, we hypothesized that the additive is not involved in the

stereochemistry-determining oxidative cyclization step. Mesitylene can weakly bind to rhodium, and could be improving catalyst turnover by displacing the cyclopentenone product following reductive elimination.[113]

Because mesitylene was having a positive effect on the yield of the APKR, we decided to screen a number of other sterically bulky hydrocarbon additives to test whether this effect could be enhanced. To this end, naphthalene, anthracene and hexamethylbenzene were tested as additives in the APKR (Table 14, entries 2-4). Reactions were performed exactly as described in Section 3.1.1, changing only the additive identity. Naphthalene, anthracene, and hexamethylbenzene additives all afforded lower yields of product **2.22c** and higher yields of aldehyde **2.23c** than the reaction with mesitylene additive (Table 14, compare entry 1 with entries 2-4). The less sterically-demanding derivatives *o*-xylene and toluene were also tested as additives (entries 5 and 6). Both resulted in lower yields, with no change in enantioselectivity when compared to mesitylene. Based upon the results of this brief additive study, the marked increase in yield of **2.22c** afforded by mesitylene was unique to this additive. Even though the enantioselectivity for anthracene was marginally higher (entry 3), we continued our optimization studies with mesitylene.

Table 14. Effects of changing identity on APKR yield and ee.

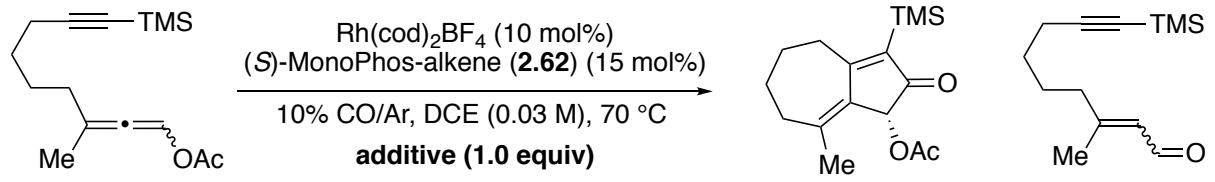

2.21c **2.22c** **2.23c**

entry	additive	yield (%)	aldehyde (%)	ee (%)
1	mesitylene	71 [a]	9	64
2	naphthalene	27 [b]	23	62
3	anthracene	24 [c]	32	70
4	hexamethylbenzene	29 [d]	24	62
5	*o*-xylene	53 [e]	- [f]	64
6	toluene	56 [e]	- [f]	62

[a] Yields were determined by integral ratio of product (5.8 ppm) and aldehyde (9.9 ppm) resonances relative to mesitylene resonance (6.8 ppm). [b] Yield was determined by integral ratios relative to naphthalene resonance (7.8 ppm). [c] Yield was determined by integral ratios relative to anthracene resonance (7.8 ppm). [c] Yield was determined by integral ratios relative to hexamethylbenzene resonance (2.1 ppm). [e] Isolated yields obtained after purification by column chromatography. [f] Data was not obtained.

Next, we hypothesized that, because addition of 1.0 equiv mesitylene improved the yield of the APKR, higher equivalents of this additive might increase the yield even further. To test this hypothesis, a series of APKRs were performed with mesitylene equivalents ranging from 5 to 50 equiv. Reactions were performed exactly as described in Section 3.1.1, with the only change being that neat mesitylene was measured by microliter syringe and added directly to the reaction. The reaction with 5.0 equiv (35 μL) of mesitylene afforded product in 82% yield and 63% ee (Table 15, entry 2). Further increases in mesitylene equivalents led to an increase in the amount of aldehyde byproduct **2.23c** formed (entries 3-5). Based on this study, the optimal amount of mesitylene under these conditions is 5 equiv. The reaction is tolerant of up to 25 equiv mesitylene (175 μL, entry 4) and the yield is decreased significantly upon addition of 50 equiv mesitylene

(17.5% v/v in DCE, entry 5), due to an increase in the amount of aldehyde byproduct **2.23c**. The enantioselectivity of the APKR is not affected by the equivalents of mesitylene.

Table 15. Determination of the optimal equivalents of mesitylene in the APKR.

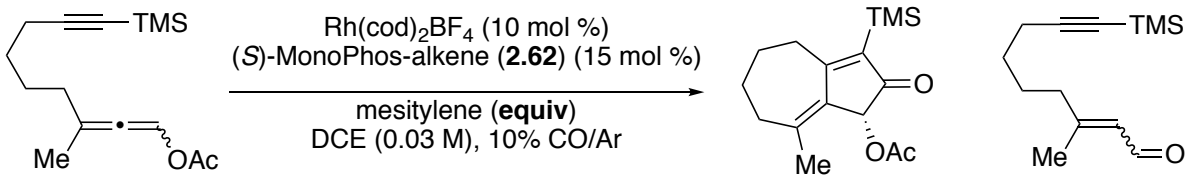

2.21c **2.22c** **2.23c**

entry	mesitylene (equiv)	yield (%) [a]	aldehyde (%)	ee (%)	mesitylene/ DCE (% v/v)
1	1	71	9	64	0.4
2	5	82	<1	63	2.1
3	10	75	9	64	4.1
4	25	70	17	62	9.6
5	50	43	39	62	17.5

[a] Yields were determined by integral ratios for product resonance (5.8 ppm) and aldehyde resonance (9.9 ppm) relative to mesitylene resonance (6.8 ppm).

3.2.3 Testing the effect of (*S*)-MonoPhos-alkene ligand to Rh ratio on the yield and ee of the APKR.

In the asymmetric APKR using Rh-phosphoramidite catalysts, a careful balance of the reaction conditions is necessary to ensure that the phosphoramidite ligand is coordinated to the catalyst. For example, under CO atmosphere, the Rh-(*S*)-MonoPhos-alkene (**2.62**) catalyst can exist as an equilibrium between three species: the "CO-only" catalyst **3.9**, the one-(*S*)-**2.62**-ligand complex **3.4** and the two-(*S*)-**2.62** ligand complex **3.5** (Scheme 39). An excess of (*S*)-MonoPhos-alkene (**2.62**) ligand is desirable to disfavor the background reaction resulting from formation of the "CO-only" Rh species **3.9** which can rapidly complex the allene-yne substrate to give **3.10** and afford

racemic product **2.22c** (see Section 2.4.4). Increasing the equivalents of ligand to Rh could shift the catalyst equilibrium away from the ligand-free Rh species; however, too much ligand could lead to a predominance of the two-(*S*)-**2.62** ligand complex **3.5**, for which the energy of substrate coordination would be high and would likely result in only recovered starting material. An optimum ligand to Rh ratio would shift the equilibrium of the catalyst resting state complexes to **3.4**, which readily coordinates the allene-yne to give **3.8**, and subsequently affords the enantioenriched product (*R*)-**2.22c**. Thus, several experiments were performed to identify the impact of the ligand to Rh ratio on the yield and ee of the APKR product.

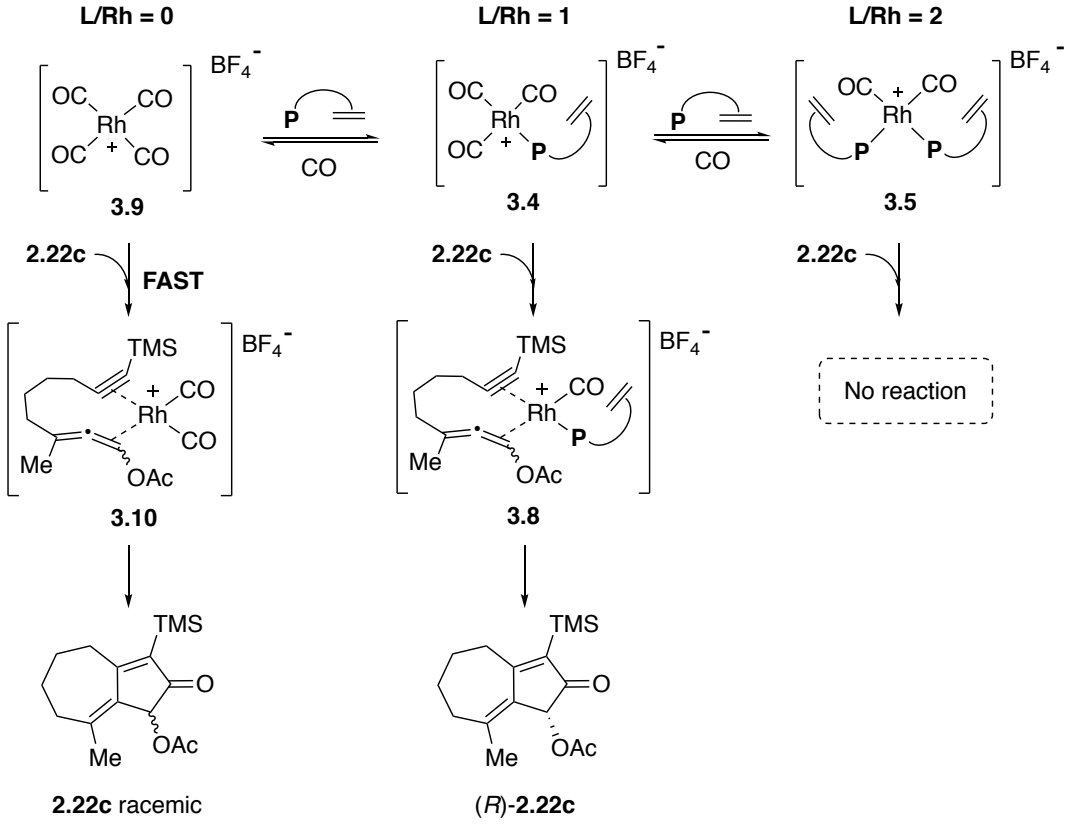

Scheme 39. Proposed dependence of APKR on ligand to Rh ratio.

Experiments to examine the effect of the ligand to Rh ratio were performed exactly as described in Section 3.1.1, changing only the equivalents of (*S*)-MonoPhos-alkene (**2.62**) ligand added. In addition, mesitylene was not used as an additive in this experiment. Reactions were performed with ligand (*S*)-**2.62** to Rh ratios of DCE under 100% CO atmosphere (Table 16). The APKR with a ligand to Rh ratio of 1.1 was complete in only 3 h, and afforded product in 50% yield and 38% ee (entry 1). The APKR with a ligand to Rh ratio of 1.5 gave product in 15 h in 49% yield and 55% ee, with 9% aldehyde byproduct formed (entry 2). The reaction with a ligand to Rh ratio of 2.2 gave no APKR product, with 5% conversion of the starting allene to aldehyde **2.23c**. These results indicate that the ligand to Rh ratio does greatly impact the APKR yield and ee, with a ligand to Rh ratio of more than 1.5 significantly reducing catalyst reactivity.

Table 16. Testing effect of ligand to Rh equivalents in APKR.

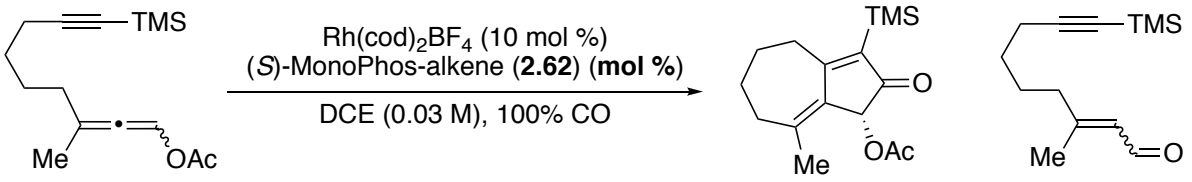

2.21c **2.22c** **2.23c**

entry	Ligand/Rh ratio	T (°C)	time (h)	yield (%) [a]	aldehyde	ee (%)
1	1.1	70	3	50	20	38
2	1.5	70	15	49	9	55
3	2.2	90	16	0 (5) [b]	5	-

[a] Isolated yields after purification by column chromatography. [b] Starting allene was recovered with 5% conversion to aldehyde **2.23c**.

3.2.4 Testing the effect of scale on the yield and ee of the APKR.

Up to this point, all APKR experiments were performed on small scale (13 mg allene, 0.05 mmol) in 8-mL test tubes. Once conditions had been identified that afforded good yields and ee's, the scale of the reaction was increased. A reaction was performed exactly as described in Section 3.1.1, with the only changes being the scale of the reaction (13 mg versus 50 mg) and the reaction vessel (test tube versus a 50-mL round-bottomed flask, Table 17, compare entries 1 and 2). The yield for the larger scale reaction was considerably lower than that of the smaller scale reaction (41% versus 71%), and more aldehyde **2.23c** was observed (35% versus 9%, compare entries 1 and 2). Because both the reaction scale and apparatus had been altered, we hypothesized that because there was only a four-fold change in the scale of the reaction, the reaction vessel may be playing a role in the reaction efficiency. Therefore, we tested the larger scale reaction in a Schlenk tube because this shape was similar to that of the reaction test tubes used during small-scale testing. Performing the APKR on a 45-mg scale in a 50-mL Schlenk tube afforded **2.22c** in a 48% yield, representing a 7% improvement over the APKR yield in the round-bottomed flask (compare entries 2 and 3). At this point, we opted to examine reaction conditions that had previously been shown to afford higher APKR yields. Under 100% CO conditions, the yield of **2.22c** was improved to 75%; however, the ee was reduced to 53% (entry 4). Next, 5.0 equiv mesitylene was added, and the yield of the APKR was improved from 41 to 79% (entry 5). These conditions were also tested on allenyl benzoate **2.21f**, which reacted in 67% yield and 66% ee (entry 6). In summary, the increase in equivalents of mesitylene and performing the larger scale reaction in a Schlenk tube led to an improved yield of the APKR on a large (50 mg) scale.

Table 17. Optimization of the APKR yield on a 50 mg scale.

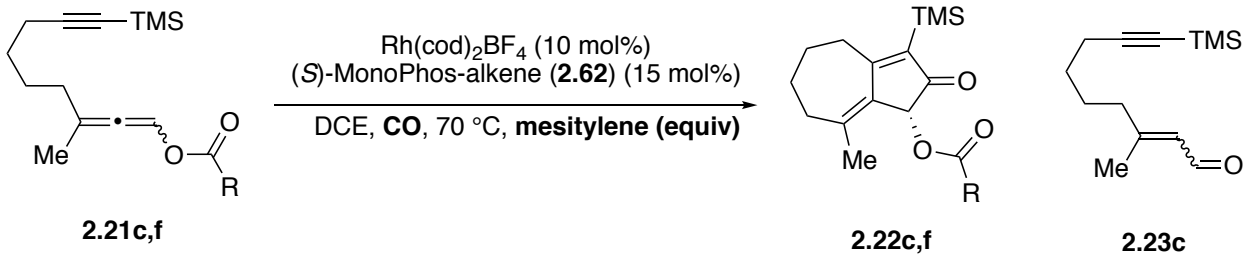

2.21c,f **2.22c,f** **2.23c**

entry	R	Scale (mg)	CO/Ar (%)	mesitylene (equiv)	apparatus	yield (%)[a]	aldehyde (%)[a]	ee (%)	Color
1	Me, **2.21c**	13	10	1	8-mL test tube	71	9	64	Orange
2	Me, **2.21c**	50	10	1	50-mL round-bottomed flask with condensor	41	35	64	Orange
3	Me, **2.21c**	45	10	1	50-mL Schlenk tube	48	17	60	Orange
4	Me, **2.21c**	50	100	5	50-mL Schlenk tube	75	0	53	Yellow
5	Me, **2.21c**	50	10	5	50-mL Schlenk tube	79 [b]	9	63	Orange
6	Ph, **2.21f**	62	10	5	50-mL Schlenk tube	67 [b]	8	66	Orange

[a] Yields were determined by integral ratios for product resonance (5.8 ppm) and aldehyde resonance (9.9 ppm) relative to mesitylene (6.8 ppm). [b] Isolated yields. Reproduced with permission from Burrows, L. C.; Jesikiewicz, L. T.; Lu, G.; Geib, S. J.; Liu, P.; Brummond, K. M., *J. Am. Chem. Soc.* **2017**, *139* (42), 15022-15032. © 2017 American Chemical Society.

3.2.5 Effect of solvent on the APKR yield and ee.

Our initial APKR experiments using a cationic Rh catalyst and a phosphoramidite ligand were performed in DCE because this was established as an optimal solvent in the first enantioselective PKR using a phosphoramidite ligand.[99] However, we expected the choice of solvent to have a significant impact on the yield and ee in the Rh-(*S*)-MonoPhos-alkene (**2.62**)-catalyzed APKR because the solvent would influence the coordination state of the hemilabile alkene group of the

ligand (Scheme 40). For example, a highly coordinating solvent such as THF may compete with the alkenyl group for a coordination site on the Rh metal, thus favoring the alkene *unbound* catalyst **3.11**, while a weakly coordinating solvent such as DCE would favor an alkene *bound* catalyst **3.7**. We set out to determine whether a correlation could be made between the APKR yield and ee and the solvent coordinating ability, polarity or polarizability. To this end, seven different solvents varying in their coordinating ability, polarity and polarizability were tested in the APKR: DCE, acetonitrile, chlorobenzene, THF, toluene, *m*-xylene and α,α,α-trifluoroethanol (Table 18). Numerical values describing each solvent's coordinating ability were obtained from Díaz-Torres *et. al*., where more negative numbers represent more non-coordinating solvents.[117] Parameters describing solvent polarity and polarizability were reported by Sheppard *et. al.* [118]

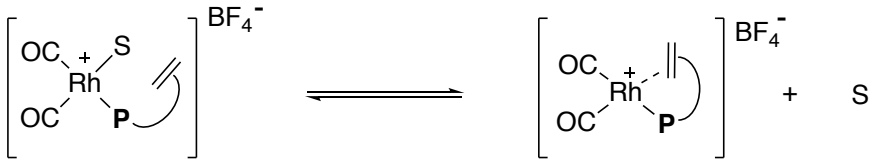

3.11 S = Coordinating solvent **3.7** S = Noncoordinating solvent

Scheme 40. Effect of solvent coordinating ability on catalyst structure.

In this solvent screening experiment, reactions were performed on a 0.025 mmol scale. $Rh(cod)_2BF_4$ was dissolved in DCM (13.6 mg in 3.8 mL) and 0.28 mL of this solution was added to seven test tubes, under nitrogen atmosphere. (*S*)-MonoPhos-alkene ligand (**2.62**) was dissolved in DCM (14.9 mg in 3.9 mL) and 0.28 mL of this solution was added to each test tube. Dichloromethane was removed from each test tube using an inlet needle attached to a vacuum manifold, leaving a red-orange solid catalyst, which was re-dissolved in the appropriate solvent (listed in Table 18). Catalyst solutions were stirred under nitrogen at rt, and then under 10% CO/Ar,

as described in Section 3.1.1. Solutions of allene-yne **2.21c** were prepared using each solvent listed and added to the reaction test tubes (6.6 mg allene **2.21c**). Mesitylene was not added to the reactions listed in entries 2-7 (Table 18).

Performing the APKR in PhCl gave **2.22c** in 62% ee and in 26% yield (Table 18, entry 2). Diminished yield (15-19%) and enantioselectivity (11-42% ee) was observed when the APKR was carried out in toluene, *m*-xylene, and trifluoroethanol (Table 18, entries 3-5). In the reactions with coordinating solvents tetrahydrofuran (THF) and acetonitrile (MeCN), only starting allene was recovered (Table 18, entries 6 and 7).

Table 18. Solvent effects in the APKR yield and ee.

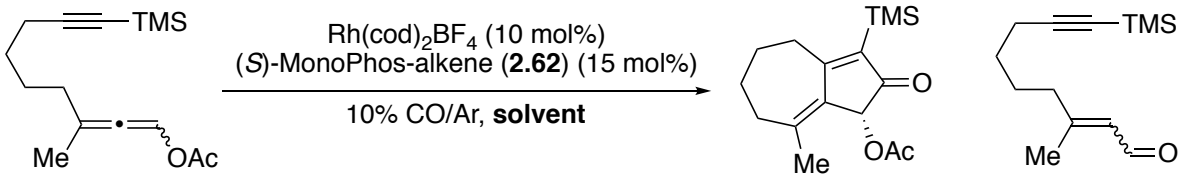

2.21c **2.22c** **2.23c**

entry	solvent	T (°C)	yield (%) [a]	Unreacted **2.21c** [b]	aldehyde **2.23c** [b]	ee (%)	coordinating ability[117]	polarity[118]	polarizability[118]
1	DCE [c]	70	71	0	9	64	-1.6	0.79	1.10
2	PhCl	70	26	0	30	62	-1.5	1.50	2.56
3	toluene	90	15	30	20	42	-1.2	0.64	0.65
4	TFE	90	19	30	40	28	-0.5	-2.97	-3.07
5	xylene	90	13	50	10	11	-0.4	2.84	1.33
6	THF	90	No reaction	100	0	-	-0.3	0.42	-1.35
7	MeCN	90	No reaction	100	0	-	-0.2	-2.18	-1.49

[a] Isolated yields after purification by column chromatography. [b] Unreacted starting allene **2.21c** and aldehyde **2.23c** were not isolated in this screening experiment. Percentages reported are rough estimates based upon TLC analysis. [c] Reaction was performed with 1.0 equiv mesitylene added.

The parameters describing solvent polarity and polarizability have been reported and are listed in Table 18. The complexity afforded by these additional parameters led us to consider a statistical software package, JMP 12.0 for the analysis of this data. Herein, we report a statistical analysis of this data to quantitatively identify which solvent parameter was most important for high yield and ee, as elucidated by the p-values in Table 19 (an individual p-value of <0.05 is statistically significant). The only variable that is statistically significant is coordinating ability, supporting our initial conclusions.

Table 19. Statistical analysis of solvent parameters in APKR.

entry	solvent parameter	p-value (yield)	p-value (% ee)
1	coordinating ability	0.011	0.001
2	polarity	0.52	0.53
3	polarizability	0.88	0.33

Because solvent coordinating ability was determined to be the most important solvent parameter with noncoordinating solvents being most effective, we hypothesized that other noncoordinating solvents might afford similarly high yields and enantioselectivities in the APKR. To test this hypothesis, the APKR was performed in dichloromethane (DCM), another noncoordinating solvent, at 30 °C (Table 20, entry 2). DCM has a solvent coordinating parameter of -1.7, which is similar to that of DCE (-1.6, Table 20, entries 1 and 2). However, DCM proved to not be a good solvent because of its low boiling point and our inability to perform this reaction at a temperature required to effect the PKR (Table 20, entry 2). α,α,α-Trifluorotoluene (TFT) is a suggested alternative to DCE based on the principle component analysis performed by Sheppard and coworkers.[118] Therefore, in a second experiment, TFT was tested in the APKR, and afforded good yield (55%) and ee (69%, Table 20, entry 3).

Table 20. Non-coordinating solvents tested in the APKR.

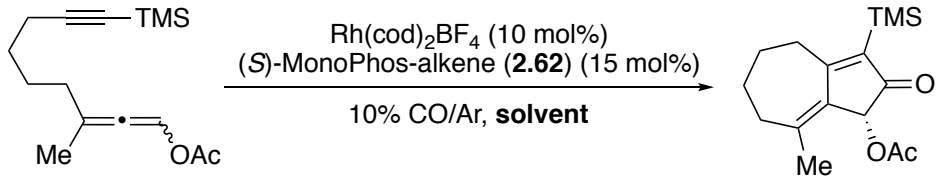

2.21c **2.22c**

entry	Solvent	Coordinating ability[117]	Polarity[118]	Polarizability[118]	T (°C)	time (h)	yield (%)	ee (%)
1	DCE	-1.6	0.79	1.10	70	15	71	64
2	DCM	-1.7	0.54	-0.42	30	14	0	-
3	TFT	-[a]	1.65	1.83	70	14	55	69

[a] Coordinating ability of trifluorotoluene (TFT) was not reported.

In summary, the three best solvents in the APKR were DCE (Table 18, entry 1), PhCl (entry 2), and TFT (Table 20, entry 3). Each of these solvents afford APKR product **2.22c** in good yield and good enantioselectivity. Therefore, these three solvents were further investigated in subsequent optimization efforts.

3.3 APPLICATION OF A DESIGN OF EXPERIMENTS STATEGY TO ENHANCE THE YIELD AND EE OF THE ASYMMETRIC APKR.

3.3.1 Rationale for using DOE to optimize the APKR yield and ee.

A typical optimization strategy for asymmetric transition metal catalyzed reactions consists of setting standard conditions and screening a library of chiral ligands for best yields and ee's; an empirical approach that has proven quite successful. However, because of the mechanistic complexity associated with the transformation of racemic allenyl acetate to enantioenriched

cyclocarbonylated product, we employed a rational approach to catalyst discovery armed with mechanistic insights gained from DFT calculations. Consequently, we successfully identified (*S*)-MonoPhos-alkene (**2.62**) ligand using a combined computational and experimental approach (Chapter 2). However, during these catalyst design studies and initial reaction optimizations, it became clear that the APKR using (*S*)-MonoPhos-alkene (**2.62**) ligand was sensitive to a number of reaction conditions, including temperature, solvent, ligand to Rh ratio, internal standard identity, internal standard amount, and CO concentration (Section 3.2). Several other unexplored factors could play a role as well, including reaction concentration, and counteranion identity. Therefore, we needed a more comprehensive approach to APKR yield and ee optimization which would take into consideration all of these factors. Statistical design of experiments (DOE) is a way to test many reaction factors simultaneously, without the need to test every possible combination.[119] This is accomplished by employing statistical software where a minimal number of points are selected to effectively sample the entire "reaction space". These results afford a mathematical model which can be used to predict ideal reaction conditions.

3.3.2 Transition metal-catalyzed reaction optimization using DOE.

DOE is growing in popularity both within the chemical industry and in academia due to improved screening technologies and increasing regulatory demands on R&D.[119-121] This popularity coincides with an increasing number publications involving DOE optimization strategies for chemical reactions.[120, 122-127] In developing our own DOE-optimization strategy for the enantioselective APKR, we were inspired by a reported enantioretentive *N*-arylation of amino acid ester **3.12** where DOE was successfully implemented (Scheme 41).[128] In this study, Buchwald and King optimized 11 different reaction conditions (refered to as factors) to enhance the yield and ee

of the *N*-arylated product **3.13** (referred to as responses), employing JMP 12.0, a statistical analysis software package from SAS. Eleven different factors were studied at two settings each to identify which had a statistically significant impact on yield and ee. Of the possible 2048 possible reaction conditions, a set of 31 discreet chemical reactions was generated using JMP software as an initial sampling of the reaction space. The runs were performed, and four significant factors were identified: temperature, equivalents of base, amount of 3 Å molecular sieves, and base identity. These four factors were subjected to a second round of DOE analysis, in which an additional 19 reactions were performed. After two rounds of DOE optimization, the yield and ee were improved from 61% yield and 84% ee to 69% yield and 89% ee. Subsequently, it was shown that by increasing the catalyst loading from 2% to 5% the *N*-arylated product **3.13** could be obtained in 93% yield and 91% ee. Because our APKR optimization involves the same two responses (yield and ee), and many reaction factors, we closely followed this two-round optimization strategy.

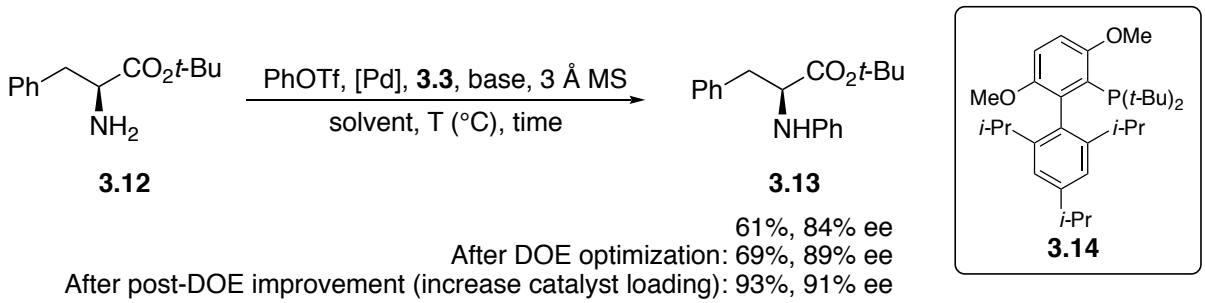

Scheme 41. DOE optimization of enantioretentive *N*-arylation.

3.3.3 Accepted nomenclature used in statistical DOE.

In the field of DOE, there is nomenclature that should be clarified.[119, 129-130] A set of *runs* placed strategically throughout the experimental space are collectively called an *experiment*. In the case of chemical reaction optimization, a *run* is a discreet chemical reaction. The *factors* are the

independent variables which influence the system. The *responses* are the dependent variables which are being optimized (in our case, yield and ee), and the *experimental region* is the multidimensional space being explored. *Continuous* factors are numeric and can have an infinite number of settings, while *categorical* factors have distinct settings and are non-ordered. *Discrete numeric* factors are numeric and have limited settings. The *model* refers to the mathematical equation (usually a linear regression) used to represent the best fit for the data points upon completion of the experiment. *Factor screening* is the process of defining which factors are important to the outcome of a system and is usually performed in the first round of experimentation. *Optimization* involves more detailed modeling and determination of optimum conditions and is usually performed in a second round of experimentation. The goal of DOE is to perform experiments to define a model which will mathematically describe the reality of the system. A model is not a perfect representation of reality, but rather, it is a tool which can be used to predict outcomes of future experiments. A well-designed experiment will span maximum area of reaction space in a minimum limited number of runs.

3.3.4 Factors and settings chosen in Experiment 1.

In our optimization of the yield and ee for the APKR, two experiments were performed in which the relative significance of seven different factors was determined in Experiment 1, and from these seven, the factors determined to be the most significant were then optimized in Experiment 2. This approach enabled a thorough investigation of the of maximum relevant reaction space with a minimum number of runs. We included in Experiment 1 seven factors which, based on both previous APKR studies and literature precedent, are influential in the APKR yield and enantioselectivity. These factors and their settings are shown in Table 21. The discreet settings

chosen for each factor were intended to sample the maximum of reaction space, while still maintaining catalyst reactivity. For example, the lowest temperature affording APKR product **2.22c** is 50 °C, while yields decreased at or above 90 °C (Section 3.2.1). Therefore, temperature settings of 50, 70 and 90 °C were selected (Table 21, entry 1). Three solvents settings were based upon previous results showing good reactivity and enantioselectivity in the APKR: 1,2-dichloroethane (DCE), chlorobenzene (PhCl), and α,α,α-trifluorotoluene (TFT) (Section 3.2.5). Previous experiments showed that the APKR proceeded in good yield with a ligand/Rh ratio of 1.1, and that ligand/Rh ratios beyond 1.5 hindered catalyst reactivity (Section 3.2.3). Therefore, the ligand/Rh ratio was tested at two settings: 1.1 and 1.5 equiv (Table 21, entry 3). In addition, the APKR has previously shown sensitivity to CO atmosphere (Section 3.2.1) and the incorporation of mesitylene as an additive (Section 3.2.2). Therefore, the effects of these two factors were explored (Table 21, entries 4 and 5), each with two settings. Our research group has previously demonstrated that concentration can play a role in the APKR, and therefore a range of concentrations were tested (Table 21, entry 6).[131] Finally, literature precedent supporting the importance of counteranion effects in the enantioselective PKR led us to test three counteranions differing in their coordinating ability (coordinating OTf, noncoordinating BF_4, and highly noncoordinating tetrakis(3,5-bis(trifluoromethyl)phenyl)borate, BAr^F_4) in the APKR (Table 21, entry 7). [132, 99, 117] Most of the numeric factors were investigated using only two settings at "high" and "low" values (Table 21, entries 3, 4, and 5), however, the ranges of temperature and concentration are large, and three settings were used to ensure that an optimal point at an intermediate value would not be excluded from the model (Table 21, entries 1 and 6).

Table 21. Factors and settings in Experiment 1.

entry	factor	type	settings
1	Temperature	Discrete numeric	50, 70, 90 °C
2	Solvent	Categorical	DCE, PhCl, TFT
3	Ligand/Rh	Discrete numeric	1.1, 1.5
4	CO atmosphere	Discrete numeric	10, 100% CO/Ar
5	Mesitylene	Discrete numeric	0, 5 equiv
6	Concentration	Discrete numeric	0.01, 0.03, 0.1 M
7	Catalyst	Categorical	BF_4, OTf, $BAr^F{}_4$,

The "Custom Design" tool of JMP 12.0 software was used to design Experiment 1. A screenshot of this Custom Design setup page is shown in Figure 15. First, the two responses, yield and ee were entered in the "Responses" panel, along with the lower and upper limits of 0 and 100 (Panel A, Figure 15) The goal of this experiment, to maximize both yield and ee, was also indicated to JMP in the "Responses" panel. Next, the seven factors being investigated were entered in Panel B. The settings for each factor were entered as described in Table 21, where temperature, ligand to Rh ratio, CO atmosphere, mesitylene (equiv) and concentration were entered as discrete numeric factors, while solvent and counteranion were entered as categorical factors.

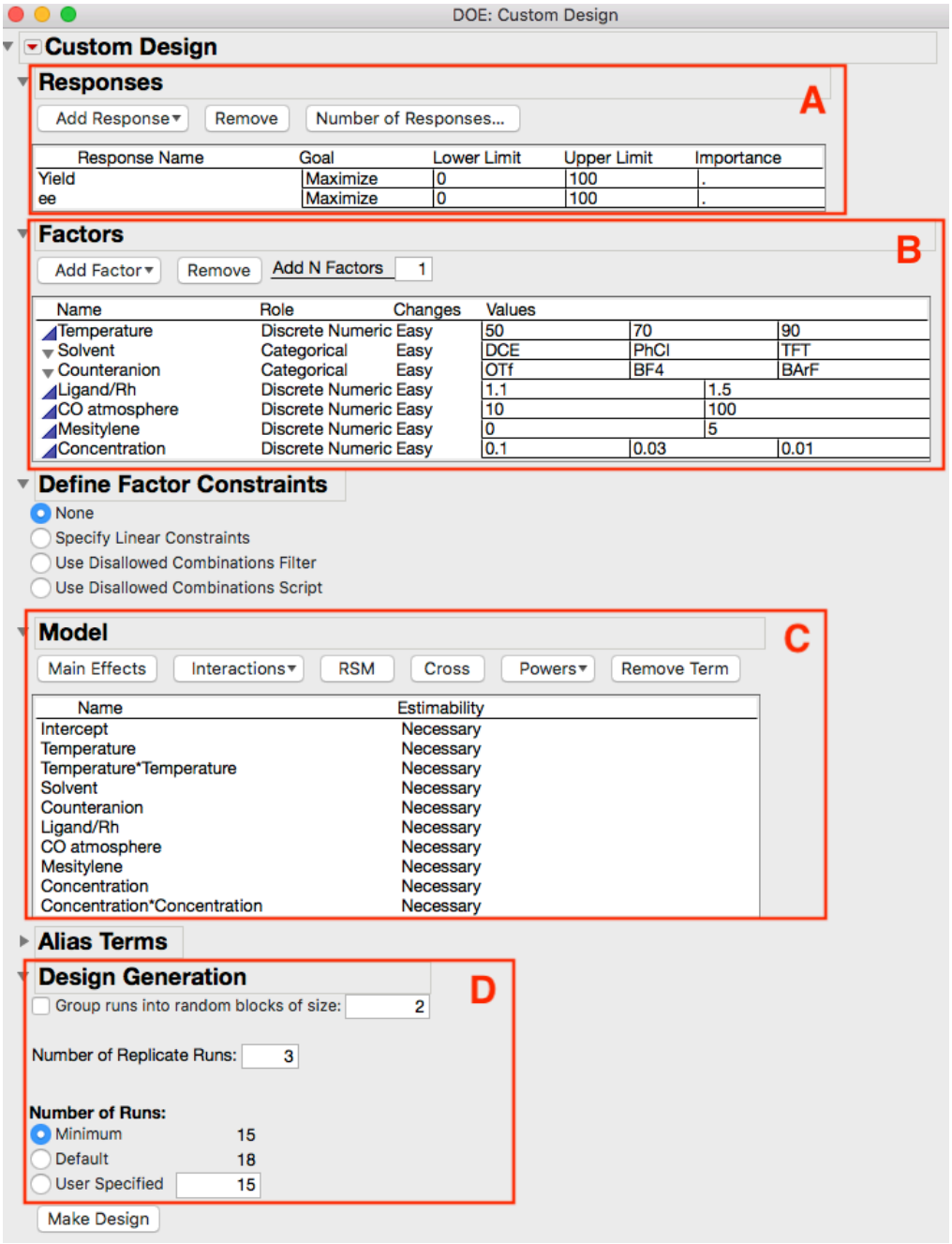

Figure 15. Screenshot of Experiment 1 of DOE setup in JMP software.

3.3.5 Choosing a model for Experiment 1.

In order to generate a set of runs that will most effectively model the reaction space, the statistical software JMP requires that an initial mathematical model be selected first. We chose to model the data in Experiment 1 using a linear regression with first order terms ($k_n x_n$, where k_n is the parameter weighing the contribution of factor x) included for all factors, and quadratic terms ($k_n x_n^2$) for temperature and concentration only (Table 21, entries 1 and 6).[129, 133] Quadratic terms ($k_n x_n^2$) introduce curvature to the model, and were necessary for modeling numeric factors with three settings. Without the quadratic term, a minimum or maximum at the intermediate settings of these factors (70 °C and 0.03 M) would not be detected. Additional terms for factor interactions were not included ($k_n x_1 x_2$) in this experiment. This model is depicted in Panel C of Figure 15.

Next, three replicate runs, which are randomly distributed repeats of individual runs, were included to measure experimental error (Figure 15, Panel D). [128, 129] Here, with our goal for this first experiment focused on establishing the relative importance of each factor, we opted to proceed with the 15 runs composing the minimum required for this experiment with seven first order terms, two second order terms, and three replicates (Figure 15, Panel D).[129] Selection of "Make Design" (bottom of Custom Design screen, Figure 15), affords a set of 15 runs was generated by the JMP software (Table 22). The factors were evenly distributed among all settings, along with three replicate runs (entries 3, 5, and 15). This design models a total of 648 different factor combinations.

Table 22. Runs in the Experiment 1.

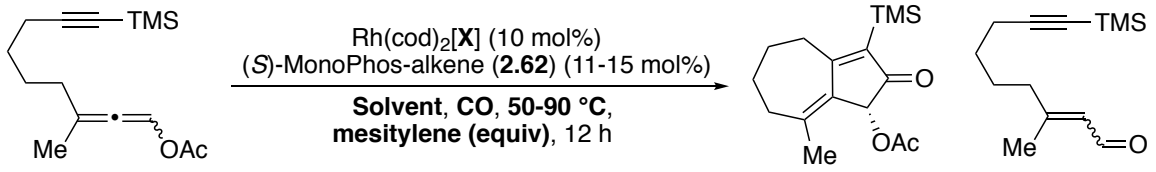

2.21c **2.22c** **2.23c**

Entry	T (°C)	Solvent	Counter-anion, X	Ligand/ Rh	CO/Ar (%)	Mesitylene (equiv)	C (M)
1	50	PhCl	BF_4	1.5	100	5	0.03
2	50	DCE	OTf	1.5	100	0	0.1
3	50	DCE	OTf	1.5	100	0	0.1
4	50	TFT	BAr^F_4	1.1	10	0	0.03
5	50	TFT	BAr^F_4	1.1	10	0	0.03
6	50	TFT	BF_4	1.1	100	5	0.01
7	70	PhCl	BAr^F_4	1.1	100	5	0.1
8	70	PhCl	OTf	1.1	10	0	0.01
9	70	DCE	BAr^F_4	1.5	10	5	0.01
10	70	TFT	BF_4	1.5	100	0	0.03
11	90	PhCl	BAr^F_4	1.5	100	0	0.01
12	90	DCE	BF_4	1.1	10	0	0.1
13	90	DCE	OTf	1.1	100	5	0.03
14	90	TFT	OTf	1.5	10	5	0.1
15	90	TFT	OTf	1.5	10	5	0.1

3.3.6 Data collection and statistical analysis of Experiment 1.

All 15 reactions listed in Table 22 were performed as described in Section 3.1.1, with a few exceptions. The cationic catalysts ($Rh(cod)_2OTf$, $Rh(cod)_2BF_4$, and $Rh(cod)_2BAr^F_4$) exhibited poor solubility in TFT and PhCl, so these three Rh catalysts were weighed into round-bottomed flasks, dissolved in dichloromethane (DCM), and the required amount of the solution delivered to the reaction test tube via syringe (0.005 mmol Rh in 0.25 mL DCM). The DCM was removed by vacuum evaporation using an inlet needle attached to a vacuum manifold, leaving the Rh catalyst as a red-orange solid. Addition of the (*S*)-MonoPhos-alkene (**2.62**) (0.0055 mmol, 0.11 equiv or

0.0075 mmol, 0.15 equiv) as a solution in the appropriate solvent afforded homogenous Rh-(*S*)-**2.62** solutions. The Rh-(*S*)-**2.62** solutions were stirred (1000 rpm) in the appropriate solvent (DCE, PhCl, or TFT) for 30 min at rt under a nitrogen atmosphere to afford red solutions. The atmosphere of each test tube was evacuated and refilled with CO (10% or 100% CO/Ar). The resulting yellow solutions were stirred under a CO (balloon of attached to an inlet needle) for 1 h at rt. Mesitylene was added by microliter syringe (35 μL, 5.0 equiv, if applicable), followed by the substrate **2.21c** dissolved in the appropriate solvent (DCE, PhCl, or TFT). The reactions were placed into a preheated oil bath (50, 70 or 90 °C) for exactly 12 h under a balloon of either 10% CO/Ar or 100% CO. After 12 h, the reactions were allowed to cool to rt, and aliquots (100 uL) were taken using a syringe, transferred to an NMR tube, and diluted with $CDCl_3$ (500 μL).[115] Yields of product **2.22c** (5.8 ppm, 1 H) and aldehyde byproduct **2.23c** (9.9 ppm, 1 H) were measured by ^{1}H NMR integrations versus internal standard mesitylene (6.8 ppm, 3 H). For experiments where the mesitylene (equiv) setting was zero, the mesitylene (35 μL, 5.0 equiv) was added to the reaction test tube for yield determination after the reaction was complete. Silica gel (0.2 g) was added to the reaction test tubes, solvent removed by rotary evaporation, and the resulting mixtures were loaded onto silica gel columns (0.7 cm diameter × 5 cm height). The products **2.22c** were isolated by flash column chromatography (10 × 1 mL fractions, eluting with 5-20% ethyl acetate/hexanes). The samples were dissolved in HPLC grade *i*PrOH/hexanes, and enantioselectivities were determined by HPLC using a Chiralpak IA-3 column (0.5% iPrOH/Hexanes, 1.0 mL/min).

The results of this first DOE experiment are shown in Table 23. The highest yield (77% yield) was obtained with $Rh(cod)_2BAr^F{}_4$ catalyst in PhCl at 90 °C, under 100% CO with 0 equiv mesitylene added at 0.01 M (Table 23, entry 11). The highest enantioselectivity (71% ee) was obtained with $Rh(cod)_2BF_4$ catalyst in PhCl solvent at 50 °C, under 100% CO with 5.0 equiv

mesitylene added at 0.03 M (entry 1). In general, reactions with triflate (OTf) counteranion gave poor yields. For example, entries 8, 13, 14 and 15 afforded yields at or below 8%. Entries 2 and 3 were replicates and gave poor yield agreement (23% and 32% yield, respectively). So, while these results call into question the reliability of the reactions performed with the $Rh(cod)_2OTf$ catalyst, it is clear that the OTf counteranion performs poorly in terms of both yield and ee. Unfortunately, a high proportion of runs performed at 90 °C were carried out using the $Rh(cod)_2OTf$ catalyst (three out of five runs, entries 13, 14, and 15) and this distribution could have incorrectly diminished a positive effect of higher temperature (90 °C) on APKR yields during the analysis.

Table 23. Results of Experiment 1.

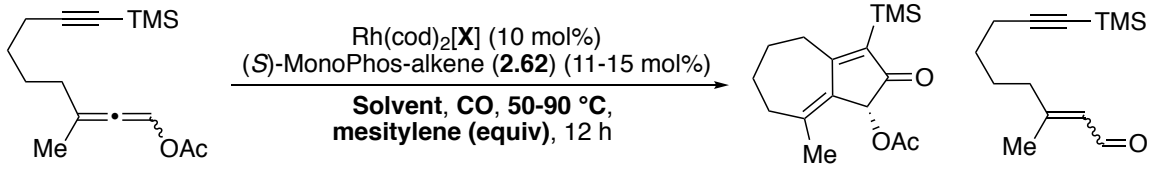

2.21c **2.22c** **2.23c**

Entry	T (°C)	Solvent	Counter-anion, X	Ligand/ Rh	CO/Ar (%)	Mesitylene (equiv)	C (M)	Yield [a]	Alde-hyde [a]	ee (%)
1	50	PhCl	BF_4	1.5	100	5	0.03	25	5	71
2	50	DCE	OTf	1.5	100	0	0.1	23	19	38
3	50	DCE	OTf	1.5	100	0	0.1	32	49	39
4	50	TFT	BAr^F_4	1.1	10	0	0.03	8	0	37
5	50	TFT	BAr^F_4	1.1	10	0	0.03	10	0	32
6	50	TFT	BF_4	1.1	100	5	0.01	25	0	36
7	70	PhCl	BAr^F_4	1.1	100	5	0.1	38	0	47
8	70	PhCl	OTf	1.1	10	0	0.01	8	20	10
9	70	DCE	BAr^F_4	1.5	10	5	0.01	10	4	56
10	70	TFT	BF_4	1.5	100	0	0.03	50	12	55
11	90	PhCl	BAr^F_4	1.5	100	0	0.01	77	5	58
12	90	DCE	BF_4	1.1	10	0	0.1	12	9	52
13	90	DCE	OTf	1.1	100	5	0.03	2	8	16
14	90	TFT	OTf	1.5	10	5	0.1	4	6	9
15	90	TFT	OTf	1.5	10	5	0.1	4	8	3

[a] Yields were determined by integral ratios for product resonance (5.8 ppm) and aldehyde resonance (9.9 ppm) relative to mesitylene (6.8 ppm).

The yields, enantioselectivities, and aldehyde amounts from the first experiment were analyzed and the set of data points were fit using the model designated in the initial experimental design. The results from analysis are summarized in the prediction profiler plots in Figure 16, where each panel represents a cross-section of a seven-dimensional mathematical model. The black lines represent responses of yield or ee for settings within each factor and the blue bars represent the 95% confidence limit of the model. The panels are depicted in the order decreasing factor significance, with counteranion being the most significant, and concentration being the least significant. The BAr^{F}_{4} and BF_4 counteranions both afforded higher yields (Figure 16, panel 1), and the BF_4 counteranion afforded highest ee's (panel 2). The OTf counteranion gave very low yields and ee's. Higher CO atmosphere gave higher yields (panel 3), and according to the model, had no effect on ee (panel 4). PhCl gave best yields (panel 5), while DCE and PhCl gave equally good ee's (panel 6). A higher ligand/Rh ratio of 1.5 afforded higher yields and ee's (panels 7 and 8). According to the model, mesitylene had a negative effect on yield (panel 9), and no effect on ee (panel 10). Higher temperature (90 °C) gave best yields (panel 11) and lower temperature (50 °C) gave better ee's (panel 12). Higher concentrations had a small negative effect on yield (panel 13) and a small positive effect on ee (panel 14).

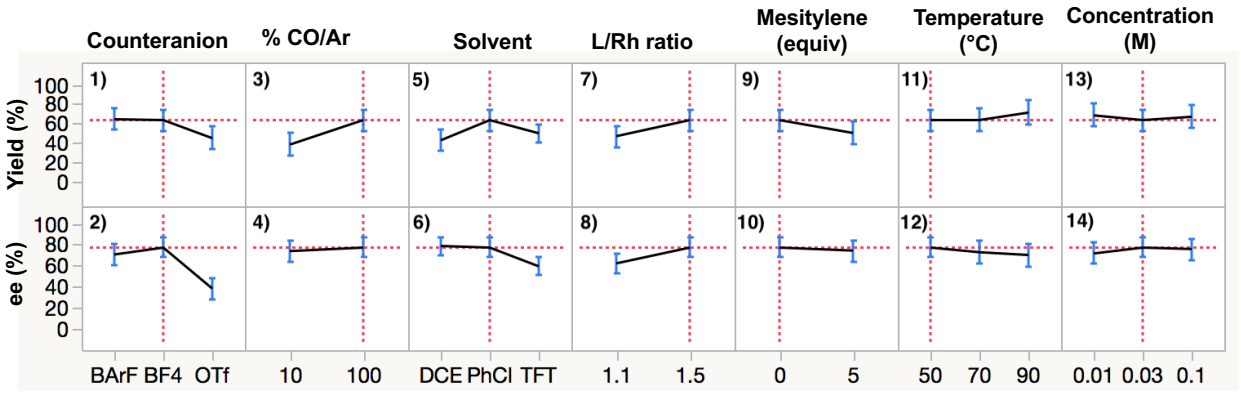

Figure 16. Experiment 1 prediction profiler plot for yield and ee, Table 23.

The percent yield of aldehyde **2.23c** in each reaction was analyzed using JMP. Amounts of aldehyde were measured by integral comparison of the aldehyde resonance at 9.9 ppm to the mesitylene peak at 6.8 ppm. The effect of each factor on the amount of aldehyde byproduct **2.23c** is summarized in the prediction profiler plots in Figure 17. The plots are arranged in order of most to least influential to aldehyde formation. The OTf counteranion gave the most aldehyde, with the $BArF^4$ counteranion resulting in the least byproduct formation (Figure 17, panel 1). More aldehyde was generated when zero equivalents of mesitylene were used (panel 2), and at a temperature of 50 °C (panel 3). Other factors had minimal effect on aldehyde formation, and their effects on aldehyde formation are within experimental error (blue bars).

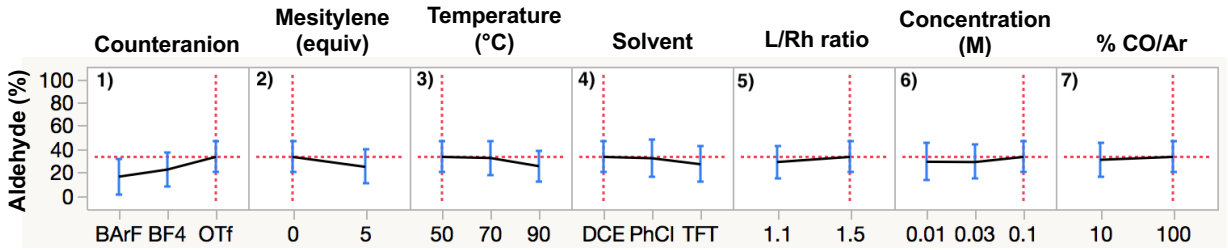

Figure 17. Experiment 1 prediction profiler plot for aldehyde amount, Table 23.

3.3.7 Effect of adding runs and center points to Experiment 1.

The model obtained from the 15-run experiment (Table 23) showed two inconsistencies with our previous experiments. First, the model predicted that CO had no effect on enantioselectivity (Figure 16, panel 4), and second, that zero equivalents of mesitylene gave better yields (Figure 16, panel 9). Previous experiments showed that adding mesitylene to the APKR resulted in a 27%

increase in yield; and that lowering the CO atmosphere to 10% afforded a 10% increase in ee (Chapter 2, Table 10, entries 1-3). These discrepancies led us to question whether the predictions of the DOE-generated model were accurate. We hypothesized that addition of more data points would improve to accuracy of the model, and potentially give predictions in better agreement with our previous experimental results. Therefore, an additional five experiments were added to the design.[133]

First, three random runs were added to the data set. This process was carried out by navigating to the JMP toolbar and selecting DOE, then "Augment Design". A screenshot of the "augment design" window is shown in Figure 18, Panel A shows the factors in settings involved in this experiment, and Panel B shows the terms included in the model, both of which were left unchanged. Under Design Generation (Panel C), the number of runs included in the experiment was changed from 15 to 18. After selecting "Make Design", three random runs were added to the data table (Table 24, entries 16-18). In addition to the three randomly added points, two center points were added to the model. Center points are added to improve the accuracy of a model, and to check for possible maxima or minima in the center of the reaction space.[133] To add these center points, the "Augment Design" function was again selected, and under "Augmentation Choices" the option to "Add Center points" was selected (Figure 19, A). Two center points were added in Window B, and entries 19 and 20 were added to the data table (Table 24).

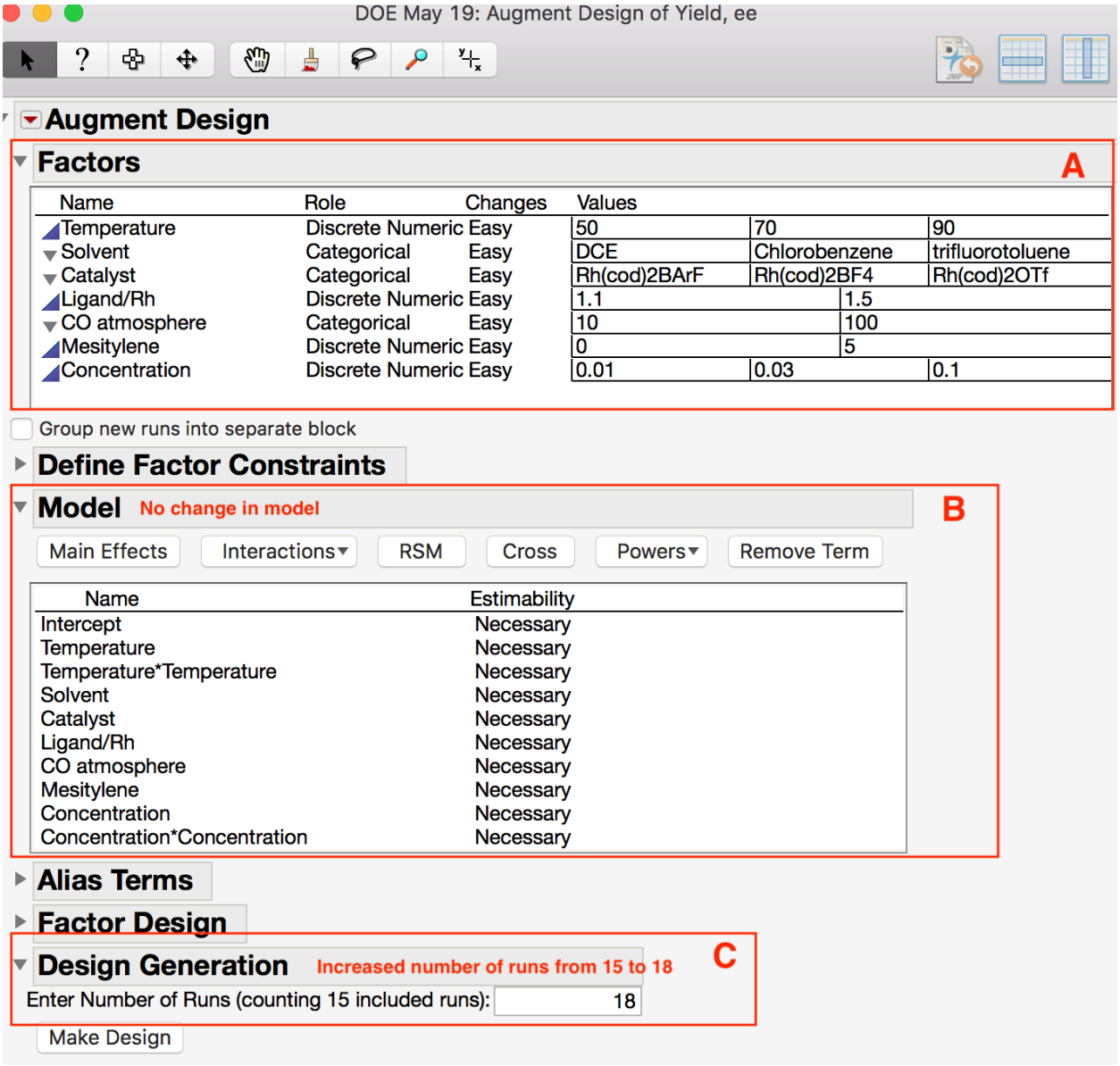

Figure 18. Process in JMP to add three random runs to Experiment 1.

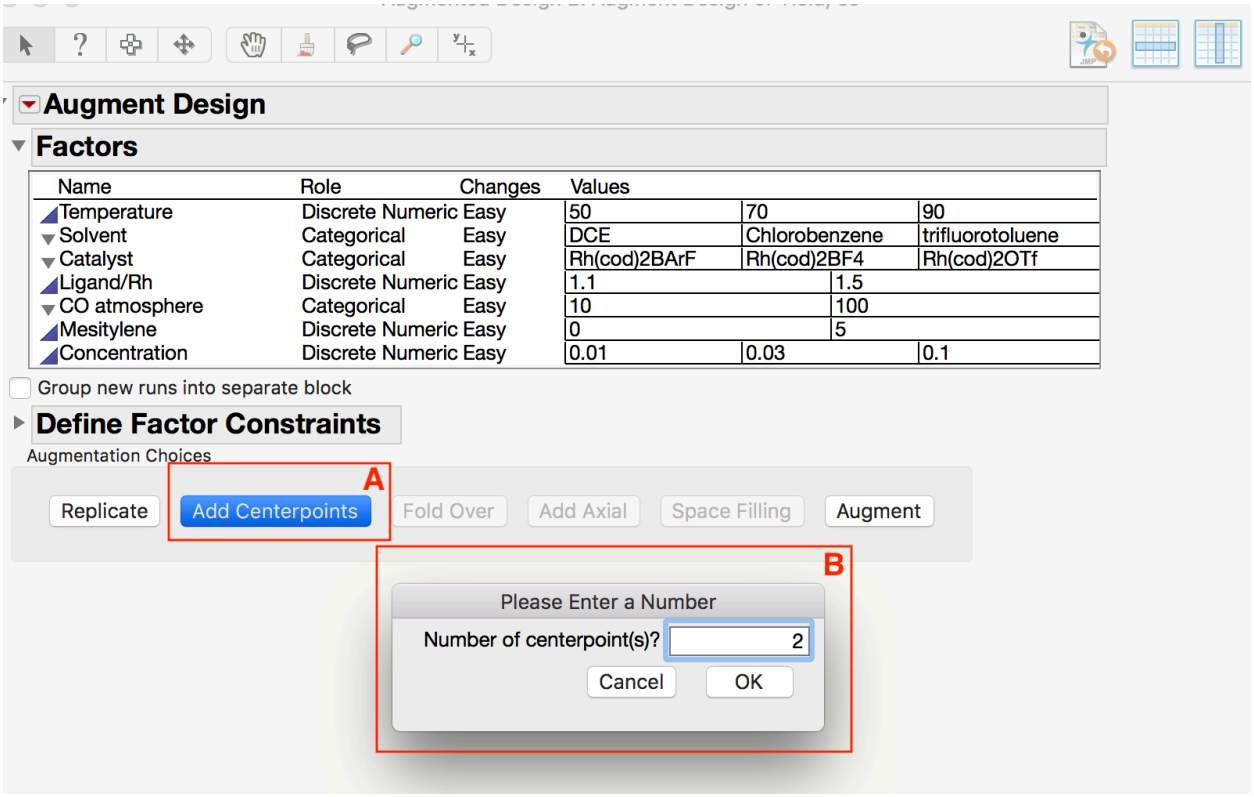

Figure 19. Addition of two center points to Experiment 1.

Table 24. Experiment 1 augmented with additional runs and center points.

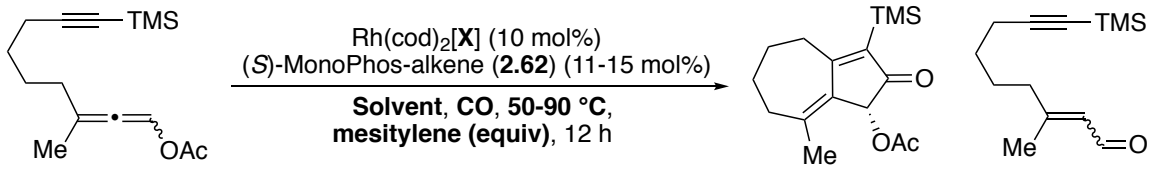

2.21c **2.22c** **2.23c**

Entry	T (°C)	Solvent	Counter-anion, X	Ligand/ Rh	CO/Ar (%)	Mesitylene (equiv)	C (M)	Yield [a]	Alde-hyde [a]	ee (%)
1	50	PhCl	BF_4	1.5	100	5	0.03	25	5	71
2	50	DCE	OTf	1.5	100	0	0.1	23	19	38
3	50	DCE	OTf	1.5	100	0	0.1	32	49	39
4	50	TFT	BArF	1.1	10	0	0.03	8	0	37
5	50	TFT	BArF	1.1	10	0	0.03	10	0	32
6	50	TFT	BF_4	1.1	100	5	0.01	25	0	36
7	70	PhCl	BArF	1.1	100	5	0.1	38	0	47
8	70	PhCl	OTf	1.1	10	0	0.01	8	20	10
9	70	DCE	BArF	1.5	10	5	0.01	10	4	56
10	70	TFT	BF_4	1.5	100	0	0.03	50	12	55
11	90	PhCl	BArF	1.5	100	0	0.01	77	5	58
12	90	DCE	BF_4	1.1	10	0	0.1	12	9	52
13	90	DCE	OTf	1.1	100	5	0.03	2	8	16
14	90	TFT	OTf	1.5	10	5	0.1	4	6	9
15	90	TFT	OTf	1.5	10	5	0.1	4	8	3
16	70	TFT	BF_4	1.1	100	0	0.1	48	10	52
17	70	PhCl	OTf	1.1	100	5	0.03	6	16	6
18	50	PhCl	BF_4	1.1	10	5	0.1	32	9	69
19	50	DCE	BArF	1.1	10	0	0.01	16	0	45
20	70	PhCl	BF_4	1.5	100	5	0.03	33	4	49

[a] Yields were determined by integral ratios for product resonance (5.8 ppm) and aldehyde resonance (9.9 ppm) relative to mesitylene (6.8 ppm).

3.3.8 Results from Experiment 1 augmented with additional runs and center points.

After these five additional runs were added to Experiment 1 (Table 24, entries 16-20), the reactions were performed and the data was re-analyzed. The prediction profiler plots illustrating

the responses of yield and ee to each factor in the augmented design are shown in Figure 20. The trends modeling aldehyde formation for each factor are shown in Figure 21. Examination of the profile plots shows no change in trends between the original design and the augmented design (compare Figure 16 with Figure 20, and Figure 17 with Figure 21). Because the addition of more data points did not change the predictions in JMP, we concluded that the original trends were accurate (Figure 16).

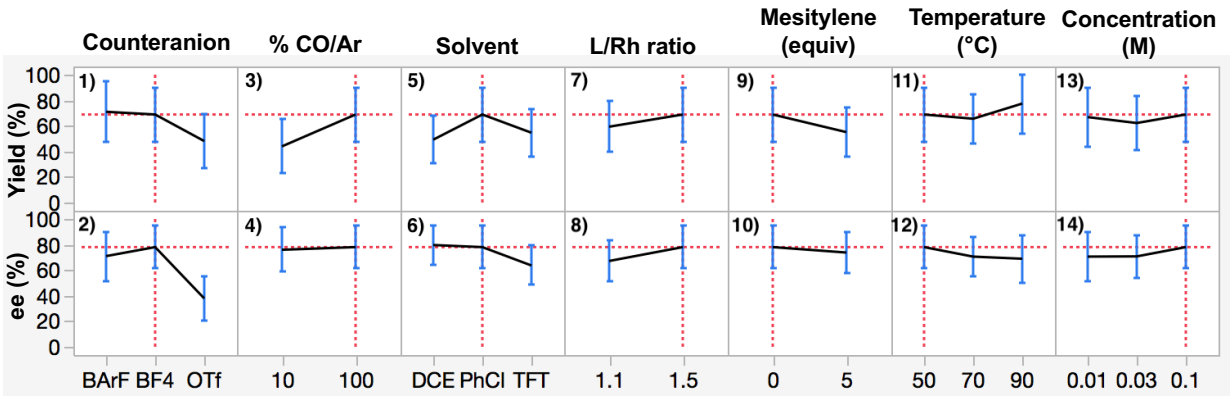

Figure 20. Experiment 1 prediction profiler plot for yield and ee, Table 24.

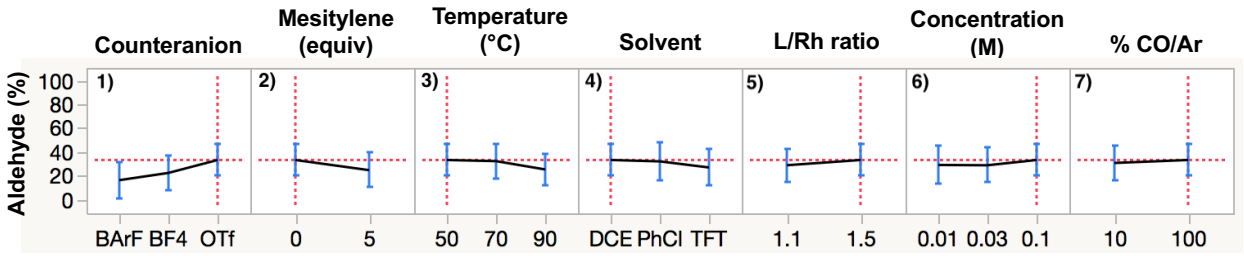

Figure 21. Experiment 1 prediction profiler plot for aldehyde amount, Table 24.

3.3.9 Conclusions from Experiment 1.

Conclusions based upon the Experiment 1 of our DOE optimization are shown in Table 25. Based upon our DOE analysis, the three most significant factors in this experiment were counteranion, CO atmosphere and solvent. Therefore, these three factors were further optimized in a second experiment. The good yields observed for both BAr^{F}_{4} and BF_4 counteranions inspired further optimization, while the poor results for OTf led us to omit that counteranion from future experiments (Table 25, entry 1). Both settings of CO atmosphere, 10 and 100% CO, were included in the second round of optimization (Table 25, entry 2). DCE and PhCl gave equally good enantioselectivity and were included in the second round of optimization. Although solvent TFT afforded higher yields, according to the model, this solvent was detrimental to enantioselectivity, and was thus omitted from optimizations (Table 25, entry 3). Both yield and ee were improved by a ligand to Rh ratio of 1.5, so this setting was kept constant for the remainder of our optimizations (Table 25, entry 4). According to the DOE model, the mesitylene setting of 0 equiv gave higher yields and enantioselectivities. Therefore, mesitylene was omitted from further optimizations, despite previous results which suggested that mesitylene improves yield (Section 3.2.2). We hypothesized that the advantageous catalyst stabilizing effect of mesitylene is limited to the noncoordinating solvent DCE, and therefore this benefit was not observed in the aromatic solvents PhCl and TFT. We chose to continue our optimization with temperature set at 50 °C because this temperature afforded better enantioselectivities. The lower yields for runs performed at 50 °C were attributed to the lower reaction conversion at this temperature combined with the limited reaction times in this experiment (12 h). We continued our optimization at the 50 °C temperature setting with the assumption that lower yields at this temperature could later be improved by increasing the reaction times (Table 25, entry 6). Finally, in Experiment 2 of DOE, the role of concentration

was examined in more detail because higher concentration gave an improvement in enantioselectivity (Table 25, entry 7).

Table 25. Conclusions from Experiment 1.

entry	Factor	Optimal setting, yield	Optimal setting, ee	Conclusion
1	Counteranion	BF_4, BArF	BF_4	Optimize further
2	CO atmosphere	100	no effect	Optimize further
3	Solvent	PhCl	DCE, PhCl	Optimize further
4	Ligand/Rh	1.5	1.5	1.5
5	Mesitylene	0	0	0
6	Temperature	90	50	50
7	Concentration	0.01, 0.1	0.1	Optimize further

3.3.10 Design of Experiment 2 using JMP.

Experiment 2 was designed based upon the conclusions made in Experiment 1, and included the factors and settings described in Table 26. A linear regression model was chosen with first order terms to model all four factors ($k_n x_n$), and an additional quadratic term to model concentration ($k_1 x_1^2$).

Table 26. Factors and settings in Experiment 2.

entry	factor	type	settings
1	Solvent	Categorical	PhCl, DCE
2	Counteranion	Categorical	BF_4 , BAr^F_4
3	CO atmosphere	Discrete Numeric	10% CO/Ar, 100% CO
4	Concentration	Continuous	0.05 to 0.15

Experiment 2 was designed using the Custom Design function of JMP. A screenshot of the design setup is shown in Figure 22. As in the set-up of Experiment 1, the responses (yield and ee)

were entered Panel A, with minimum and maximum values of 0 and 100, with the goal being to maximize both values. The four factors described in Table 26 were entered in the "Factors" section (Figure 22, Panel B). Solvent and counteranion were designated as categorical factors, CO atmosphere was designated as a discrete numeric factor, and concentration as a continuous factor. Next, the model was specified, with main effects included for all four factors (solvent, counteranion, CO atmosphere and concentration, $k_n x_n$), and a quadratic term included for concentration (concentration*concentration, kx^2), to check for curvature in the response of this continuous variable (Panel C). In the "Design Generation" section, two center points were added, and one replicate run was added. The option to generate a data table with the minimum number of runs to accommodate this design (9 runs) was selected (Panel D).

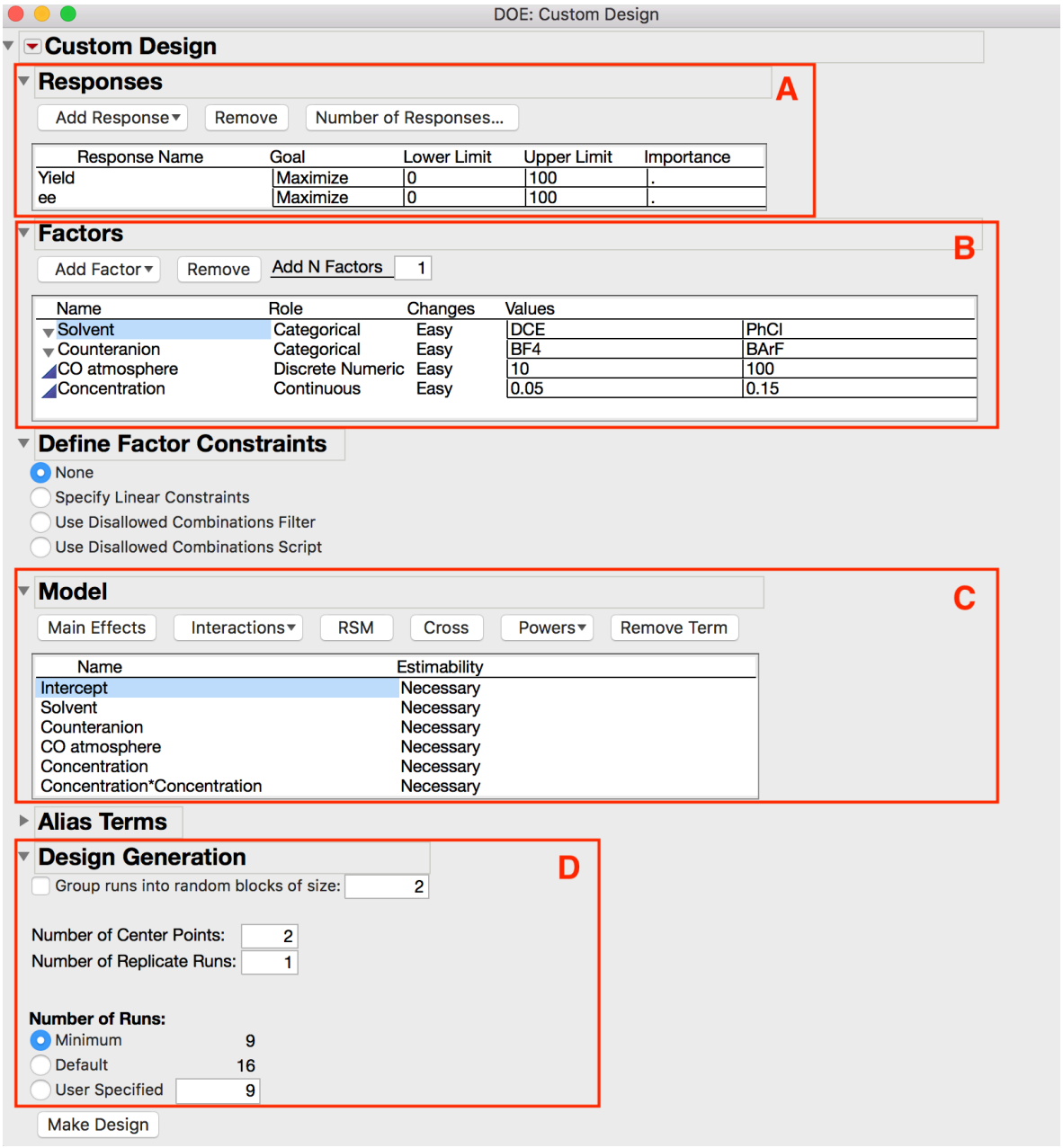

Figure 22. Design of Experiment 2 using JMP.

A design of 8 runs was generated, and one replicate was added, to give an experiment consisting of 9 runs (Table 27). The design included all eight possible combinations of solvent, counteranion and CO atmosphere and were distributed among different concentrations of 0.05 M, 0.10 M, and 0.15 M by JMP. Reactions were performed in the same manner as those in the

experiment, as described in Section 3.3.6, with the reaction time extended from 12 h to 18 h to ensure reaction progress at lower temperatures. The results of Experiment 2 are summarized in Table 27.

Table 27. Runs in Experiment 2.

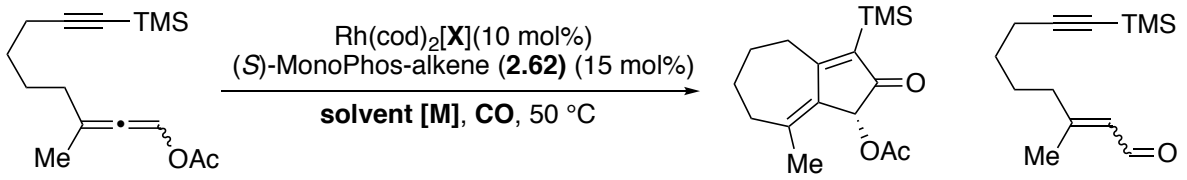

2.21c **2.22c** **2.23c**

Entry	Solvent	Conc. (M)	Counter anion	CO/Ar (%)	yield **2.22c** (%) [a]	aldehyde **2.23c** (%) [a]	Unreacted **2.21c** (%) [b]	ee (%)
1	PhCl	0.05	BF_4	10	35	5	61	70
2	PhCl	0.10	BAr^F_4	10	3	1	71	35
3	PhCl	0.10	BF_4	100	20	24	52	41
4	PhCl	0.15	BAr^F_4	100	34	3	65	25
5	DCE	0.05	BAr^F_4	100	24	1	79	24
6	DCE	0.10	BAr^F_4	10	3	1	90	22
7	DCE	0.10	BF_4	100	39	3	61	33
8	DCE	0.15	BF_4	10	18	1	82	55
9	DCE	0.15	BF_4	10	13	3	88	56

[a] Yields were determined by integral ratios for product resonance (5.8 ppm) and aldehyde resonance (9.9 ppm) relative to mesitylene (6.8 ppm). [b] Approximate amount of unreacted starting allene **2.21c** determined by integral ratio for starting material resonance (0.3 ppm) relative to mesitylene (6.8 ppm).

Despite the increased reaction time in the Experiment 2, most of the reactions did not proceed to completion. Approximate amounts of unreacted starting allene-yne **2.21c** are listed in the Table 27. The highest yield (39%) was obtained with $Rh(cod)_2BF_4$ catalyst, DCE solvent (0.10 M) under 10% CO/Ar. The highest enantioselectivity (70% ee) was obtained with $Rh(cod)_2BF_4$ catalyst, PhCl (0.05 M) solvent, under 10% CO/Ar. In general, low amounts of aldehyde **2.23c**

were formed, with the exception of entry 3, in which 24% aldehyde was afforded from the reaction of $Rh(cod)_2BF_4$ catalyst, and PhCl (0.10 M) solvent under 10% CO/Ar. The replicate runs, entries 8 and 9, demonstrate good agreement between yield and ee (entries 8 and 9).

The results of the Experiment 2 were examined using JMP prediction profiler plots (Figure 23). The uncertainty associated with yield in this analysis was high, as evidenced by the large error bars in the prediction profiler plots for yield (blue). This indicates that the model chosen (main effects plus one quadratic term, concentration*concentration) is not sufficient to describe the relationship between yield and the four factors. The low linear correlation between "actual yield" and "predicted yield" ($R^2 = 0.40$) was another indication of the low accuracy of this initial model (Figure 24).

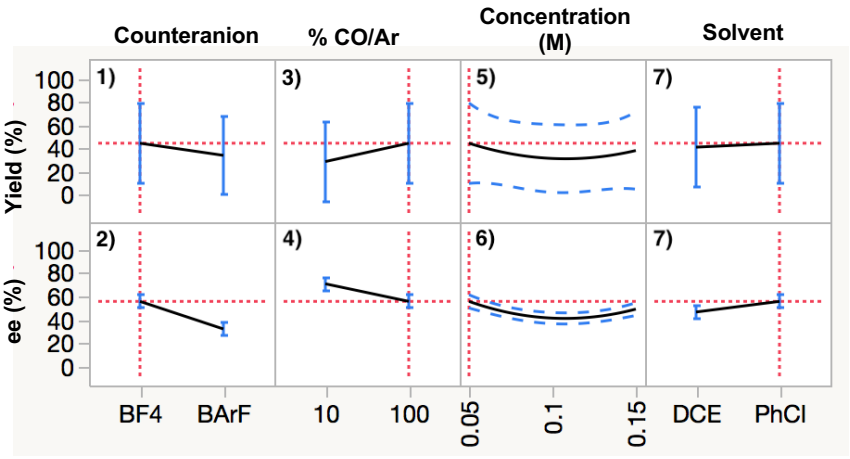

Figure 23. Experiment 2 prediction profiler plot of yield and ee, Table 27.

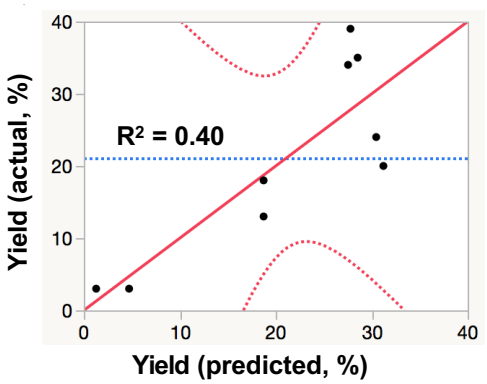

Figure 24. Experiment 2 actual vs. predicted yield for model without cross terms.

3.3.11 Effect of adding cross terms to Experiment 2.

The poor correlation between the actual and predicted yields indicated that additional terms needed to be added to the linear regression model to better describe the system. The JMP factor screening tool was used to determine which cross terms should be added. This tool shows the relative influence of each factor in the model, including terms which were not originally part of the model.[133] Screenshots of the factor screening analysis for yield and ee are shown in Figure 25 and Figure 26. The cross terms which were among the most important, but were not part of the original model, are highlighted with red boxes. These cross terms include CO atmosphere*concentration, CO atmosphere*counteranion, CO atmosphere*solvent, and counteranion*solvent. We also noted that the quadratic term concentration*concentration was *not* included among the most significant terms.

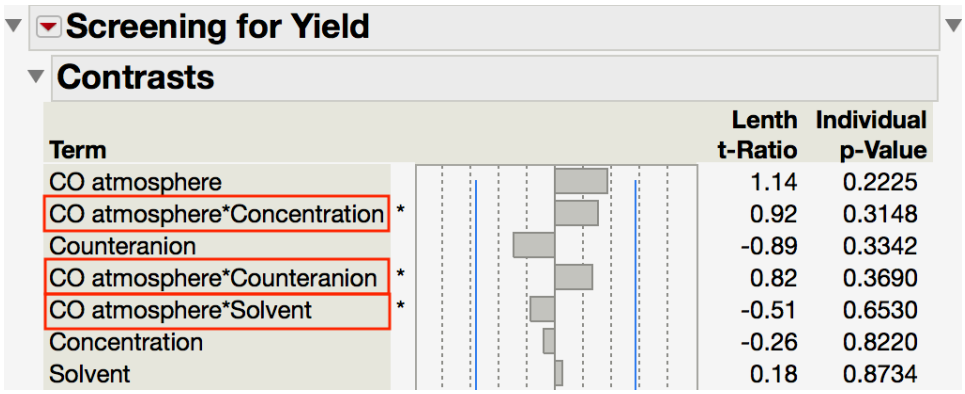

Figure 25. Experiment 2 effect screening for yield.

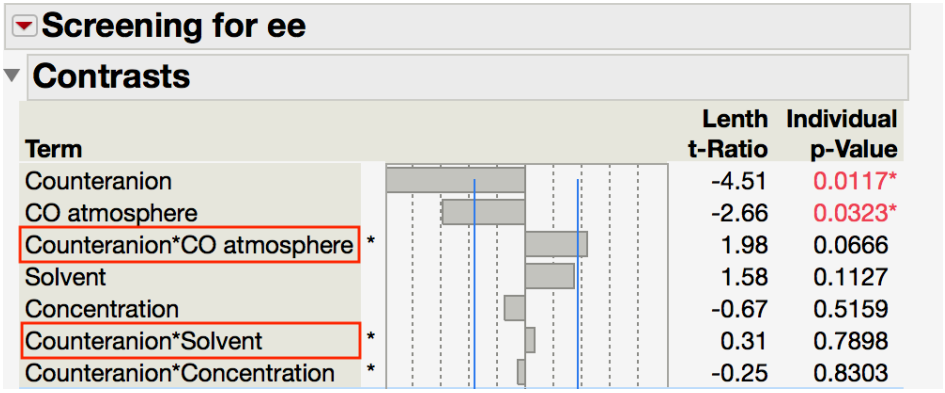

Figure 26. Experiment 2 effect screening for ee.

Next, the design was modified to include the significant cross terms indicated by the factor screening tool, and to omit insignificant terms. This modification was performed using the JMP Augment Design function (screenshot shown in Figure 27). In the Augment Design window, the factors and settings included in this experiment were left unchanged (Panel A). In Panel B, the terms included in the linear regression model are listed. Here, four cross terms were added: CO atmosphere*concentration, CO atmosphere*counteranion, CO atmosphere* solvent, and counteranion*solvent. The added cross terms are highlighted by a red box. Next, the concentration*concentration term was removed. A net addition of three more terms to the model

(added four, removed one) required addition of three runs to the experiment. These runs were generated using the JMP software (Table 28, entries 10-12).

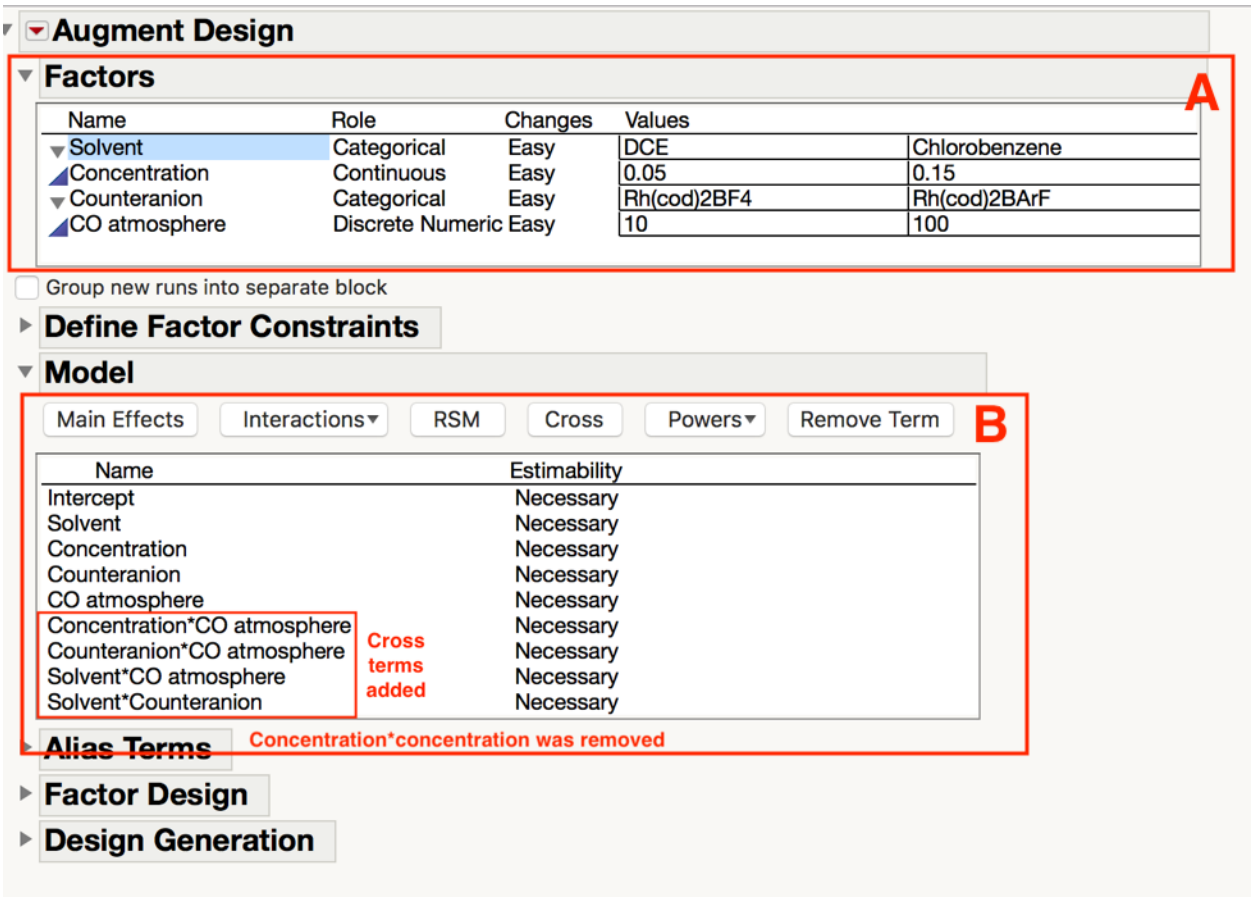

Figure 27. Augment design function of JMP used to add cross terms.

Table 28. Experiment 2 augmented with four cross terms.

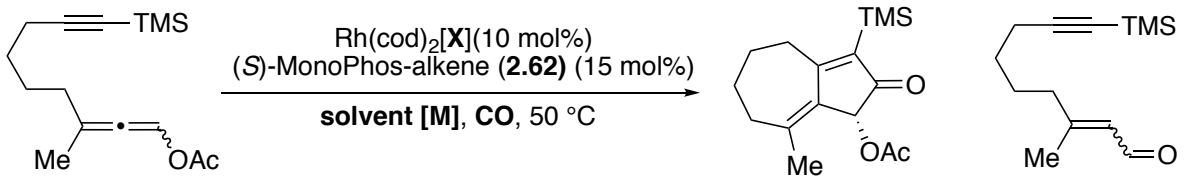

2.21c **2.22c** **2.23c**

Entry	Solvent	Conc. (M)	Counter anion	CO/Ar (%)	yield **2.22c** (%) [a]	aldehyde **2.23c** (%) [a]	Unreacted **2.21c** (%) [b]	ee (%)
1	PhCl	0.05	BF_4	10	35	5	61	70
2 [c]	PhCl	0.10	BAr^F_4	10	3	1	71	35
3	PhCl	0.10	BF_4	100	20	24	52	41
4	PhCl	0.15	BAr^F_4	100	34	3	65	25
5	DCE	0.05	BAr^F_4	100	24	1	79	24
6	DCE	0.10	BAr^F_4	10	3	1	90	22
7	DCE	0.10	BF_4	100	39	3	61	33
8	DCE	0.15	BF_4	10	18	1	82	55
9	DCE	0.15	BF_4	10	13	3	88	56
10	PhCl	0.15	BAr^F_4	10	9	1	62	47
11	DCE	0.15	BF_4	100	42	18	31	28
12	PhCl	0.05	BF_4	100	22	10	78	40

[a] Yields were determined by integral ratios for product resonance (5.8 ppm) and aldehyde resonance (9.9 ppm) relative to mesitylene (6.8 ppm). [b] Amount of unreacted starting 2.21c determined by integral ratio for starting material resonance (0.3 ppm) relative to mesitylene (6.8 ppm). [c] Omitted from analysis in Figure 28 and Figure 29.

The three additional runs were performed and the data added to Table 28 (entries 10-12). Although the reaction conditions for entries 2 and 10 are exactly the same except for concentration (0.10 versus 0.15 M), these runs afforded substantially different results. The run described in entry 2 gave a 6% yield and 35% ee, while the run described in entry 10 gave a 15% yield and 47% ee. Because the only difference between these two runs is concentration, the inclusion of both points in the model could have inaccurately amplified the role of concentration in the reaction. Therefore, entry 2 was omitted from the subsequent analysis. With the new model including four cross terms,

and entry 2 omitted, the analysis showed a much better correlation between predicted and actual yields ($R^2 = 0.99$, Figure 28, compare to Figure 24, $R^2 = 0.40$).

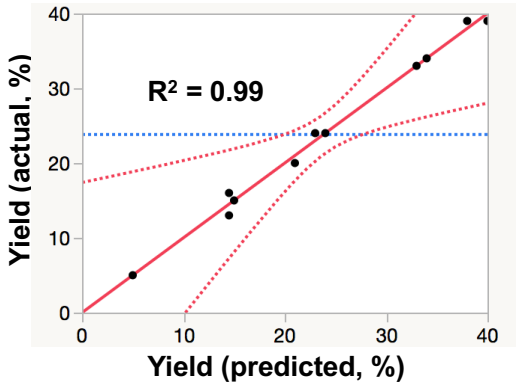

Figure 28. Actual versus predicted plot of DOE yield with four cross terms added.

The augmented design of Experiment 2 (which included four new cross terms), with entry 2 omitted, was analyzed using JMP profiler plots (Figure 29). The plots in Figure 29 are arranged from left to right in order of decreasing factor significance. In Experiment 2, catalyst counteranion had the greatest impact on the responses, with BF_4 counteranion giving both higher yields and higher enantioselectivities (Figure 29, panels 1 and 2). According to the DOE model, the higher CO atmosphere of 100% CO gave higher yields, while a CO atmosphere of 10% CO/Ar gave higher ee (panel 4). The solvent PhCl gave slightly higher yields (panel 5), however, the error bars for this trend are large compared to the change in yield, therefore this effect is not significant. PhCl solvent did effect a substantial improvement in enantioselectivity (panel 6). Finally, the least important factor was concentration, with higher concentrations affording lower yields (panel 7) and slightly higher enantioselectivities (panel 8).

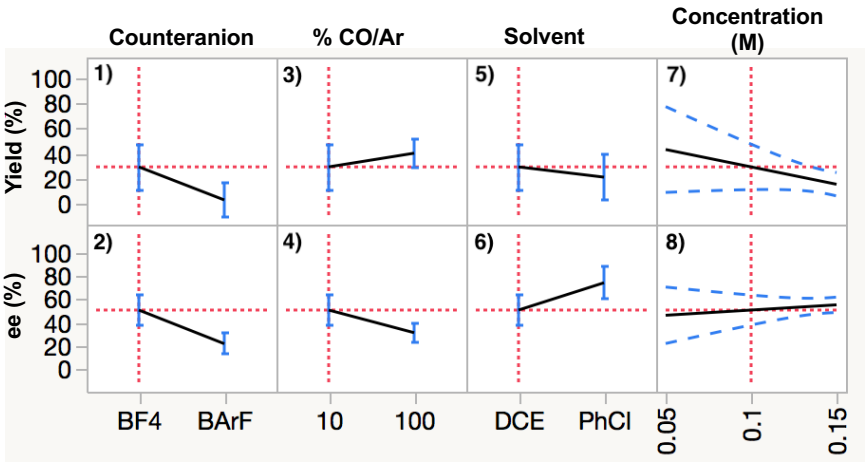

Figure 29. Experiment 2 prediction profiler plot for Yield and ee, Table 28.

3.3.12 Conclusions from Experiment 2.

The results of the Experiment 2 are summarized in Table 29. The BF_4 counteranion was the optimal setting for both yield and ee (Table 29, entry 1). The higher setting for CO atmosphere (100% CO) afforded overall better yields, but the lower setting (10% CO/Ar) afforded higher ee's (entry 2). DCE as a solvent gave better yields, while PhCl solvent gave higher ee's (entry 3). The effect of concentration was the least pronounced, but according to the DOE model, lower concentrations (0.05 M) provided higher yields, and higher concentration (0.15 M) provided higher ee's.

Table 29. Conclusions from Experiment 2.

entry	Factor	Optimal setting, yield	Optimal setting, ee
1	Counteranion	BF_4	BF_4
2	CO atmosphere	100	10
3	Solvent	DCE	PhCl
4	Concentration	0.05	0.15

3.3.13 Final post-DOE optimizations.

We continued the optimization of the APKR with a focus on the most enantioselective conditions predicted by the DOE. Based on the final DOE model, the most enantioselective conditions for the APKR are: 10% CO/Ar, $Rh(cod)_2BF_4$ catalyst, PhCl solvent, at 0.15 M concentration at 50 ° C (Table 29). These conditions were tested experimentally, and afforded product **2.22c** in 27% yield and 70% ee (with 18% recovered starting material) and 10% aldehyde byproduct (Table 30, entry 1). Although we were pleased with the increase in enantioselectivity over the original conditions (which afforded product **2.22c** in 64% ee), further efforts were undertaken to improve the low yield. First, we hypothesized that lowering the concentration would improve the yield. This hypothesis was based upon the trends predicted through DOE analysis wherein lower concentrations gave improved yields and had minimal effect on enantioselectivity (Figure 29, panels 7 and 8). The APKR was performed under the same conditions as described in entry 1, except that the concentration was changed from 0.15 M to 0.05 M (Table 30, entry 2). The reaction time slowed to 62 h, and product was obtained in only 26% yield, with 11% aldehyde. We suspected that the low yield observed, and high amount of aldehyde formation was caused by catalyst degradation during this long reaction time. During our DOE analysis, we hypothesized that low APKR yields after 12 h at 50 °C could be addressed by increasing the reaction time (Section 3.3.9). The low yield observed here with longer reaction times (62 h, 26% yield, Table 30, entry 2) suggests that the previous hypothesis was inaccurate, and perhaps temperature should have been included as a significant factor in Experiment 2.

Table 30. Optimized conditions of the APKR.

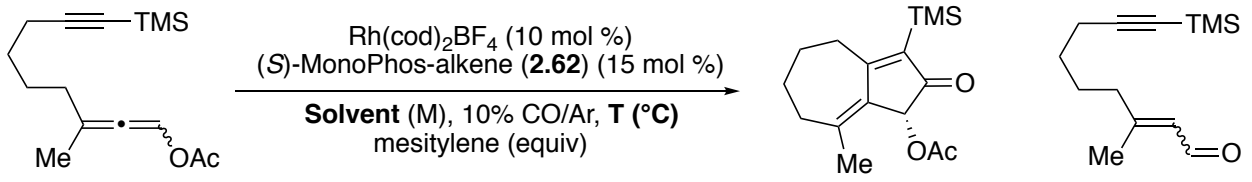

2.21c **2.22c** **2.23c**

entry	solvent	Conc. (M)	Mesitylene (equiv)	T (°C)	time (h)	yield **2.22c** (%) [a]	aldehyde **2.23c** (%)	ee (%)
1	PhCl	0.15	0	50	21	27 (18)	10	70
2	PhCl	0.05	0	50	62	26 (0)	11	70
3	PhCl	0.15	0	55	17	55(0)	10	71
4	PhCl	0.15	5	55	40	23(0)	21	70
5	*o*-DCB	0.15	0	55	16	76 (0)	trace	67

[a] Isolated yields after purification by column chromatography.

Continuing our optimization of the most enantioselective conditions, the concentration was returned to 0.15 M and the poor conversion observed at 50 °C was addressed by increasing the temperature to 55 °C (Table 30, entry 3). This modest change in temperature more than doubled the yield of **2.22c** (with no starting allene recovered) and maintained the enantioselectivity of 71% ee (entry 3). Because the DOE model was unclear regarding the effect of mesitylene on the APKR yield (Figure 20, panel 9), we tested the effect of mesitylene on the APKR yield. The reaction was performed at 55 °C in PhCl (0.15 M) with 5.0 equiv mesitylene added. Under these conditions, the reaction time slowed to 40 h, and product was formed in only 23% yield, with 21% aldehyde byproduct (Table 30, entry 4). This result supports our hypothesis that the mesitylene additive is not necessary in aromatic solvents (Section 3.3.9). In fact, under these concentrated conditions mesitylene slowed the reaction and was detrimental to the yield. Under these concentrated conditions (0.15 M, 0.33 mL PhCl), 5.0 equiv of mesitylene amounts to 10% v/v of the volume of solvent, a percentage which was previously shown to decrease APKR yield, even when DCE was

used as the solvent (Table 15).

Because DCE afforded higher APKR yields (71% yield, 64% ee) and PhCl affords higher enantioselectivities (55% yield, 71% ee, Table 30, entry 3), we hypothesized that a third solvent could combine advantageous properties of each. DCE is more polar than PhCl, as evidenced by their respective dielectric constants of 10.4 and 5.6 (Table 31, compare entries 1 and 2). *o*-Dichlorobenzene (*o*-DCB) is similar in structure to PhCl and has a dielectric constant similar to that of DCE (9.9 versus 10.4). We tested *o*-DCB as a solvent in the APKR and were pleased to observe an increase in yield to 76%, and high enantioselectivity of 67% (Table 31, entry 3).

Table 31. Summary of optimized enantioselective APKR conditions.

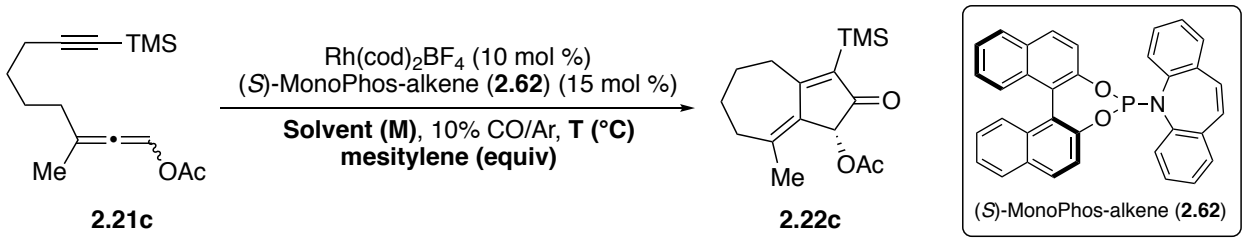

entry		Solvent	dielectric constant	Conc. (M)	Mesitylene (equiv)	T (°C)	yield (%)[a]	ee (%)
1	Conditions A	DCE	9.9	0.03	1	70	71	64
2	Conditions B	PhCl	5.6	0.15	0	55	55	71
3	Conditions C	*o*-DCB	10.4	0.15	0	55	76	67

[a] Isolated yields after purification by column chromatography.

3.3.14 Summary of DOE optimization of APKR.

Upon initial discovery that (*S*)-MonoPhos-alkene (**2.62**) ligand is an efficient and enantioselective ligand for the APKR, we demonstrated that reaction in DCE (0.03 M) with catalyst $Rh(cod)_2BF_4$

(10 mol %), (*S*)-MonoPhos-alkene ligand (15 mol %), and mesitylene additive under 10% CO/Ar atmosphere, at 70 °C provided cyclopentenone product **2.22c** in 71% yield and 64% ee (Conditions A, entry 1, Table 31). Because of the sensitivity of the APKR to many different reaction conditions, and our desire to test the entirety of the APKR "reaction space" to find optimal settings, we used a statistical design of experiments approach to determine conditions which would improve yield and ee. As a result, we found that reaction conditions affording the highest APKR enantioselectivity comprise PhCl (0.15 M) as a solvent, with 10% CO/Ar atmosphere at 55 °C (55% yield, 71% ee, Conditions B, Table 31, entry 2). Further efforts to improve yield led us to discover a third set of conditions involving *o*-DCB as a solvent, which, (compared to the original Conditions A) enabled improvements to both yield and ee (Conditions C, Table 31, entry 3).

Statistical DOE was successful in improving the enantioselectivity of the APKR. However, this study highlights the difficulty of optimizing two responses simultaneously. For example, we found that CO atmosphere was an important factor influencing the two responses, but each response was affected in the opposite manner: decreasing CO atmosphere had a positive effect on enantioselectivity and a negative effect on yield. Therefore, simultaneous optimization of both responses was not possible. Fortunately, we were able to discover conditions using *o*-DCB as a solvent which afford both good yield and enantioselectivity in the APKR. These Conditions C, along with the most enantioselective Conditions B, were applied in the APKR of a variety of allene-yne substrates.

3.4 EXPLORING THE SUBSTRATE SCOPE OF THE ENANTIOSELECTIVE APKR.

We hypothesized that the conditions developed in our design of experiments optimization would improve yields and enantioselectivities for substrates beyond the model allene-yne **2.21c**. In order to determine whether the DOE optimized conditions would be successful in expanding the scope of the APKR, we tested several different substrates by varying the alkyne and carboxy ester groups, and the tether length.

3.4.1 Testing the substrate scope of the APKR by varying the alkyne and carboxy ester groups.

The optimized conditions were tested on a variety of APKR precursors differing in their alkyne and carboxy ester substituents. The APKR of **2.21c** with a TMS-substituted alkyne and an allenyl carboxy acetate afforded the highest yield of **2.22c** under Conditions C (76%, Table 32, entry 3), and highest enantioselectivity under Conditions B (71%, entry 2). Reaction of allenyl carboxy pivalate **2.21d**, under the original APKR conditions, Conditions A, afforded **2.22d** in 50% yield and 72% ee (Table 32, entry 4). Application of Conditions B to this substrate afforded **2.22d** in 29% yield and 74% ee (entry 5), representing the highest enantioselectivity observed in our studies of the APKR. Allenyl carboxy benzoate **2.21f** afforded **2.22f** in 57% yield and 70% ee when reacted under conditions B (entry 7) and 61% yield and 70% ee under Conditions C (entry 8). Conditions B afforded **2.22g** in 38% yield and 60% ee, representing a 7% increase in ee (compare entries 9 and 10). The phenyl-substituted alkyne afforded product **2.22a** in 51% yield and 72% ee (entry 11). The TIPS substituted alkyne **2.21b** under conditions B afforded product **2.22b** in only

3% and 0% yield, respectively (entries 12 and 13). In both cases, mostly recovered starting allene, and some degradation products were observed.

Table 32. Scope of the enantioselective APKR of allenyl carboxy esters.

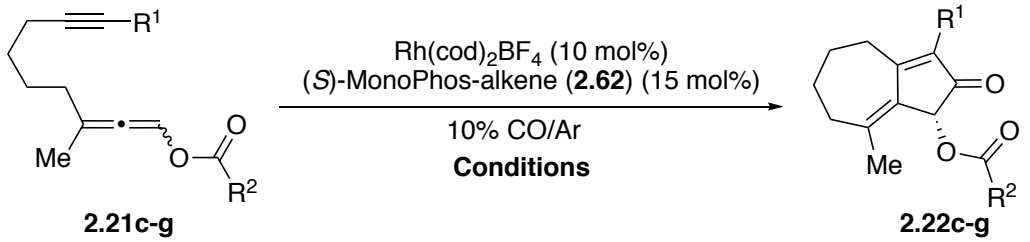

2.21c-g **2.22c-g**

entry	R^1	R^2	SM	Conditions [a]	time (h)	yield (%)[b]	ee (%)
1 [c]	TMS	Me	**2.21c**	A	15	**2.22c** 71	64
2	TMS	Me	**2.21c**	B	17	**2.22c** 55[d]	71
3	TMS	Me	**2.21c**	C	19	**2.22c** 76[d]	67
4[c]	TMS	*t*-Bu	**2.21d**	A	15	**2.22d** 50	72
5	TMS	*t*-Bu	**2.21d**	B	48	**2.22d** 29[d]	74
6 [c]	TMS	Ph	**2.21f**	A	20	**2.22f** 77	70
7	TMS	Ph	**2.21f**	B	20	**2.22f** 57[d]	72
8	TMS	Ph	**2.21f**	C	18	**2.22f** 61[d]	70
9	TMS	4-NO_2Ph	**2.21g**	A	20	**2.22g** 45	53
10	TMS	4-NO_2Ph	**2.21g**	B	24	**2.22g** 38[d]	60
11 [c]	Ph	Me	**2.21a**	A	18	**2.22a** 51	72
12	TIPS	Me	**2.21b**	A	24	**2.22b** 3	-
13	TIPS	Me	**2.21b**	B	24	**2.22b** 0	-

[a] Conditions A: mesitylene (1.0 equiv), DCE (0.03 M), 70 °C. Conditions B: PhCl (0.15 M), 55 °C. Conditions C: *o*-DCB (0.15 M), 55 °C. [b] Unless otherwise indicated, yields were determined by integral comparison to product resonance (5.7 ppm) to mesitylene resonance (6.8 ppm). [c] Results previously reported in *J. Am. Chem. Soc.* **2017**, *139* (42), 15022-15032 [d] Isolated yield.

The APKR affords the highest ee's with sterically bulky carboxy ester substituents such as carboxy pivalate and carboxy benzoate groups, with ee's ranging from 70% to 74% ee under all reaction conditions. Electron deficient substituents such as *p*-nitrobenzoate **2.21g** afforded significantly lower ee's. Sterically demanding alkynes such as TIPS-alkyne **2.21b** are unreactive. The poor reactivity of sterically demanding alkynes is likely due to the large steric interaction

between the (*S*)-MonoPhos-alkene (**2.62**) ligand and the alkyne substituent, which is observed in the calculated lowest-energy transition state structures (Chapter 2, Figure 11). In summary, the substrate imposed a substantial effect on both the ee and yield of the APKR. Conditions B resulted in slightly increased ee (a range of +2 to +7% ee) at a substantial cost to yield (−7 to −21% yield), depending on the substrate. Conditions C represent a compromise between Conditions A and Conditions B, affording high ee's in somewhat lower yields.

3.4.2 APKR of methyl-substituted alkynes.

After testing TMS, TIPS and Ph-alkynes in the APKR, we wondered whether the scope of the APKR could be extend to alkyl-substituted alkynes. A methyl-alkyne substitution was chosen for this experiment because APKR of a Me-alkyne would afford the cyclopentenone product in a substitution pattern consistent with that of Thapsigargin (**1.9**). A series of three Me-alkynes differing in their substitution at the allenyl carboxy position were synthesized and tested in the APKR. To access these substrates, 5-hexyn-1-ol was subjected to potassium *tert*-butoxide in DMSO to afford the methyl-alkyne **3.15** (Scheme 42). The alcohol **3.15** was converted to mesylate **3.16** by reaction with mesityl chloride and triethylamine, which was subsequently reacted with sodium iodide in acetone to provide the iodide **3.17**. Exposure of iodide **3.17** to the sodium salt of *tert*-butyl acetoacetate, followed immediately by reaction with catalytic *p*-toluene sulfonic acid hydrate afforded methyl ketone **3.18** in 54% yield. Addition of ethynylmagnesium bromide to ketone **3.18**, followed either by acetyl chloride or aqueous ammonium chloride gave propargyl acetate **3.19a** or propargyl alcohol **3.20**, respectively. Propargyl carboxy pivalate **3.19b** was accessed by reacting propargyl alcohol **3.9** with catalytic scandium triflate and pivalic anhydride

in acetonitrile (Scheme 43). Propargyl benzoate **3.19c** was obtained by reaction of propargyl alcohol **3.20** with benzoic anhydride, triethyl amine, 4-dimethylaminopyridine in DCM for 3 d.

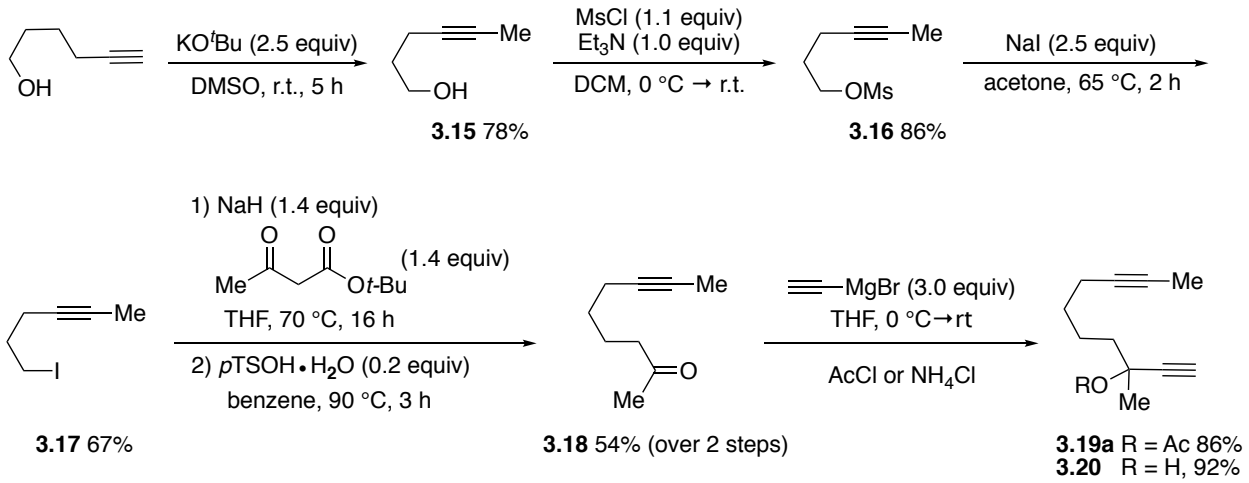

Scheme 42. Synthesis of propargyl acetate 3.8a and propargyl alcohol 3.9.

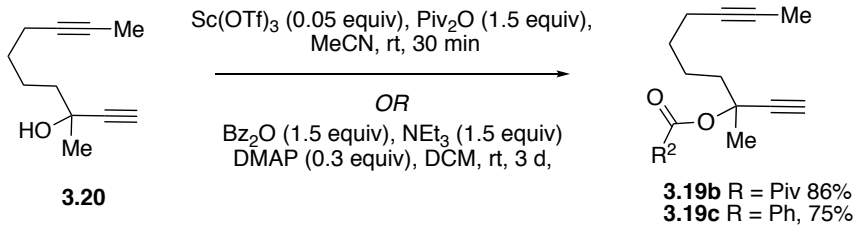

Scheme 43. Synthesis of propargyl carboxy pivalate 3.8b and propargyl carboxy benzoate 3.8c.

Synthesis of allenyl carboxy ester APKR precursors was accomplished by reacting propargyl carboxy esters **3.19a-c** with rhodium(II) trifluoroacetate dimer (5 mol %) in toluene at 50 °C (Scheme 44). Reaction of propargyl acetate **3.19a** afforded allenyl acetate **3.21a** in 79% yield. Allenyl carboxy pivalate **3.19b** and allenyl carboxy benzoate **3.19c** were obtained in 84 and 81% yield, respectively.

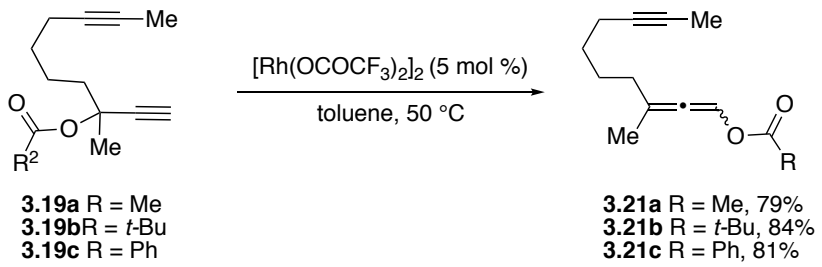

3.19a R = Me
3.19bR = *t*-Bu
3.19c R = Ph

3.21a R = Me, 79%
3.21b R = *t*-Bu, 84%
3.21c R = Ph, 81%

Scheme 44. Synthesis of allenyl carboxy esters 3.10a-c.

With methyl-alkyne APKR precursors **3.21a-c** in hand, we tested these substrates in the APKR using both our initial Conditions A, and DOE-optimized Conditions C (Table 33). The APKR of allenyl acetate **3.21a** in DCE (0.03 M), mesitylene (1.0 equiv) at 70 °C (Conditions A) afforded cyclopentenone product **3.22a** in 57% yield and 55% ee (Table 33, entry 1). The DOE-optimized Conditions C using *o*-DCB (0.15 M) at 55 °C improved the ee by 10%, without significant reduction in yield (compare entries 1 and 2). Under Conditions A, reaction of allenyl carboxy pivalate **3.21b** provides product **3.22b** in 43% yield and 50% ee (entry 3). These results were improved to 50% yield and 61% ee under DOE-optimized Conditions C (entry 4). Finally, the APKR of benzoate **3.21c** under initial Conditions A afforded product in 32% yield and 57% ee. In this case, the yield was improved by 11% and the ee improved by 14% using the DOE-optimized Conditions C (compare entries 5 and 6). In the APKR of benzoate **3.21c**, a nonpolar byproduct was observed by TLC. Analysis of this byproduct by mass spectrometry indicated that the compound has a mass which is approximately double that of the starting allene-yne, indicating that a dimerization process could be competing with the APKR (byproduct m/z = 537.2980). The low yield of benzoate **3.21c** is attributed to the formation of this hypothesized dimer, and thus, the yield could potentially be improved by decreasing the concentration of the reaction.[131] In summary, the APKR of all three Me-substituted alkynes proceeded in comparable or higher yields, and higher

enantioselectivities under the DOE-optimized Conditions C. These results demonstrate the ability of DOE optimization to expand the scope of the enantioselective APKR.

Table 33. APKR of Me-substituted alkynes using optimized conditions.

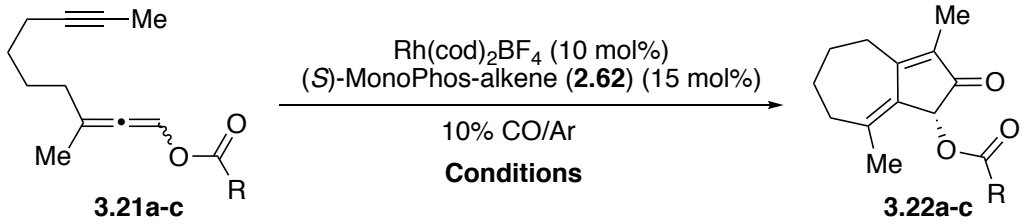

entry	R		Conditions [a, b c]	time (h)	yield (%)[d]	ee (%)
1	Me	**3.21a**	A	18	**3.22a** 57	55
2	Me	**3.21a**	C	24	**3.22a** 54	65
3	*t*-Bu	**3.21b**	A	16	**3.22b** 42	46
4	*t*-Bu	**3.21b**	C	22	**3.22b** 50[e]	61
5	Ph	**3.21c**	A	4	**3.22c** 32	57
6	Ph	**3.21c**	C	19	**3.22c** 43	71

[a]All reactions were carried out on a 0.05 mmol (13-20 mg) scale. [b] Conditions A: mesitylene (1.0 equiv), DCE (0.03 M), 70 °C. [c] Conditions C: *o*-DCB (0.15 M), 55 °C. [d] Unless otherwise indicated, yields were determined by integral comparison of product resonance (5.7 ppm) to mesitylene resonance (6.8 ppm). [e] Isolated yield.

Interestingly, the HPLC retention times for the major and minor enantiomers of Me-benzoate APKR product **3.21c** do not correlate with the retention times of other products accessed using the same (*S*)-MonoPhos-alkene (**2.62**) ligand. For example, in the reaction with Rh-(*S*)-MonoPhos (**2.62**)-alkene catalyst, the TMS-benzoate product **2.22f** was obtained in 70% ee, and eluted on a Chiralcel IA-3 column with retention times of 14.5 min (minor) and 16.3 min (major) (Figure 30, A). The major enantiomer of TMS-benzoate **2.22f** which eluted *second*, at 16.3 min was unambiguously assigned as (*R*) by X-ray crystallography (Figure 12, Chapter 2). All other α-carboxy cyclopentenone products obtained from reaction with the (*S*)-MonoPhos-alkene (**2.62**)

catalyst gave the major product also eluting *second* on the Chiralcel column (**2.22a-f**, **3.10a** and **3.10b**). Therefore, all of these products **2.21a-f**, **3.10a** and **3.10b**) were assigned as (*R*). We observed however, that Me-benzoate product **3.21c** eluted on the Chiralcel column with retention times of 52.7 min (major) and 66.6 min (minor), with the major product eluting *first* (Figure 30, B). Either the (*S*)-MonoPhos-alkene (**2.62**) catalyst affords a different major enantiomer of the Me-benzoate product, or the enantiomers of Me-benzoate product simply interact differently with the chiral packing material of the column, changing their relative elution times. Because the absolute configurations of APKR products were assigned by analogy to the retention times of TMS-benzoate product **2.22f**, this absolute configuration of Me-benzoate product **3.22c** will be confirmed by hydrolyzing the acetoxy ester of **3.22c** converting it to the benzoyloxy ester **2.22f**, using the enantioretentive hydrolysis conditions described in Section 3.5.

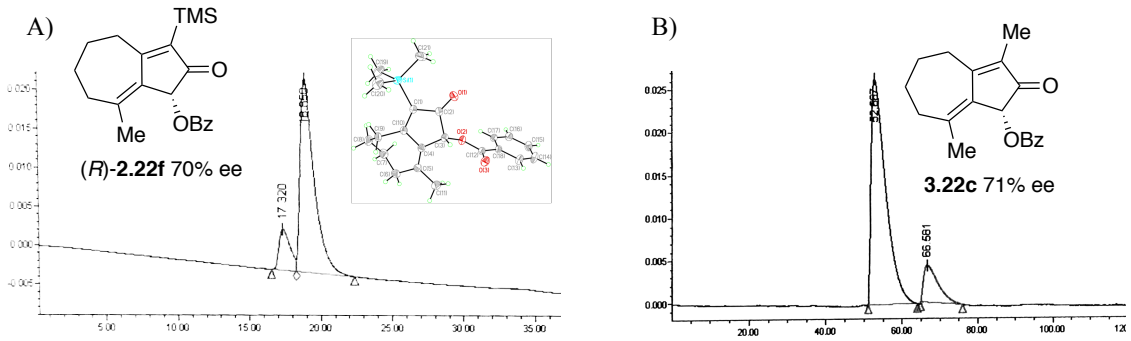

$[\alpha]^{20}_D$ = +52.0 (*c.* = 1.0, $CHCl_3$)

$[\alpha]^{20}_D$ = + 45.0 (*c.* = 0.53, $CHCl_3$)

Figure 30. HPLC traces of benzoate products.

3.4.3 Expanding the scope of the asymmetric APKR to the preparation of chiral α-acetoxy cyclopentenones with a [6, 5] ring system.

The Ph-substituted, *O*-tethered enyne **1.50** reacts in the enantioselective Rh-catalyzed PKR in high yields and ee's under a number of conditions (Section 4.1.2). Therefore, we hypothesized that an allene-yne with an *O*-tethered allene-yne such as **3.28** might also react in the APKR in high yields and enantioselectivity. Efforts were undertaken to synthesize allenyl acetate **3.28** from enyne **1.50**. *O*-Tethered enyne **1.50** was subjected to Wacker oxidation conditions, which gave no product **3.24** and resulted only in decomposition (Scheme 45). The analogous methylene-tethered enyne **3.23** was also subjected to these conditions, but methyl ketone **3.14** was isolated in an unsatisfactory 8% yield. In both cases, we expect that over-oxidation products could have formed due to competition with the electron-rich phenyl alkyne.

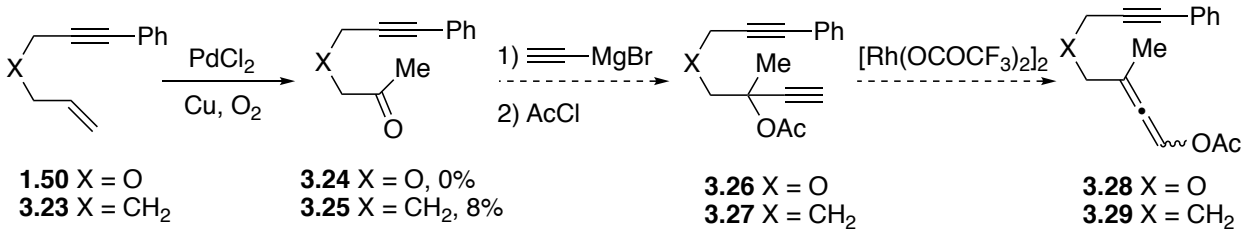

Scheme 45. Unsuccessful approach to a three-carbon tethered allenyl acetate.

Because of the poor yield of the Wacker oxidation process, an alternative strategy to access a three-carbon tethered alkyne-one was taken. Using methodology developed by Dudley, we postulated that a three-carbon tethered allenyl acetate containing a geminal dimethyl group could be synthesized using dimedone **3.30** as a starting material (Scheme 46). [134-135] We anticipated that

the gem-dimethyl group would increase the reactivity of the allene-yne **3.36** in the APKR through a Thorpe-Ingold effect.

The synthesis of three-carbon-tethered propargyl acetate **3.35** is shown in Scheme 46. Dimedone **3.30** was reacted with triflic anhydride and pyridine to afford vinylogous enol triflate **3.31** in 94% yield. Addition of methyllithium (1.0 equiv) and warming from -78 °C to 60 °C gave alkyne-one **3.32** in 72% yield. Reaction of the alkynyl group of **3.32** under Sonagashira coupling conditions provided Ph-alkyne **3.33** in 74% yield. Addition of ethynylmagnesium bromide to ketone **3.33** afforded propargyl alcohol **3.34** in 91% yield, which was subsequently reacted with acetic anhydride, 4-*N*,*N*-dimethlyaminopyridine and trimethylamine to afford propargyl acetate **3.35** in 72% yield.

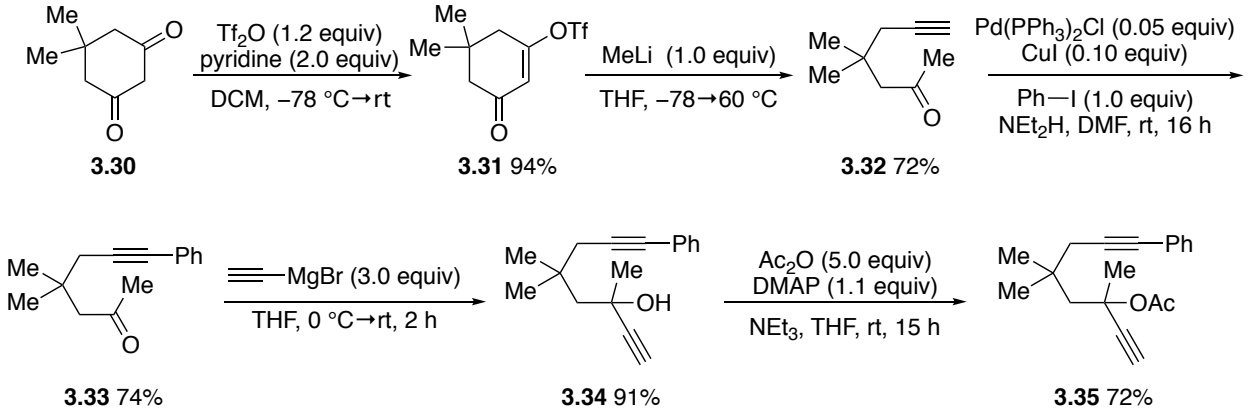

Scheme 46. Synthesis of three-carbon tethered propargyl acetate 3.24.

Reaction of propargyl acetate **3.35** with Rh(II)-trifluoroacetate dimer (5 mol %) in toluene afforded allenyl acetate **3.36** in low yield (36%, Table 34, entry 1). Two alternative catalysts were tested in an effort to improve this yield. Previous results in our group suggest that allenes with substituted tethers are formed in higher yields using gold(III) catalysis.[71] Reaction of propargyl

acetate **3.35** with gold(III) chloride afforded allenyl acetate **3.36** in only 14% yield (Table 34, entry 2). Reaction of **3.35** with platinum(II) chloride gave no reaction after 4 d (entry 3). The synthesis of allenyl acetate **3.36** was not optimized beyond 36%. The low yield of this transformation is attributed to steric interference from the gem-dimethyl group.

Table 34. Conditions tested in the [3,3]-rearrangement of propargyl acetate 3.24.

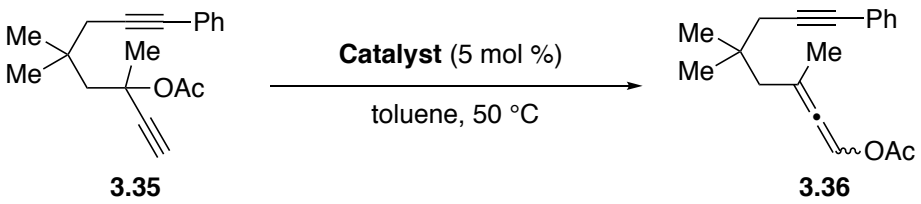

3.35 **3.36**

entry	catalyst	T (°C)	time	yield (%)
1	$[Rh(OCOCF_3)_2]_2$	50	90 min	36
2	$AuCl_3$	rt	10 min	14
3	$PtCl_2$	40	4 d	0

To test the feasibility of the asymmetric APKR with a three-carbon tethered allene-yne, allenyl acetate **3.36** was first subjected to standard APKR conditions. Cationic rhodium catalyst $Rh(cod)_2BF_4$ with triphenylphosphine ligand in DCE afforded product **3.37** in 55% yield (Table 35, entry 1). The reaction was complete in only 40 min at 50 °C, representing a six-fold decrease in reaction time when compared to that of the four carbon-tethered Ph-alkyne substrate **2.21a** under the same conditions.[114] This decreased reaction time demonstrates the impact of the shorter tether length, and the gem-dimethyl group. When subjected to asymmetric APKR conditions using (*S*)-MonoPhos alkene (**2.62**) ligand in DCE at 50 °C, the allene-yne **3.36** reacted in 33% yield and only 10% ee (Table 35, entry 2). When using the DOE-optimized Conditions C using *o*-DCB as a solvent, the yield was increased to 69%, but the enantioselectivity remained low at 7% ee (entry 3). The low enantioselectivity of this substrate **3.36** is likely due to decreased interaction between the

acetate group and the chiral ligand compared to the interaction of the four-carbon tethered substrates.

Table 35. Conditions tested in the APKR of allenyl acetate 3.25.

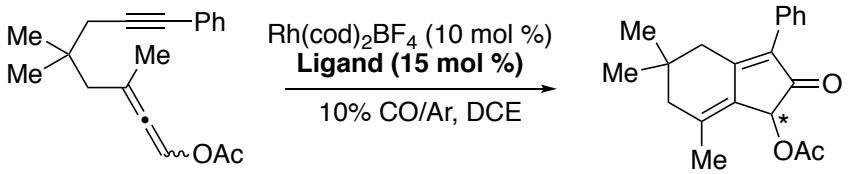

3.36 **3.37**

entry	ligand	Solvent (M)	T (°C)	Time	yield (%)[a]	ee (%)
1	PPh_3	DCE (0.03)	50	40 min	55	-
2	(*S*)- **2.62**	DCE (0.03)	50	4.5 h	33	10
3	(*S*)-**2.62**	*o*-DCB (0.15)	55	10 h	69	7

[a] Isolated yields after purification by column chromatography.

3.5 HYDROLYSIS OF THE APKR PRODUCT TO AFFORD ALPHA-HYDROXY CYCLOPENTEONES.

A variety of biologically interesting natural products contain a chiral α-hydroxy cyclopentenones.[17, 19, 21, 136-137] In order to access this functionality the APKR, an enantioretentive protocol for the hydrolysis of chiral α-acyloxy cyclopentenones is necessary. Previously, our group had demonstrated a successful hydrolysis of the racemic [6,5] α-acyloxy cyclopentenone **3.39** with potassium carbonate in water and methanol afforded alcohol **3.40** in 59% yield. [71] The analogous [7,5] ring system **2.22c** underwent hydrolysis with potassium carbonate to afford alcohol **3.41** in 49% yield. This low yield prompted a search for conditions which would improve yield and hydrolyze chiral carboxy esters while retaining the stereochemical integrity of the

resulting α-hydroxyl stereocenter. To this end, conditions developed by Kajiro and coworkers for the hydrolysis of chiral carboxy esters alpha to coordinating groups were tested. Reaction of chiral cyclopentenone (*R*)-**2.22c** (64% ee, Scheme 47, b) with substoichiometric scandium triflate in 20% water/MeOH gave the desired hydrolysis product **3.41** in 81% yield and 65% ee.[138] Thus, the reaction occurred with retention of stereochemistry. Stereoretention observed attributed to a tridentate coordination of the scandium(III) catalyst to the ketone and the acetate groups (intermediate **3.42**), preventing epimerization of either the starting material or product.

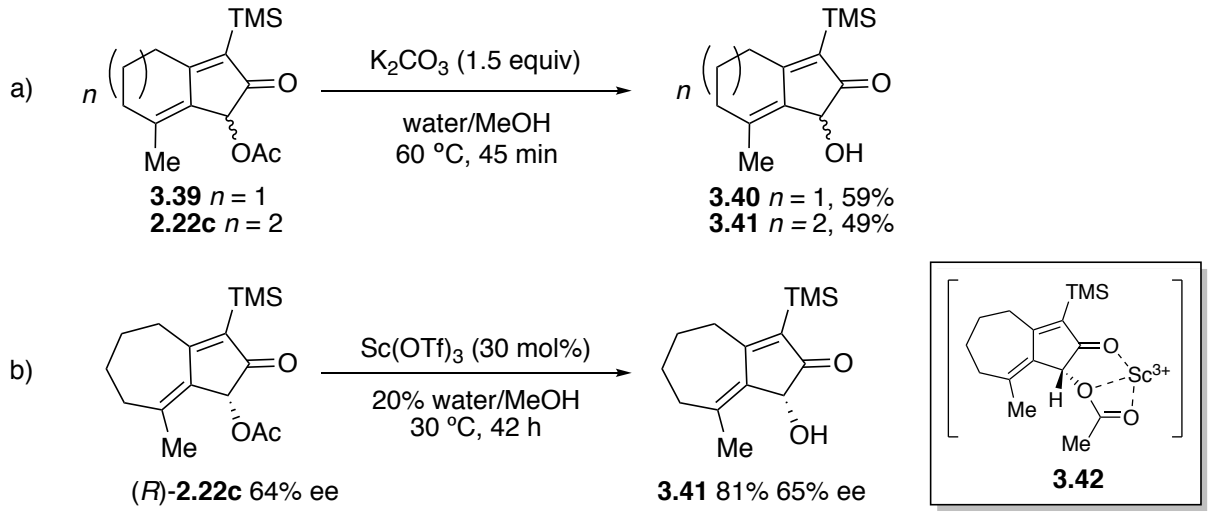

Scheme 47. Base-mediated and Lewis acid-catalyzed hydrolysis of α-acylyoxy cyclopentenones.

3.6 CONCLUSIONS FROM APKR OPTIMIZATION AND SCOPE STUDIES.

After identifying the (*S*)-MonoPhos-ligand (**2.62**) which afforded good yields and enantioselectivities in the APKR, experiments were performed to probe the effects of CO concentration, additive identity and equivalents, ligand to Rh ratio, solvent and scale. Following

these initial experiments which indicated that many reaction factors influenced APKR yield and ee, a statistical design of experiments strategy was employed to optimize both APKR yield and ee by testing seven different reaction conditions simultaneously. We concluded that conditions affording the highest APKR enantioselectivity include PhCl (0.15 M) as a solvent, with 10% CO/Ar atmosphere at 55 °C (55% yield, 71% ee, Conditions B). Further efforts to improve yield led us to discover a third set of conditions employing *o*-DCB as a solvent, which, (compared to the original Conditions A) enabled improvements to both yield and ee (Conditions C).

These conditions were applied to several substrates beyond the model allene-yne **2.21c**. The APKR affords the highest ee's with sterically bulky carboxy ester substituents such as carboxy pivalate and carboxy benzoate groups, with ee's ranging from 70% to 74% ee. Electron deficient substituents such as *p*-nitrobenzoate **2.21g** afforded significantly lower ee's, while sterically demanding alkynes such as TIPS-alkyne **2.21b** were unreactive. The enantioselectivities of the APKR with methyl substituted alkynes was improved substantially (+10-15%) by the DOE-optimized Conditions C, compared to the original APKR Conditions A. The APKR of a three-carbon tethered allene-yne was effected in 67% yield, and enantioretentive hydrolysis conditions were applied to access chiral α-hydroxy cyclopentenones.

SUPPORTING INFORMATION

CHAPTER 3

General Methods

Unless otherwise indicated, all reactions were performed in flame-dried glassware under an inert atmosphere of dry nitrogen and stirred with Teflon-coated magnetic stir bars. All commercially available compounds were purchased and used as received unless otherwise specified. The solvents tetrahydrofuran (THF) and dichloromethane (DCM) were purified by passing through alumina using the Sol-Tek ST-002 solvent purification system. Toluene, acetonitrile (MeCN), and triethylamine (Et_3N) were distilled from calcium hydride prior to use. Deuterated chloroform ($CDCl_3$) was dried over 3 Å molecular sieves. Gasses N_2, 100% CO, and 10% CO/Ar, were purchased from Matheson Tri Gas. All ligands were stored and weighed in a nitrogen-filled glovebox. Purification of compounds by flash column chromatography was performed using silica gel (40-63 μm particle size, 60 Å pore size). TLC analyses were performed on silica gel F_{254} glass-backed plates (250 μm thickness). Preparatory TLC separations were performed on silica gel glass-backed plates with UV254 (1000 μm thickness, Sorbent catalog number 1617124). ^{1}H NMR, ^{13}C NMR and ^{31}P NMR spectra were recorded on Bruker Avance 300, 400, or 500 MHz spectrometers. Spectra were referenced to residual chloroform (7.26 ppm, ^{1}H; 77.16 ppm, ^{13}C). Chemical shifts (δ) are reported in ppm and multiplicities are indicated by s (singlet), d (doublet), t (triplet), q (quartet), quint (quintet), and m (multiplet). Coupling constants, *J*, are reported in hertz (Hz). All NMR spectra were obtained at room temperature. IR spectra were obtained using a Nicolet Avatar E.S.P. 360 FT-IR. EI mass spectroscopy was performed on a Waters Micromass GCT high

resolution mass spectrometer, while ES mass spectroscopy was performed on a Waters Q-TOF Ultima API, Micromass UK Limited high resolution mass spectrometer. HPLCs were performed using a Waters 600 series solvent delivery module with a photodiode array with an injection volume of 50 μL and a flow rate of 1.0 mL/min. Optical rotations (reported in 10 $deg^{-1}cm^2\ g^{-1}$) were measured at 589 nm (sodium D line) using a Perkin Elmer 241 spectropolarimeter.

General methods for DOE studies: Reactions were performed in oven-dried, 8-mL screw-top test tubes, sealed with Teflon caps (ChemGlass, CG-4910, PTFE septa) using an InnovaSyn condenser. Anhydrous dichloroethane (99.8%) was purchased from Acros Organics and trifluorotoluene (>99%) were purchased from Sigma Aldrich and were used as received. Chlorobenzene was distilled over calcium hydride prior to use. $Rh(cod)_2OTf$ and $Rh(cod)_2BArF$ were purchased from Sigma Aldrich and stored in a 0 °C freezer and opened only in a nitrogen-filled glovebox. $Rh(cod)_2BF_4$ was purchased from Strem and stored in a nitrogen-filled glovebox. at rt. (*S*)-MonoPhos-alkene ligand (**2.62**) was prepared as previously reported,[114] and was stored in a nitrogen-filled glovebox at rt.

Example procedure for DOE studies

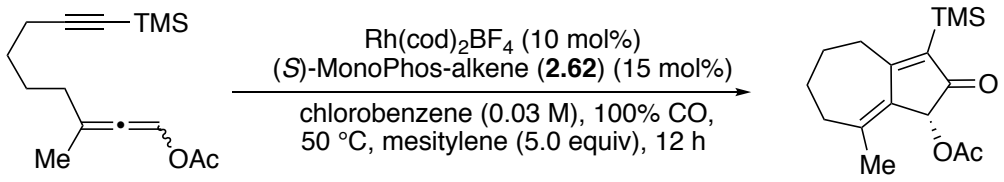

2.21c **2.22c**

General Procedure C: In a nitrogen-filled glovebox, rhodium(I) bis(1,5-cyclooctadiene) tetrafluoroborate (6.5 mg) was weighed into a 15-mL round-bottomed flasks and sealed with rubber septa. In a separate 15- mL, round-bottomed flask, (*S*)-MonoPhos-alkene (10 mg) was

weighed and sealed with a rubber septum. The flasks were removed from the glovebox and placed in a fume hood. Rhodium bis(1,5-cyclooctadiene) tetrafluoroborate was dissolved in dichloromethane (1.6 mL) and a portion of this solution (0.50 mL, containing 2.0 mg Rh, 0.10 equiv) was added to the reaction test tube. The dichloromethane was removed using a needle attached to a vacuum manifold, and the atmosphere in the test tube replaced with nitrogen. (*S*)-MonoPhos-alkene was dissolved in chlorobenzene (2.9 mL), and a portion of this solution (1.1 mL containing 3.8 mg (*S*)-MonoPhos-alkene (**2.62**), 0.15 equiv) was added to the test tube. The resulting catalyst-ligand solution was stirred under nitrogen for 30 min at rt. The Teflon cap of the test tube was pierced with a needle attached to a balloon containing 10% CO/Ar, and the test tube was evacuated and refilled with 10% CO/Ar (3 ×), and the reaction was stirred under CO for 1 h at rt. Mesitylene (35 μL, 5.0 equiv) was added via syringe. Into a separate 15-mL flask was weighed allenyl acetate **2.21c** (32 mg). The flask was evacuated and refilled with nitrogen, and chlorobenzene was added (1.3 mL) was added. A portion of this solution (0.55 mL containing 13 mg allenyl acetate **2.21c**, 1.0 equiv) was added to the test tube. The test tube was lowered into a preheated oil bath (50 °C) and the reaction mixture stirred under 10% CO/Ar for 12 h. When complete, an aliquot of the reaction mixture (0.2 mL) were taken via syringe, added to an NMR tube, and diluted with $CDCl_3$ (0.4 mL).[115] The samples were submitted for yield determination by ^1H NMR via integral comparison of the α-keto hydrogen peak of the product (5.8 ppm) to the aromatic peak (6.8 ppm) of mesitylene. Silica gel (0.2 g) was added to the reaction test tube, DCE removed by rotary evaporation, and the resulting mixture was loaded onto a silica gel column (0.7 cm diameter × 5 cm height). The product **2.22c** was isolated by flash column chromatography (10 × 1 mL fractions, eluting with 5-20% ethyl acetate/hexanes). Fractions containing product **2.22c** were combined, the solvent removed by rotary evaporation, and the residue re-dissolved in HPLC-

grade *i*PrOH/hexanes. Enantiomeric excess was determined by HPLC using a ChiralPak IA-3 column, eluting with 0.5% *i*PrOH/hexanes and detecting at 298 nm.

[1]H NMR spectra for DOE Experiment 1:

Round 1, Entry 1, LCB 5-009

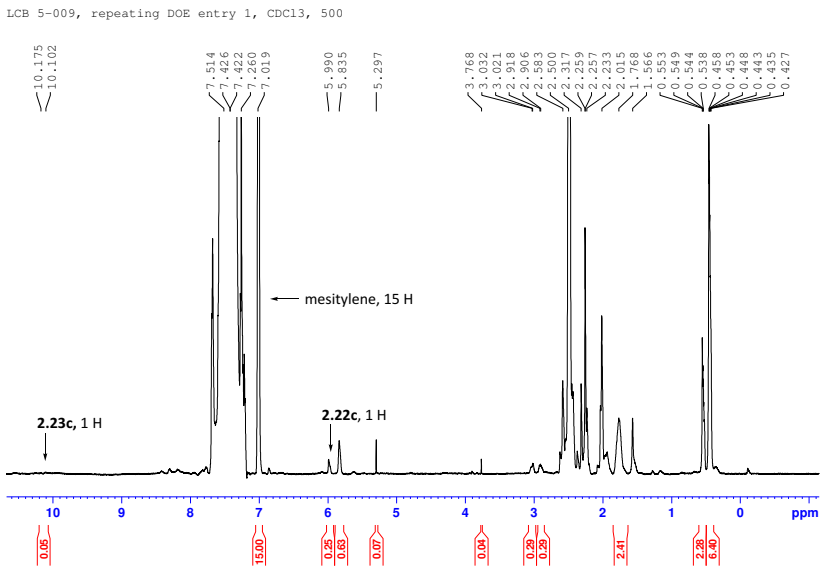

Round 1, Entry 2, LCB 4-190

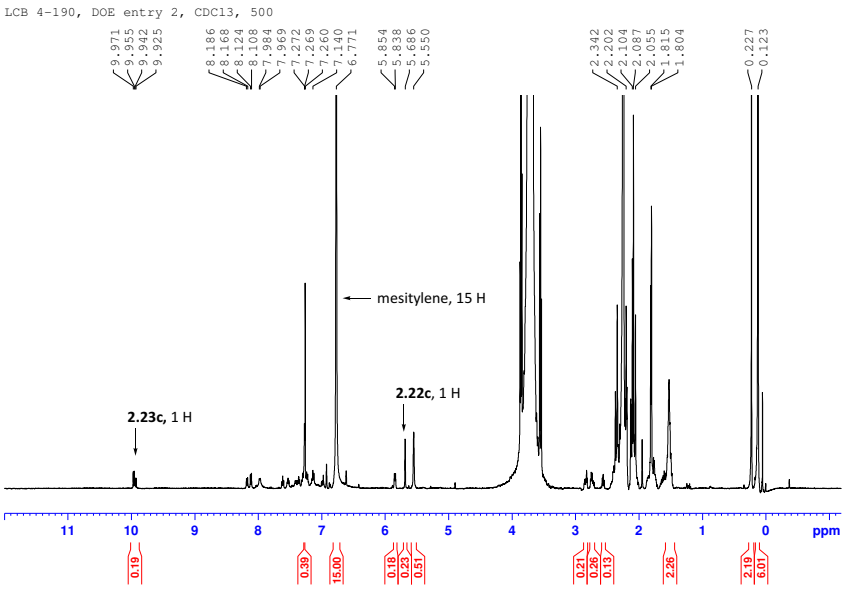

Round 1, Entry 3, LCB 4-187

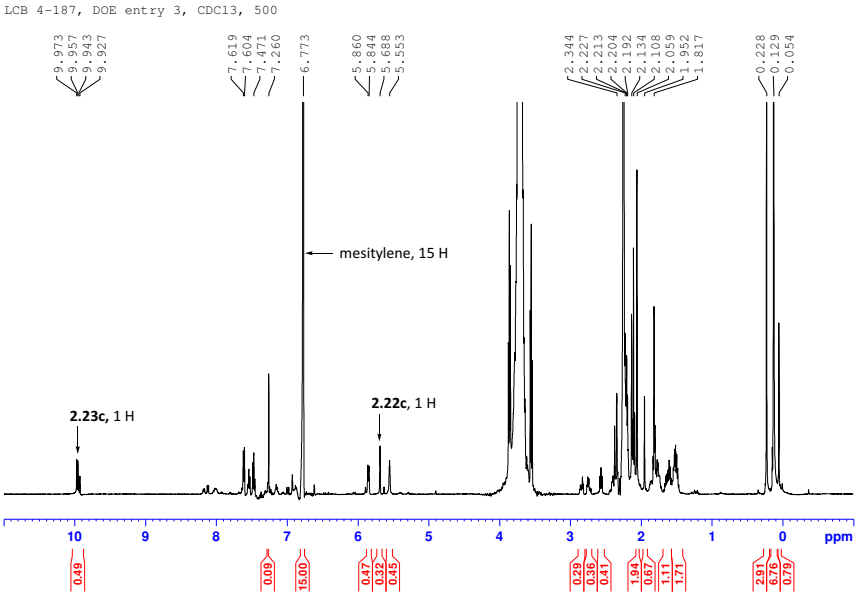

Round 1, Entry 4, LCB 4-191

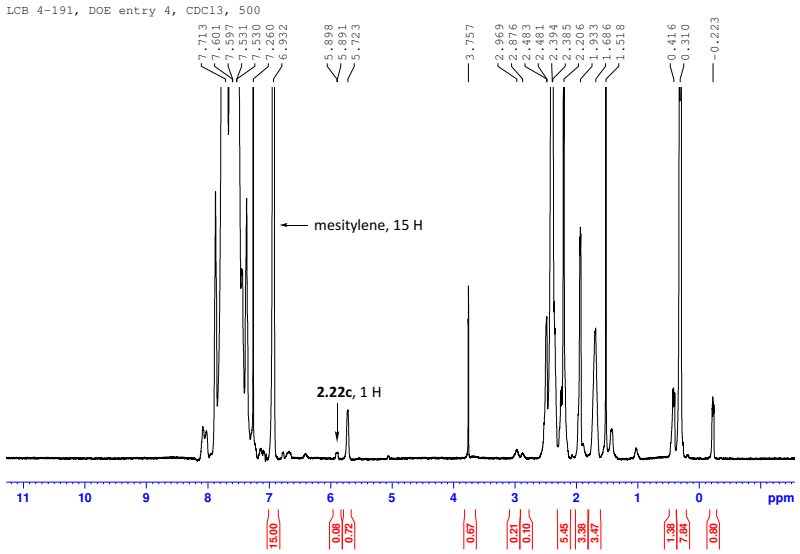

Round 1, Entry 5, LCB 4-188

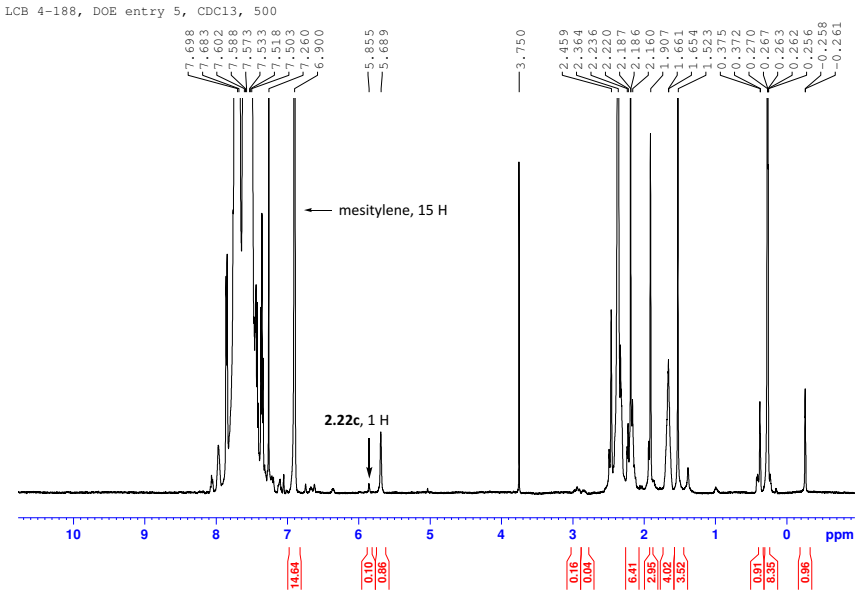

Round 1, Entry 6, LCB 4-159

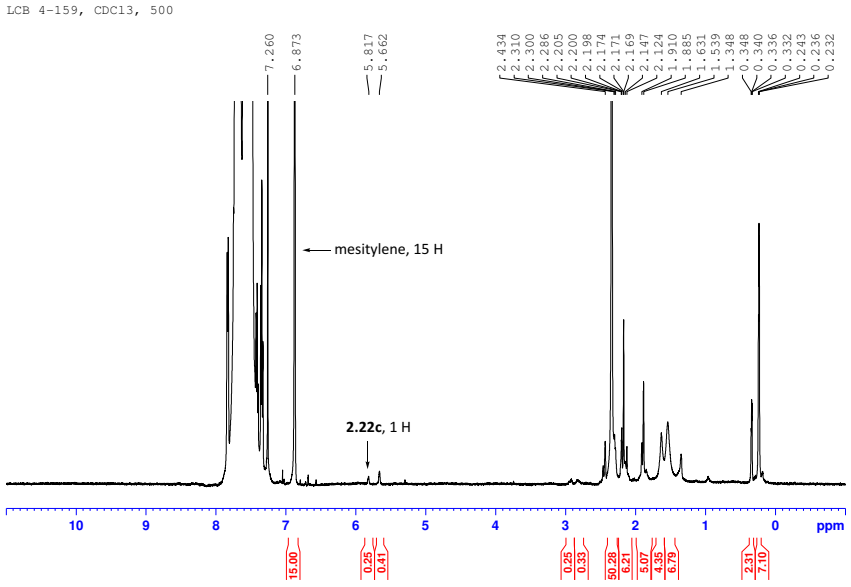

Round 1, Entry 7, LCB 4-161

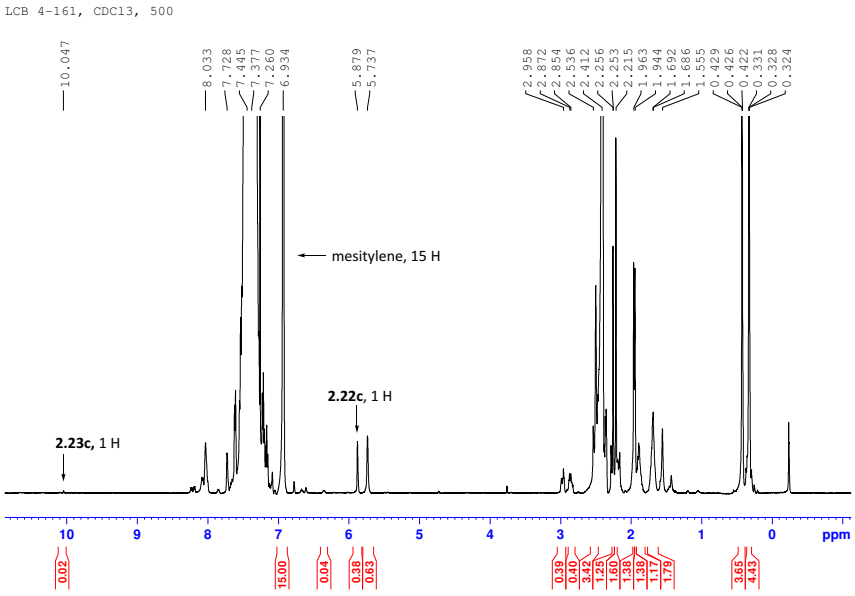

Round 1, Entry 8, LCB 4-162

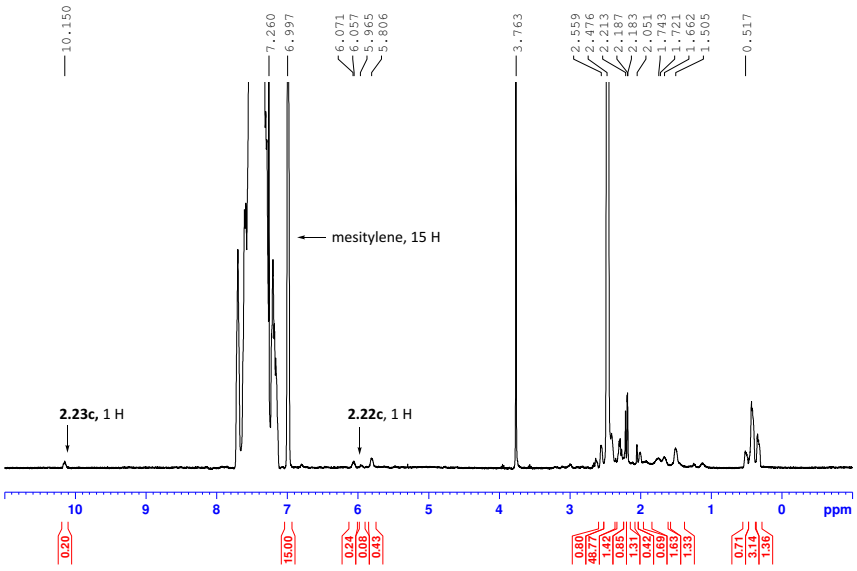

Round 1, Entry 9, LCB 4-167

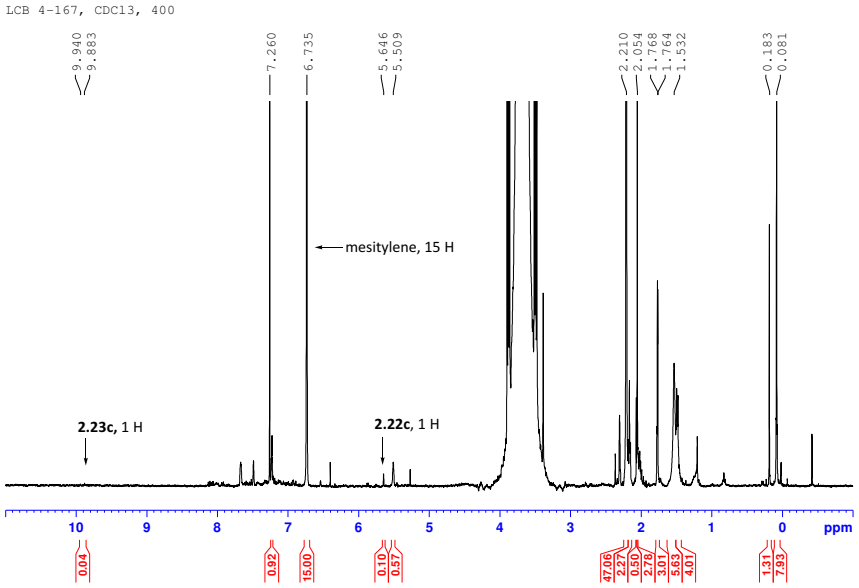

Round 1, Entry 10, LCB 4-160

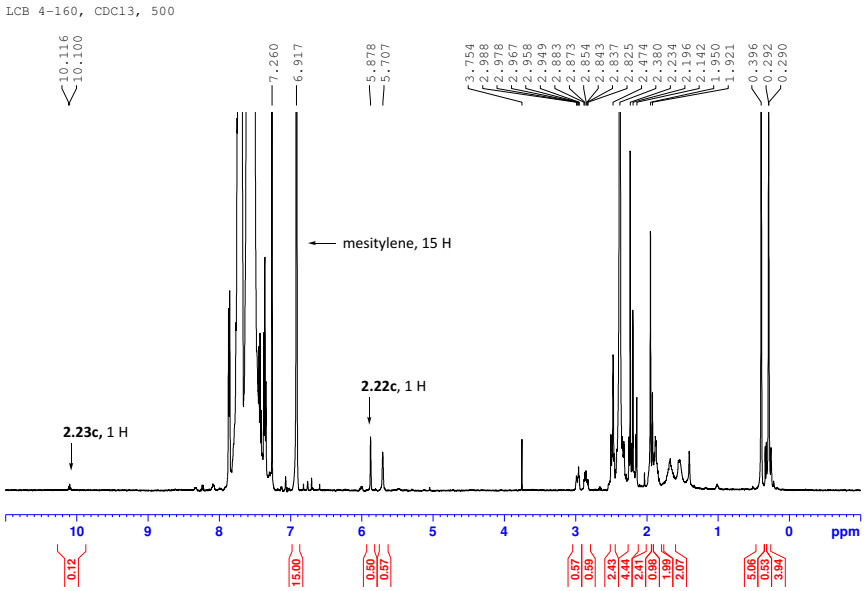

Round 1, Entry 11, LCB 5-001

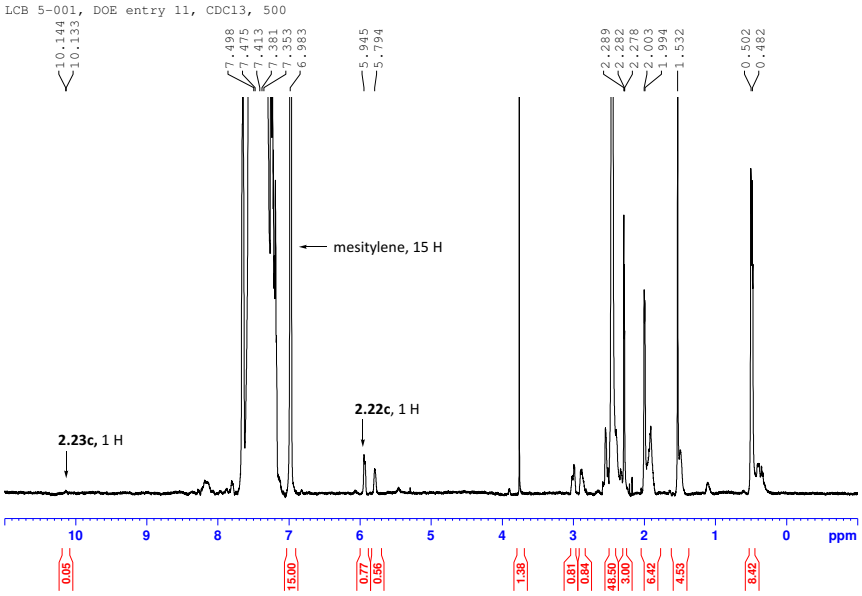

Round 1, Entry 12, LCB 5-002

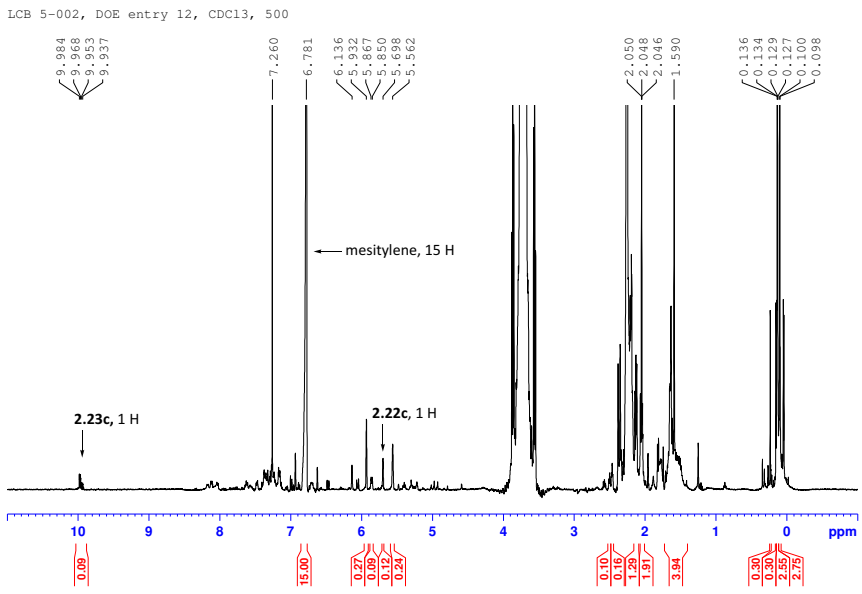

Round 1, Entry 13, LCB 5-003

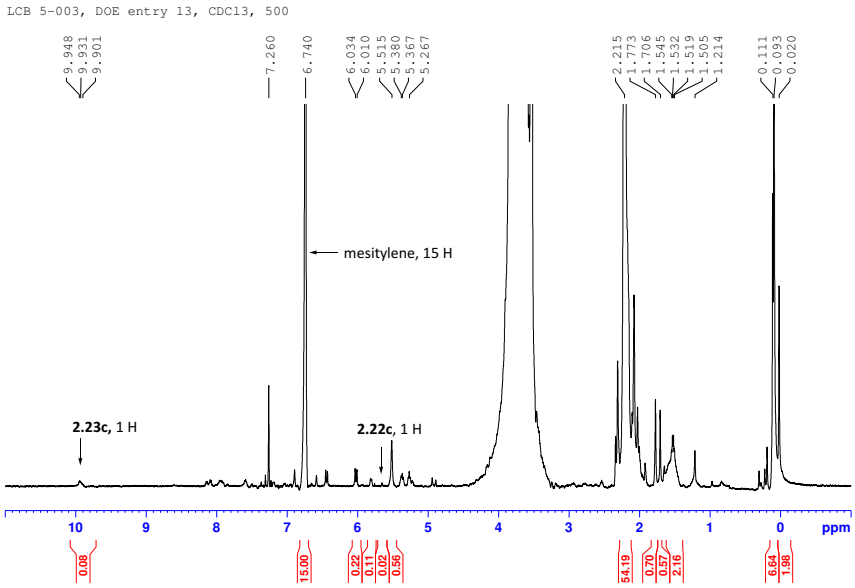

Round 1, Entry 14, LCB 5-004

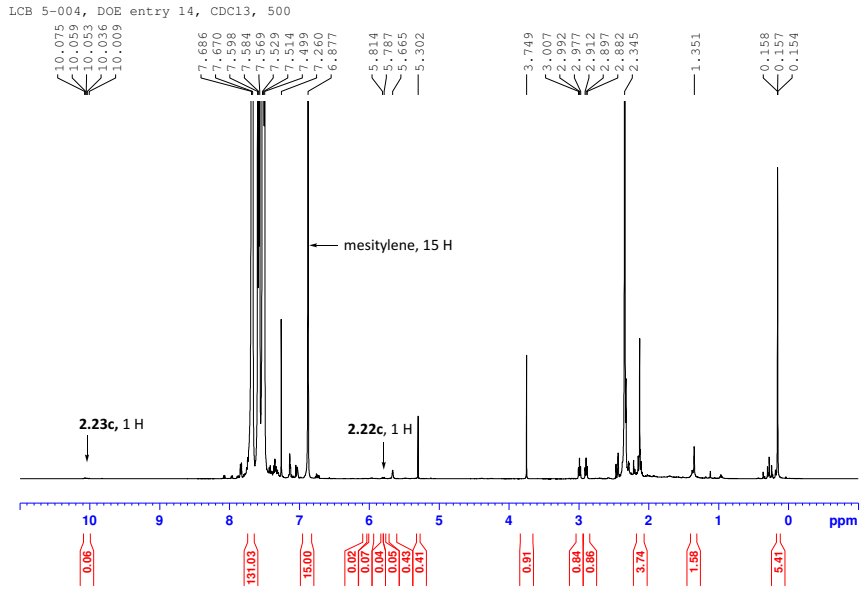

Round 1, Entry 15, LCB 5-005

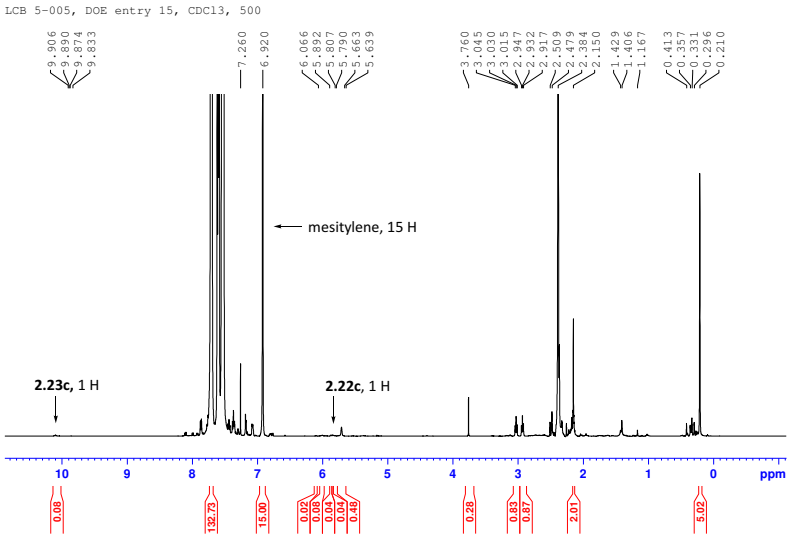

Round 1, Entry 16, LCB 5-012

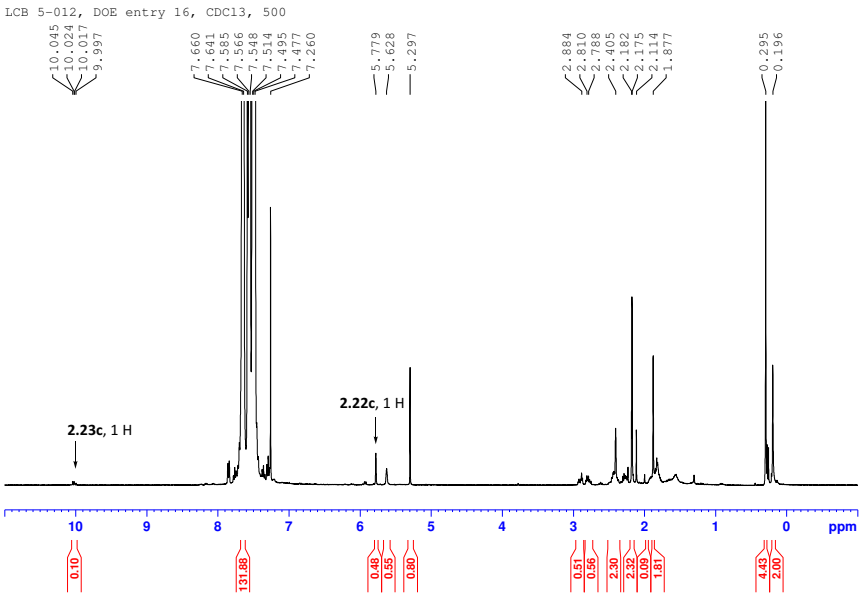

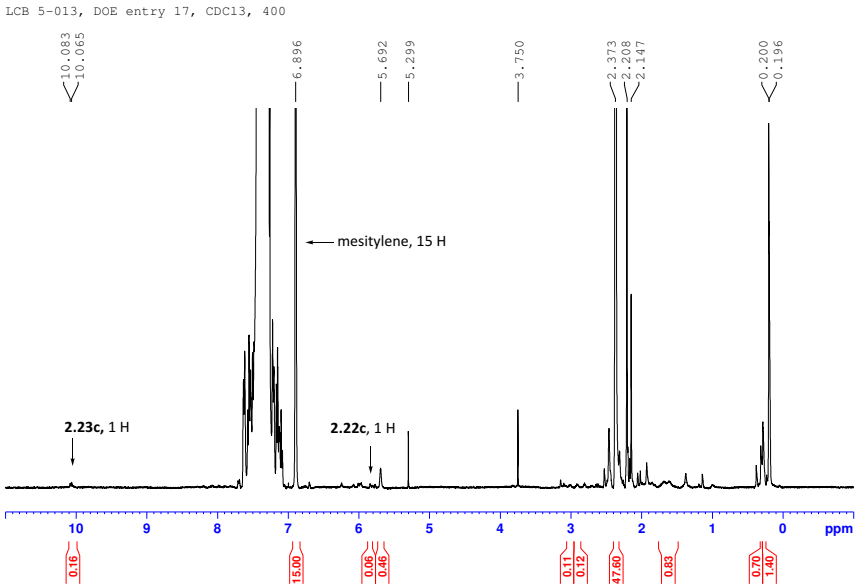

Round 1, Entry 18, LCB 5-010

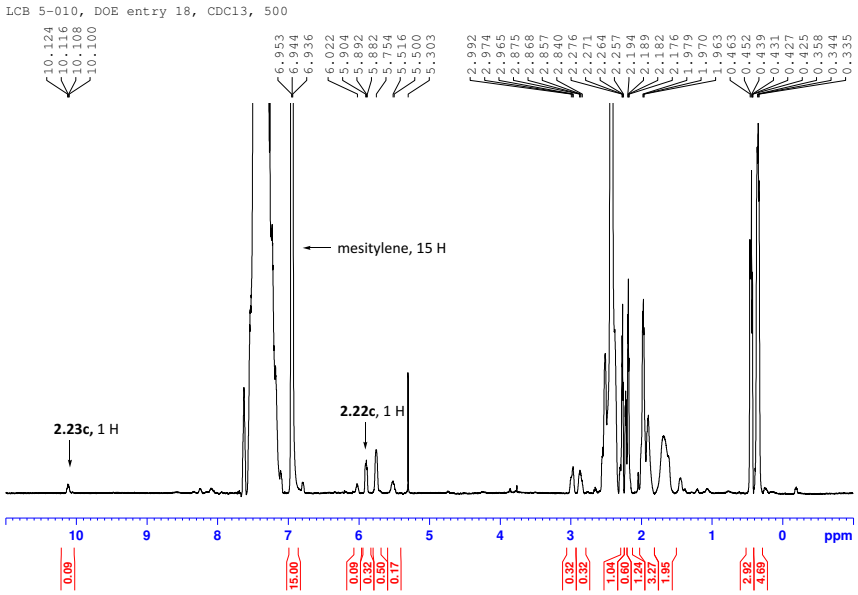

Round 1, Entry 19, LCB 5-011

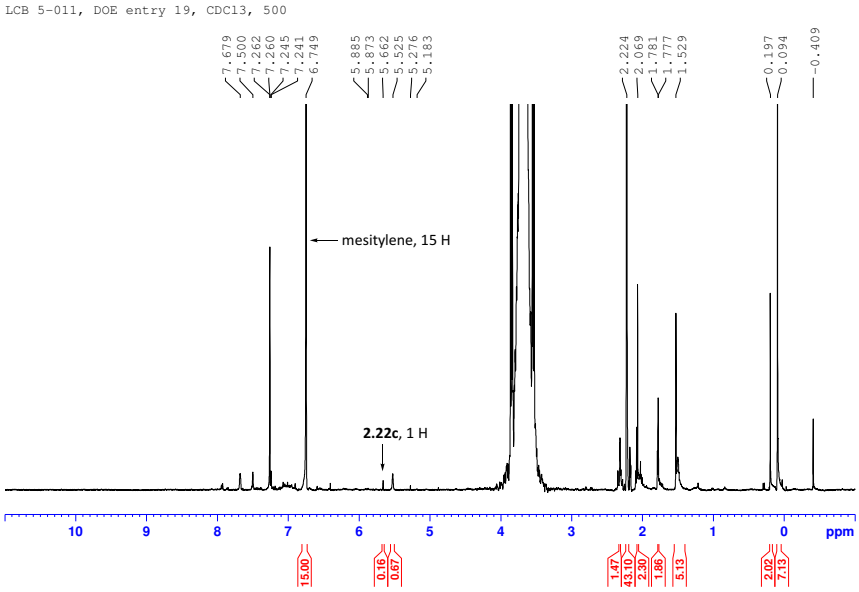

Round 1, Entry 20, LCB 5-014

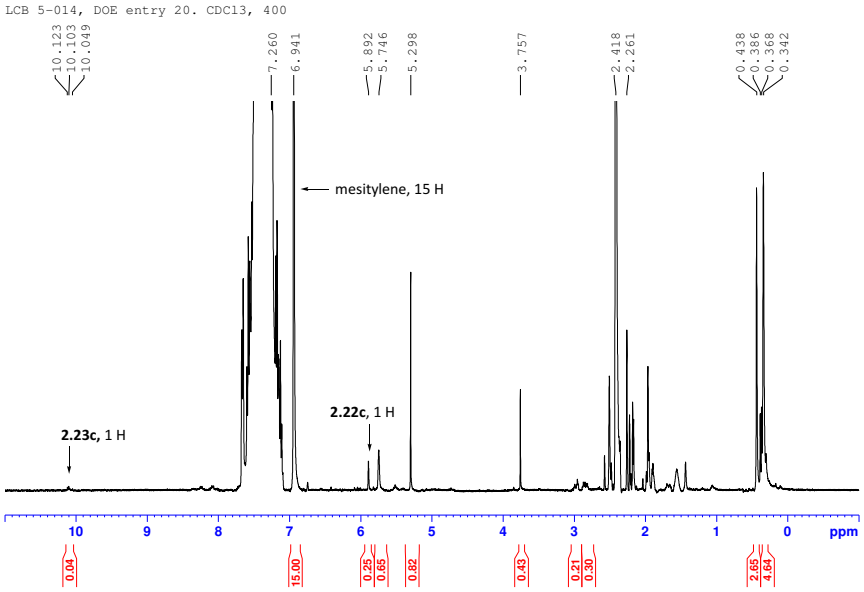

[1]H NMR spectra for DOE Experiment 2:

Round 2, Entry 1, LCB 5-056

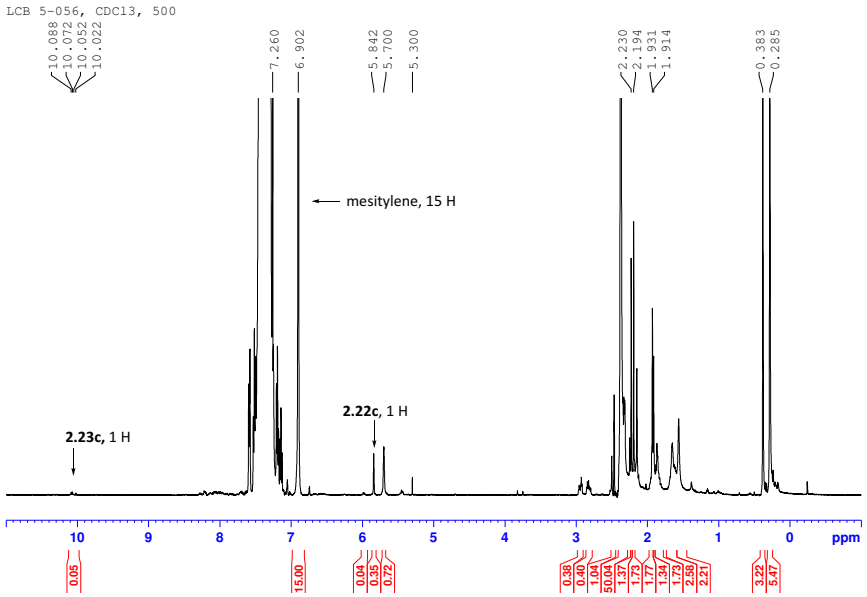

Round 2, Entry 2, LCB 5-061

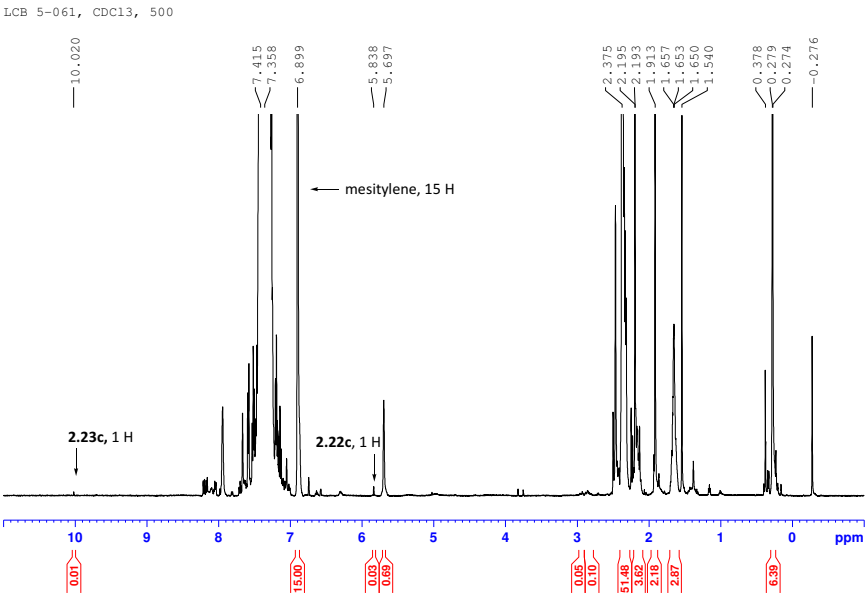

Round 2, Entry 3, LCB 5-058

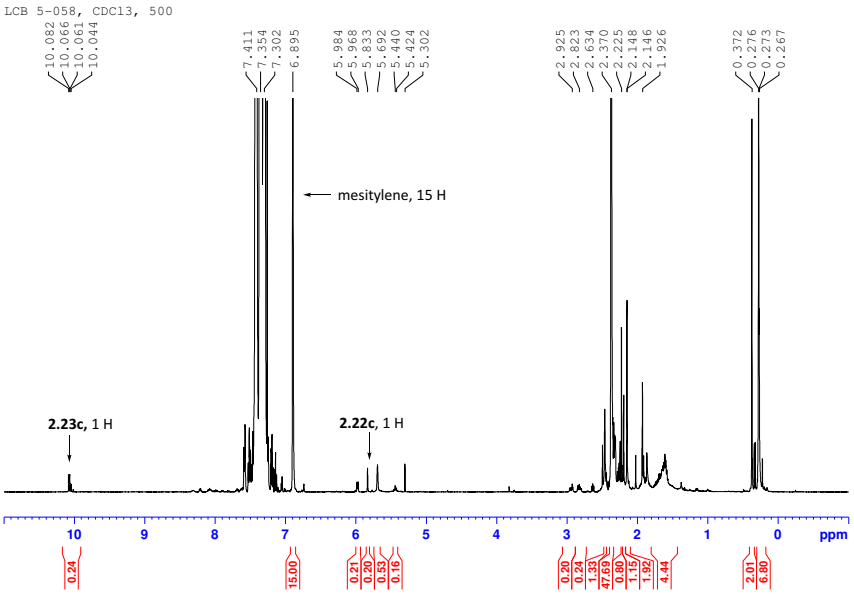

Round 2, Entry 4, LCB 5-059

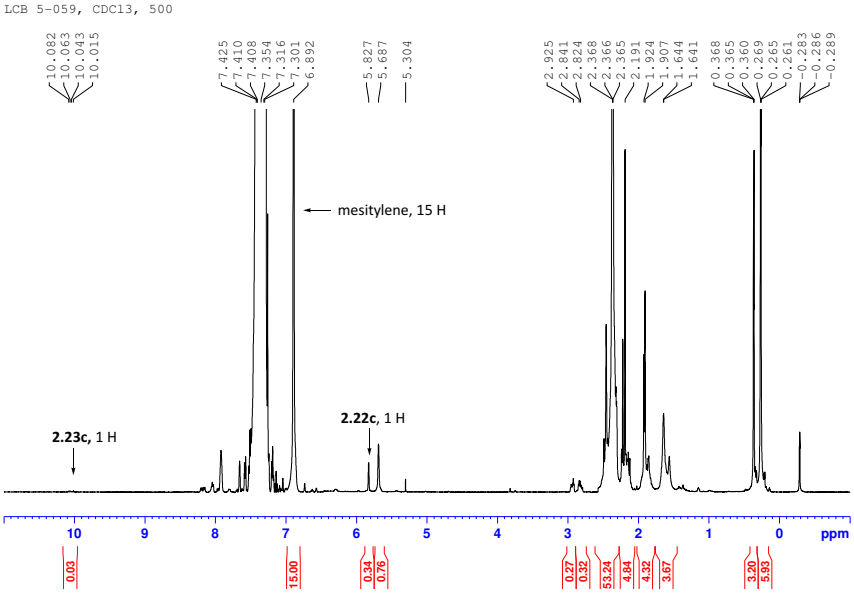

Round 2, Entry 5, LCB 5-062

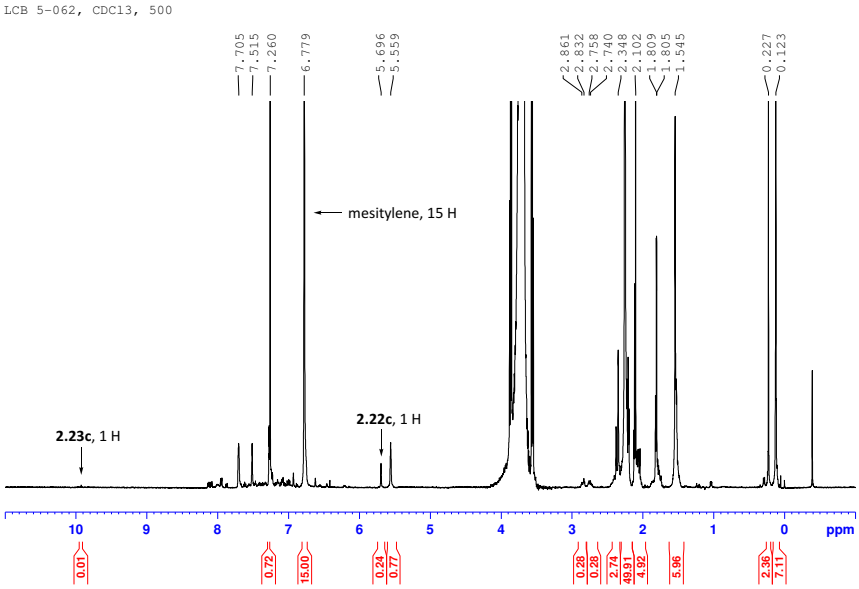

Round 2, Entry 6, LCB 5-063

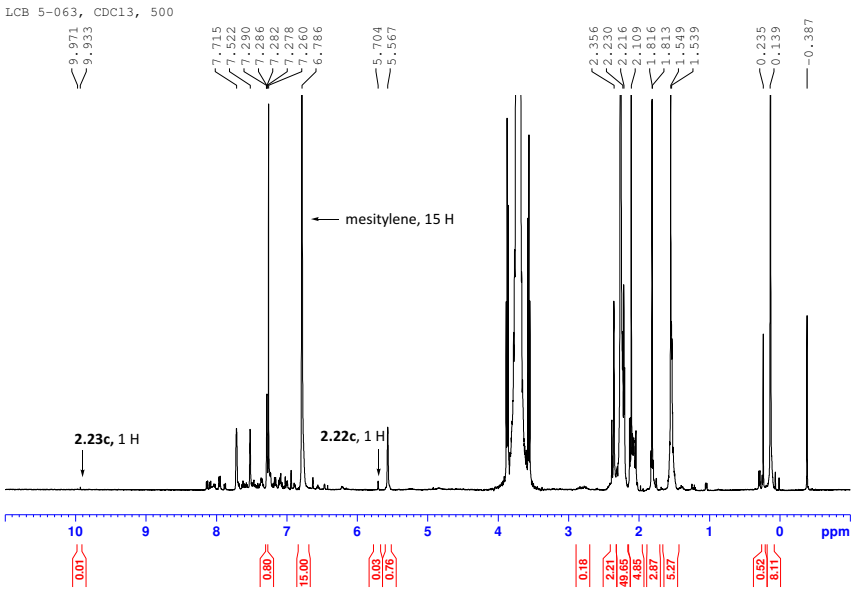

Round 2, Entry 7, LCB 5-064

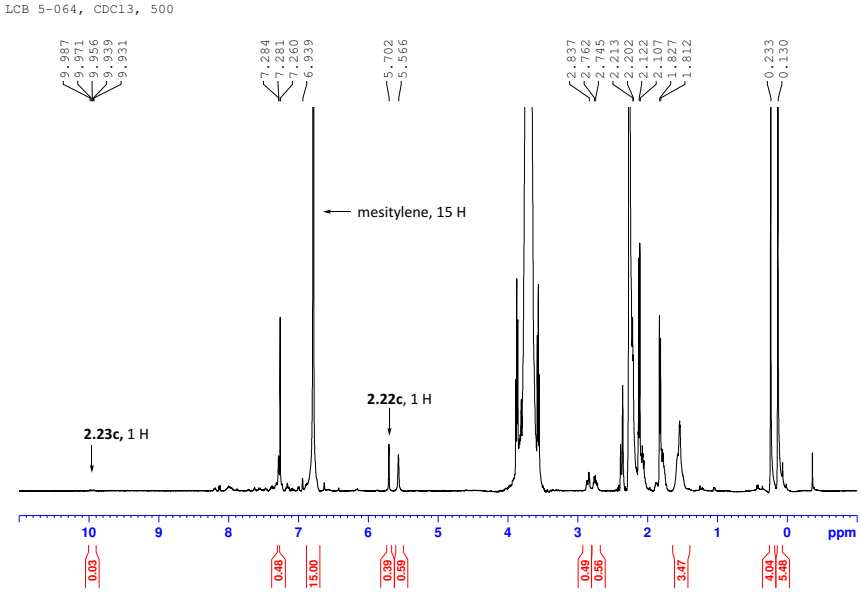

Round 2, Entry 8, LCB 5-065

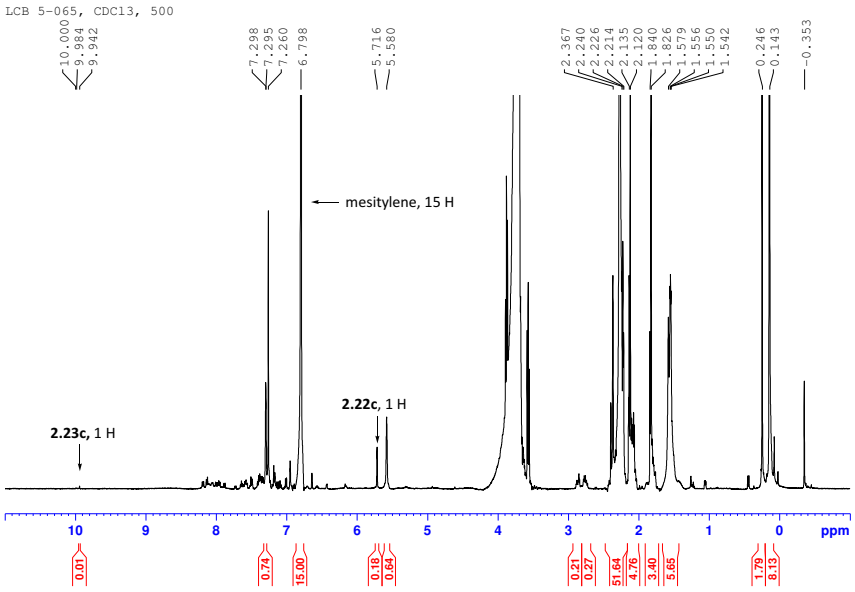

Round 2, Entry 9, LCB 5-040

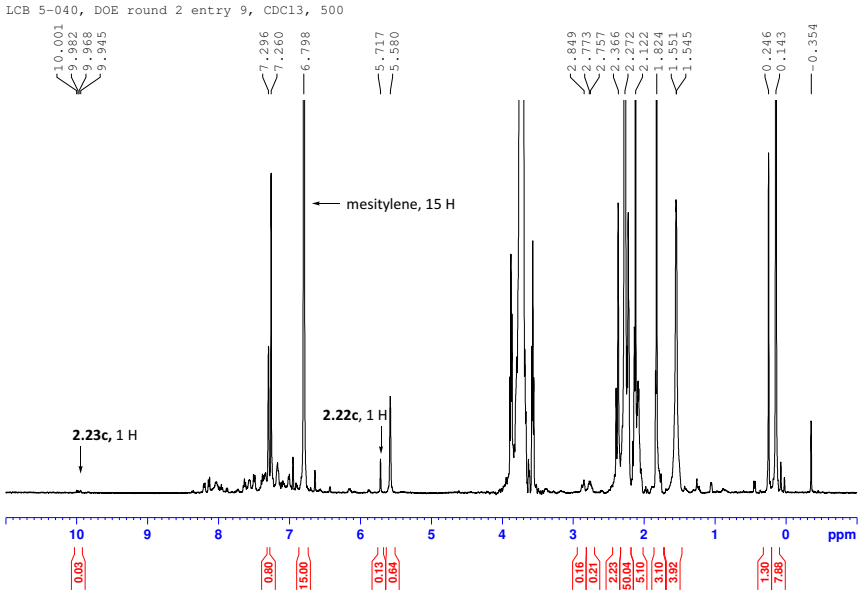

Round 2, Entry 10, LCB 5-086

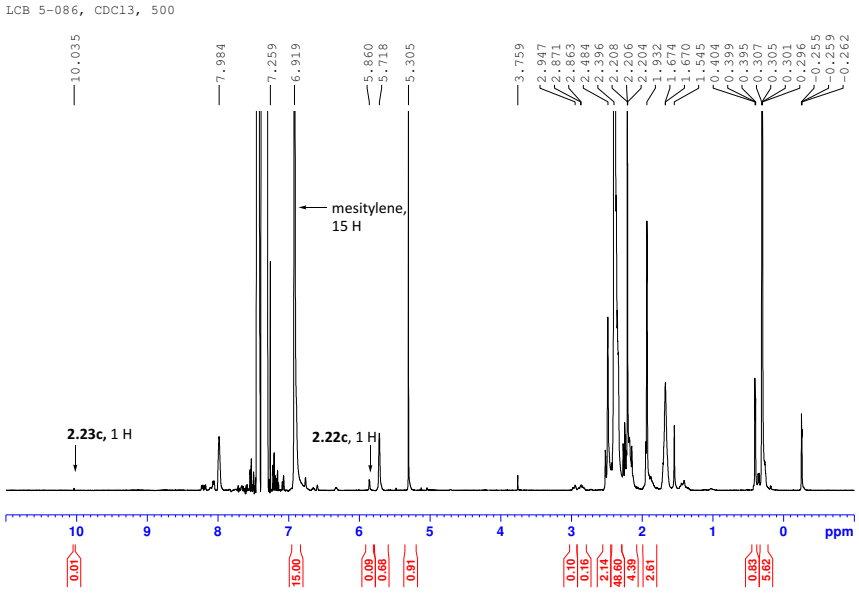

Round 2, Entry 11, LCB 5-087

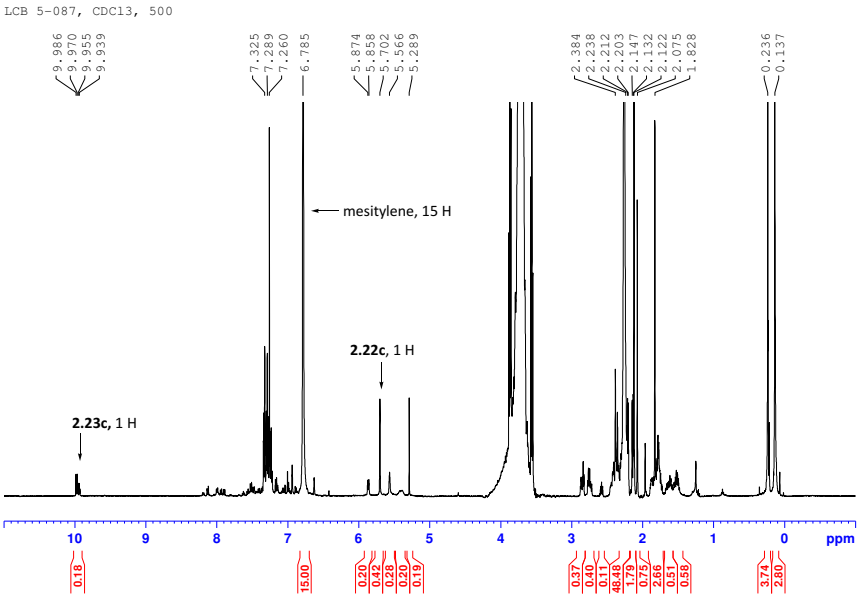

Round 2, Entry 12, LCB 5-088

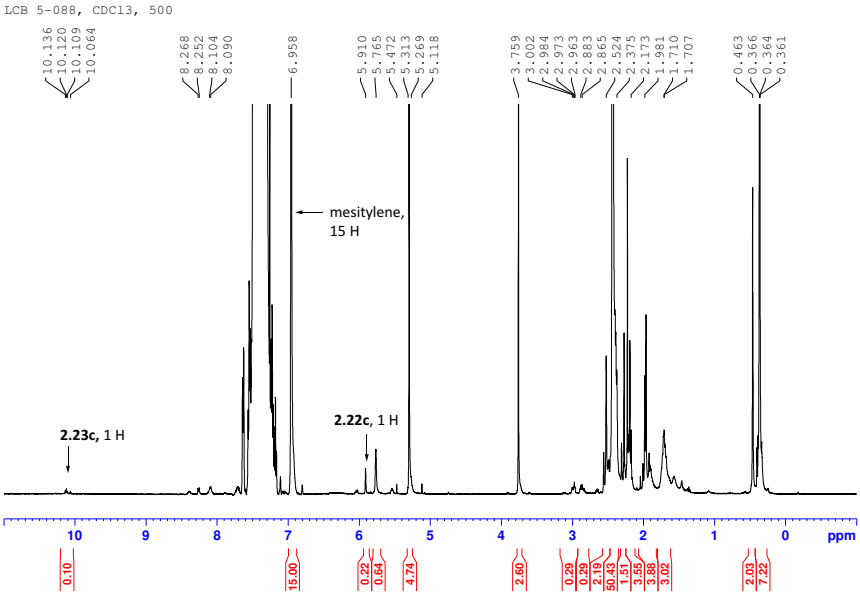

HPLC traces for DOE Experiment 1, entries 1-4

LCB 5-009

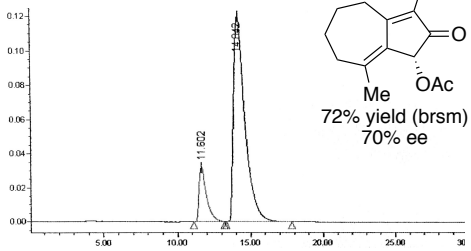

72% yield (brsm)
70% ee

Entry 1	Ret. Time (min)	Area (%)
Peak 1	11.602	14.86
Peak 2	14.042	85.14

LCB 4-190

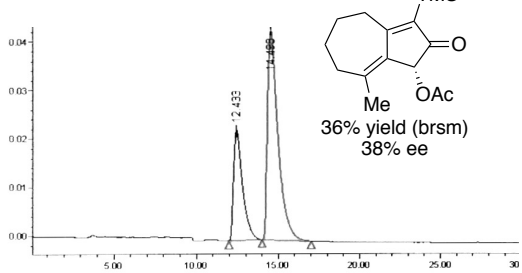

36% yield (brsm)
38% ee

Entry 2	Ret. Time (min)	Area (%)
Peak 1	12.433	30.94
Peak 2	14.498	69.06

LCB 4-187

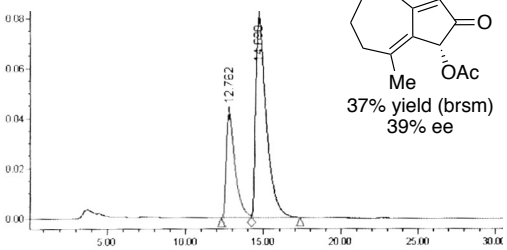

37% yield (brsm)
39% ee

Entry 3	Ret. Time (min)	Area (%)
Peak 1	12.762	30.42
Peak 2	14.690	69.58

LCB 4-191

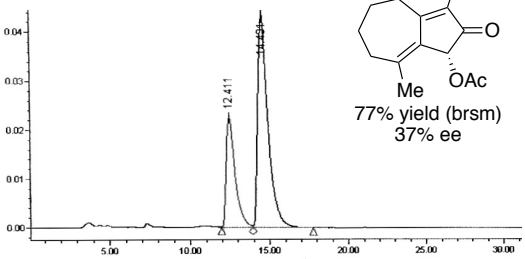

77% yield (brsm)
37% ee

Entry 4	Ret. Time (min)	Area (%)
Peak 1	12.411	31.26
Peak 2	14.431	68.74

HPLC traces for DOE Experiment 1, entries 5-8

LCB 4-188

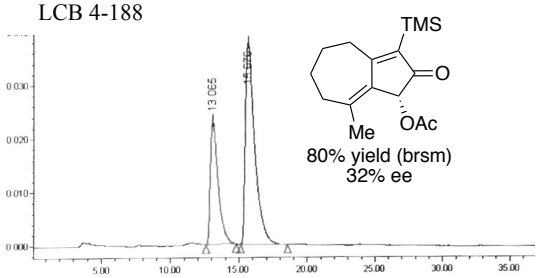

Entry 5	Ret. Time (min)	Area (%)
Peak 1	13.065	34.13
Peak 2	15.676	65.87

LCB 4-159

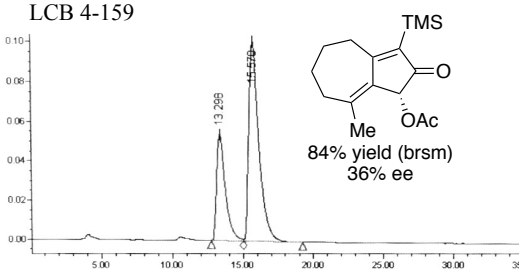

Entry 6	Ret. Time (min)	Area (%)
Peak 1	13.298	31.93
Peak 2	15.570	68.07

LCB 4-161

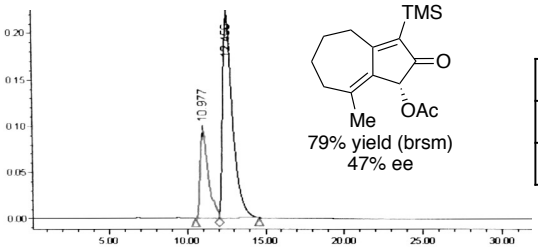

Entry 7	Ret. Time (min)	Area (%)
Peak 1	10.977	26.59
Peak 2	12.456	73.41

LCB 4-162

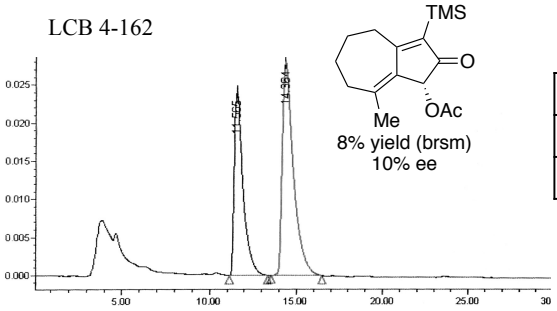

Entry 8	Ret. Time (min)	Area (%)
Peak 1	11.565	40.75
Peak 2	14.364	59.25

HPLC traces for DOE Experiment 1, entries 9-12

LCB 4-167

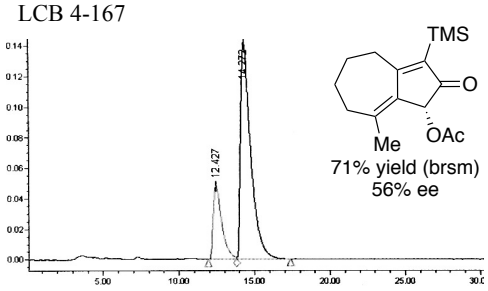

Entry 9	Ret. Time (min)	Area (%)
Peak 1	12.427	22.22
Peak 2	14.272	77.78

LCB 4-160

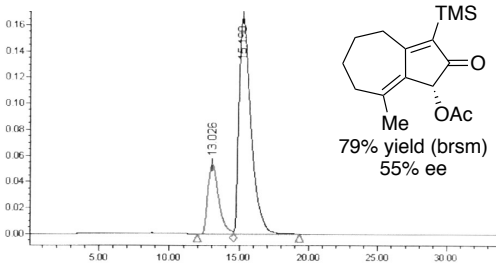

Entry 10	Ret. Time (min)	Area (%)
Peak 1	13.026	22.50
Peak 2	15.198	77.50

LCB 5-001

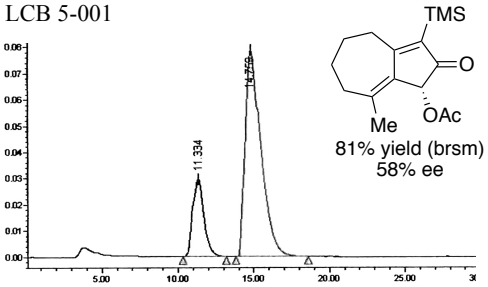

Entry 11	Ret. Time (min)	Area (%)
Peak 1	11.334	21.17
Peak 2	14.759	78.83

LCB 5-002

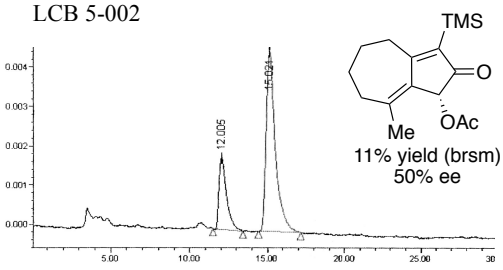

Entry 12	Ret. Time (min)	Area (%)
Peak 1	12.005	24.79
Peak 2	15.012	75.21

HPLC traces for DOE Experiment 1, entries 13-16

LCB 5-003

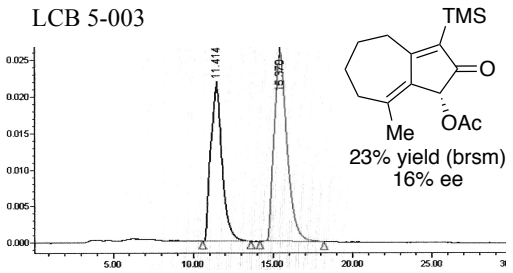

Entry 13	Ret. Time (min)	Area (%)
Peak 1	11.414	42.03
Peak 2	15.378	57.97

LCB 5-004

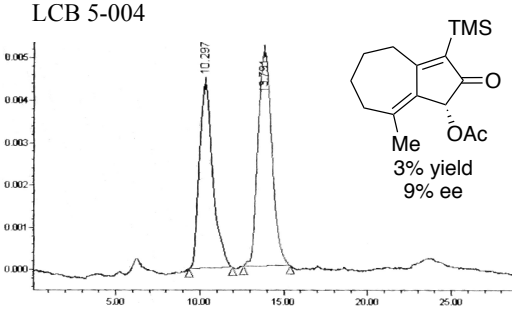

Entry 14	Ret. Time (min)	Area (%)
Peak 1	10.297	45.42
Peak 2	13.791	54.58

LCB 5-005

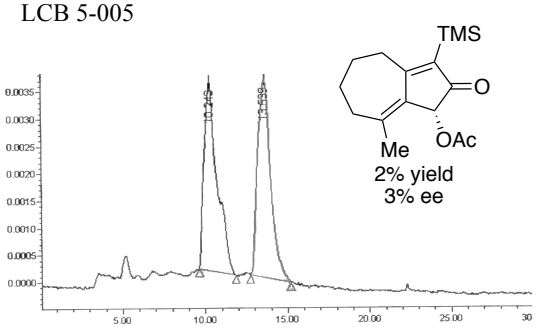

Entry 15	Ret. Time (min)	Area (%)
Peak 1	10.243	48.75
Peak 2	13.539	51.25

LCB 5-012

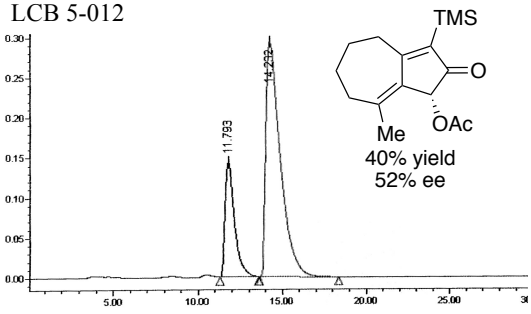

Entry 16	Ret. Time (min)	Area (%)
Peak 1	11.793	23.78
Peak 2	14.232	76.22

HPLC traces for DOE Experiment 1, entries 17-20

LCB 5-013

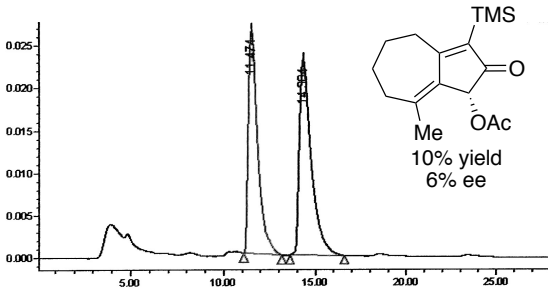

Entry 17	Ret. Time (min)	Area (%)
Peak 1	11.474	47.17
Peak 2	14.304	52.83

LCB 5-010

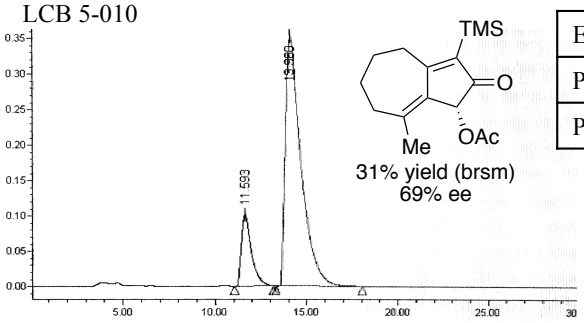

Entry 18	Ret. Time (min)	Area (%)
Peak 1	11.593	15.49
Peak 2	13.988	84.51

LCB 5-011

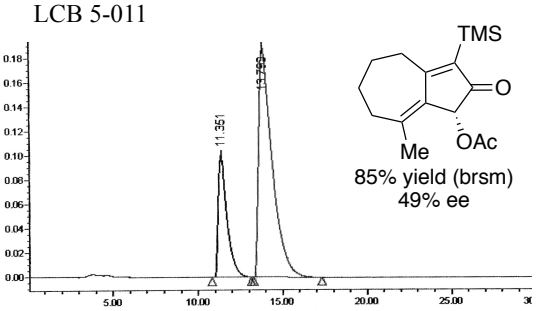

Entry 19	Ret. Time (min)	Area (%)
Peak 1	11.351	25.68
Peak 2	13.793	74.32

LCB 5-014

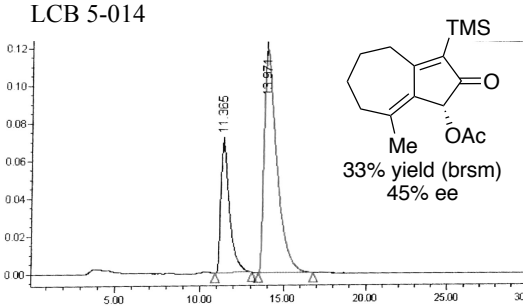

Entry 20	Ret. Time (min)	Area (%)
Peak 1	11.365	26.60
Peak 2	13.971	71.40

HPLC traces for DOE Experiment 2, entries 1-4

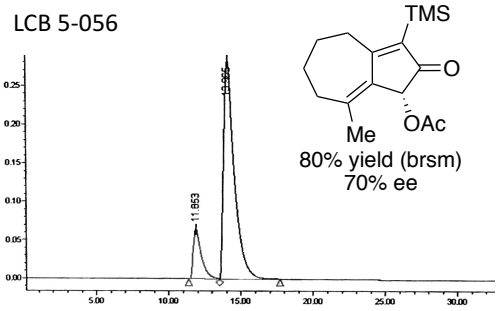

Entry 1	Ret. Time (min)	Area (%)
Peak 1	11.653	14.90
Peak 2	13.965	85.10

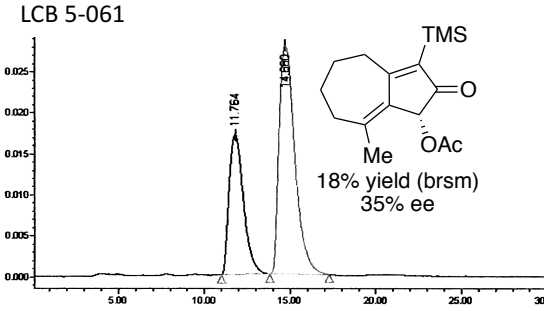

Entry 2	Ret. Time (min)	Area (%)
Peak 1	11.764	35.87
Peak 2	14.660	64.13

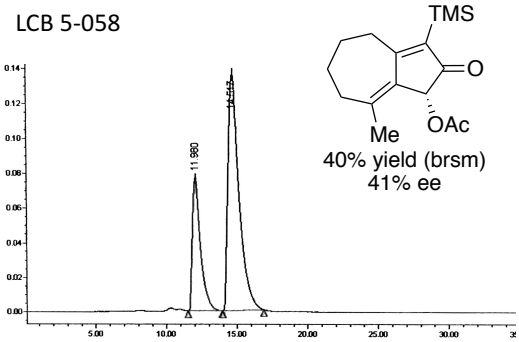

Entry 3	Ret. Time (min)	Area (%)
Peak 1	11.980	29.27
Peak 2	14.517	70.73

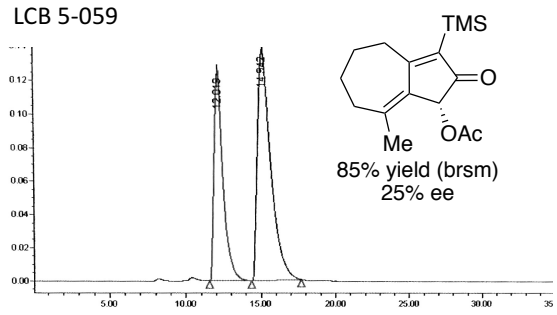

Entry 4	Ret. Time (min)	Area (%)
Peak 1	12.019	37.66
Peak 2	14.942	62.34

HPLC traces for DOE Experiment 2, entries 5-8

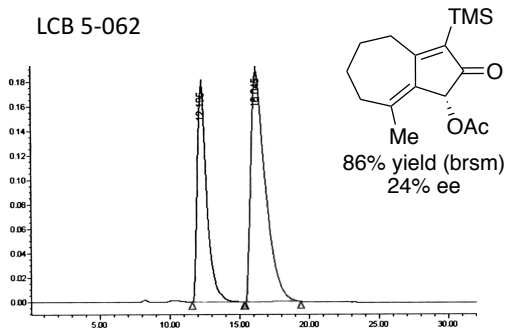

Entry 5	Ret. Time (min)	Area (%)
Peak 1	12.195	38.07
Peak 2	16.045	61.93

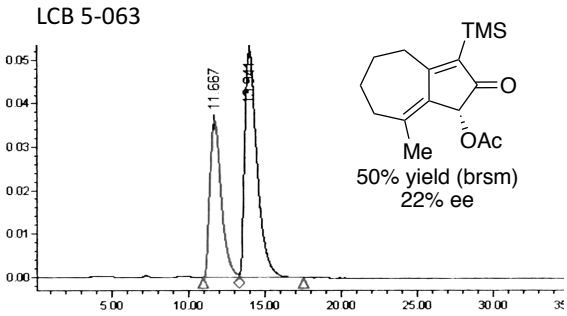

Entry 6	Ret. Time (min)	Area (%)
Peak 1	11.667	39.06
Peak 2	13.941	60.94

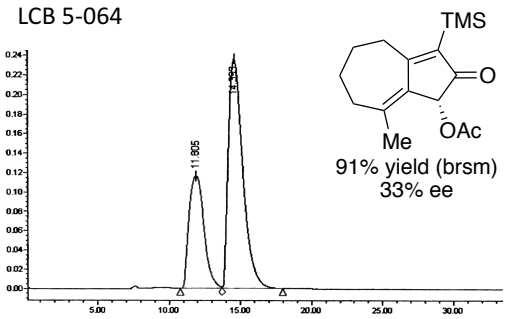

Entry 7	Ret. Time (min)	Area (%)
Peak 1	11.805	33.70
Peak 2	14.393	66.30

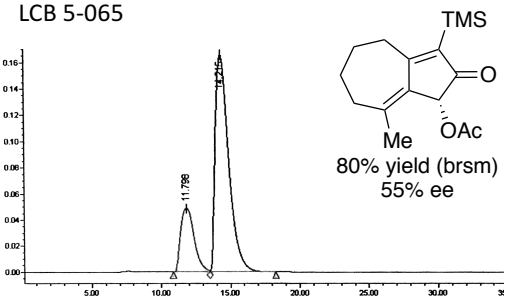

Entry 8	Ret. Time (min)	Area (%)
Peak 1	11.798	22.62
Peak 2	14.215	77.38

HPLC traces for DOE Experiment 2, entries 9-12

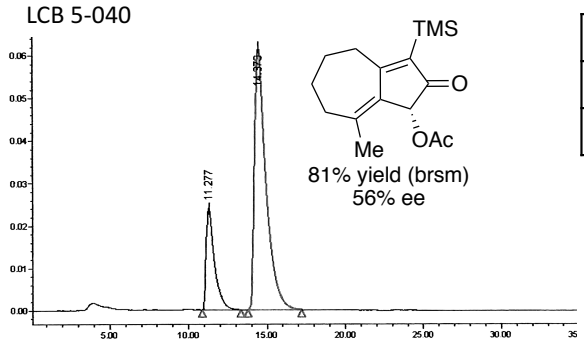

Entry 9	Ret. Time (min)	Area (%)
Peak 1	11.277	22.09
Peak 2	14.373	77.91

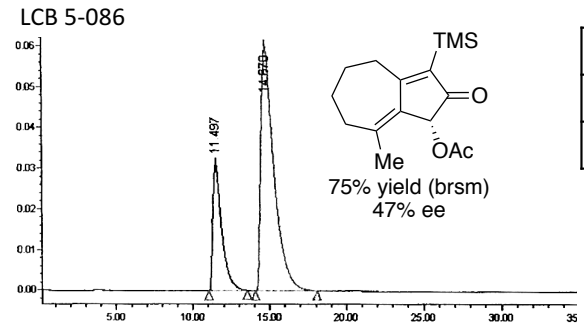

Entry 10	Ret. Time (min)	Area (%)
Peak 1	11.497	26.44
Peak 2	14.670	73.56

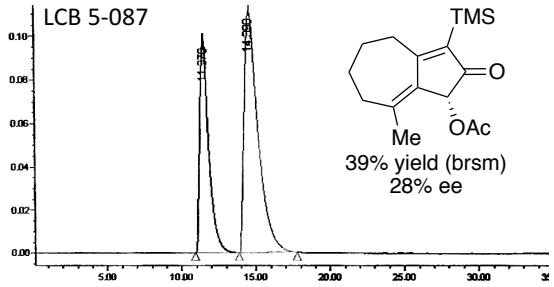

Entry 11	Ret. Time (min)	Area (%)
Peak 1	11.378	36.19
Peak 2	14.390	63.61

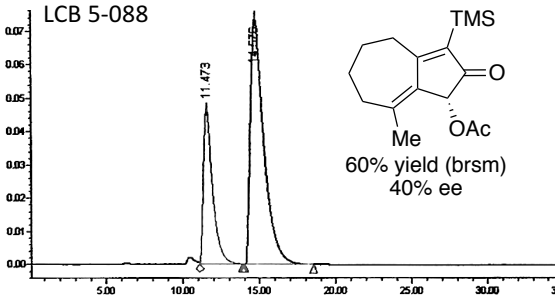

Entry 12	Ret. Time (min)	Area (%)
Peak 1	11.473	30.13
Peak 2	14.576	69.87

Synthesis of methyl-substituted propargyl acetate 3.19a and alcohol 3.20.

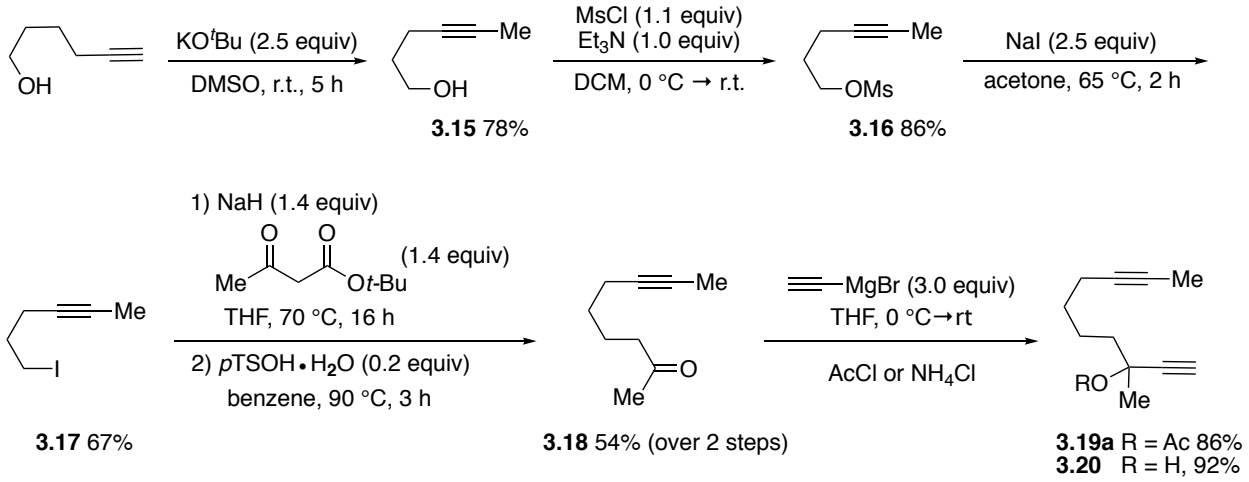

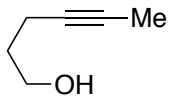

3.15

Hex-4-yn-1-ol (3.15). To a three-necked, 1-L round-bottomed flask equipped with two septa and nitrogen inlet adaptor was added 5-hexyn-1-ol (7.0 g, 71.4 mmol, 1.0 equiv), followed by DMSO (270 mL, 0.26 M). Potassium *tert*-butoxide (20.0 g, 178 mmol, 2.5 equiv) was added portion-wise over 5 min at rt, affording an orange reaction mixture. After 5 h at rt, complete consumption of starting alkyne was observed by TLC. The flask was cooled to 0 °C using an ice/water bath and 1 M HCl (300 mL) was added and stirred 30 min. The reaction was transferred to a 1 L separatory funnel and diluted with diethyl ether (200 mL). The aqueous layer was extracted with diethyl ether (4 × 200 mL). The combined organic layers were dried over magnesium sulfate, gravity filtered, and concentrated by rotary evaporation with a water bath temperature of 15 °C. Due to volatility concerns, the product was not exposed to high vacuum. The crude product was purified by passing through a short plug of silica gel using diethyl ether (300 mL) to yield the title compound **3.15** as a clear oil (7.0 g, 78%). ^{1}H NMR shows residual *t*-butanol. LCB 5-123

^{1}H NMR (300 MHz, $CDCl_3$)

3.74 (t, J = 6.2 Hz, 2 H), 2.28-2.21 (m, 2 H), 1.77 (t, J = 2.6 Hz, 3 H), 1.72 (quint, J = 6.2 Hz, 2 H), 1.61 (br s, 1 H) ppm

Contains *t*-butanol impurity at 1.26 (s) ppm

IR (thin film)

3346, 2921, 2864, 1437, 1057, 931 cm^{-1}

TLC R_f = 0.6 (40% ethyl acetate/hexanes) [silica gel, $KMnO_4$ stain]

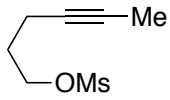

3.16

Hex-4-yn-1-yl methanesulfonate (3.16). To a two-necked, 250-mL round-bottomed flask equipped with a septum and nitrogen inlet adaptor was added alcohol **3.4** (7.0 g, 71.4 mmol, 1.0 equiv) in DCM (94 mL, 0.76 M). Triethylamine (10.2 mL, 73.0 mmol, 1.0 equiv) was added, and the flask was cooled to 0 °C using an ice/water bath. Methanesulfonyl chloride (5.2 mL, 67.3 mmol, 1.1 equiv) was added dropwise over 20 min. The flask was allowed to warm to rt. After 1 h at rt, complete consumption of starting alcohol was observed by TLC. The reaction mixture was transferred to a separatory funnel with diethyl ether (100 mL). The organic layer was washed with water (200 mL) and brine (200 mL) and the combined aqueous layers were back-extracted with diethyl ether (100 mL). The combined organic layers were dried over magnesium sulfate, gravity filtered and concentrated by rotary evaporation. The crude product was purified by passing through a short plug of silica gel using diethyl ether (400 mL) to yield the title compound **3.16** as a yellow oil (11 g, 86%). LCB 5-124

^{1}H NMR (300 MHz, $CDCl_3$)

4.33 (t, J = 6.3 Hz, 2 H), 3.01 (s, 3 H), 2.31-2.25 (m, 2 H), 1.89 (quint, J = 6.3 Hz, 2 H), 1.76 (t, J = 2.7 Hz, 3 H) ppm

^{13}C NMR (125 MHz, $CDCl_3$)

77.2, 76.9, 68.8, 37.4, 28.4, 15.1, 3.5 ppm

IR (thin film)

2923, 1353, 1174, 1008, 975, 931, 836 cm^{-1}

TLC R_f = 0.4 (50% ethyl acetate/hexanes) [silica gel, *p*-anisaldehyde stain]

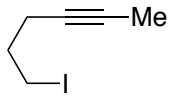

3.17

6-Iodohex-2-yne (3.17). To a two-necked, 500-mL round-bottomed flask equipped with a condenser with nitrogen inlet adaptor, and a septum was added acetone (152 mL, 0.4 M), followed by sodium iodide (22.8 g, 152 mmol, 2.5 equiv). The suspension was stirred 10 min at rt, until sodium iodide was fully dissolved. Mesylate **3.16 (**10.7 g, 60.8 mmol, 1.0 equiv**)** was added to the reaction in a single portion. The flask was lowered into a preheated oil bath (75 °C) After refluxing 2 h, complete consumption of starting mesylate was observed by TLC. The oil bath was removed and the flask cooled to rt. Water (150 mL) was added to the flask, and the mixture was transferred to a 500-mL separatory funnel. The aqueous layer was extracted with diethyl ether (3 × 150 mL) and the combined organic layers were washed with brine (200 mL), dried over magnesium sulfate, filtered and concentrated by rotary evaporation. The crude product was purified by passing through a short plug of silica gel using diethyl ether (300 mL) to yield the title compound **3.17** as a yellow oil (8.44 g, 67%). LCB 5-126

^{1}H NMR (300 MHz, $CDCl_3$)

3.29 (td, *J* = 0.9, 6.6 Hz, 2 H), 2.28-2.23 (m, 2 H), 1.94 (quint, *J* = 6.6 Hz, 2 H), 1.78-1.76 (m, 3 H) ppm

^{13}C NMR (125 MHz, $CDCl_3$)

77.1, 76.9, 32.7, 19.9, 5.7, 3.6 ppm

IR (thin film)

2916, 2841, 1716, 1430, 1222, 1168, 847 cm^{-1}

TLC R_f = 0.9 (10% ethyl acetate/hexanes) [silica gel, *p*-anisaldehyde stain]

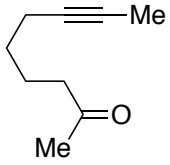

3.18

Non-7-yn-2-one (3.18). To a two-necked, 250-mL, round-bottomed flask equipped with a reflux condenser with nitrogen inlet adaptor and a septum was added sodium hydride (60% dispersion in mineral oil, 2.33 g, 58.2 mmol, 1.4 equiv), followed by THF (132 mL, 0.30 M). The flask was cooled to 0 °C using an ice/water bath. *Tert*-butylacetoacetate (9.6 mL, 58.2 mmol, 1.4 equiv) was added dropwise over 20 minutes. The flask was allowed to warm to rt. After 2 h, iodide **3.17** (8.40 g, 40.4 mmol, 1.0 equiv) was added all at once, and the flask was lowered in to a preheated oil bath (70 °C). After refluxing 16 h, complete consumption of starting iodide was observed by TLC. The oil bath was removed and the flask cooled to rt. Sat'd aq. ammonium chloride (100 mL) was added to the flask and the mixture was transferred to a 500-mL separatory funnel. The aqueous layer was extracted with diethyl ether (3× 150 mL) and the combined organic layers were dried over magnesium sulfate, filtered, and concentrated by rotary evaporation to afford the crude product as a yellow oil (12.5 g), which was taken on immediately to the next step. To a two-necked, 250-mL, round-bottomed flask equipped with a reflux condenser with nitrogen inlet adaptor and a septum was added β-ketoester (12.4 g, 52.1 mmol, 1.0 equiv) in benzene (176 mL, 0.3 M). *Para*-Toluenesulfonic acid monohydrate (2.01 g, 10.6 mmol, 0.20 equiv) was added in one portion, and the flask was lowered into a preheated oil bath (90 °C). After refluxing 3 h, complete consumption of starting β-ketoester was observed by TLC. The oil bath was removed and the flask cooled to rt. Sat'd aq. sodium bicarbonate (200 mL) was added to the flask and the mixture was transferred to a 500-mL separatory funnel. The aqueous layer was extracted with diethyl ether (3 × 100 mL) and the combined organic layers were

washed with brine (100 mL), dried over magnesium sulfate, filtered and concentrated to a volume of approximately 150 mL by rotary evaporation. The remaining benzene was removed by simple distillation. The crude product was purified by silica gel flash column chromatography (10-50% diethyl ether/pentane) to yield the title compound **3.18** as a yellow oil (3.93 g, 54%) LCB 5-128

^{1}H NMR (300 MHz, $CDCl_3$)

2.41 (t, J = 7.2 Hz, 2 H), 2.14-2.07 (m, 5 H), 1.72 (t, J = 2.4 Hz, 3 H), 1.65 (quint, J = 7.2 Hz, 2 H), 1.43 (quint, 6.9 Hz, 2 H) ppm

^{13}C NMR (125 MHz, $CDCl_3$)

208.8, 78.7, 75.9, 43.3, 29.9, 28.5, 23.1, 18.6, 3.5 ppm

IR (thin film)

2921, 2862, 1716, 1436, 1359, 1158, 955 cm^{-1}

HRMS (FTMS + p ESI)

[M+H] calcd for $C_9H_{15}O$, 139.1117; found, 139.1117

TLC R_f = 0.5 (10% ethyl acetate/hexanes) [silica gel, *p*-anisaldehyde stain]

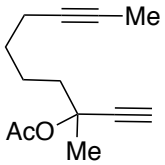

3.19a

3-methyldeca-1,8-diyn-3-yl acetate (3.19a). The synthesis of **3.19a** was performed in a manner analogous to that previously reported.[71] To a two-necked, 250-mL, round-bottomed flask equipped with a reflux condenser with nitrogen inlet adaptor and a septum was added methyl ketone **3.18** (0.51 g, 3.7 mmol, 1.0 equiv). The flask was evacuated and refilled with nitrogen and THF (12 mL, 0.30 M) was added via syringe. The flask was cooled to 0 °C using an ice/water bath. Ethynylmagnesium bromide (22 mL of a 0.5 M solution in THF, 10.9 mmol, 3.0 equiv) was added dropwise via syringe. After 45 min at 0 °C, complete consumption of starting ketone was observed by TLC. Acetyl chloride (0.76 mL, 19

mmol, 5.0 equiv) was added via syringe, and after 90 min, the reaction was complete as evidenced by TMC. The reaction mixture was allowed to warm to rt, diluted with diethyl ether (100 mL) and transferred to a separatory funnel. The organic layer was washed with water (100 mL) and brine (100 mL), dried over magnesium sulfate, gravity filtered, and concentrated under reduced pressure. The crude product was purified by silica gel flash column chromatography (0-20% diethyl ether/hexanes) to yield the title compound **3.19a** as a yellow oil (0.65 g, 86%). LCB 5-129

^{1}H NMR (500 MHz, $CDCl_3$)

2.54 (d, J = 1 Hz, 1 H), 2.15-2.13 (m, 2 H), 2.02 (d, J = 1.0 Hz, 3 H), 1.76-1.75 (m, 3 H), .56-1.48 (m, 4 H) ppm

^{13}C NMR (125 MHz, $CDCl_3$)

169.4, 84.0, 79.0, 75.8, 74.9, 73.3, 41.0, 29.0, 26.5, 23.5, 22.0, 18.9, 3.5 ppm

IR (thin film)

3284, 2941, 2865, 1746, 1439, 1243, 1168, 1017 cm^{-1}

HRMS (FTMS + p ESI)

[M+H] calcd for $C_{13}H_{19}O_2$, 207.1380; found, 207.1382

TLC R_f = 0.5 (15% ethyl acetate/hexanes) [silica gel, *p*-anisaldehyde stain]

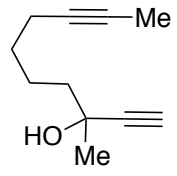

3.20

3-Methyldeca-1,8-diyn-3-ol (3.20). The synthesis of **3.20** was performed in a manner analogous to that previously reported.[71] To a 250-mL, three-necked, round-bottomed flask equipped with a React-IR probe, nitrogen inlet adaptor, and addition funnel with septum, was added methyl ketone **3.18** (1.0 g, 7.2 mmol, 1.0 equiv) in THF (72 mL, 0.1 M). The solution was cooled to 0 °C using an ice/water bath. Ethynylmagnesium bromide (37 mL, 0.5 M in THF, 18 mmol, 3.0 equiv) was added via addition

funnel, dropwise over 15 min syringe. After 1 h at 0 °C and 20 min at rt, complete consumption of methyl ketone **3.7** was observed by React-IR (monitored disappearance of ketone peak at 1720 cm^{-1}). Sat'd aq. ammonium chloride (100 mL) was added to the flask and the reaction stirred an addition al 30 min. mixture was transferred to a 500-mL separatory funnel and the aqueous layer extracted (3 × 100 mL) with diethyl ether. The combined organic layers were washed with brine (200 mL), dried over magnesium sulfate, collected by vacuum filtration, and concentrated by rotary evaporation to yield the title compound **3.20** as a yellow oil (1.1 g, 92%). LCB 5-139

^{1}H NMR (500 MHz, $CDCl_3$)

2.43 (s, 1 H), 2.17-2.14 (m, 2 H), 1.96 (br s, 1 H), 1.77 (t, J = 2.5 H, 3 H), 1.68-1.65 (m, 2 H), 1.62-1.57 (m, 2 H), 1.53-1.49 (m, 5 H) ppm

^{13}C NMR (125 MHz, $CDCl_3$)

87.8, 79.1, 75.8, 71.4, 68.1, 43.1, 29.9, 29.2, 24.0, 18.8, 3.6 ppm

IR (thin film)

2942, 2921, 2863, 1455, 1372, 1335, 1116, 1109, 929 cm^{-1}

HRMS (FTMS + p ESI)

[M+H] calcd for $C_{11}H_{17}O$, 165.1274; found, 165.1271

TLC R_f = 0.4 (20% ethyl acetate/hexanes) [silica gel, *p*-anisaldehyde stain]

Synthesis of propargyl carboxy pivalate 3.19b and benzoate 3.19c.

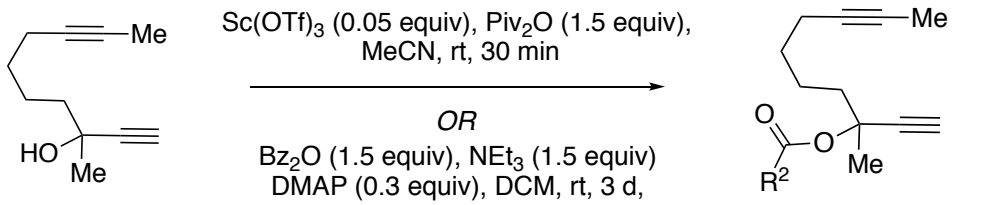

3.20

3.19b R = Piv 86%
3.19c R = Ph, 75%

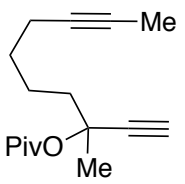

3.19b

3-Methyldeca-1,8-diyn-3-yl pivalate (3.19b). The synthesis of **3.19b** was performed in a manner similar to that previously reported.[114] To a two-necked, 25-mL round-bottomed flask equipped with a septum and nitrogen inlet adaptor was added propargyl alcohol **3.20** (0.30 g, 1.8 mmol, 1.0 equiv) in MeCN (7.3mL, 0.25 M) via cannula. Pivalic anhydride (0.56 mL, 3.4 mmol, 1.5 equiv) was added via syringe at rt. Scandium(III) trifluoromethanesulfonate (18 mg, 0.037 mmol, 0.02 equiv) was dissolved in MeCN (1.8 mL, 0.02 M) was added slowly via syringe. After 30 min at rt, complete consumption of starting alcohol **3.20**was observed by TLC. Sat'd aq sodium bicarbonate (10 mL) was added slowly and stirred for an additional 30 min. The solution was transferred to a 250-mL separatory funnel and diluted with diethyl ether (80 mL) and water (80 mL). The aqueous layer was extracted with diethyl ether (2 x 80 mL), dried over magnesium sulfate, gravity filtered, and concentrated under reduced pressure. The crude product was purified by silica gel flash column chromatography (5% ethyl acetate/hexanes) to yield the title compound **3.19b** as a clear oil (0.39 g, 86%). LCB 5-144

^{1}H NMR (500 MHz, $CDCl_3$)

2.51 (s, 1 H), 2.18-2.12 (m, 2 H), 1.95-1.85 (m, 1 H), 1.84-1.79 (m, 1 H), 1.76 (t, *J* = 2.8 Hz, 3 H), 1.65 (s, 3 H), 1.63-1.47 (m, 4 H), 1.18 (s, 9 H) ppm

^{13}C NMR (125 MHz, $CDCl_3$)

176.7, 84.19, 79.0, 75.8, 74.3, 73.0, 41.2, 39.3, 29.0, 27.2 (3 C), 26.5, 23.3, 18.7, 3.5 ppm

IR (thin film)

3282, 2938, 2870, 1820, 1737, 1480, 1370, 1285, 1098, 1042, 1007, 661 cm^{-1}

HRMS (FTMS + p ESI)

[M+H] calcd for $C_{16}H_{25}O_2$, 249.1855; found, 249.1863

TLC R_f = 0.9 (20% ethyl acetate/hexanes) [silica gel, *p*-anisaldehyde stain]

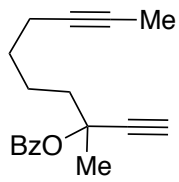

3.19c

3-Methyldeca-1,8-diyn-3-yl benzoate (3.19c). To a two-necked, 10-mL round-bottomed flask equipped with a septum and nitrogen inlet adaptor was added a propargyl alcohol **3.20** (0.38 g, 2.3 mmol, 1.0 equiv). The flask was evacuated and refilled with nitrogen, and DCM (3.9 mL, 0.6 M) was added via syringe. Triethylamine (0.49 mL, 3.5 mmol, 1.5 equiv) was added via syringe, followed by 4-dimethylaminopyridine (85 mg, 0.69 mmol, 0.3 equiv). The solution was cooled to 0 °C using an ice/water bath. Benzoic anhydride (0.83 g, 6.0 mmol, 1.5 equiv) was added as a solid all at once. The flask was allowed to warm to rt and monitored by TLC. After 3 d, sat'd aq ammonium chloride (10 mL) was added and the mixture was transferred to a 60-mL separatory funnel. The aqueous layer was extracted with diethyl ether (3 × 20 mL). The combined organic layers were dried over magnesium sulfate, vacuum filtered and concentrated under reduced pressure. The crude product was purified by silica gel flash column chromatography (5% ethyl acetate/hexanes) to yield the title compound **3.19c** as a light-yellow oil (0.46 g, 75%). LCB 5-141

^{1}H NMR (500 MHz, $CDCl_3$)

8.01 (d, J = 8.0 Hz, 2 H), 7.54 (t, J = 8.0 Hz, 1 H), 7.42 (t, J = 8.0 Hz, 2 H), 2.20-2.17 (ddd, J = 2.5, 5.0, 7 Hz, 2 H), 2.10 (ddd, J = 4.5, 11.5, 13.0 Hz, 1 H), 1.97 (ddd, J = 5.0, 11.5, 13.5, 1 H), 1.82 (s, 3 H), 1.76 (t, J = 2.5 Hz, 3 H), 1.73-1.66 (m, 2 H), 1.58 (quint, 7.0 Hz, 2 H) ppm

^{13}C NMR (125 MHz, $CDCl_3$)

164.9, 133.0, 131.1, 129.7, 128.4, 84.0, 79.0, 75.9, 75.5, 73.6, 41.3, 29.0, 26.7, 23.5, 18.8, 3.5 ppm

IR (thin film)

3293, 2940, 2864, 1723, 1601, 1314, 1279, 1069, 1026, 712, 569 cm^{-1}

HRMS (FTMS + p ESI)

[M+H] calcd for $C_{18}H_{21}O_2$,269.1542; found, 269.1539

TLC R_f = 0.8 (20% ethyl acetate/hexanes) [silica gel, *p*-anisaldehyde stain]

Synthesis of allenyl carboxy acetate 3.21a, benzoate 3.21b and pivalate 3.21c.

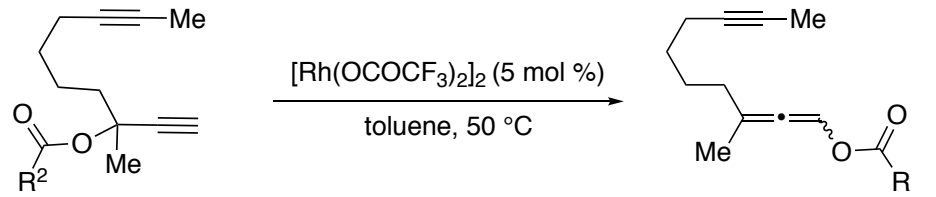

3.19a R = Me
3.19bR = *t*-Bu
3.19c R = Ph

3.21a R = Me, 79%
3.21b R = *t*-Bu, 84%
3.21c R = Ph, 81%

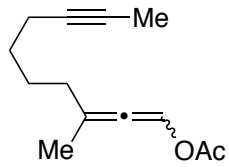

3.21a

3-methyldeca-1,2-dien-8-yn-1-yl acetate (3.21a). Follows general procedure A: rhodium(II) trifluoroacetate dimer (200 mg, 0.09 mmol, 0.05 equiv), propargyl acetate **3.19a** (0.20 g, 0.97 mmol, 1.0 equiv), toluene (4.9 mL, 0.2 M). After 90 min, complete consumption of propargyl acetate was observed by TLC. The crude product was purified by silica gel flash column chromatography (2% ethyl acetate/hexanes) to yield the title compound **3.21a** as a clear oil (0.16 g, 79%). LCB 5-130

^{1}H NMR (500 MHz, $CDCl_3$)

7.28 (septet, *J* = 2.0, 1 H), 2.12-2.00 (m, 7 H), 1.81-1.80 (m, 3 H),

^{13}C NMR (125 MHz, $CDCl_3$)

189.5, 168.9, 115.9, 109.8, 79.0, 75.7, 34.8, 28.6, 26.5, 21.0, 20.6, 18.7, 3.5 ppm

IR (thin film)

3065, 2938, 2860, 1975, 1753, 1443, 1368, 1219, 1040, 922, 789, 599 cm^{-1}

HRMS (FTMS + p ESI)

[M+H] calcd for $C_{13}H_{19}O_2$, 207.1380; found, 207.1383

TLC R_f = 0.6 (15% ethyl acetate/hexanes) [silica gel, *p*-anisaldehyde stain]

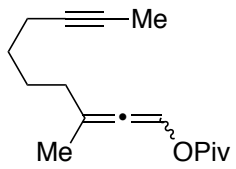

3.21b

3-Methyldeca-1,2-dien-8-yn-1-yl pivalate (3.21b). Follows general procedure A: rhodium(II) trifluoroacetate dimer (26 mg, 0.040 mmol, 0.05 equiv), propargyl pivalate **3.19b** (0.20 g, 0.81 mmol, 1.0 equiv), toluene (4.0 mL, 0.2 M). After 60 min, complete consumption of propargyl acetate was observed by TLC. The crude product was purified by silica gel flash column chromatography (2% ethyl acetate/hexanes) to yield the title compound **3.21b** as a clear oil (0.162 g, 81%). LCB 5-147

^{1}H NMR (500 MHz, $CDCl_3$)

7.25 (sextet, J = 2.0 Hz, 1 H), 1 H), 2.13-2.56 (m, 4 H), 1.81 (d, J = 2.0 Hz, 3 H), 1.76 (t, J = 2.5 Hz, 3 H), 1.57-1.48 (m, 4 H), 1.24 (s, 9 H) ppm

^{13}C NMR (125 MHz, $CDCl_3$)

190.0, 176.7, 115.3, 110.1, 79.3, 75.8, 39.3, 34.9, 28.6, 27.3, 26.5, 20.7, 18.8, 3.7 ppm

IR (thin film)

2936, 2862, 1976, 1741, 1459, 1281, 1134, 1036, 761 cm^{-1}

HRMS (FTMS + p ESI)

[M+H] calcd for $C_{16}H_{25}O_2$, 249.1849; found, 249.1852

TLC R_f = 0.7 (10% ethyl acetate/hexanes) [silica gel, *p*-anisaldehyde stain]

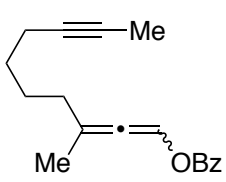

3.21c

3-Methyldeca-1,2-dien-8-yn-1-yl benzoate (3.21c). Follows general procedure A: rhodium(II) trifluoroacetate dimer (26 mg, 0.040 mmol, 0.05 equiv), propargyl benzoate **3.19c** (0.22 g, 0.81 mmol, 1.0 equiv), toluene (4.0 mL, 0.2 M). After 45 min, complete consumption of propargyl acetate was observed by TLC. The crude product was purified by silica gel flash column chromatography (2% ethyl acetate/hexanes) to yield the title compound **3.21c** as a clear oil (0.18 g, 84%). LCB 5-146

^{1}H NMR (500 MHz, $CDCl_3$)

8.09 (d, J = 7.0 Hz, 2 H), 7.57 (t, J = 7.0 Hz, 1 H), 7.54 (sextet, J = 2.0 Hz, 1 H), 7.45 (t, J = 7.5 Hz, 2 H), 2.18-2.07 (m, 4 H), 1.87 (d, J = 2.0 Hz, 3 H), 1.76 (t, J = 2.5 Hz, 3 H), 1.62-1.53 (m, 4 H) ppm

^{13}C NMR (125 MHz, $CDCl_3$)

190.2, 164.7, 133.4, 130.0, 129.8, 128.5, 115.9, 110.2, 79.2, 75.7, 34.8, 28.6, 26.5, 20.7, 18.7, 3.6 ppm

IR (thin film)

3066, 2937, 2859, 1977, 1728, 1601, 1451, 1271, 1096, 1026, 996, 709 cm^{-1}

HRMS (FTMS + p ESI)

[M+H] calcd for $C_{18}H_{21}O_2$,269.1536; found, 269.1545

TLC R_f = 0.5 (10% ethyl acetate/hexanes) [silica gel, *p*-anisaldehyde stain]

Racemic APKR to afford α-carboxy acetate 3.22a, benzoate 3.22b and pivalate 3.22c.

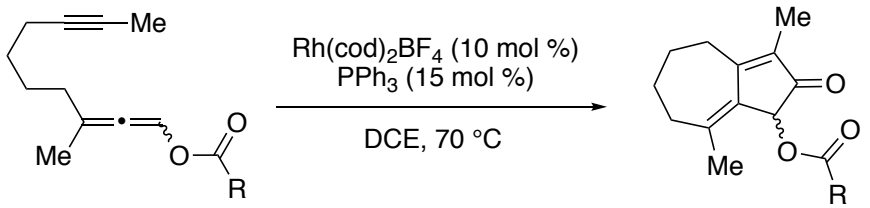

3.21a R = Me
3.21b R = *t*-Bu
3.21c R = Ph

3.22a R = Me
3.22b R = *t*-Bu
3.22c R = Ph

General Procedure D: Reactions were performed in oven-dried, 8-mL screw-top test tubes, sealed with Teflon caps (ChemGlass, CG-4910, PTFE septa, Figure 14) using an InnovaSyn condenser. In a nitrogen glovebox, rhodium(I) bis(1,5-cyclooctadiene) tetrafluoroborate (11 mg) was weighed into a 15-mL round-bottomed flask and sealed with a rubber septum. In a separate 15- mL, round-bottomed flask, triphenylphosphine (10 mg) was weighed and sealed with a rubber septum. The flasks were removed from the glovebox and placed in a fume hood. Rhodium bis(1,5-cyclooctadiene) tetrafluoroborate was dissolved in DCE (3.0 mL, 0.0091 M) and a portion of this solution (0.55 mL, containing 2.0 mg Rh, 0.10 equiv) was added to the reaction test tube. Triphenylphosphine was dissolved in DCE (2.9 mL, 0.0014 M), and a portion of this solution (0.55 mL containing 2.0 mg triphenylphosphine, 0.15 equiv) was added to the test tube. The catalyst-ligand solution was stirred under nitrogen for 30 min at rt. The Teflon cap of the test tube was pierced with a needle attached to a balloon containing 100% CO, and the reaction was stirred under CO for 1 h at rt. Mesitylene (86 mg) was weighed into a 15-mL round-bottomed flask and sealed with a septum. The flask was evacuated and refilled with nitrogen, and DCE was added to dissolve mesitylene (3.6 mL, 0.20 M). A portion of this solution (0.25 mL containing 6.0 mg mesitylene, 1.0 equiv) was added to the test tube. Allenyl ester (1.0 equiv) was weighed in a separate flask and sealed with a septum. The flask was evacuated and refilled with nitrogen, and DCE (0.17 M) was

added. Allenyl ester in DCE (0.3 mL, containing 0.05 mmol allene, 1.0 equiv) was added to the reaction test tube. The test tube was lowered into a preheated oil bath (70 °C) and the reaction mixture stirred under 100% CO, monitoring by TLC. When complete, aliquots of the reaction mixture (0.3 mL) were taken via syringe, added to an NMR tube, and diluted with CDCl3 (0.3 mL).[115] The samples were submitted for yield determination by ^{1}H NMR via integral comparison of the α-keto hydrogen peak of the product. Silica gel (0.2 g) was added to the reaction test tube, DCE removed by rotary evaporation, and the resulting mixture was loaded onto a silica gel column (0.7 cm diameter × 5 cm height). The product **2.22c** was isolated for characterization by flash column chromatography (10 × 1 mL fractions, eluting with 5-20% ethyl acetate/hexanes) to afford the title compounds.

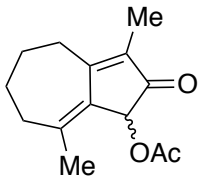

3.22a

3,8-Dimethyl-2-oxo-1,2,4,5,6,7-hexahydroazulen-1-yl acetate (3.22a). Follows general procedure D: allenyl acetate **3.21a** (10 mg, 0.05 mmol,1.0 equiv), rhodium(I) bis(1,5-cyclooctadiene) tetrafluoroborate (2.0 mg, 0.005 mmol, 0.10 equiv), triphenylphosphine (2.0 mg, 0.0075 mmol, 0.15 equiv), mesitylene (35 μL, 0.25 mmol, 5.0 equiv), DCE (0.03 M, 1.7 mL). The flask was placed in a preheated oil bath (70 °C) under a balloon of 100% CO, and the solution stirred for 4 h. The crude product was purified by silica gel flash column chromatography (5-20% ethyl acetate/hexanes) to yield the title compound **3.22a** as a yellow sticky solid (6.8 mg, 58%). LCB 5-132

^{1}H NMR (400 MHz, $CDCl_3$)

5.66 (s, 1 H), 2.72 (t, J = 6.0 Hz, 2 H), 2.44-2.36 (m, 2 H), 2.13 (s, 3 H), 1.89-1.73 (m, 4H), 1.82 (s, 3 H), 1.78 (s, 3 H) ppm

^{13}C NMR (100 MHz, $CDCl_3$)

200.3, 170.0, 169.3, 140.5, 134.9, 131.9, 72.2, 35.6, 29.0, 26.5, 24.2, 23.5, 20.9, 8.3 ppm

IR (thin film)

2925, 2858, 1748, 1706, 1597, 1455, 1372, 1228, 1031 cm^{-1}

TLC R_f = 0.3 (20% ethyl acetate/hexanes) [silica gel, *p*-anisaldehyde stain]

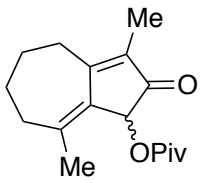

3.22b

3,8-dimethyl-2-oxo-1,2,4,5,6,7-hexahydroazulen-1-yl pivalate (3.22b). Follows general procedure D: allenyl pivalate **3.21b** (20 mg, 0.08 mmol, 1.0 equiv), rhodium(I) bis(1,5-cyclooctadiene) tetrafluoroborate (3.0 mg, 0.008 mmol, 0.10 equiv), triphenylphosphine (3.9 mg, 0.012 mmol, 0.15 equiv), mesitylene (9.6 mg, 0.08 mmol, 1.0 equiv), DCE (0.03 M, 1.7 mL). The flask was placed in a preheated oil bath (70 °C) under a balloon of 10% CO/Ar, and the solution stirred for 2 h. The crude product was purified by silica gel flash column chromatography (5-20% ethyl acetate/hexanes) to yield the title compound **3.22b** as a yellow solid (3.8 mg, 17%, mp = 78-90 °C).

LCB 5-199

^{1}H NMR (500 MHz, $CDCl_3$)

5.62 (s, 1 H), 2.72 (t, J = 6 Hz, 2 H), 2.46-2.35 (m, 2 H), 1.90-1.84 (m, 2 H), 1.82 (s, 3 H), 1.79-1.74 (m, 5 H), 1.24 (s, 9 H) ppm

^{13}C NMR (125 MHz, $CDCl_3$)

200.4, 177.5, 168.7, 140.0, 134.7, 132.2, 72.3, 39.1, 35.4, 28.8, 27.4 (3 C), 26.5, 24.2, 23.6, 8.3 ppm

IR (thin film)

2933, 2866, 1736, 1704, 1595, 1456, 1394, 1272, 1148, 1033 cm^{-1}

HRMS (FTMS + p ESI)

[M+H] calcd for $C_{17}H_{25}O_3$, 277.1798; found, 277.1803

TLC R_f = 0.4 (10% ethyl acetate/hexanes) [silica gel, *p*-anisaldehyde stain]

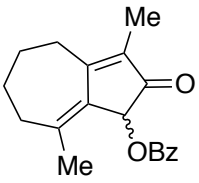

3.22c

3,8-dimethyl-2-oxo-1,2,4,5,6,7-hexahydroazulen-1-yl benzoate (3.22c). Follows general procedure D: allenyl benzoate **3.21c** (27 mg, 0.10 mmol, 1.0 equiv), rhodium(I) bis(1,5-cyclooctadiene) tetrafluoroborate (4.1 mg, 0.010 mmol, 0.10 equiv), triphenylphosphine (3.9 mg, 0.015 mmol, 0.15 equiv), mesitylene (12 mg, 1.0 mmol, 1.0 equiv), DCE (0.03 M, 1.7 mL). The flask was placed in a preheated oil bath (70 °C) under a balloon of 10% CO/Ar, and the solution stirred for 2 h. The crude product was purified by silica gel flash column chromatography (5-20% ethyl acetate/hexanes) to yield the title compound **3.22c** as a yellow sticky solid (7.5 mg, 25%). LCB 5-201

^{1}H NMR (500 MHz, $CDCl_3$)

8.06 (d, *J* = 7.0 Hz, 2 H), 7.55 (t, *J* = 7.5 Hz, 1 H), 7.42 (t, *J* = 7.5 Hz, 2 H), 5.84 (s, 1 H), 2.77 (t, *J* = 7.5 Hz, 1 H), 2.43-2.41 (m, 2 H), 1.91-1.89 (m, 2 H), 1.85-1.78 (m, 8 H) ppm

^{13}C NMR (125 MHz, $CDCl_3$)

200.1, 168.9, 165.7, 140.6, 134.9, 133.2, 132.1, 130.1, 130.0, 128.5, 72.9, 35.7, 29.0, 26.6, 24.2, 23.6, 8.4 ppm

IR (thin film)

2931, 2863, 1724, 1702, 1599, 1451, 1261, 1109, 1026, 711 cm^{-1}

HRMS (FTMS + p ESI)

[M+H] calcd for $C_{19}H_{21}O_3$,297.1485; found, 297.1493

TLC R_f = 0.7 (10% ethyl acetate/hexanes) [silica gel, *p*-anisaldehyde stain]

Synthesis of three-carbon-tethered allenyl acetate 3.36.

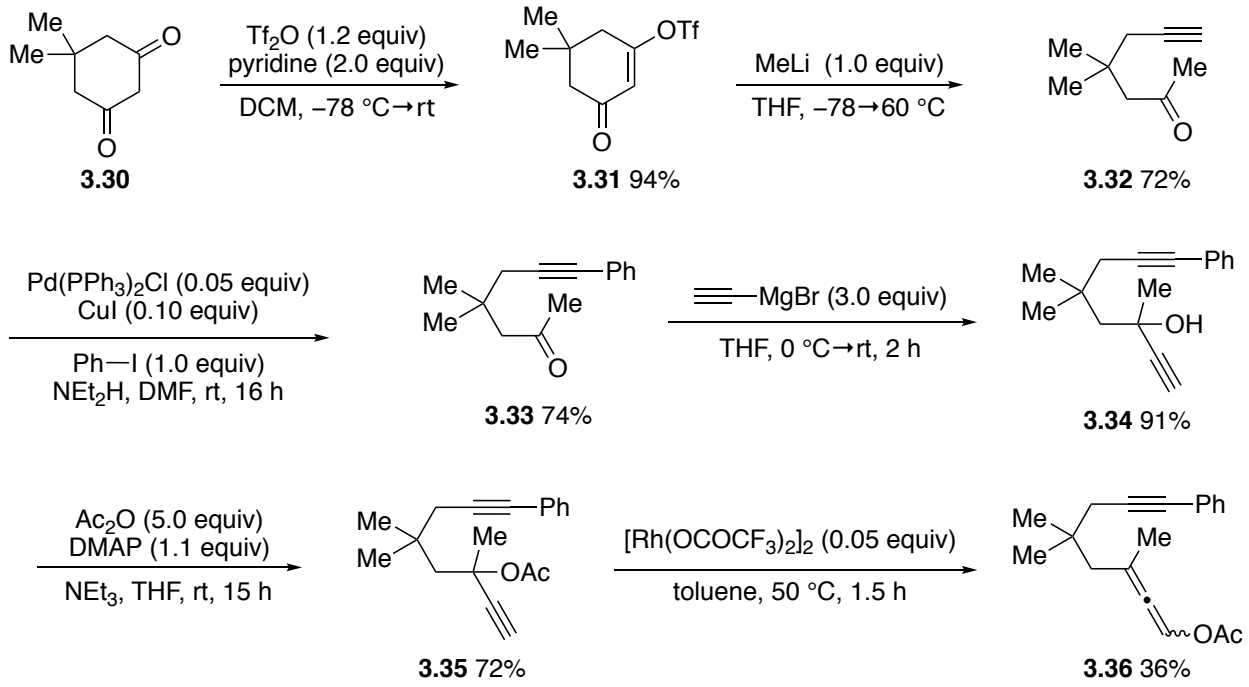

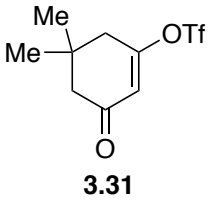

3.31

5,5-Dimethyl-3-oxocyclohex-1-en-1-yl trifluoromethanesulfonate (3.31). The synthesis of **3.31** was performed in a manner analogous to that previously reported.[134] To a two-necked, 1 L round bottomed flask equipped with a nitrogen inlet adaptor, and septum,was added dimedone (7.0 g, 0.05 mol, 1.0 equiv) and DCM (300 mL, 0.17 M). The flask was sealed with a septum and evacuated and refilled with nitrogen three times. Pyridine (8.0 mL, 0.10 mol, 2.0 equiv) was added via syringe, and the solution was cooled to -78 °C using a dry ice/acetone bath. Trifluoromethanesulfonic anhydride (10.0 mL, 0.60 mol, 0.06 mol, 1.2 equiv) was added dropwise over 10 minutes. The reaction was allowed to stir 1 h at -78 °C. The dry ice/acetone bath was removed, and the reaction was allowed to warm to rt, and stirred another 30 min, monitoring by TLC. Aqueous HCl (100 mL, 1 M, aq.)

was added to the flask, and the reaction mixture was transferred to a 500 mL separatory funnel. The organic layer was collected, and the aqueous layer was extracted with Et_2O (2 X 100 mL). The combined organic layers were washed with brine (200 mL), dried over magnesium sulfate, collected by vacuum filtration, and concentrated by rotary evaporation. The resulting red oil was purified by passing through a silica gel plug with 30% ethyl acetate/hexanes and concentrated to yield the title compound as a light-yellow oil (12.8 g, 94% yield). The product **3.31** was previously characterized and all spectral data match those reported.[134] LCP 3-160

^{1}H NMR (500 MHz, $CDCl_3$)

6.07 (t, J = 1.5 Hz, 1 H), 2.55 (d, J = 2.0 Hz, 2 H), 2.31 (s, 2 H), 1.14 (s, 6 H) ppm

^{13}C NMR 197.5, 166.1, 118.5, 50.7, 42.5, 33.5, 28.1 (2 C) ppm

TLC R_f = 0.5 (15% ethyl acetate/hexanes) [silica gel, $KMnO_4$ stain]

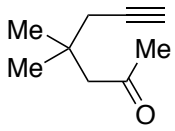

3.32

4,4-Dimethylhept-6-yn-2-one (3.32). The synthesis of **3.32** was performed in a manner analogous to that previously reported.[134] To a two-necked 500 mL round-bottomed flask, equipped with a nitrogen inlet adaptor, and septum was added vinyl triflate **3.31** (12.8 g, 47.0 mmol, 1.0 equiv) and THF (160 mL, 0.3 M). The solution was cooled to -78 °C using a dry ice/acetone bath. Methyl lithium (1.6 M in Et_2O, 29 mL, 47.0 mmol, 1.0 equiv) was added dropwise over 10 min. The reaction was stirred at -78 °C for 10 min. The dry ice/acetone bath was replaced with an ice/water bath, and the reaction stirred at 0 °C for 10 min. The ice/water bath was removed and the reaction allowed to warm to rt and stirred for 30 min. The flask was lowered into a preheated oil bath (60 °C) and stirred 30 min, monitoring by TLC. Sat'd aqueous ammonium chloride (100 mL) was added, and the mixture was transferred to

a 500-mL separatory funnel. The organic layer was isolated and washed with water (100 mL) and brine (100 mL), dried over magnesium sulfate, filtered and concentrated by rotary evaporation. The crude product (6.4 g) was purified by passing through a plug of silica gel with 20% ethyl acetate/hexanes (300 mL) and concentrated by rotary evaporation to yield the title compound as a yellow oil (4.7 g, 72%). The product **3.32** was previously characterized and all spectral data match those reported.[134] LCP 3-161

^{1}H NMR (400 MHz, $CDCl_3$)

2.48 (s, 2 H), 2.26 (dd, J = 0.8, 2.4 Hz, 2 H), 2.16, (s, 3 H), 2.00 (td, J = 0.8, 2.4 Hz, 1 H), 1.08 (s, 6 H) ppm

^{13}C NMR (100 MHz, $CDCl_3$)

208.4, 82.3, 70.5, 52.4, 33.4, 32.3, 31.4, 27.2 ppm

TLC R_f = 0.6 (15% ethyl acetate/hexanes) [silica gel, $KMnO_4$ stain]

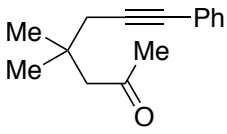

3.33

4,4-Dimethyl-7-phenylhept-6-yn-2-one (3.33). The synthesis of **3.33** was performed in a manner analogous to that previously reported.[139] To a 100-mL Schlenk flask, equipped with a nitrogen inlet adaptor and septum, was added alkyne **3.32** (4.6 g, 33 mmol, 1.0 equiv) and DMF (8.3 mL, 4.0 M). Copper(I) iodide (0.63 g, 3.3 mmol, 0.10 equiv) was added as a solid all at once. The flask was evacuated and refilled with nitrogen. Diethylamine (freshly distilled over potassium hydroxide, 33 mL, 1.0 M) was added via syringe. Tetrakis(triphenylphosphine) palladium(0) (1.9 g, 1.7 mmol, 0.05 equiv) was added as a solid, and the flask was evacuated and refilled with nitrogen. Phenyl iodide (6.8 g, 3.7 mL, 33 mmol, 1.0 equiv) was added via syringe. After 16 h at rt, complete consumption of alkyne **3.32** was observed by TLC. The reaction mixture was diluted with ether (100 mL) and transferred to a

500-mL separatory funnel. The organic layer was washed with sat'd aq ammonium chloride (150 mL), water (150 mL) and brine (150 mL), dried over magnesium sulfate, gravity filtered, and concentrated by rotary evaporation. The crude product was purified by silica gel flash column chromatography (2-10% ethyl acetate/hexanes) to yield the title compound **3.33** as a light-yellow oil (5.3 g, 74%). LCP 3-162

^{1}H NMR (400 MHz, $CDCl_3$)

7.41-7.39 (m, 2 H), 7.30-7.28 (m, 3 H), 2.53 (s, 2 H), 2.49 (s, 2 H), 2.17 (s, 3 H), 1.14 (s, 6 H) ppm

^{13}C NMR (100 MHz, $CDCl_3$)

208.6, 131.7, 128.4, 127.8, 124.0, 88.0, 82.9, 52.8, 34.1, 32.5, 32.4, 27.4 ppm

IR (thin film)

2925, 1694, 1472, 1347, 1143, 748, 685 cm^{-1}

HRMS (FTMS + p ESI)

$[M + H]^+$ calcd for $C_{15}H_{19}O$: 215.1436, found 215.1474

TLC R_f = 0.6 (15% ethyl acetate/hexanes) [silica gel, UV, *p*-anisaldehyde stain]

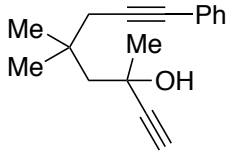

3.34

3,5,5-Trimethyl-8-phenylocta-1,7-diyn-3-ol (3.34). The synthesis of **3.34** was performed in a manner analogous to that previously reported.[71] To a two-necked, 100-mL round-bottomed flask, equipped with a nitrogen inlet adaptor and septum, was added methyl ketone **3.33**(0.80 g, 3.8 mmol, 1.0 equiv) and THF (19 mL, 0.2 M). The solution was cooled to 0 °C using an ice/water bath. Ethynylmagnesium bromide (22 mL, 0.5 M in THF, 3.0 equiv) was added via syringe, in two portions, dropwise over 10 min. The reaction was allowed to warm to rt. After 2 h at rt, complete consumption of methyl ketone **3.33** was

observed by TLC. The reaction mixture was transferred to a 250-mL separatory funnel and diluted with ether (50 mL) and water (50 mL). The organic layer was separated, and the aqueous layer was extracted with ether (2 x 50 mL). The combined organic layers were washed with brine (50 mL), dried over magnesium sulfate, gravity filtered, and concentrated by rotary evaporation. The crude product was purified by passing through a plug of silica gel (20% ethyl acetate/hexanes) to yield the title compound **3.34** as a yellow oil (0.82 g, 91%). LCP 3-163

^{1}H NMR (400 MHz, $CDCl_3$)

7.42-7.40 (m, 2 H), 7.30-7.27 (m, 3 H), 2.56 (d, J = 4 Hz, 2 H), 2.53 (s, 1 H), 2.12 (s, 1 H), 1.87 (s, 2 H), 1.58 (s, 3 H), 1.26 (s, 3 H), 1.24 (s, 3 H) ppm

^{13}C NMR (100 MHz, $CDCl_3$)

131.7 (2 C), 128.4 (2 C), 127.7, 124.1, 88.8, 88.5, 83.1, 73.0, 67.5, 52.1, 34.8, 34.0, 33.8, 28.8, 28.5 ppm

IR (thin film)

3396, 3263, 2926, 1624, 1472, 1351, 1174, 1056, 748, 684 cm^{-1}

HRMS (FTMS + p ESI)

$[M + H]^+$ calcd for $C_{17}H_{21}O$: 241.1592, found 241.1660

TLC R_f = 0.5 (15% ethyl acetate/hexanes) [silica gel, $KMnO_4$ stain]

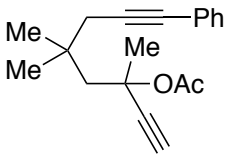

3.35

3,5,5-Trimethyl-8-phenylocta-1,7-diyn-3-yl acetate (3.35). The synthesis of **3.35** was performed in a manner analogous to that previously reported.[71] To a two-necked, 25-mL round-bottomed flask equipped with a septum and nitrogen inlet adaptor was added propargyl alcohol **3.34** (0.82 g, 3.4 mmol, 1.0 equiv). The flask was evacuated and refilled with nitrogen and triethylamine (4.9 mL, 0.7 M) and 4-

dimethylaminopyridine (DMAP, 0.46 g, 3.8 mmol, 1.1 equiv) and THF (6.0 mL) were added. The solution was cooled to 0 °C using an ice/water bath and acetic anhydride (1.6 mL, 17 mmol, 5.0 equiv) was added via syringe dropwise over 5 min. After 30 min at 0 °C, the ice/water bath was removed and the reaction mixture allowed to warm to rt. After 14 h at rt, complete consumption of propargyl alcohol **3.23** was observed by TLC. The reaction mixture was diluted with ether (50 mL) and transferred, to a 250-mL separatory funnel, and washed with sat'd aq. ammonium chloride (50 mL), water (50 mL) and brine (50 mL). The combined aqueous layers were extracted with ether (50 mL). The combined organic layers were dried over magnesium sulfate, gravity filtered, passed through a short plug of silica gel, and concentrated to yield the title compound **3.35** as a clear oil (0.70 g, 72%). LCP 3-164

^{1}H NMR (500 MHz, $CDCl_3$)

7.42-7.40 (m, 2 H), 7.31-7.27 (m, 3 H), 2.65 (s, 1 H), 2.51 (ABq, J_{AB} = 16.5 Hz, $\Delta\delta_{AB}$ = 20.7 Hz , 2 H), 2.05(ABq, J_{AB} = 15.0 Hz, $\Delta\delta_{AB}$ = 96.3 Hz , 2 H), 2.04 (s, 3 H), 1.79 (s, 3 H), 1.23 (d, J = 1.0 Hz, 6 H) ppm

^{13}C NMR (125 MHz, $CDCl_3$)

169.3, 131.7, 128.4, 127.7, 124.2, 88.5, 84.4, 82.9, 75.1, 74.4, 50.7, 34.8, 34.2, 29.5, 28.5, 28.4, 22.4 ppm

IR (thin film)

2927, 1726, 1473, 1352, 1225, 1048, 748, 684 cm^{-1}

HRMS (FTMS + p ESI)

$[M + H]^+$ calcd for $C_{19}H_{23}O_2$: 283.1698, found 283.1745

TLC R_f = 0.6 (15% ethyl acetate/hexanes) [silica gel, $KMnO_4$ stain]

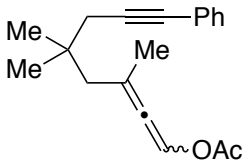

3.36

3,5,5-Trimethyl-8-phenylocta-1,2-dien-7-yn-1-yl acetate (3.36). Follows general procedure A: rhodium(II) trifluoroacetate dimer (23 mg, 0.035 mmol, 0.05 equiv), propargyl acetate **3.35** (201 mg, 0.14 mmol), toluene (3.5 mL, 0.2 M). After 90 min, complete consumption of propargyl acetate was observed by TLC. The crude product was purified by silica gel flash column chromatography (2% ethyl acetate/hexanes) to yield the title compound **3.36** as a yellow oil (72 mg, 36%). LCP 3-165

^{1}H NMR (500 MHz, $CDCl_3$)

7.41-7.39 (m, 2 H), 7.30-7.27 (m, 3 H), 2.37 (s, 2 H), 2.19 (dd, J = 6.5, 2.0, Hz, 2 H), 2.13 (s, 3 H), 1.91 (d, J = 2.0 Hz, 3 H), 1.10 (s, 6 H) ppm

^{13}C NMR (125 MHz, $CDCl_3$)

192.1, 169.0, 131.7, 128.8, 127.7, 126.0, 124.2, 112.7, 109.2, 88.3, 82.8, 46.3, 35.3, 32.7, 27.3, 23.4, 21.1 ppm

IR (thin film)

3062, 2959, 1975, 1785, 1490, 1368, 1215, 1047, 757, 692 cm^{-1}

HRMS (FTMS + p ESI)

$[M + H]^+$ calcd for $C_{19}H_{23}O_2$: 283.1693, found 283.1702

TLC R_f = 0.4 (10% ethyl acetate/hexanes) [silica gel, $KMnO_4$ stain]

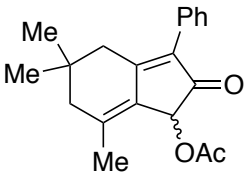

3.37

5,5,7-trimethyl-2-oxo-3-phenyl-2,4,5,6-tetrahydro-1H-inden-1-yl acetate (3.26). Follows general procedure D: allenyl acetate **3.377** (14 mg, 0.05 mmol, 1.0 equiv), rhodium(I) bis(1,5-cyclooctadiene) tetrafluoroborate (2.0 mg, 0.005 mmol, 0.10 equiv), triphenylphosphine (1.2 mg, 0.0075 mmol, 0.15 equiv), mesitylene (6.0 mg, 0.05 mmol, 1.0 equiv) DCE (0.02 M, 1.5 mL). The flask was placed in a preheated oil

bath (50 °C) under a balloon of 100% CO, and the solution stirred for 4 h. The crude product was purified by silica gel flash column chromatography (10-30% ethyl acetate/hexanes) to yield the title compound **3.36** as a yellow oil (5.1 mg, 55%) LCP 3-168

^{1}H NMR (500 MHz, $CDCl_3$)

7.44-7.39 (m, 4 H), 7.32 (tt, J = 1.5, 7.0 Hz, 1 H), 5.37 (s, 1 H), 2.58 (ABq, J_{AB} = 16.5 Hz, $\Delta\delta_{AB}$ = 51.6 Hz, 2 H), 2.21-2.08 (m, 5 H), 1.88 (s, 3 H), 1.04 (s, 3 H), 0.95 (s, 3 H) ppm

^{13}C NMR (125 MHz, $CDCl_3$)

198.8, 169.9, 165.1, 137.4, 134.2, 131.3, 129.2 (2 C), 128.8, 128.3 (2 C), 127.9, 70.8, 46.2, 39.1, 31.8, 29.5, 27.5, 20.8, 20.5 ppm

IR (thin film)

2956, 2867, 1747, 1706, 1585, 1369, 1231, 1054, 697 cm^{-1}

HRMS (FTMS + p ESI)

$[M + H]^+$ calcd for $C_{20}H_{23}O_3$: 311.1642, found 311.1649

TLC R_f = 0.2 (10% ethyl acetate/hexanes) [silica gel, $KMnO_4$ stain]

Hydrolysis of α-acyloxy cyclopentenone 2.22c to afford 3.41.

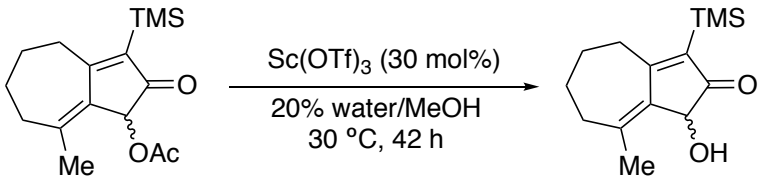

2.22c **3.41**

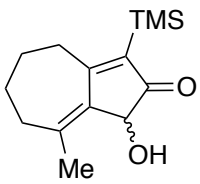

3.41

1-Hydroxy-8-methyl-3-(trimethylsilyl)-4,5,6,7-tetrahydroazulen-2(1*H*)-one (3.41). The synthesis of **3.41** was performed in a manner similar to that previously reported.[140] To a flame-dried test tube equipped with a stirbar and Teflon screw cap and nitrogen inlet needle was added scandium(III) triflluoromethane sulfonate (3.4 mg, 0.0069 mmol, 0.3 equiv) dissolved in water/MeOH (20 v/v%, 0.5mL, 0.014 M), via syringe. α-carboxy cyclopentenone **2.22c** (7.2 mg, 0.025 mmol, 1.0 equiv) was dissolved in water/MeOH (20 v/v%, 0.5 mL, 0.05 M) and added to the test tube via syringe. Complete consumption of acetate **2.22c** was observed by TLC after 42 h. The solution was diluted with water (5 mL), transferred to a separatory funnel, and extracted with DCM (3 x 5 mL). The combined organic layers were dried over magnesium sulfate, gravity filtered, and concentrated under reduced pressure to yield the title compound **3.41** as a sticky solid (5.0 mg, 81%). LCP 3-183

^{1}H NMR (500 MHz, $CDCl_3$)

4.44 (s, 1 H), 2.87 (dt, J = 15.0, 6.0 Hz, 1 H), 2.79-2.74 (m, 1 H), 2.67 (s, 1 H), 2.42 (t, J = 4.5 Hz, 2 H), 2.08 (s, 3 H), 1.88-1.77 (m, 4 H), 0.25 (s, 9 H) ppm

^{13}C NMR (125 MHz, $CDCl_3$)

210.3, 182.6, 144.6, 137.1, 135.3, 73.8, 34.3, 31.0, 26.1, 24.2, 0.0 (3 C) ppm

IR (thin film)

3412, 2934, 2863, 1680, 1522, 1248, 842 cm^{-1}

HRMS (FTMS + p ESI)

$[M + H]^+$ calcd for $C_{14}H_{23}O_2Si$: 251.1462, found 251.1463

TLC R_f = 0.4 (20% ethyl acetate/hexanes)[silica gel, *p*-anisaldehyde stain]

APKR of allenyl acetate 2.21c.

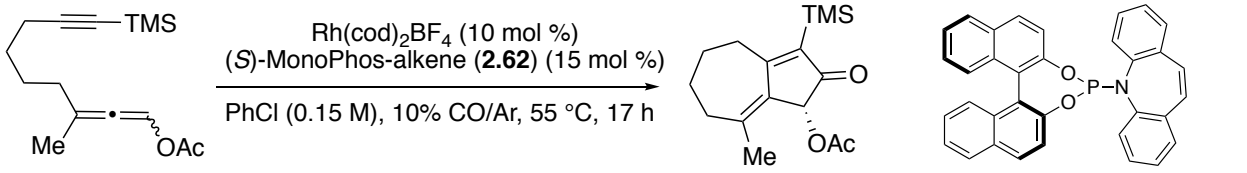

2.21c

2.22c 55%, 71% ee (*S*)-MonoPhos-alkene (**2.62**)

Follows general procedure C: Allenyl acetate **2.21c** (13 mg, 0.05 mmol, 1.0 equiv), rhodium(I) bis(1,5-cyclooctadiene) tetrafluoroborate (2.0 mg, 0.005 mmol, 0.10 equiv), (*S*)-MonoPhos-alkene (**2.62**) (3.8 mg, 0.0075 mmol, 0.15 equiv), chlorobenzene (0.15 M, 0.33 mL). The test tube was placed in a preheated oil bath (55 °C) under a balloon of 10% CO/Ar. After 17 h, consumption of allene starting material was observed by TLC. The crude product was purified by silica gel flash column chromatography (5-20% ethyl acetate/hexanes) to yield the title compound **2.22c** as a yellow oil (9.4 mg, 55%). LCB 5-074

Waters 600 HPLC, UV/PDA detector, 298 nm
Daicel CHIRALPAK-IA3, 25 cm column
0.5% *i*PrOH/hexanes, Flow rate: 1 mL/min

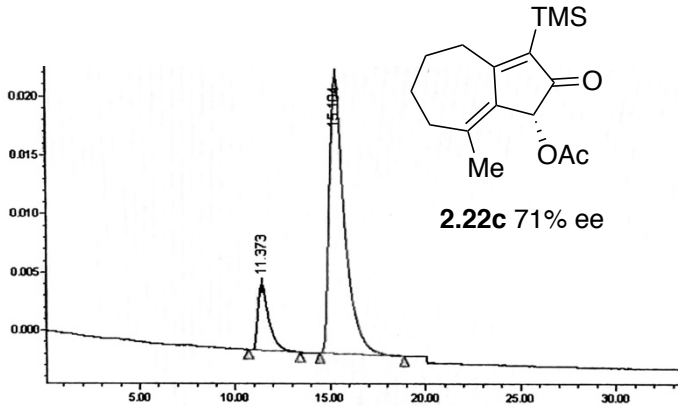

2.22c 71% ee

	Ret. Time (min)	Area (%)
Peak 1	11.373	14.64
Peak 2	15.104	85.36

APKR of allenyl acetate 2.21c.

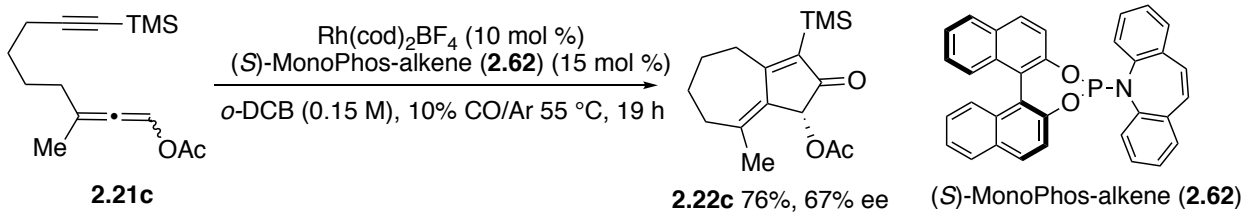

2.21c **2.22c** 76%, 67% ee (*S*)-MonoPhos-alkene (**2.62**)

Follows general procedure C: Allenyl acetate **2.21c** (13 mg, 0.05 mmol, 1.0 equiv), rhodium(I) bis(1,5-cyclooctadiene) tetrafluoroborate (2.0 mg, 0.005 mmol, 0.10 equiv), (*S*)-MonoPhos-alkene (**2.62**) (3.8 mg, 0.0075 mmol, 0.15 equiv), *o*-dichlorobenzene (0.15 M, 0.33 mL). The test tube was placed in a preheated oil bath (55 °C) under a balloon of 10% CO/Ar. After 19 h, consumption of allene starting material was observed by TLC. The crude product was purified by silica gel flash column chromatography (5-20% ethyl acetate/hexanes) to yield the title compound **2.22c** as a yellow oil (11.0 mg, 76%). LCB 5-111

Waters 600 HPLC, UV/PDA detector, 298 nm
Daicel CHIRALPAK-IA3, 25 cm column
0.5% *i*PrOH/hexanes, Flow rate: 1 mL/min

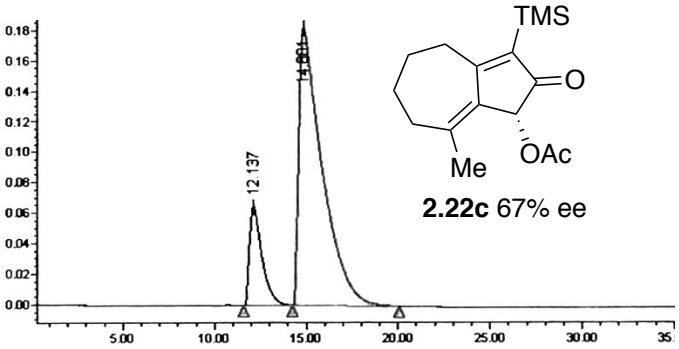

	Ret. Time (min)	Area (%)
Peak 1	12.137	16.33
Peak 2	14.881	83.67

APKR of allenyl pivalate 2.21d.

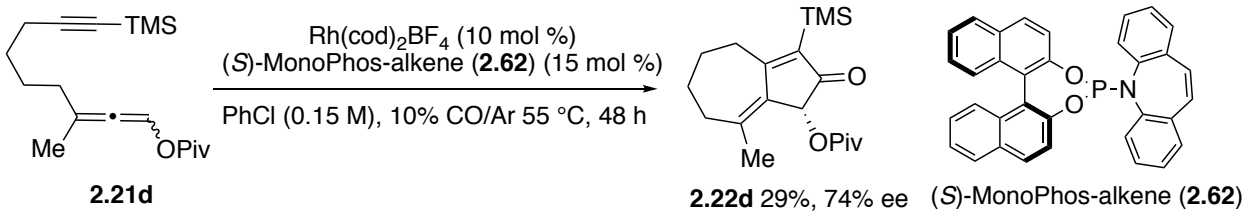

2.21d **2.22d** 29%, 74% ee (*S*)-MonoPhos-alkene (**2.62**)

Follows general procedure C: Allenyl carboxy pivalate **2.21d** (15 mg, 0.05 mmol, 1.0 equiv), rhodium(I) bis(1,5-cyclooctadiene) tetrafluoroborate (2.0 mg, 0.005 mmol, 0.10 equiv), (*S*)-MonoPhos-alkene (**2.62**) (3.8 mg, 0.0075 mmol, 0.15 equiv), chlorobenzene (0.15 M, 0.33 mL). The test tube was placed in a preheated oil bath (55 °C) under a balloon of 10% CO/Ar. After 48 h, consumption of allene starting material was observed by TLC. The crude product was purified by silica gel flash column chromatography (5-20% ethyl acetate/hexanes) to yield the title compound **2.22d** as a yellow oil (4.9 mg, 29%). LCB 5-084

Waters 600 HPLC, UV/PDA detector, 298 nm
Daicel CHIRALPAK-IA3, 25 cm column
0.3% *i*PrOH/hexanes, Flow rate: 1 mL/min

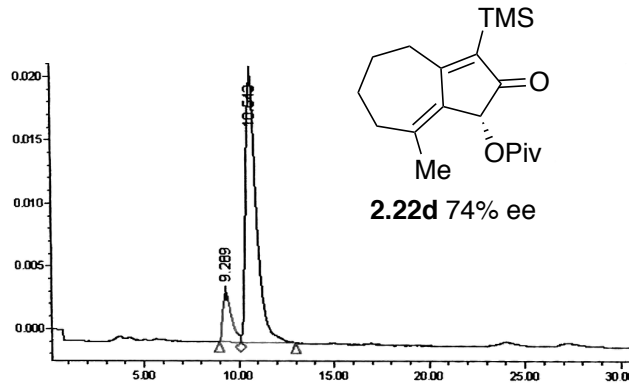

2.22d 74% ee

	Ret. Time (min)	Area (%)
Peak 1	9.289	13.11
Peak 2	10.543	86.89

APKR of allenyl benzoate 2.21f.

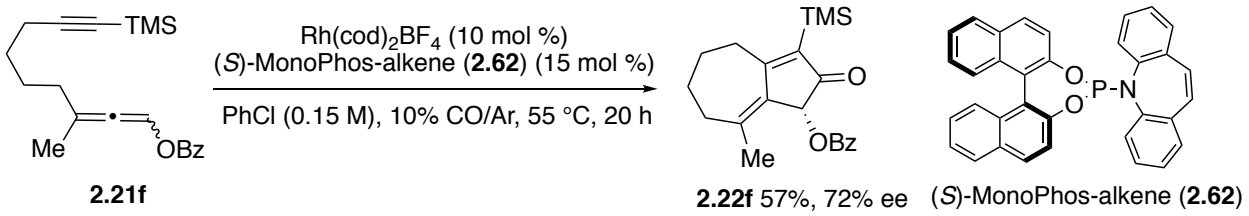

Follows general procedure C: Allenyl benzoate **2.21f** (16 mg, 0.05 mmol, 1.0 equiv), rhodium(I) bis(1,5-cyclooctadiene) tetrafluoroborate (2.0 mg, 0.005 mmol, 0.10 equiv), (*S*)-MonoPhos-alkene (**2.62**) (3.8 mg, 0.0075 mmol, 0.15 equiv), chlorobenzene (0.15 M, 0.33 mL). The test tube was placed in a preheated oil bath (55 °C) under a balloon of 10% CO/Ar. After 20 h, consumption of allene starting material was observed by TLC. The crude product was purified by silica gel flash column chromatography (5-20% ethyl acetate/hexanes) to yield the title compound **2.22f** as a yellow sticky solid (10 mg, 57%). LCB 5-083

Waters 600 HPLC, UV/PDA detector, 298 nm
Daicel CHIRALPAK-IA3, 25 cm column
0.5% *i*PrOH/hexanes, Flow rate: 1 mL/min

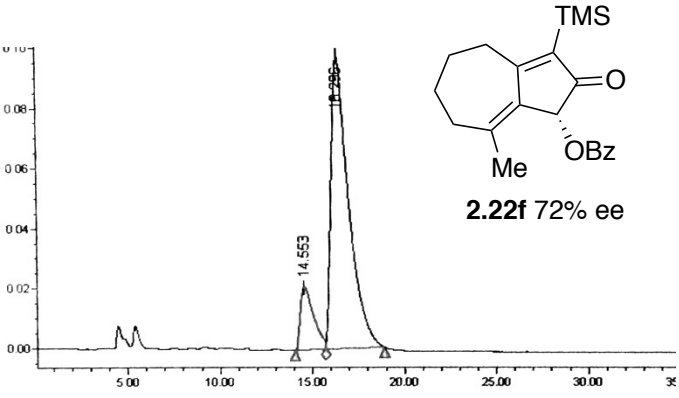

	Ret. Time (min)	Area (%)
Peak 1	14.553	14.28
Peak 2	16.296	85.72

APKR of allenyl benzoate 2.21f.

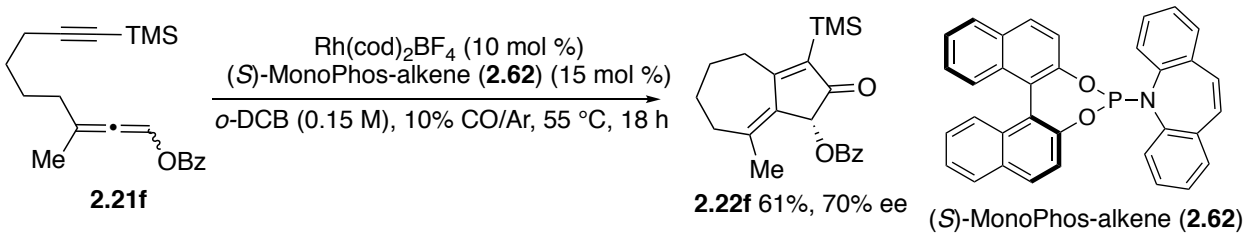

Follows general procedure C: Allenyl benzoate **2.21f** (16 mg, 0.05 mmol, 1.0 equiv), rhodium(I) bis(1,5-cyclooctadiene) tetrafluoroborate (2.0 mg, 0.005 mmol, 0.10 equiv), (*S*)-MonoPhos-alkene (**2.62**) (3.8 mg, 0.0075 mmol, 0.15 equiv), *o*-DCB (0.15 M, 0.33 mL). The test tube was placed in a preheated oil bath (55 °C) under a balloon of 10% CO/Ar. After 18 h, consumption of allene starting material was observed by TLC. The crude product was purified by silica gel flash column chromatography (5-30% ethyl acetate/hexanes) to yield the title compound **2.22** as a yellow sticky solid (10.3 mg, 61%). LCB 6-002

Waters 600 HPLC, UV/PDA detector, 298 nm
Daicel CHIRALPAK-IA3, 25 cm column
0.5% *i*PrOH/hexanes, Flow rate: 1 mL/min

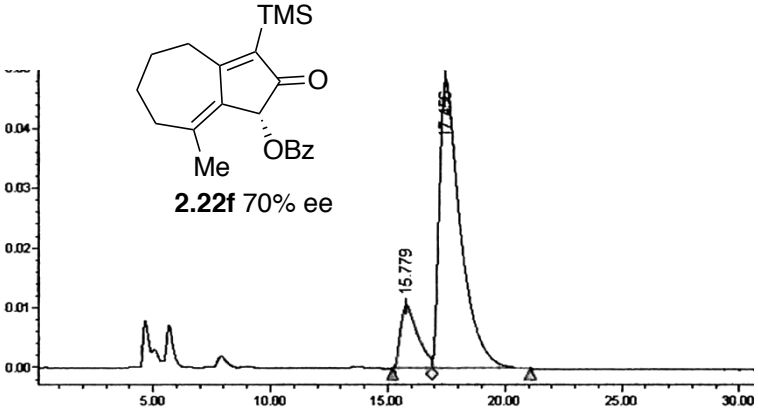

	Ret. Time (min)	Area (%)
Peak 1	15.779	15.22
Peak 2	17.456	84.78

APKR of allenyl *p*-nitrobenzoate 2.21g.

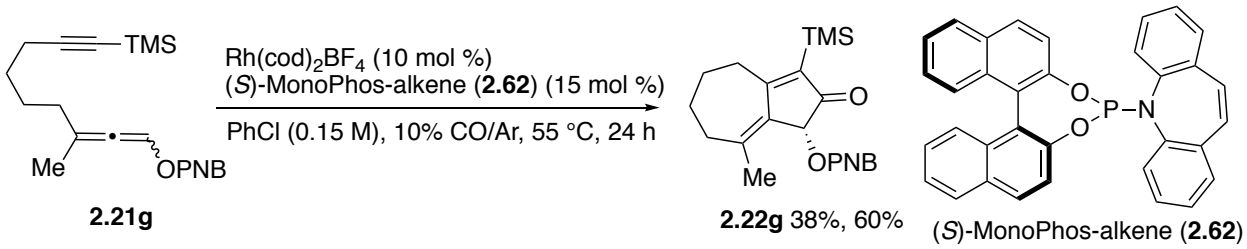

Follows general procedure C: Allenyl *p*-nitrobenzoate **2.21g** (19 mg, 0.05 mmol, 1.0 equiv), rhodium(I) bis(1,5-cyclooctadiene) tetrafluoroborate (2.0 mg, 0.005 mmol, 0.10 equiv), (*S*)-MonoPhos-alkene (**2.62**) (3.8 mg, 0.0075 mmol, 0.15 equiv), chlorobenzene (0.15 M, 0.33 mL). The test tube was placed in a preheated oil bath (55 °C) under a balloon of 10% CO/Ar. After 24 h, consumption of allene starting material was observed by TLC. The crude product was purified by silica gel flash column chromatography (5-30% ethyl acetate/hexanes) to yield the title compound **2.22g** as a yellow sticky solid (7.8 mg, 38%). LCB 5-112

Waters 600 HPLC, UV/PDA detector, 298 nm
Daicel CHIRALPAK-IA3, 25 cm column
1.0% *i*PrOH/hexanes, Flow rate: 1 mL/min

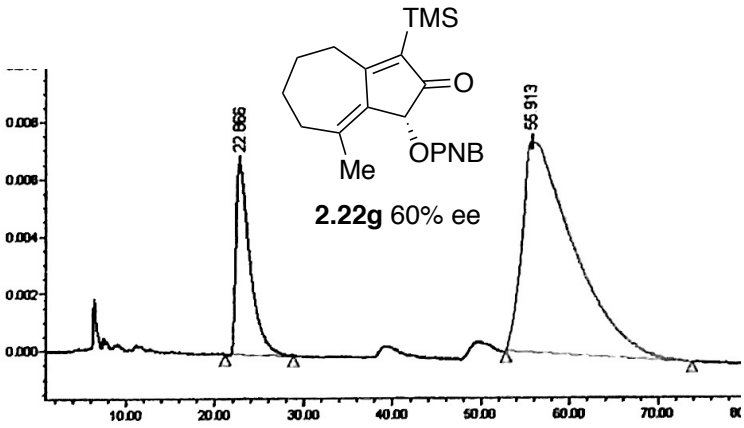

	Ret. Time (min)	Area (%)
Peak 1	22.866	19.87
Peak 2	55.913	80.13

APKR of allenyl acetate 3.21a.

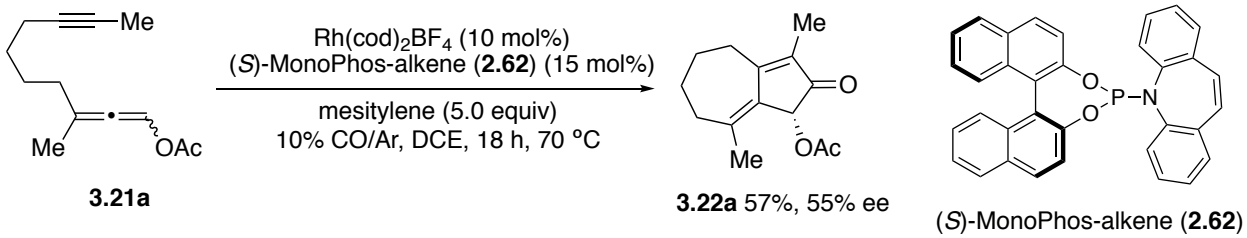

3.21a

3.22a 57%, 55% ee

(*S*)-MonoPhos-alkene (**2.62**)

Follows general procedure C: Allenyl acetate **3.21a** (10 mg, 0.05 mmol, 1.0 equiv), rhodium(I) bis(1,5-cyclooctadiene) tetrafluoroborate (2.0 mg, 0.005 mmol, 0.10 equiv), (*S*)-MonoPhos-alkene (**2.62**) (3.8 mg, 0.0075 mmol, 0.15 equiv), mesitylene (35 μL 0.25 mmol, 5.0 equiv), DCE (0.03 M, 1.7 mL). The test tube was placed in a preheated oil bath (70 °C) under a balloon of 10% CO/Ar. After 18 h, consumption of allene starting material was observed by TLC. The crude product was purified by silica gel flash column chromatography (5-20% ethyl acetate/hexanes) to yield the title compound **3.22a** as a yellow sticky solid (6.8 mg, 57%). LCP 5-131

Waters 600 HPLC, UV/PDA detector, 298 nm
Daicel CHIRALPAK-IA3, 25 cm column
0.5% *i*PrOH/hexanes, Flow rate: 1 mL/min

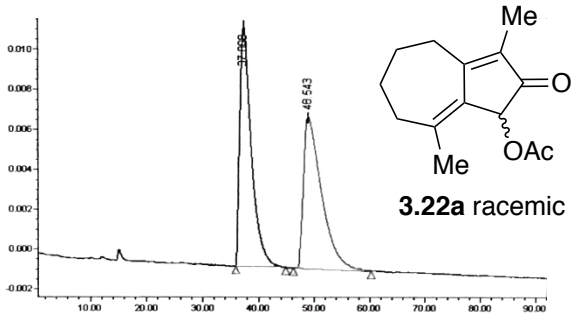

3.22a racemic

	Ret. Time (min)	Area (%)
Peak 1	37.008	49.91
Peak 2	48.543	50.09

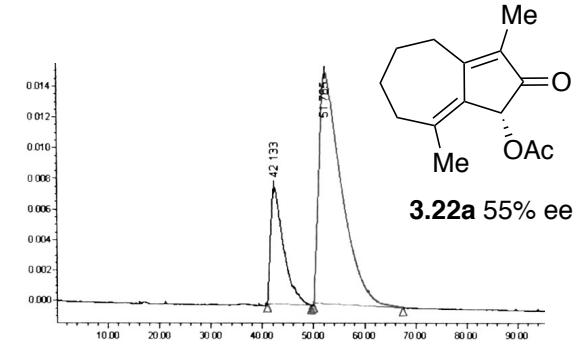

3.22a 55% ee

	Ret. Time (min)	Area (%)
Peak 1	42.133	22.45
Peak 2	51.765	77.55

APKR of allenyl acetate 3.21a.

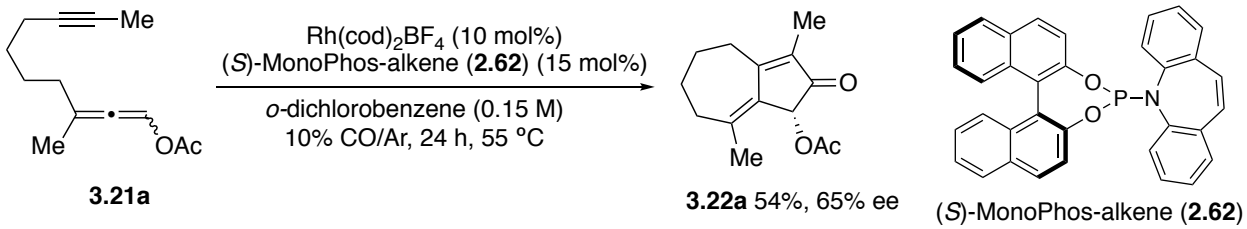

Follows general procedure C: Allenyl acetate **3.21a** (10 mg, 0.05 mmol, 1.0 equiv), rhodium(I) bis(1,5-cyclooctadiene) tetrafluoroborate (2.0 mg, 0.005 mmol, 0.10 equiv), (*S*)-MonoPhos-alkene (**2.62**) (3.8 mg, 0.0075 mmol, 0.15 equiv), *o*-dichlorobenzene (0.15 M, 0.33 mL). The test tube was placed in a preheated oil bath (55 °C) under a balloon of 10% CO/Ar. After 24 h, consumption of allene starting material was observed by TLC. Yield was determined by integral comparison to the internal standard mesitylene (54%). LCB-158

$[\alpha]^{20}_{D} = +53.1$ (*c.* = 0.58, $CHCl_3$)

Waters 600 HPLC, UV/PDA detector, 298 nm
Daicel CHIRALPAK-IA3, 25 cm column
0.5% *i*PrOH/hexanes, Flow rate: 1 mL/min

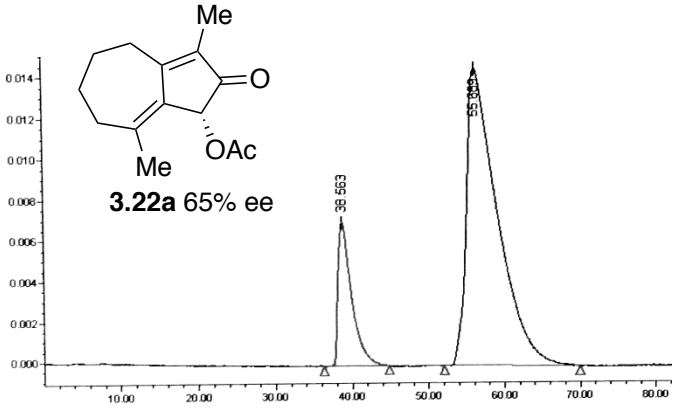

	Ret. Time (min)	Area (%)
Peak 1	38.563	17.44
Peak 2	55.689	82.56

APKR of allenyl carboxy pivalate 3.21b.

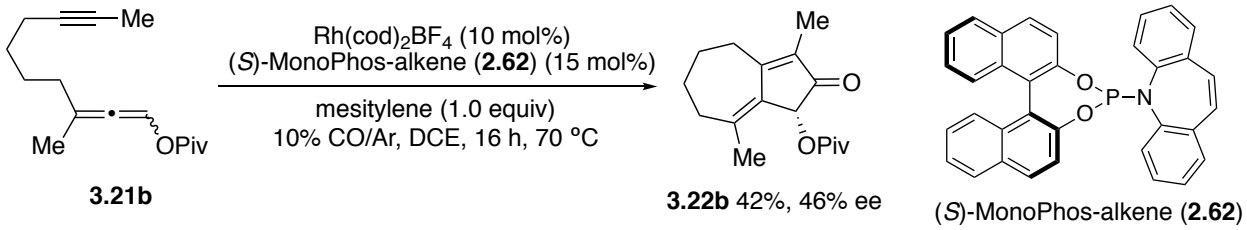

Follows general procedure C: Allenyl carboxy pivalate **3.21b** (12 mg, 0.05 mmol, 1.0 equiv), rhodium(I) bis(1,5-cyclooctadiene) tetrafluoroborate (2.0 mg, 0.005 mmol, 0.10 equiv), (*S*)-MonoPhos-alkene (**2.62**) (3.8 mg, 0.0075 mmol, 0.15 equiv), mesitylene (6.0 mg, 0.05 mmol, 1.0 equiv) DCE (0.03 M, 1.7 mL). The test tube was placed in a preheated oil bath (70 °C) under a balloon of 10% CO/Ar. After 16 h, consumption of allene starting material was observed by TLC. Yield was determined by integral comparison to the internal standard mesitylene (42%). LCB 5-198

Waters 600 HPLC, UV/PDA detector, 298 nm
DaiceChiralcel OD, 25 cm column
0.5% *i*PrOH/hexanes, Flow rate: 1 mL/min

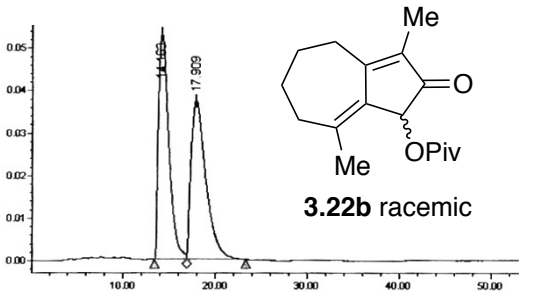

	Ret. Time (min)	Area (%)
Peak 1	14.163	49.82
Peak 2	17.909	50.18

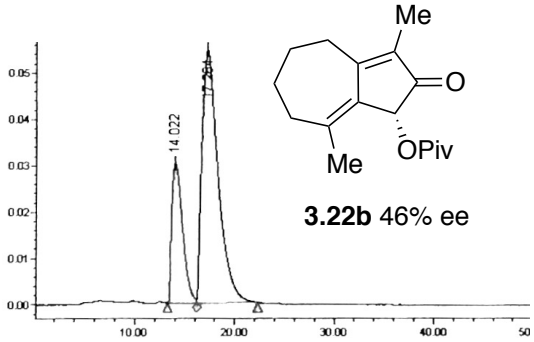

	Ret. Time (min)	Area (%)
Peak 1	14.022	27.01
Peak 2	17.264	72.99

APKR of allenyl pivalate 3.21b.

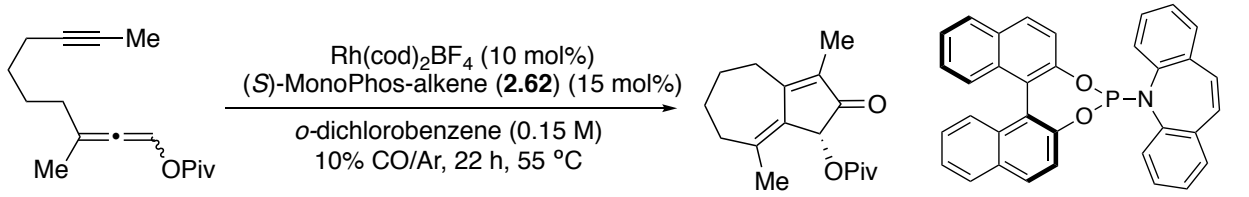

3.21b

3.22b 50%, 61% ee (*S*)-MonoPhos-alkene (**2.62**)

Follows general procedure C: Allenyl carboxy pivalate **3.21b** (25 mg, 0.10 mmol, 1.0 equiv), rhodium(I) bis(1,5-cyclooctadiene) tetrafluoroborate (4.0 mg, 0.01 mmol, 0.10 equiv), (*S*)-MonoPhos-alkene (**2.62**) (7.6mg, 0.015 mmol, 0.15 equiv), *o*-dichlorobenzene (0.15 M, 0.66 mL). The test tube was placed in a preheated oil bath (55 °C) under a balloon of 10% CO/Ar. After 22 h, consumption of allene starting material was observed by TLC. The crude product was purified by silica gel flash column chromatography (5-20% ethyl acetate/hexanes) to yield the title compound **3.22b** as a light-yellow solid (14 mg, 50%). LCB 5-204

Waters 600 HPLC, UV/PDA detector, 298 nm
DaiceChiralcel OD, 25 cm column
0.5% *i*PrOH/hexanes, Flow rate: 1 mL/min

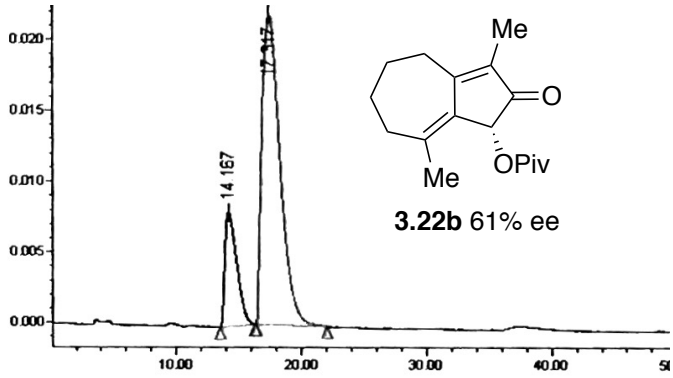

3.22b 61% ee

	Ret. Time (min)	Area (%)
Peak 1	14.167	19.41
Peak 2	17.317	80.59

APKR of allenyl benzoate 3.21c.

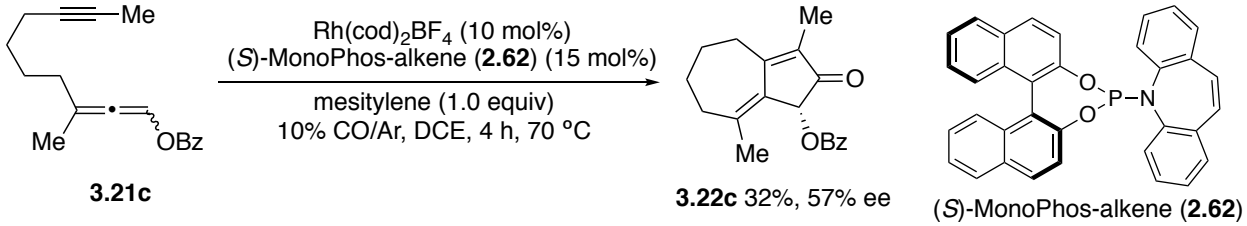

Follows general procedure C: Allenyl benzoate **3.21c** (13 mg, 0.05 mmol, 1.0 equiv), rhodium(I) bis(1,5-cyclooctadiene) tetrafluoroborate (2.0 mg, 0.005 mmol, 0.10 equiv), (*S*)-MonoPhos-alkene (**2.62**) (3.8 mg, 0.0075 mmol, 0.15 equiv), mesitylene (35 μL 0.25 mmol, 5.0 equiv), DCE (0.03 M, 1.7 mL). The test tube was placed in a preheated oil bath (70 °C) under a balloon of 10% CO/Ar. After 18 h, consumption of allene starting material was observed by TLC. Yield was determined by integral comparison to the internal standard mesitylene (32%). LCB 5-200

Waters 600 HPLC, UV/PDA detector, 298 nm
Daicel CHIRALPAK-IA3, 25 cm column
0.5% *i*PrOH/hexanes, Flow rate: 1 mL/min

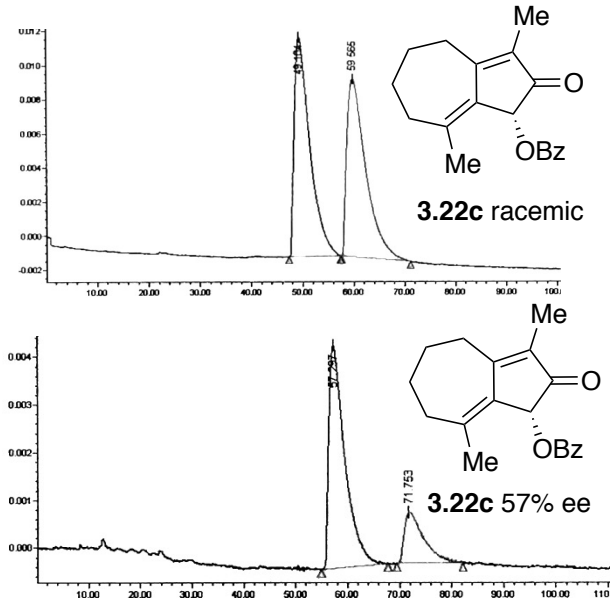

	Ret. Time (min)	Area (%)
Peak 1	49.104	50.23
Peak 2	59.565	49.77

	Ret. Time (min)	Area (%)
Peak 1	57.297	78.53
Peak 2	71.753	21.47

APKR of allenyl benzoate 3.21c.

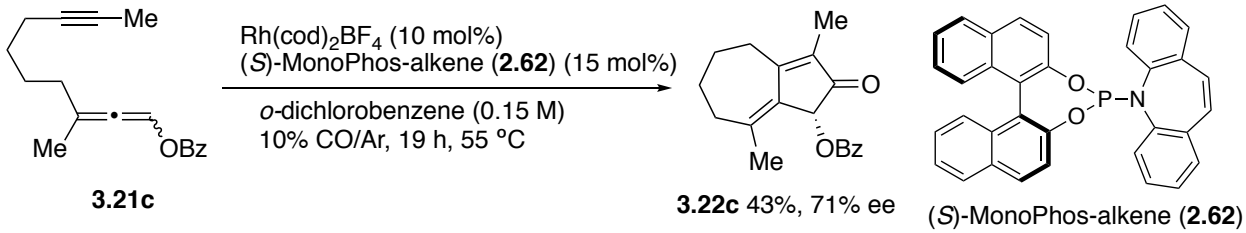

Follows general procedure C: Allenyl benzoate **3.21c** (13 mg, 0.05 mmol, 1.0 equiv), rhodium(I) bis(1,5-cyclooctadiene) tetrafluoroborate (2.0 mg, 0.005 mmol, 0.10 equiv), (*S*)-MonoPhos-alkene (**2.62**) (3.8 mg, 0.0075 mmol, 0.15 equiv), *o*-dichlorobenzene (0.15M, 0.33 mL). The test tube was placed in a preheated oil bath (55 °C) under a balloon of 10% CO/Ar. After 19 h, consumption of allene starting material was observed by TLC. Yield was determined by integral comparison to the internal standard mesitylene (43%). A proposed dimeric byproduct was isolated in 36% yield. LCB 5-159

$[\alpha]^{20}_{D} = +45.0$ (*c.* = 0.53, $CHCl_3$)

Waters 600 HPLC, UV/PDA detector, 298 nm
Daicel CHIRALPAK-IA3, 25 cm column
0.5% *i*PrOH/hexanes, Flow rate: 1 mL/min

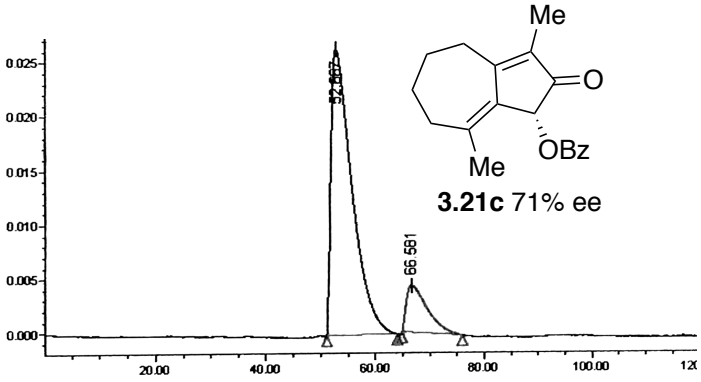

	Ret. Time (min)	Area (%)
Peak 1	52.667	85.69
Peak 2	66.581	14.31

APKR of allenyl acetate 3.25.

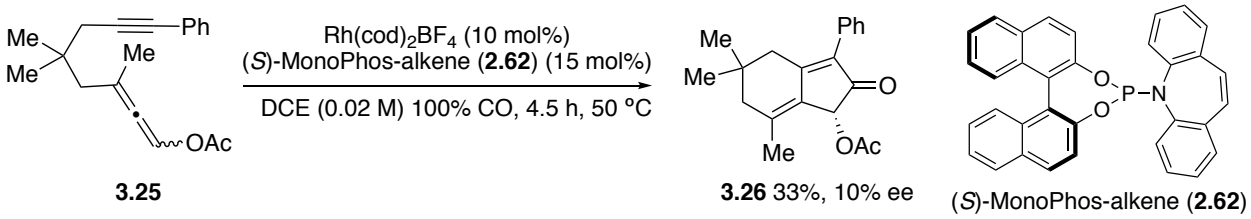

3.25 **3.26** 33%, 10% ee (*S*)-MonoPhos-alkene (**2.62**)

Follows general procedure C: Allenyl acetate **3.25** (9 mg, 0.05 mmol, 1.0 equiv), rhodium(I) bis(1,5-cyclooctadiene) tetrafluoroborate (1.2 mg, 0.003 mmol, 0.10 equiv), (*S*)-MonoPhos-alkene (**2.62**) (2.3 mg, 0.0075 mmol, 0.15 equiv), DCE (0.02 M, 1.5 mL). The test tube was placed in a preheated oil bath (50 °C) under a balloon of 100% CO. After 4.5 h, consumption of allene starting material was observed by TLC. The crude product was purified by silica gel flash column chromatography (5-30% ethyl acetate/hexanes) to yield the title compound **3.26** as a yellow sticky solid (3.1 mg, 33%). LCB 3-169

Waters 600 HPLC, UV/PDA detector, 298 nm
Daicel CHIRALPAK-IA3, 25 cm column
1.0% *i*PrOH/hexanes, Flow rate: 1 mL/min

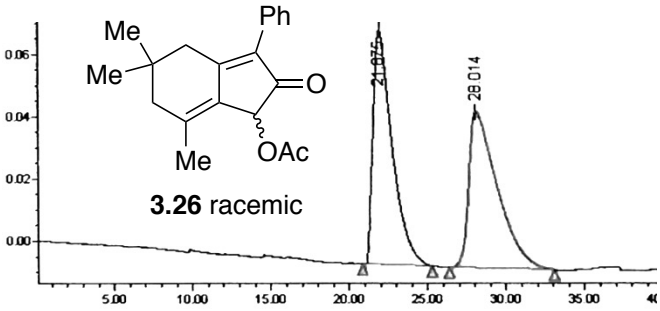

3.26 racemic

	Ret. Time (min)	Area (%)
Peak 1	21.875	50.21
Peak 2	28.014	49.79

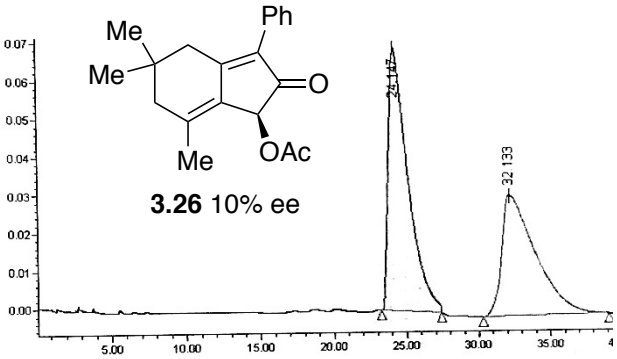

3.26 10% ee

	Ret. Time (min)	Area (%)
Peak 1	24.147	55.18
Peak 2	32.133	44.82

APKR of allenyl acetate 3.25.

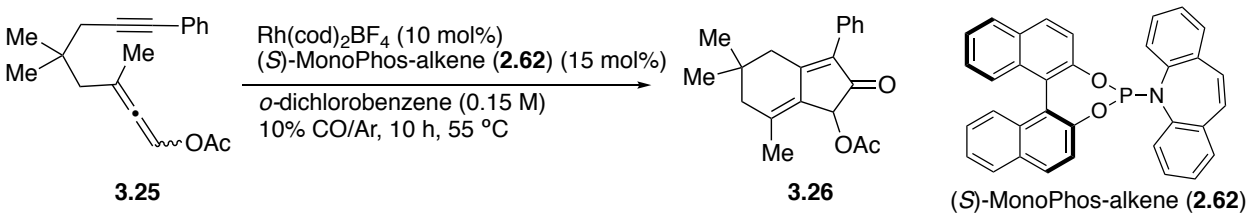

3.25 **3.26** (*S*)-MonoPhos-alkene (**2.62**)

Follows general procedure C: Allenyl acetate **3.25** (28 mg, 0.10 mmol, 1.0 equiv), rhodium(I) bis(1,5-cyclooctadiene) tetrafluoroborate (4.1 mg, 0.01 mmol, 0.10 equiv), (*S*)-MonoPhos-alkene (**2.62**) (7.6 mg, 0.015 mmol, 0.15 equiv), *o*-dichlorobenzene (0.66 mL, 0.15 M). The test tube was placed in a preheated oil bath (55 °C) under a balloon of 10% CO/Ar. After 10 h, consumption of allene starting material was observed by TLC. The crude product was purified by silica gel flash column chromatography (5-30% ethyl acetate/hexanes) to yield the title compound **3.26** as a yellow sticky solid (22 mg, 69%). LCB 5-203

Waters 600 HPLC, UV/PDA detector, 306 nm
Daicel CHIRALPAK-IA3, 25 cm column
1.0% *i*PrOH/hexanes, Flow rate: 1 mL/min

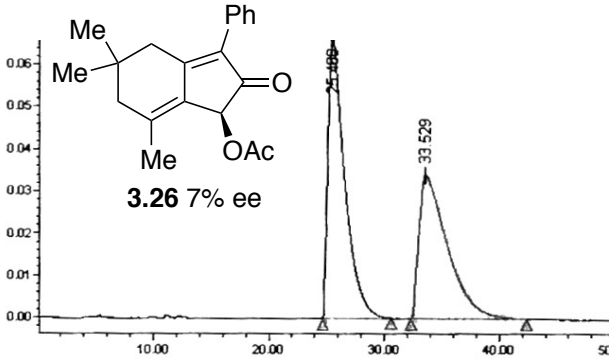

	Ret. Time (min)	Area (%)
Peak 1	25.468	53.59
Peak 2	33.529	46.41

Determination of the stereoretention of the hydrolysis product 3.54. Enantioenriched α-acyloxy cyclopentenone **2.22c** (64% ee) was subjected to $Sc(OTf)_3$ -catalyzed hydrolysis. The resulting α-hydroxy cyclopentenone **3.54** enantiomers were separated by HPLC using a Daicel CHIRALPAK-IA3 column. LCP 3-192

Waters 600 HPLC, UV/PDA detector, 298 nm
Daicel CHIRALPAK-IA3, 25 cm column
0.5% *i*PrOH/hexanes, Flow rate: 1 mL/min

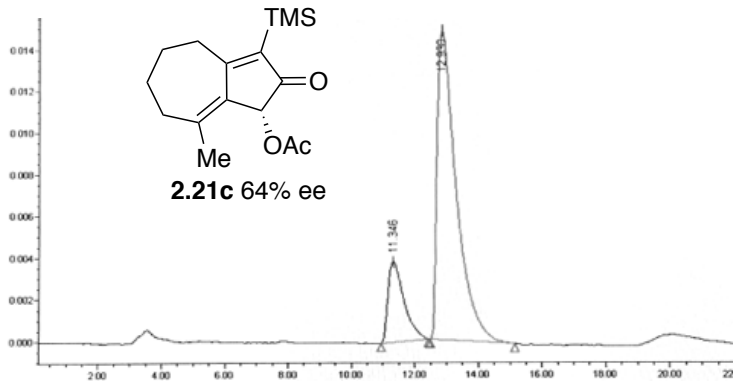

	Ret. Time (min)	Area (%)
Peak 1	11.346	17.90
Peak 2	12.938	82.10

Waters 600 HPLC, UV/PDA detector, 298 nm
Daicel CHIRALPAK-IA3, 25 cm column
0.5% *i*PrOH/hexanes, Flow rate: 1 mL/min

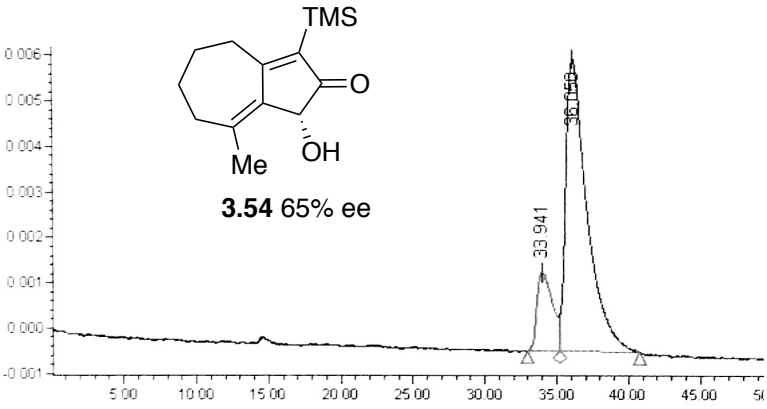

	Ret. Time (min)	Area (%)
Peak 1	33.941	16.49
Peak 2	36.050	83.51

4.0 EXPERIMENTAL AND COMPUTATIONAL MECHANISTIC STUDIES OF THE ENANTIOSELECTIVE PAUSON-KHAND REACTION OF 1,6-ENYNES.

The synthesis of complex natural products having, or involving as intermediates, cyclopentenones has been realized through diastereoselective Co- and Rh-catalyzed Pauson–Khand reactions.[141] Additionally, Rh has been identified as an effective catalyst for the enantioselective PKR (Section 1.3.7).[75, 142] However, a Rh-catalyzed enantioselective PKR has not been used to establish absolute stereochemistry in a total synthesis, and an enantioselective Co-catalyzed PKR has only been applied once in a total sysnthesis.[143-144] Further, the enantioselective Rh-catalyzed PKR is limited to 1,6-enynes having O, NTs or $C(CO_2Et)_2$ tethers, a limitation which challenges the general utility of this reaction.[145]

We propose that a detailed understanding of the PKR mechanism, coupled with an investigation of new chiral catalysts, can lead to the development of new catalytic conditions applicable to an expanded substrate scope. DFT calculations offer the ability to examine catalytic mechanisms in detail, however, the complexity of enantioselective transition metal-catalyzed reactions makes it difficult to make predictions with a high level of accuracy.[91] Specifically, the PKR is a hallmark of complexity with four distinct intermediates in the progression from precursor to product. The complexity of the reaction affords opportunities for accessing alternative products via interruption and pathway divergence; however, it is for this reason that the PKR is highly sensitive to the reaction conditions.[146] Therefore, we sought to study the mechanism of the enantioselective Rh-catalyzed PKR using a combination of experiments and DFT calculations. In this way, calculations could be verified by experiment, and experiments guided by calculations.

Atropisomeric *bidentate* phosphine ligands are the most widely applied ligands in the enantioselective Rh-catalyzed PKR. [142] These catalysts have been studied extensively, with experiments probing solvent effects,[147] ligand electronic effects,[148] and internal chelation by various tethers.[149] Although these *bidentate* ligands are generally considered to be more effective chiral ligands because of their lower conformational freedom,[150] we have shown the first and only example of an enantioselective Rh-catalyzed PKR of a substrate that is not a 1,6-enyne using a *monodentate* phosphoramidite ligand.[114] In a single report, *monodentate* phosphoramidites were shown to afford enantioselectivities up to 84% in the Rh-catalyzed PKR of 1,6-enynes, but the mechanism of these catalysts in the PKR of enynes remains unexplored.[99] Because of these initial successes of monodentate phosphoramidites, and the limited substrate scope of Rh-bisphosphine catalysts, we propose that a detailed study of Rh-phosphoramidite catalysts in the PKR is needed. Phosphoramidites are significantly more π-accepting and less sterically demanding than bisphosphine ligands and could therefore show significant deviations in their effect on mechanistic steps. For example, because of their lower steric demand, we hypothesize that phosphoramidite ligand class could enable coordination of more sterically demanding substrates. A comparative study of the bisphosphine and phosphoramidite ligand classes could identify advantages and disadvantages of each catalyst system, so that catalysts can be rationally designed for a given substrate.

Herein, we report a comparison of the ligand effects of (*R*)-BINAP (**2.24**) and (*S*)-MonoPhos (**2.27**) on the mechanism of the Rh(I)-catalyzed PKR. (*R*)-BINAP (**2.24**) was chosen because of its previous success in the enantioselective PKR, and its low conformational freedom, which simplifies computational analysis. (*S*)-MonoPhos (**2.27**) was chosen because it is the simplest member of the phosphoramidite class, and afforded high yields in the enantioselective

PKR of allene-ynes.[114] We focused our study on a well-known substrate, *O*-tethered 1,6-enyne **1.50** which generally affords excellent yields and ee's in the PKR across different ligand classes.

This report represents the first computational study of the cationic Rh-catalyzed enantioselective PKR of 1,6-enynes using chiral phosphorous ligands.[114, 151] In addition, we report the first computational and experimental mechanistic study of PKR using a monodentate phosphoramidite ligand. The effects of ligand identity on reaction rate and enantioselectivity were compared both experimentally and computationally. In addition, we demonstrate the first PKR of a 1,6-enyne using a hybrid phosphine-phosphoramidite ligand (*S*)-MeAnilaPhos (**2.50**).

4.1 LIGANDS AND SUBSTRATES IN THE PKR OF ENYNES.

4.1.1 Ligands in the enantioselective PKR of enynes.

All ligands previously applied in the PKR of enynes are shown in Figure 31. The majority of these ligands are atropisomeric bisphosphine ligands; however, several other classes have been demonstrated as well. The first enantioselective PKR was effected using (*S*)-BINAP (**2.24**) and cationic Rh catalyst in THF.[75] Soon thereafter, (*S*)-tol-BINAP (**4.1**) was applied in the enantioselective PKR using cinnamaldehyde as a CO source.[152] (*S*)-tol-BINAP (**4.1**) was effective under neutral Rh(I) conditions at high reaction temperatures (120 °C). Bis-pyridyl ligand (*S*)-P-Phos (**4.2**) is an efficient ligand in water as a solvent with cinnamaldehyde as a CO source.[153] In 2005, the spirocyclic phosphoramidite ligand (*R*)-SIPHOS (**2.42**) was demonstrated in the PKR by Zhou and coworkers.[99] (*R*)-SIPHOS (**2.42**) was the first monodentate phosphoramidite ligand to be applied in the PKR. The spirocyclic bisphosphine derivative of (*R*)-SIPHOS (**2.42**), (*R*)-SDP

(**4.4**) was also applied in the enantioselective PKR with marginally improved yields and enantioselectivities over (*R*)-SIPHOS (**2.42**).[154] (*S*)-SynPhos, which has a narrower dihedral angle than BINAP gave good ee's for some *O*-tethered substrates.[148] A more electron deficient ligand, (*S*)-Difluorphos (**4.6**) afforded high yields for NTs-tethered substrates.[148] The more sterically bulky ligand (*R*)-3,5-diC_6H_4-BINAP (**4.7**) effected the PKR in high enantioselectivities, and in many cases, at room temperature.[155] The relatively electron rich, biphenyl ligand (*S*)-DTBM-MeO-BINAP (**4.8**) affords higher yields and enantioselectivities for $C(CO_2Et)_2$ -tethered enynes.[156] Most recently, (*R*)-MaxPhos, a P-stereogenic ligand with a wide bite angle was applied in the PKR. This ligand is most efficient in reactions with *N*-tosyl-tethered enynes.[157]

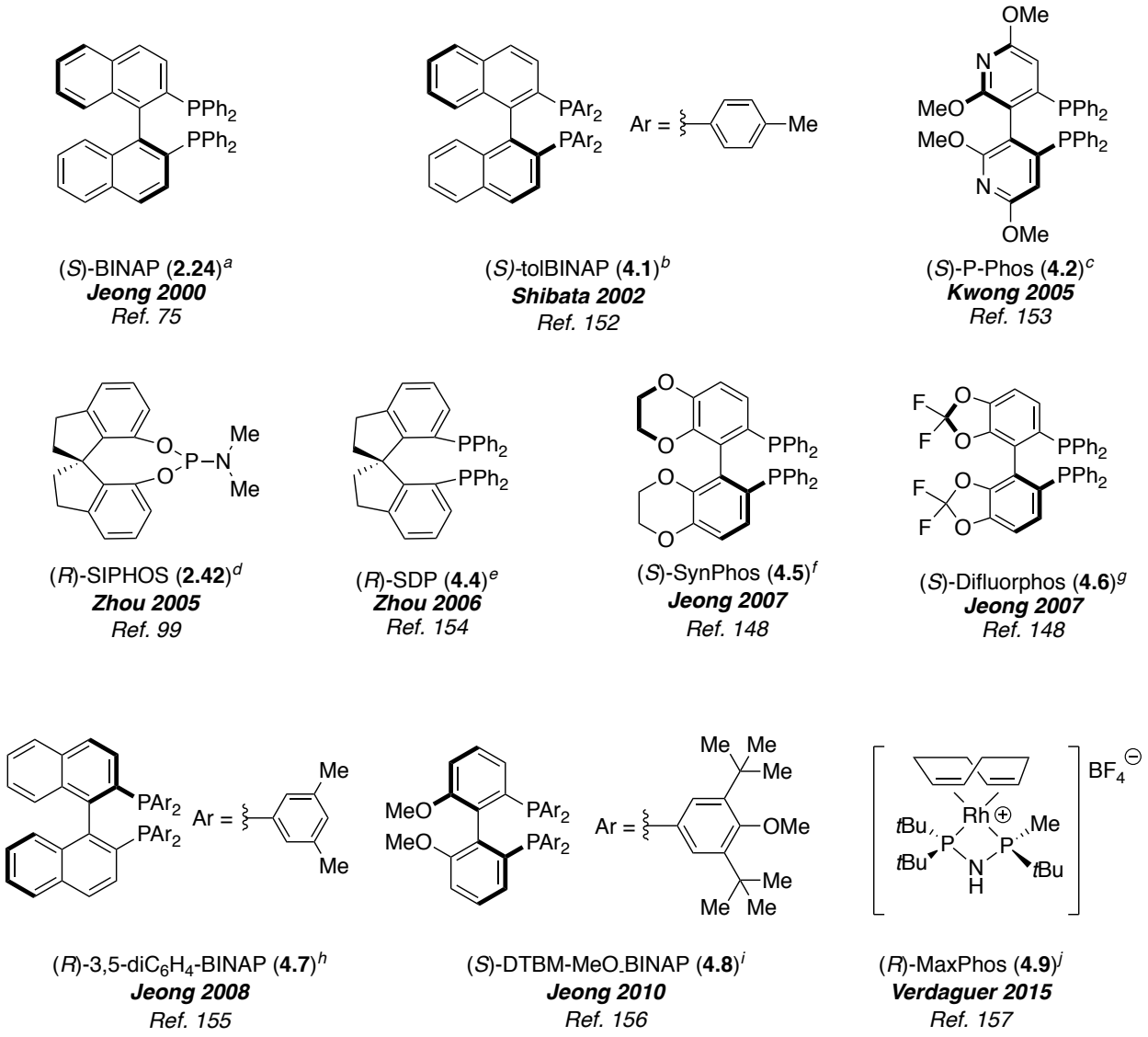

Figure 31. Ligands applied in the enantioselective Rh-catalyzed PKR of enynes.

[a] $[Rh(CO)_2Cl]_2$ AgOTf, THF, CO, 90-130 °C [b] $[Rh(cod)Cl]_2$, cinnamaldehyde, 120 °C [c] $[Rh(cod)Cl]_2$, cinnamaldehyde, water, 100 °C [d] $[Rh(CO)_2Cl]_2$, $AgSbF_6$, DCE, CO, 90 °C [e] $[Rh(CO)_2Cl]_2$, $AgSbF_6$, DCE, CO, 90 °C [f] $[Rh(cod)Cl]_2$, cinnamaldehyde, *t*-amyl alcohol, 100 °C MW [g] $[Rh(CO)_2Cl]_2$, AgOTf, THF, CO, 80 °C [h] $[Rh(CO)_2Cl]_2$, AgOTf, THF, CO, 80 °C [i] $[Rh(CO)_2Cl]_2$, AgOTf, THF, 10: 1 Ar : CO [j] Rh-(*R*)-MaxPhos, CO, DME, 120 °C

4.1.2 Scope of the Pauson−Khand reaction of enynes.

Even within the limited substrate scope of O-, N-tosyl-, and $C(CO_2Et)_2$ -tethered 1,6-enynes, no single catalyst system can give high yields and enantioselectivity for all substrates. Table 36 shows the complete substrate scope of all ligands reported in the enantioselective, Rh(I)-catalyzed PKR.

Table 36. Scope of the enantioselective Rh(I)-catalyzed PKR.

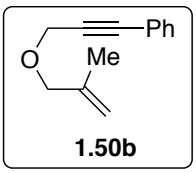

1.50b

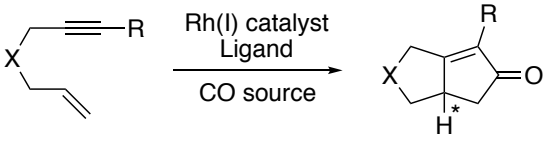

	Yield (%), ee (%)
	≥90, ≥98
	≥90, ≥90
	≥80, ≥80

Entry	X	R		**2.24**	**4.1**	**4.2**	**2.42**	**4.4**	**4.5**	**4.6**	**4.7**	**4.8**	**4.9**
1	O	Ph	**1.50a**	88, 81	-	82, 84	56, 84	80, 81	73, 89	81, 87	99, 92	92, 92	35, 67
2	O	Ph	**1.50b**	-	41, 82	71, 90	-	-	-	-	-	-	-
3	O	4-CH_3Ph	**1.50c**	-	-	92, 88	44, 80	56, 86	-	-	95, 90	-	-
4	O	4-CH_3OPh	**1.50d**	-	86, 81	93, 93	37, 82	86, 82	-	70, 91	82, 92	92, 95	-
5	O	4-CF_3Ph	**1.50e**	-	-	-	46, 77	96, 78	-	80, 90	99, 84	95, 84	-
6	O	4-F-Ph	**1.50f**	-	-	90, 82	-	-	52, 87	-	-	-	-
7	O	4-Cl-Ph	**1.50g**	-	82, 79	91, 77	-	-	73, 82	-	95, 90	-	-
8	O	4-NO_2Ph	**1.50h**	-	-	-	62, 56	96, 70	-	-	-	-	-
9	O	2-ClPh	**1.50i**	-	-	-	-	-	-	-	-	99, 77	-
10	O	3,5-diCH_3Ph	**1.50j**	-	-	-	-	83, 69	-	-	-	-	-
11	O	3,5-diCF_3Ph	**1.50k**	-	-	-	-	99, 74	-	-	-	-	-
12	O	2-thienyl	**1.50l**	-	-	-	-	-	58, 90	-	-	-	-
13	O	CH_3	**1.50m**	40, 96	-	82, 95	-	-	-	38, 98	44, 99	90, 99	-
14	O	Et	**1.50n**	-	-	-	-	-	60, 95	-	-	-	-
15	O	C_4H_9	**1.50o**	60, 65	-	-	-	-	-	-	-	-	-
16	O	allyl	**1.50p**	-	-	-	-	-	-	-	-	83, 86	-
17	O	H	**1.50q**	-	-	-	-	-	-	-	18, 99	94, 98	-
18	NTs	Ph	**4.15a**	93, 74	99, 56	96, 80	58, 62	95, 77	53, 80	90, 70	99, 72	96, 91	62, 82
19	NTs	4-CH_3OPh	**4.15b**	-	-	-	-	-	-	90, 75	99, 75	90, 93	-
20	NTs	4-CF_3OPh	**4.15c**	-	-	-	-	-	-	90, 71	-	96, 99	-
21	NTs	CH_3	**4.15d**	80, 84	-	98, 88	-	95, 75	-	62, 89	96, 98	90, 99	55, 81
22	NTs	allyl	**4.15e**	-	-	-	-	-	-	-	-	94, 84	-
23	NTs	H	**4.15f**	-	-	-	-	-	-	-	27, 99	94, 60	-
24	$C(CO_2Me)_2$	Ph	**4.16a**	78, 42	79, 45	-	-	-	-	-	-	-	-
25	$C(CO_2Me)_2$	Me	**4.16b**	91, 62	-	-	-	-	-	-	-	-	-
26	$C(CO_2Et)_2$	Ph	**4.16c**	67, 61	-	-	73, 47	82, 50	-	-	40, 68	98, 93	-
27	$C(CO_2Et)_2$	4-CH_3OPh	**4.16d**	-	-	-	-	-	-	-	98, 74	91, 91	-
28	$C(CO_2Et)_2$	4-CF_3Ph	**4.16e**	-	-	-	-	-	-	-	96, 63	99, 87	-
29	$C(CO_2Et)_2$	CH_3	**4.16f**	70, 70	-	91, 77	-	92, 65	40, 89	-	50, 96	55, 70	16, 72
30	$C(CO_2Et)_2$	allyl	**4.16g**	-	-	-	-	-	-	-	-	62, 75	-
31	$C(CO_2Et)_2$	H	**4.16h**	-	-	-	-	-	-	-	60, 99	82, 91	39, 79
32	$C(CO_2iPr)_2$	Ph	**4.16i**	80, 58	-	-	-	-	-	-	-	-	-
33	$C(CO_2iPr)_2$	CH_3	**4.16j**	40, 90	-	-	-	-	-	-	-	-	-
34	CH_2	Ph	**4.16k**	61, 51	-	-	-	-	-	-	-	-	-

One of the most widely applied substrates in the enantioselective PKR is Ph-substituted, O-tethered enyne **1.50a**. Bulky, electron-rich ligands (*R*)-3,5-diC_6H_4-BINAP (**4.7**) and (*S*)-DTBM-MeO-BIPHEP (**4.8**) afforded highest yields and enantioselectivities for this substrate (Table 36, entry 1). The enantioselective PKR of methyl-substituted alkene **1.50b** was demonstrated using (*S*)-tol-BINAP (**4.1**) and dipyridyldiphosphane (*S*)-P-Phos (**4.2**) (entry 2). This substrate **1.50b** remains the only enyne demonstrated in the enantioselective PKR which contains a methyl substituent on the alkene group. Various substitutions in the *para*-position of the aryl alkyne were all well-tolerated, including methyl- **1.50c**, methoxy- **1.50d**, trifluoromethyl- **1.50e**, fluoro- **1.50f**, and chloro- **1.50g**- substituents (entries 3-7), however, the strongly electron-withdrawing nitro group in the *para* position of **1.50h** afforded product in lower enantioselectivities (entry 8). 2-Thienyl-alkyne **1.50l** reacted in lower yield (58%) but high enantioselectivity (90%) with *(S)*-SynPhos (**4.5**) (entry 12)**.** Methyl-alkyne **1.50m** was tested in reactions with five different ligands, and in all cases, cyclopentenone product was obtained in over 95% ee (entry 13). The highest combined yield and enantioselectivity of **1.50m** was achieved using (*S*)-DTBM-MeO-BIPHEP (**4.8**), which afforded product in 90% yield and 99% ee. Ethyl-substituted alkyne **1.50n** was tested in the PKR using (*S*)-SynPhos (**4.5**) and provided product in 60% yield and 95% ee (entry 14). The high enantioselectivities observed in reactions of methyl **1.50m** and ethyl **1.50n** alkynes were not observed in the PKR of an *n*-butyl substituted alkyne. In the PKR using (*S*)-BINAP (**2.24**)**,** *n*-butyl-alkyne **1.50o** reacted in 60% yield and 65% ee (entry 15). An allyl group on the alkyne (**1.50p**) gave PKR product in 83% yield and 86% ee. Finally, terminal alkyne **1.50q** affords a high yield (94%) and enantiopure product (99% ee) in the reaction with (*S*)-DTBM-MeOBINAP (**4.8**) (entry 17).

The PKR of NTs-tethered Ph-alkyne substrate **4.15a** has been tested as a model system in every report of a new PKR ligand (entry 18). This substrate **4.15a** affords yields of over 90% in seven out of the ten ligands reported. Enantioselectivites for this substrate **4.15a** are generally moderate (56- 82% ee), except in the case of (*S*)-DTBM-MeO-BINAP (**4.8**), which afforded *NTs*-cyclopenenone product in 91% ee (entry 18). *p*-Methoxy (**4.15b**) and *p*-trifluoromethoxy (**4.15c**) substitutions on the phenyl group also afforded high yields and ee's when (*S*)-DTBM-MeO-BINAP (**4.8**) ligand was employed (entries 19 and 20). Methyl-substituted alkyne **4.15d** affords high enantioselectivities when bulky bisphosphine ligands (*R*)-3,5-diC_6H_4-BINAP (**4.7**) and (*S*)-DTBM-MeO-BINAP (**4.8**) (95-99% ee) were applied (entry 21). Allyl-alkyne **4.15e** was tested once using (*S*)-DTBM-MeO-BINAP (**4.8**) ligand and the reaction proceeded in 94% yield and 84% ee (entry 22). Terminal alkyne **4.15f** gave high enantioselectivity (99% ee) but low yield (27%) in the PKR using (*R*)-3,5-diC_6H_4-BINAP (**4.7**) (entry 23).

The majority of carbon-tethered PKR substrates contain diester groups to enhance reactivity. Methyl diesters **4.16a** and **4.16b** gave low enantioselectivities in the PKR using (*S*)-BINAP (**2.24**) (42 and 62% ee, respectively, entries 24 and 25). Ethyl diesters gave improved results in reactions with certain alkyne substituents. For example, in reaction with (*S*)-DTBM-MeO-BINAP (**4.8**), phenyl (**4.16c**), *p*-methoxyphenyl (**4.16d**), and *p*-trifluoromethylphenyl (**4.16e**) alkynes afforded product in high yields (>91%) and ee's (93, 91, and 87% ee, respectively, entries 26-28). Methyl-substituted alkyne **4.16f** gave high enantioselectivity (91% ee) at the expense of yield (50%) in the PKR with (*R*)-3,5-diC_6H_4-BINAP (**4.7**) (entry 29). Allyl alkyne **4.16g** reacted in 62% yield and 75% ee in the PKR with (*S*)-DTBM-MeO-BINAP (**4.8**) (entry 30). Terminal alkyne afforded enantiopure product (99% ee) in the reaction with (*R*)-3,5-diC_6H_4-BINAP (**4.7**) (entry 31). Isopropyl esters were only tested using (*S*)-BINAP (**2.24**) ligand. Ph-

alkyne **4.16i** afforded product in 80% yield and 58% ee, while methyl-alkyne **4.16j** afforded product in 40% yield and 90% ee (entries 32 and 33). Methylene-tethered enyne **4.16k** reacted in the PKR with (*S*)-BINAP (**2.24**), providing cyclopentenone product in 61% yield and 51% ee (entry 34).

In summary, the PKR of O and NTs-tethered enynes affords products in high yields and enantioselectivities across a variety of alkyne substitutions. In general, the sterically bulky bisphosphine ligands (*R*)-3,5-diC_6H_4-BINAP (**4.7**) and (*S*)-DTBM-MeO-BINAP (**4.8**) provide the highest enantioselectivities for these substrates. (*S*)-DTBM-MeO-BINAP (**4.8**) also provides good yields and enantioselectivities in the PKR of carbon-tethered enynes. Although many of these model systems perform well using these ligands, only one example of a substituted alkene (**1.50b**), and one example of a methylene-tethered enyne **4.16k** has only been tested in the enantioselective PKR. We propose that alternative catalyst systems to complement the enantioselective bisphosphines should be further studied in order to expand the substrate scope of the PKR.

4.2 PREVIOUS MECHANISTIC STUDIES OF BISPHOSPHINE LIGANDS IN THE RHODIUM(I)-CATALYZED PKR OF ENYNES.

4.2.1 Accepted general mechanism of the PKR of 1,6-enynes.

A general mechanism of the enantioselective PKR has been proposed previously, and we used this as our starting point for our computational studies (Scheme 48).[158] The cationic catalyst exists in equilibrium as a mixture of solvent- and carbon-monoxide coordinated species **4.17**, **4.18** and **4.19**. Coordination of 1,6-enyne **1.50g** to active catalyst **4.19** affords complex **4.20**, and oxidative

cyclization gives Rh(III) metallacycle **4.21**. Subsequent CO insertion affords Rh(III)-acyl complex **4.22**, followed by reductive elimination and product dissociation, which provide the desired cyclopentenone product **1.51g**.

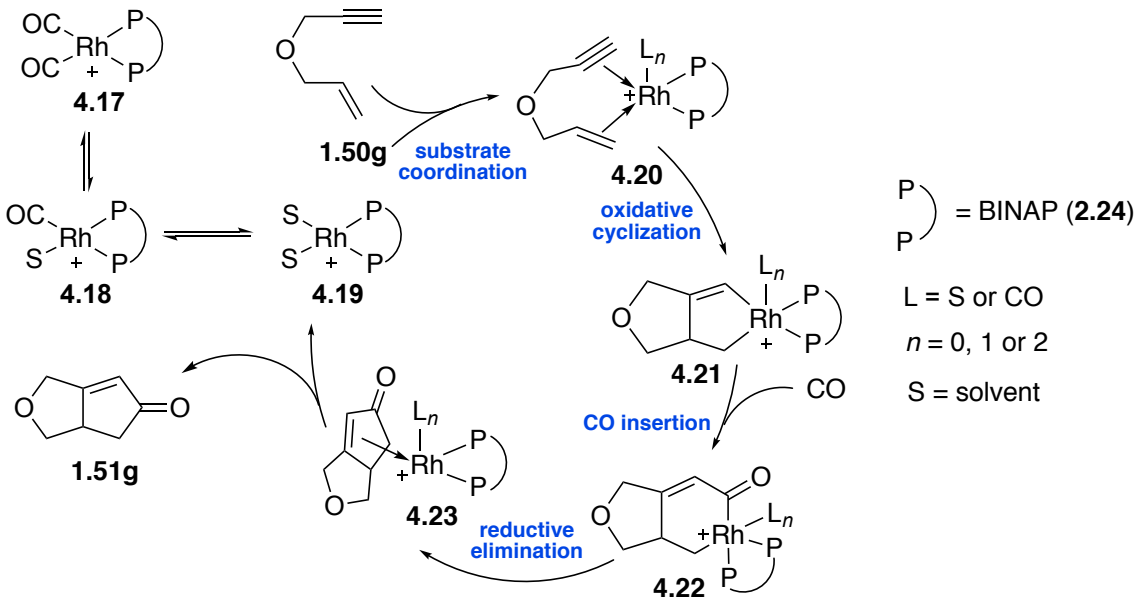

Scheme 48. Mechanism of the enantioselective cationic Rh-BINAP-catalyzed PKR.

4.2.2 Investigation of the role of solvent coordination.

Previous experimental studies have probed the structure of the PKR transition state. For example, Jeong and coworkers investigated the role of solvent coordination in the PKR transition state. The authors observed that the PKR using THF as a solvent proceeded rapidly and at low temperature when coordinating solvent (THF) was employed.[147] Under 10% CO/Ar atmosphere in THF, the PKR of **1.50** proceeds in 80% yield and 90% ee in only 1 h at 30 °C (Table 37, entry 1). Because the coordinating solvent THF afforded higher ee's than less coordinating solvents such as toluene,

the authors hypothesized that THF was coordinating to the Rh catalyst and facilitating the reaction. In order to test whether THF was coordinated to Rh during the enantioselectivity-determining transition state, a series of test reactions were performed using a chiral THF derivative, (+)-(*S*)-2-methyltetrahydrofuran **4.24** as a solvent.[147] In the PKR using (*R*)-BINAP (**2.24**) as a ligand and (+)-(*S*) **4.24** as a solvent, product (*R*)-**1.51** was obtained in 93% ee, which is approximately the same ee as obtained in the reaction with THF as a solvent (compare entries 1 and 2). Next, the reaction with (+)-(*S*)- **4.24** was performed with (*S*)-BINAP (**2.24**) as a ligand. The (*S*)-product **1.51** was obtained, again in similar enantioselectivity (91% ee) as the reaction performed in THF (90% ee). The observation of the same degree of enantioselectivity upon changing the ligand configuration indicated that there were no relevant diastereomeric interactions occurring between the ligand and the chiral solvent. The absence of any change in product ee upon use of the chiral solvent demonstrated that the solvent is not coordinated to Rh in the enantioselectivity determining step. Instead, the coordinating THF solvent could be serving to displace CO from the resting catalyst to enable substrate coordination.

Table 37. Experiment reported by Jeong testing solvent coordination.

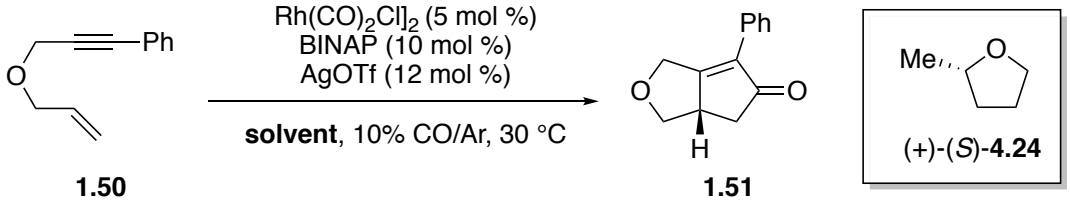

1.50 **1.51**

entry	Solvent	BINAP	time (h)	yield (%)	ee (%)
1	THF	*R*	1	80	90, *R*
2	(+)-(*S*)-**4.24**	*R*	3	62	93, *R*
3	(+)-(*S*)-**4.24**	*S*	3	60	91, *S*

4.2.3 Proposed inactivity of $Rh(CO)_2$-bisphosphine catalysts.

The PKR using Rh-bidentate phosphine ligands has been investigated in detail through various experimental mechanistic studies. Consiglio and coworkers examined the structure of the active PKR catalyst using ^{31}P NMR. Initial rate studies showed a minus 2 order with respect to CO pressure (in the range of 0.75-2.55 bar).[132] Therefore, the authors hypothesized that the CO-dissociation to enable solvent coordination was rate determining. This hypothesis was tested by reacting the [Rh(cod)(*R*)-BiPhemp (**4.25**)]OTf catalyst dissolved in deuterated methanol in an NMR tube with hydrogen to remove the cod ligand (not shown) and provide the solvent-coordinated complex **4.27**, which was readily observed by ^{31}P NMR (Scheme 49, a). Addition of substoichiometric enyne **4.16h** afforded the substrate-bound complex **4.28**, which upon exposure to CO at −70 °C, provided product **4.26h** in 90% ee. The low temperature at which the PKR proceeded (−70 °C) demonstrates the high reactivity of the solvent-bound catalyst **4.27**. Alternatively, when the solution was placed under CO prior to substrate addition, the CO-bound complexes **4.29** and **4.30** were observed by ^{31}P NMR (Scheme 49, b), and addition of enyne **4.16h** to the solution of CO-bound complexes **4.29** and **4.30** gave no reaction. Taken together, these experiments suggest that the rate of the reaction is governed by the distribution of starting catalyst species **4.27**, **4.29** and **4.30**. Therefore, we included this step in our computational mechanistic considerations.

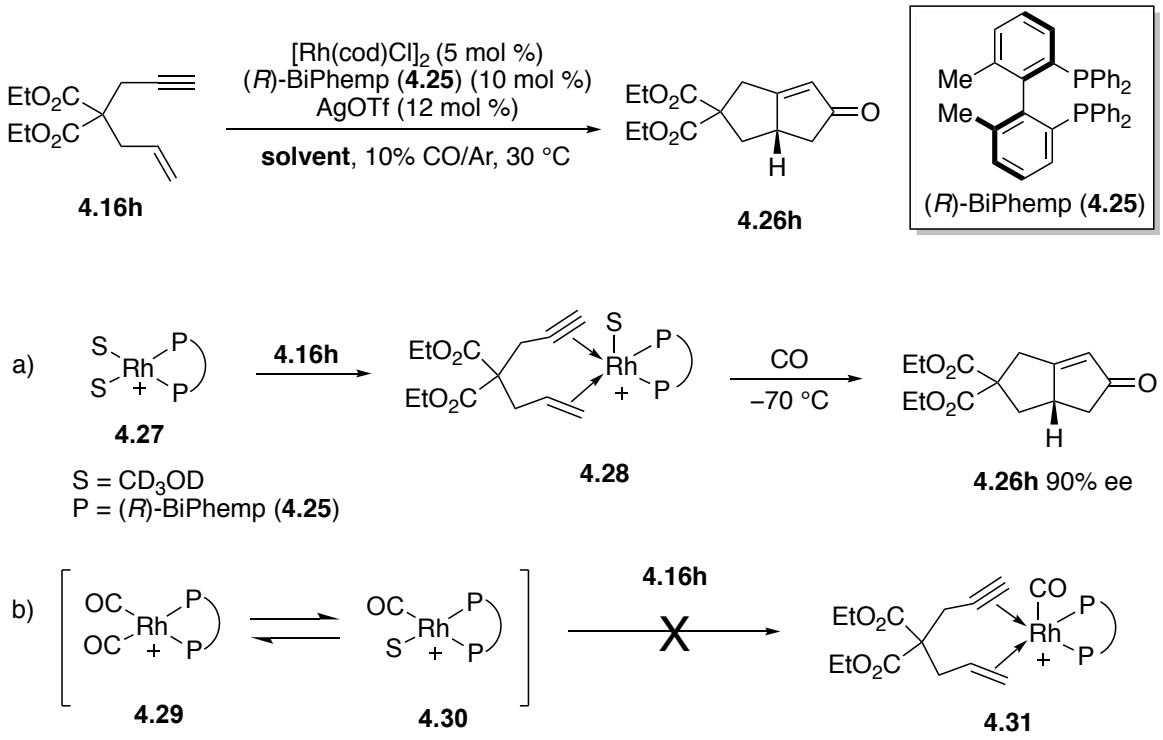

Scheme 49. Experiment demonstrating reactivity of solvent-bound PKR resting catalyst.

4.2.4 Proposed internal chelation by oxygen.

Another experimental study which addressed the structure of PKR reactive intermediates was performed by Jeong to elucidate the role of the enyne tether. Enyne substrates with oxygen tethers react faster in the PKR than other substrates.[155] For example, in a competition where equimolar amounts of O-tethered enyne **1.50,** NTs-tethered enyne **4.15a**, and $C(CO_2Et)_2$-tethered enyne **4.16c** were reacted in THF with $[Rh(CO)_2Cl]_2$ and (*R*)-3,5-xylylBINAP (**4.7**) for 2 h. The O-tethered product **1.51** was obtained in 86% yield, while the NTs and $C(CO_2Et)_2$ –tethered reacted in only 15 and 6% yield, respectively (Scheme 50). At the conclusion of the experiment, 85 and 93% of unreacted NTs and $C(CO_2Et)_2$ enynes were recovered. In addition to the enhanced reactivity

observed for the O-tethered substrate **1.50**, the enantioselectivity of this substrate was also superior. Product **1.51** was obtained in 87% ee, while the NTs and $C(CO_2Et)_2$ products **4.32a** and **4.26c** were obtained in 68 and 77% ee, respectively. A proposed explanation for the faster reaction and higher enantioselectivity of the O-tethered substrate **1.50** is that the oxygen can coordinate to Rh more efficiently than the NTs or $C(CO_2Et)_2$ groups. This interaction, which is illustrated in Figure 32, would serve to increase the reaction rate by facilitating substrate coordination, and enhance the rigidity of the enantio-determining transition state, thus improving enantioselectivity. Several additional experiments were conducted to rule out alternative explanations for the rate and enantioselectivity increase, but ultimately, it is difficult to prove or disprove this proposed tether chelation interaction using experiments. DFT calculations can provide lowest-energy catalyst structures which can help elucidate the role of the oxygen tether in the PKR mechanism.

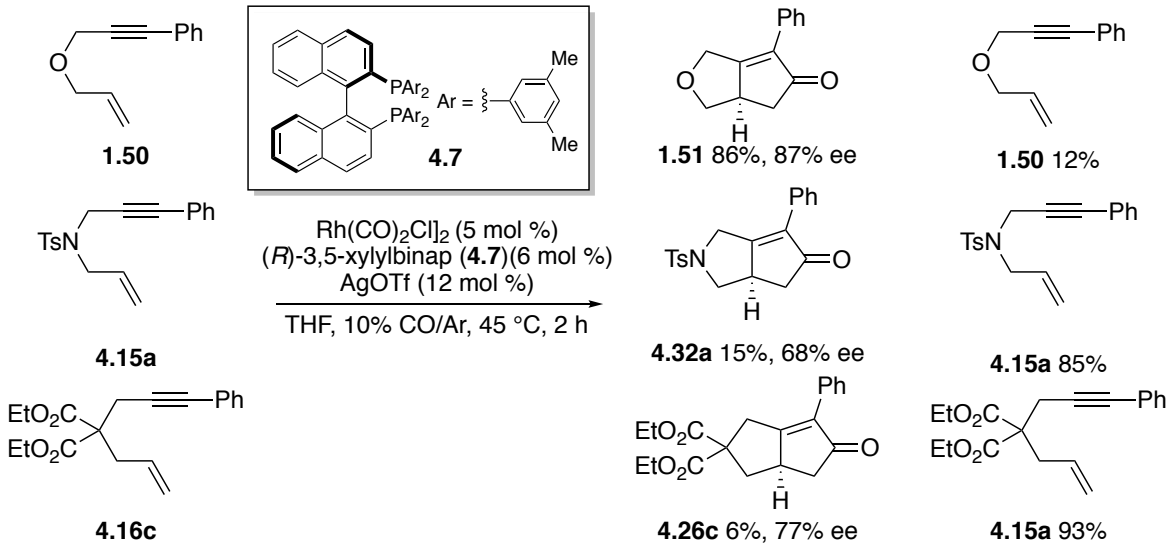

Scheme 50. Experiment comparing reactivity of O-, NTs- and $C(CO_2Et)_2$-tethered enynes.

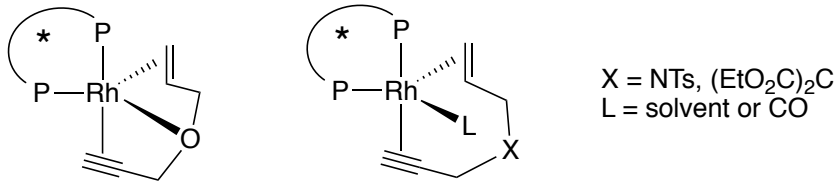

Figure 32. Proposed chelation of oxygen tethers in PKR.

4.2.5 Previous mechanistic experiments investigating the effect of ligand electron density on the identity of the rate-determining step.

Jeong and coworkers examined the effect of ligand electron donating ability on the reaction in an effort to determine which mechanistic step, substrate coordination or oxidative cyclization, was rate determining. The authors reasoned that electron-donating phosphine ligands would facilitate oxidative cyclization by increasing the electron density on the forming Rh(III) species but would hinder substrate coordination by increasing back-bonding to CO (therefore increasing the energy needed to displace CO with the substrate). Alternatively, electron withdrawing phosphine ligands would facilitate substrate coordination and hinder oxidative cyclization. A series of six ligands differing in their electron donating ability, as quantified by their ^{31}P NMR shifts, were tested in the PKR to elucidate the rate-determining step (Table 38). Electron donating ligand (*S*)-**4.33** with para-methoxy phenyl groups on the phosphorus reacted quickly (0.5 h) but in lower yield and ee (67% yield, 64% ee, Table 38, entry 1). When more deshielded phosphorous ligands were employed, the reaction slowed and product was afforded in higher yields and ee's (~90% yield, 90% ee, entries 4-6). Because electron-donating ligands afforded faster reaction, the authors concluded that oxidative cyclization is the rate-determining step of the PKR of enyne **1.50**.

Table 38. Study of ligand electronic effects in the PKR.

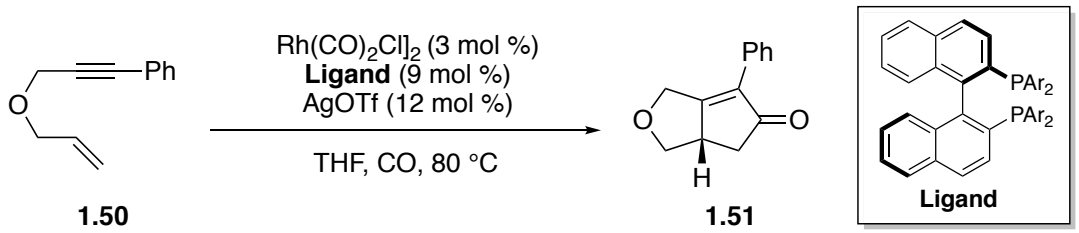

entry	Ar	ligand	^{31}P NMR shift	time (h)	Yield (%)	ee (%)
1	4-$MeOC_6H_4$	(*S*)-**4.33**	−16.9	0.5	67	64
2	4-MeC_6H_4	(*S*)-**4.34**	−15.8	1	78	86
3	Ph	(*S*)-**2.24**	−14.4	1.5	72	85
4	4-CF_3H_4	(*S*)-**4.35**	−13.8	3	89	90
5	3-$CF_3C_6H_4$	(*S*)-**4.36**	−13.7	3.5	90	90
6	3,5-$Me_2C_6H_4$	(*S*)-**4.7**	−13.6	3	89	90

In this study of ligand electronic effects, the authors state that the outcome of the enantioselective PKR can be modulated substantially by tuning the electronic effects of the ligand. More deshielded ligands afforded higher yields and enantioselectivities. In this study, however, the ligands tested were limited to phosphine ligands, and spanned a small range of electron donating ability (δ ^{31}P = −16.9 to −13.6). A more thorough look at the significantly more deshielded phosphoramidite ligands (δ ^{31}P = 125 to 145 ppm) could reveal novel and effective PKR catalysts.

4.3 COMPUTATIONAL STUDIES OF THE ENANTIOSELECTIVE RHODIUM-CATALYZED PKR

4.3.1 Substrate coordination energies of Rh-BINAP catalysts.

As a first step in our efforts towards gaining a more rigorous understanding of the mechanism of the asymmetric PKR, the reaction energy profile for Rh-BINAP catalyzed PKR was investigated using DFT calculations. We used the previously proposed mechanism of the PKR as the starting point for our computational studies (Scheme 48). The complexity of the PKR is evidenced by the first step of the reaction: coordination of enyne **1.50** to the rhodium catalyst. To determine the energy required for this step, one needs to know the structural identity of the Rh complex to which the enyne is binding. Structural conformation is complicated by the Rh-BINAP complexes existing in solution as a number of interconverting species with a distribution that is dependent upon CO atmosphere, solvent coordinating ability and choice of Rh-precatalyst. To establish the identity of the initial Rh-complex to which the enyne coordinates, ground state calculations were performed on four different Rh-BINAP catalysts, where X = CO **4.37a**, 1,5-cyclooctadiene (cod) **4.37b**, THF **4.37c** and DCE, **4.37d** (Scheme 51). These ligands were selected to represent a range of coordinating abilities, with CO being a strongly coordinating Rh ligand and DCE being a weakly coordinating Rh ligand, to establish the relative energies of these species.

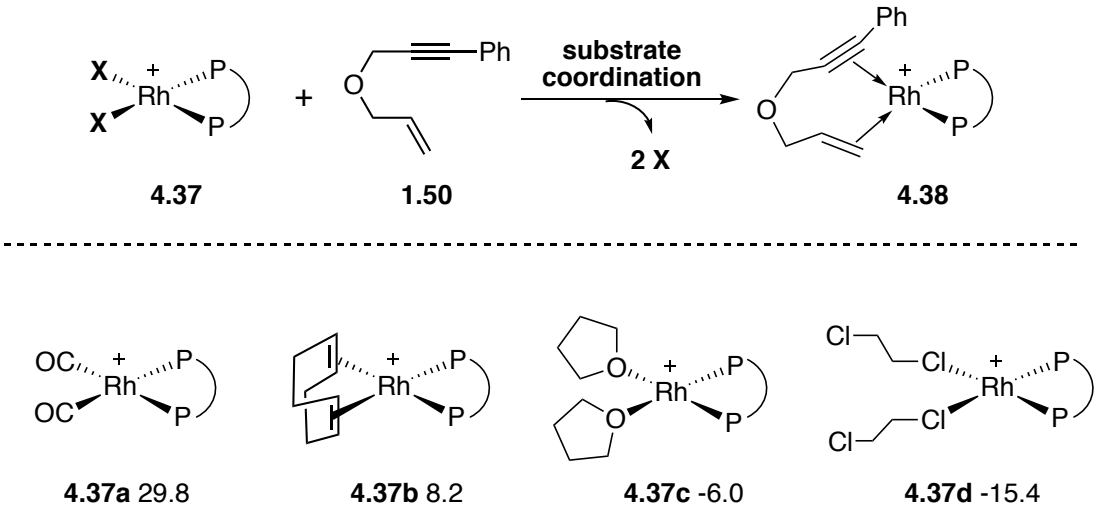

Scheme 51. Substrate coordination energies of Rh-BINAP catalysts.

The calculated energies required for substrate coordination to these four complexes are depicted in Scheme 51. The CO-bound Rh-BINAP complex **4.37a** requires 29.8 kcal/mol of energy for the replacement of two CO ligands with enyne **1.50**; while the cod ligand of complex **4.37c** can be replaced with only 8.2 kcal/mol of energy. Replacement of two THFs of **4.37c** by the substrate **1.50** is energetically favored by 6.0 kcal/mol; while replacement of two DCEs of **4.37d** is favored by 15.4 kcal/mol.

These calculated values reflect the relative coordinating ability of these ligands (CO > cod > THF > DCE) and in turn illustrate the importance of the starting catalyst identity on the reaction energy profile.[117] For example, it can be assumed based upon these relative energies that the Rh-DCE complex **4.37d** does not exist in the presence of CO and does not contribute to the reaction pathway. Further, the CO-bound catalyst **4.37a** is highly stable and is likely the resting state of the Rh catalyst. Under certain reaction conditions, coordination to this species could be rate-determining. Previous experimental studies by Jeong have demonstrated the importance of CO atmosphere and solvent on the rate of the PKR, with lower CO atmospheres, (10% CO, 90%

Argon) showing significantly faster reaction rates. The authors invoked an equilibrium shift of the resting state of the catalyst from CO-bound to solvent-bound complexes.[155]

4.3.2 Calculated reaction energy profile of the cationic Rh-(*R*)-BINAP catalyzed PKR.

Next, the relative energies of the remaining PKR transition states and intermediates were calculated. These calculations were performed using a correction for CO atmosphere (0.1 atm CO), solubility of CO in DCE (0.0055 M),[159] and a thermal correction for temperature (80 °C). Because substrate coordination can proceed from several different structures, the energies of subsequent steps are reported relative to the substrate-coordinated complex **4.38** (Scheme 52). The first step following substrate coordination, the oxidative cyclization step, can proceed with Rh being either four- or five-coordinated. We hypothesized that the oxidative cyclization step would proceed through the five-coordinated, 18-electron complex **4.41-TS**. This hypothesis was based upon two previous computational studies wherein the PKR proceeded via a five-coordinated transition state: a neutral Rh-catalyzed PKR of a 1,6-enyne,[151] and the cationic Rh-catalyzed enantioselective PKR of an allene-yne.[114] Here, our calculations show that the five-coordinated complex **4.39**, which is formed from square-pyramidal complex **4.38** by coordination of a molecule of CO in the apical position, undergoes oxidative cyclization with a lowest-energy transition state of 19.7 kcal/mol (**4.40-TS**). Alternatively, oxidative cyclization directly into the square planar, 16-electron complex has a lowest-energy transition state of 16.0 kcal/mol (**4.41-TS**). Therefore, in contrast to previous studies, the four-coordinated pathway is 3.7 kcal/mol more favorable than the five-coordinated pathway in the Rh-(*R*)-BINAP (**2.24**) catalyzed PKR.

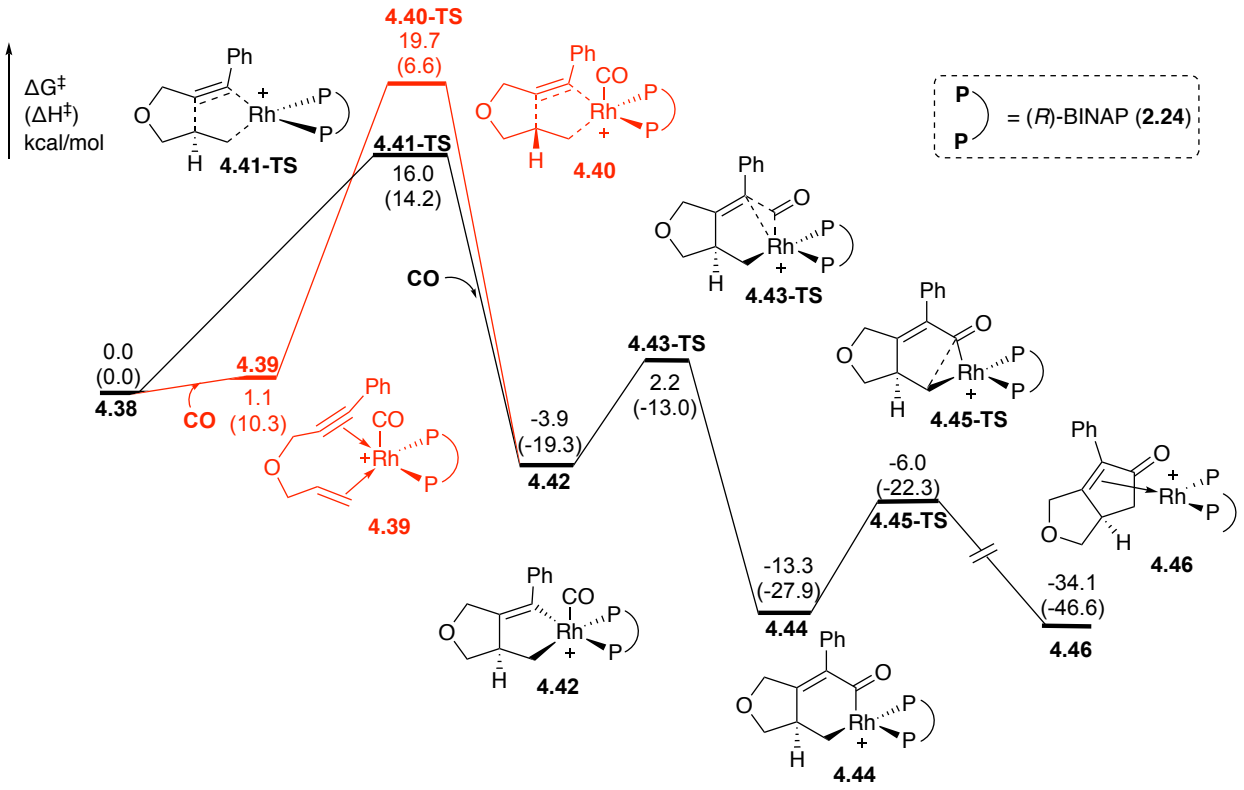

Scheme 52. Lowest-energy reaction profile of the Rh-(*R*)-BINAP-catalyzed PKR

Geometry optimization was performed using B3LYP/6-31G(d)−LANL2DZ (Rh) and single point energy performed using M06/6-311+G(d,p)−SDD(Rh) /SMD(DCE). Counteranions are omitted from the calculations

Oxidative cyclization and coordination of an additional molecule of CO provides Rh(III)-intermediate **4.42** in an overall exothermic process (−3.9 kcal/mol). Subsequent CO insertion proceeds with a low barrier (+6.1 kcal/mol) via **4.43-TS** to afford Rh(III)-acyl intermediate **4.44**. A highly exothermic reductive elimination via **4.45-TS** provides the product-coordinated complex **4.46**.

4.3.3 Transition state isomers in the Rh-BINAP-catalyzed PKR.

Examination of this calculated mechanism reveals that the oxidative cyclization step has the highest-energy transition state (**4.41-TS**, 16.0 kcal/mol), and is therefore the rate-determining step. In addition, because the reverse reaction (**4.42** to **4.41-TS,** +19.9 kcal/mol) is much higher in energy than the CO insertion step (**4.42** to **4.43-TS**, +6.1 kcal/mol), the oxidative cyclization is irreversible. Therefore, because the new stereocenter is formed during this step, the oxidative cyclization is the enantioselectivity-determining step. The lowest-energy transition state structure leading to the (*R*)-product **1.51** is four-coordinated transition state **4.41-TS**, while the lowest-energy transition state structure leading to the (*S*)-product **1.51** is the four-coordinated complex **4.47-TS** (Figure 33). The energies of all five-coordinated complexes are higher in energy (**4.48-TS**, **4.40-TS**, **4.49-TS**, **4.50-TS**, **4.51-TS** and **4.52-TS**, Figure 33). Therefore, in this calculated mechanism of the PKR using (*R*)-BINAP (**2.24**) catalyst, (*R*)- **1.51** is preferred by 1.4 kcal/mol.

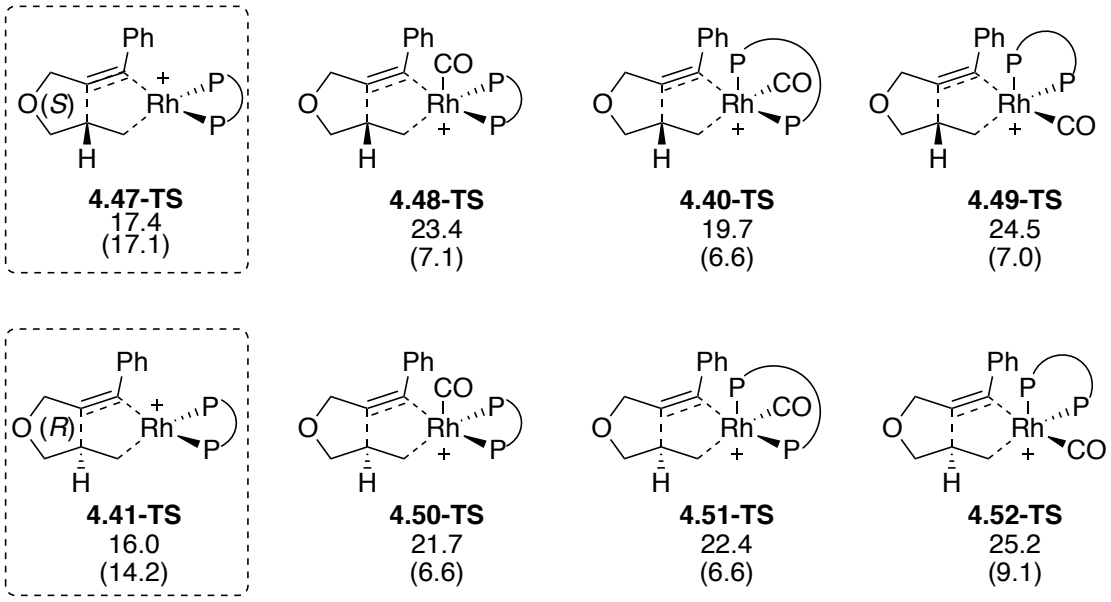

Figure 33. Transition state isomers considered in the Rh-BINAP oxidative cyclization.

4.3.4 Origin of BINAP enantioselectivity in the PKR.

The lowest-energy oxidative cyclization transition state isomers are shown in Figure 34. Rhodium is shown in blue, phosphorous is shown in orange, and oxygen is shown in red. Several key interactions between the (*R*)-BINAP (**2.24**) ligand and the enyne substrate **1.50** were identified which contribute to the observed enantioselectivity. For example, the transition state leading to the minor enantiomer of the product, **4.47TS** (Figure 34, right) has an unfavorable steric interaction between a terminal hydrogen on the alkene, and the phenyl groups on the ligand backbone. One phenyl group is 2.10 Å from the terminal hydrogen, and the other is 2.46 Å away. In the transition state structure leading to the major enantiomer, **4.41TS** (Figure 34, left), the distances between the terminal hydrogen atom and the phenyl groups of the ligand are longer (2.68 and 2.35 Å). These key bond distances illustrate the importance of the aryl groups on the phosphorous atom of the ligand for effecting enantioselectivity, which is further supported by several examples of highly enantioselective BINAP-derived PKR ligands with sterically bulky aryl groups on the phosphorous.[155, 160]

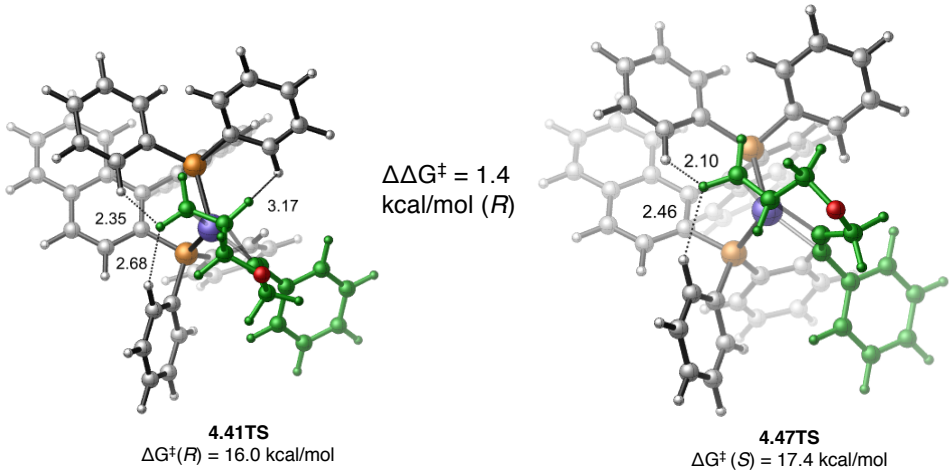

Figure 34. Lowest-energy transition state structures of Rh-(*R*)-BINAP-catalyzed PKR.

4.4 CONFIRMATION OF ABLOLUTE STEREOCHEMISTRY OF PKR PRODUCT

4.4.1 Previous stereochemical assignment of PKR product.

Next, our attention turned to comparing the absolute configuration of **1.51** predicted by calculation with that reported in the literature. However, there was some uncertainty in the literature regarding the stereochemical assignment of this compound. For example, (+)-**1.51** (obtained from (*S*)-BINAP), was initially assigned as (*R*)-**1.51** based upon analogous optical rotations to an NTs-containing PKR product **4.53**, which was characterized by X-ray crystallography, and a series of $(CO_2Et)_2$ -containing PKR products (+)-**4.26d**, (+)-**4.26l**, (+)- **4.26m**, and (+)-**4.26n**, which were characterized by Mosher ester analysis (Figure 35). These compounds were all assigned as (*R*) and had (+) optical rotations.[161] Therefore, (+)-**1.51**, obtained from the PKR with (*S*)-BINAP ligand, was also assigned as (*R*) (Scheme 53).[75] More recently, (+)-**1.51** (obtained from (*S*)-Difluorophos (**4.6**)) was assigned as (*S*)-**1.51** based upon a crystal structure of a derivative of **1.51**; a derivative prepared from (+)-**1.51** in three steps: 1) hydrogenation of the alkene, 2) reduction of the ketone, and 3) esterification with (*S*)-N-2-nitrophenyl)proline (Scheme 54).[149] These opposite assignments inspired us to seek out a more direct method of determining the absolute configuration for compound **1.51**.

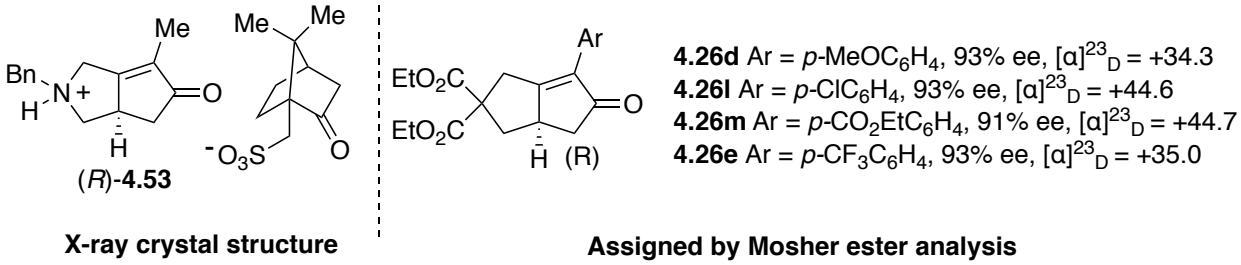

Figure 35. Assignment of absolute stereochemistry of PKR products by Buchwald.

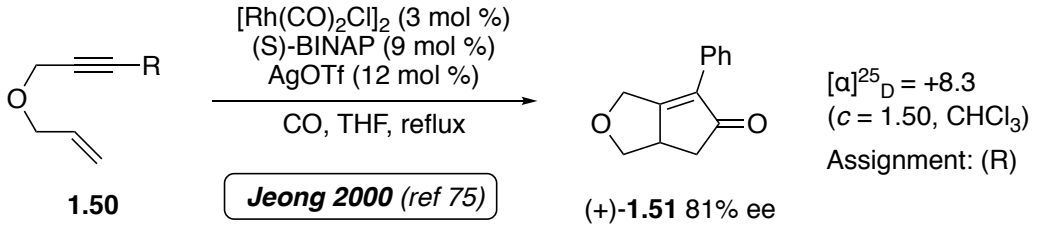

Scheme 53. Previous assignment of absolute stereochemistry of 1.51 by analogy to optical rotations.

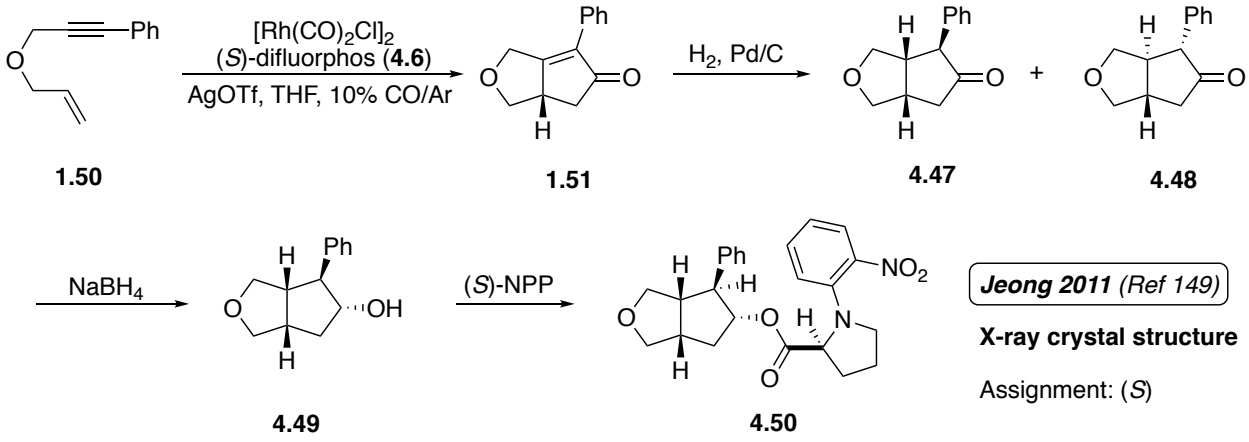

Scheme 54. Synthesis of crystalline ester reported by Jeong for stereochemical assignment of PKR product.

4.4.2 Introduction to vibrational circular dichroism (VCD).

In the present study, the absolute configuration of cyclopentenone **1.51** was validated directly using vibrational circular dichroism (VCD).[162-163] VCD is used to measure the differential absorption of left- and right-handed circularly polarized infrared radiation by a chiral sample in solution. This method is considered a reliable method for stereochemical assignment by the pharmaceutical industry and regulatory agencies such as the Food and Drug Administration.[163] VCD is advantageous for determination of absolute stereochemistry because samples can be evaluated either as a neat liquids or solutions, eliminating the need for growing crystals. Enantiomers generate VCD spectra which are mirror images of each other. The absorbance of circularly polarized radiation is on the order of 10^4 times less than the absorbance of IR radiation. Therefore, VCD is highly sensitive and it is difficult to draw conclusions about molecular structure from the VCD spectrum alone. Instead, a VCD spectrum can be considered a "fingerprint" which can be used for identification but cannot be predicted or assigned accurately. In order to use VCD for assignment of absolute stereochemistry, DFT calculations are used to calculate a theoretical VCD spectrum for each enantiomer, then the experimental spectrum is matched to either the (*R*) or (*S*) calculated spectrum. Because VCD measures infrared absorption of compounds in the ground state, the calculations required for assignment are straightforward and can be considered reliable.[162] The reliability of the calculations is for stereochemical assignment is checked for each sample by first calculating the IR spectrum of the molecule, which is independent of absolute stereochemistry. If the calculated and experimental IR spectra match, this supports the credibility of the calculated VCD spectra.

4.4.3 Confirmation of absolute stereochemistry of PKR product.

We set out to experimentally confirm the absolute stereochemistry of the PKR product of the Rh (*R*)-BINAP (**2.24**) catalyst, which was the subject of our computational mechanistic study (Scheme 52). First, in order to confirm the optical rotation of the PKR product obtained from (*R*)-BINAP (**2.24**), the reaction was performed according to the procedure described by Jeong.[75] Enyne **1.51** was reacted with rhodium biscarbonyl chloride dimer $[Rh(CO)_2Cl]_2$, (*R*)-BINAP (**2.24**), and silver triflate in THF under 100% CO atmosphere (Scheme 55, a). Cyclopentenone **1.51** was obtained in 56% yield and 82% ee (HPLC retention times 11.3 min (major) and 15.0 min (minor)).

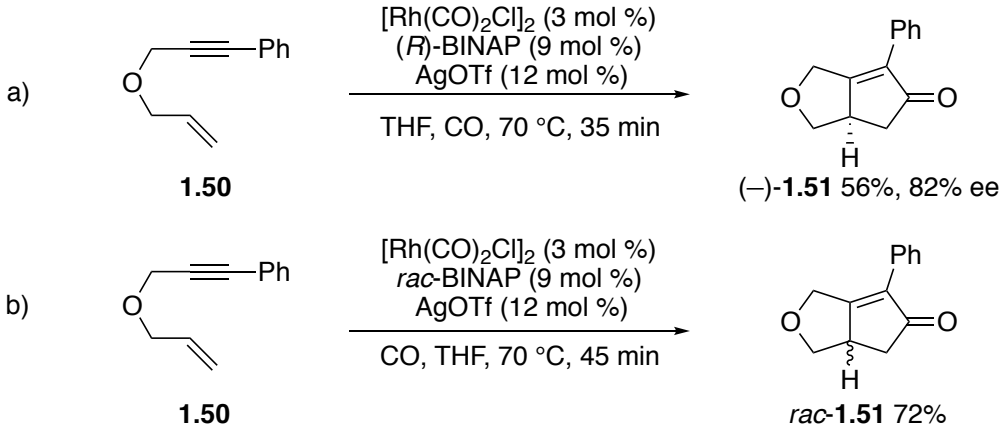

Scheme 55. Enantioselective (a) and racemic (b) PKR.

VCD analyses are most reliable when both enantiomers are examined.[163] Therefore, racemic PKR product **1.51** was obtained by reacting enyne **1.50** with racemic BINAP (**2.24**) (Scheme 55, b) and enantiomers (−)-**1.51** and (+)-**1.51** were separated by HPLC using a chiral column. The enantiomer with a retention time of 11 min had an optical rotation of −23.7° and the enantiomer a with retention time of 15 min had an optical rotation of +24.0° (Figure 36).

Enantiopure samples (>97% ee) of each enantiomer were subjected to VCD analysis. The experimental VCD spectra were obtained from BioTools, Inc. Samples were dissolved in carbon tetrachloride (5 mg/150 μL) and analyzed in a 100 μL BaF_2 cell using a ChiralIR-2X™ VCD spectrometer. *In silico* VCD spectra for each compound were generated by first performing a conformational search using ComputeVOA software, available from BioTools. Initial conformational search provided two low energy conformers, but upon subsequent geometry optimization (using B3LYP functional with 6-31G(d) basis set), these two conformers converged to the same lowest-energy conformer. Therefore, only one lowest-energy conformer was located for this rigid molecule. The VCD spectra of the lowest-energy conformer for each enantiomer was generated using B3LYP basis set with TZVP basis set, as described by Jiminez-Oses.[164]

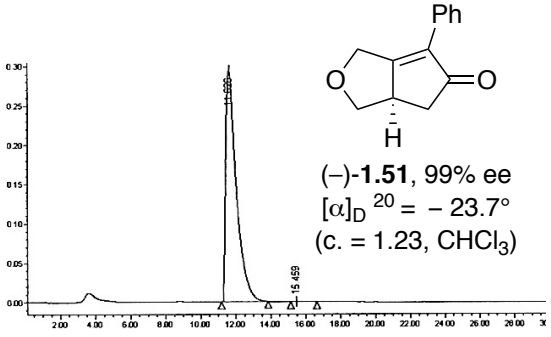

	Ret. Time (min)	Area (%)
Peak 1	11.626	99.78
Peak 2	15.458	0.22

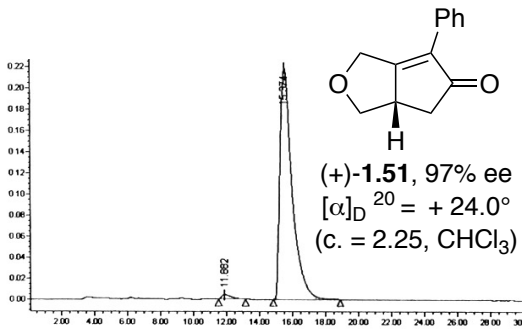

	Ret. Time (min)	Area (%)
Peak 1	11.882	1.46
Peak 2	15.374	98.54

Figure 36. Separation of enantiomers by HPLC for VCD analysis.

The reliability of the calculation was tested by first comparing the calculated IR spectrum with the experimental IR spectrum. Indeed, the calculated IR spectrum shows good correlation with the experimental IR spectrum, with peaks only being shifted to higher wavenumbers in the calculated spectrum. For example, the carbonyl absorption appears at 1710 cm^{-1} in the

experimental spectrum (Figure 37, A, peak 17, blue), and at 1805 cm^{-1} in the calculated spectrum (Figure 37, A, peak 17, red). Peaks in the fingerprint region (850-1500 cm^{-1}) exhibit a similar shift to higher wavenumbers in the calculated IR spectrum. To assign absolute configuration of enantiomers of **1.51**, the same shifts and scaling needed to overlay the computational and experimental IR spectra were also applied to the VCD spectra, using an algorithm contained in CompareVOA software, from BioTools.[165] After shifts and scaling were applied, the degree of similarity between the calculated VCD spectrum and the experimental spectrum were quantified by the enantiomeric similarity index (ESI). The major enantiomer obtained from the PKR using (*R*)-BINAP, (−)-**1.51**, had an ESI of 60.6 (97% confidence level) with the calculated VCD spectrum of (*R*)-**1.51**; and the (+)-**1.51** enantiomer had an ESI of 44.7 (90% confidence level) with the calculated VCD spectrum of (*S*)-**1.51**. Visual inspection of the calculated VCD spectrum of (*R*)-**1.51** (Figure 37, B, red) and the experimental VCD spectrum of (-)-**1.51** (Figure 37, B, blue) shows a clear correlation between the signs of the carbonyl stretches (peak 33, both negative). Similarly, the carbonyl stretches of the calculated and experimental VCD spectra of (+)-**1.51** are both positive (peak 52, Figure 37, C).

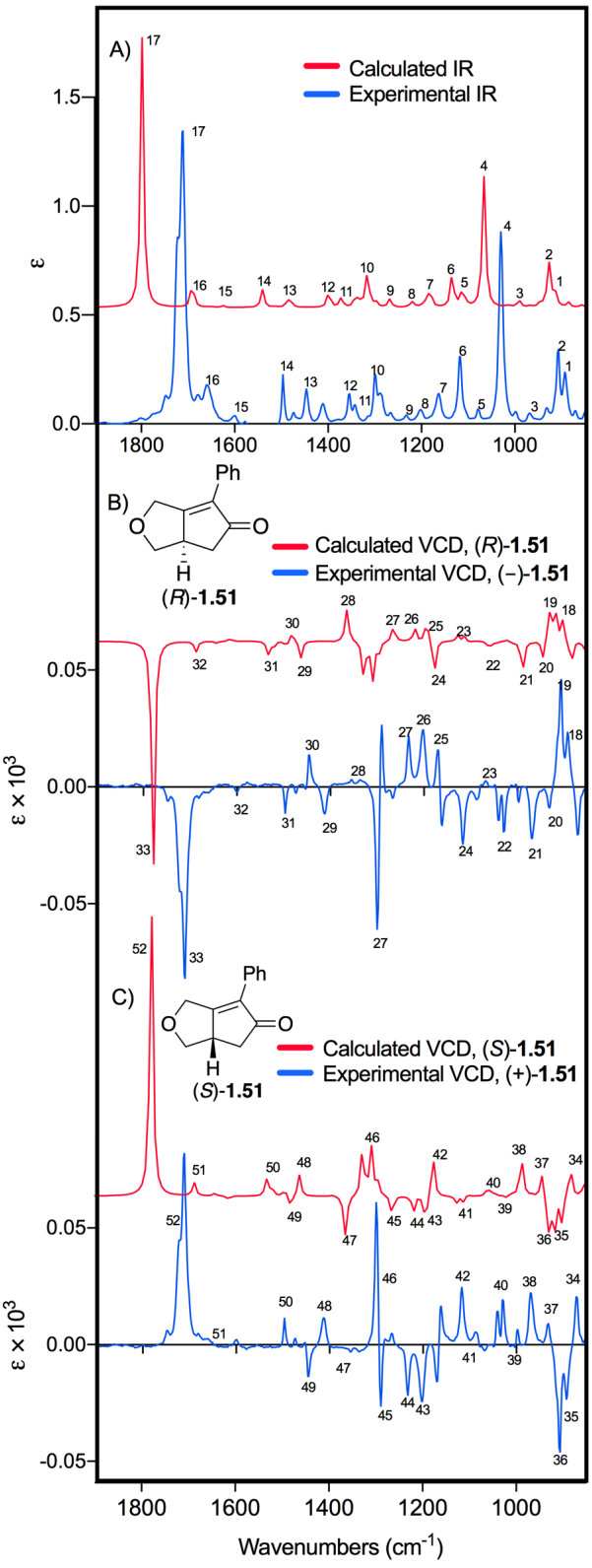

Figure 37. Calculated (red) and experimental (blue) VCD spectra of PKR product.

In summary, VCD analysis confirmed that (−)-**1.51** is the (*R*)-enantiomer of **1.51**, and (+)-**1.51** is the (*S*)-enantiomer of **1.51**. These results corroborate the results obtained by Jeong's crystal structure of **4.50** (Scheme 54). Therefore, the product of the PKR using (*S*)-BINAP (**2.42**) is (*S*)-(+)-**1.51**,[75] and the product of the PKR with (*R*)-BINAP (**2.42**) is (*R*)-(−)-**1.51**. This assignment corroborates our computational prediction of absolute stereochemistry of **1.51** (Scheme 52).

4.5 CALCULATED MECHANISM OF (*S*)-MONOPHOS IN THE PKR

Next, the lowest-energy PKR mechanism with a monodentate phosphoramidite ligand was calculated. Monodentate ligands have higher conformational flexibility and are therefore more difficult to predict computationally. Despite this flexibility, monodentate phosphoramidites have been previously demonstrated as enantioselective ligands in the PKR,[99] and other Rh-catalyzed reactions.[166] For this computational study, (*S*)-MonoPhos (**2.27**) was chosen as the simplest representative of the phosphoramidite ligand class. We hypothesized that the lower steric demand of (*S*)-MonoPhos (**2.27**) compared to (*R*)-BINAP (**2.42**) could lower the energy required for substrate coordination, while still providing electron density to facilitate the oxidative cyclization step. We performed DFT calculations on this ligand for the most important steps, substrate coordination and oxidative cyclization, to determine the ligand effects of this ligand class relative to Rh-BINAP catalysts. Pathways were considered which included one or two monodentate ligands on the catalyst, and four- or five- coordinated transition states.

4.5.1 Substrate coordination energies of Rh-(*S*)-MonoPhos catalysts.

The energy required for coordination to the resting catalyst is dependent on the structure of the resting catalyst. In the presence of CO and an excess of (*S*)-MonoPhos ligand to Rh, the Rh catalyst can exist as one-, two- or three-(*S*)-MonoPhos (**2.27**) coordinated species. The four-(*S*)-MonoPhos (**2.27**) complex can also be formed, but this species is unlikely to facilitate the reaction and was not considered here.[166] We hypothesized that, due to the lower steric demand of monodentate phosphoramidite ligands compared to bisphosphine ligands, the substrate coordination energies of the Rh-(*S*)-MonoPhos (**2.27**) would be lower than those of the Rh-BINAP catalyst (Scheme 51, Rh(BINAP)$(CO)_2$ complex **4.37a**, +29.8 kcal/mol).

The calculated substrate coordination energies for these three complexes are summarized in Scheme 56. The energy required to replace two CO molecules on the one-(*S*)-MonoPhos (**2.27**) resting catalyst (**4.51**) to afford the substrate-coordinated complex **4.52** is +6.2 kcal/mol (Scheme 56, a). The energy required for the substrate to displace two CO molecules on the two-(*S*)-MonoPhos (**2.27**) resting catalyst (**4.53**) to afford substrate-coordinated complex **4.54** is +14.4 kcal/mol (Scheme 56, b). With three (*S*)-MonoPhos (**2.27**) ligands coordinated to the resting catalyst (complex **4.55**), the energy required for the substrate to coordinate and replace one CO molecule and one (*S*)-MonoPhos (**2.27**) ligand is +17.6 kcal/mol (Scheme 56, c).

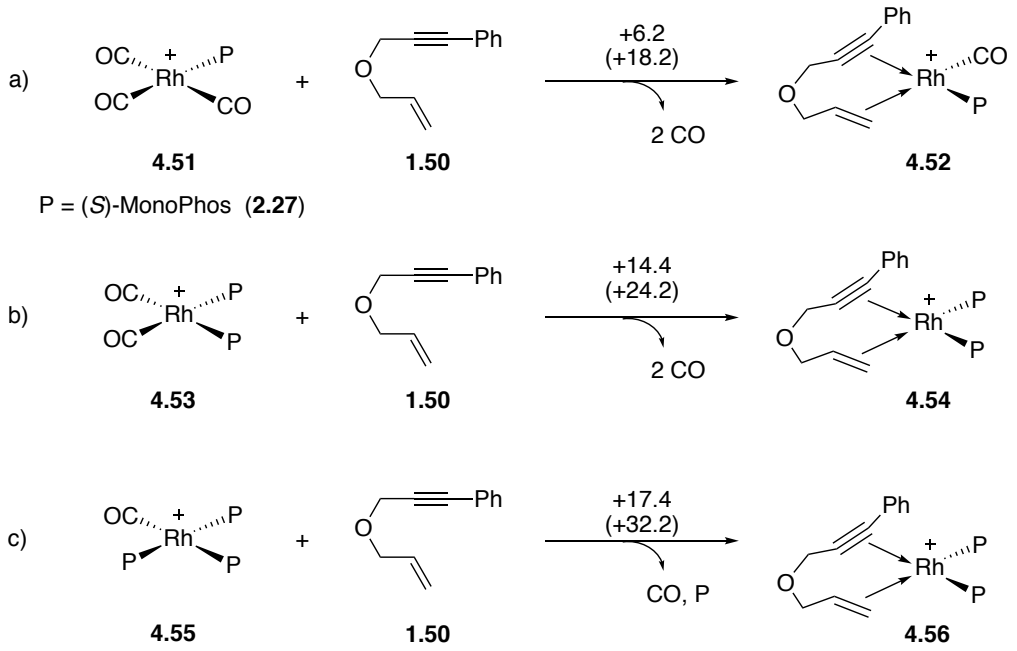

Scheme 56. Substrate coordination energies for Rh-(*S*)-MonoPhos resting catalysts.

The energies required for substrate coordination to Rh-(*S*)-MonoPhos catalysts **4.51** (+6.2 kcal/mol), **4.53** (+14.4 kcal/mol), and **4.55** (+17.7 kcal/mol) are all lower than that of the analogous CO-bound Rh-BINAP catalyst (+29.8 kcal/mol). This finding supports our hypothesis that the monodentate phosphoramidite ligands could facilitate substrate coordination. The lower substrate coordination energies of Rh-(*S*)-MonoPhos catalysts compared to Rh-(*R*)-BINAP is likely both steric and electronic in nature. The monodentate phosphoramidites are less sterically demanding than bisphosphine ligands, making them better able to accommodate the substrate. Electronically, phosphoramidites are less electron-donating than phosphine ligands, which leads to a lesser degree of backbonding in to the Rh-CO bonds, and facilitates dissociation of CO.[167] Because of these lower substrate coordination energies compared to BINAP catalysts, phosphoramidite ligands could be an advantageous ligand class in the PKR of sterically demanding substrates.

4.5.2 Oxidative cyclization of Rh-(*S*)-MonoPhos catalysts.

Next, the oxidative cyclization step of the Rh-(*S*)-MonoPhos-catalyzed PKR was investigated. In the calculated mechanism of Rh-(*S*)-MonoPhos catalysts, both the one-(*S*)-MonoPhos (**2.27**) and two-(*S*)-MonoPhos (**2.27**) pathways were considered (Scheme 57). The free energies shown in Scheme 57 are reported relative to the one-(*S*)-**2.27** substrate-coordinated complex **4.54**. The "one-(*S*)-MonoPhos" pathway is shown on the left, and the "two-(S)-MonoPhos" pathway is shown on the right. The substrate-coordinated one-(*S*)-**2.27** complex **4.52** is 1.7 kcal/mol lower in energy than the substrate-coordinated two-(*S*)-**2.27** complex **4.54**. From the one-(*S*)-**2.27** complex **4.52**, the oxidative cyclization step can proceed either via a four- or five-coordinated transition state (Scheme 57, left). The lowest-energy four-coordinated transition state has an activation energy of 17.7 kcal/mol (**4.55-TS**), while the lowest-energy five-coordinated transition state has an activation energy of 20.4 kcal/mol (**4.56-TS**). Therefore, in the one-(*S*)-MonoPhos (**2.27**) pathway, the four-coordinated transition state **4.55-TS** is favored by 2.7 kcal/mol.

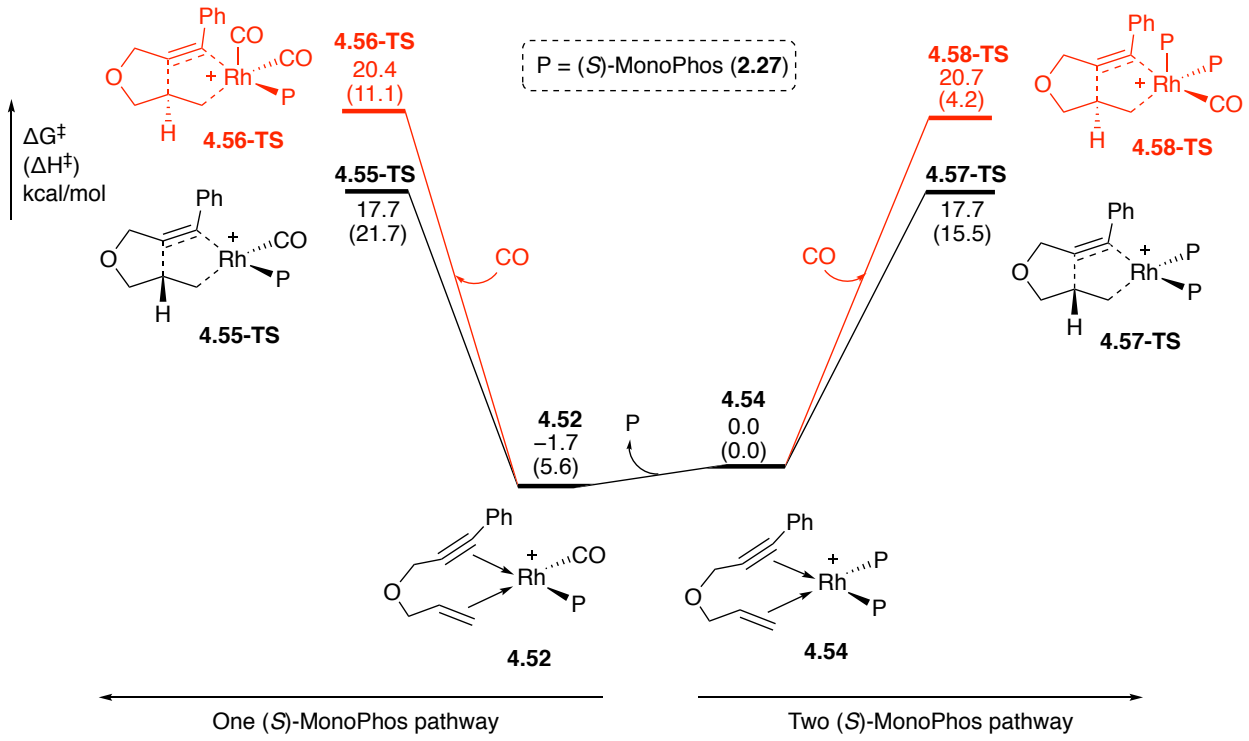

Scheme 57. Calculated lowest-energy reaction profiles of (*S*)-MonoPhos-catalyzed PKR.

Geometry optimization was performed using B3LYP/6-31G(d)−LANL2DZ (Rh) and single point energy performed using M06/6-311+G(d,p)−SDD(Rh) /SMD(DCE). Counteranions are omitted from the calculations

The two-(*S*)-**2.27** pathway can also proceed via a four-coordinate or five-coordinate pathway (Scheme 57, right). The lowest-energy four-coordinated transition state has an activation energy of 17.7 kcal/mol (**4.57-TS**), while the lowest-energy five-coordinated transition state has an activation energy of 20.7 kcal/mol (**4.58-TS**). Therefore, in the one-(*S*)-MonoPhos (**2.27**) pathway, the four-coordinated transition state **4.57-TS** is favored by 3.0 kcal/mol. According to these calculations, the oxidative cyclization step of the Rh-(*S*)-MonoPhos (**2.27**)-catalyzed PKR proceeds with exactly the same activation energy (17.7 kcal/mol), regardless of whether there are one or two (*S*)-MonoPhos (**2.27**) ligands on the Rh catalyst (Scheme 57).

4.5.3 Summary of Rh-(*S*)-MonoPhos transition states considered.

In calculating the activation energy of the oxidative cyclization step for the enantioselective PKR using (*S*)-MonoPhos (**2.27**), a total of 34 transition state structures were considered. One- and two-coordinated Rh catalysts were examined, and two rotamers each about the Rh-P bond were calculated for each one-(*S*)-**2.27**-coordinated catalyst. The total number of calculated transition states includes: eight four-coordinated, one-(*S*)-**2.27** transition states, eight four-coordinated two-(*S*)-**2.27** transition states, 12 five-coordinated one-(*S*)-**2.27** transition states, and six five-coordinated two-(*S*)-**2.27** transition states. The activation energies of these calculated transition states are summarized in Figure 38, where each point represents a transition state structure. In Figure 38. Summary of transition state energies of the Rh-(*S*)-MonoPhos-catalyzed PKR., a, b and c, the transition states are sorted according to: a) number of (*S*)-MonoPhos ligands, b), Rh coordination number, and c) the product enantiomer.

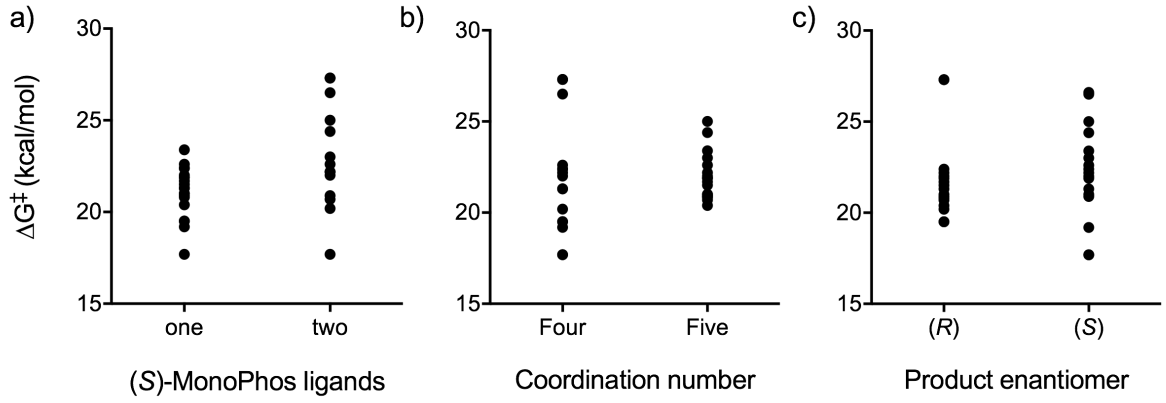

Figure 38. Summary of transition state energies of the Rh-(*S*)-MonoPhos-catalyzed PKR.

The lowest-energy transition states for both one- and two-(*S*)-**2.27** pathways are energetically indistinguishable. Rh-(*S*)-MonoPhos pathways with one or two (S)-MonoPhos ligands have exactly the same lowest-energy transition states (17.7 kcal/mol). Therefore, the number of ligands on the Rh-(*S*)-MonoPhos transition state structure is likely dependent on the equivalents of ligand to Rh present in the reaction mixture. The lowest-energy four-coordinated transition state (**4.55-TS**, 17.7 kcal/mol) is favored over the lowest energy five-coordinated transition state (**4.56-TS**, 20.4 kcal/mol) by 2.7 kcal/mol (Figure 38, b). This preference for the four-coordinated transition state was also demonstrated by Rh-BINAP catalyst (Scheme 52, **4.41-TS,** 16.0 kcal/mol). Finally, the lowest-energy transition state leading to (*S*)-**1.51** is preferred over the lowest-energy transition state leading to (*R*)-**1.51** by 1.8 kcal/mol (Figure 38, c). Therefore, our calculations show that (*S*)-**1.51** is predicted as the major product of the PKR using (*S*)-MonoPhos (**2.27**) ligand.

4.5.4 Optimization of conditions for Rh-(*S*)-MonoPhos-catalyzed PKR.

In order to validate the computational prediction that the (*S*)-**1.51** product is afforded by the PKR using (*S*)-MonoPhos (**2.27**) ligand, the reaction was performed experimentally. Some optimization was necessary in order to obtain the product in satisfactory yield. We began our experimental studies of the PKR using (*S*)-MonoPhos (**2.27**) ligand by first applying the same conditions reported by Zhou in the PKR using (*R*)-SIPHOS, where PKR product **1.51** was formed in 56% yield and 84% ee: $[Rh(CO)_2Cl]_2$ (3 mol %), ligand (13.2 mol %), using DCE as a solvent, silver hexafluoroantimonate (12 mol %) as an activator (Table 39, entry 1).[99] Under the conditions described by Zhou, the PKR proceeded very quickly (10 min) and afforded **1.51** in 15% yield, along with many reaction byproducts as observed by TLC. Because lowering the CO atmosphere

is known to reduce PKR byproducts in some cases, we tested an atmosphere of 10% CO/Ar (entry 2).[155] Upon lowering the CO atmosphere, the reaction time slowed to 14 h and product was obtained in 36% yield (entry 2). We hypothesized that the silver salt could be contributing to substrate decomposition, and therefore, cationic precatalyst rhodium(I) bis(1,5)-cyclooctadiene hexafluoroantimonate ($Rh(cod)_2SbF_6$) was employed, which gave an improved yield of 65% and 83% ee (entry 3). We hypothesized that lowering the temperature could improve enantioselectivity further. We also desired conditions which included an internal standard for determination of yield by ^1H NMR spectroscopy. Therefore, the PKR was performed at 60 °C with mesitylene (1.0 equiv) as an internal standard (entry 4). Although only 49% yield was obtained after 2 d, the high recovery of unreacted starting material (45%) was encouraging. An increase in catalyst loading resulted in improved conversion to afford product in 63% yield and 78% ee (entry 5). These conditions were employed in subsequent studies of the Rh-(S)-MonoPhos-catalyzed PKR. Enantioselectivities were determined by HPLC using a chiral column. All reactions with (*S*)-MonoPhos (**2.27**) ligand afforded product with the enantiomer eluting 11 min being the minor product and the enantiomer eluting at 15 min being the major product. The specific rotation of the product of the PKR with (*S*)-MonoPhos (**2.27**) ligand was +17.9. Therefore, according to our VCD assignment, (*S*)-**1.51** was obtained, which corroborates our computational prediction.

Table 39. Optimization of conditions for Rh-(*S*)-MonoPhos-catalyzed PKR.

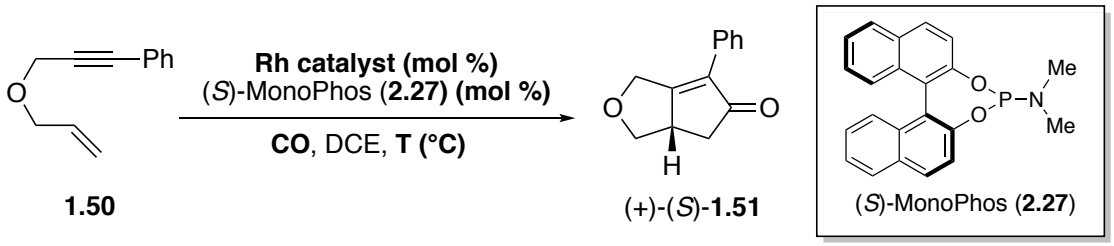

1.50 (+)-(*S*)-**1.51**

entry	Rh catalyst (mol %)	(*S*)-**2.27** (mol %)	CO/Ar (%)	T (° C)	time	yield (%)	ee (%)
1	$[Rh(CO)_2Cl]_2$ (3), $AgSbF_6$ (12)	13.2	100	90	10 min	15 [a]	-
2	$[Rh(CO)_2Cl]_2$ (3) $AgSbF_6$ (12)	13.2	10	80	14 h	36 [a]	77 (*S*)
3	$[Rh(cod)_2SbF_6$ (5)	6	10	80	6 h	65 (0) [b]	83 (*S*)
4	$[Rh(cod)_2SbF_6$ (5), mesitylene (1.0 equiv)	6	10	60	2 d	49 (45) [b]	78 (*S*)
5	$[Rh(cod)_2SbF_6$ (10), mesitylene (1.0 equiv)	12	10	60	3 d	63 (7) [b]	78 (*S*) [c]

[a] Isolated yields. [b] Yields were determined by integral comparison of product resonance (4.9 ppm) to mesitylene resonance (6.8 ppm). Percent recovered starting enyne is indicated in parentheses. [c] $[\alpha]^{20}_D$ = +17.9 (0.67 $CHCl_3$).

4.6 COMPARISON OF PHOSPHOROUS LIGAND-CONTAINING AND PHOSPHOROUS LIGAND-FREE PKR CONDITIONS

4.6.1 Long reaction time of cationic Rh catalyst in PKR.

In our synthesis of the racemic cyclopentenone **1.51**, we noted that the Rh-catalyzed PKR in the absence of a phosphorous ligand reacted slowly. For example, the PKR of **1.50** using $Rh(cod)_2SbF_6$ and in DCE at 60 °C degrees afforded only 20% yield of product **1.51**, with 64% recovered starting enyne **1.50** after reacting 5 days (Scheme 58). This observed slow reactivity was in stark contrast to the rapid reactivity of cationic Rh catalysts in the APKR (Section 2.4.4). Therefore, we were

inspired to investigate the relative activation energies of the cationic Rh catalyst computationally to determine the origin of this poor reactivity.

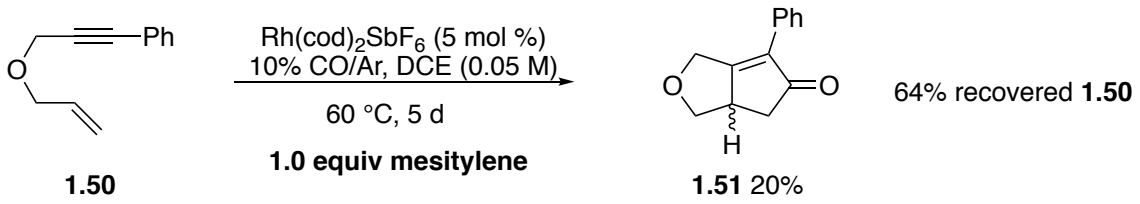

Scheme 58. Cationic Rh PKR conditions in the absence of phosphine ligand.

4.6.2 Comparison of oxidative cyclization activation energies among BINAP, (*S*)-MonoPhos, and cationic CO-only catalysts.

The lowest-energy reaction profile of the oxidative cyclization step of the cationic Rh "CO-only" catalyst, was calculated, and compared to the oxidative cyclization energies of the Rh-(*R*)-BINAP and Rh-(*S*)-MonoPhos catalysts (Scheme 59). Beginning from the substrate-coordinated complex **4.59** (L = CO), coordination of an additional CO affords the square pyramidal complex **4.60** which is 1.2 kcal/mol lower in energy. Oxidative cyclization from **4.60** via **4.61-TS** requires an activation energy of 24.3 kcal/mol to afford the Rh(III)-metallacycle **4.62**.

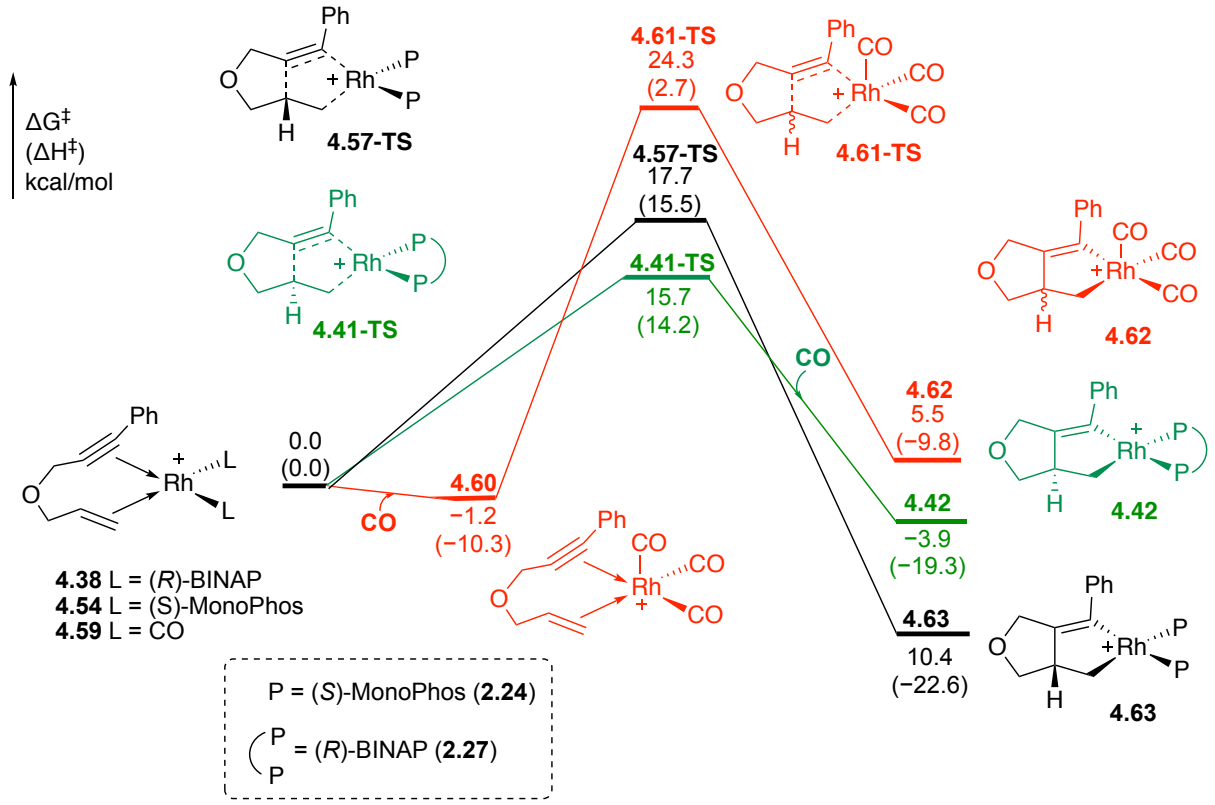

Scheme 59. Activation energies of (*R*)-BINAP, (*S*)-MonoPhos, and CO-only catalysts.

Geometry optimization was performed using B3LYP/6-31G(d)−LANL2DZ (Rh) and single point energy performed using M06/6-311+G(d,p)−SDD(Rh) /SMD(DCE). Counteranions are omitted from the calculations.

A comparison of the rate-determining steps of the two lowest-energy reaction profiles demonstrates that the Rh-"CO-only" catalyst has an overall activation energy which is 8.6 kcal/mol higher than that of the Rh-(*R*)-BINAP (**2.24**) catalyst (Scheme 59, compare **4.61-TS** and **4.41-TS**), and 6.6 kcal/mol higher than that of the Rh-(*S*)-MonoPhos (**2.27**) (catalyst compare **4.61-TS** and **4.57-TS**). The high activation energy for the Rh-CO only catalyst explains the poor reactivity observed for this catalyst. This energetic difference between the cationic Rh "CO-only" catalyst and the phosphorus ligand-containing catalysts is likely due to the ability of the σ-donating phosphorous ligand to increase electron density on the Rh catalyst and facilitate the oxidative cyclization process.

4.6.3 Screening counteranions for the PKR of enyne 1.50.

During studies exploring optimal conditions for the enantioselective PKR, we noted that the reactivity of the catalyst in the absence of any ligand was poor (Scheme 58). Noting that ligand acceleration is advantageous for asymmetric catalysis when the rate- and stereochemistry-determining steps are the same, we were inspired to investigate this possible effect through further experiments.[168] A series of cationic catalysts was tested to determine which counteranion would offer the most enhanced difference in reactivity in the presence and absence of a ligand. Our goal was to identify a Rh precatalyst which would afford long reaction times with good recovery of starting material in the absence of a phosphorous ligand, and a short reaction time with high product yield in the presence of a phosphorous ligand.

To this end, several Rh-bis-cyclooctadiene precatalysts with different counteranions were tested in the PKR of **1.50** using (*S*)-MonoPhos (**2.27**) ligand. Reactions were performed simultaneously in 8-mL test tubes using an InnovaSyn condenser and monitored by TLC. Enantioselectivities were not determined in this screening experiment. Precatalysts containing four different counteranions were tested: Tetrafluoroborate (BF_4), trifluoromethanesulfonate (OTf), hexafluoroantimonate (SbF_6) and tetrakis[3,5-bis(trifluoromethyl)phenyl]borate ($BAr^F{}_4$). Among all four counteranions tested, the reactions containing 22 mol % (*S*)-MonoPhos (**2.27**) ligand (Table 40, entries 2, 4, 6 and 8) all proceeded in higher yields than the reactions with 0 mol% (*S*)-MonoPhos (**2.27**) (entries 1, 3, 5, and 7). The PKR with BF_4 counteranion reacted in 84% yield in the presence of (*S*)-MonoPhos (**2.27**), while the reaction without ligand afforded only 38% yield of product, with 51% unreacted starting material after 96 h (Table 40, entries 1 and 2). In the PKR with the OTf counteranion, the reaction with 22 mol % (*S*)-MonoPhos (**2.27**) proceeded in good yield (77%), but the reaction without ligand afforded 33% yield of product with no recovered

enyne after 20 h (entries 3 and 4). The SbF_6 counteranion afforded a 77% yield of cyclopentenone product after 40 h with ligand, while the catalyst without ligand afforded only 24% yield of **1.51**, with 65% enyne remaining after 96 h (entries 5 and 6). The noncoordinating BAr^F_4 catalyst with 22 mol% ligand afforded 60% yield of **1.51** than the other catalysts tested (entries 7 and 8).

Table 40. Effect of counteranion on ligand acceleration in the PKR.

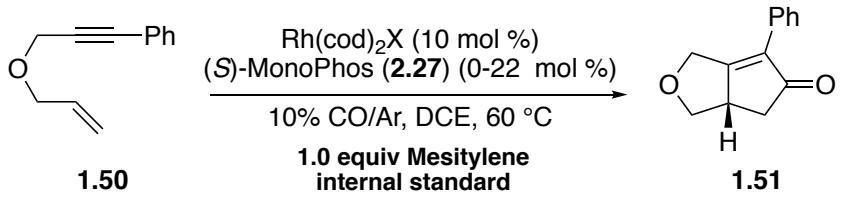

1.50 **1.51**

entry	X	(*S*)-**2.27** (mol%)	Time (h)[a]	Yield (SM) [b]
1	BF_4	22	96	84 (10)
2	BF_4	0	96	38 (51)
3	OTf	22	40	77 (10)
4	OTf	0	20	33 (0)
5	SbF_6	22	40	77 (10)
6	SbF_6	0	96	24 (65)
7	BAr^F_4	22	96	60 (5)
8	BAr^F_4	0	96	27 (62)

[a] Yields were determined by integral comparison of product resonance (4.9 ppm) to mesitylene resonance (6.8 ppm). Percent recovered starting enyne is indicated in parentheses.

In summary, the SbF_6 counteranion afforded the greatest difference in reactivity between reactions in the presence and in the absence of (*S*)-MonoPhos (**2.27**) ligand. With 22 mol % (S)-MonoPhos, the SbF_6 catalyst afforded a high yield of product (77%) in a shorter reaction time (40 h) compared to the phosphorous ligand-free conditions, which provided only 24% yield of product and good recovery of starting material (65%) after 96 h.

4.7 RATE STUDIES INDICATING LIGAND ACCELERATED CATALYSIS IN THE CATIONIC RHODIUM-CATALYZED PKR

To effect enantioselectivity in a catalytic transformation, chiral ligands need to have sufficient steric influence on the substrate. This steric crowding usually decreases reactivity compared to the chiral-ligand-free catalyst.[168] This ligand deceleration effect presents a challenge in developing asymmetric catalysts because the racemic background reaction can dominate product formation, resulting in low enantioselectivities. The term "ligand-accelerated catalysis" first coined by Sharpless, refers to acceleration of an existing catalytic transformation by addition of a ligand.[168] Ligand-accelerated catalysis is most relevant when many interconverting catalysts can exist in the reaction mixture. If the most enantioselective, ligand-bound catalyst also reacts at the fastest rate, the reaction will proceed with high enantioselectivity, even in the presence of unselective catalytic species which exist in the reaction mixture. Ligand acceleration will be particularly advantageous in the PKR using monodentate ligands because they are prone to displacement by CO (Scheme 29). In an accelerated PKR, this potential lability of the monodentate chiral ligand would not negatively impact catalyst enantioselectivity.

4.7.1 Experimental rates correlated with oxidative cyclization energies.

With the information in hand that the oxidative cyclization transition state of the "CO only" Rh catalyst was 8.6 kcal/mol higher in energy than transition state of the Rh-BINAP catalyst, we conducted a quantitative rate study of the PKR to compare the reaction rates quantitatively. Optimized conditions include cationic $Rh(cod)_2SbF_6$ 10 mol %), (*R*)-BINAP (**2.24**) (11 mol %), and internal standard mesitylene (1.0 equiv) under 10% CO/Ar in DCE solvent. The Rh precatalyst

and (*R*)-BINAP (**2.24**) were first stirred 1 h under nitrogen atmosphere at 60 °C, followed by another 1 h under 10% CO/Ar, at which time the temperature of the oil bath was increased to 80 °C, followed by addition of the enyne substrate **1.50**. Reaction progress was closely monitored by removing aliquots from the reaction and measuring the disappearance of the starting enyne (**1.50**, 5.9 ppm, 1 H) relative to mesitylene, the internal standard (6.8 ppm, 3 H) by ^{1}H NMR spectroscopy. The amounts of reaction byproducts were approximated by comparing the ratio of the sum of the integration of alkenyl resonances in the range of 6.5 to 4.5 ppm and the integration of the product peak at 5.4 ppm (Table 41).

Table 41. Rate studies of cationic Rh catalysts in the PKR of enyne 1.50.

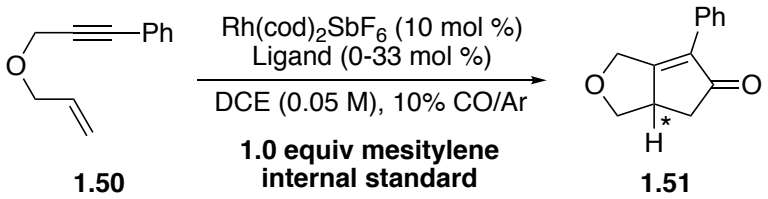

1.50 **1.51**

entry	Ligand(L/Rh)	rate (s^{-1})	time (h)[a]	$t_{1/2}$ (h)	yield (SM) [b]	ee (%)	**1.51**:byproduct [b]
1	none	6.39×10^{-7}	245	301	11 (56)	-	1:1
2	(*R*)-**2.24** (1.1)	1.88×10^{-3}	1.0	0.10	41 (0)	79 (*R*)	1:2
3	PPh_3 (2.2)	7.92×10^{-6}	141	24.3	15 (23)	-	1:1
4	(*S*)-**2.27** (0.5)	3.03×10^{-5}	48	6.4	59 (1)	79 (*S*)	2:1
5	(*S*)-**2.27** (1.1)	1.10×10^{-4}	18	1.6	61 (4)	82 (*S*)	1:1
6	(*S*)-**2.27** (2.2)	1.15×10^{-4}	18	1.7	60 (0)	83 (*S*)	1:1
7	(*S*)-**2.27** (3.3)	6.32×10^{-6}	101	30.5	90 (0)	79 (*S*)	20:1

[a] Time reaction was monitored. [b] Yields were determined by integral comparison of product resonance (4.9 ppm) to mesitylene resonance (6.8 ppm). Percent recovered starting enyne is indicated in parentheses. Ratio of integration (x100) of peaks in range 6.5-4.5 ppm which do not correspond to enyne **1.50**, product **1.51** or cyclooctadiene.

Reaction of **1.50** with $Rh(cod)_2SbF_6$ in DCE in a 10% CO/Ar atmosphere at 80 °C proceeded slowly, with a half-life of 301 h (12 days, Table 41, entry 1); whereas, performing this same reaction with added (*R*)-BINAP (L/Rh = 1.1) resulted in complete consumption of starting material in only 1 h with a half-life of 6 min and an enantiomeric excess of 79% ee (entry 2). Comparison of the reaction rates for (*R*)-BINAP (**2.24**) ($k = 6.39 \times 10^{-7}$ s^{-1}, entry 2) and ligand-free (1.88×10^{-3} s^{-1}, entry 1) conditions show a 3000-fold increase for the BINAP reaction rate! To test the generality of this ligand acceleration effect, the reaction was performed using an achiral ligand, triphenylphosphine (PPh_3, entry 3). Although the reaction was accelerated compared to the ligand-free cationic catalyst (compare entries 1 and 3), the PKR with the triphenylphosphine ligand was low-yielding (15%). In the reaction with added (*R*)-BINAP (**2.24**), a significantly higher ratio of byproducts to product were formed in comparison to the reactions with ligand-free and the achiral monodentate ligand (compare **1.51**: byproduct ratios for entries 1, 2 and 3).

These rate studies confirm that phosphorous ligands accelerate the PKR when using a cationic rhodium catalyst, an acceleration not observed for neutral Rh(I) catalysts and to our knowledge has not previously been reported.[75] In the case of BINAP, the disappearance of starting material was very fast but the product **1.51**:byproduct ratio was low (1:2). This reaction time was shorter than that reported by Jeong when THF was used as a solvent (5 h), the yield was lower (41% yield vs. 88% yield) and the enantioselectivity was approximately the same (81 vs 79% ee).[75] The extended reaction time and low yield when triphenylphosphine was used is attributed to by the large cone angle of this ligand (145°), which causes the two phosphine ligands coordinate to the Rh(I) *trans* to one another; preventing substrate coordination.[169] The good correlation between the rates of the Rh-(*R*)-BINAP and Rh-CO only catalysts validates the computational mechanism and supports the conclusion that the oxidative cyclization is rate-determining.

4.7.2 Rate experiments with changing (*S*)-MonoPhos equivalents.

Next, the effect of the (*S*)-MonoPhos (**2.27**) ligand on the PKR rate was examined. We questioned whether the reaction rate of the active catalyst would be dependent on the number of (*S*)-MonoPhos ligands coordinated to Rh. Therefore, a series of reactions were performed using varying ligand to Rh ratios. Plots depicting the change in concentration of starting enyne and product over time in reactions of different (*S*)-MonoPhos (**2.27**) equivalents are shown in Figure 39 and Figure 40. The reactions with 1.1 and 2.2 equiv of ligand/Rh proceeded at similar rates and afforded product with nearly the same enantioselectivies (Table 41, entries 3 and 4, Figure 39 and Figure 40, yellow and green). These reactions occurred approximately 180 times faster than the reaction with no phosphorous ligand (compare to Table 41, entry 1, Figure 39 and Figure 40, red). The reaction with a ligand to Rh ratio of proceeded in a marginally faster rate (1.15×10^{-4}) and the reaction with a ligand to Rh ratio of 2.2 proceeded in higher enantioselectivity (83%, Table 41, entry 6).

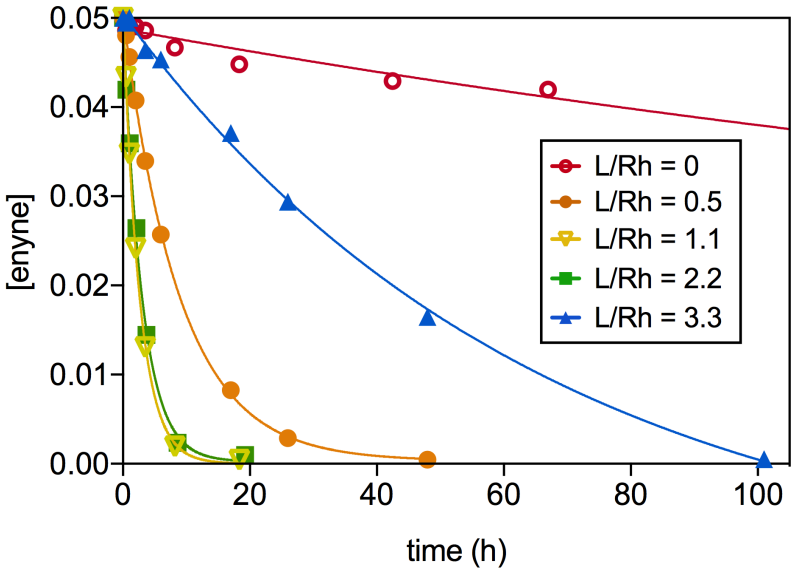

Figure 39. Change in concentration (M) of starting enyne 1.50 over time.

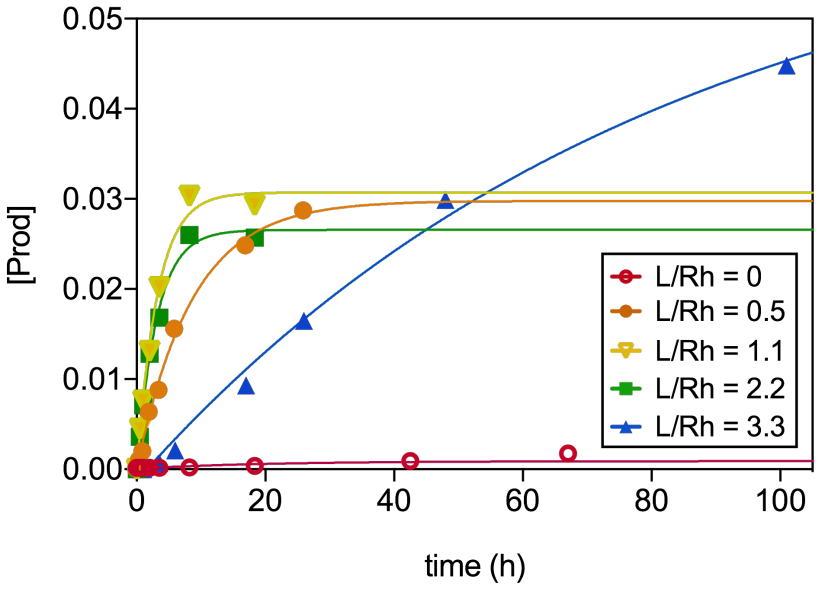

Figure 40. Change in concentration (M) of product 1.51 over time.

Because of the similar reaction rates of the reactions with a ligand to Rh ratio of one and two, reactions with ligand to Rh ratios of 0.5 and 3.3 were also performed to differentiate between the reactions with one and two ligands on the catalyst. The reaction performed with a ligand to Rh ratio of 0.5 was intended to ensure that only one ligand was bound to the active catalyst, while the reaction performed with a ligand to Rh ratio of 3.3 was intended to ensure that two ligands were bound to the active catalyst (Table 41, entries 2 and 5). The reaction performed with L/Rh = 0.5, occurred 4 times slower than the reaction performed with L/Rh = 1.1 (compare Table 41, entries 4 and 5). Alternatively, the reaction performed with L/Rh = 3.3 proceeded at a much slower rate. This slow rate could be because of hindered substrate coordination in the three or four-(*S*)-MonoPhos (**2.24**)-coordinated species.[166] Interestingly, a significant improvement in yield resulted from increasing the ligand to Rh ratio to 3.3 (90% yield, Table 41, entry 7). We propose that the presence of excess ligand could be preventing the undesired side reactions.

4.7.3 Experiment to determine coordination number of (*S*)-MonoPhos.

In the rate studies using (*S*)-MonoPhos (**2.27**) ligand described in Table 41, approximately the same enantioselectivity of the product was obtained, regardless of the (*S*)-MonoPhos/Rh ratio employed ((*S*)-**2.27**, 79-83% ee, Table 41, entries 4-7). Based on this observation, we hypothesized that regardless of the L/Rh equivalents in the reaction mixture, only one active catalytic species, either one or two-(*S*)-**2.27**-coordinated Rh, was undergoing the enantioselectivity determining oxidative cyclization step.[166] The calculations suggest that the one- and two-(*S*)-**2.27** pathways have the same activation energies (Scheme 57, right). Because good reactivity was exhibited by the L/Rh = 0.5 catalyst system, conditions in which the amount of two-(*S*)-**2.27**-coordinated complex present was assumed to be negligible, we initially postulated that the PKR proceeds via the one-(*S*)-**2.21** pathway

We tested the hypothesis that the one-(*S*)-**2.27**-coordinated Rh catalyst was effecting the enantioselectivity-determining oxidative cyclization by conducting an experiment in which the enantiomeric excess of the (*S*)-MonoPhos (**2.27**) ligand was varied from 0 to 100% ee, and the dependence of the product ee examined. A linear response of product %ee to ligand %ee would support the hypothesis that only a catalyst with one ligand is involved in the PKR mechanism.[170] The same conditions employed in the rate experiment using L/Rh = 1.1 (Table 41, entry 5) were applied in the nonlinear experiment. Reactions were performed simultaneously in 8-mL test tubes using an InnovaSyn condenser. A 0.05 M solution of mesitylene in DCE was prepared and degassed by freeze-pump-thaw (3 ×). This solution of DCE containing internal standard mesitylene was used for preparation of Rh, ligand and substrate solutions in this experiment. Solutions of Rh catalyst in DCE were added to each reaction test tube, under nitrogen. Solutions of (*S*)-MonoPhos of varying ee's were prepared, their ee's verified by HPLC, and added to the catalyst solutions. As

described in Section 4.7.1, Rh-ligand solutions were stirred 1 h at 60 °C under nitrogen atmosphere, followed by 1 h at 60 °C under 10% CO/Ar atmosphere. Enyne **1.50**, dissolved in DCE, was added to each test tube, and after 6 h at 80 °C, aliquots (100 μL) were removed from the reactions and yields were determined by ^{1}H NMR integral comparison to the internal standard, mesitylene (Table 42).

Table 42. Response of PKR product ee to changing (*S*)-MonoPhos ee.

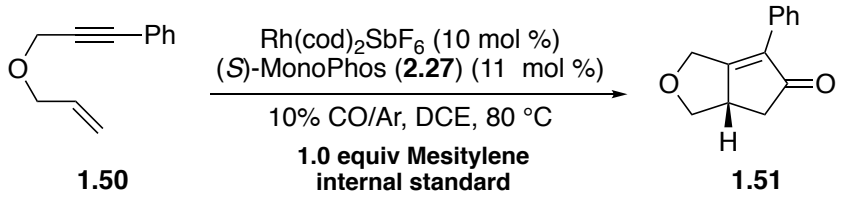

1.50 **1.51**

entry	(*S*)-MonoPhos (**2.27**) ee (%)	Yield (SM)[a]	ee (%)
1	-13	62 (12)	-11
2	9	66 (16)	5
3	31	67 (18)	20
4	52	65 (15)	39
5	76	63 (17)	58
6	100	64 (21)	83

[a] Yields were determined by integral comparison of product resonance (4.9 ppm) to mesitylene resonance (6.8 ppm). Percent recovered starting enyne is indicated in parentheses.

A plot of the response of the product ee (%) to the ligand ee (%) is shown in Figure 41. A linear correlation between the ligand ee and the product ee was observed. Based on these results, we conclude that the reaction with a ligand to Rh ratio of 1.1 most likely proceeds with one ligand in the catalytic active species.[171] Because our calculations show that the one- and two-(*S*)-MonoPhos catalysts have exactly the same activation energies (17.7 kcal/mol, Scheme 57), the number of ligands on the catalyst is likely determined by the ligand to Rh ratio employed in the reaction.

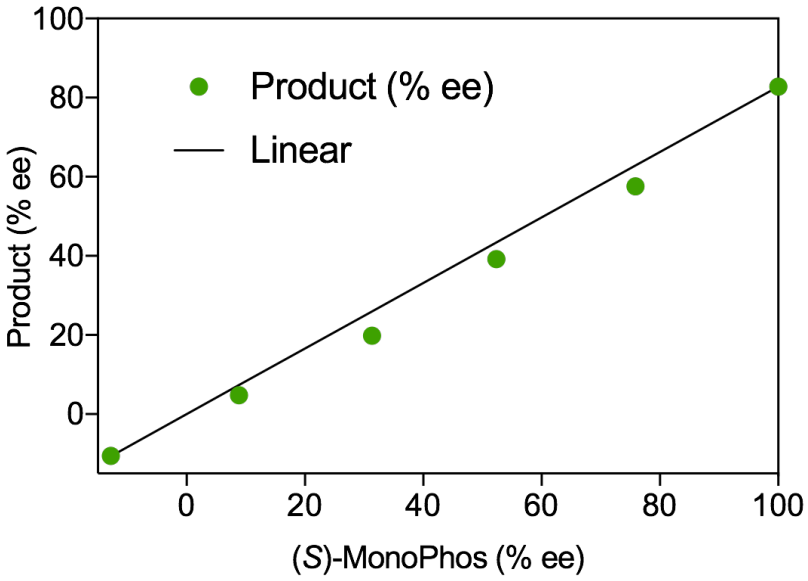

Figure 41. Linear response of product ee (%) to (*S*)-MonoPhos ee (%).

4.8 OPTIMIZATION OF (*S*)-MEANILAPHOS IN THE PKR OF ENYNES

Because of the efficiency of both phosphine and phosphoramidites ligands in the PKR, we hypothesized that a hybrid bidentate phosphine-phosphoramidite ligand would also be effective. Examples in which hybrid phosphine-phosphoramidite ligands afforded high enantioselectivity in asymmetric hydroformylations inspired us to test this hybrid ligand class in the PKR.[103]

4.8.1 Ligand loading and CO atmosphere in PKR with (*S*)-MeAnilaPhos.

We set out to test the feasibility of this hybrid catalyst system by first testing conditions previously demonstrated using (*S*)-SIPHOS (**2.42**) as a ligand. [99] At 90 °C with 100% CO, product was obtained in 34% yield and 69% ee (Table 43, entry 1). When the CO atmosphere was lowered to 10% CO/Ar, the reaction proceeded at a lower temperature (60 °C) with no improvement in yield

(entry 2). The cationic precatalyst $Rh(cod)_2SbF_6$ reacted at 80 °C in 6 h to afford product in 60% yield and 73% ee (entry 3). Lowering the temperature to 60 °C resulted in improved enantioselectivity (entry 4). The slow conversion observed at 60 °C in the presence of mesitylene prompted an increase in catalyst loading. The reaction with 10 mol % $Rh(cod)_2SbF_6$ afforded product in 77% yield and 77% ee (entry 5).

Table 43. Screening ligand loading and CO atmosphere in the PKR of (*S*)-MeAnilaPhos.

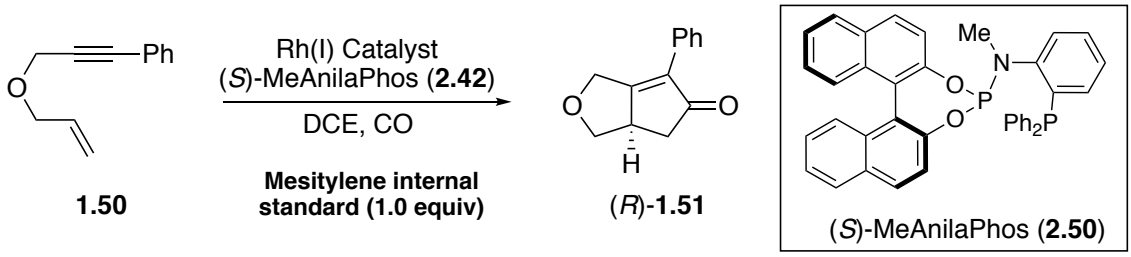

entry	Rh(I) Catalyst (mol %)	(*S*)-**2.50** (mol %)	CO/Ar (%)	T (°C)	time	yield [a]	ee (%)
1	$[Rh(CO)_2Cl]_2$ (3), $AgSbF_6$ (12)	7.2	100	90	30 m	34 (0)	69
2	$[Rh(CO)_2Cl]_2$ (3), $AgSbF_6$ (12)	7.2	10	60	30 m	31 (0)	67
3	$Rh(cod)_2SbF_6$ (5)	6	10	80	6 h	60 (0)	73
4	$Rh(cod)_2SbF_6$ (5), mesitylene (1 equiv)	6	10	60	5 d	67 (25)	76
5	$Rh(cod)_2SbF_6$ (10), mesitylene (1 equiv)	12	10	60	20 h	77 (0)	77

[a] Yields were determined by integral comparison of product resonance (4.9 ppm) to mesitylene resonance (6.8 ppm). Percent recovered starting enyne is indicated in parentheses.

4.8.2 Solvents and counteranions in the PKR with (*S*)-MeAnilaPhos.

In addition to the hexafluoroantimonate catalysts shown in Table 43, several alternative solvents and counteranions were tested in the PKR using (*S*)-MeAnilaPhos (**2.50**). No reaction occurred in coordinating solvent THF (Table 44, entries 1-3). Product was observed in moderately

coordinating solvent toluene with the noncoordinating BArF anion (entry 6), and in all three reactions in noncoordinating solvent DCE (entries 7-9). Enantioselectivities from 75 to 67% ee were achieved, with the highest enantioselectivity achieved in DCE with triflate counteranion (75%, entry 7). None of the conditions tested in this study offered improved yield or enantioselectivity over the hexafluoroantimonate catalyst with DCE solvent (Table 44). In summary, phosphine-phosphoramidite ligand (*S*)-MeAnilaPhos (**2.50**) provided cyclopentenone product (*R*)-**1.51** in 77% yield, and 77% ee (entry 5). This enantioselectivity is similar to that obtained by the (*S*)-MonoPhos (**2.27**) ligand.

Table 44. Solvents and Rh counteranions tested in the PKR of (*S*)-MeAnilaPhos.

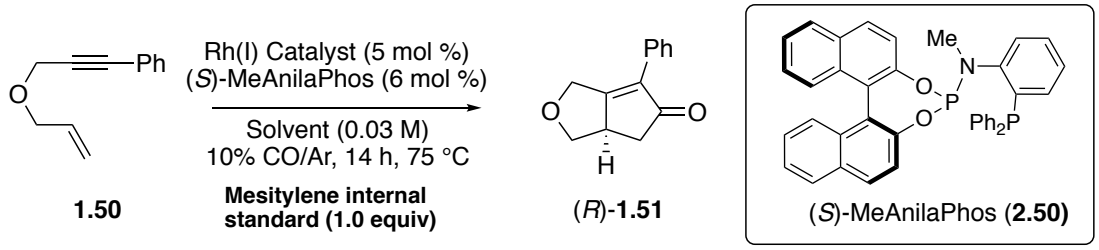

entry	solvent	Rh(I) Catalyst	yield (%)[a]	ee (%)
1	THF	$Rh(cod)_2OTf$	NR	-
2	THF	$Rh(cod)_2BF_4$	NR	-
3	THF	$Rh(cod)_2BArF$	NR	-
4	Toluene	$Rh(cod)_2OTf$	trace	-
5	Toluene	$Rh(cod)_2BF_4$	trace	-
6	Toluene	$Rh(cod)_2BArF$	16 (60)	67
7	DCE	$Rh(cod)_2OTf$	19 (48)	75
8	DCE	$Rh(cod)_2BF_4$	27 (39)	72
9	DCE	$Rh(cod)_2BArF$	20 (59)	70

[a] Yields were determined by integral comparison of product resonance (4.9 ppm) to mesitylene resonance (6.8 ppm). Percent recovered starting enyne is indicated in parentheses.

4.9 CONCLUSIONS FROM COMPUTATIONAL AND EXPERIMENTAL STUDIES OF THE ENANTIOSELECTIVE PKR

We have demonstrated a combined experimental and computational approach to study the mechanism of the enantioselective PKR of enyne **1.50**. A thorough investigation of the lowest-energy PKR mechanisms for cationic Rh-(*R*)-BINAP (**2.24**), Rh-(*S*)-MonoPhos (**2.27**), and Rh-CO only catalysts was performed. Lower substrate coordination energies were observed for the Rh-(*S*)-MonoPhos (**2.27)** catalysts (compared to the Rh-(*R*)-BINAP (**2.24**)-CO catalyst (Scheme 51 and Scheme 56). This lower substrate coordination energy be beneficial in the application of monodentate phosphoramidite ligands in PKRs of sterically demanding substrates.

Calculation of the reaction energy profile of the Rh-(*R*)-BINAP catalyst revealed that oxidative cyclization is the rate- and enantioselectivity-determining step. The four-coordinated Rh-(*R*)-BINAP oxidative cyclization transition state was preferred over the five-coordinated transition state by 3.7 kcal/mol, and affords (*R*)-**1.51** product (Scheme 52), a prediction which was validated by VCD spectroscopy (Figure 37). A comparison of the activation energies of Rh-(*R*)-BINAP (**2.24**) and Rh-(*S*)-MonoPhos (**2.27**) catalysts with the Rh-CO only catalyst revealed a higher activation energy for the ligand-free catalyst ($\Delta\Delta G^{\ddagger}$ = 8.6 kcal/mol). This computational result was quantified experimentally by rate studies of the two ligand classes and a substantial ligand acceleration effect was observed. For example, the PKR was accelerated approximately 3000-fold in the presence of BINAP ligand, and 180-fold in the presence of (*S*)-MonoPhos (**2.27**) ligand. This ligand acceleration effect is especially advantageous in the PKR using monodentate ligands, wherein a mixture of catalyst structures exists.[168]

The Rh-(*S*)-MonoPhos-catalyzed PKR exhibits a linear response to changing the ee of the ligand (Figure 41). This result demonstrates that, under reaction conditions with a ligand to Rh

ratio of 1.1, the PKR most likely proceeds with one (*S*)-MonoPhos (**2.27**) ligand on the catalyst.[171] Therefore, good enantioselectivity can be achieved in the PKR using (*S*)-MonoPhos ligands when only one ligand is bound to the catalyst. We anticipate that these mechanistic studies will encourage the application of phosphoramidite ligands in the PKR of new substrates.

SUPPORTING INFORMATION

CHAPTER 4

General Methods

Unless otherwise indicated, all reactions were performed in flame-dried glassware under an inert atmosphere of dry nitrogen and stirred with Teflon-coated magnetic stir bars. All commercially available compounds were purchased and used as received unless otherwise specified. Tetrahydrofuran (THF) and was purified by passing through alumina using the Sol-Tek ST-002 solvent purification system. 1,2-dichloroethane (DCE) was distilled from calcium hydride prior to use. Deuterated chloroform ($CDCl_3$) was dried over 3 Å molecular sieves. Gasses N_2, O_2, 100% CO, and 10% CO/Ar, were purchased from Matheson Tri Gas. Ligands (*S*)-MonoPhos, (*R*)-MonoPhos, and (*R*)-BINAP were purchased from Strem Chemicals and used as received. Absolute configurations of purchased chiral ligands (*S*)-MonoPhos and (*R*)-BINAP were checked using a Perkin Elmer 241 spectropolarimeter, and the observed optical rotations matched those reported. Ligands were stored and weighed in a nitrogen-filled glovebox. Purification of compounds by flash column chromatography was performed using silica gel (40-63 μm particle size, 60 Å pore size). TLC analyses were performed on silica gel F_{254} glass-backed plates (250 μm thickness). ^{1}H NMR, ^{13}C NMR and ^{31}P NMR spectra were recorded on Bruker Avance 400, or 500 MHz spectrometers. Spectra were referenced to residual chloroform (7.26 ppm, ^{1}H; 77.16 ppm, ^{13}C). Chemical shifts (δ) are reported in ppm and multiplicities are indicated by s (singlet), d (doublet), t (triplet), q (quartet), quint (quintet), and m (multiplet). Coupling constants, *J*, are reported in hertz (Hz). All

NMR spectra were obtained at room temperature. HPLCs were performed using a Waters 600 series solvent delivery module with a photodiode array detector and a Daicel CHIRALPAK IA-3 column with an injection volume of 50 μL and a flow rate of 1.0 mL/min. Optical rotations (reported in 10 $deg^{-1}cm^2\ g^{-1}$) were measured at 589 nm (sodium D line) using a Perkin Elmer 241 spectropolarimeter.

Synthesis of enyne 1.50.

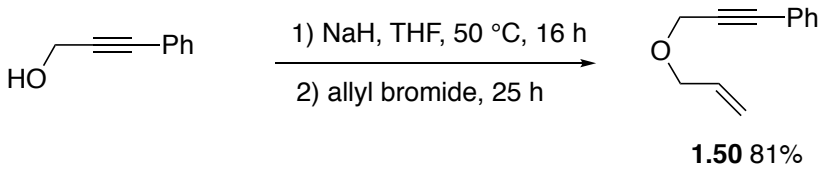

1.50 81%

1-(Allyloxy)but-2-yne (1.50). The synthesis of **1.50** was performed in a manner analogous to that previously reported.[172] To a flame-dried, two-necked 25-mL, round-bottomed flask equipped with a nitrogen inlet adaptor, a septum and a stirbar, was added NaH (0.63 g, 26 mmol, 1.4 equiv) as a solid under a stream of nitrogen, followed by THF (7.5 mL, 2.5 M) via syringe. 3-Phenylprop-2-yn-1-ol (2.5 g, 19.1 mmol, 1.0 equiv) was added to the stirred solution via syringe. The reaction was lowered into a preheated oil bath (50 °C). After 16 h, the reaction was cooled to rt and allyl bromide (2.8 g, 23 mmol, 1.2 equiv) was added via syringe. After another 24 h at 50 °C, complete consumption of starting alcohol was observed by TLC. The reaction was cooled to rt and poured into 20 mL water. The mixture was transferred to a 250-mL separatory funnel and extracted with ether (2 × 50 mL). The combined organic layers were dried over magnesium sulfate, gravity filtered and concentrated under reduced pressure. The crude product was purified by vacuum distillation (10 mmHg, 80 °C) to yield the title compound as a clear oil (2.2 g, 81%). The product **1.50** was previously characterized and all spectral data match those reported. LCP 1-138

^{1}H NMR (300 MHz, $CDCl_3$)

7.47-7.44 (m, 2 H), 7.38-7.30 (m, 3 H), 5.95 (ddt, J = 5.7, 10.5, 11.4), 5.34 (dq, J = 1.5, 15.6 Hz, 1 H), 5.24 (dd, J = 1.2, 10.2, 1 H) 4.15 (dt, J = 1.2, 5.7, 2 H) ppm

TLC: R_f = 0.8 (20% ethyl acetate in hexanes) [Silica gel, UV, *p*-anisaldehyde]

Racemic PKR of enyne 1.51.

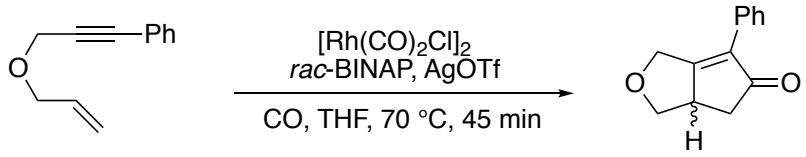

1.50 **1.51** 72%

6-Phenyl-3a,4-dihydro-1*H*-cyclopenta[*c*]furan-5(3*H*)-one (1.51). The synthesis of **1.51** was performed in a manner analogous to that previously reported.[75] To a flame-dried, two-necked 10 mL round-bottomed flask equipped with a condenser, stir bar and septa was added a solution of rhodium biscarbonyl chloride dimer (5.8 mg, 0.015 mmol, 0.03 equiv) in THF (0.5 mL) under argon atmosphere. A solution of *rac*-BINAP (20.8 mg, 0.045 mmol, 0.09 equiv) in THF (2 mL) was added via syringe. After 15 min at rt, a solution of silver trifluoromethanesulfonate (15.4 mg, 0.03 mmol, 0.06 equiv) in THF (0.5 mL) was added via syringe. After another 15 min, the atmosphere was evacuated and refilled with CO (3 ×) using a needle attached to a vacuum manifold. After 15 min under a balloon of CO, enyne **1.50** (86 mg, 0.50 mmol, 1 equiv) in THF (0.5 mL) was added dropwise. The reaction was lowered into a preheated oil bath (70 °C). After 45 min, complete consumption of starting enyne was observed by TLC. The oil bath was removed and the reaction allowed to cool to room temperature. The crude reaction was passed through a plug of silica gel with DCM (20 mL) and concentrated under reduced pressure. The crude residue

was purified by silica gel column flash chromatography (10-30% ethyl acetate/hexanes) to yield the title compound as a clear oil (72 mg, 72%). The product **1.51** was previously characterized and all spectral data match those reported. LCB 5-019

^{1}H NMR (400 MHz, $CDCl_3$)

7.54 (dd, J = 1.6, 8.8 Hz, 2 H), 7.42 (t, J = 7.2 Hz, 2 H), 7.36 (m, 1 H), 4.94 (d, J = 16.4 Hz, 1 H), 4.70 (d, J = 16.4 Hz, 1 H), 4.39 (t, J = 7.6 Hz, 1 H), 3.25 (dd,J = 8.0, 11.2, 1 H), 2.86 (dd, J = 6.4, 17.6 Hz, 1 H), 2.35 (dd, J = 3.6, 17.6 Hz, 1 H)

TLC: R_f = 0.2 (20% ethyl acetate in hexanes) [Silica gel, UV, *p*-anisaldehyde]

General Procedure E: Enantioselective PKR of enyne 1.50.

Preparation of solvent containing internal standard. To a 50-mL Schlenk flask, was added mesitylene (77 mg) and DCE (12.7 mL) to afford a solution of mesitylene in DCE (0.05 M). This solution was degassed by freeze-pump-thaw (3 ×) and was used for preparation of all solutions in rate experiments.

General procedure for PKR rate experiments. In a nitrogen-filled glovebox, rhodium(I) bis(1,5-cyclooctadiene) hexafluoroantimonate (20 mg) was weighed into a 15-mL round-bottomed flask and sealed with a rubber septum. In a separate 15-mL, round-bottomed flask, (*S*)-MonoPhos (**2.27**) (14 mg) was weighed and sealed with a rubber septum. The flasks were removed from the glovebox and placed in a fume hood. PKRs were performed in oven-dried, 8-mL screw-top test tubes, sealed with Teflon caps (ChemGlass, CG-4910, PTFE septa) using an InnovaSyn condenser. Rhodium bis(1,5-cyclooctadiene) hexafluoroantimonate was dissolved in the prepared DCE/mesitylene solution (2.4 mL, 0.015 M) and a portion of this solution (0.67 mL, containing

5.6 mg Rh, 0.10 equiv) was added to each test tube under nitrogen. (*S*)-MonoPhos (**2.27**) was dissolved in the prepared DCE/mesitylene solution (1.2 mL, 0.033 M), and a portion of this solution (0.67 mL containing 7.9 mg (*S*)-MonoPhos (**2.27**), 0.22 equiv) was added to the test tube. The test tubes were lowered into a preheated oil bath (60 °C). After 1 h, the atmosphere was evacuated and refilled with 10% CO/Ar (3 ×) using a needle attached to a vacuum manifold. The test tubes remained under balloons of 10% CO/Ar attached to inlet needles at 60 °C for another 1 h. The test tubes were removed from the oil bath and the temperature of the oil bath was increased to 80 °C. Enyne **1.51** (55 mg) was weighed in a separate 15-mL round-bottomed flask and sealed with a septum and placed under nitrogen. The prepared DCE/mesitylene solution was added (2.2 mL, 0.15 M). A portion of this enyne/DCE/mesitylene solution was added to the test tube (0.67 mL solution, containing 17.2 mg enyne, 0.10 mmol, 1.0 equiv). The final volume of each reaction mixture was 2 mL, containing 0.10 mmol of mesitylene, or 1.0 equiv mesitylene with respect to enyne substrate. The test tubes were lowered into the preheated oil bath (80 °C) and a timer started. The reaction mixtures were stirred at a rate of 1000 rpm under balloons of 10% CO/Ar.

Aliquots for analysis by ^1H NMR. At the time points indicated in Tables 45-51, aliquots of the reaction mixtures (100 μL) were removed using a 250 μL syringe, added to an oven-dried NMR tube, and diluted with $CDCl_3$ (500 μL). The samples were submitted for yield determination by ^1H NMR via integral comparison of the vinyl proton peak of the product (ddt, 5.9 ppm, 1 H) to the mesitylene internal standard aromatic peak (6.8 ppm, 3 H). The large DCE solvent peak at 3.7 ppm did not interfere with integrations of the mesitylene, enyne and cyclopentenone peaks.

Removal of catalyst and determination of enantiomeric excess by HPLC. Silica gel (0.2 g) was added to the reaction test tube, DCE removed by rotary evaporation, and the resulting mixture was loaded onto a silica gel plug and the product **1.51** was eluted with 50% ethyl acetate/hexanes (10 mL). The resulting crude product solution was concentrated by rotary evaporation and redissolved in 10% *i*PrOH/hexanes (HPLC grade). The enantiomeric ratios of products were determined by HPLC using a Daicel CHIRALPAK IA-3 column (25 cm), eluting with 10% *i*PrOH/hexanes with a flow rate of 1.0 mL/min and detecting at 254 nm.

PKR of enyne 1.50 using cationic Rh catalyst with no phosphorous ligand.

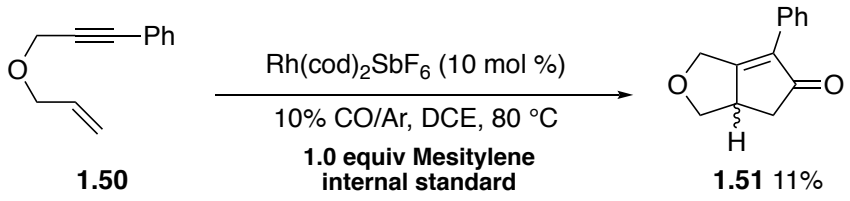

1.50 **1.51** 11%

Follows general procedure E. Enyne **1.50** (17 mg, 0.10 mmol, 1.0 equiv), rhodium(I) bis(1,5-cyclooctadiene hexafluoroantimonate (5.6 mg, 0.01 mmol, 0.10 equiv), prepared solution of DCE/mesitylene (2.0 mL, containing 12.0 mg mesitylene, 0.10 mmol, 1.0 equiv). The test tube was placed in a preheated oil bath (80 °C) under a balloon of 10% CO/Ar and aliquots were removed periodically for analysis by ^{1}H NMR spectroscopy. Yield was determined by integral comparison to the internal standard mesitylene (11% after 245 h). LCB 5-180

Table 45. ^{1}H NMR monitoring of PKR with no phosphorous ligand.

time (h)	time (min)	SM (%)	[SM]	Prod (%)	[Prod]
0.033	2	1.000	0.05	0	0
8.17	490	0.934	0.0467	0.000943	0.0000472
18.33	1100	0.896	0.0448	0.00443	0.000222
42.5	2550	0.858	0.0429	0.0156	0.000778
67	4020	0.840	0.0420	0.0317	0.00158
137.75	8265	0.708	0.0354	0.0415	0.00207
244.50	14760	0.557	0.0278	0.113	0.00566

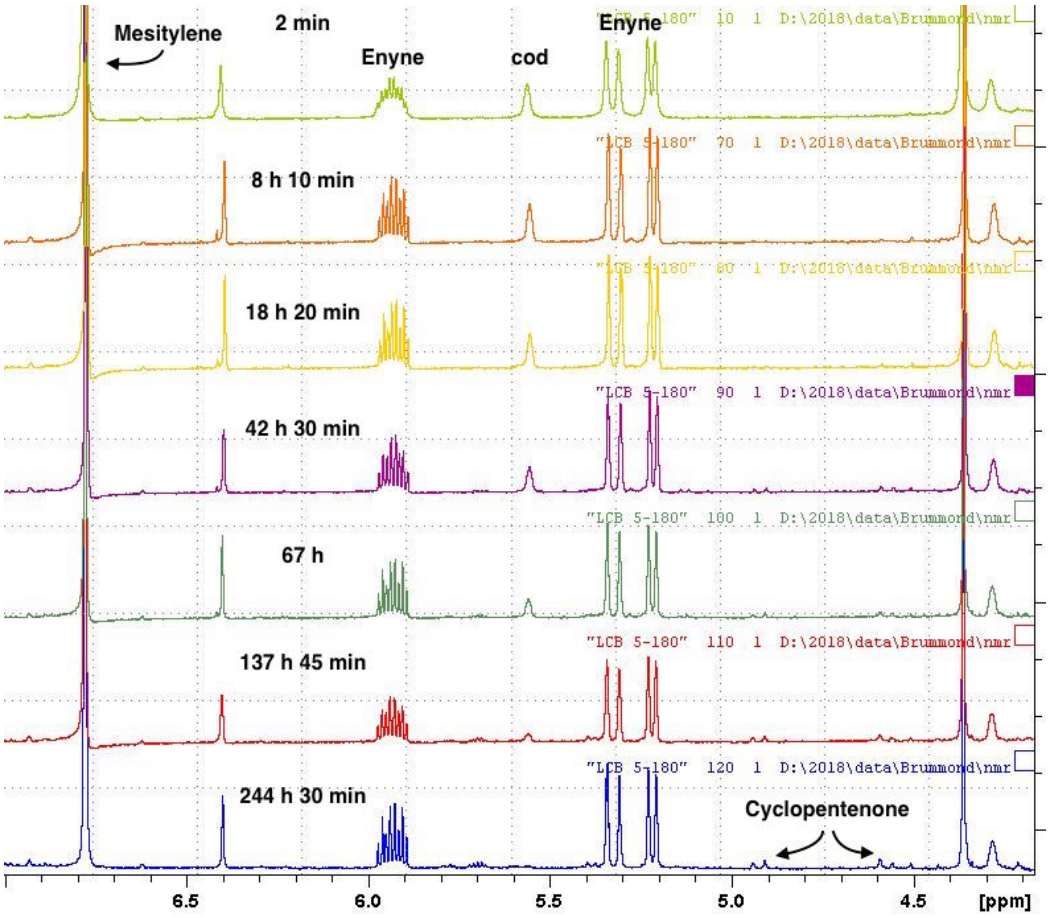

Figure 42. Peaks monitored in rate experiment with no phosphorous ligand.

Enantioselective PKR of enyne 1.50 with (*R*)-BINAP ligand.

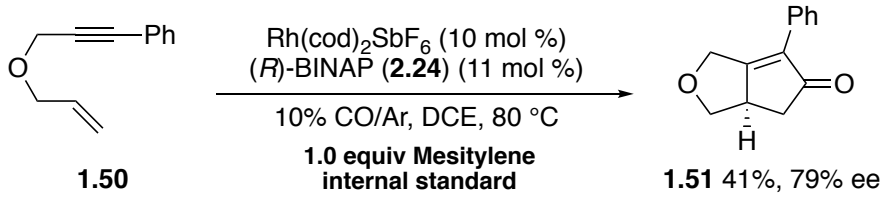

1.50 **1.51** 41%, 79% ee

Follows general procedure E. Enyne **1.50** (17 mg, 0.10 mmol, 1.0 equiv), rhodium(I) bis(1,5-cyclooctadiene hexafluoroantimonate (5.6 mg, 0.01 mmol, 0.10 equiv), (*R*)-BINAP (**2.24**) (6.8 mg, 0.011 mmol, 0.11 equiv), prepared solution of DCE/mesitylene (2.0 mL, containing 12.0 mg mesitylene, 0.10 mmol, 1.0 equiv). The test tube was placed in a preheated oil bath (80 °C) under a balloon of 10% CO/Ar and aliquots were removed periodically for analysis by ^{1}H NMR spectroscopy. Yield was determined by integral comparison to the internal standard mesitylene (41% after 1 h). LCB 5-195

Table 46. ^{1}H NMR monitoring of PKR with (*R*)-BINAP.

time (h)	time (min)	SM (%)	[SM]	Prod (%)	[Prod]
0.03	2	0.691	0.0346	0.1760	0.0088
0.50	30	0.042	0.0021	0.3620	0.0181
1.00	60	0.001	0.0001	0.4060	0.0203

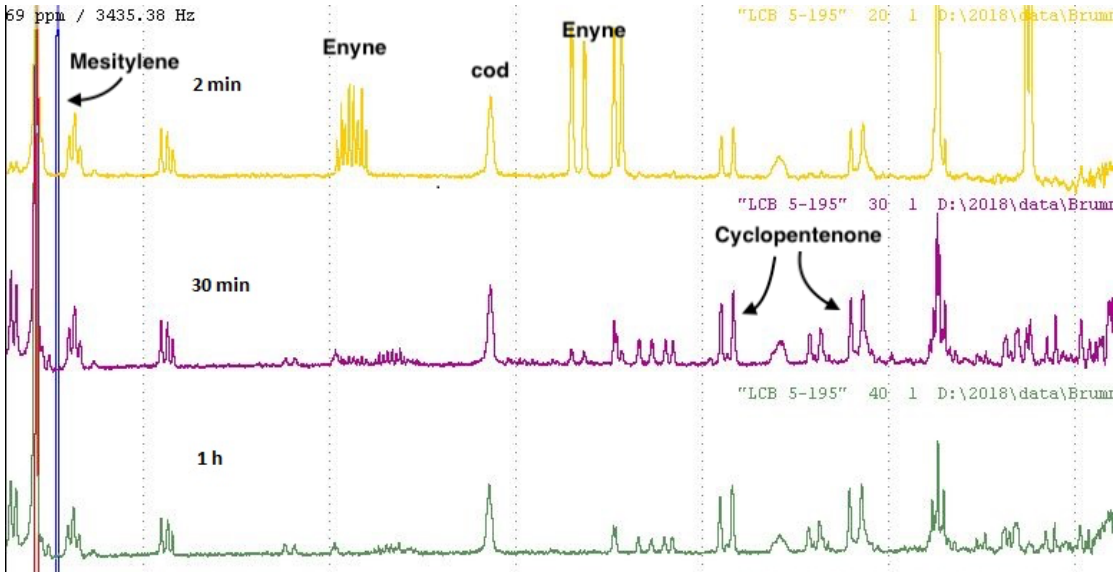

Figure 43. Peaks monitored in rate experiment with (*R*)-BINAP.

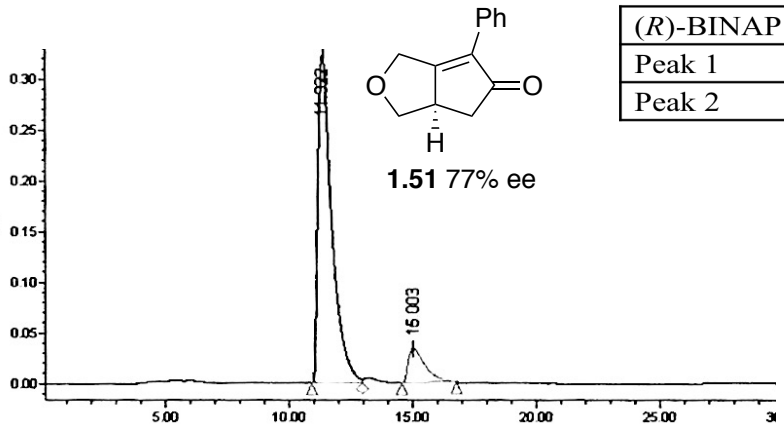

(*R*)-BINAP	Ret. Time (min)	% Area
Peak 1	11.322	88.65
Peak 2	15.003	11.35

PKR of enyne 1.50 with PPh_3 ligand.

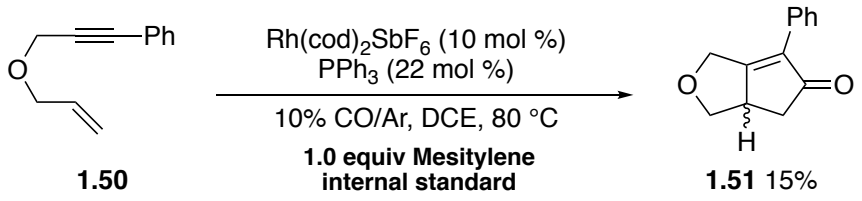

1.50 **1.51** 15%

Follows general procedure E. enyne **1.50** (17 mg, 0.10 mmol, 1.0 equiv), rhodium(I) bis(1,5-cyclooctadiene hexafluoroantimonate (5.6 mg, 0.01 mmol, 0.10 equiv), triphenylphosphine (5.8 mg, 0.022 mmol, 0.22 equiv), prepared solution of DCE/mesitylene (2.0 mL, containing 12.0 mg mesitylene, 0.10 mmol, 1.0 equiv). The test tube was placed in a preheated oil bath (80 °C) under a balloon of 10% CO/Ar and aliquots were removed periodically for analysis by ^{1}H NMR spectroscopy. Yield was determined by integral comparison to the internal standard mesitylene (15% after 141 h).

Table 47. ^{1}H NMR monitoring of PKR with PPh_3.

time (h)	time (min)	SM (%)	[SM]	Prod (%)	[Prod]
0.03	2	1.000	0.0500	0.00000	0.00000
0.50	30	0.942	0.0471	0.00000	0.00000
1.00	60	0.923	0.0435	0.00000	0.00000
2.00	120	0.846	0.0368	0.00000	0.00000
3.67	220	0.760	0.0280	0.00962	0.00048
7.67	460	0.654	0.0183	0.02885	0.00144
18.42	1105	0.519	0.0095	0.06731	0.00337
52	3120	0.375	0.0036	0.14423	0.00721
141	8460	0.231	0.0008	0.15385	0.00769

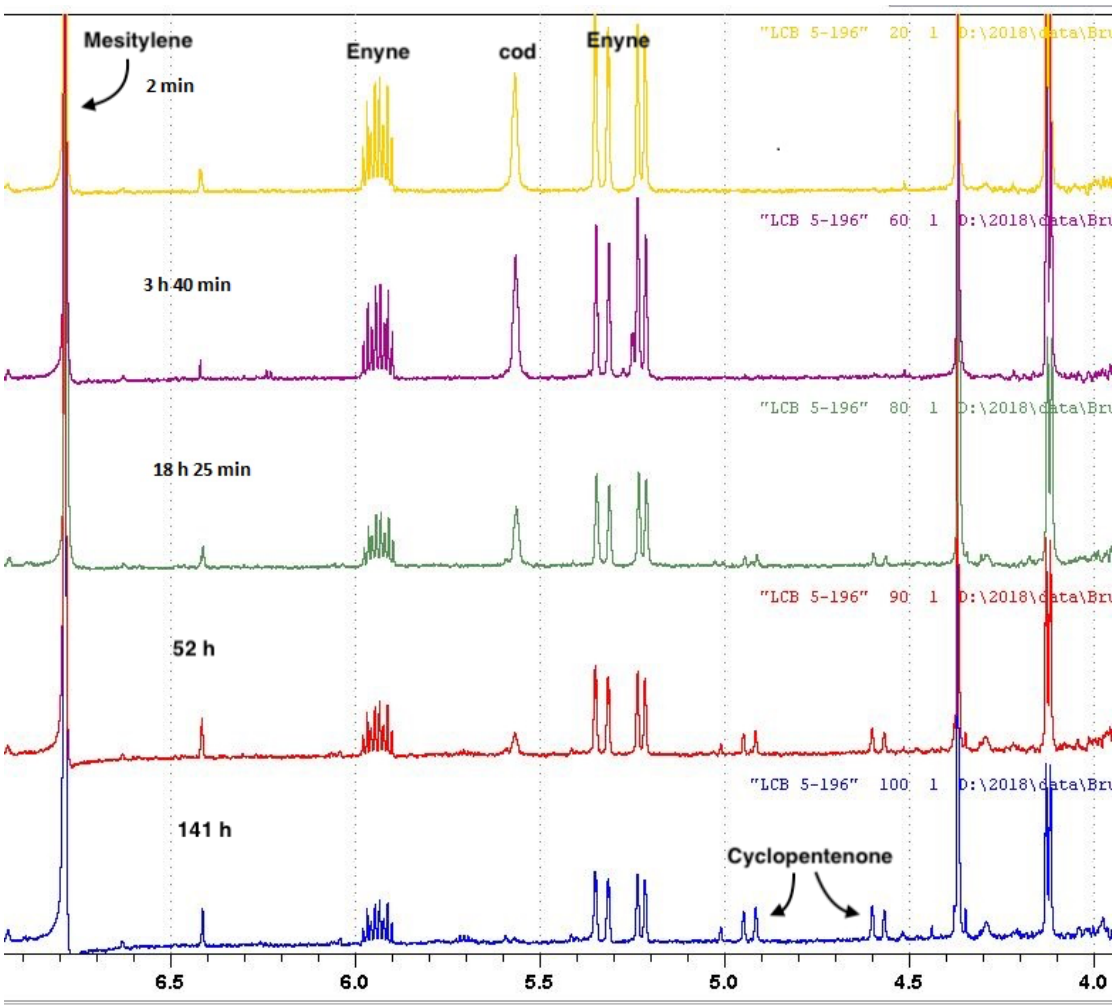

Figure 44. Peaks monitored in rate experiment with PPh_3.

Enantioselective PKR of enyne 1.50 with (*S*)-MonoPhos to Rh ratio of 0.5.

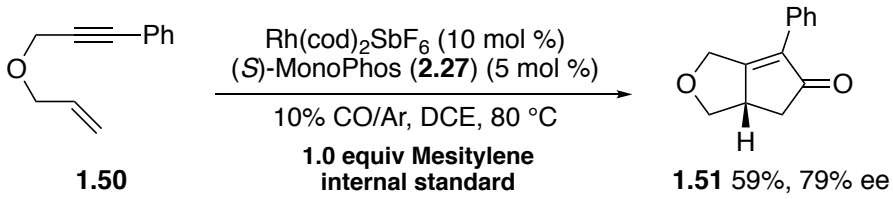

1.50 **1.51** 59%, 79% ee

Follows general procedure E. enyne **1.50** (17 mg, 0.10 mmol, 1.0 equiv), rhodium(I) bis(1,5-cyclooctadiene hexafluoroantimonate (5.6 mg, 0.01 mmol, 0.10 equiv), (*S*)-MonoPhos (**2.27**) (1.8 mg, 0.005 mmol, 0.05 equiv), prepared solution of DCE/mesitylene (2.0 mL, containing 12.0 mg mesitylene, 0.10 mmol, 1.0 equiv). The test tube was placed in a preheated oil bath (80 °C) under a balloon of 10% CO/Ar and aliquots were removed periodically for analysis by ^{1}H NMR spectroscopy. Yield was determined by integral comparison to the internal standard mesitylene (59% after 48 h). LCB 5-184

Table 48. ^{1}H NMR monitoring of PKR with (*S*)-MonoPhos to Rh ratio of 0.5.

time (h)	time (min)	SM (%)	[SM]	Prod (%)	[Prod]
0.05	3	1.000	0.0500	0.000	0.0000
0.5	30	0.961	0.0481	0.019	0.0010
1	60	0.913	0.0456	0.039	0.0019
2	120	0.816	0.0408	0.126	0.0063
3.5	210	0.680	0.0340	0.175	0.0087
6	360	0.515	0.0257	0.311	0.0155
17	1020	0.165	0.0083	0.495	0.0248
26	1560	0.058	0.0029	0.573	0.0286
48	2880	0.010	0.0005	0.592	0.0296

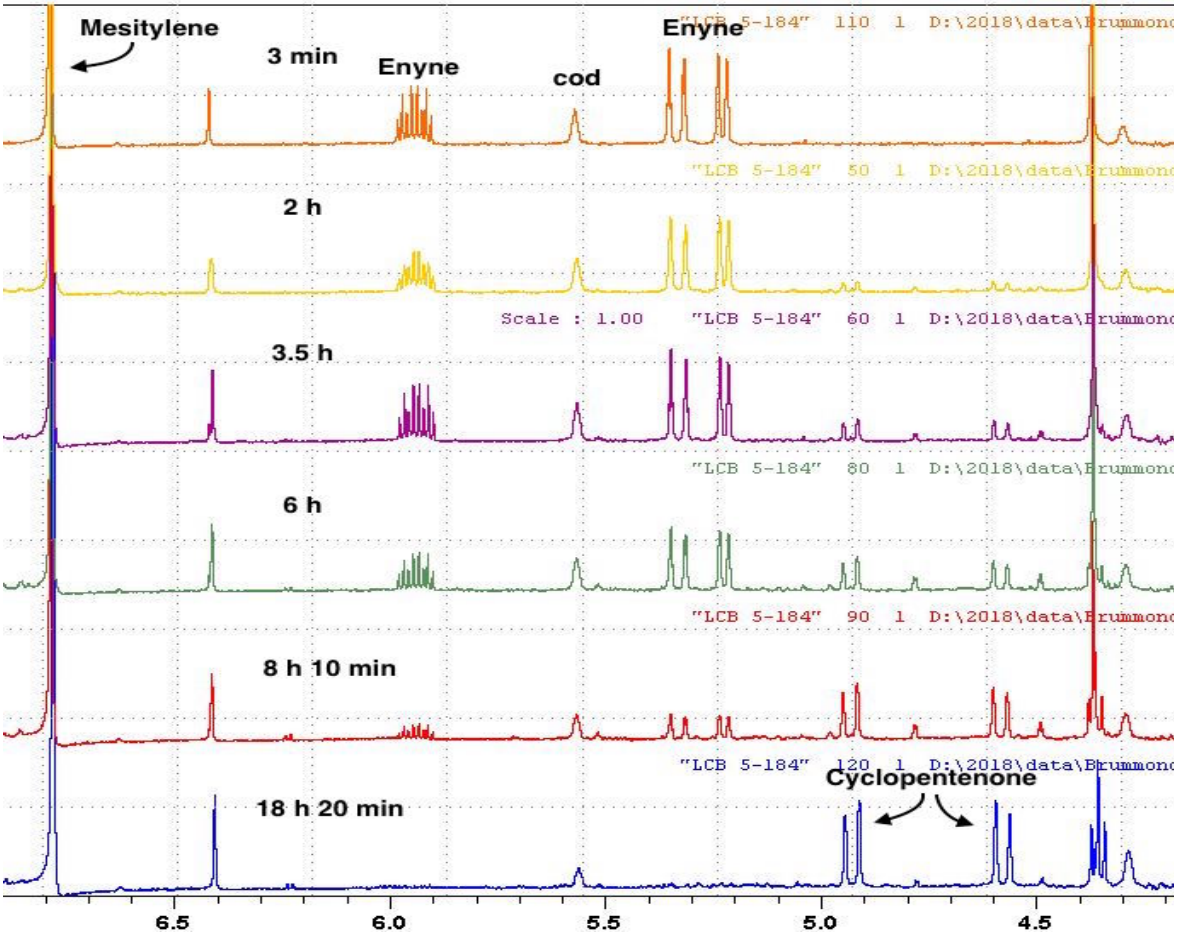

Figure 45. Peaks monitored in rate experiment with (*S*)-MonoPhos to Rh ratio of 0.5.

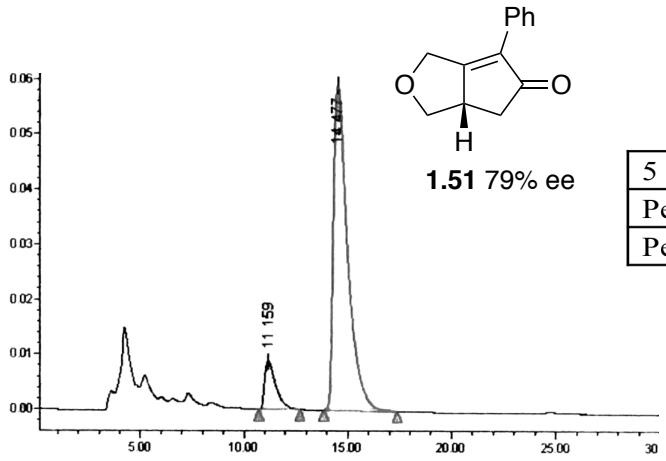

1.51 79% ee

5 mol % **2.27**	Ret. Time (min)	% Area
Peak 1	11.159	10.43
Peak 2	14.477	89.57

Enantioselective PKR with (*S*)-MonoPhos to Rh ratio of 1.1.

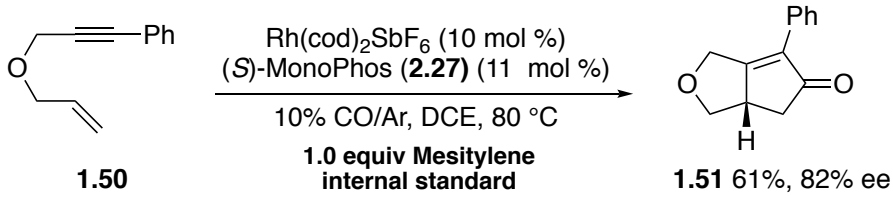

1.50 **1.51** 61%, 82% ee

Follows general procedure E. Enyne **1.50** (17 mg, 0.10 mmol, 1.0 equiv), rhodium(I) bis(1,5-cyclooctadiene hexafluoroantimonate (5.6 mg, 0.01 mmol, 0.10 equiv), (*S*)-MonoPhos (**2.27**) (4.0 mg, 0.011 mmol, 0.11 equiv), prepared solution of DCE/mesitylene (2.0 mL, containing 12.0 mg mesitylene, 0.10 mmol, 1.0 equiv). The test tube was placed in a preheated oil bath (80 °C) under a balloon of 10% CO/Ar and aliquots were removed periodically for analysis by ^{1}H NMR spectroscopy. Yield was determined by integral comparison to the internal standard mesitylene (61% after 8.2 h). LCB 5-179

Table 49. ^{1}H NMR monitoring of PKR with (*S*)-MonoPhos to Rh ratio of 1.1.

time (h)	time (min)	SM (%)	[SM]	Prod (%)	[Prod]
0.033	2	1.000	0.0500	0	0
0.5	30	0.869	0.0434	0.091	0.0045
1	60	0.697	0.0348	0.152	0.0076
2	120	0.485	0.0242	0.263	0.0131
3.5	210	0.263	0.0131	0.404	0.0202
8.17	490	0.040	0.0020	0.606	0.0303
18.3	1100	0.010	0.0005	0.586	0.0293

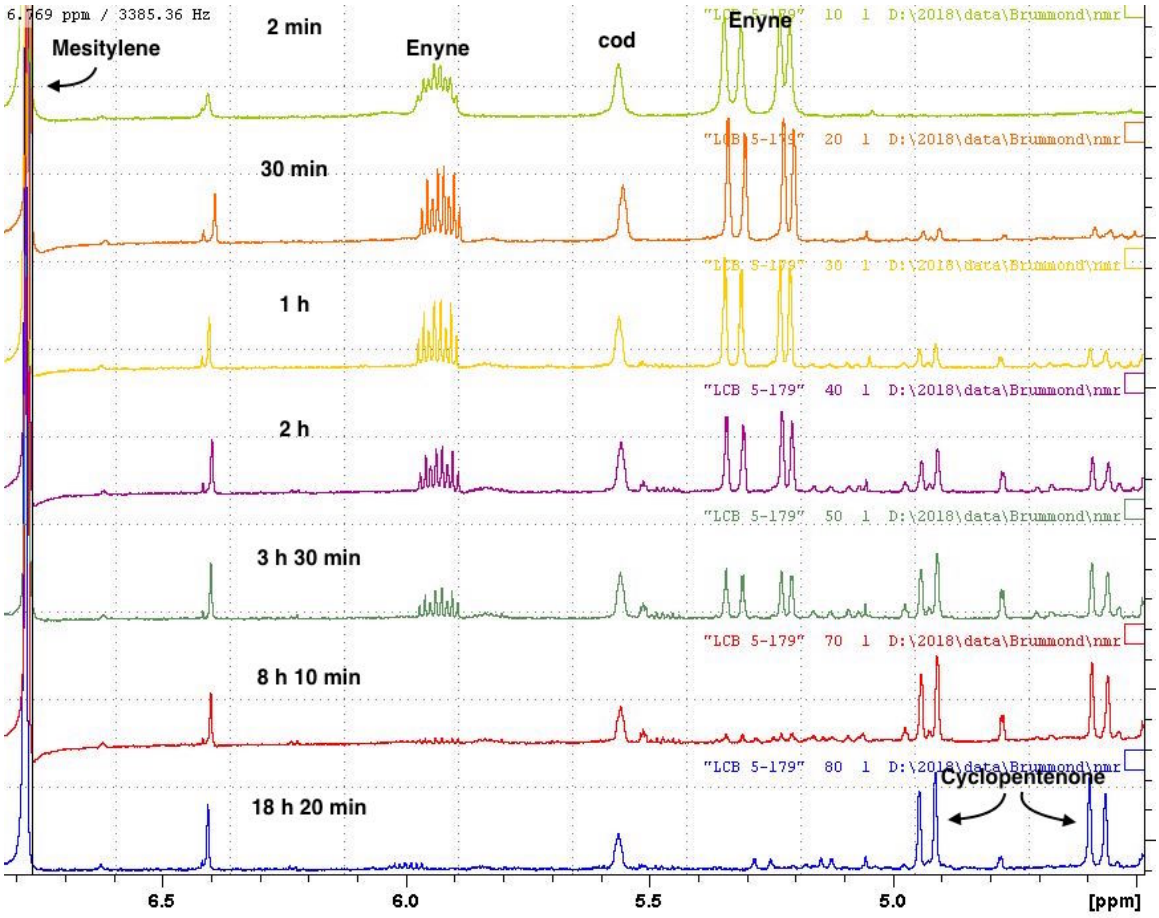

Figure 46. Peaks monitored in rate experiment with (*S*)-MonoPhos to Rh ratio of 1.1.

11 mol % **2.27**	Ret. Time (min)	% Area
Peak 1	11.338	8.88
Peak 2	14.787	91.12

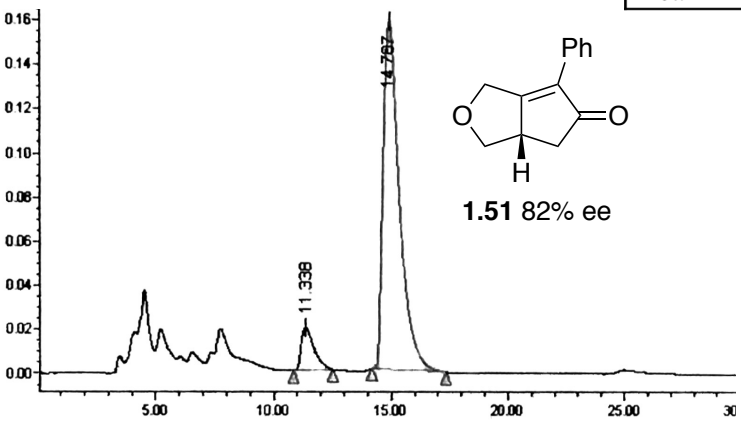

1.51 82% ee

Enantioselective PKR with (*S*)-MonoPhos to Rh ratio of 2.2.

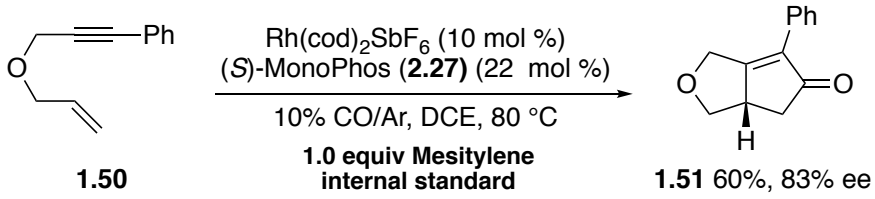

1.50 **1.51** 60%, 83% ee

Follows general procedure E. Enyne **1.50** (17 mg, 0.10 mmol, 1.0 equiv), rhodium(I) bis(1,5-cyclooctadiene hexafluoroantimonate (5.6 mg, 0.01 mmol, 0.10 equiv), (*S*)-MonoPhos (**2.27**) (7.9 mg, 0.022 mmol, 0.22 equiv), prepared solution of DCE/mesitylene (2.0 mL, containing 12.0 mg mesitylene, 0.10 mmol, 1.0 equiv). The test tube was placed in a preheated oil bath (80 °C) under a balloon of 10% CO/Ar and aliquots were removed periodically for analysis by ^{1}H NMR spectroscopy. Yield was determined by integral comparison to the internal standard mesitylene (60% after 7.7 h). LCB 5-194

Table 50. ^{1}H NMR monitoring of PKR with (*S*)-MonoPhos to Rh ratio of 2.2.

	time (min)	SM (%)	[SM]	Prod (%)	[Prod]
0.03	2	1.000	0.0500	0.0010	0.0000
0.50	30	0.865	0.0433	0.0858	0.0037
1.00	60	0.702	0.0351	0.1896	0.0082
2.00	120	0.470	0.0235	0.3393	0.0147
3.67	220	0.227	0.0113	0.4900	0.0212
7.67	460	0.001	0.0000	0.5978	0.0259
18.4	1105	0.001	0.0000	0.5689	0.0246

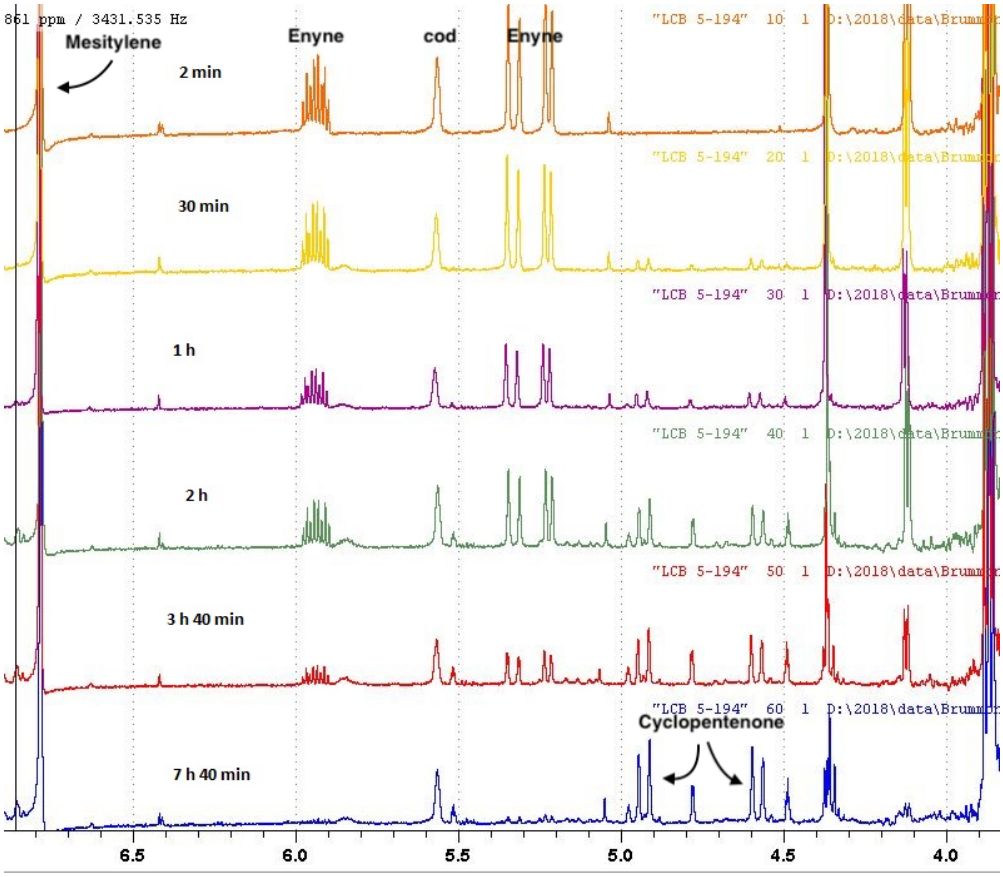

Figure 47. Peaks monitored in rate experiment with (*S*)-MonoPhos to Rh ratio of 2.2.

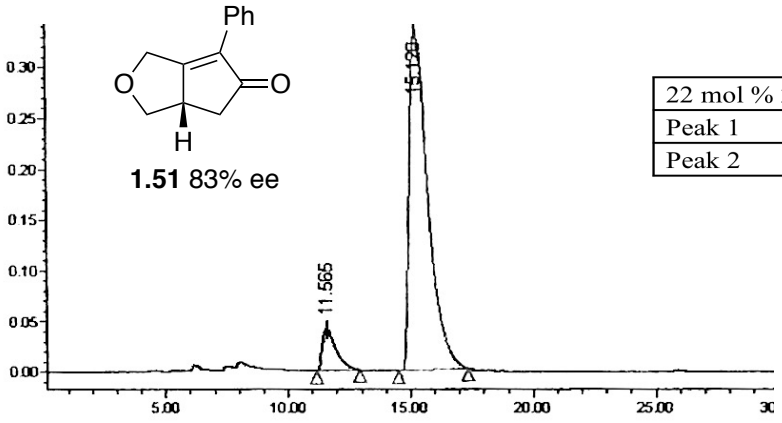

22 mol % **2.27**	Ret. Time (min)	% Area
Peak 1	11.565	8.27
Peak 2	15.128	91.73

Enantioselective PKR with (*S*)-MonoPhos to Rh ratio of 3.3.

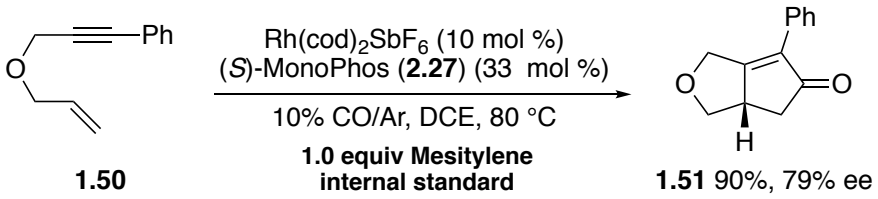

1.50 **1.51** 90%, 79% ee

Follows general procedure E. Enyne **1.50** (17 mg, 0.10 mmol, 1.0 equiv), rhodium(I) bis(1,5-cyclooctadiene hexafluoroantimonate (5.6 mg, 0.01 mmol, 0.10 equiv), (*S*)-MonoPhos (**2.27**) (11.9 mg, 0.033 mmol, 0.33 equiv), prepared solution of DCE/mesitylene (2.0 mL, containing 12.0 mg mesitylene, 0.10 mmol, 1.0 equiv). The test tube was placed in a preheated oil bath (80 °C) under a balloon of 10% CO/Ar and aliquots were removed periodically for analysis by ^{1}H NMR spectroscopy. Yield was determined by integral comparison to the internal standard mesitylene (90% after 101 h). LCB 5-185

Table 51. ^{1}H NMR monitoring of PKR with 33 mol % (*S*)-MonoPhos.

time (h)	time (min)	SM (%)	[SM]	Prod (%)	[Prod]
0.05	3	1.000	0.0500	0.000	0.0000
0.5	30	0.990	0.0495	0.000	0.0000
1	60	1.000	0.0500	0.000	0.0000
3.5	210	0.928	0.0464	0.013	0.0007
6	360	0.907	0.0454	0.041	0.0021
17	1020	0.742	0.0371	0.186	0.0093
26	1560	0.588	0.0294	0.330	0.0165
48	2880	0.330	0.0165	0.598	0.0299
101	6060	0.010	0.0005	0.897	0.0448

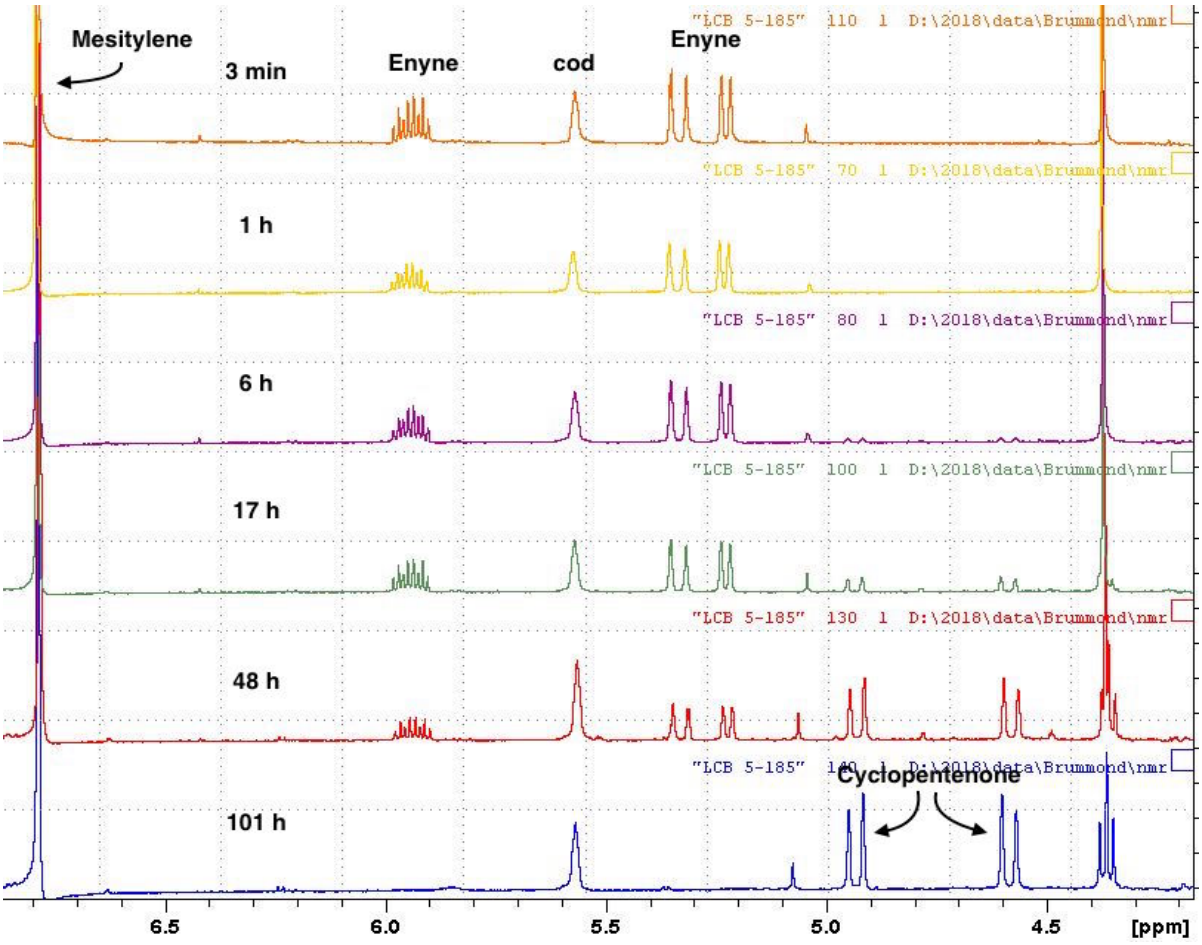

Figure 48. Peaks monitored in rate experiment with (*S*)-MonoPhos to Rh ratio of 3.3.

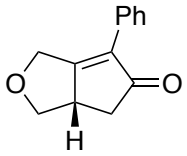

1.51 79% ee

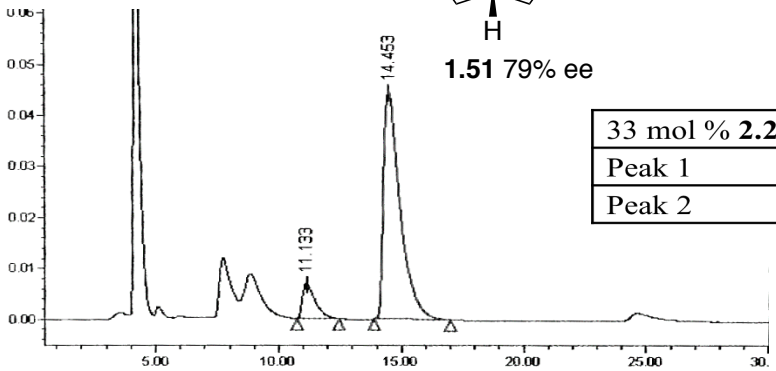

33 mol % **2.27**	Ret. Time (min)	% Area
Peak 1	11.133	10.54
Peak 2	14.453	89.46

Experiment to investigate (*S*)-MonoPhos coordination number.

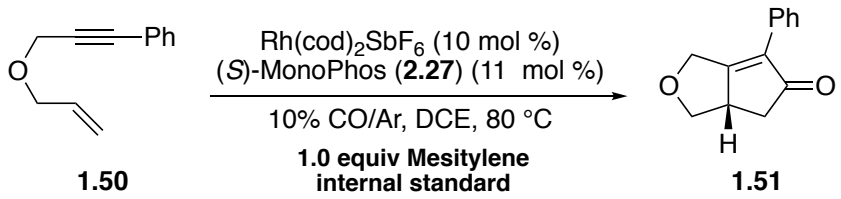

1.50 **1.51**

Preparation of (S)-MonoPhos solutions with varying ee. (*S*)-MonoPhos and (*R*)-MonoPhos were weighed in a nitrogen-filled glovebox into separate 10-mL round-bottomed flasks. The flasks were sealed with septa and removed from the glovebox. A prepared DCE/mesitylene solution was added to each to afford solutions of (*S*)-MonoPhos (0.011 M) and (*S*)-MonoPhos (0.011 M). To six different test tubes were added the necessary amounts of each of these solutions to provide (*S*)-MonoPhos ligand ranging from 0 to 100% ee (2.0 mL each, Table 52). An aliquot of each MonoPhos solution was removed (100 uL), added to a separate vial, the solvent removed by rotary evaporation, and the ligand re-dissolved in HPLC-grade solvent (toluene 0.1%/0.4% iPrOH/99.5% hexanes, 2 mL). The enantiomeric excesses of each MonoPhos sample was determined by HPLC using a ChiralPak IA-3 column, eluting with toluene/0.4% iPrOH/99.5% hexanes at a flow rate of 1.0 mL/min and detecting at 300 nm (Figure 49).

PKR: Follows general procedure E. Rhodium bis(1,5-cyclooctadiene) hexafluoroantimonate (22 mg) was dissolved in a prepared DCE/mesitylene solution (2.0 mL, 0.015 M) and a portion of this solution (0.25 mL, containing 2.8 mg Rh, 0.10 equiv) was added to each test tube under nitrogen. Solutions of (*S*)-MonoPhos of various ee's (0.5 mL, containing 2.0 mg, 0.11 equiv) were added to each of the six test tubes. The test tubes were lowered into a preheated oil bath (60 °C). After 1 h, the atmosphere was evacuated and refilled with 10% CO/Ar (3 ×) using a

needle attached to a vacuum manifold. The test tubes remained under balloons of 10% CO/Ar attached to inlet needles at 60 °C for another 1 h. Enyne **1.50** (80 mg) was weighed in a 15-mL round-bottomed flask, and the prepared DCE/mesitylene solution was added (2.3 mL, 0.2 M M). A portion of this enyne/DCE/mesitylene solution was added to each test tube (0.25 mL solution, containing 8.6 mg enyne, 0.05 mmol, 1.0 equiv). The final volume of each reaction mixture was 1 mL, containing 0.05 mmol of mesitylene, or 1.0 equiv mesitylene with respect to enyne substrate. The test tubes were lowered into the preheated oil bath (80 °C). The reaction mixtures were stirred at a rate of 1000 rpm under balloons of 10% CO/Ar. After 6 h, aliquots (100 μL) were removed from the reactions and yields were determined by ^{1}H NMR integral comparison to the internal standard mesitylene. The enantiomeric ratios of products were determined by HPLC using a Daicel CHIRALPAK IA-3 column (25 cm), eluting with 10% *i*PrOH/hexanes with a flow rate of 1.0 mL/ min and detecting at 254 nm (Figure 41, Figure 50).

Table 52. Preparation of enantioimpure (*S*)-MonoPhos solutions.

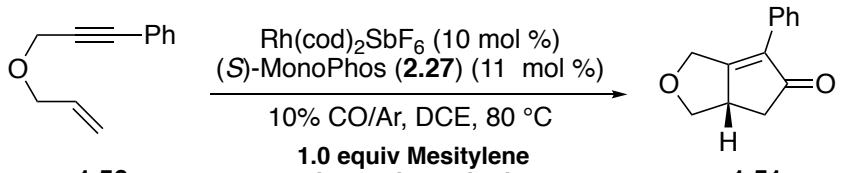

1.50 **1.51**

entry	(*S*)-**2.27** (mL)[a]	(*R*)-**2.27** (mL)[b]	(*S*)-**2.27** ee (%)	Yield (SM)[c]	ee (%)
1	1.0	1.0	-13	62 (12)	-11
2	1.2	0.8	9	66 (16)	5
3	1.4	0.6	31	67 (18)	20
4	1.6	0.4	52	65 (15)	39
5	1.8	0.2	76	63 (17)	58
6	2.0	0	100	64 (21)	83

[a] Amount of prepared (*S*)-MonoPhos solution (0.011 M) added. [b] Amount of prepared (*R*)-MonoPhos solution (0.011 M) added. [c] Yields were determined by integral comparison of product resonance (4.9 ppm) to mesitylene resonance (6.8 ppm).

Chiralcel OD column, 300 nm
99.5% hexanes, 0.4% iPrOH, 0.1% toluene
1.0 mL/min

entry 1	Ret. Time (min)	% Area
Peak 1	9.311	56.41
Peak 2	13.649	43.59

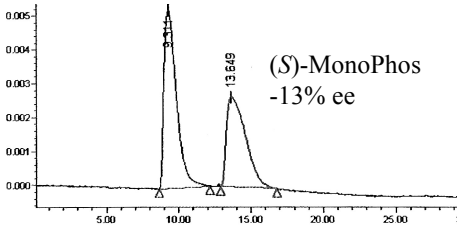

entry 2	Ret. Time (min)	% Area
Peak 1	9.658	45.57
Peak 2	14.457	54.43

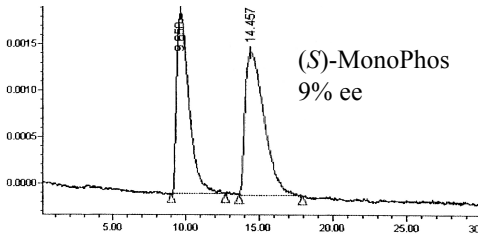

entry 3	Ret. Time (min)	% Area
Peak 1	8.244	34.34
Peak 2	11.746	65.66

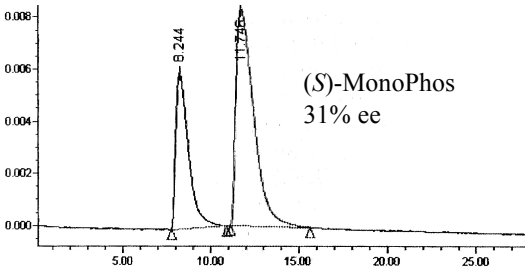

entry 4	Ret. Time (min)	% Area
Peak 1	8.193	23.82
Peak 2	11.331	23.82

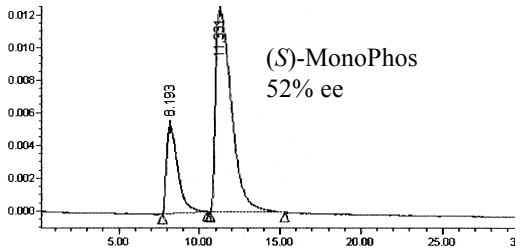

entry 5	Ret. Time (min)	% Area
Peak 1	8.093	12.05
Peak 2	11.318	87.95

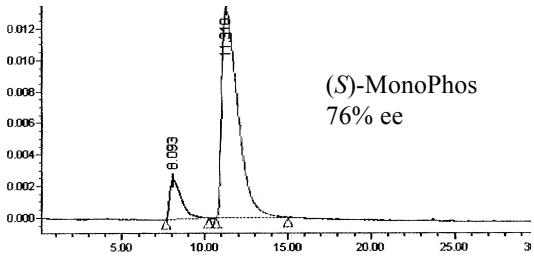

entry 6	Ret. Time (min)	% Area
Peak 1	-	0
Peak 2	12.220	100

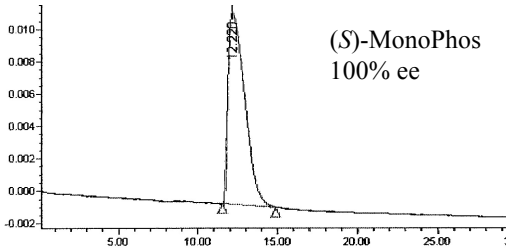

Figure 49. HPLC traces of enantioimpure (*S*)-MonoPhos.

entry 1	Ret. Time (min)	% Area
Peak 1	11.253	55.29
Peak 2	14.777	44.71

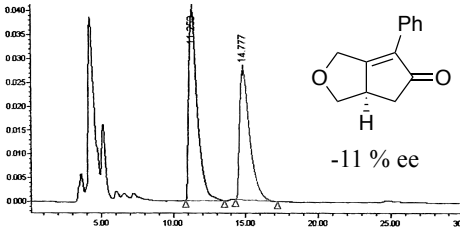

entry 2	Ret. Time (min)	% Area
Peak 1	11.252	47.50
Peak 2	14.737	52.40

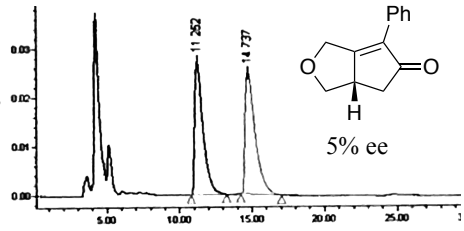

entry 3	Ret. Time (min)	% Area
Peak 1	11.251	40.09
Peak 2	14.747	59.91

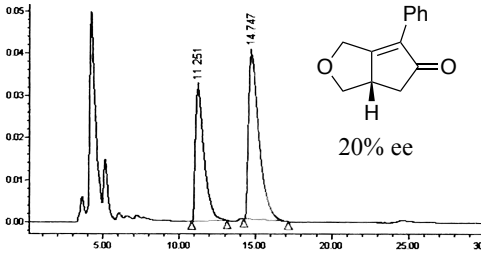

entry 4	Ret. Time (min)	% Area
Peak 1	11.321	30.38
Peak 2	14.789	69.62

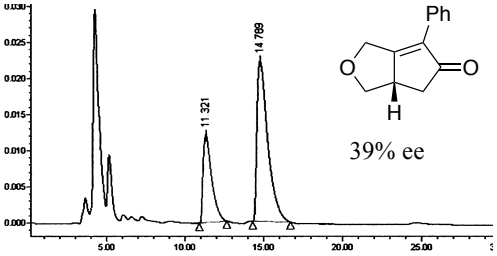

entry 5	Ret. Time (min)	% Area
Peak 1	11.334	21.19
Peak 2	14.815	78.81

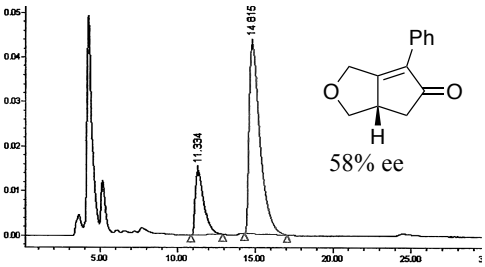

entry 6	Ret. Time (min)	% Area
Peak 1	11.436	8.59
Peak 2	14.950	91.41

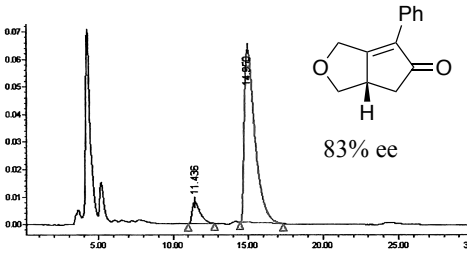

Figure 50. HPLC traces of products obtained from PKR with enantioimpure (*S*)-MonoPhos.

Confirmation of absolute stereochemistry using vibrational circular dichroism (VCD).

Separation of cyclopentenone enantiomers by HPLC. The PKR of enyne **1.50** was performed using racemic BINAP. Each enantiomer was isolated by HPLC (3 mg/200 uL injections, 10% *i*PrOH/Hex). Each enantiomer was collected in a separate vial and the solvent removed by rotary evaporation. Both enantiomers (−)-**1.51** (5.3 mg), and (+)-**1.51** (5.4 mg) were isolated in >97% ee.

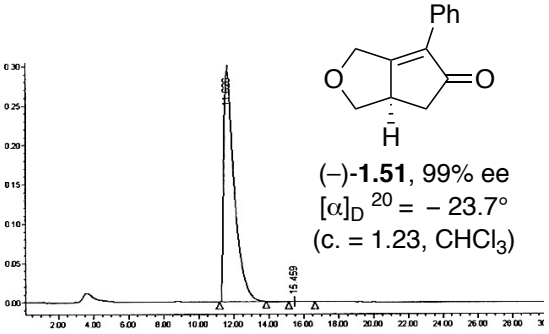

	Ret. Time (min)	Area (%)
Peak 1	11.626	99.78
Peak 2	15.458	0.22

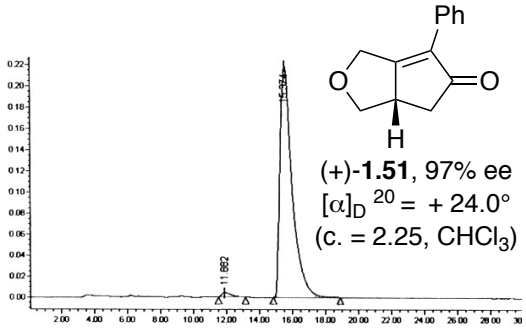

	Ret. Time (min)	Area (%)
Peak 1	11.882	1.46
Peak 2	15.374	98.54

Collection of IR and VCD data for (−)-1.51 and (+)-1.51. The IR and VCD spectra were recorded using a ChiralIR™ VCD spectrometer equipped with a Dual PEM accessory (BioTools, Jupiter, FL). Samples were dissolved in carbon tetrachloride (150 uL) and added to a BaF_2 cell with a 0.1 mm path length. The samples were analyzed by FT-IR and the from the resulting IR spectra were subtracted IR spectra of carbon tetrachloride. Measurements were performed for 12 h each in 1 h blocks and averaged. VCD spectra were corrected using the half difference method (Peak 1 Half difference = (Peak 1 VCD – Peak 2 VCD)/2). This method has lower noise and an improved

baseline compared to solvent or racemic subtraction The baseline of each spectrum is the half sum of each VCD spectrum ([Peak 1 + Peak 2]/2). The experimental noise spectra are shown in Figure 51 and Figure 52, black.

*Calculation of (R)-**1.51** and (S)-**1.51** IR and VCD spectra and comparison to experimental spectra.* Calculations were performed using Gaussian 09. The VCD spectra of the lowest-energy conformer for each enantiomer was generated using B3LYP basis set with TZVP basis set, as described by Jiminez-Oses.[164] Output of frequency calculations included IR and VCD spectra. These calculated IR and VCD spectra were compared to experimental IR and VCD spectra using Compute VOA software, available from BioTools. Enantiomeric similarity indexes (ESI's) were calculated for both (*R*) and (*S*)-**1.51** with a frequency range of 850 to 1800 cm^{-1}. The major enantiomer obtained from the PKR using (*R*)-BINAP, (−)-**1.51**, had an ESI of 60.6 (97% confidence level) with the calculated VCD spectrum of (*R*)-**1.51**; and the (+)-**1.51** enantiomer had an ESI of 44.7 (90% confidence level) with the calculated VCD specrum of (*S*)-**1.51** (Table 53).

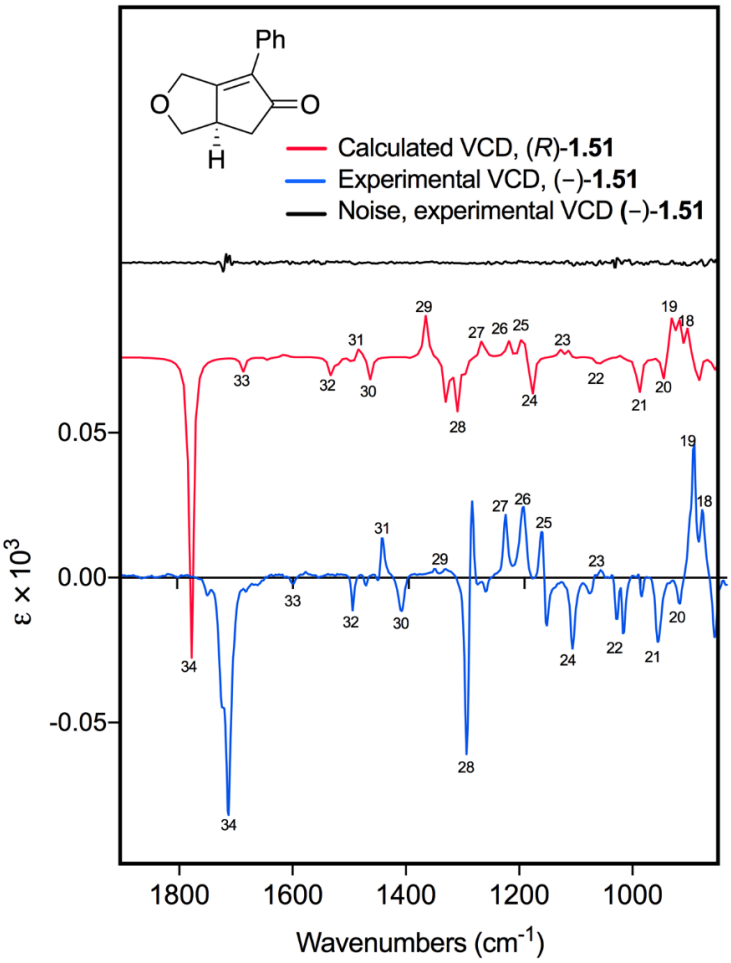

Figure 51. VCD analysis of cyclopentenone product (−)-1.51.

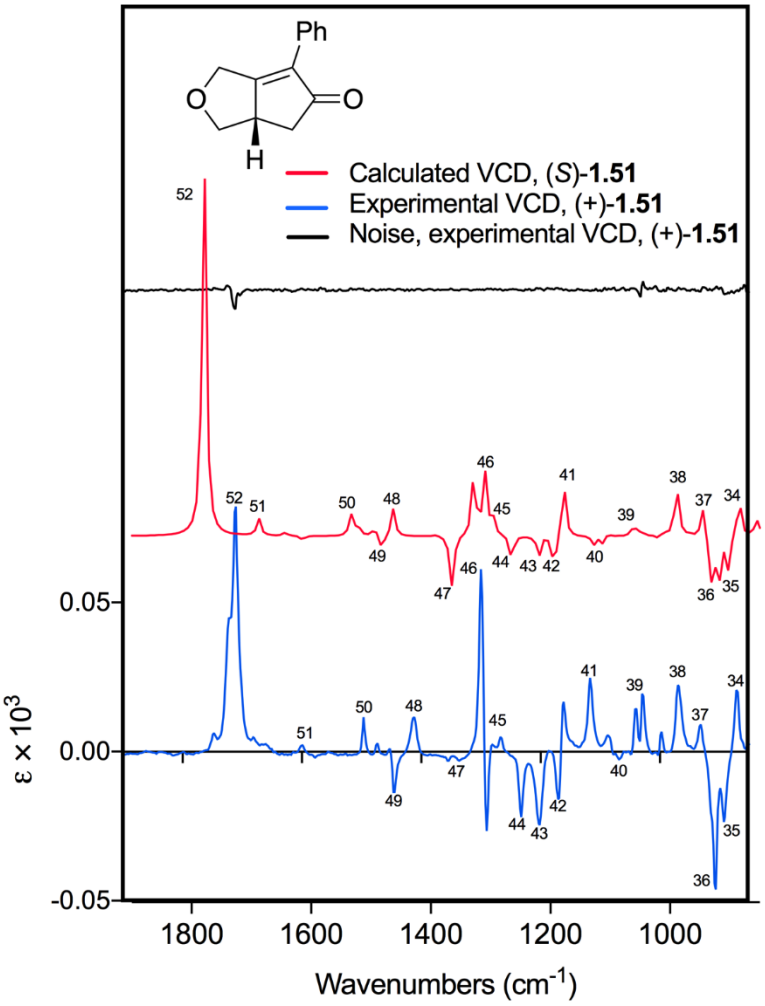

Figure 52. VCD analysis of cyclopentenone product (+)-1.51.

Table 53. Assignments of absolute configuration of enantiomers of 1.51.

entry	Experimental VCD	Calculated VCD	ESI	Confidence level
1	(−)-1.51	(*R*)-**1.51**	60.6	97%
2	(+)-1.51	(*S*)-**1.51**	44.7	90%

NMR SPECTRA

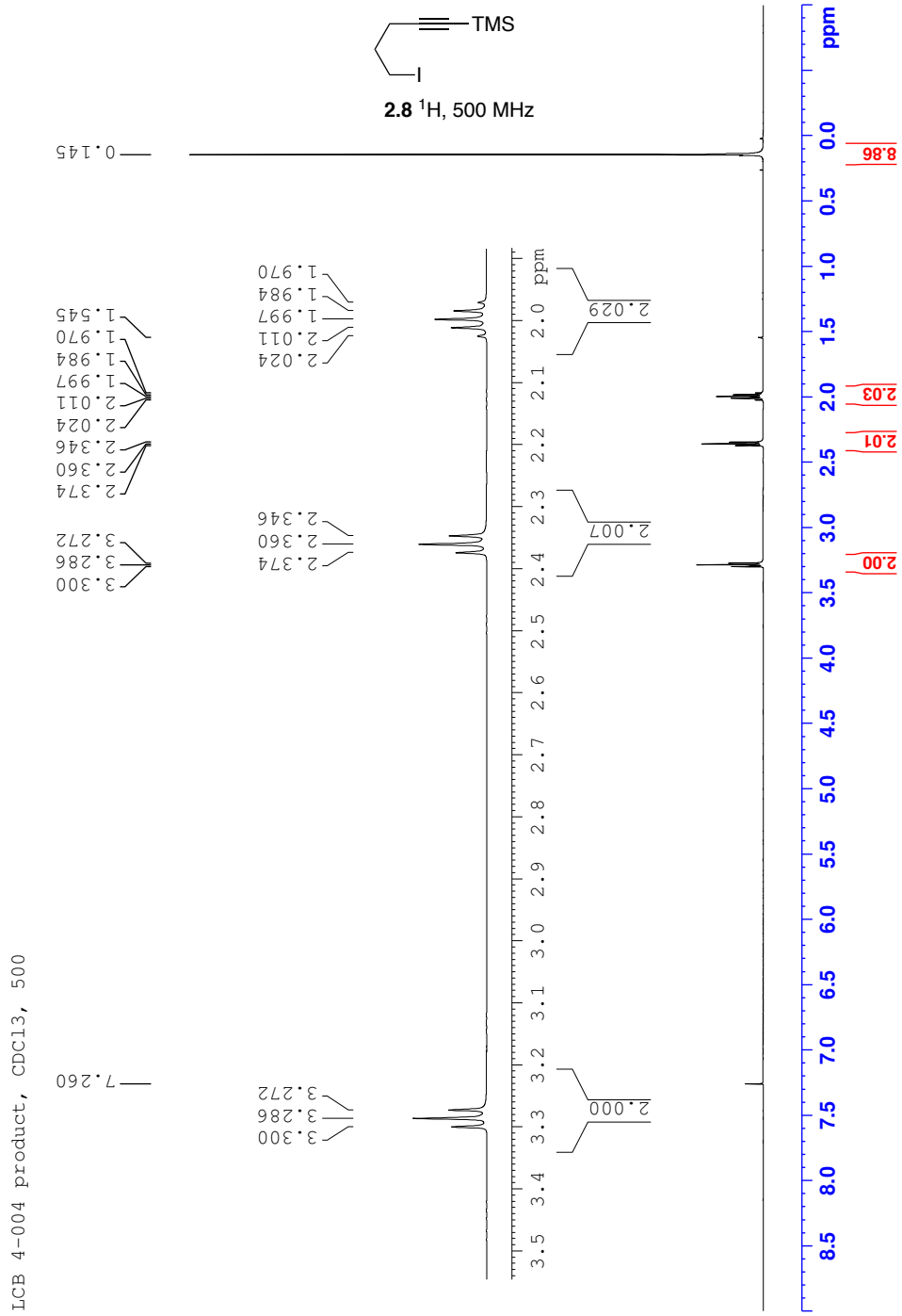
TMS
I
2.8 1H, 500 MHz
LCB 4-004 product, CDC13, 500
0.145
7.260
3.300
3.286
3.272
2.374
2.360
2.346
2.024
2.011
1.997
1.984
1.970
1.545
2.029
2.007
2.000
8.86
2.03
2.01
2.00
ppm

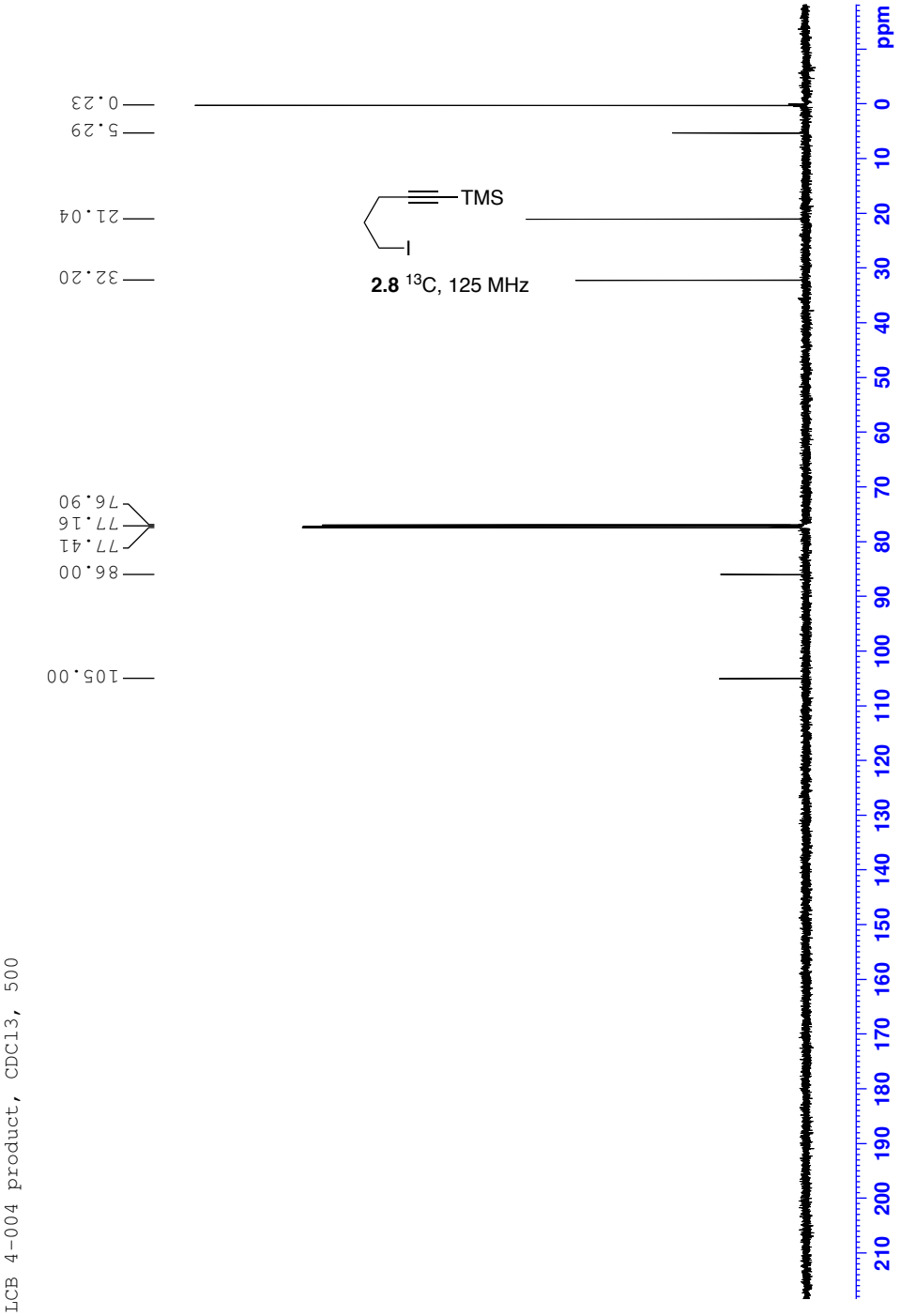
0.23
5.29
21.04
32.20
76.90
77.16
77.41
86.00
105.00
TMS
I
2.8 13C, 125 MHz
ppm
0
10
20
30
40
50
60
70
80
90
100
110
120
130
140
150
160
170
180
190
200
210
LCB 4-004 product, CDCl3, 500

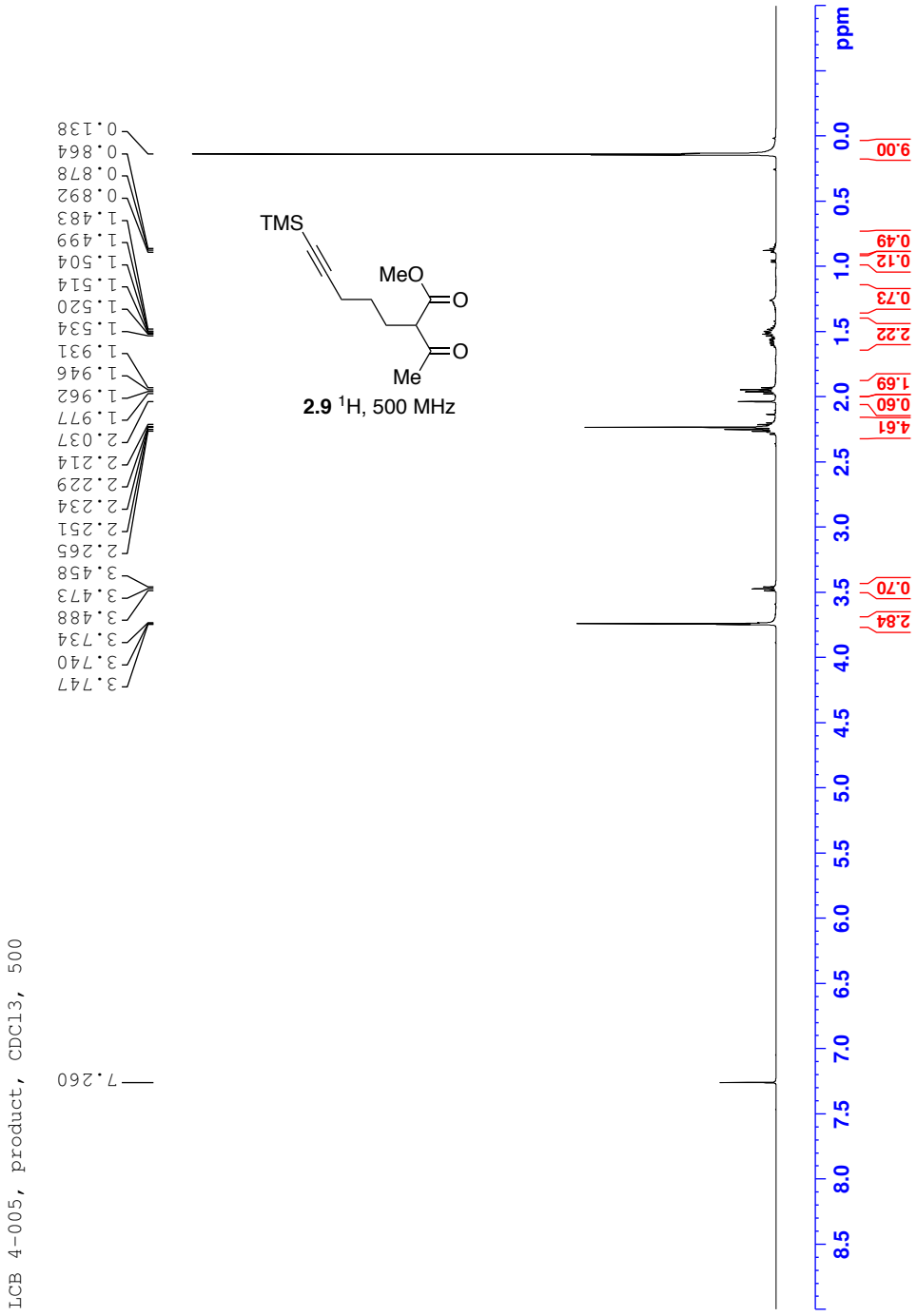
LCB 4-005, product, CDCl3, 500
0.138
0.864
0.878
0.892
1.483
1.499
1.504
1.514
1.520
1.534
1.931
1.946
1.962
1.977
2.037
2.214
2.229
2.234
2.251
2.265
3.458
3.473
3.488
3.734
3.740
3.747
7.260
TMS
MeO
O
O
Me
2.9 1H, 500 MHz
ppm
9.00
0.49
0.12
0.73
2.22
1.69
0.60
4.61
0.70
2.84

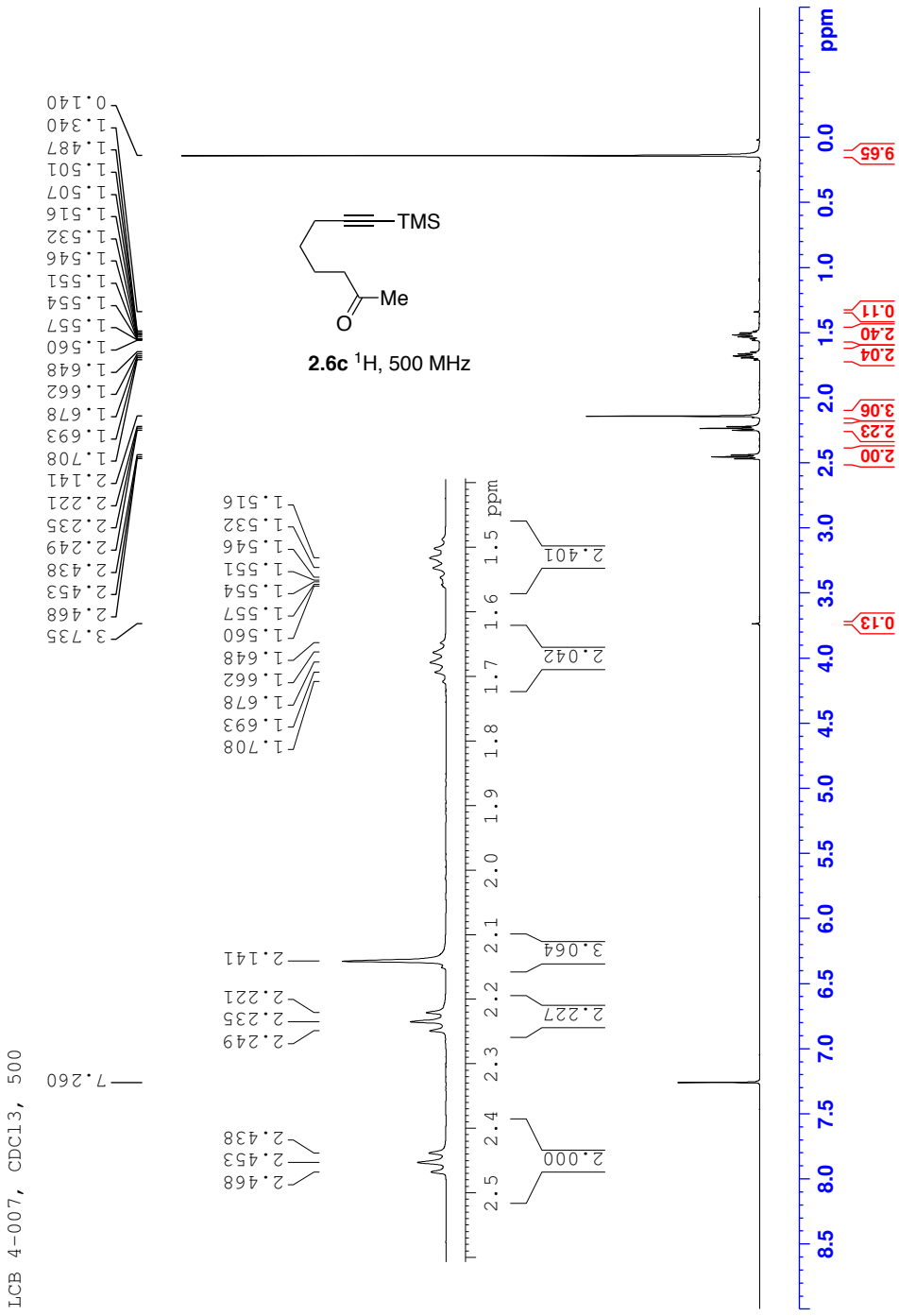
LCB 4-007, CDCl3, 500
7.260
3.735
2.468
2.453
2.438
2.249
2.235
2.221
2.141
1.708
1.693
1.678
1.662
1.648
1.560
1.557
1.554
1.551
1.546
1.532
1.516
1.507
1.501
1.487
1.340
0.140
TMS
Me
O
2.6c 1H, 500 MHz
2.000
2.227
3.064
2.042
2.401
9.65
0.11
2.40
2.04
3.06
2.23
2.00
0.13
ppm

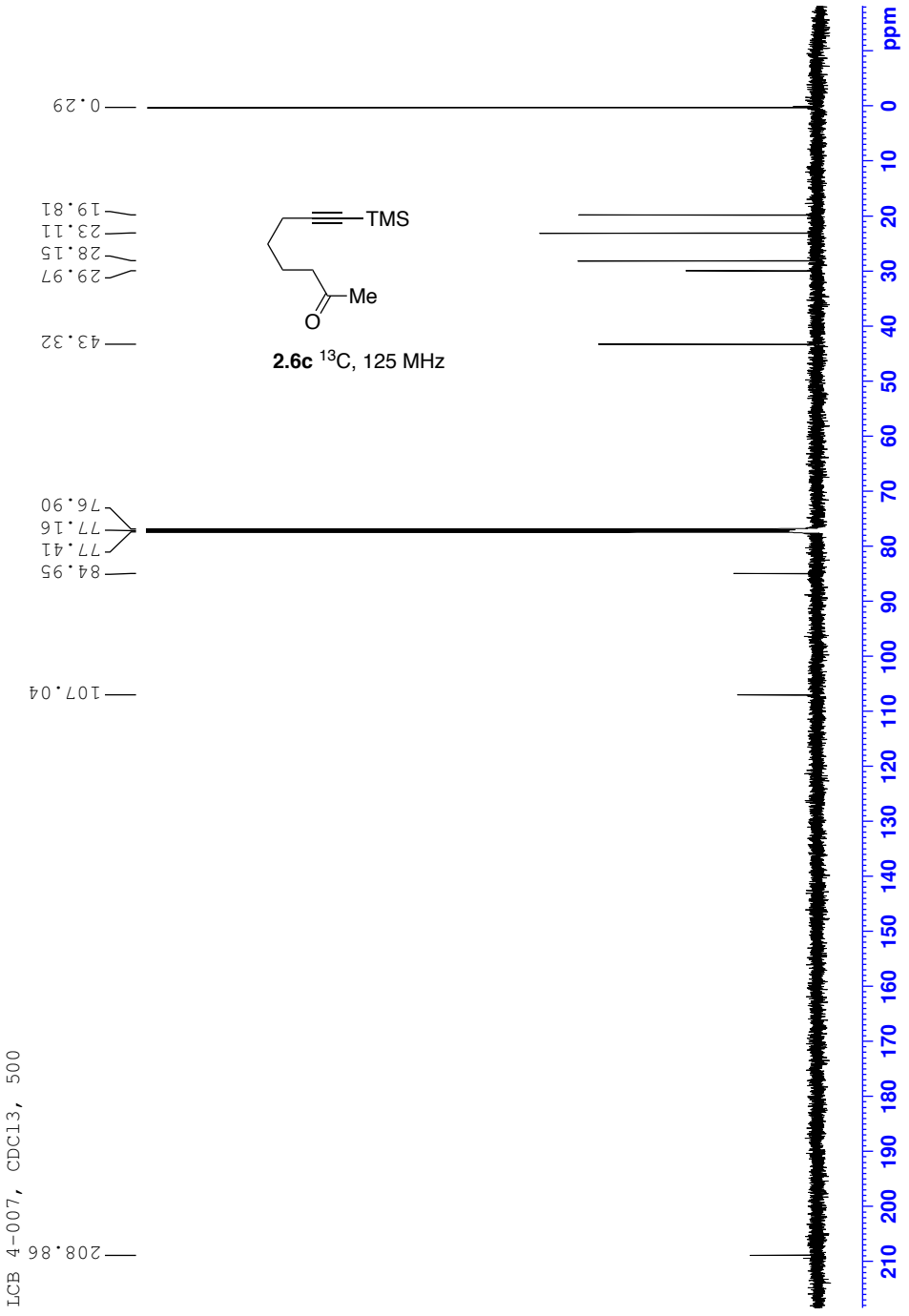

2.6c ^{13}C, 125 MHz

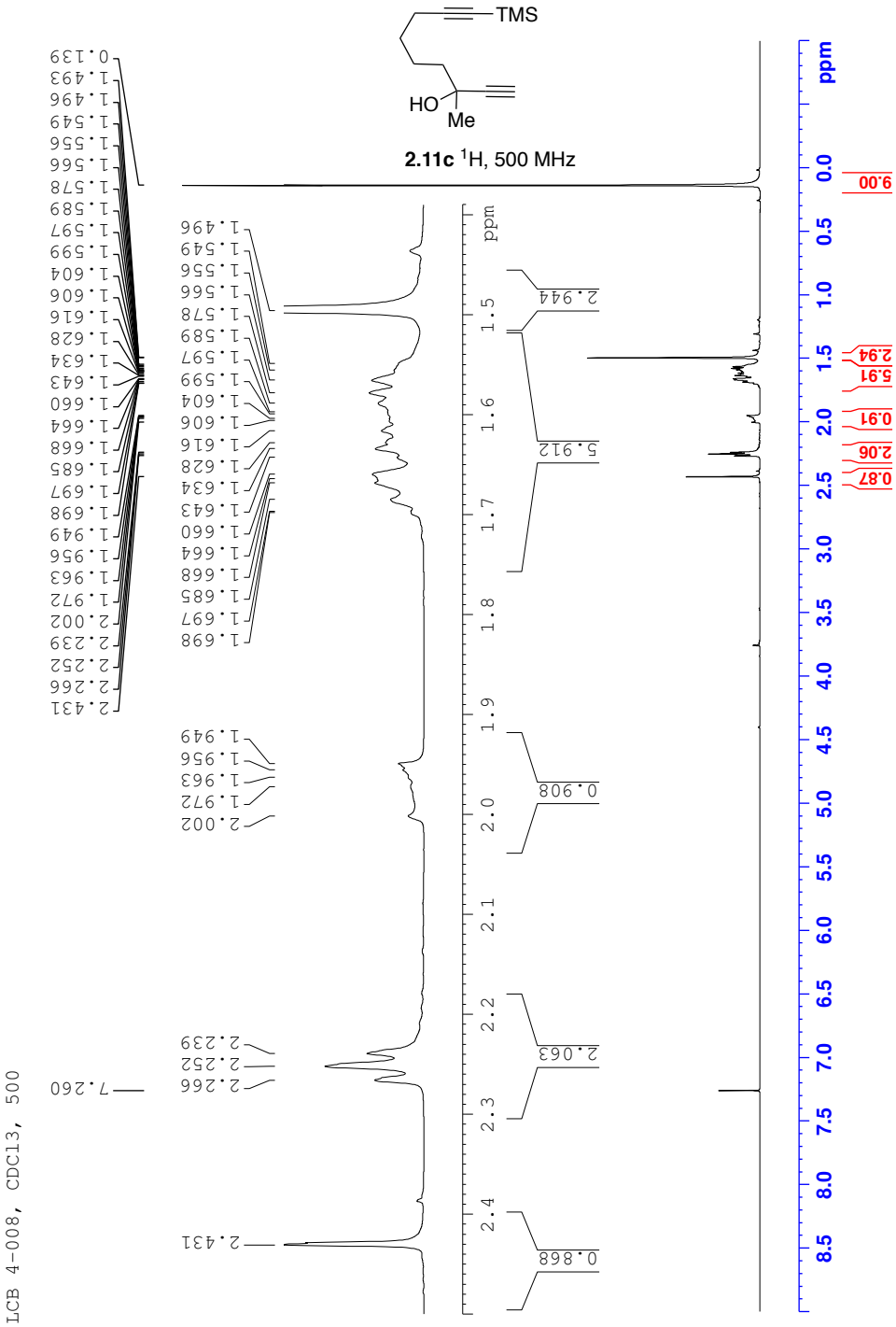
TMS
HO
Me
2.11c ^{1}H, 500 MHz
LCB 4-008, CDCl3, 500
ppm

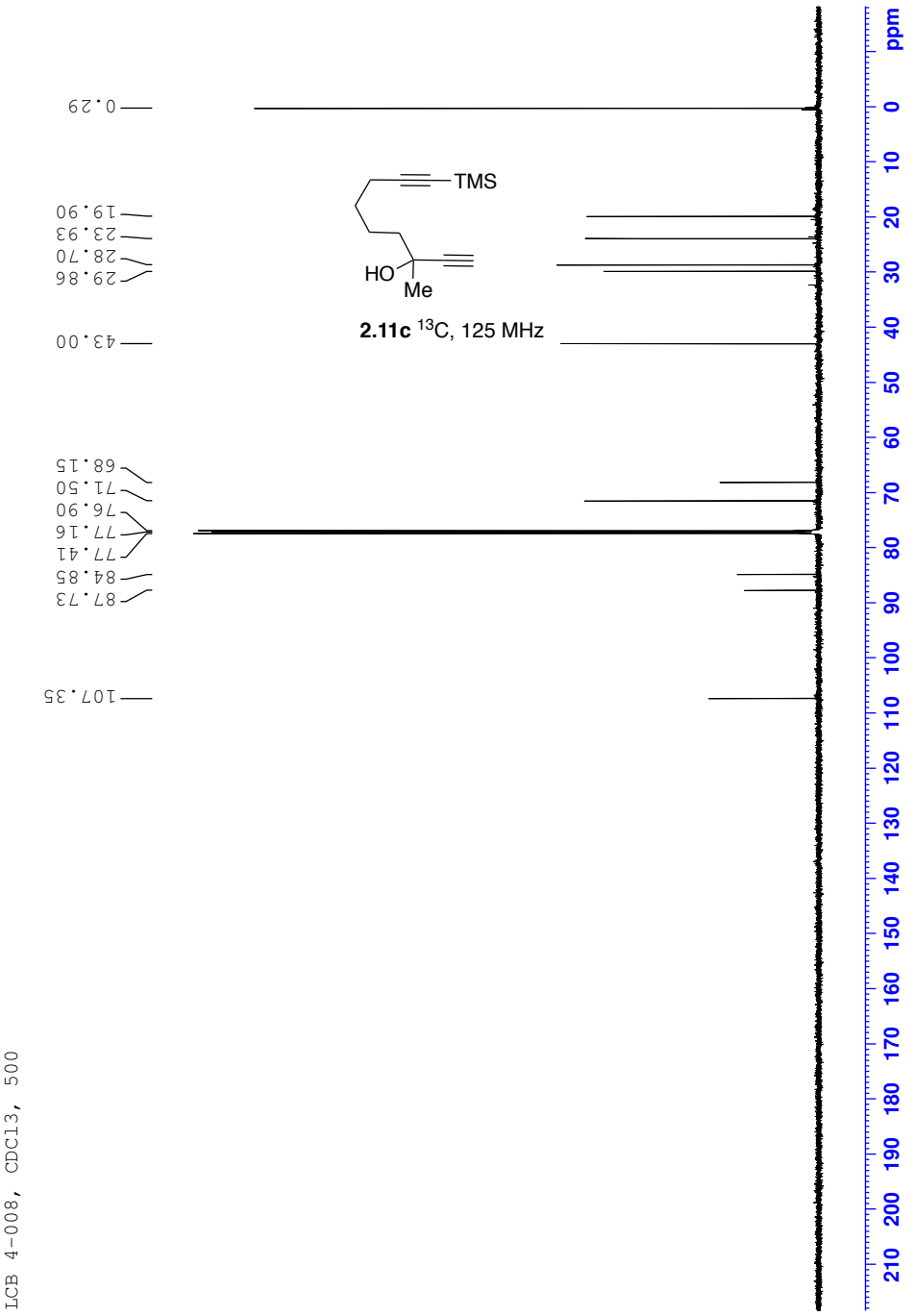
0.29
19.90
23.93
28.70
29.86
43.00
68.15
71.50
76.90
77.16
77.41
84.85
87.73
107.35
TMS
HO
Me
2.11c 13C, 125 MHz
LCB 4-008, CDCl3, 500
ppm
0
10
20
30
40
50
60
70
80
90
100
110
120
130
140
150
160
170
180
190
200
210

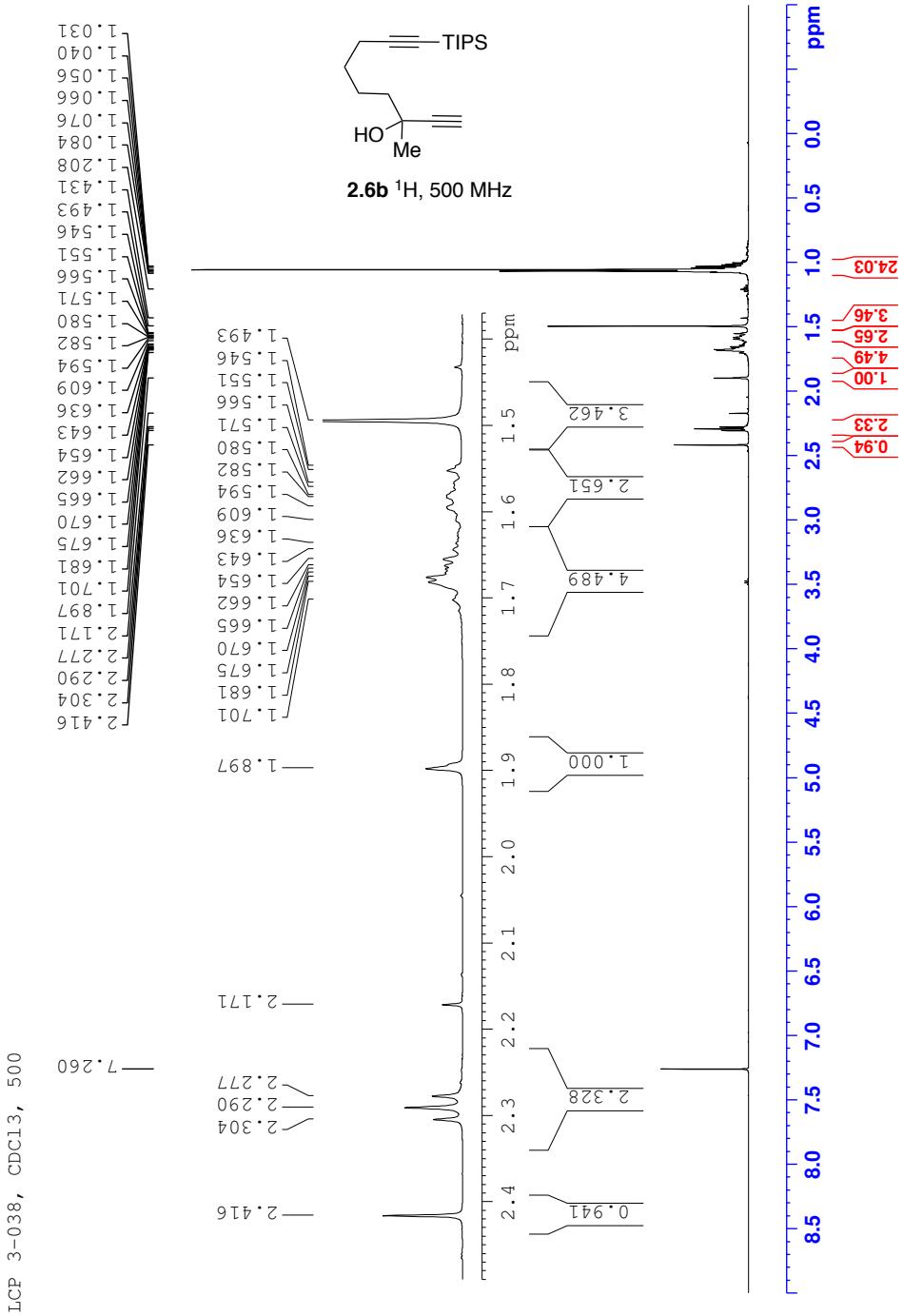
TIPS
HO
Me
2.6b 1H, 500 MHz
LCP 3-038, CDC13, 500
ppm

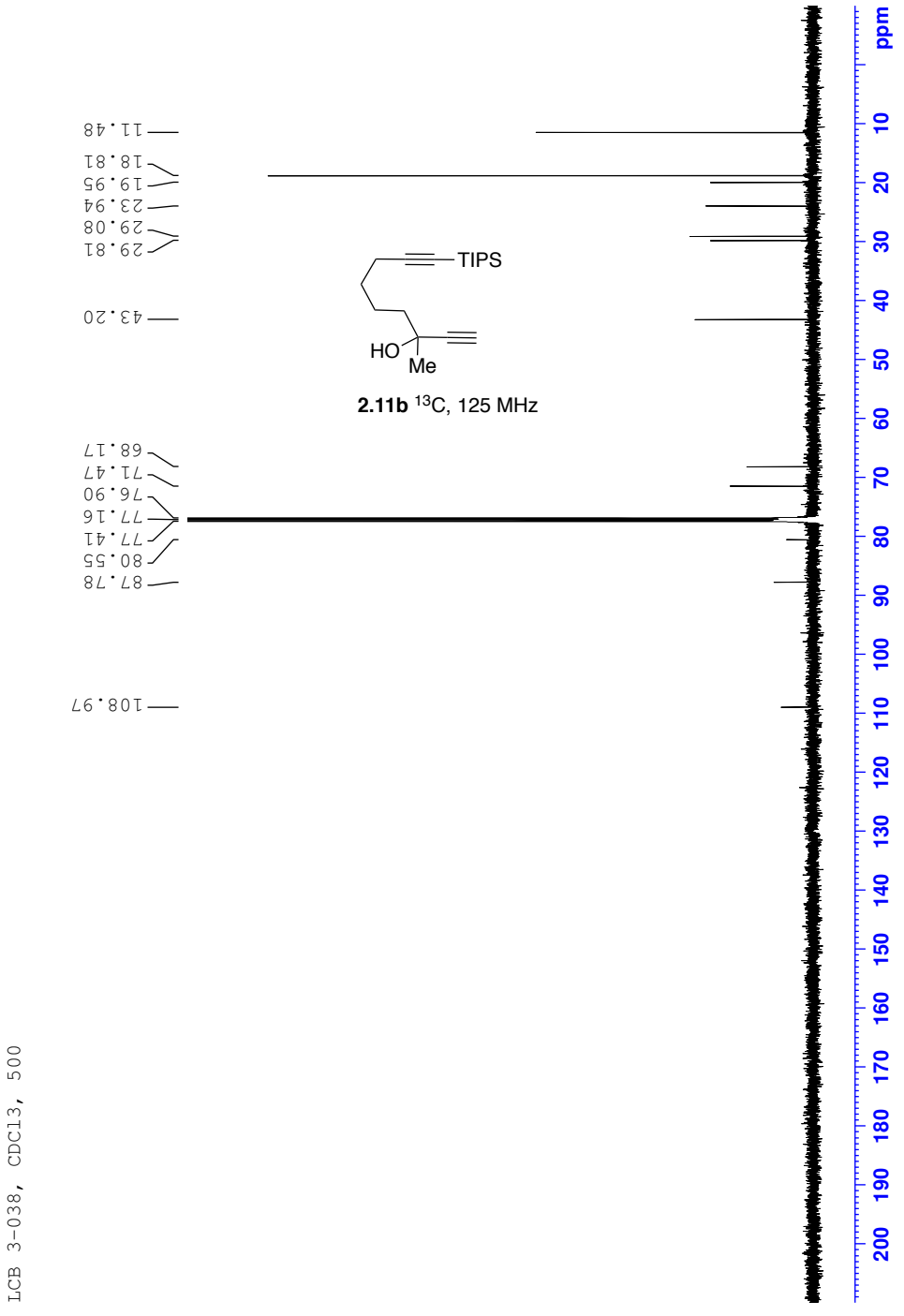

2.11b ^{13}C, 125 MHz

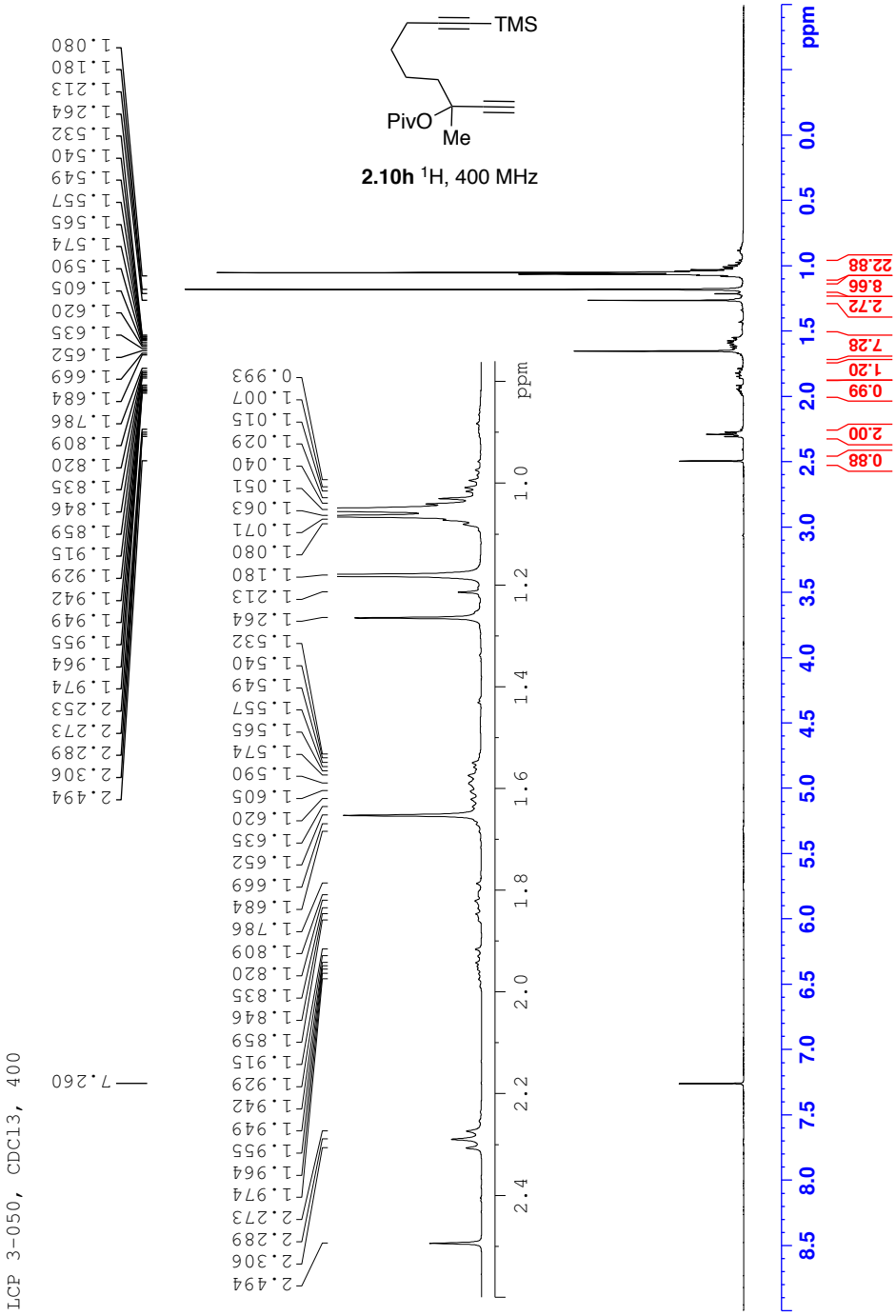
TMS
PivO
Me
2.10h 1H, 400 MHz
LCP 3-050, CDC13, 400
ppm

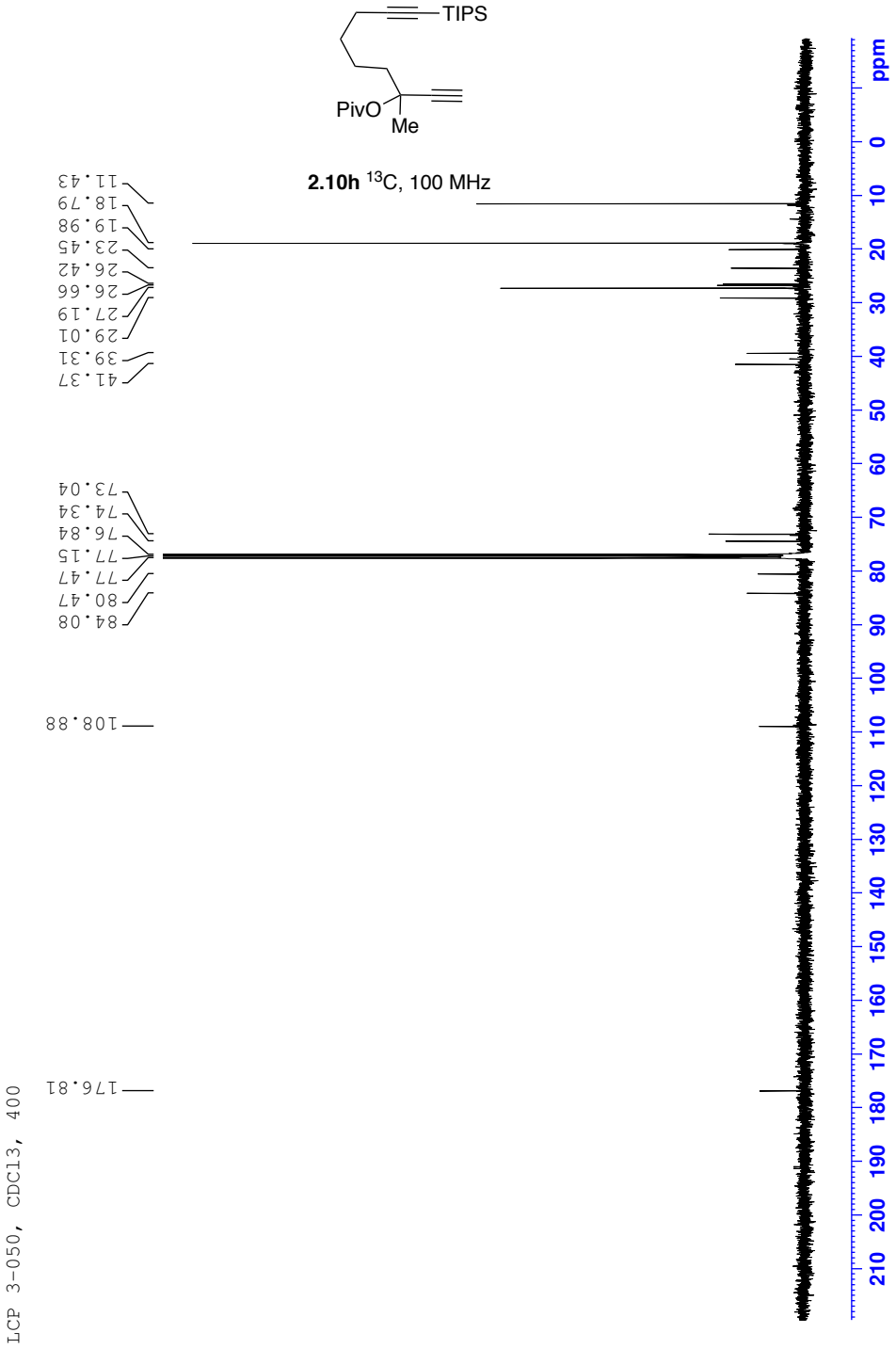
TIPS
PivO
Me
2.10h 13C, 100 MHz
11.43
18.79
19.98
23.45
26.42
26.66
27.19
29.01
39.31
41.37
73.04
74.34
76.84
77.15
77.47
80.47
84.08
108.88
176.81
LCP 3-050, CDCl3, 400
ppm
0
10
20
30
40
50
60
70
80
90
100
110
120
130
140
150
160
170
180
190
200
210

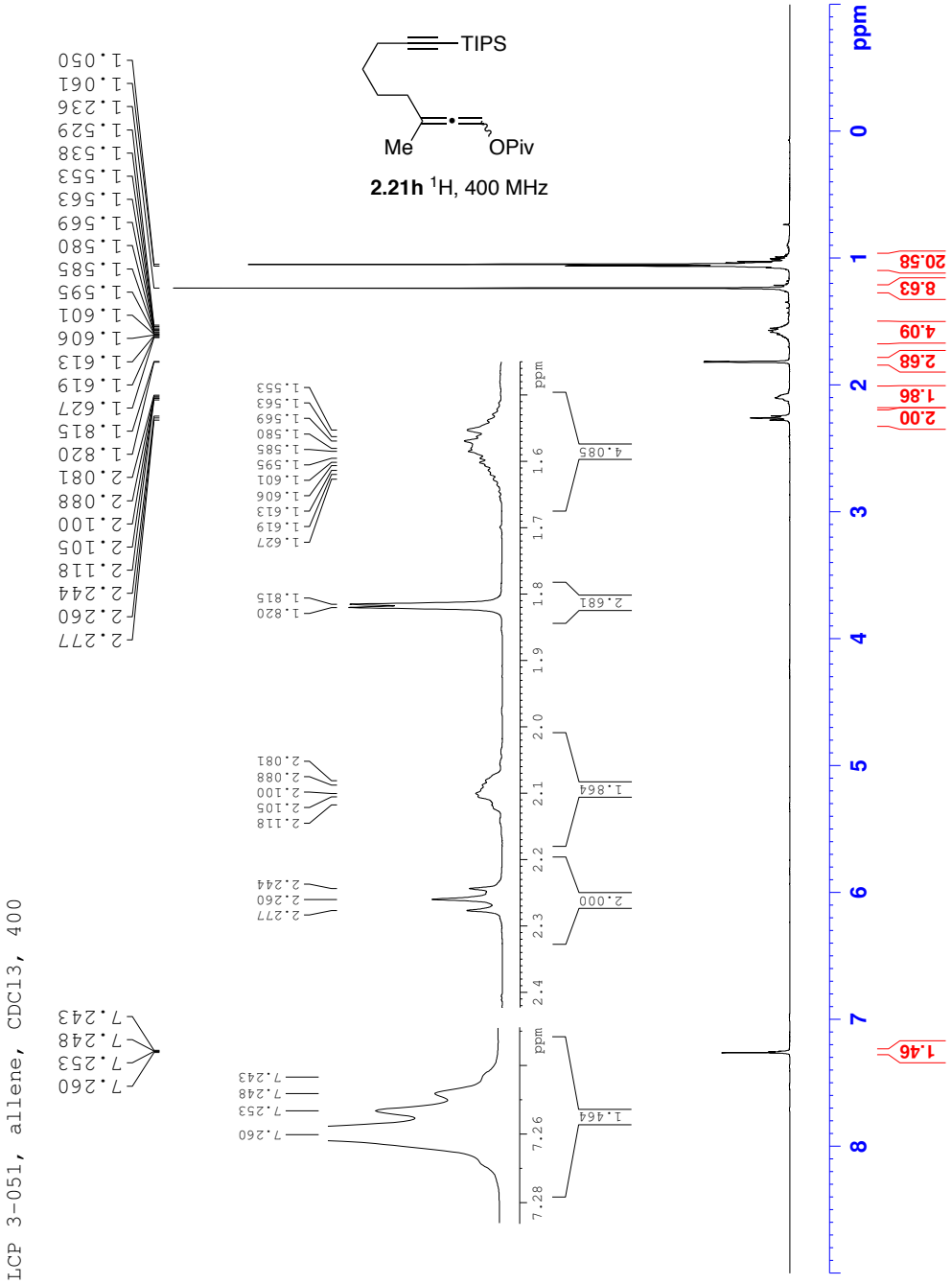
TIPS
Me
OPiv
2.21h 1H, 400 MHz
LCP 3-051, allene, CDCl3, 400
ppm
20.58
8.63
4.09
2.68
1.86
2.00
1.46

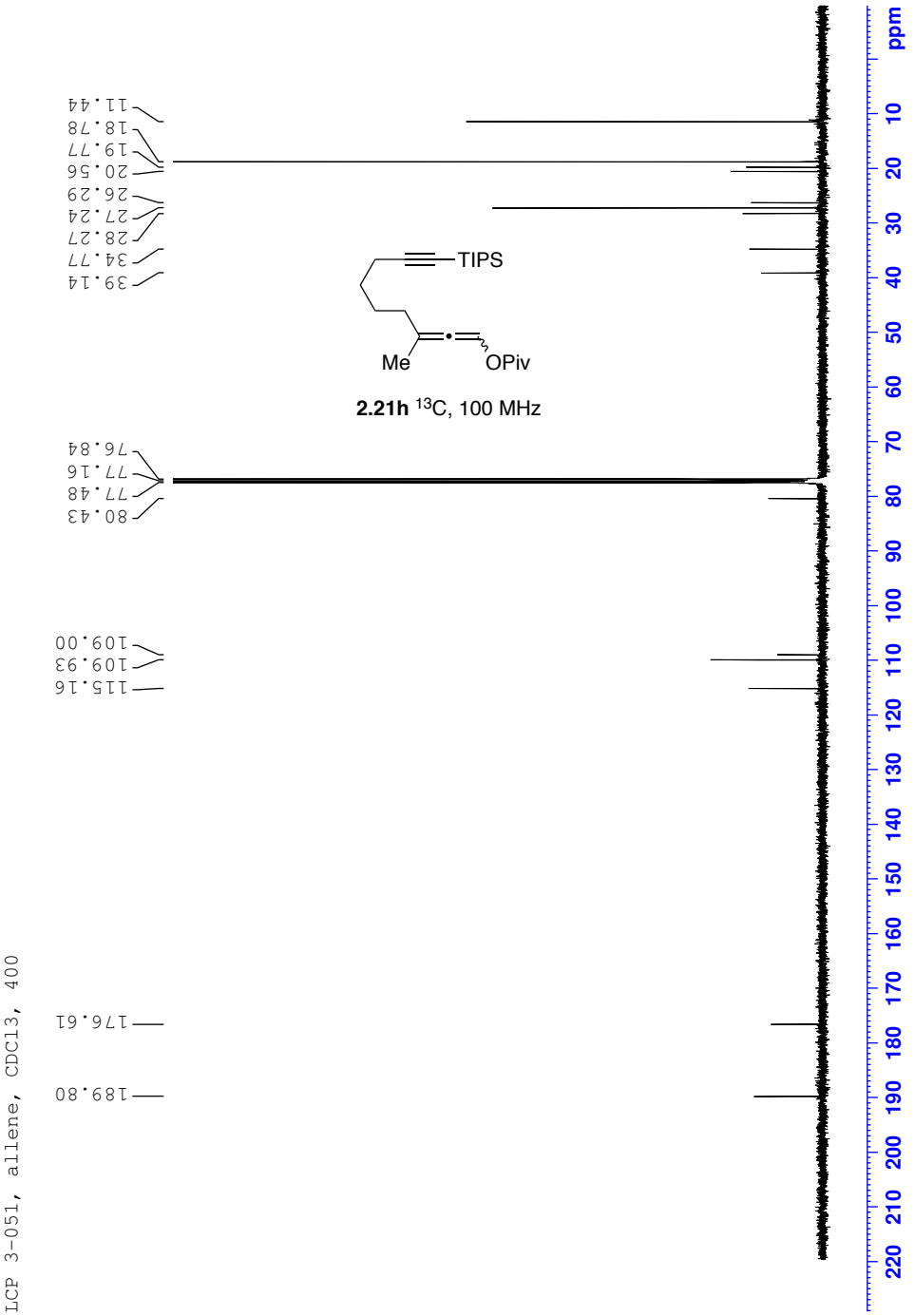
LCP 3-051, allene, CDCl3, 400
11.44
18.78
19.77
20.56
26.29
27.24
28.27
34.77
39.14
76.84
77.16
77.48
80.43
109.00
109.93
115.16
176.61
189.80
TIPS
Me
OPiv
2.21h 13C, 100 MHz
ppm

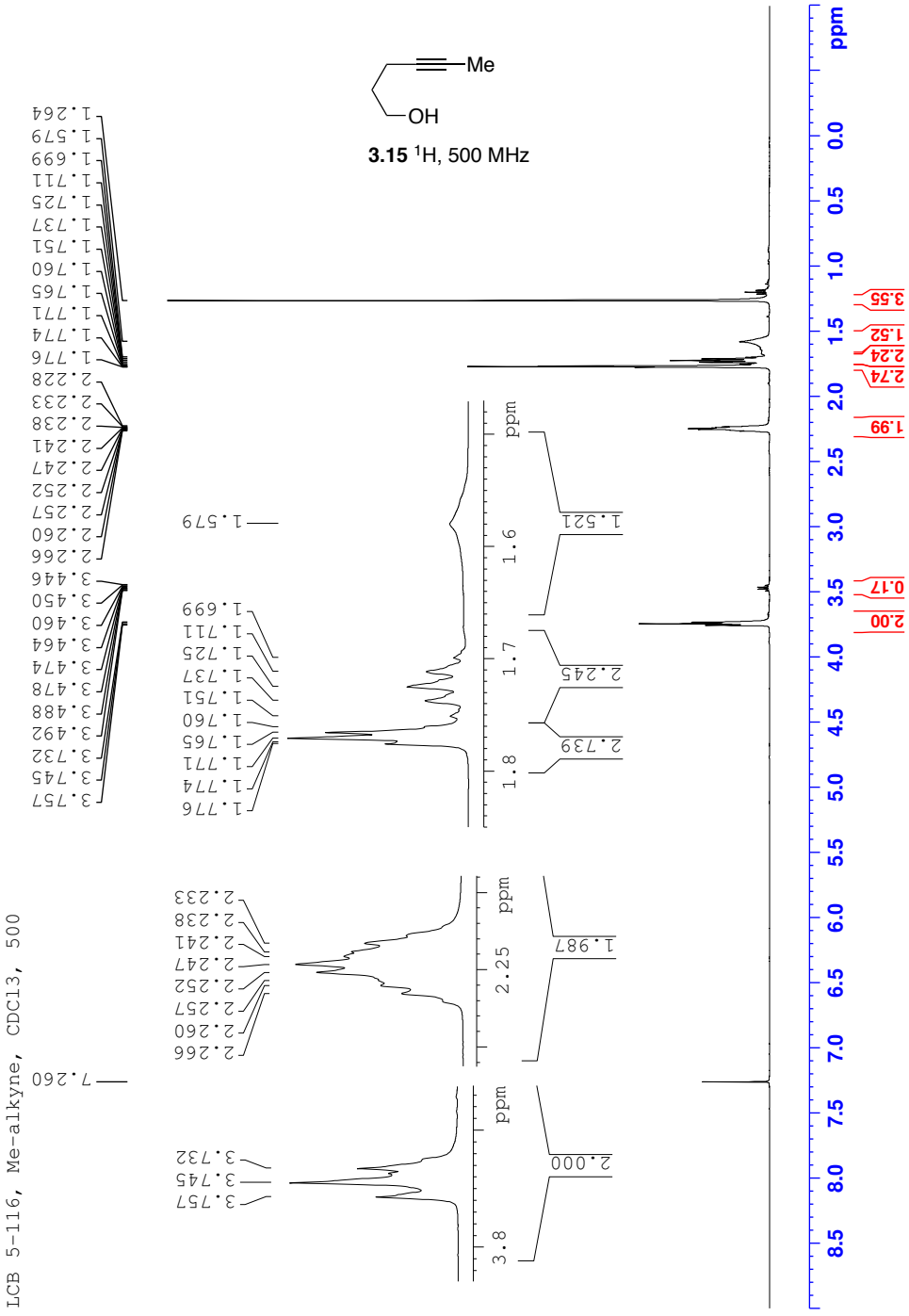
LCB 5-116, Me-alkyne, CDC13, 500
Me
OH
3.15 1H, 500 MHz
ppm
8.5
8.0
7.5
7.0
6.5
6.0
5.5
5.0
4.5
4.0
3.5
3.0
2.5
2.0
1.5
1.0
0.5
0.0
3.55
2.74
2.24
1.52
1.99
0.17
2.00
7.260
3.757
3.745
3.732
2.266
2.260
2.257
2.252
2.247
2.241
2.238
2.233
2.228
1.776
1.774
1.771
1.765
1.760
1.751
1.737
1.725
1.711
1.699
1.579
1.264
3.446
3.450
3.460
3.464
3.474
3.478
3.488
3.492
2.000
2.25
1.987
1.8
1.7
1.6
2.739
2.245
1.521

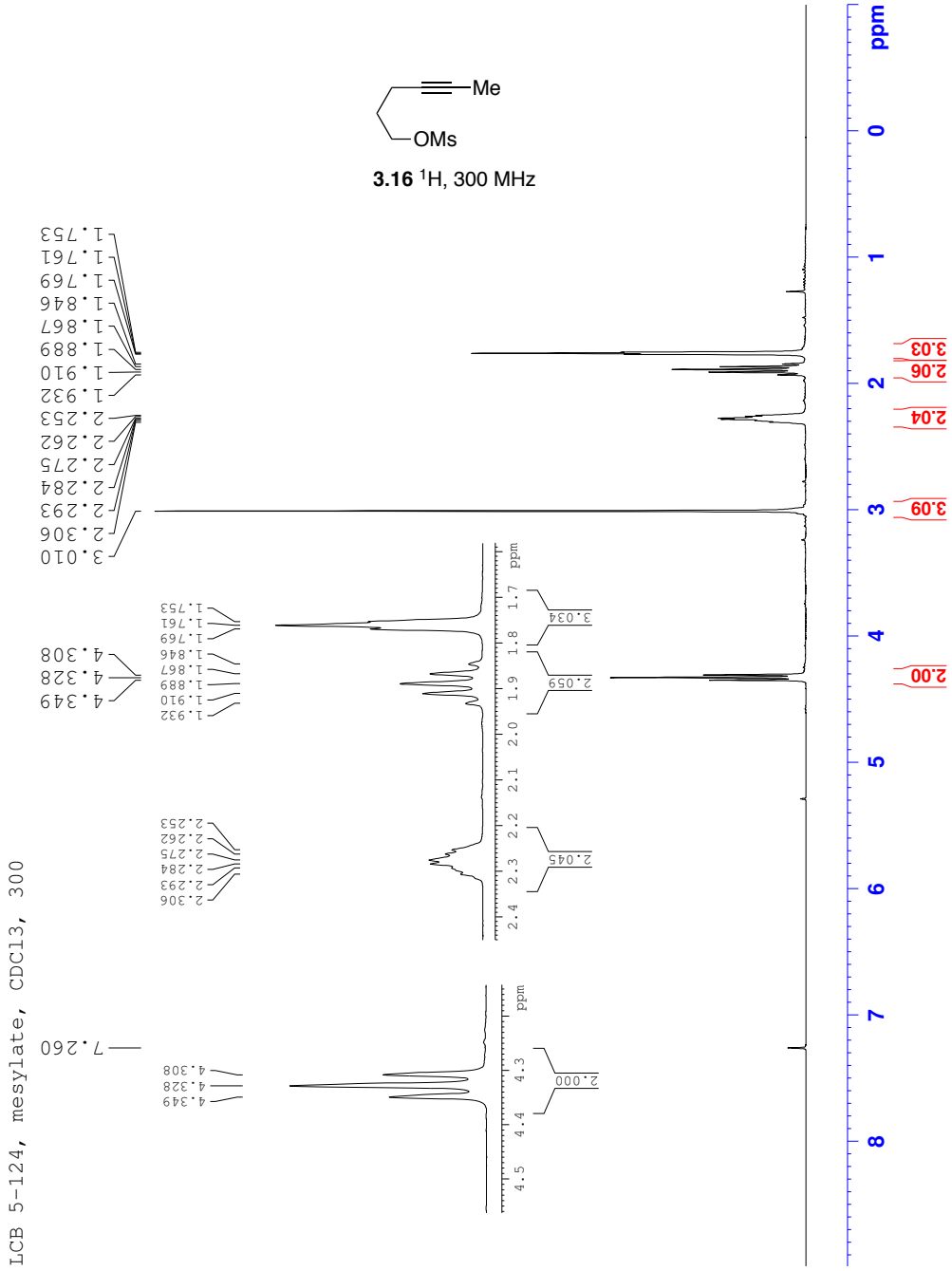
Me
OMs
3.16 1H, 300 MHz
LCB 5-124, mesylate, CDCl3, 300
7.260
4.349
4.328
4.308
2.000
2.045
2.059
3.034
2.306
2.293
2.284
2.275
2.262
2.253
1.932
1.910
1.889
1.867
1.846
1.769
1.761
1.753
3.010
2.306
2.293
2.284
2.275
2.262
2.253
1.932
1.910
1.889
1.867
1.846
1.769
1.761
1.753
4.349
4.328
4.308
3.09
2.06
2.04
3.03
2.00
ppm

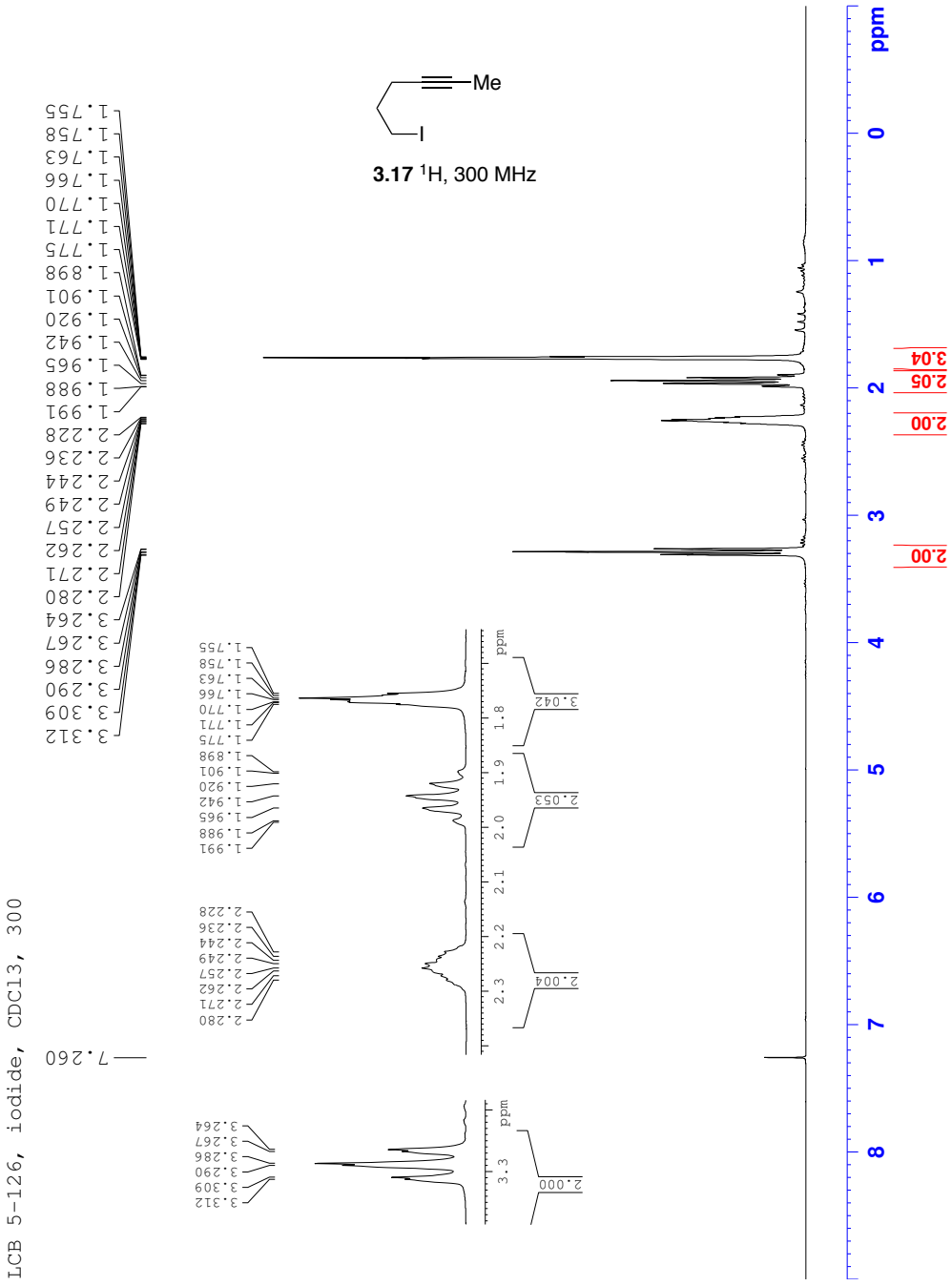
LCB 5-126, iodide, CDCl3, 300
7.260
3.312
3.309
3.290
3.286
3.267
3.264
2.280
2.271
2.262
2.257
2.249
2.244
2.236
2.228
1.991
1.988
1.965
1.942
1.920
1.901
1.898
1.775
1.771
1.770
1.766
1.763
1.758
1.755
Me
I
3.17 1H, 300 MHz
ppm
3.042
2.053
2.004
2.000
3.04
2.05
2.00
2.00

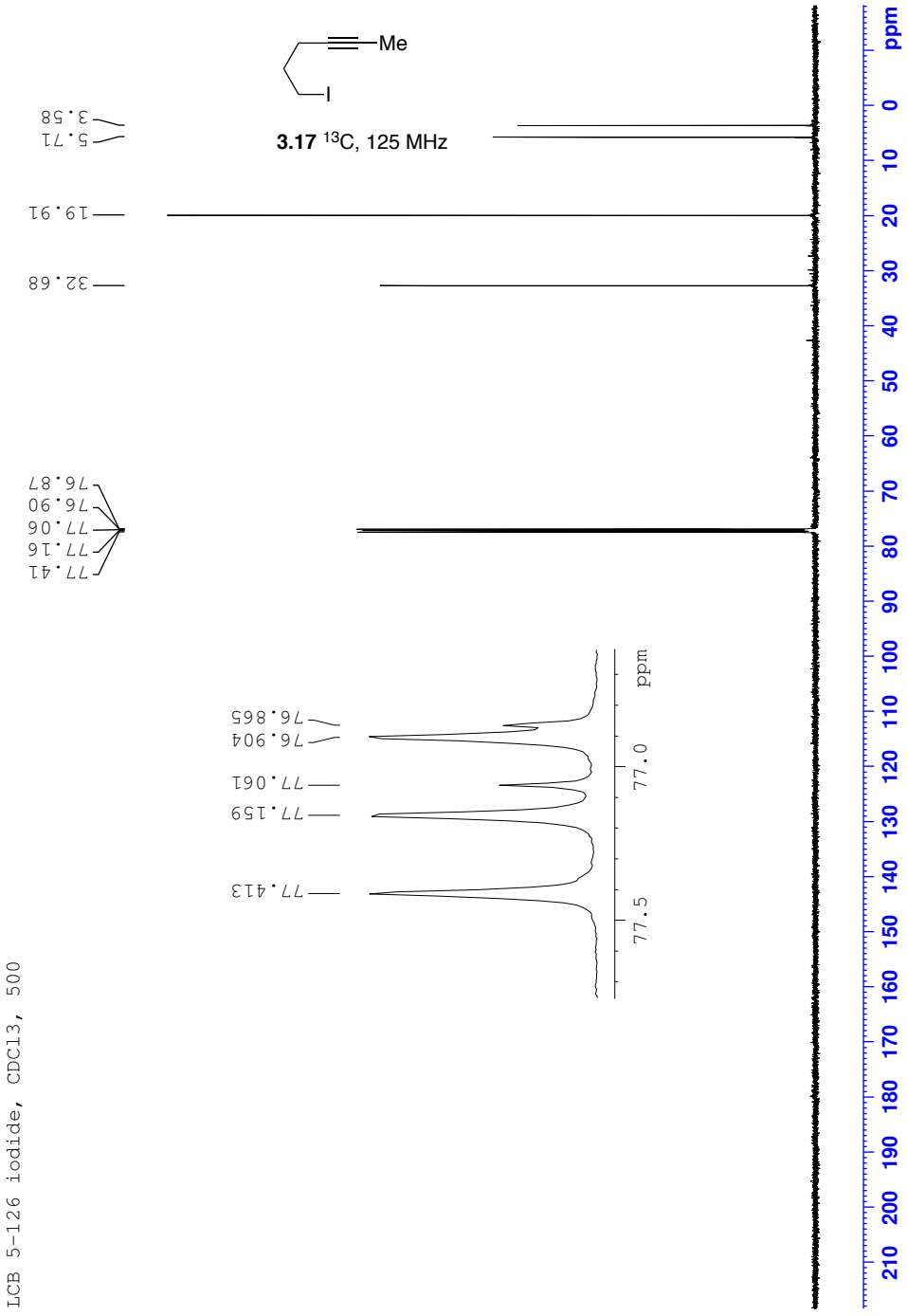
LCB 5-126 iodide, CDCl3, 500
3.17 13C, 125 MHz
Me
I
3.58
5.71
19.91
32.68
76.87
76.90
77.06
77.16
77.41
76.865
76.904
77.061
77.159
77.413
77.5
77.0
ppm
ppm

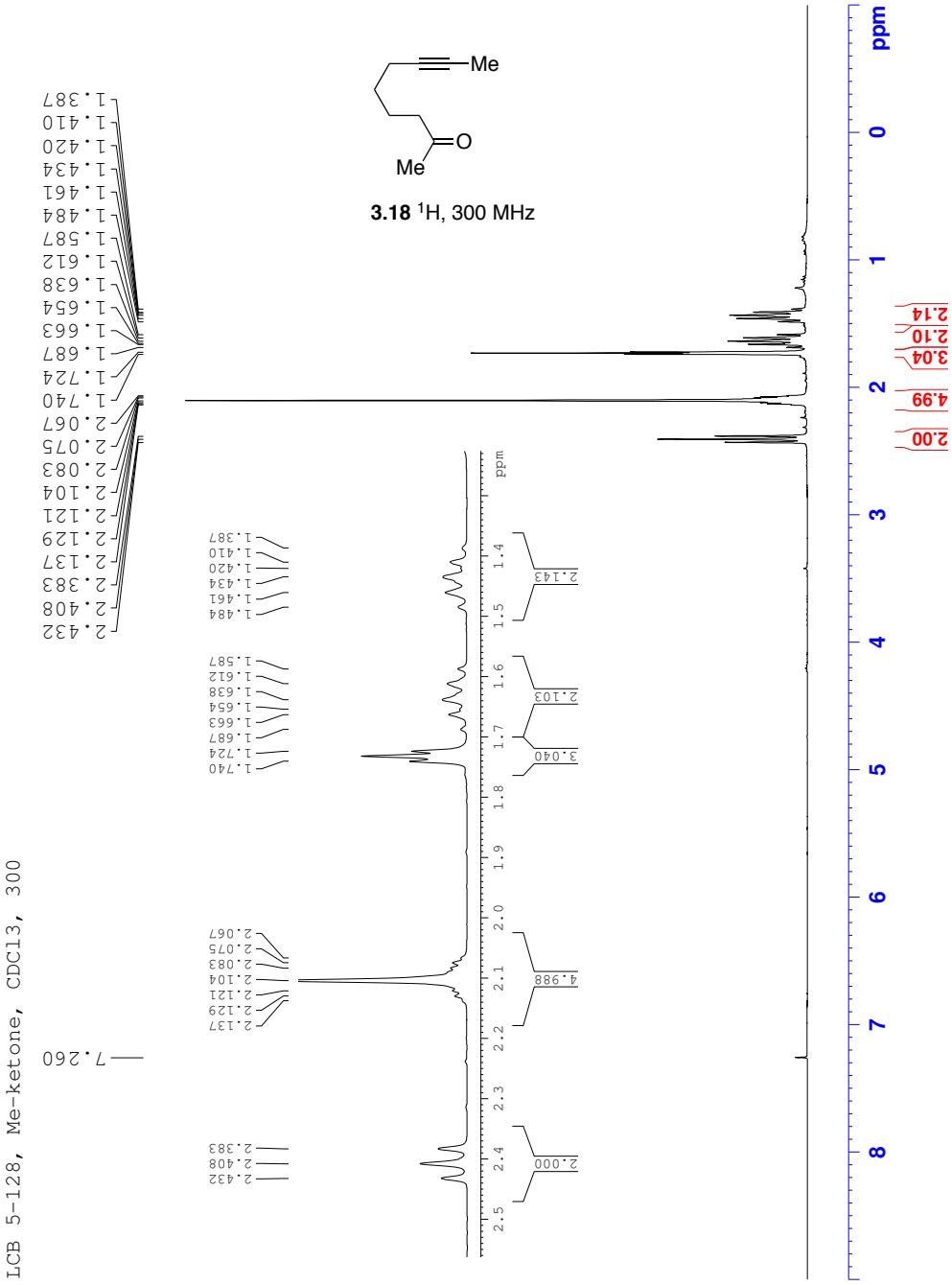
LCB 5-128, Me-ketone, CDCl3, 300
Me
O
Me
3.18 1H, 300 MHz
ppm
2.00
4.99
3.04
2.10
2.14
2.000
4.988
3.040
2.103
2.143
7.260

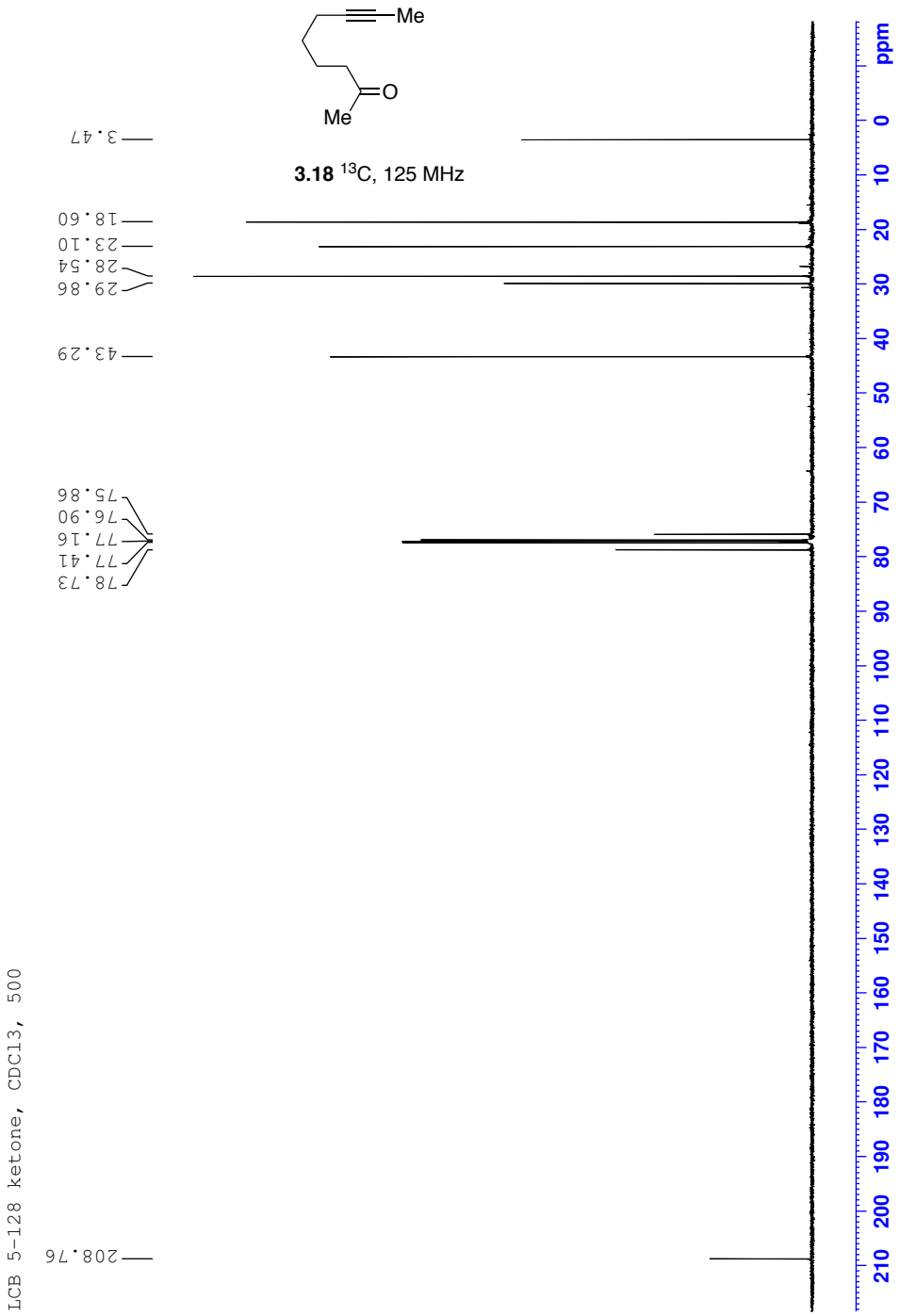
Me
O
Me
3.18 13C, 125 MHz
3.47
18.60
23.10
28.54
29.86
43.29
75.86
76.90
77.16
77.41
78.73
208.76
LCB 5-128 ketone, CDCl3, 500
ppm
0
10
20
30
40
50
60
70
80
90
100
110
120
130
140
150
160
170
180
190
200
210

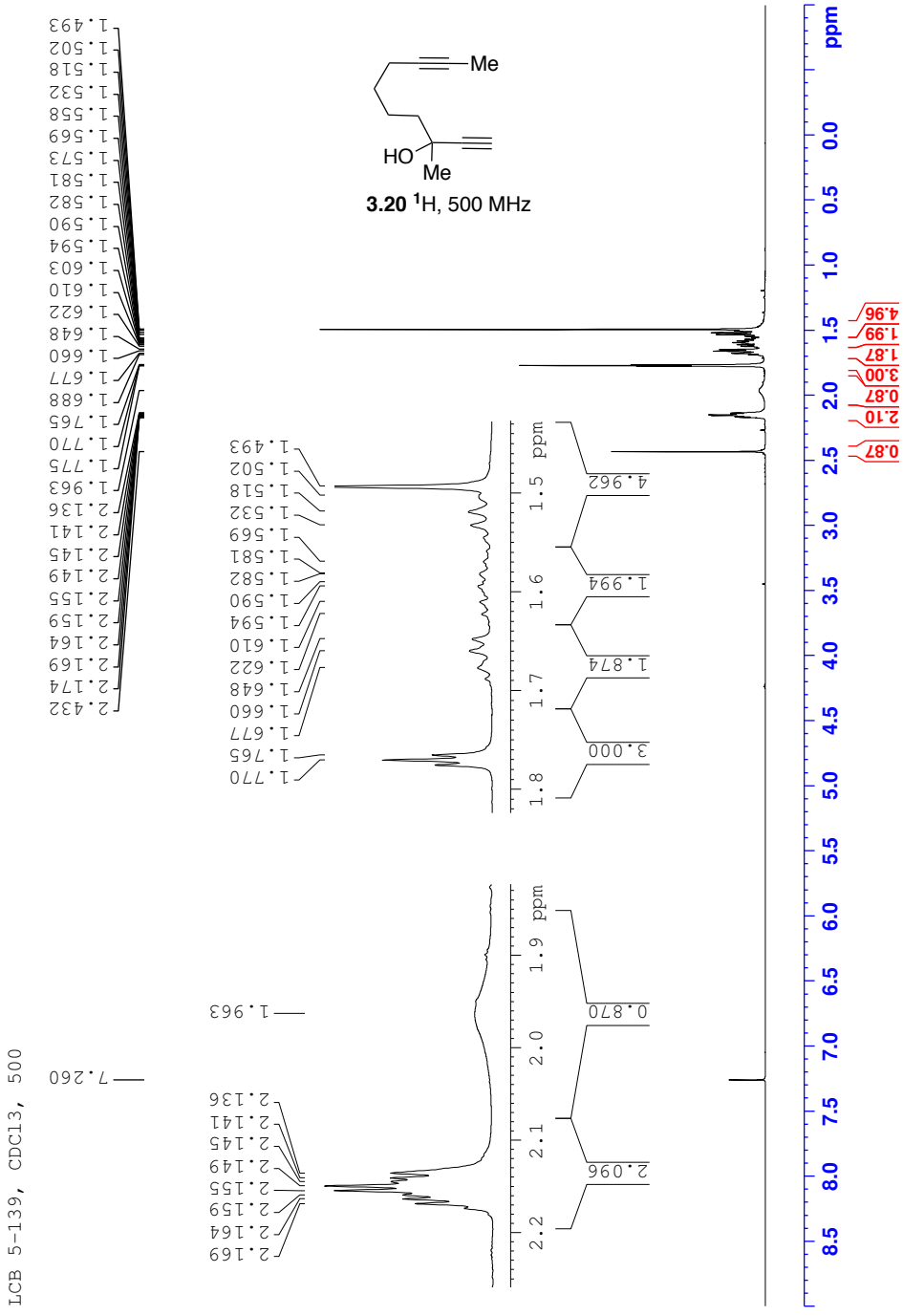
LCB 5-139, CDCl3, 500
Me
HO
Me
3.20 1H, 500 MHz
ppm

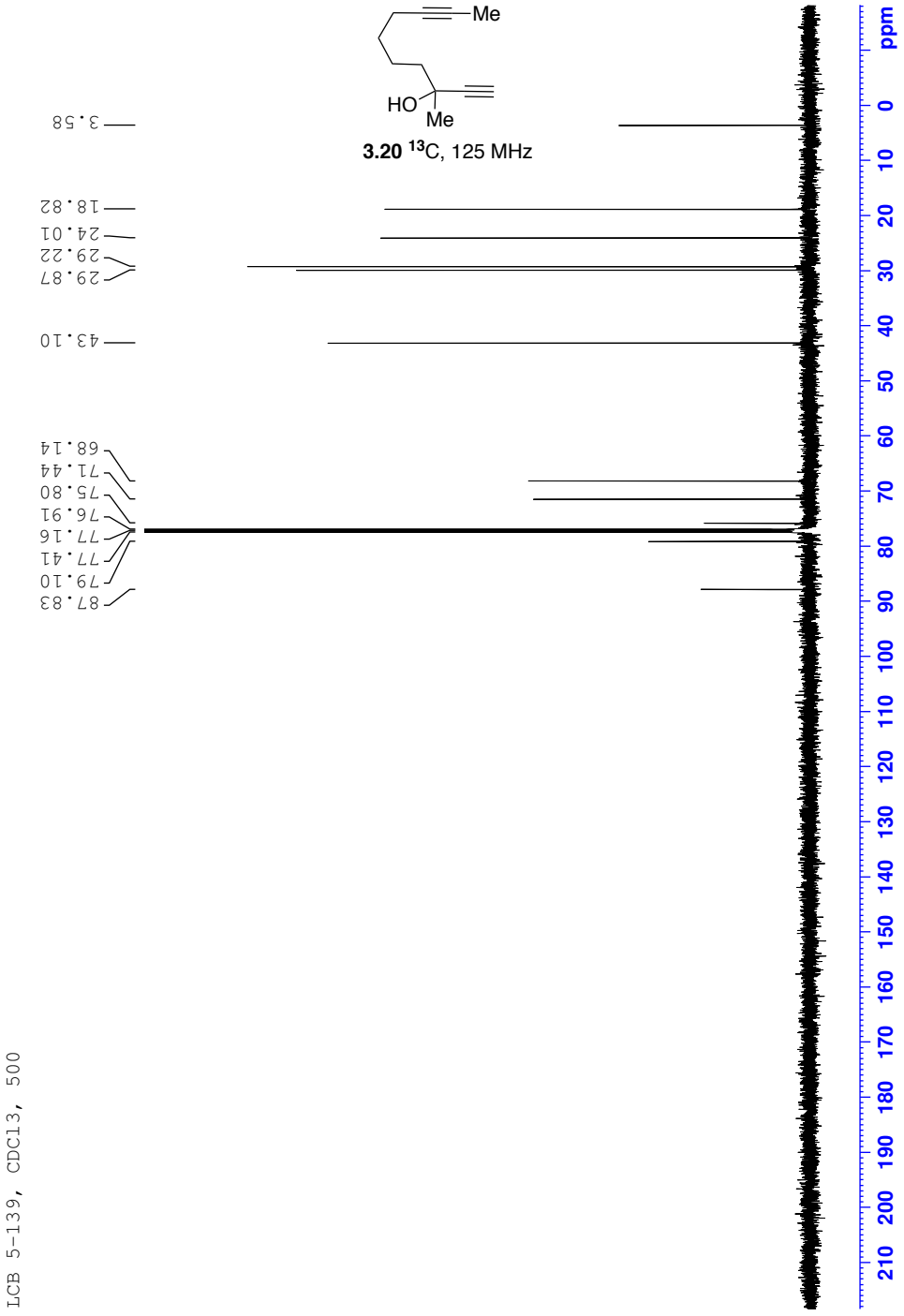
Me
HO
Me
3.20 13C, 125 MHz
3.58
18.82
24.01
29.22
29.87
43.10
68.14
71.44
75.80
76.91
77.16
77.41
79.10
87.83
ppm
0
10
20
30
40
50
60
70
80
90
100
110
120
130
140
150
160
170
180
190
200
210
LCB 5-139, CDCl3, 500

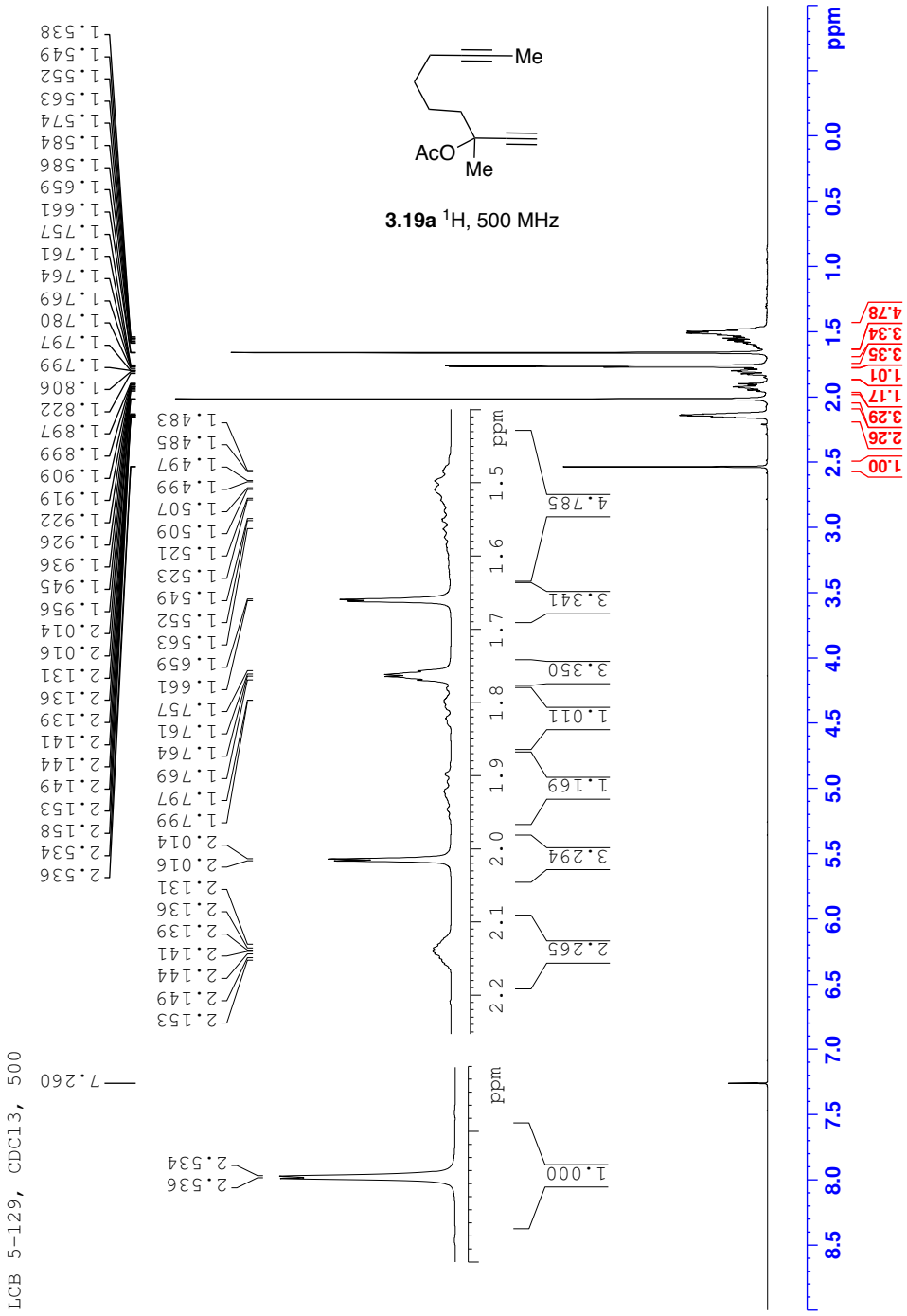
Me
AcO
Me
3.19a 1H, 500 MHz
LCB 5-129, CDC13, 500
ppm

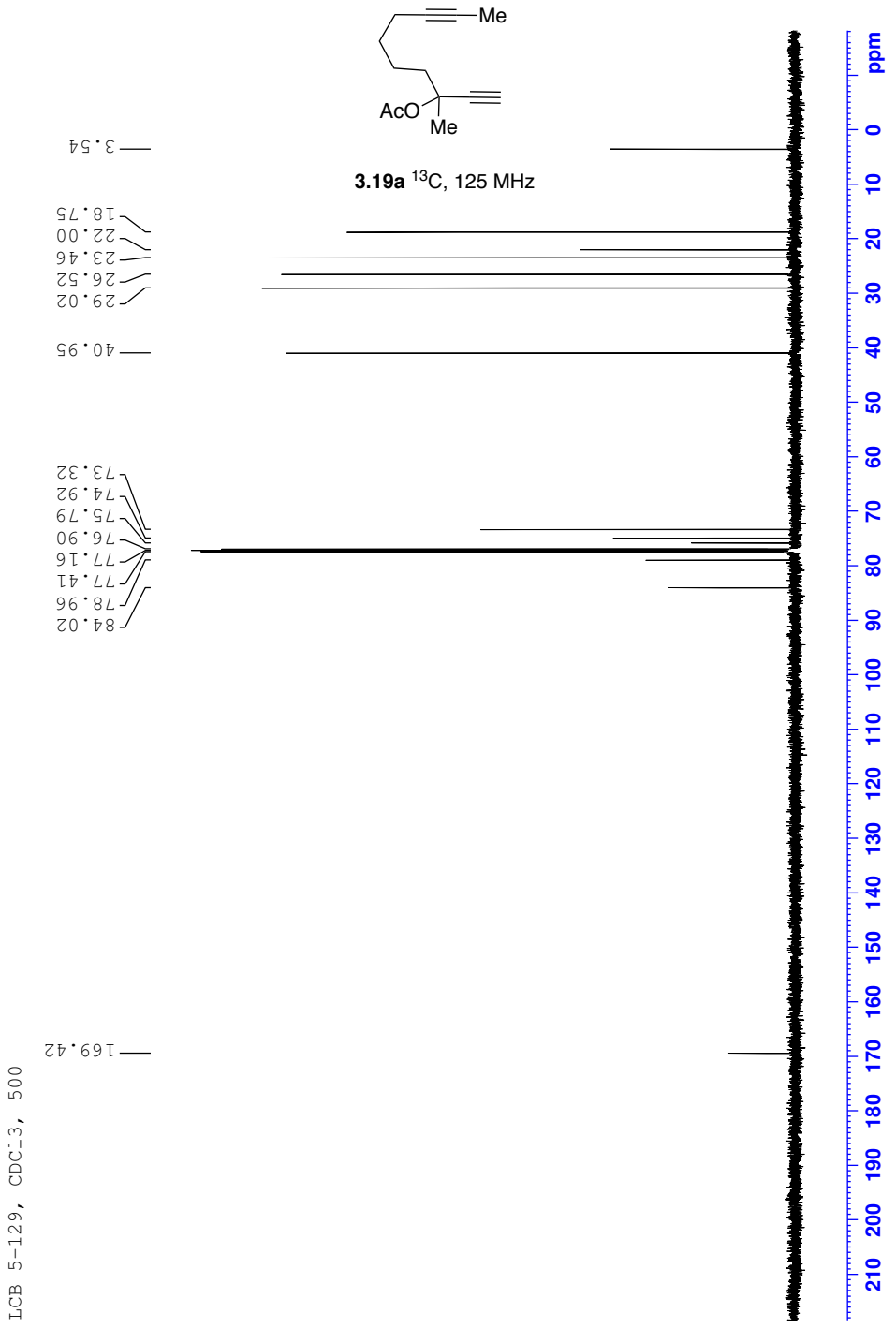
Me
AcO
Me
3.19a 13C, 125 MHz
3.54
18.75
22.00
23.46
26.52
29.02
40.95
73.32
74.92
75.79
76.90
77.16
77.41
78.96
84.02
169.42
LCB 5-129, CDCl3, 500
ppm
0
10
20
30
40
50
60
70
80
90
100
110
120
130
140
150
160
170
180
190
200
210

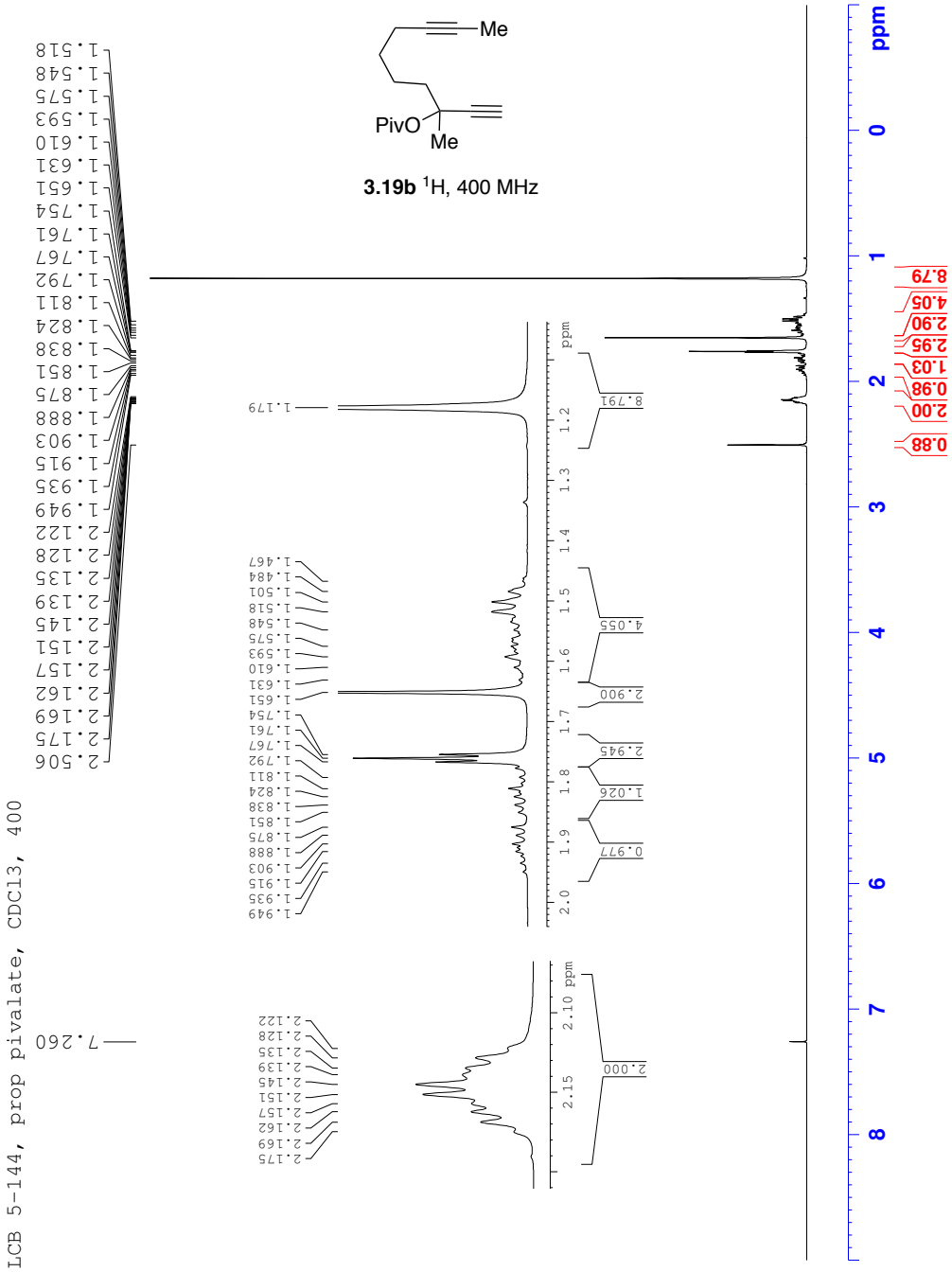
LCB 5-144, prop pivalate, CDCl3, 400
Me
PivO
Me
3.19b 1H, 400 MHz
ppm

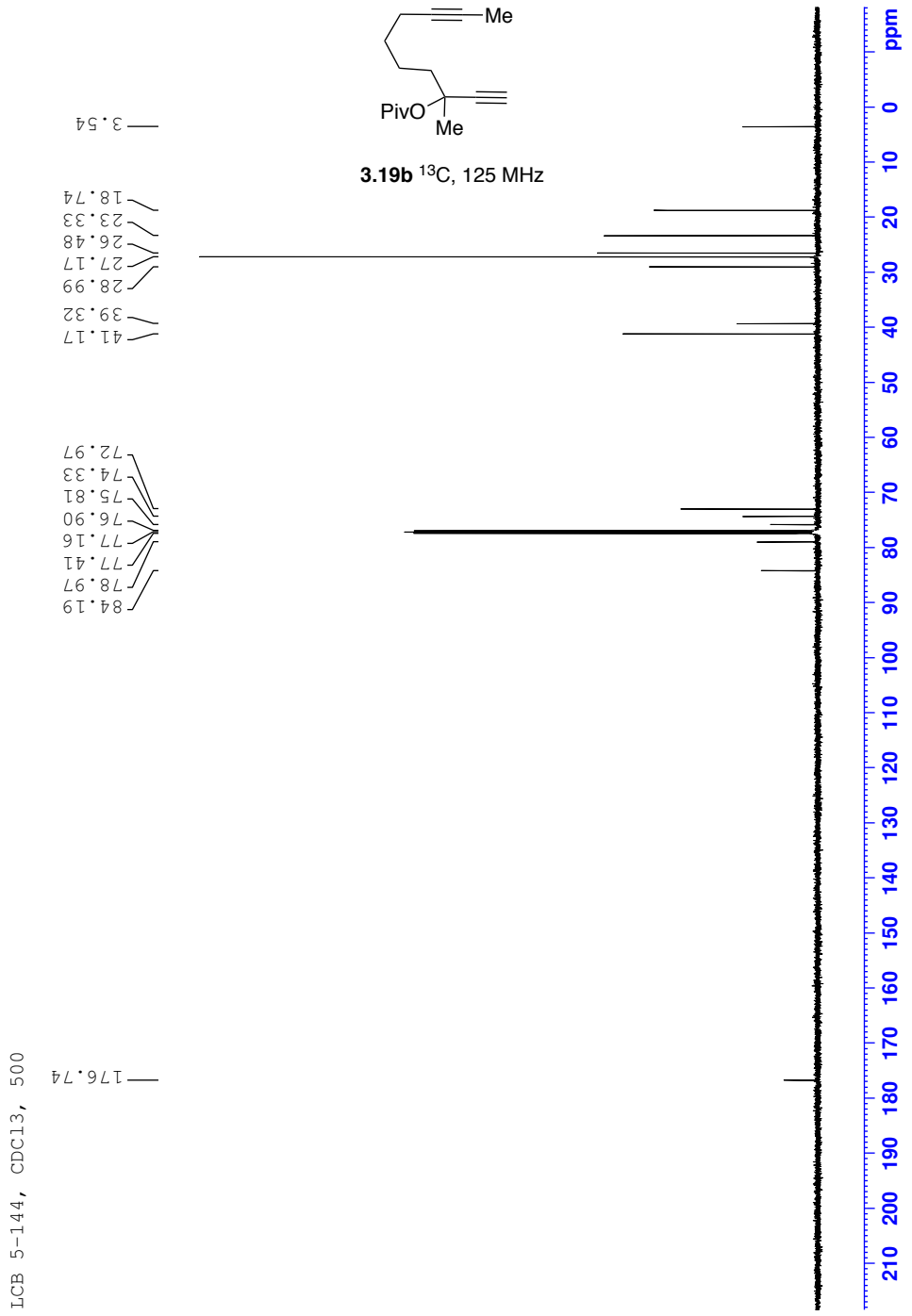
Me
PivO
Me
3.19b ^{13}C, 125 MHz
3.54
18.74
23.33
26.48
27.17
28.99
39.32
41.17
72.97
74.33
75.81
76.90
77.16
77.41
78.97
84.19
176.74
LCB 5-144, CDC13, 500
ppm
0
10
20
30
40
50
60
70
80
90
100
110
120
130
140
150
160
170
180
190
200
210

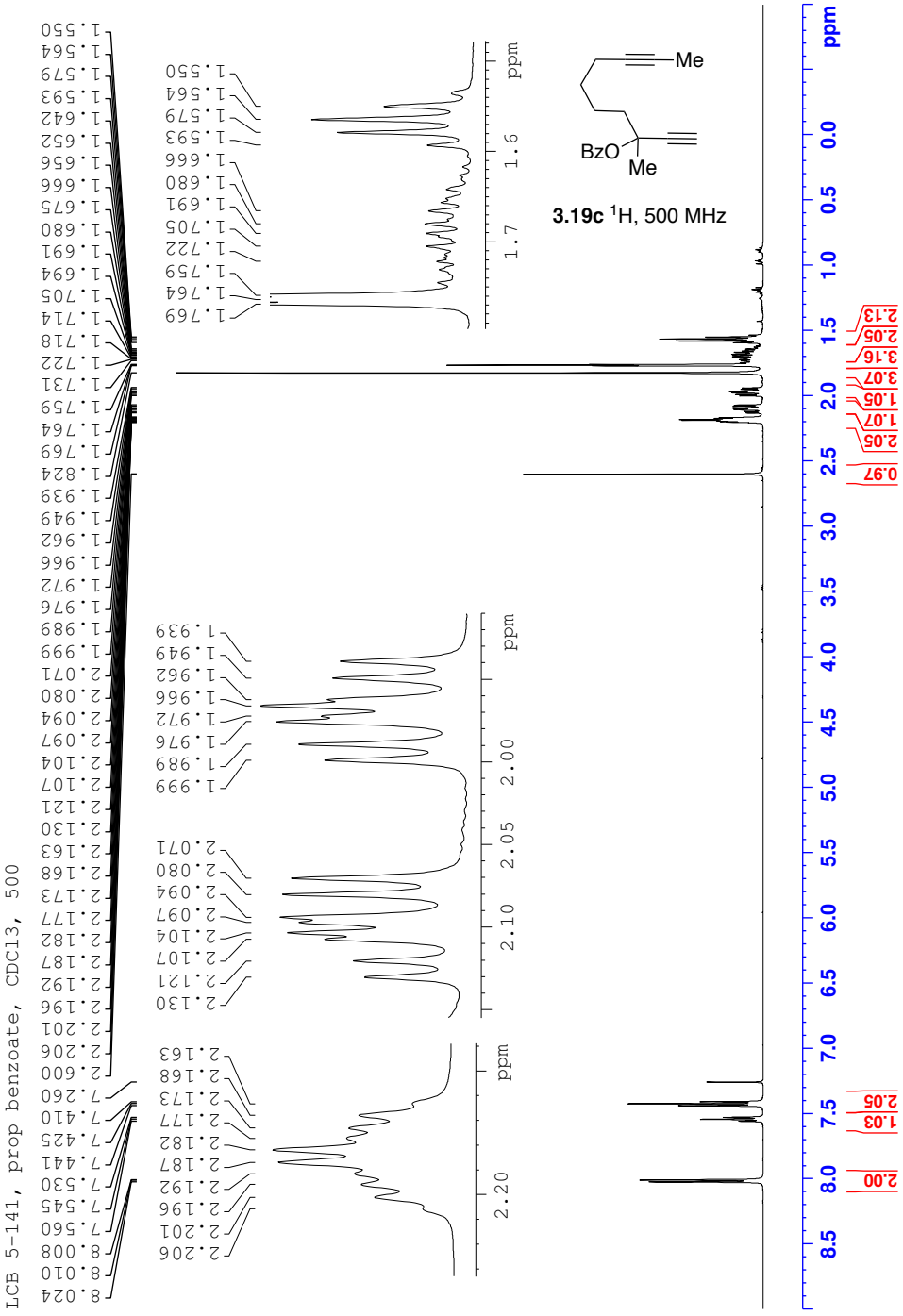
LCB 5-141, prop benzoate, CDCl3, 500
Me
BzO
Me
3.19c 1H, 500 MHz
ppm

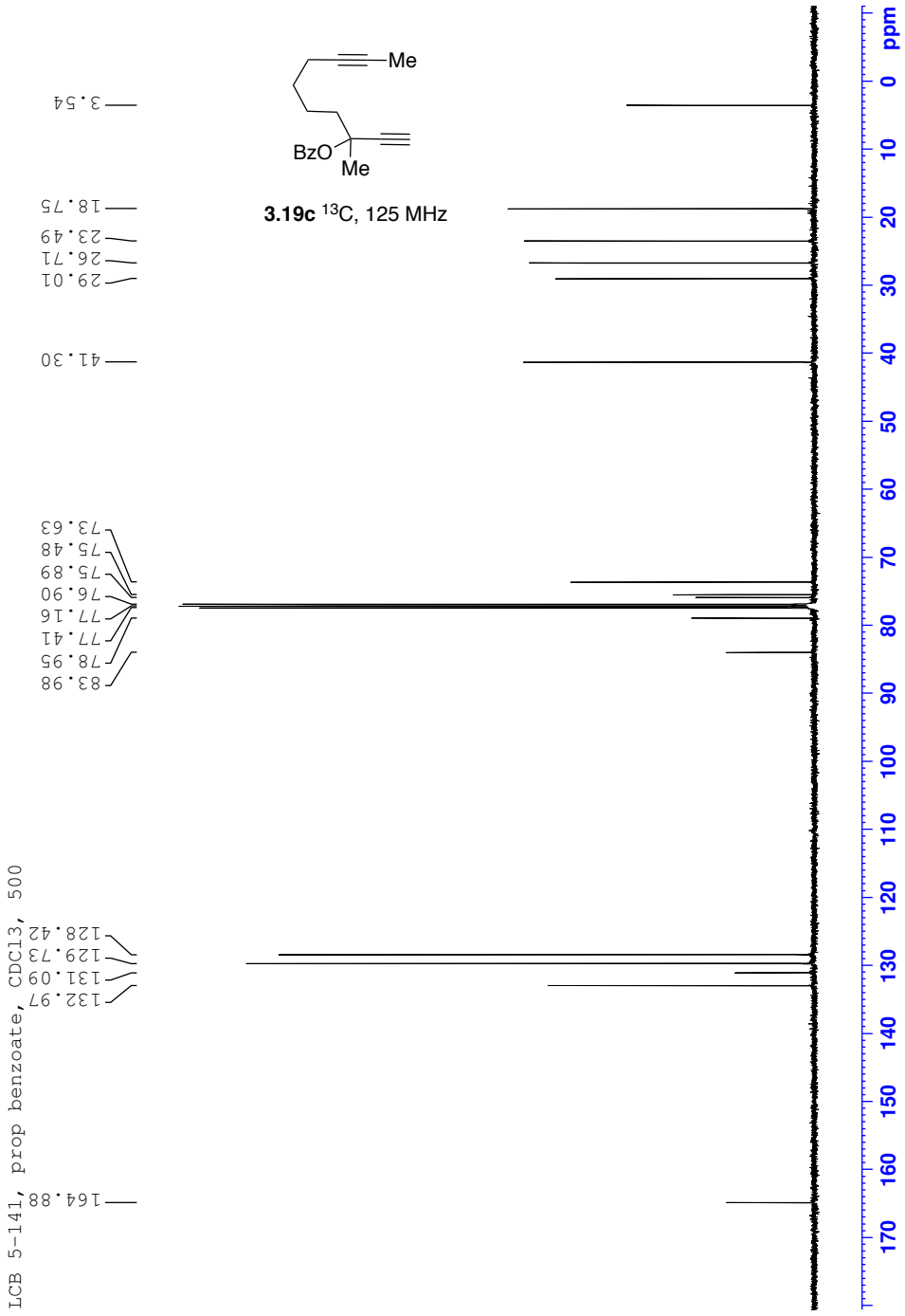

3.19c ^{13}C, 125 MHz

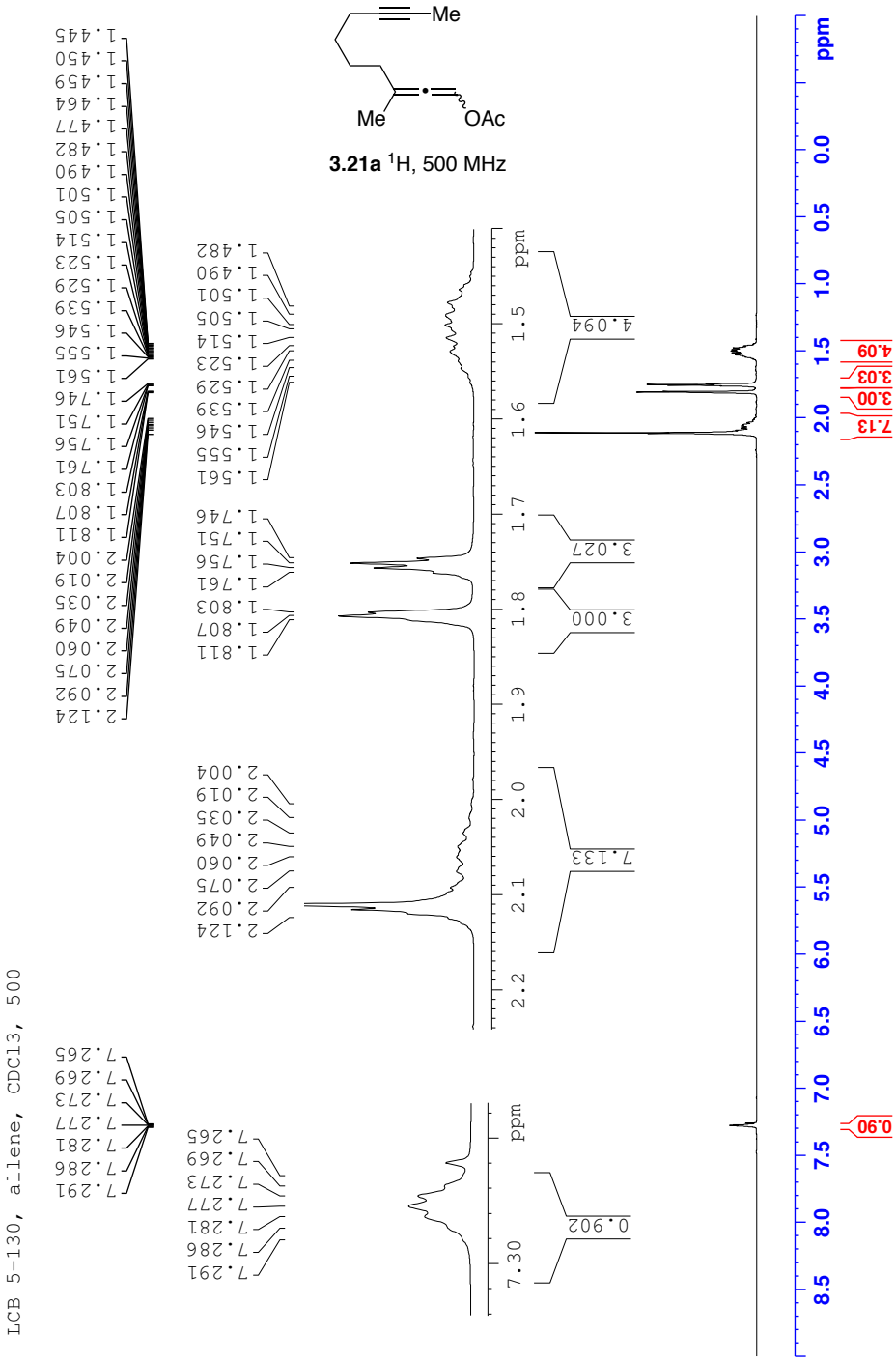
LCB 5-130, allene, CDCl3, 500
Me
Me
OAc
3.21a 1H, 500 MHz
ppm
0.90
4.09
3.03
3.00
7.13
4.094
3.027
3.000
7.133
0.902

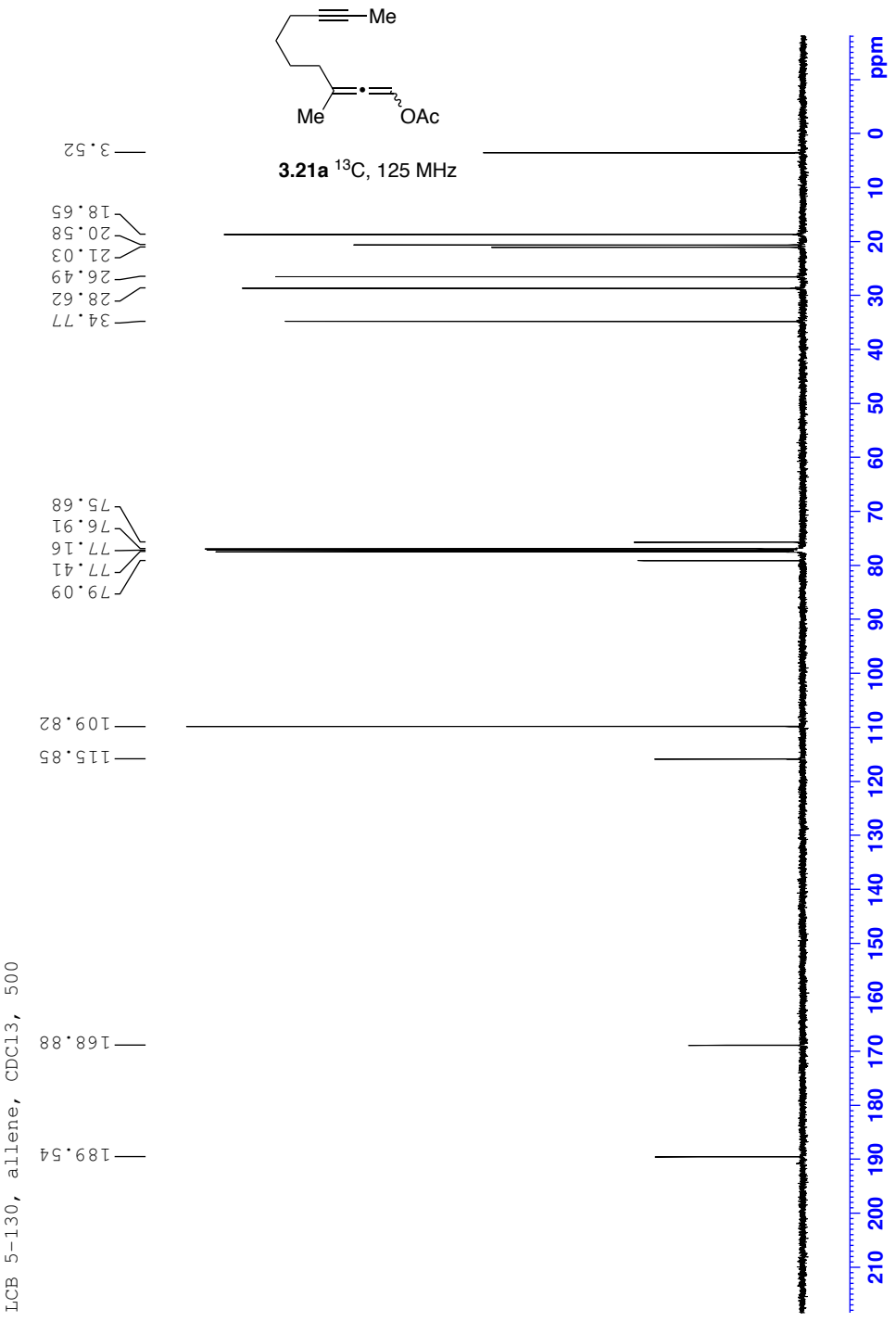
Me
Me
OAc
3.21a 13C, 125 MHz
3.52
18.65
20.58
21.03
26.49
28.62
34.77
75.68
76.91
77.16
77.41
79.09
109.82
115.85
168.88
189.54
LCB 5-130, allene, CDCl3, 500
ppm
0
10
20
30
40
50
60
70
80
90
100
110
120
130
140
150
160
170
180
190
200
210

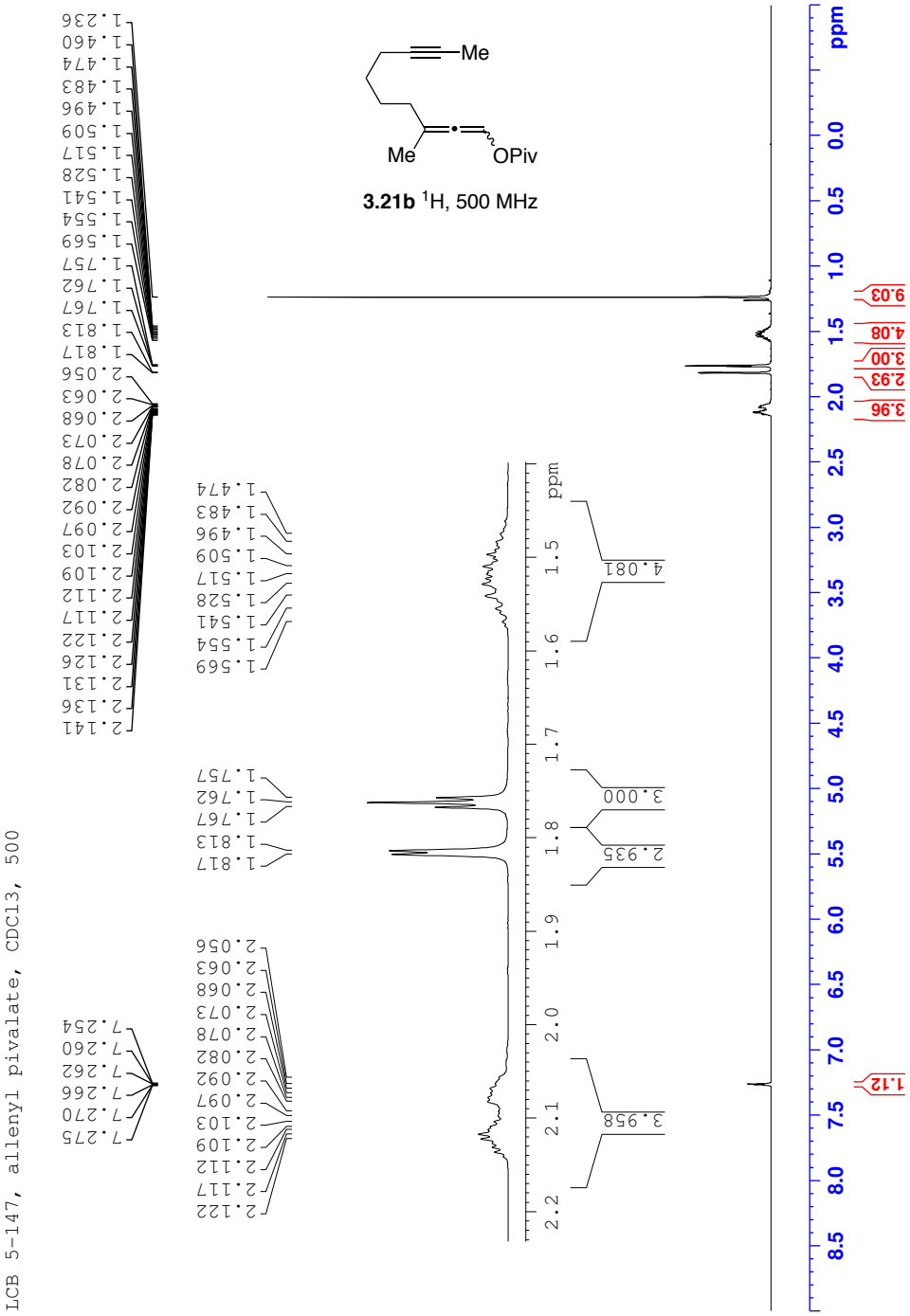
LCB 5-147, allenyl pivalate, CDCl3, 500
Me
Me
OPiv
3.21b 1H, 500 MHz
ppm
9.03
4.08
3.00
2.93
3.96
1.12
4.081
3.000
2.935
3.958

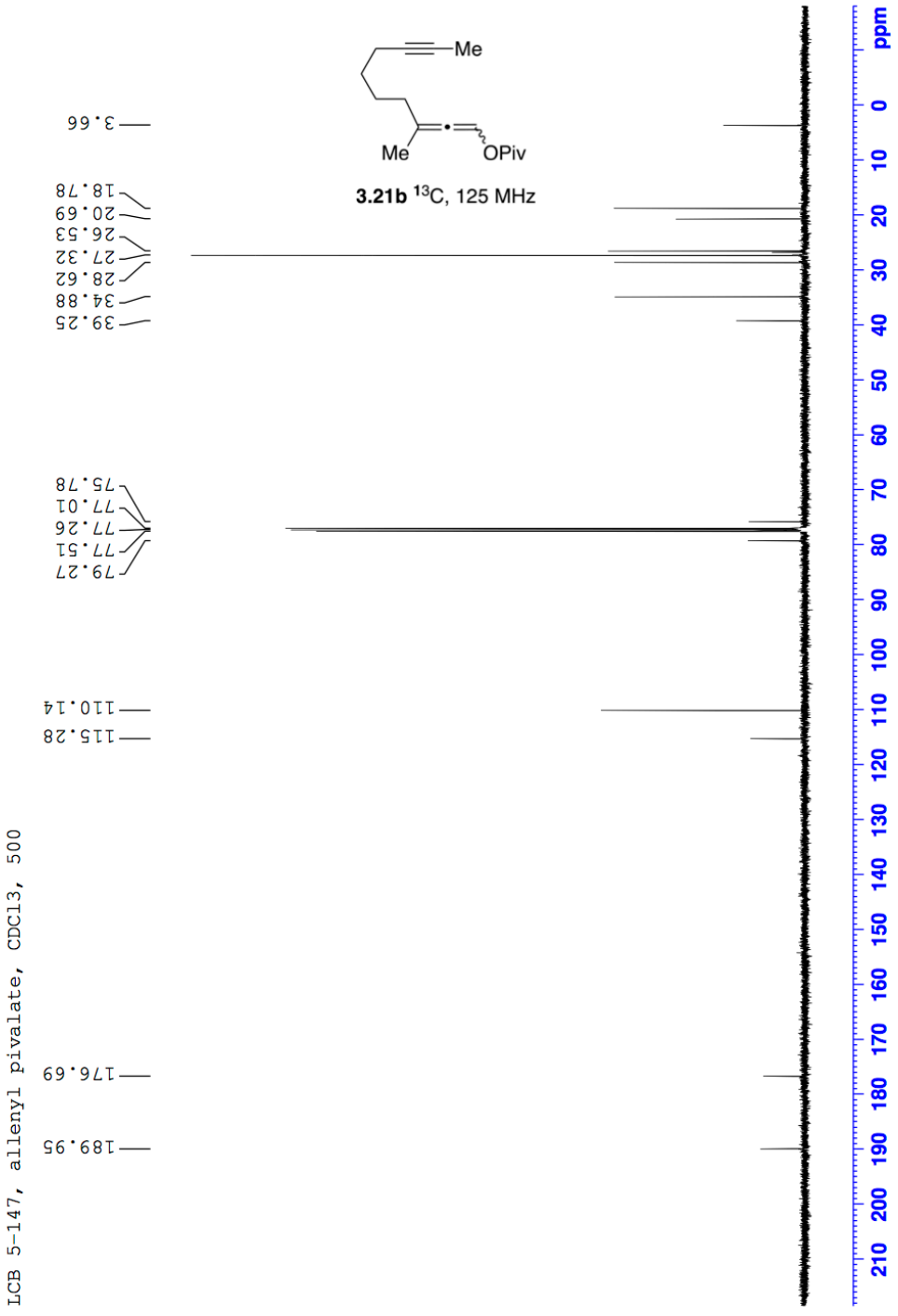
LCB 5-147, allenyl pivalate, CDCl3, 500
3.66
18.78
20.69
26.53
27.32
28.62
34.88
39.25
75.78
77.01
77.26
77.51
79.27
110.14
115.28
176.69
189.95
Me
Me
OPiv
3.21b 13C, 125 MHz
ppm
0
10
20
30
40
50
60
70
80
90
100
110
120
130
140
150
160
170
180
190
200
210

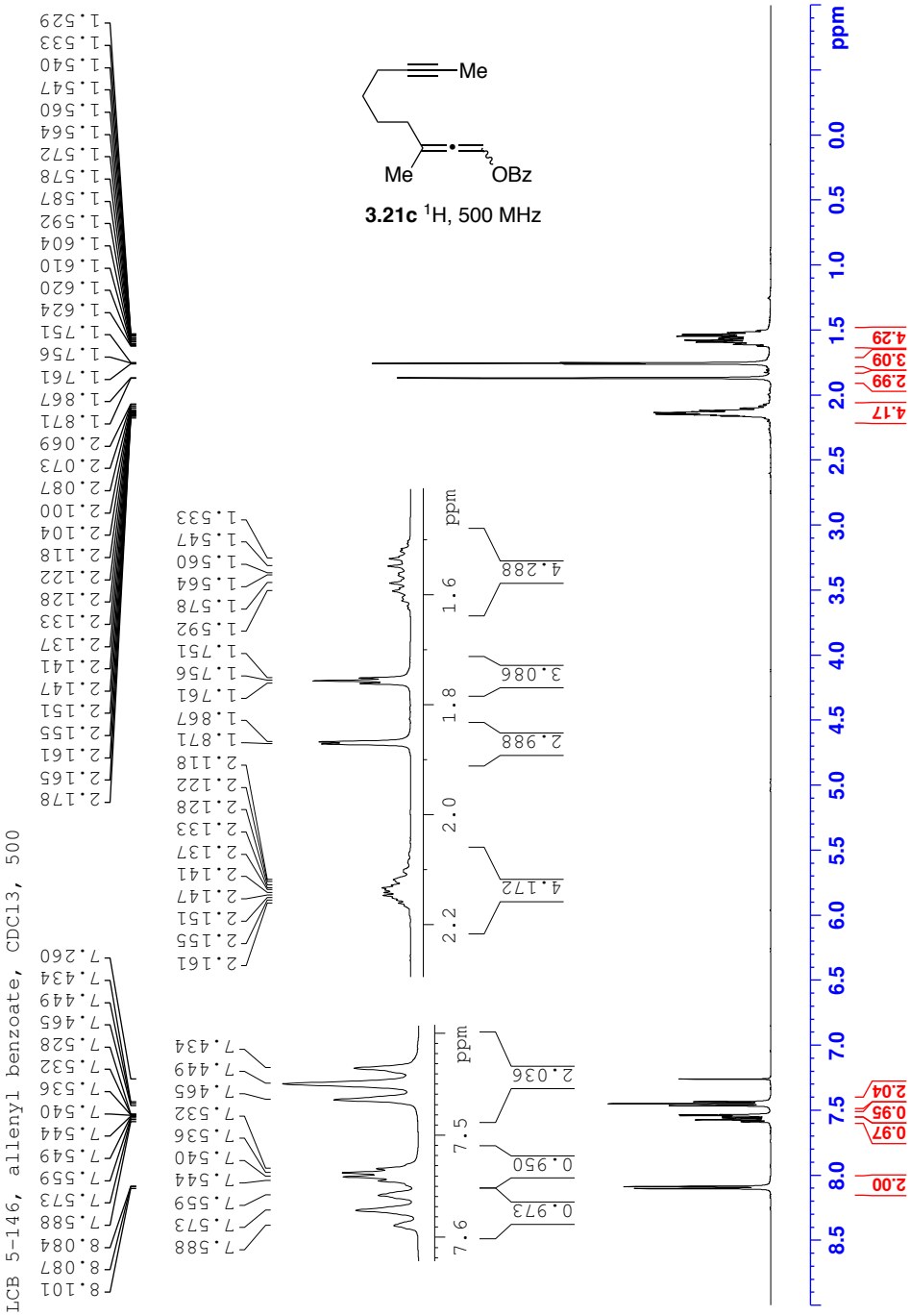
LCB 5-146, allenyl benzoate, CDCl3, 500
Me
Me
OBz
3.21c 1H, 500 MHz
ppm

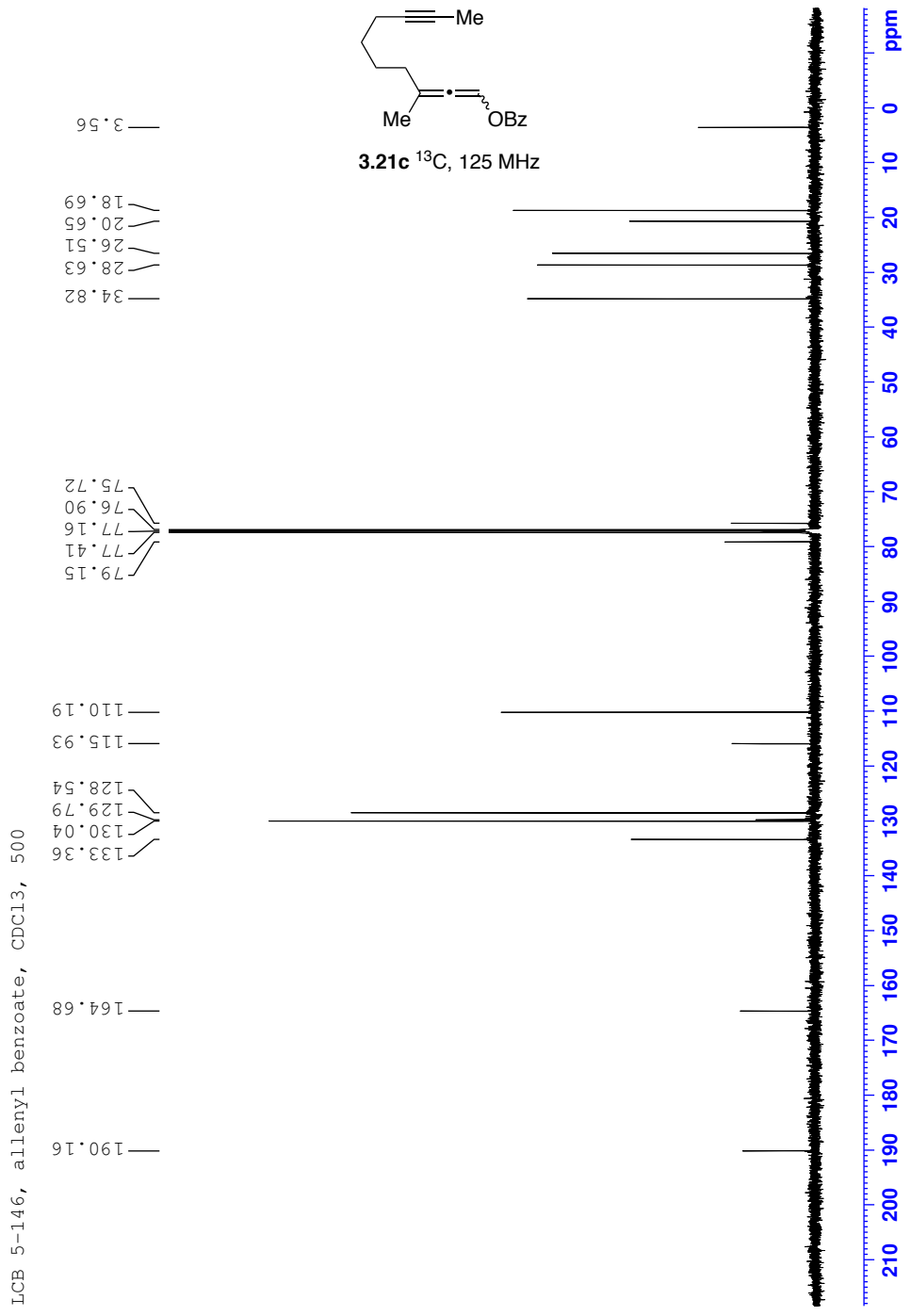
Me
Me
OBz
3.21c 13C, 125 MHz
3.56
18.69
20.65
26.51
28.63
34.82
75.72
76.90
77.16
77.41
79.15
110.19
115.93
128.54
129.79
130.04
133.36
164.68
190.16
LCB 5-146, allenyl benzoate, CDCl3, 500
ppm
0
10
20
30
40
50
60
70
80
90
100
110
120
130
140
150
160
170
180
190
200
210

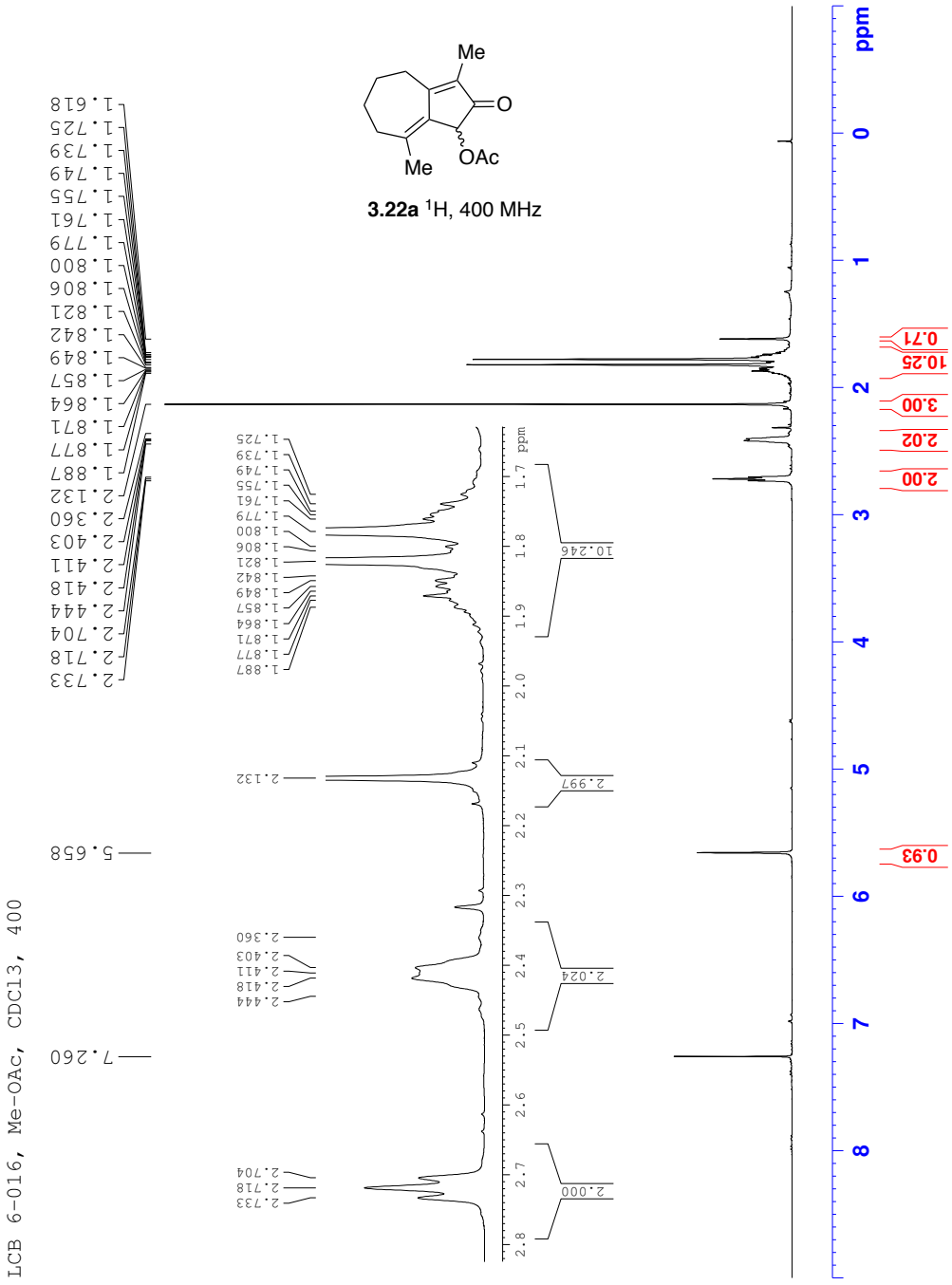
Me
O
OAc
Me
3.22a 1H, 400 MHz
LCB 6-016, Me-OAc, CDCl3, 400
ppm
0.71
10.25
3.00
2.02
2.00
0.93

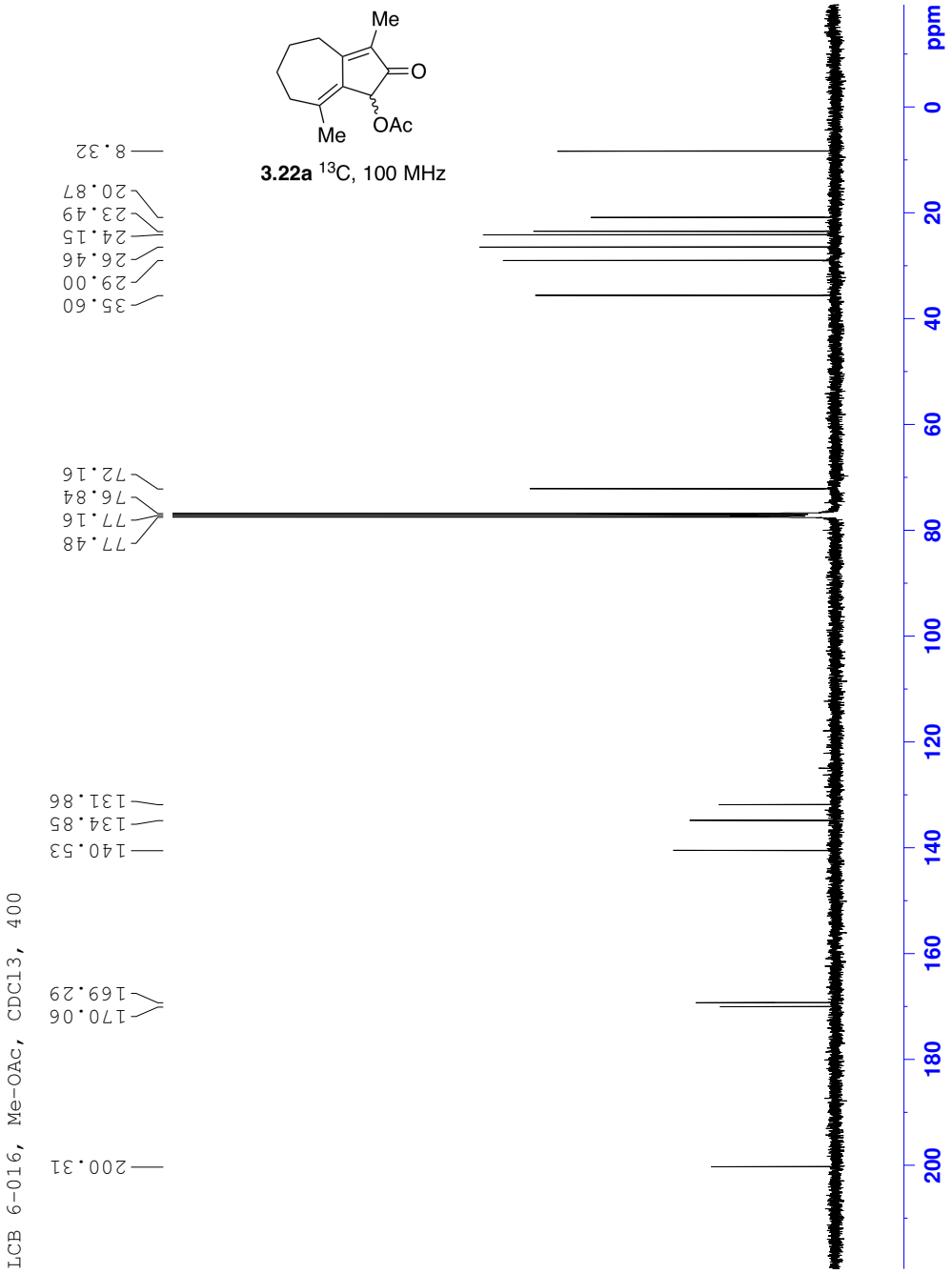
Me
O
OAc
Me
3.22a 13C, 100 MHz
8.32
20.87
23.49
24.15
26.46
29.00
35.60
72.16
76.84
77.16
77.48
131.86
134.85
140.53
169.29
170.06
200.31
LCB 6-016, Me-OAc, CDCl3, 400
ppm
0
20
40
60
80
100
120
140
160
180
200

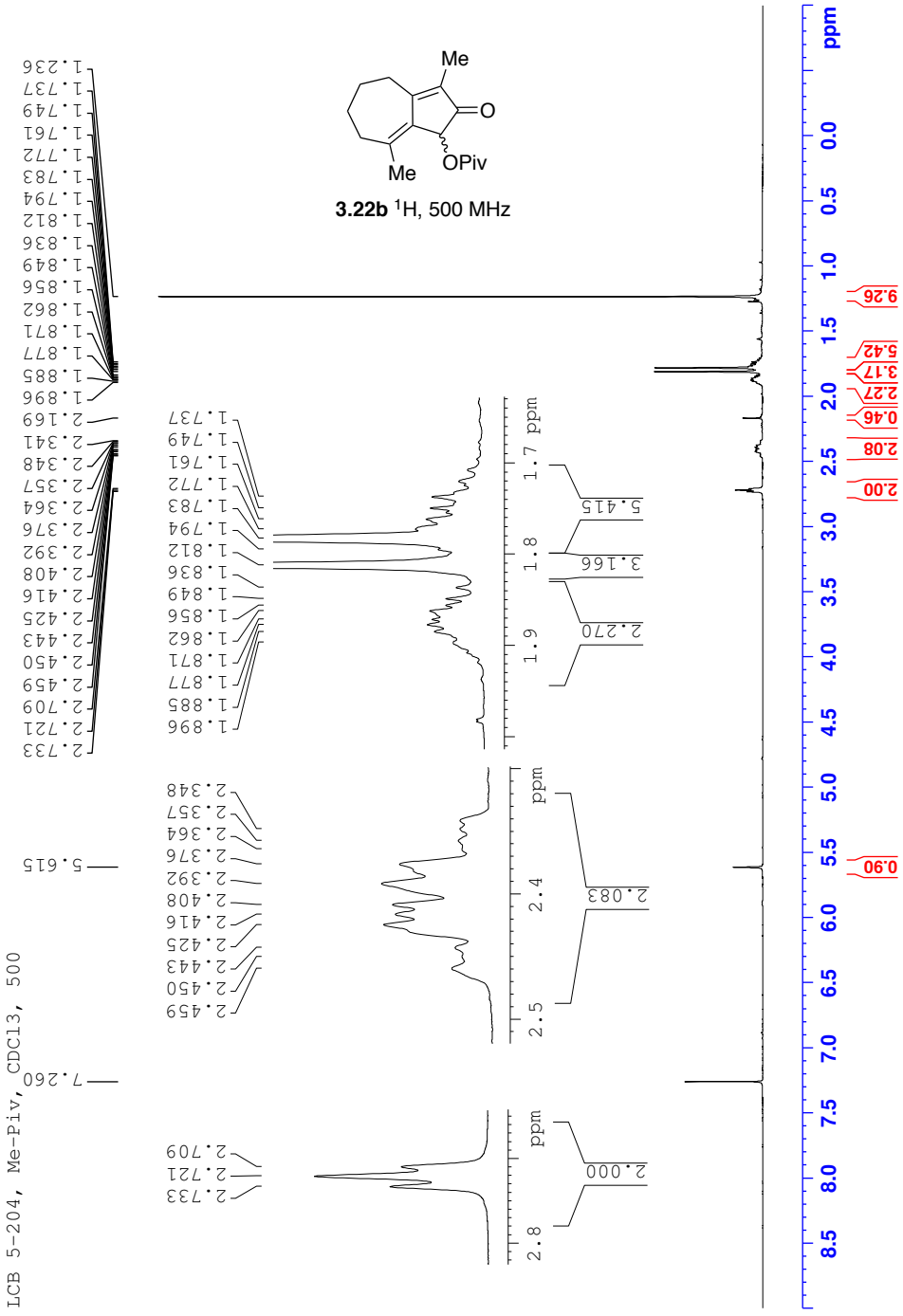
Me
O
OPiv
Me
3.22b ^{1}H, 500 MHz
LCB 5-204, Me-Piv, CDCl3, 500
ppm

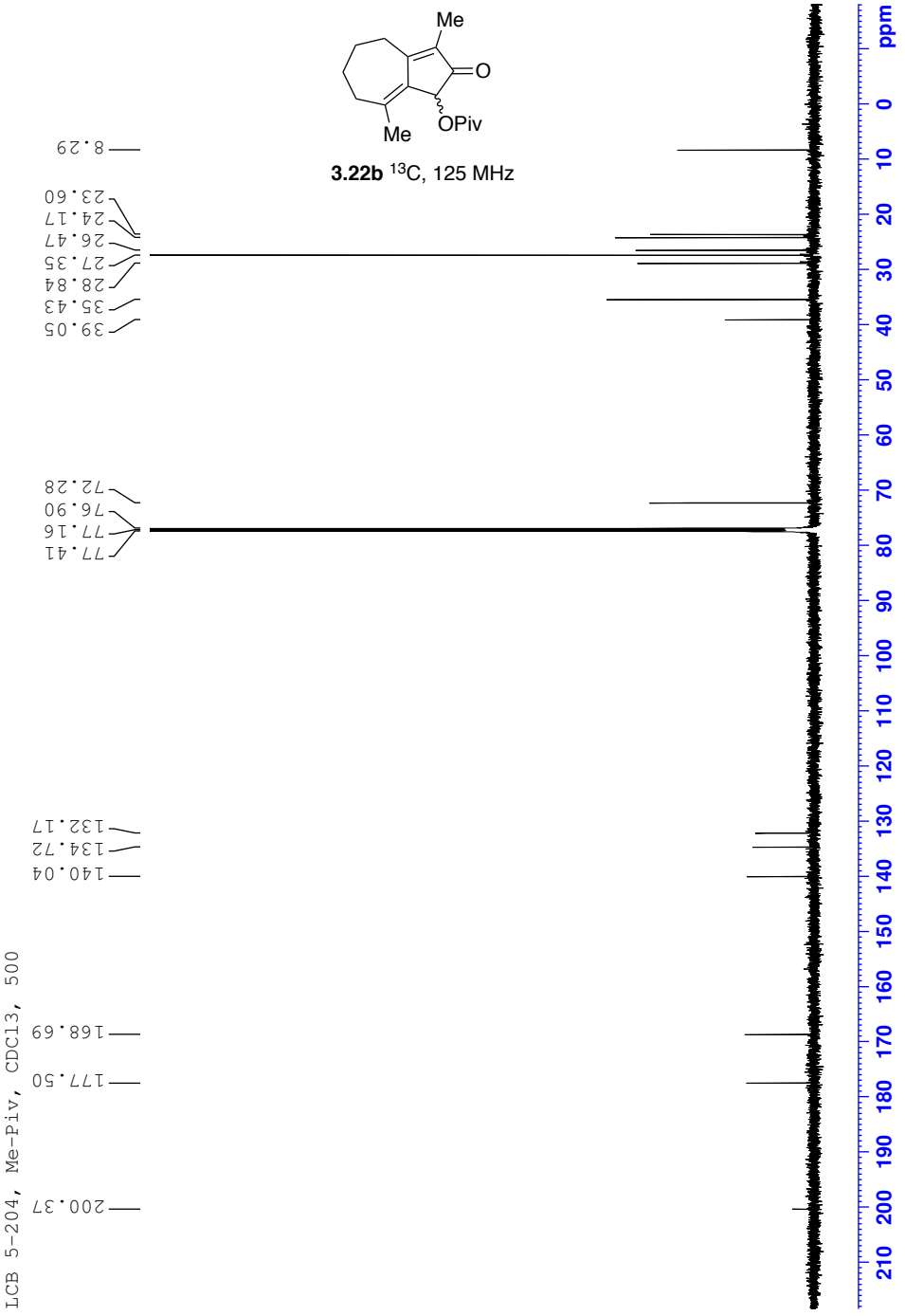
Me
O
OPiv
Me
3.22b ^{13}C, 125 MHz
8.29
23.60
24.17
26.47
27.35
28.84
35.43
39.05
72.28
76.90
77.16
77.41
132.17
134.72
140.04
168.69
177.50
200.37
LCB 5-204, Me-Piv, CDCl3, 500
ppm
0
10
20
30
40
50
60
70
80
90
100
110
120
130
140
150
160
170
180
190
200
210

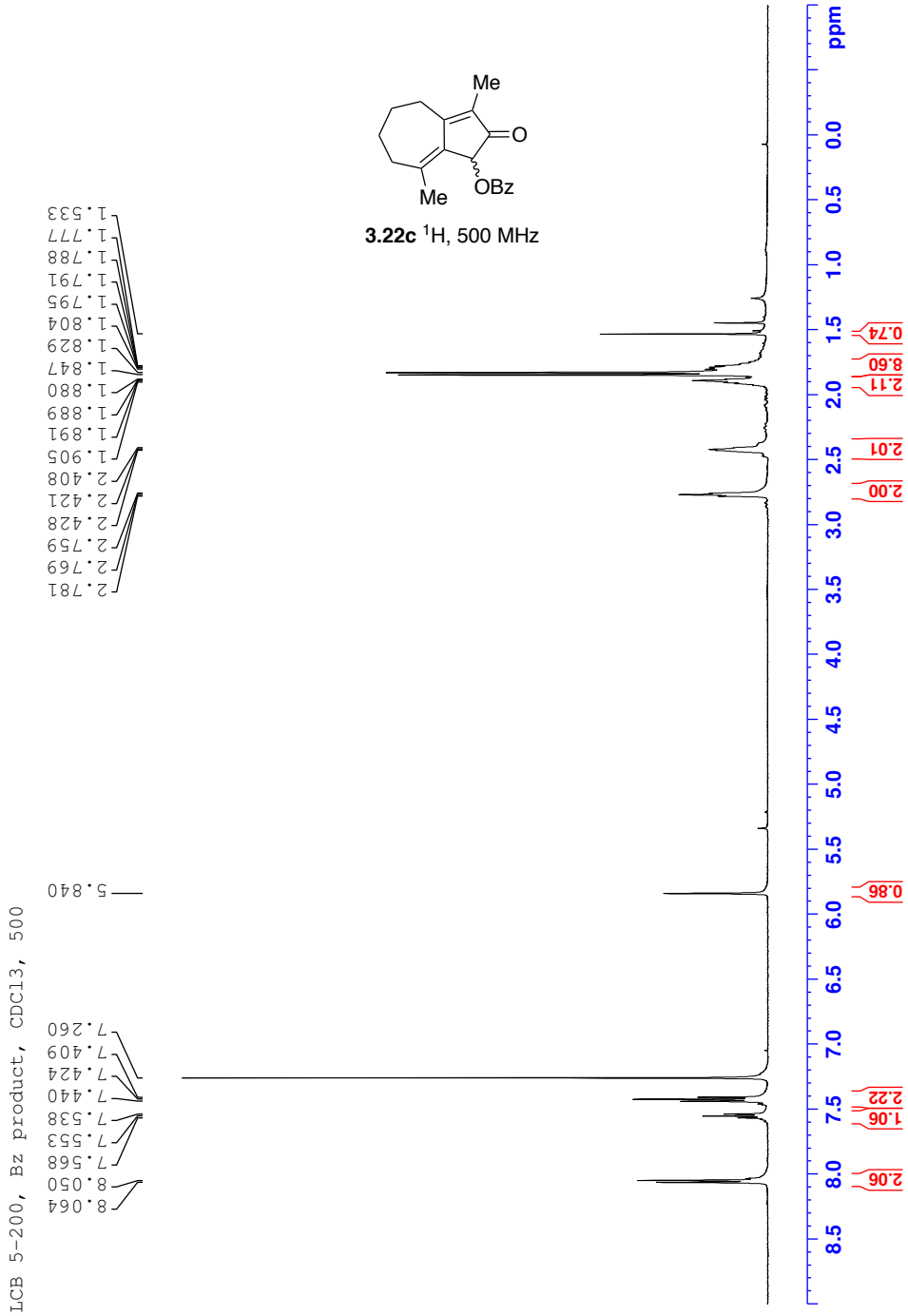
Me
O
OBz
Me
3.22c 1H, 500 MHz
LCB 5-200, Bz product, CDCl3, 500
ppm
0.0
0.5
1.0
1.5
2.0
2.5
3.0
3.5
4.0
4.5
5.0
5.5
6.0
6.5
7.0
7.5
8.0
8.5
0.74
8.60
2.11
2.01
2.00
0.86
2.22
1.06
2.06
1.533
1.777
1.788
1.791
1.795
1.804
1.829
1.847
1.880
1.889
1.891
1.905
2.408
2.421
2.428
2.759
2.769
2.781
5.840
7.260
7.409
7.424
7.440
7.538
7.553
7.568
8.050
8.064

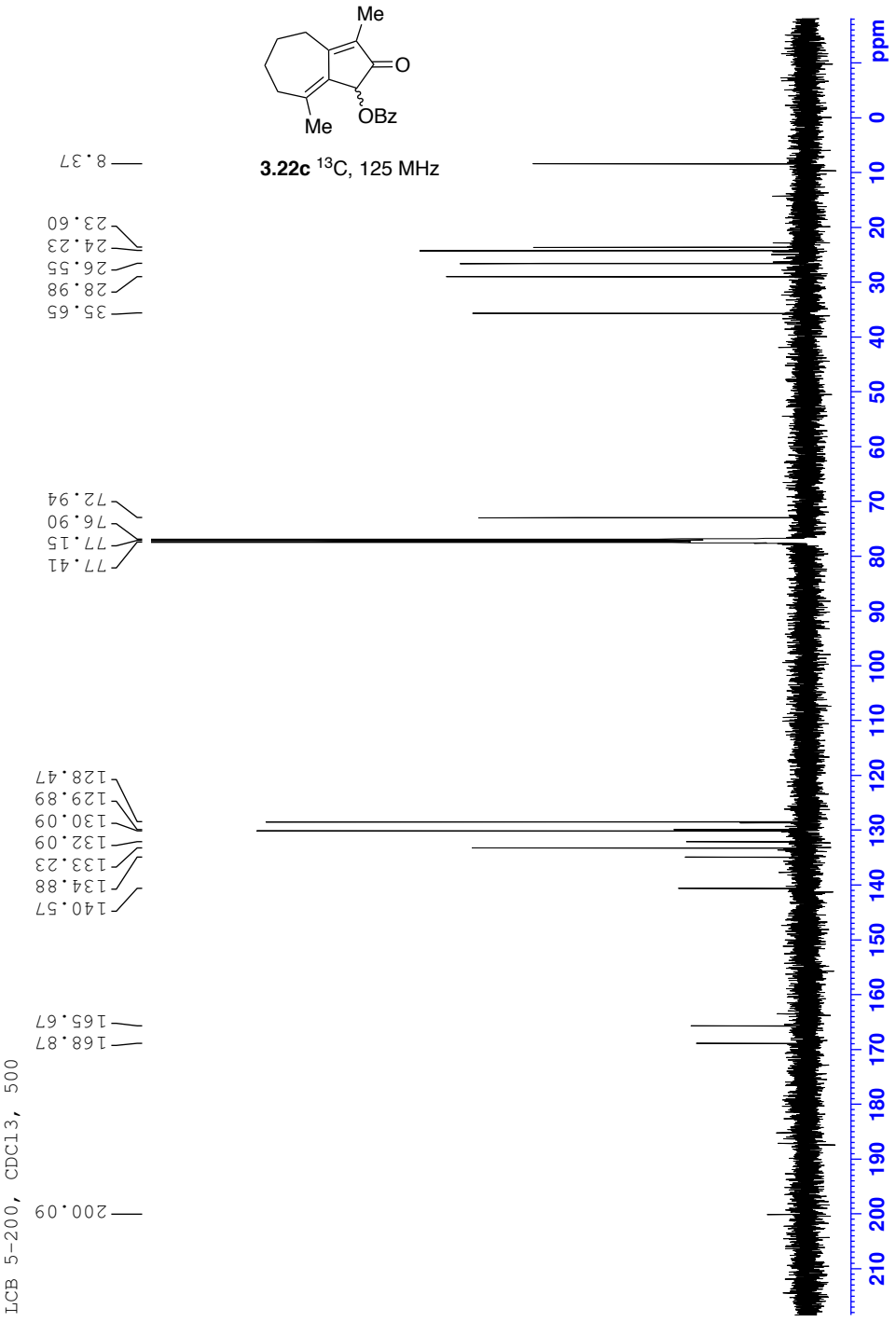
Me
O
OBz
Me
3.22c 13C, 125 MHz
8.37
23.60
24.23
26.55
28.98
35.65
72.94
76.90
77.15
77.41
128.47
129.89
130.09
132.09
133.23
134.88
140.57
165.67
168.87
200.09
LCB 5-200, CDCl3, 500
ppm
0
10
20
30
40
50
60
70
80
90
100
110
120
130
140
150
160
170
180
190
200
210

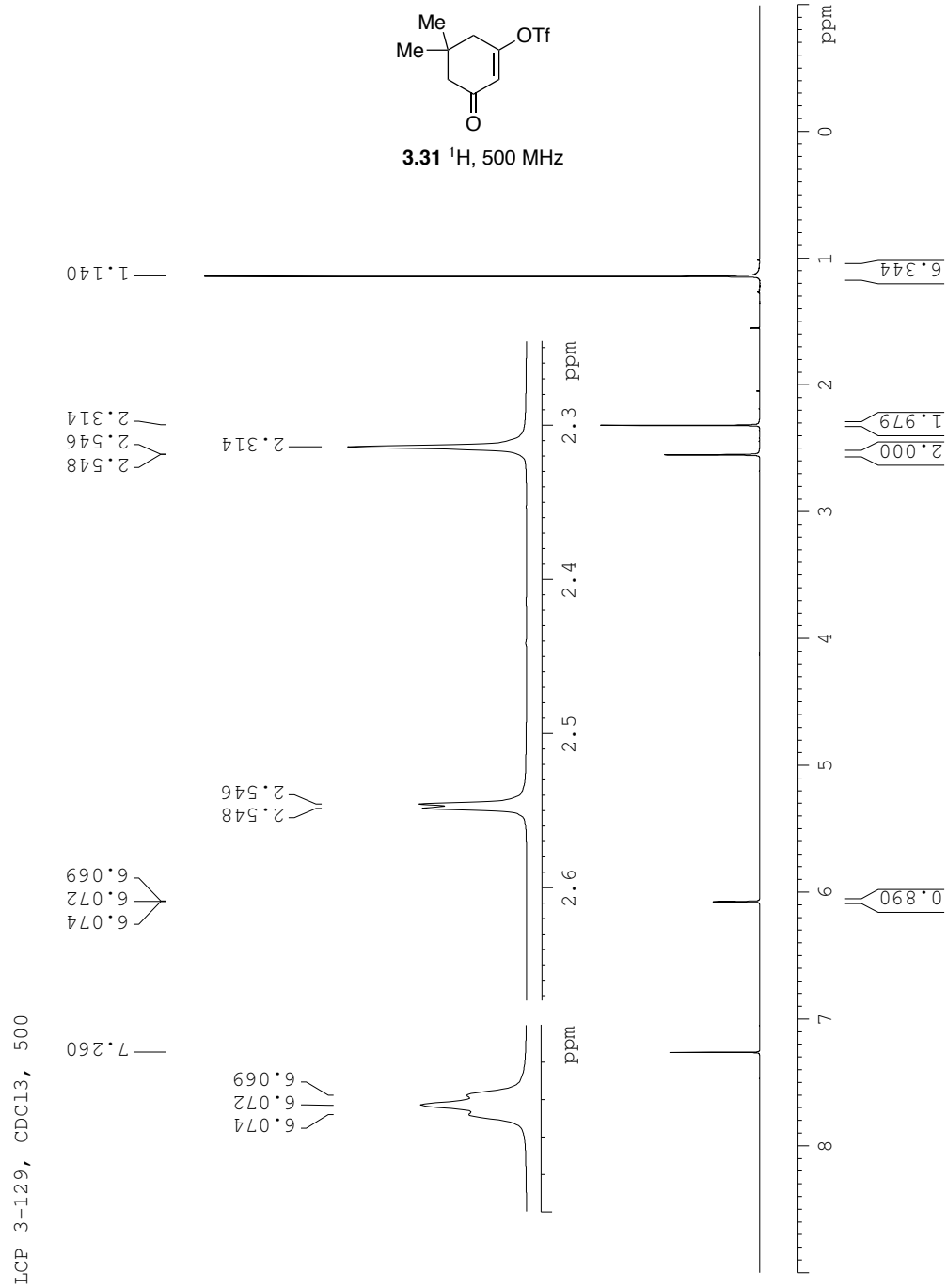
Me
Me
OTf
O
3.31 1H, 500 MHz
LCP 3-129, CDC13, 500
7.260
6.074
6.072
6.069
2.548
2.546
2.314
1.140
6.344
1.979
2.000
0.890
ppm

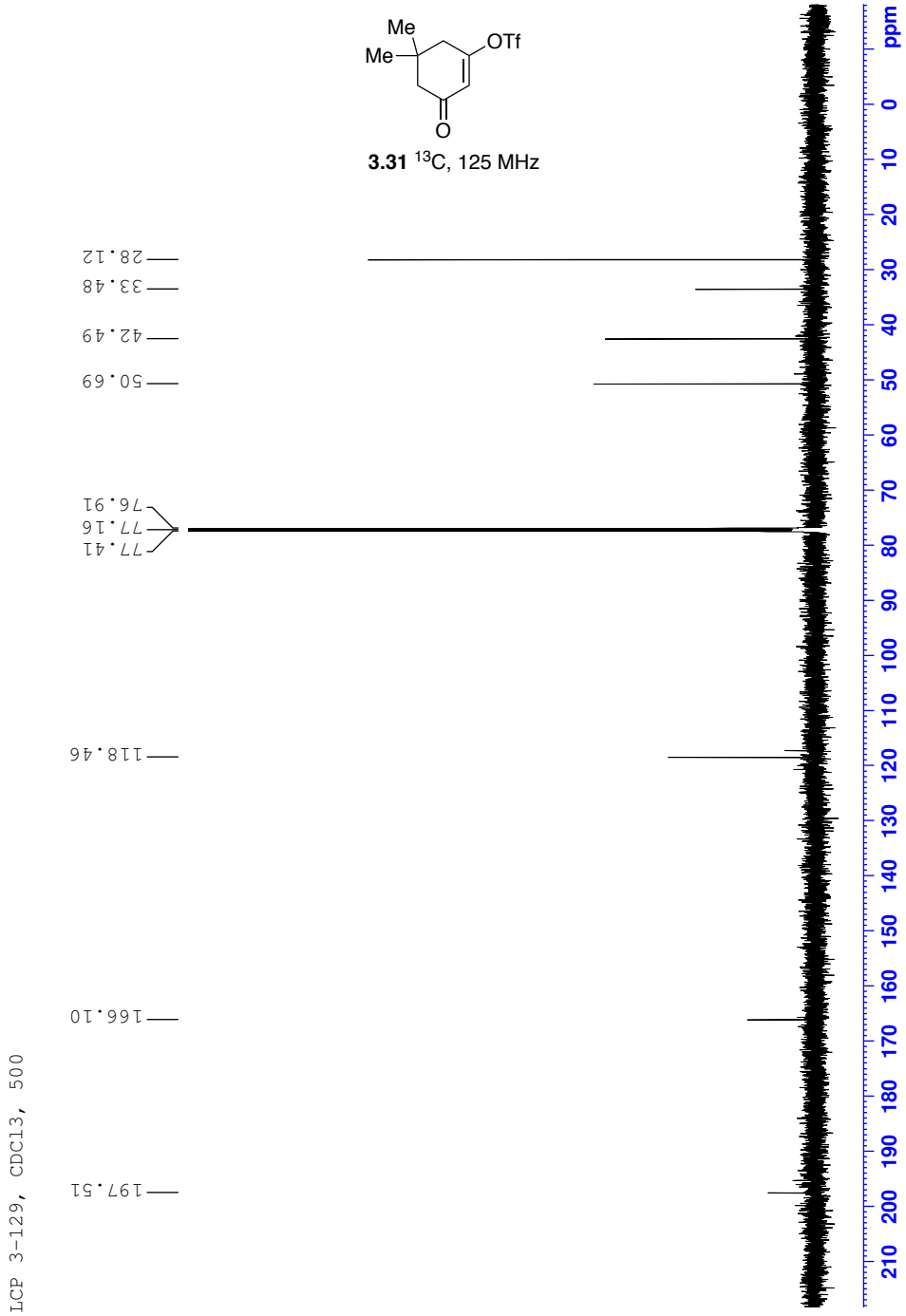
Me
Me
OTf
O
3.31 13C, 125 MHz
28.12
33.48
42.49
50.69
76.91
77.16
77.41
118.46
166.10
197.51
LCP 3-129, CDC13, 500
ppm
0
10
20
30
40
50
60
70
80
90
100
110
120
130
140
150
160
170
180
190
200
210

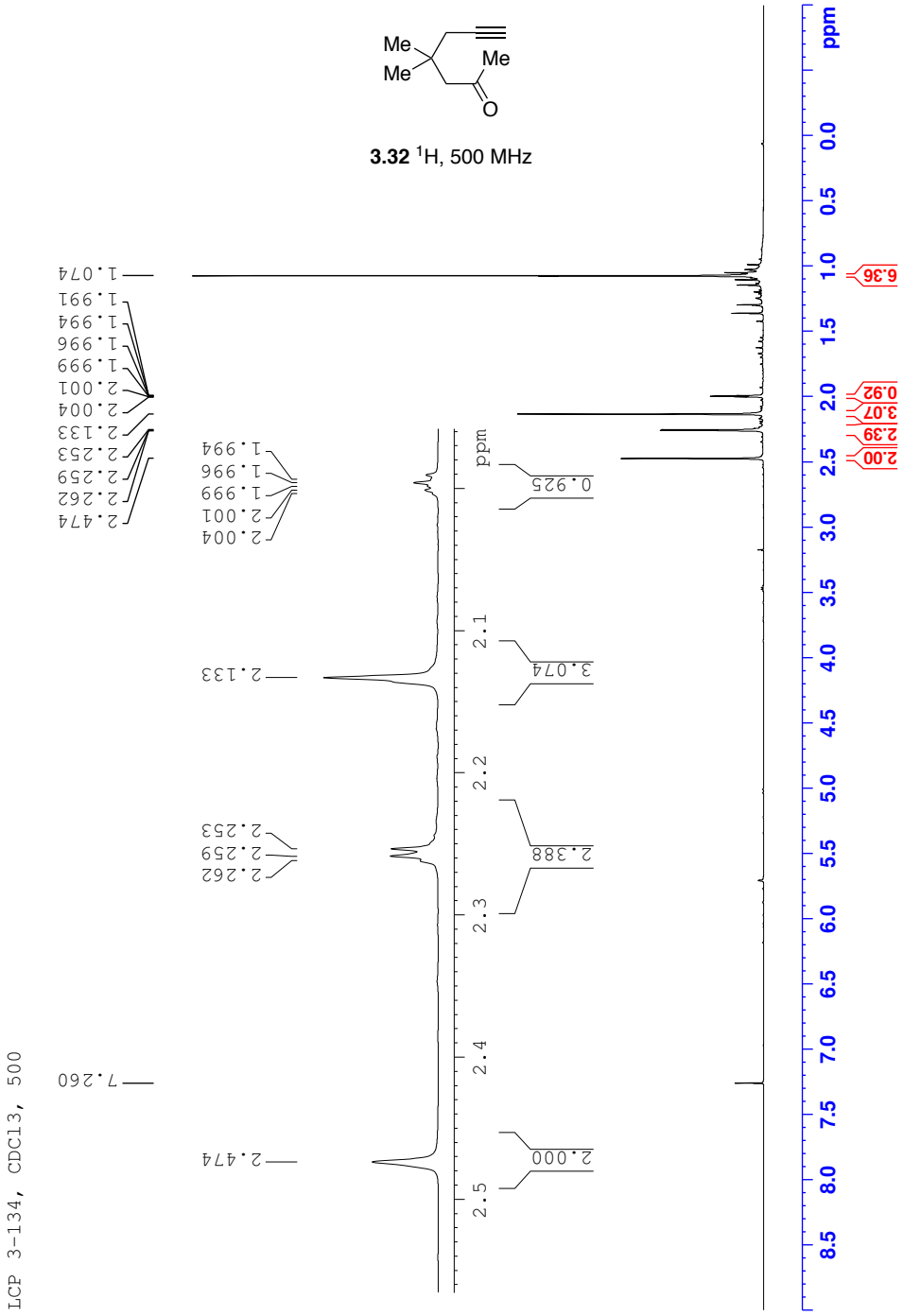
Me
Me
Me
O
3.32 1H, 500 MHz
LCP 3-134, CDC13, 500
7.260
2.474
2.133
2.253
2.259
2.262
1.074
1.991
1.994
1.996
1.999
2.001
2.004
2.133
2.253
2.259
2.262
2.474
1.994
1.996
1.999
2.001
2.004
0.925
3.074
2.388
2.000
ppm
6.36
0.92
3.07
2.39
2.00

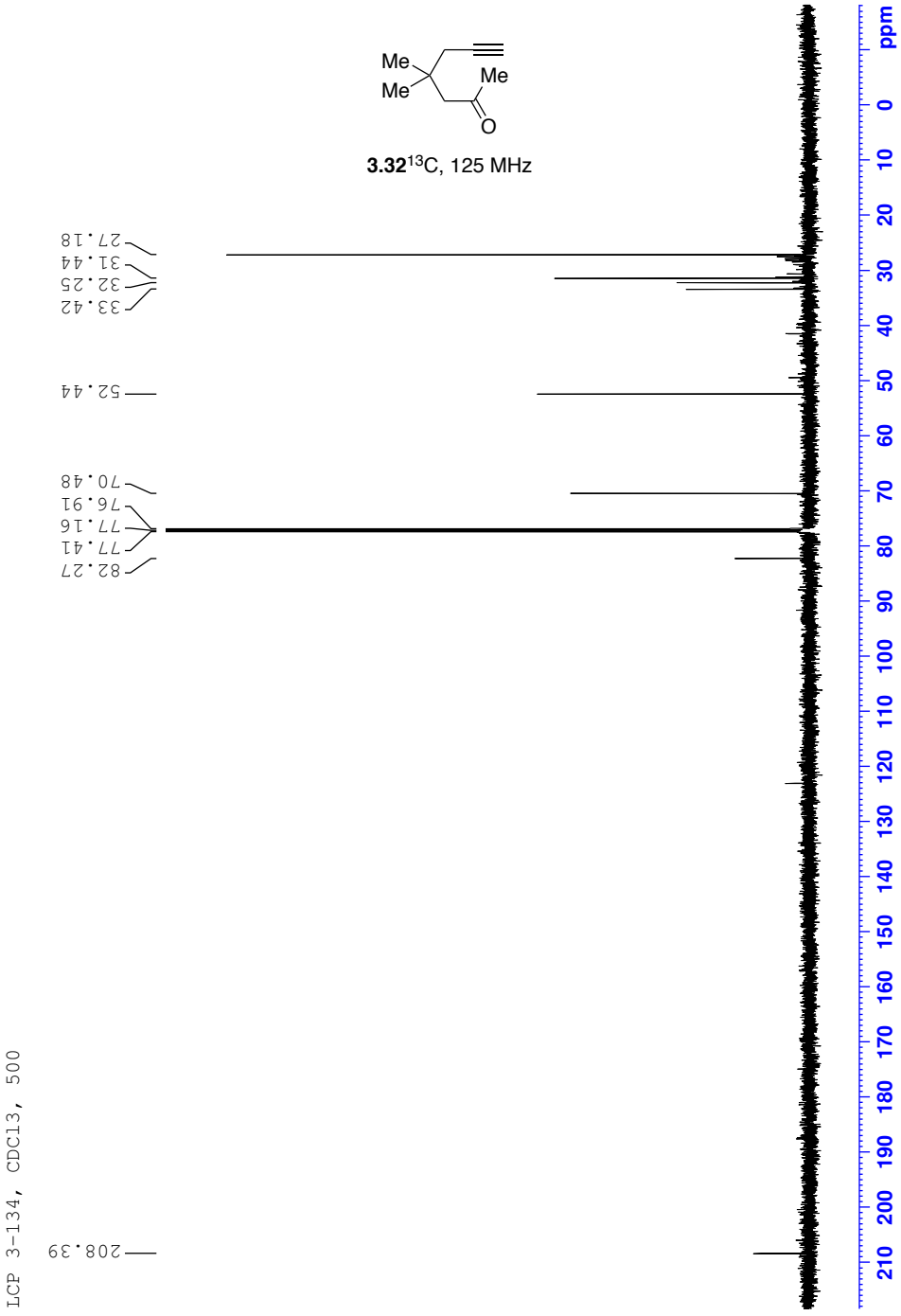
Me
Me
Me
O
3.32 13C, 125 MHz
LCP 3-134, CDC13, 500
208.39
82.27
77.41
77.16
76.91
70.48
52.44
33.42
32.25
31.44
27.18
ppm
0
10
20
30
40
50
60
70
80
90
100
110
120
130
140
150
160
170
180
190
200
210

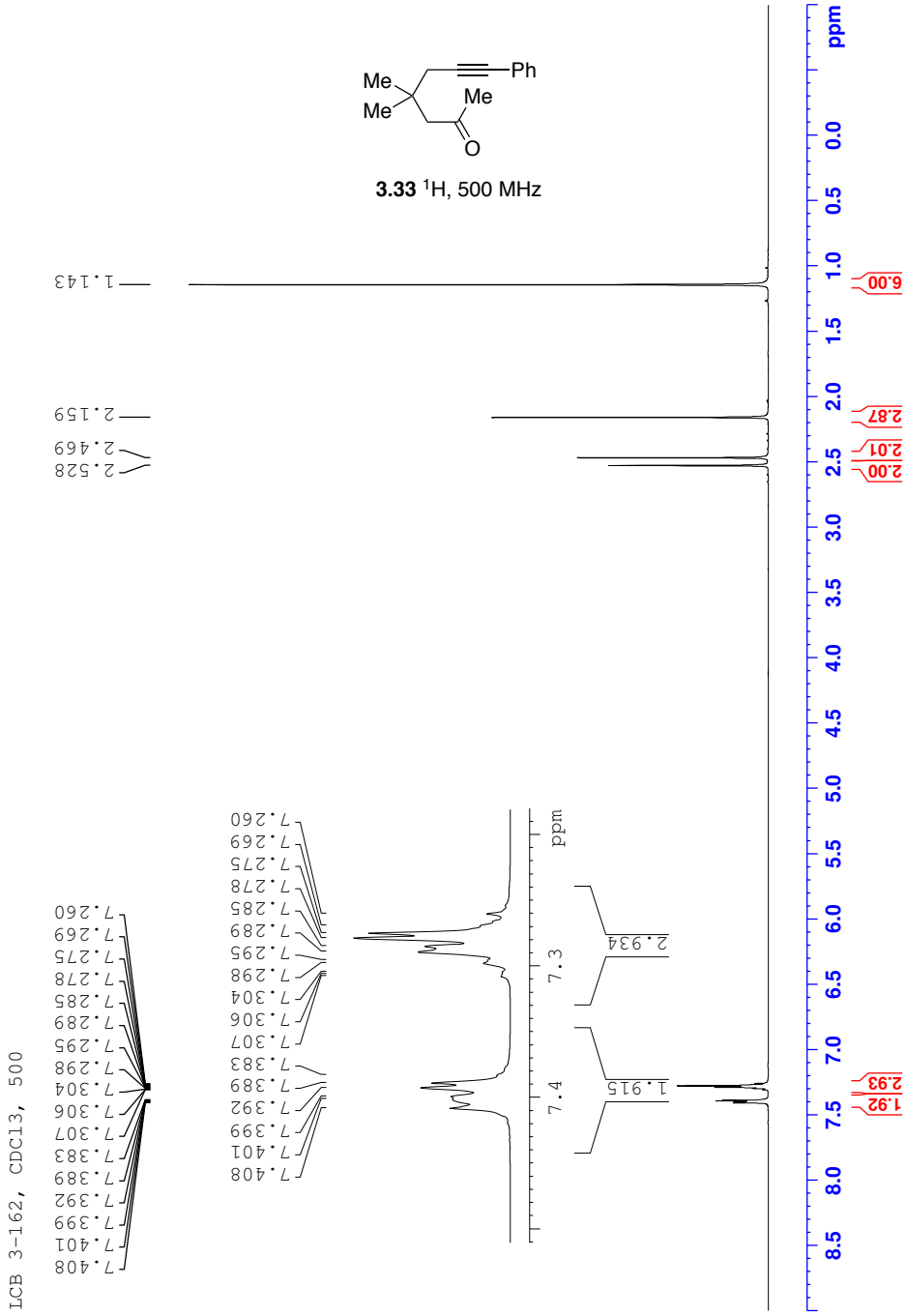
Me
Me
Me
Ph
O
3.33 1H, 500 MHz
1.143
2.159
2.469
2.528
6.00
2.87
2.01
2.00
2.93
1.92
ppm
0.0
0.5
1.0
1.5
2.0
2.5
3.0
3.5
4.0
4.5
5.0
5.5
6.0
6.5
7.0
7.5
8.0
8.5
7.3
7.4
1.915
2.934
LCB 3-162, CDCl3, 500
7.260
7.269
7.275
7.278
7.285
7.289
7.295
7.298
7.304
7.306
7.307
7.383
7.389
7.392
7.399
7.401
7.408

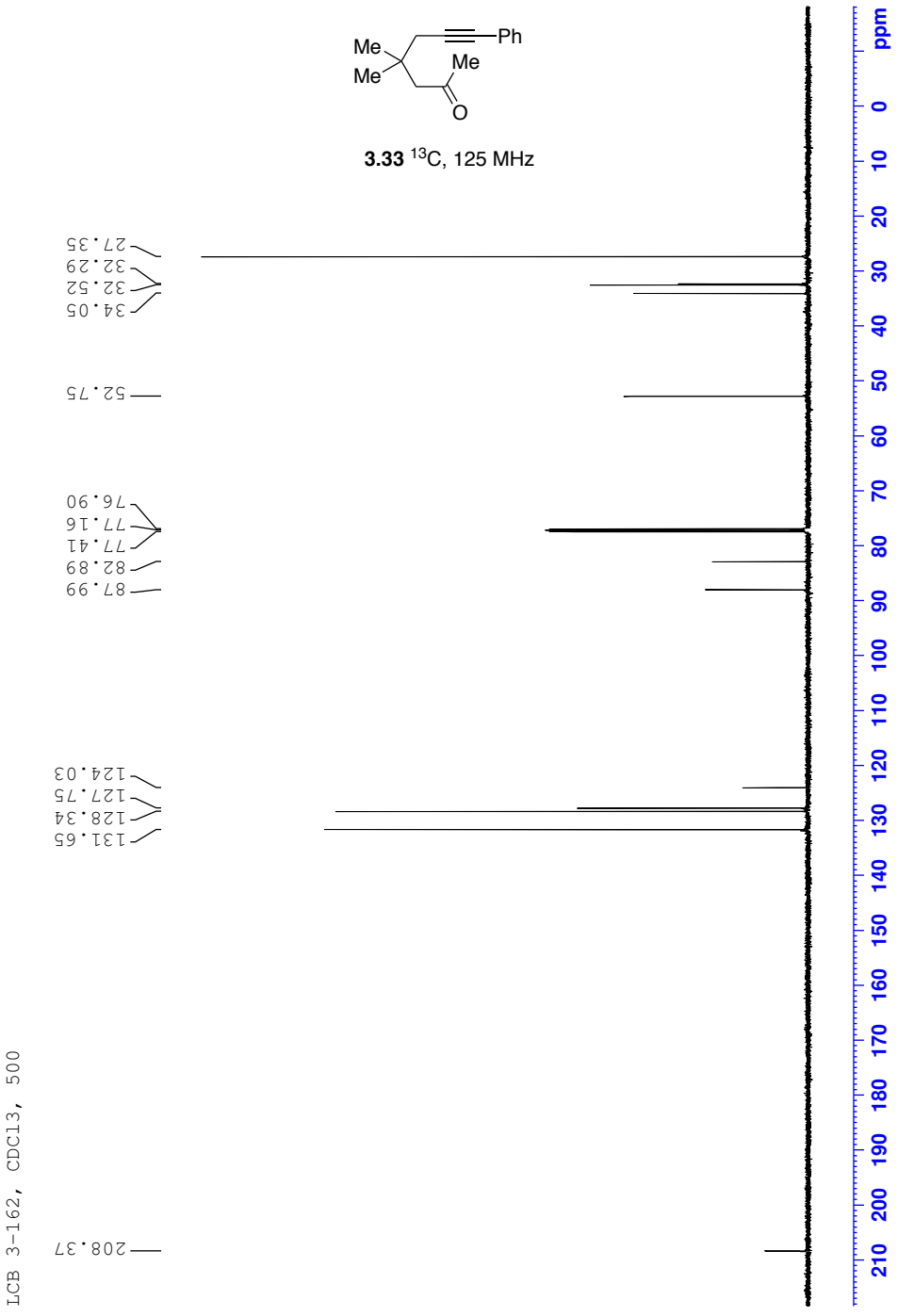
Me
Me
Me
Ph
O
3.33 13C, 125 MHz
27.35
32.29
32.52
34.05
52.75
76.90
77.16
77.41
82.89
87.99
124.03
127.75
128.34
131.65
208.37
ppm
0
10
20
30
40
50
60
70
80
90
100
110
120
130
140
150
160
170
180
190
200
210
LCB 3-162, CDC13, 500

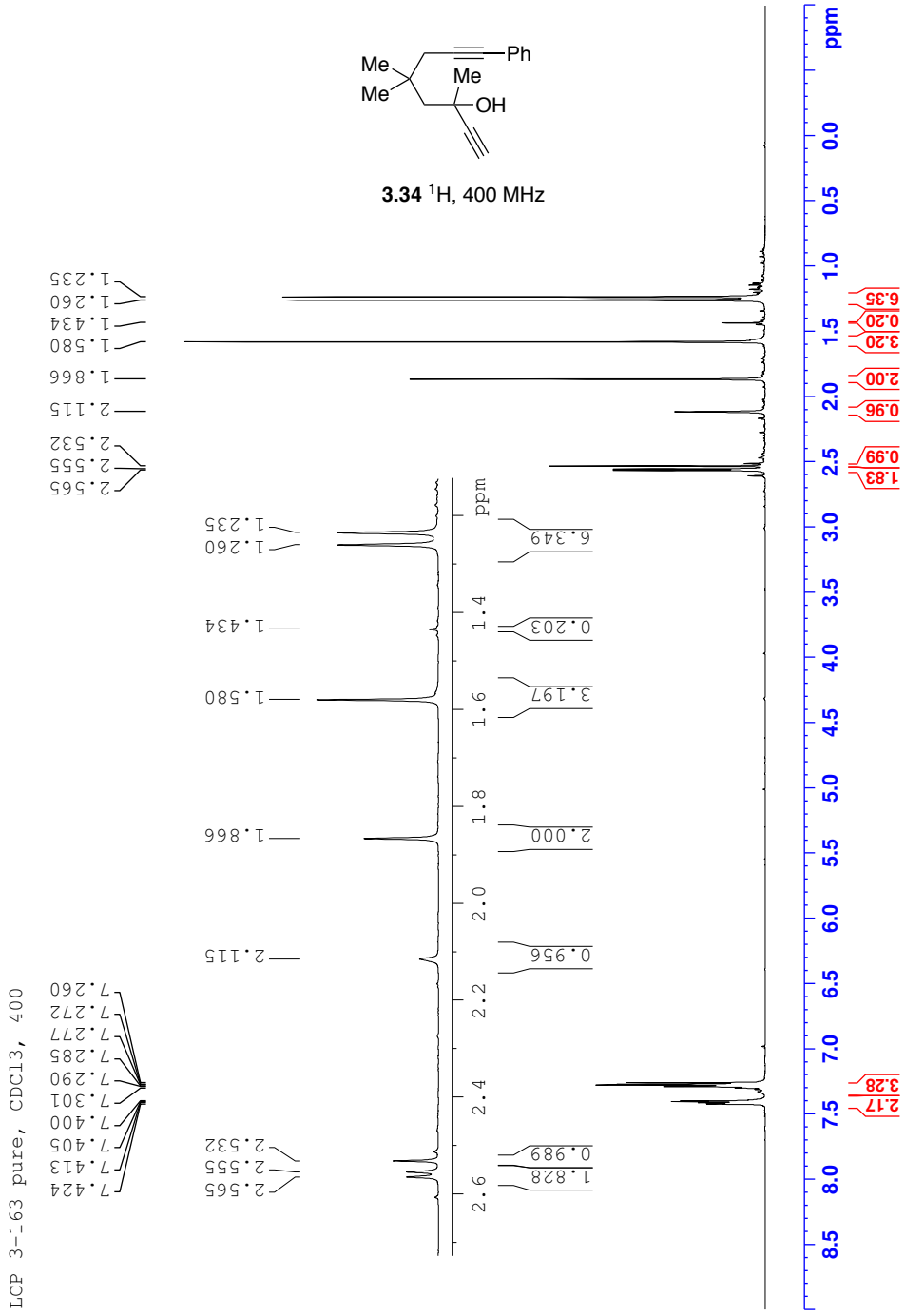
Me
Me
Me
OH
Ph
3.34 1H, 400 MHz
LCP 3-163 pure, CDCl3, 400
7.424
7.413
7.405
7.400
7.301
7.290
7.285
7.277
7.272
7.260
2.565
2.555
2.532
2.115
1.866
1.580
1.434
1.260
1.235
6.349
0.203
3.197
2.000
0.956
1.828
0.989
6.35
0.20
3.20
2.00
0.96
1.83
0.99
3.28
2.17
ppm

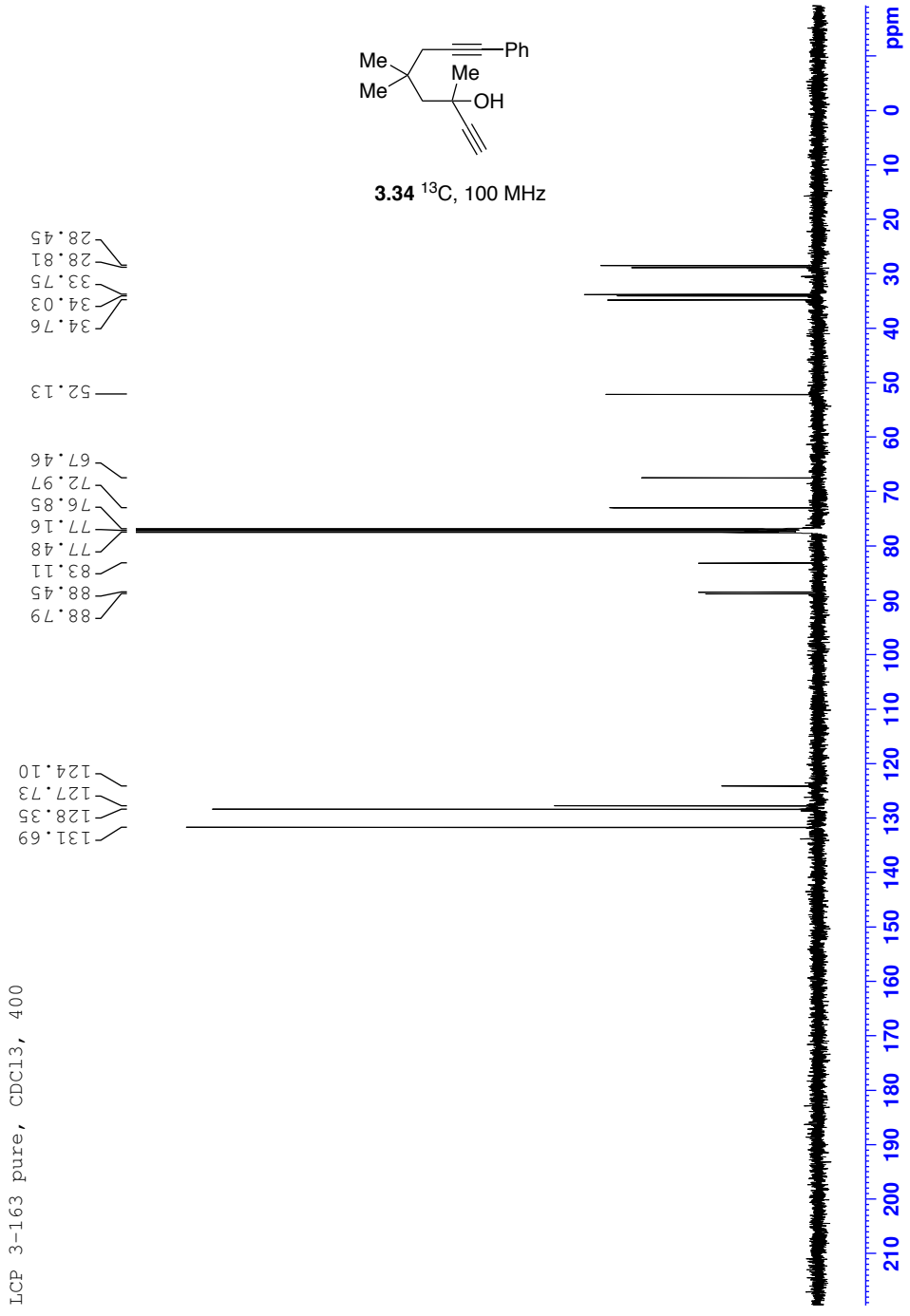
Me
Me
Me
OH
Ph
3.34 13C, 100 MHz
28.45
28.81
33.75
34.03
34.76
52.13
67.46
72.97
76.85
77.16
77.48
83.11
88.45
88.79
124.10
127.73
128.35
131.69
LCP 3-163 pure, CDCl3, 400
ppm
0
10
20
30
40
50
60
70
80
90
100
110
120
130
140
150
160
170
180
190
200
210

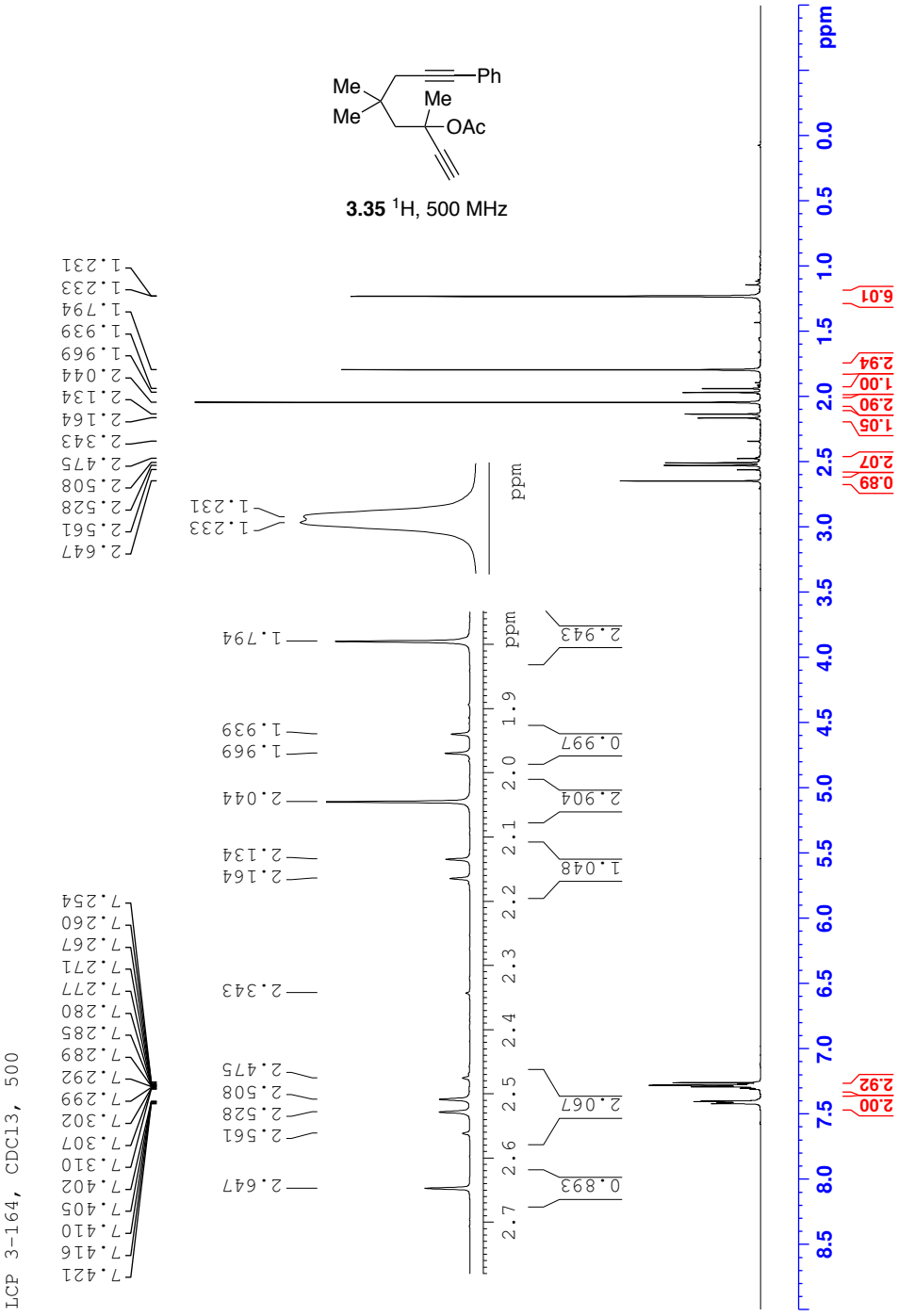
Me
Me
Me
Ph
OAc
3.35 1H, 500 MHz
LCP 3-164, CDCl3, 500
ppm

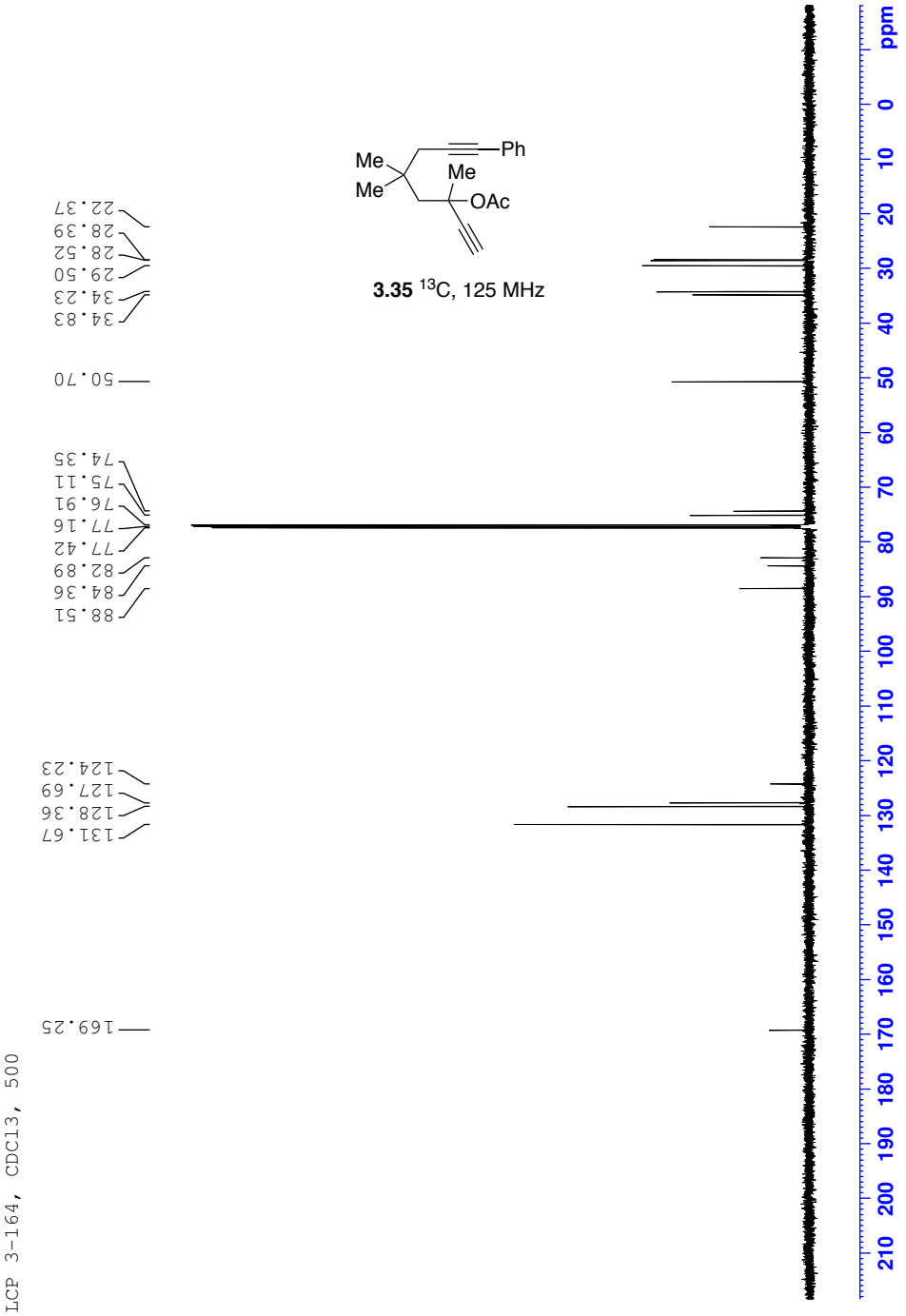
Me
Me
Me
Ph
OAc
3.35 13C, 125 MHz
LCP 3-164, CDC13, 500
22.37
28.39
28.52
29.50
34.23
34.83
50.70
74.35
75.11
76.91
77.16
77.42
82.89
84.36
88.51
124.23
127.69
128.36
131.67
169.25
ppm
0
10
20
30
40
50
60
70
80
90
100
110
120
130
140
150
160
170
180
190
200
210

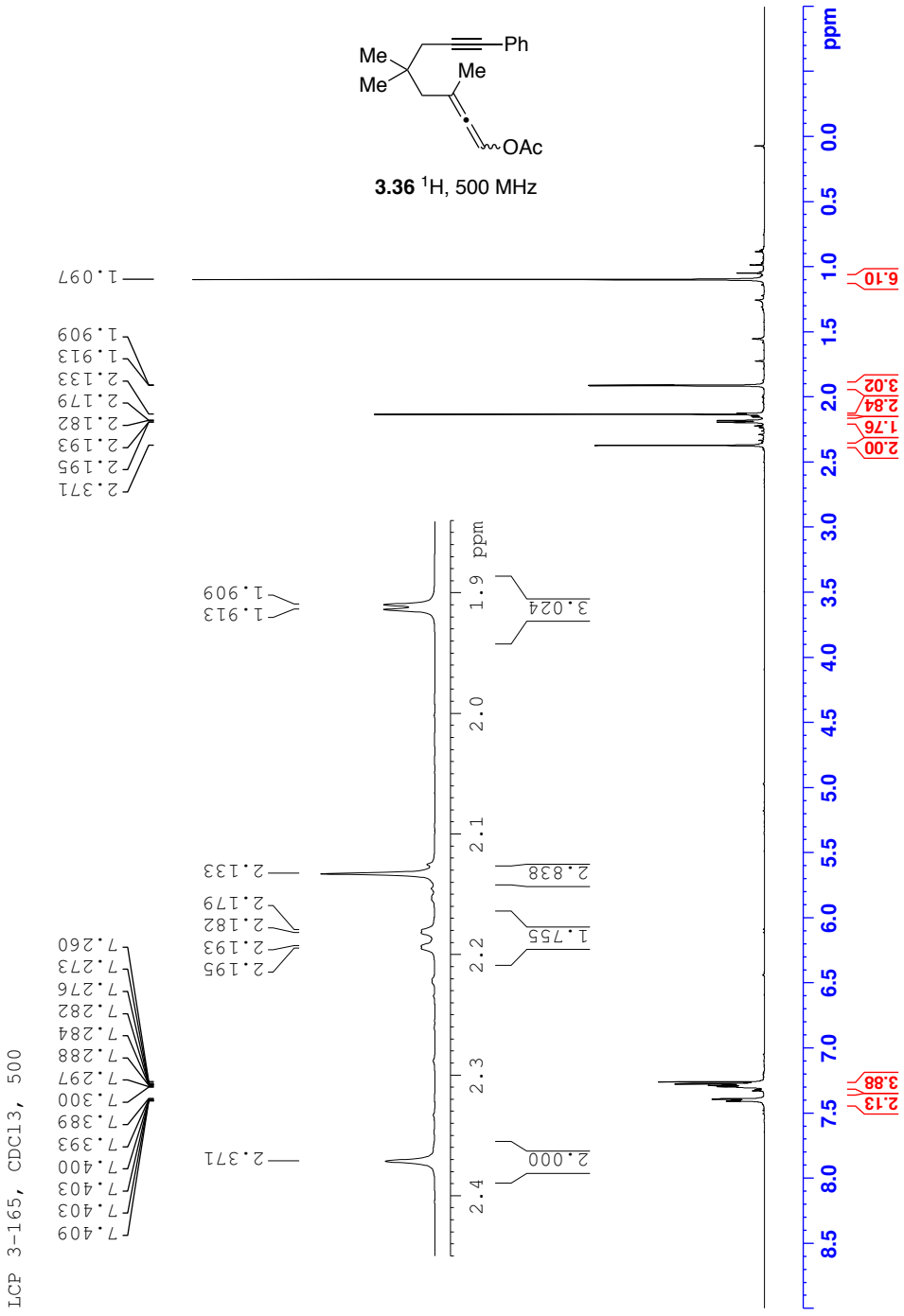
Me
Me
Me
Ph
OAc
3.36 1H, 500 MHz
LCP 3-165, CDCl3, 500
ppm

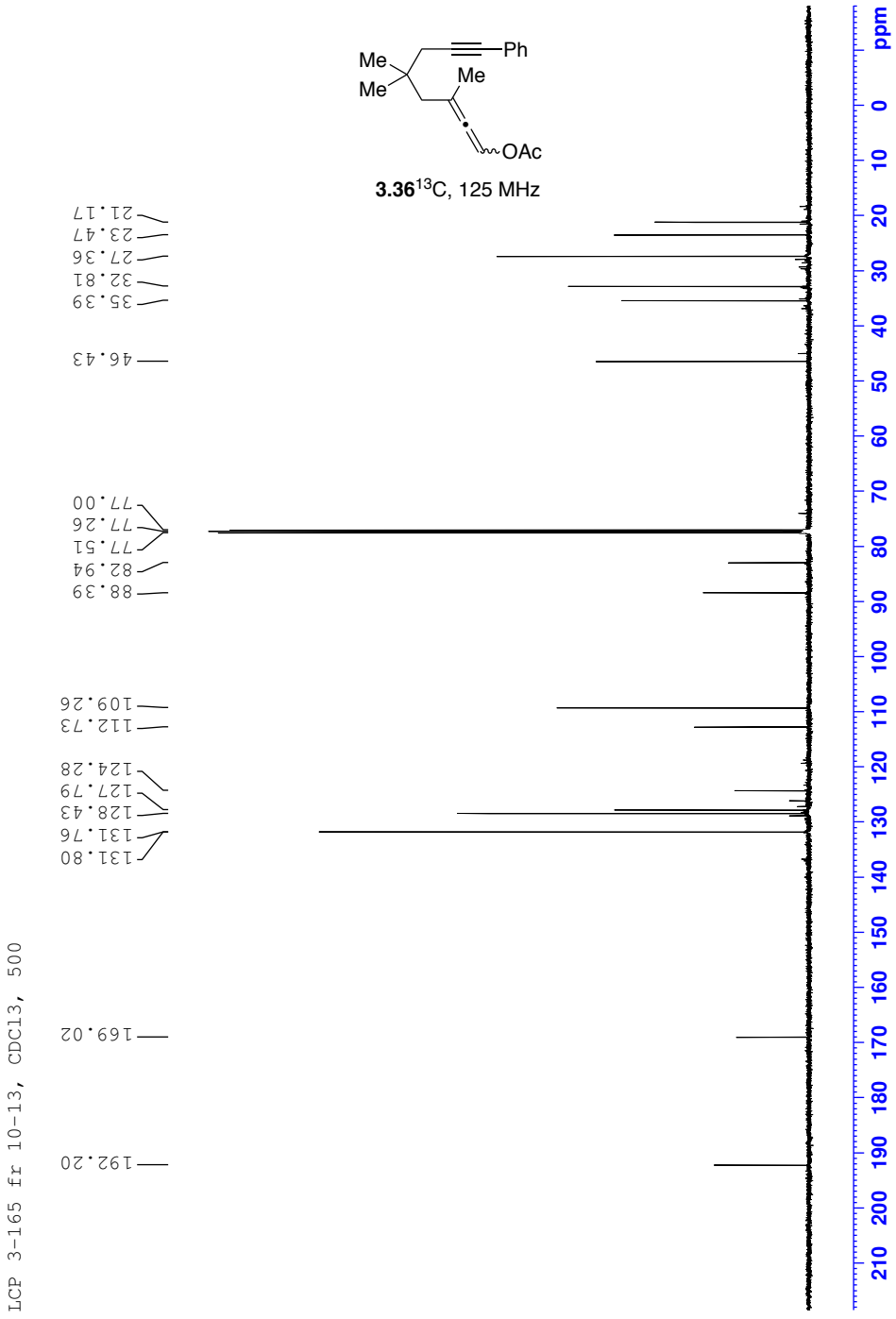
Me
Me
Me
Ph
OAc
3.36 13C, 125 MHz
LCP 3-165 fr 10-13, CDCl3, 500
21.17
23.47
27.36
32.81
35.39
46.43
77.00
77.26
77.51
82.94
88.39
109.26
112.73
124.28
127.79
128.43
131.76
131.80
169.02
192.20
ppm
0
10
20
30
40
50
60
70
80
90
100
110
120
130
140
150
160
170
180
190
200
210

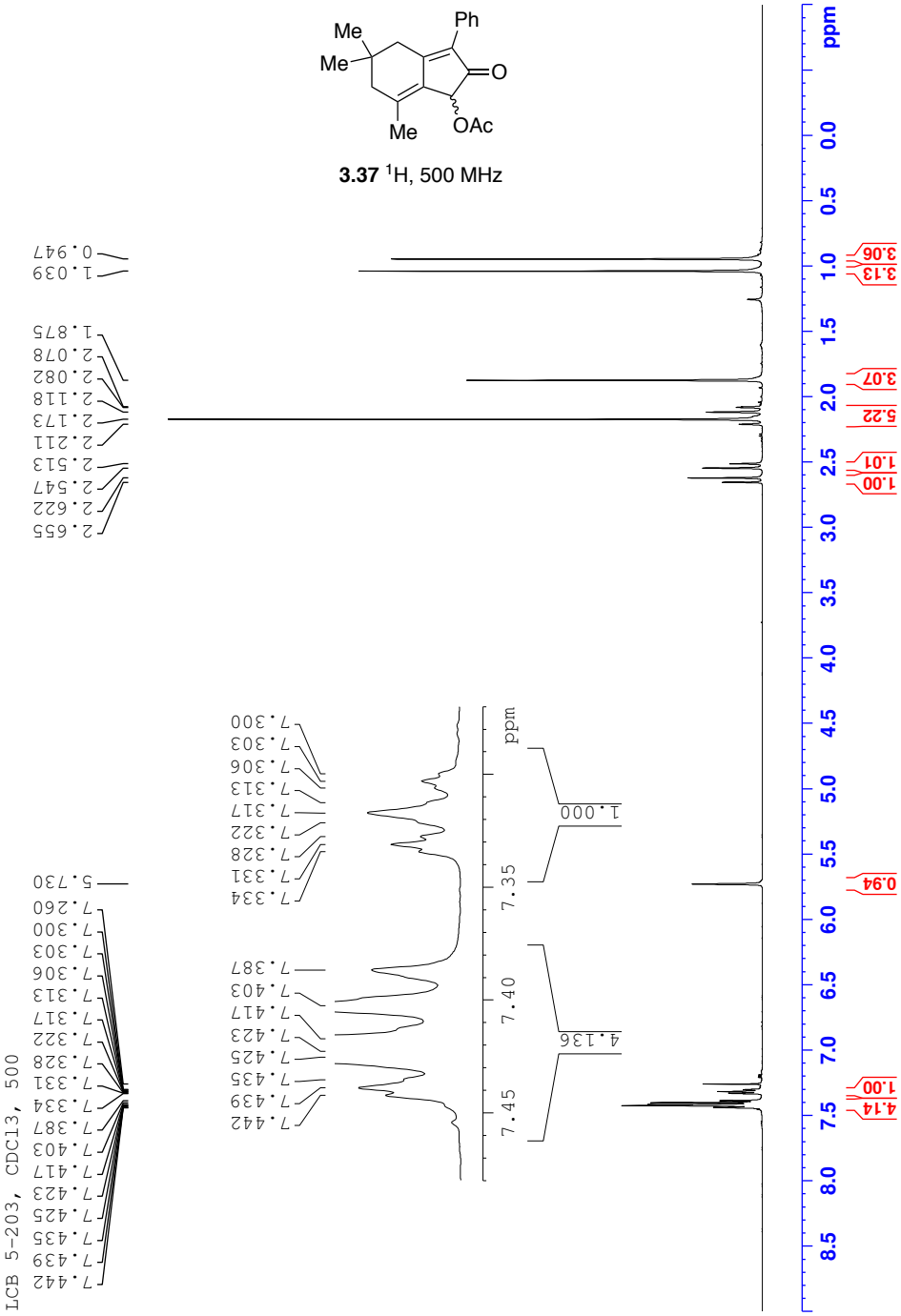
Me
Me
Me
Ph
O
OAc
3.37 1H, 500 MHz
LCB 5-203, CDC13, 500
ppm
7.35
7.40
7.45
4.136
1.000
3.06
3.13
3.07
5.22
1.01
1.00
0.94
1.00
4.14

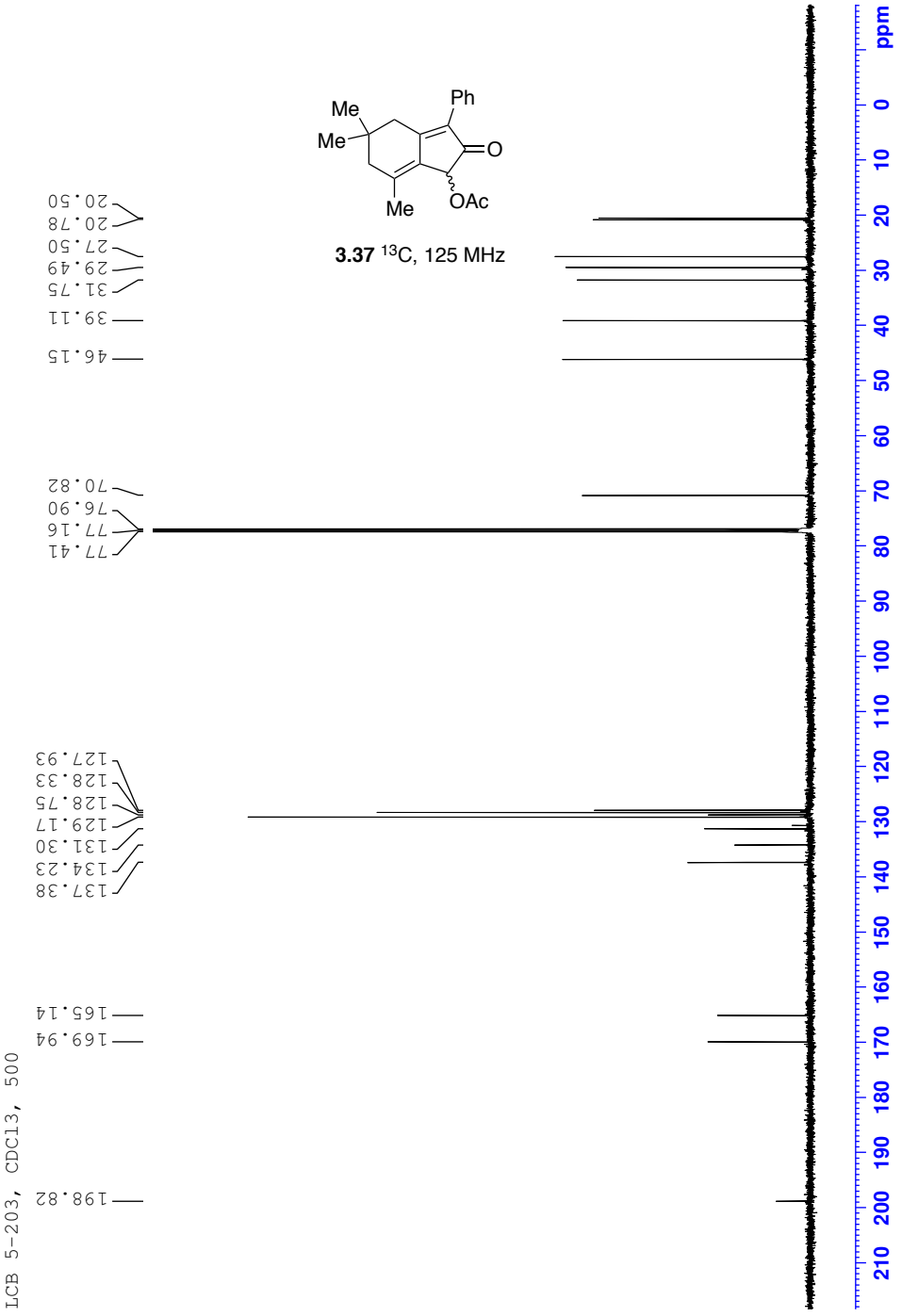
Me
Me
Ph
O
Me
OAc
3.37 13C, 125 MHz
LCB 5-203, CDC13, 500
20.50
20.78
27.50
29.49
31.75
39.11
46.15
70.82
76.90
77.16
77.41
127.93
128.33
128.75
129.17
131.30
134.23
137.38
165.14
169.94
198.82
ppm
0
10
20
30
40
50
60
70
80
90
100
110
120
130
140
150
160
170
180
190
200
210

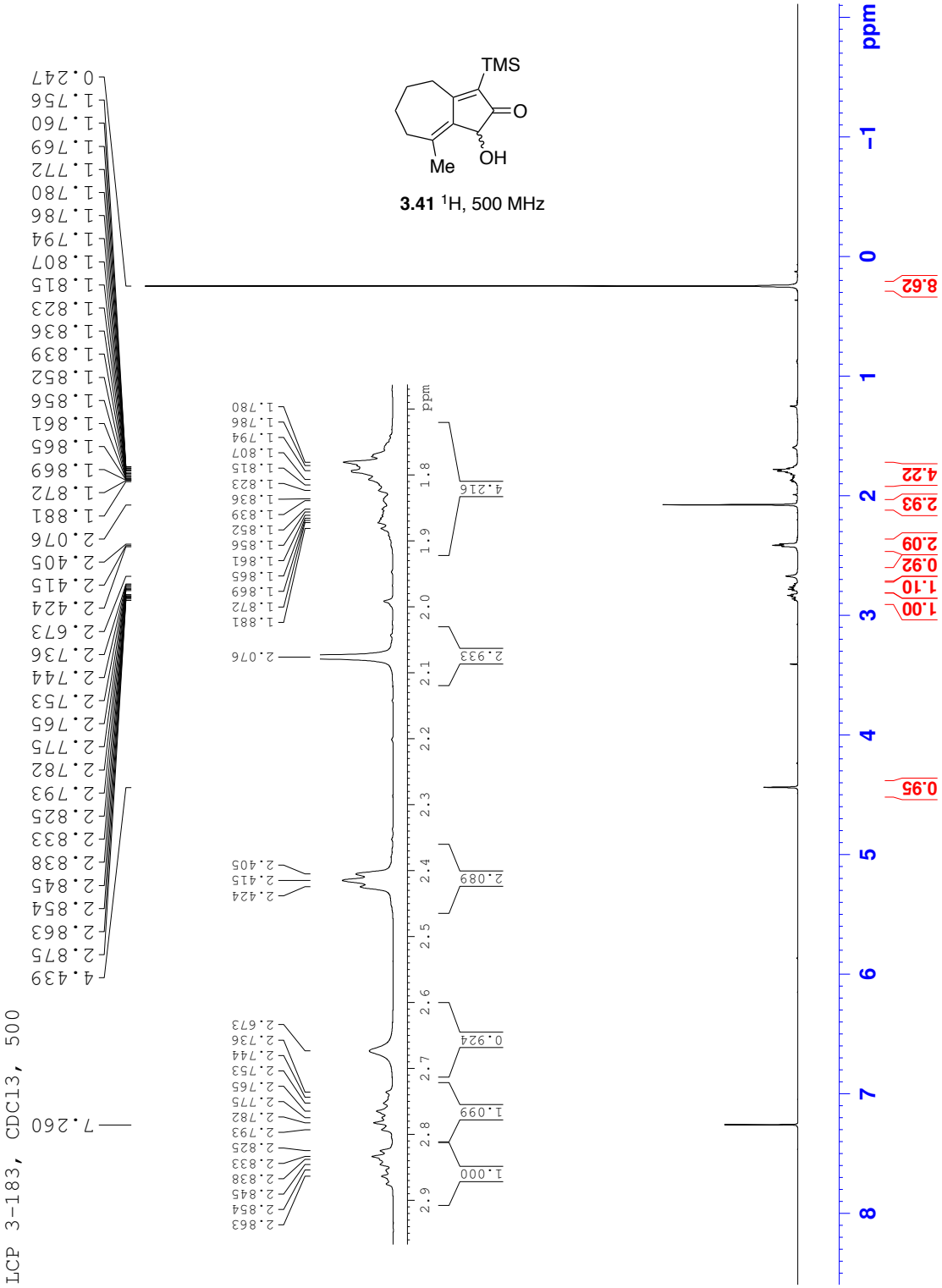
TMS
O
OH
Me
3.41 1H, 500 MHz
LCP 3-183, CDCl3, 500
ppm

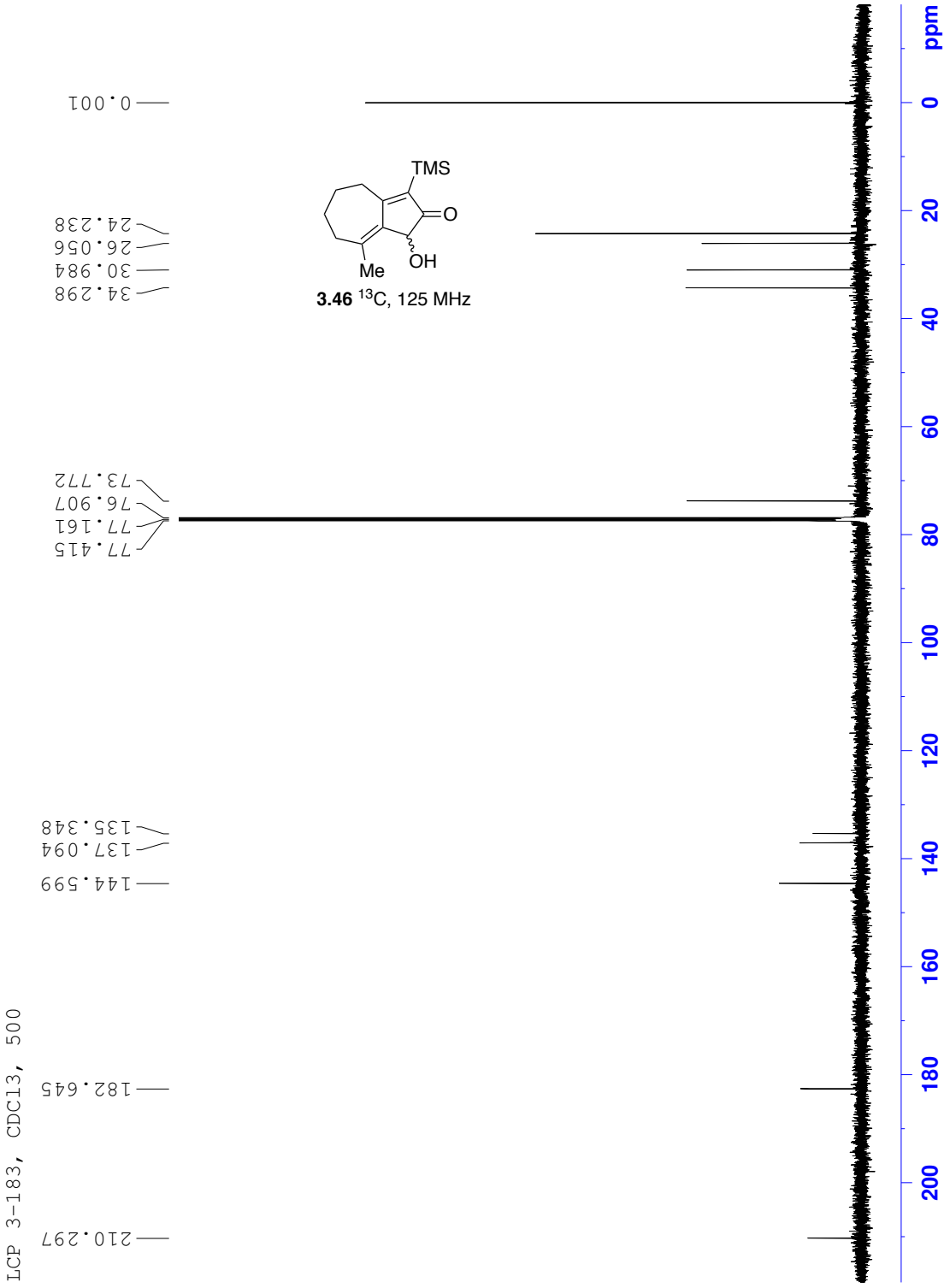
LCP 3-183, CDC13, 500
0.001
24.238
26.056
30.984
34.298
73.772
76.907
77.161
77.415
135.348
137.094
144.599
182.645
210.297
TMS
O
OH
Me
3.46 13C, 125 MHz
ppm
0
20
40
60
80
100
120
140
160
180
200

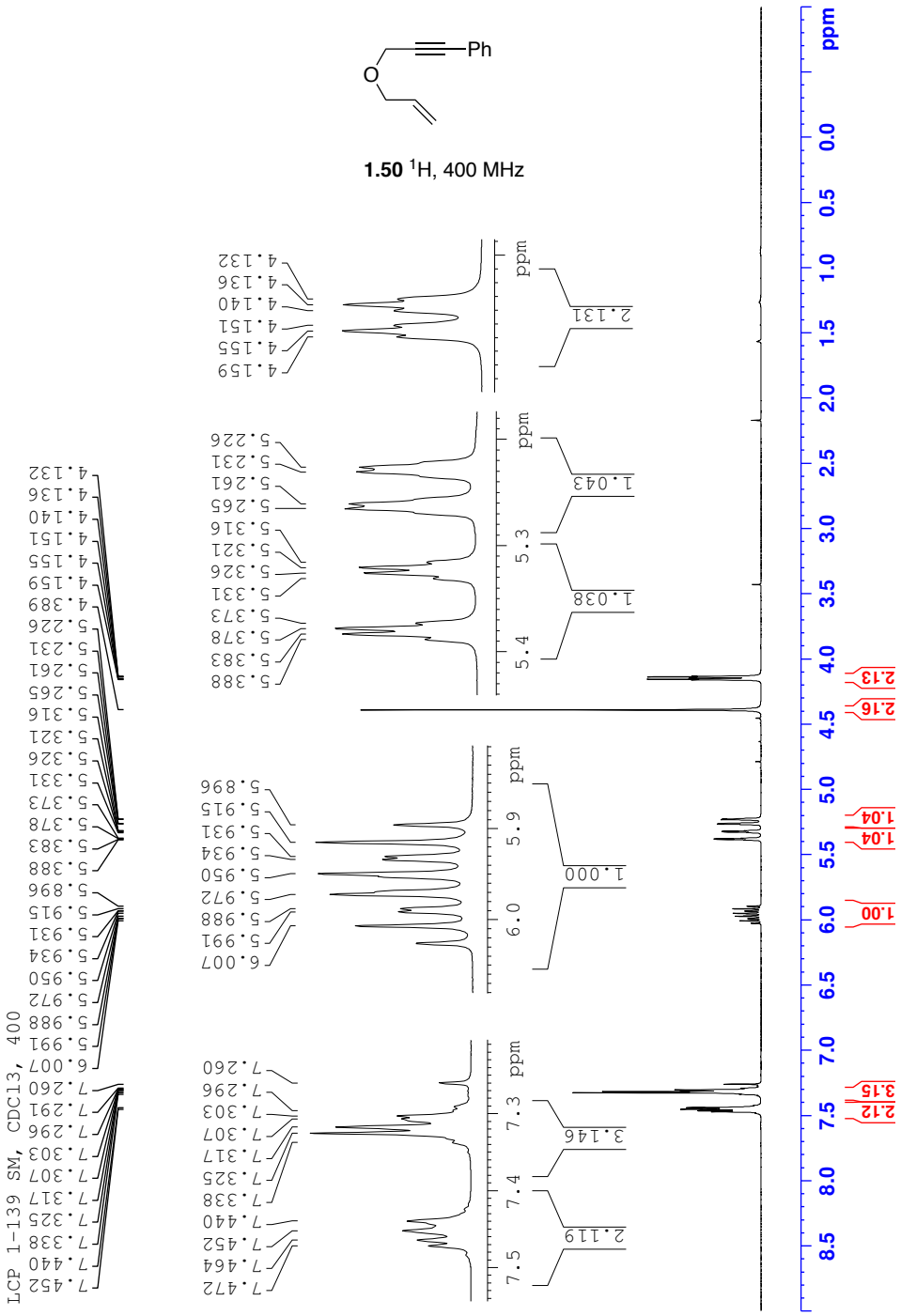
Ph
O
1.50 1H, 400 MHz
LCP 1-139 SM, CDC13, 400
7.452
7.440
7.338
7.325
7.317
7.307
7.303
7.296
7.291
7.260
6.007
5.991
5.988
5.972
5.950
5.934
5.931
5.915
5.896
5.388
5.383
5.378
5.373
5.331
5.326
5.321
5.316
5.265
5.261
5.231
5.226
4.389
4.159
4.155
4.151
4.140
4.136
4.132
ppm
2.131
1.043
1.038
1.000
2.119
3.146
2.13
2.16
1.04
1.04
1.00
2.12
3.15
ppm

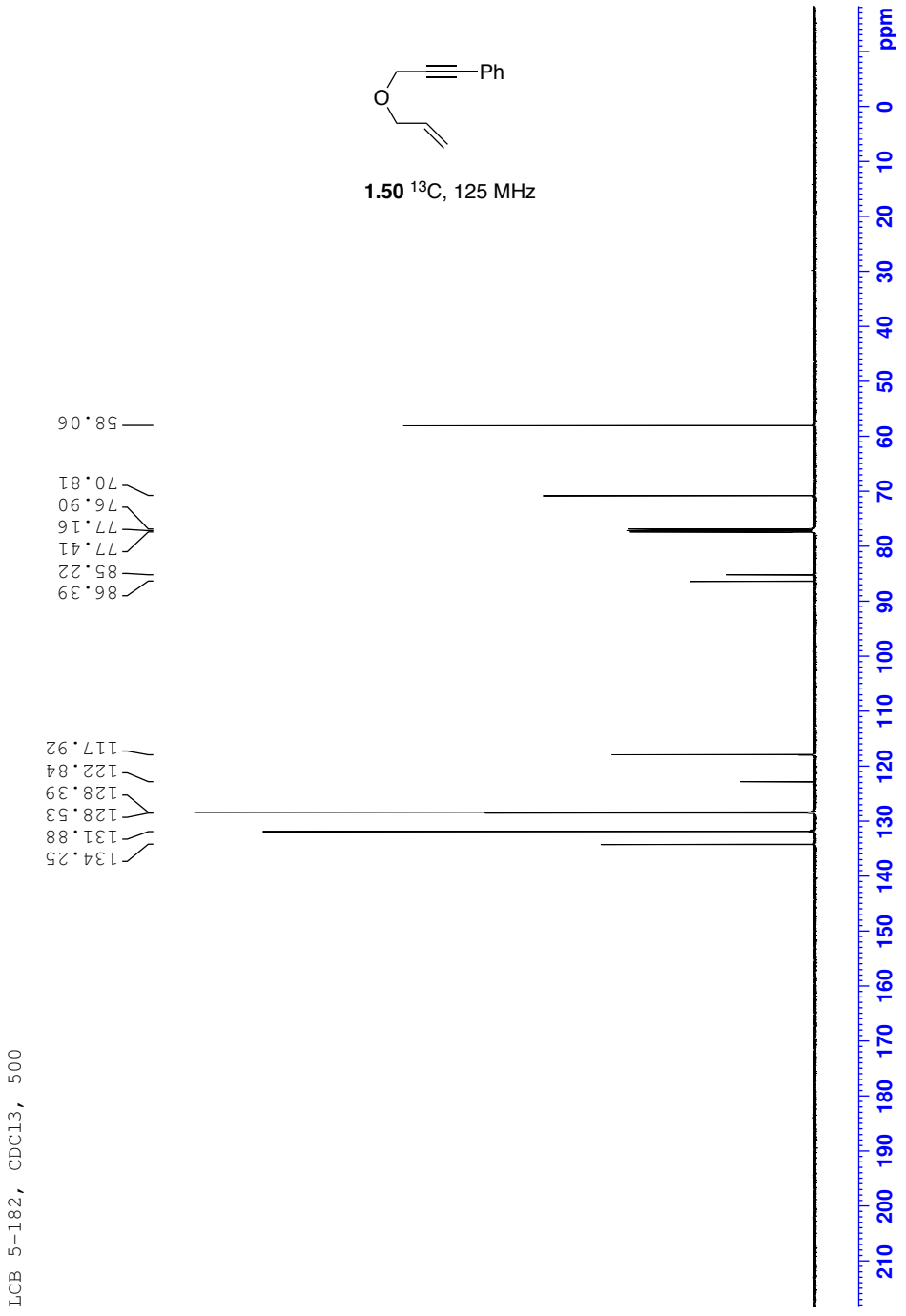
Ph
O
1.50 13C, 125 MHz
LCB 5-182, CDCl3, 500
58.06
70.81
76.90
77.16
77.41
85.22
86.39
117.92
122.84
128.39
128.53
131.88
134.25
ppm
0
10
20
30
40
50
60
70
80
90
100
110
120
130
140
150
160
170
180
190
200
210

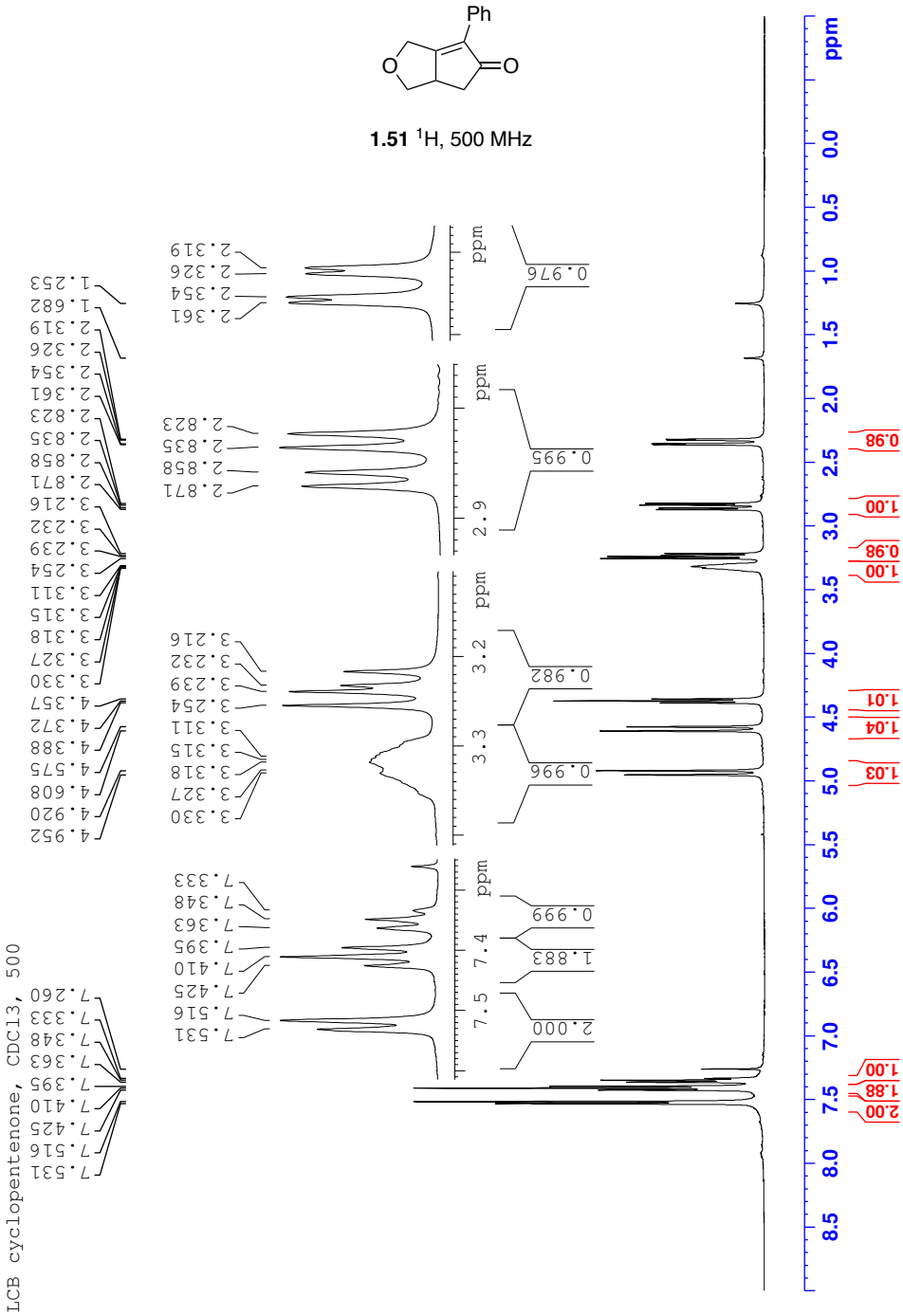
Ph
O
O
1.51 1H, 500 MHz
LCB cyclopentenone, CDCl3, 500
ppm

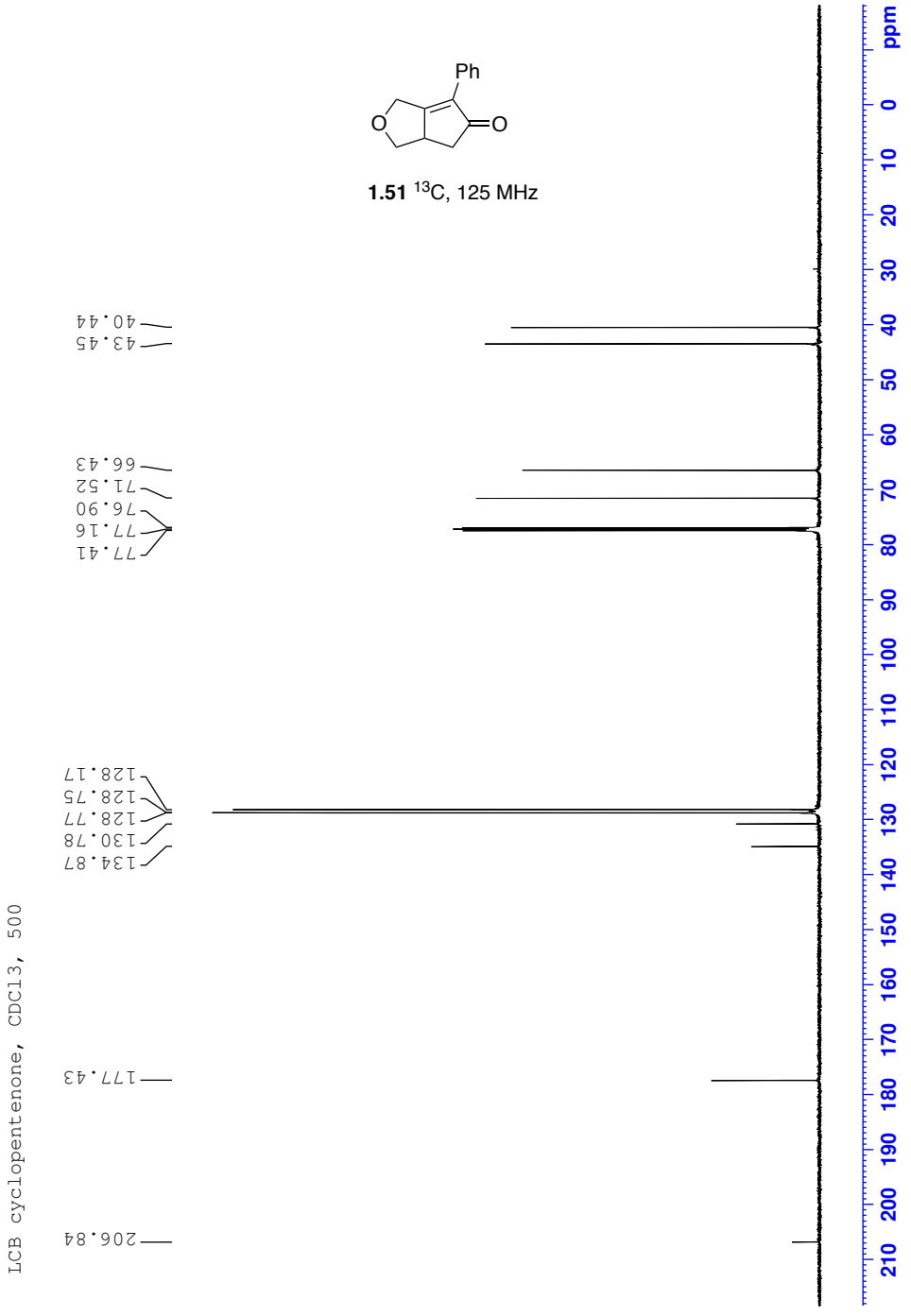

1.51 ^{13}C, 125 MHz

BIBLIOGRAPHY

1. Aitken, D. J.; Eijsberg, H.; Frongia, A.; Ollivier, J.; Piras, P. P., Recent Progress in the Synthetic Assembly of 2-Cyclopentenones. *Synthesis* **2014**, *46*, 1

2. Ellison, R. A., Methods for the Synthesis of 3-Oxocyclopentenes. *Synthesis* **1973**, *7*, 397

3. Gerdil, R.; Liu, H. Y.; Bernardinelli, G., Organic Reactions in the Solid State: Reactions of Enclathrated 3,4-epoxyclopentanone (=6-oxobicyclo[3.1.0]hexan-3-one) in Tri-o-thymotide and Absolute Configuration of 4-hydroxy- and 4-chlorocyclopent-2-en-1-one. *Helv. Chim. Acta* **1999**, 82, 418

4. Simeonov, S. P.; Nunes, J. P. M.; Guerra, K.; Kurteva, V. B.; Afonso, C. A. M., Synthesis of Chiral Cyclopentenones. *Chem. Rev*. **2016**, *116*, 5744

5. Gibson, S. E.; Lewis, S. E.; Mainolfi, N., Transition Metal-mediated Routes to Cyclopentenones. *J. Organomet. Chem.* **2004**, *689*, 3873

6. Shibatomi, K.; Kobayashi, F.; Narayama, A.; Fujisawa, I.; Iwasa, S., A Diels-Alder Approach to the Enantioselective Construction of Fluoromethylated Stereogenic Carbon Centers. *Chem. Commun.* **2012**, *48*, 413

7. Sezer, S.; Gumrukcu, Y.; Sahin, E.; Tanyeli, C., Stereoselective Synthesis of Spirocyclic Cyclopentapyrans by the Pauson-Khand Reaction on Camphor Tethered Enynes. *Tetrahedron: Asymmetry* **2008**, *19*, 2705

8. Jamison, T. F.; Shambayati, S.; Crowe, W. E.; Schreiber, S. L., Tandem Use of Cobalt-mediated Reactions to Synthesize (+)-epoxydictymene, A Diterpene Containing a Trans-fused 5-5 Ring System. *J. Am. Chem. Soc*. **1997**, *119*, 4353

9. Miyagawa, T.; Nagai, K.; Yamada, A.; Sugihara, Y.; Fukuda, T.; Fukuda, T.; Uchida, R.; Tomoda, H.; Omura, S.; Nagamitsu, T., Total Synthesis of Citridone A. *Org. Lett.* **2011**, *13*, 1158

10. Metz, P.; Bertels, S.; Frohlich, R., An Enantioselective Approach to 3-Alpha-Hydroxy-15-Rippertene - Construction of the Tetracyclic Ring-System. *J. Am. Chem. Soc.* **1993**, *115*, 12595

11. Srikrishna, A.; Dethe, D. H., Enantiospecific First Total Synthesis of cucumin-H. *Indian J. Chem., Sect. B: Org. Chem. Incl. Med. Chem.* **2011**, *50*, 1092

12. Krautwald, S.; Carreira, E. M., Stereodivergence in Asymmetric Catalysis. *J. Am. Chem. Soc.* **2017**, *139*, 5627

13. Brady, S. F.; Singh, M. P.; Janso, J. E.; Clardy, J., Guanacastepene, a Fungal-Derived Diterpene Antibiotic with a New Carbon Skeleton. *J. Am. Chem. Soc.* **2000**, *122*, 2116

14. Zhao, Y.-M.; Gu, P.; Tu, Y.-Q.; Fan, C.-A.; Zhang, Q., An Efficient Total Synthesis of (±)-Stemonamine. *Org. Lett.* **2008**, *10*, 1763

15. Iizuka, H.; Irie, H.; Masaki, N.; Osaki, K.; Uyeo, S., X-Ray Crystallographic Determination of the Structure of Stemonamine, A New Alkaloid from Stemona Japonica miq.: Isolation of Isostemonamine. *J. Chem. Soc., Chem. Commun.* **1973**, 125

16. Hao, H.-D.; Trauner, D., Furans as Versatile Synthons: Total Syntheses of Caribenol A and Caribenol B. *J. Am. Chem. Soc.* **2017**, *139*, 4117

17. Wei, X.; Rodríguez, I. I.; Rodríguez, A. D.; Barnes, C. L., Caribenols A and B, Sea Whip Derived Norditerpenes with Novel Tricarbocyclic Skeletons. *J. Org. Chem.* **2007**, *72*, 7386

18. Brown, C. D., Resiniferatoxin: The Evolution of the "Molecular Scalpel" for Chronic Pain Relief. *Pharmaceuticals* **2016**, *9*, 47

19. Hergenhahn, M.; Adolf, W.; Hecker, E., Resiniferatoxin and Other Esters of Novel Polyfunctional Diterpenes from Euphorbia Resinifera and Unispina. *Tetrahedron Lett.* **1975**, *16*, 1595

20. Wender, P. A.; Jesudason, C. D.; Nakahira, H.; Tamura, N.; Tebbe, A. L.; Ueno, Y., The First Synthesis of a Daphnane Diterpene: The Enantiocontrolled Total Synthesis of (+)-Resiniferatoxin. *J. Am. Chem. Soc.* **1997**, *119*, 12976

21. Pettersen, R. C.; Ferguson, G.; Crombie, L.; Games, M. L.; Pointer, D. J., The structure and Stereochemistry of Phorbol, Diterpene Parent of Co-carcinogens of Croton Oil. *Chem. Commun.* **1967**, 716

22. Wang, H.-B.; Wang, X.-Y.; Liu, L.-P.; Qin, G.-W.; Kang, T.-G., Tigliane Diterpenoids from the Euphorbiaceae and Thymelaeaceae Families. *Chem. Rev.* **2015**, *115*, 2975

23. Kawamura, S.; Chu, H.; Felding, J.; Baran, P. S., Nineteen-step Total Synthesis of (+)-phorbol. *Nature* **2016**, *532*, 90.

24. Rogers, E. F.; Koniuszy, F. R.; Shavel, J.; Folkers, K., Plant Insecticides. I. Ryanodine, A New Alkaloid from Ryania Speciosa Vahl. *J. Am. Chem. Soc.* **1948**, *70*, 3086

25. Xu, C.; Han, A.; Virgil, S. C.; Reisman, S. E., Chemical Synthesis of (+)-Ryanodine and (+)-20-Deoxyspiganthine. *ACS Cent. Sci.* **2017**, *3*, 278

26. Chuang, K. V.; Xu, C.; Reisman, S. E., A 15-step Synthesis of (+)-ryanodol. *Science* **2016**, *353*, 912

27. Ogawa, K.; Koyama, Y.; Ohashi, I.; Sato, I.; Hirama, M., Total Synthesis of a Protected Aglycon of the Kedarcidin Chromophore. *Angew. Chem. Int. Ed.* **2009**, *48*, 1110

28. Ren, F.; Hogan, P. C.; Anderson, A. J.; Myers, A. G., Kedarcidin Chromophore: Synthesis of Its Proposed Structure and Evidence for a Stereochemical Revision. *J. Am. Chem. Soc.* **2007**, *129*, 5381

29. Chu, H.; Dünstl, G.; Felding, J.; Baran, P. S., Divergent Synthesis of Thapsigargin Analogs. *Bioorg. Med. Chem. Lett.* **2018**, *In Press*

30. Christensen, S. B.; Andersen, A.; Poulsen, J.-C. J.; Treiman, M., Derivatives of thapsigargin as probes of its binding site on endoplasmic reticulum Ca2+ ATPase. *FEBS Lett.* **1993**, *335*, 345

31. Doan, N. T. Q.; Christensen, S. B., Thapsigargin, Origin, Chemistry, Structure-Activity Relationships and Prodrug Development. *Curr. Pharm. Des.* **2015**, *21*, 5501

32. Mahalingam, D.; Wilding, G.; Denmeade, S.; Sarantopoulas, J.; Cosgrove, D.; Cetnar, J.; Azad, N.; Bruce, J.; Kurman, M.; Allgood, V. E.; Carducci, M., Mipsagargin, A Novel Thapsigargin-based PSMA-activated Prodrug: Results of a First-in-man Phase I Clinical Trial in Patients with Refractory, Advanced or Metastatic Solid Tumours. *Br. J. Cancer* **2016**, *114*, 986

33. Andersen, B. T.; López, Q. C.; Manczak, T.; Martinez, K.; Simonsen, T. H., Thapsigargin—From Thapsia L. to Mipsagargin. *Molecules* **2015**, *20, 6113*

34. Christensen, S. B.; Dorthe Mondrup, S.; Samuel, R. D.; Craig, D.; Jesper Vuust, M.; Poul, N.; John, T. I., A Trojan Horse in Drug Development: Targeting of Thapsigargins Towards Prostate Cancer Cells. *Anti-Cancer Agents Med. Chem.* **2009**, *9*, 276

35. Winther, A.-M. L.; Liu, H.; Sonntag, Y.; Olesen, C.; le Maire, M.; Soehoel, H.; Olsen, C.-E.; Christensen, S. B.; Nissen, P.; Møller, J. V., Critical Roles of Hydrophobicity and Orientation of Side Chains for Inactivation of Sarcoplasmic Reticulum Ca2+-ATPase with Thapsigargin and Thapsigargin Analogs. *J. Biol. Chem.* **2010**, *285*, 28883

36. Skytte, D. M.; Møller, J. V.; Liu, H.; Nielsen, H. Ø.; Svenningsen, L. E.; Jensen, C. M.; Olsen, C. E.; Christensen, S. B., Elucidation of the Topography of the Thapsigargin Binding Site in the Sarco-endoplasmic Calcium ATPase. *Bioorg. Med. Chem.* **2010**, *18*, 5634

37. Brøgger Christensen, S.; Norup, E.; Rasmussen, U.; Øgaard Madsen, J., Structure of histamine releasing guaianolides from Thapsia species. *Phytochemistry* **1984**, *23*, 1659

38. Ollivier, A.; Grougnet, R.; Cachet, X.; Meriane, D.; Ardisson, J.; Boutefnouchet, S.; Deguin, B., Large Scale Purification of the SERCA Inhibitor Thapsigargin from Thapsia Garganica L. Roots Using Centrifugal Partition Chromatography. *J. Chromatogr. B: Anal. Technol. Biomed. Life Sci.***2013**, *926*, 16

39. Oliver, S. F.; Högenauer, K.; Simic, O.; Antonello, A.; Smith, M. D.; Ley, S. V., A Route to the Thapsigargins from (S)-Carvone Providing a Substrate-Controlled Total Synthesis of Trilobolide, Nortrilobolide, and Thapsivillosin F. *Angew. Chem. Int. Ed.* **2003**, *42*, 5996

40. Chu, H.; Smith, J. M.; Felding, J.; Baran, P. S., Scalable Synthesis of (-)-Thapsigargin. *ACS Cent. Sci.* **2017**, *3*, 47

41. Chen, D.; Evans, P. A., A Concise, Efficient and Scalable Total Synthesis of Thapsigargin and Nortrilobolide from (R)-(−)-Carvone. *J. Am. Chem. Soc.* **2017**, *139*, 6046

42. Chen, B.-C.; Zhou, P.; Davis, F. A.; Ciganek, E., α-Hydroxylation of Enolates and Silyl Enol Ethers. In *Organic Reactions*, John Wiley & Sons, Inc.: **2004**.

43. Rubottom, G. M.; Gruber, J. M., *m*-Chloroperbenzoic Acid Oxidation of 2-Trimethylsilyloxy-1,3-Dienes - Synthesis of α-Hydroxy and α-Acetoxy Enones. *J. Org. Chem.* **1978**, *43*, 1599

44. Rubottom, G. M.; Gruber, J. M.; Boeckman, R. K.; Ramaiah, M.; Medwid, J. B., Clarification of Mechanism of Rearrangement of Enol Silyl Ether Epoxides. *Tetrahedron Lett.* **1978**, *19*, 4603

45. Mandal, M.; Yun, H. D.; Dudley, G. B.; Lin, S. N.; Tan, D. S.; Danishefsky, S. J., Total Synthesis of Guanacastepene A: A Route to Enantiomeric Control. *J. Org. Chem.* **2005**, *70*, 10619

46. Davis, F. A.; Jenkins, R.; Yocklovich, S. G., 2-Arenesulfonyl-3-Aryloxaziridines - New Class of Aprotic Oxidizing-Agents (Oxidation of Organic Sulfur-Compounds). *Tetrahedron Lett*. **1978**, *19*, 5171

47. Davis, F. A.; Chen, B. C., Asymmetric Hydroxylation of Enolates with N-Sulfonyloxaziridines. *Chem Rev.* **1992**, *92*, 919

48. Marín-Barrios, R.; García-Cabeza, A. L.; Moreno-Dorado, F. J.; Guerra, F. M.; Massanet, G. M., Acyloxylation of Cyclic Enones: Synthesis of Densely Oxygenated Guaianolides. *J. Org. Chem.* **2014**, *79*, 6501

49. Demir, A. S.; Reis, O.; Igdir, A. C., Reinvestigation of the synthetic and mechanistic aspects of Mn(III) acetate mediated oxidation of enones. *Tetrahedron* **2004**, *60*, 3427

50. Kerr, W. J., The Pauson-Khand Reaction – an Introduction. In *The Pauson-Khand Reaction*, John Wiley & Sons, Ltd: **2012**; pp 1-21.

51. Khand, I. U.; Knox, G. R.; Pauson, P. L.; Watts, W. E., Cobalt Induced Cleavage Reaction and a New Series of Arenecobalt Carbonyl Complexes. *J. Chem. Soc. D.* **1971**, 36

52. Wang, K.-Y.; Liu, D.-D.; Sun, T.-W.; Lu, Y.; Zhang, S.-L.; Li, Y.-H.; Han, Y.-X.; Liu, H.-Y.; Peng, C.; Wang, Q.-Y.; Chen, J.-H.; Yang, Z., Asymmetric Total Synthesis of Lancifodilactone G Acetate. 2. Final Phase and Completion of the Total Synthesis. *J. Org. Chem.* **2018**, *83*, 6907

53. Zhao, N.; Yin, S.; Xie, S.; Yan, H.; Ren, P.; Chen, G.; Chen, F.; Xu, J., Total Synthesis of Astellatol. *Angew. Chem. Int. Ed.* **2018**, *57*, 3386

54. Lopez-Perez, B.; Maestro, M. A.; Mourino, A., Total Synthesis of 1[α],25-dihydroxyvitamin D3 (calcitriol) Through a Si-assisted Allylic Substitution. *Chem. Commun.* **2017**, *53*, 8144

55. Abd El-Gaber, M. K.; Yasuda, S.; Iida, E.; Mukai, C., Enantioselective Total Synthesis of (+)-Sieboldine A. *Org. Lett.* **2017**, *19*, 320

56. Volpin, G.; Vepřek Nynke, A.; Bellan Andreas, B.; Trauner, D., Enantioselective Synthesis and Racemization of (−)-Sinoracutine. *Angew. Chem. Int. Ed.* **2016**, *56*, 897

57. Kerr, W. J.; McLaughlin, M.; Pauson, P. L.; Robertson, S. M., The Utility of Vinyl Ethers and Vinyl Esters in the Khand Reaction. The Value of Vinyl Esters as Ethylene Equivalents and a Modified Synthesis of (+)-taylorione as an Example. *J. Organomet. Chem.* **2001**, *630*, 104

58. Koga, Y.; Kobayashi, T.; Narasaka, K., Rhodium-catalyzed Intramolecular Pauson-Khand Reaction. *Chem. Lett.* **1998**, *27*, 249

59. Ying, J.; Brown, K. B.; Sandridge, M. J.; Hering, B. A.; Sabat, M.; Pu, L., Rh(I)-Catalyzed Chemo- and Stereoselective Domino Cycloaddition of Optically Active Propargyl 2,4-Hexadienyl Ethers. *J. Org. Chem.* **2015**, *80*, 3195

60. Brummond, K. M.; Chen, H. F.; Fisher, K. D.; Kerekes, A. D.; Rickards, B.; Sill, P. C.; Geib, S. J., An Allenic Pauson-Khand-type Reaction: A Reversal in π-bond Selectivity and the Formation of Seven-membered Rings. *Org. Lett.* **2002**, *4*, 1931

61. Kent, J. L.; Wan, H. H.; Brummond, K. M., A New Allenic Pauson-Khand Cycloaddition for the Preparation of α-Methylene Cyclopentenones. *Tetrahedron Lett.* **1995**, *36*, 2407

62. Brummond, K. A.; Chen, D. T.; Davis, M. A., A General Synthetic Route to Differentially Functionalized Angularly and Linearly Fused [6-7-5] Ring Systems: A Rh(I)-catalyzed Cyclocarbonylation Reaction. *J. Org. Chem.* **2008**, *73*, 5064

63. Jorgensen, L.; McKerrall, S. J.; Kuttruff, C. A.; Ungeheuer, F.; Felding, J.; Baran, P. S., 14-Step Synthesis of (+)-Ingenol from (+)-3-Carene. *Science* **2013**, *341*, 878

64. Siller, G.; Rosen, R.; Freeman, M.; Welburn, P.; Katsamas, J.; Ogbourne, S. M., PEP005 (ingenol mebutate) Gel for the Topical Treatment of Superficial Basal Cell Carcinoma: Results of a Randomized Phase IIa Trial. *Australas. J. Dermatol.* **2010**, *51*, 99

65. Grillet, F.; Huang, C. F.; Brummond, K. M., An Allenic Pauson-Khand Approach to 6,12-Guaianolides. *Org. Lett.* **2011**, *13*, 6304

66. Singh, J.; Petter, R. C.; Baillie, T. A.; Whitty, A., The Resurgence of Covalent Drugs. *Nat. Rev. Drug Discovery* **2011**, *10*, 307

67. Hirose, T.; Miyakoshi, N.; Mukai, C., Total Synthesis of (+)-achalensolide Based on the Rh(I)-catalyzed Allenic Pauson-Khand-type Reaction. *J. Org. Chem.* **2008**, *73*, 1061

68. Donaldson, W. A.; Gone, J. R.; Wallock, N. J.; Pandey, R. K., ORGN 466-Preparation of Functionalized Cycloheptadienes via Organoiron Methodology. *Abstr. Pap. Am. Chem. Soc.* **2009**, 237.

69. Lee, E.; Lim, J. W.; Yoon, C. H.; Sung, Y. S.; Kim, Y. K.; Yun, M.; Kim, S., Total Synthesis of (+)-cladantholide and (-)-estafiatin: 5-exo,7-endo Radical Cyclization Strategy for the Construction of Guaianolide Skeleton. *J. Am. Chem. Soc.* **1997**, *119*, 8391

70. Wen, B.; Hexum, J. K.; Widen, J. C.; Harki, D. A.; Brummond, K. M., A Redox Economical Synthesis of Bioactive 6,12-Guaianolides. *Org. Lett.* **2013**, *15*, 2644

71. Brummond, K. M.; Davis, M. M.; Huang, C., Rh(I)-Catalyzed Cyclocarbonylation of Allenol Esters To Prepare Acetoxy 4-Alkylidenecyclopent-3-en-2-ones. *J. Org. Chem.* **2009**, *74*, 8314

72. Barriere, F.; Geiger, W. E., Generation of the 15-electron Rhodium(II) Complex [RhCl(PPh3)(3)](+) by 1-electron Oxidation of Wilkinson's catalyst. *Organometallics* **2001**, *20*, 2133

73. Schlossarczyk, H.; Seiber, W.; Hesse, M.; Hansen, H.; Schmid, H., Geltunsvereich und Mechanisums der durch Silverionen katalysierten Propargylester-allenylester Umlagerung nach. *Helv. Chim. Acta* **1973**, *56*, 875

74. Hicks, F. A.; Buchwald, S. L., Highly Enantioselective Catalytic Pauson-Khand Type Formation of Bicyclic Cyclopentenones. *J. Am. Chem. Soc.* **1996**, *118*, 11688

75. Jeong, N.; Sung, B. K.; Choi, Y. K., Rhodium(I)-Catalyzed Asymmetric Intramolecular Pauson−Khand-Type Reaction. *J. Am. Chem. Soc.* **2000**, *122*, 6771

76. Jeong, N.; Lee, S.; Sung, B. K., Rhodium(I)-catalyzed Intramolecular Pauson-Khand Reaction. *Organometallics* **1998**, *17*, 3642

77. Derdau, V.; Laschat, S.; Dix, I.; Jones, P. G., Cobalt-alkyne Complexes with Diphosphine Ligands as Mechanistic Probes for the Pauson-Khand Reaction. *Organometallics* **1999**, *18*, 3859

78. Bhat, V.; Welin, E. R.; Guo, X.; Stoltz, B. M., Advances in Stereoconvergent Catalysis from 2005 to 2015: Transition-Metal-Mediated Stereoablative Reactions, Dynamic Kinetic Resolutions, and Dynamic Kinetic Asymmetric Transformations. *Chem. Rev.* **2017**, *117*, 4528

79. Madin, A.; Overman, L. E., Controlling Stereoselection in Intramolecular Heck Reactions by Tailoring the Palladium Catalyst. *Tetrahedron Lett.* **1992**, *33*, 4859

80. Trost, B. M.; Thaisrivongs, D. A., Palladium-Catalyzed Regio-, Diastereo-, and Enantioselective Benzylic Allylation of 2-Substituted Pyridines. *J. Am. Chem. Soc.* **2009**, *131*, 12056

81. Wang, Y.-M.; Kuzniewski, C. N.; Rauniyar, V.; Hoong, C.; Toste, F. D., Chiral (Acyclic Diaminocarbene)Gold(I)-Catalyzed Dynamic Kinetic Asymmetric Transformation of Propargyl Esters. *J. Am. Chem. Soc.* **2011**, *133*, 12972

82. Faber, K., Non-sequential Processes for the Transformation of a Racemate into a Single Stereoisomeric Product: Proposal for Stereochemical Classification. *Chem. – Eur. J.* **2001**, *7*, 5004

83. Zhang, Z. B.; Bender, C. F.; Widenhoefer, R. A., Gold(I)-catalyzed Dynamic Kinetic Enantioselective Intramolecular Hydroamination of Allenes. *J. Am. Chem. Soc.* **2007**, *129*, 14148

84. Osborne, J. D.; Randell-Sly, H. E.; Currie, G. S.; Cowley, A. R.; Willis, M. C., Catalytic Enantioselective Intermolecular Hydroacylation: Rhodium-Catalyzed Combination of beta-S-Aldehydes and 1,3-Disubstituted Allenes. *J. Am. Chem. Soc.* **2008**, *130*, 17232

85. Chen, M.; Roush, W. R., Enantioconvergent Hydroboration of a Racemic Allene: Enantioselective Synthesis of (E)-δ-Stannyl-anti-homoallylic Alcohols via Aldehyde Crotylboration. *J. Am. Chem. Soc.* **2011**, *133*, 5744

86. Tran, D. N.; Cramer, N., Rhodium-Catalyzed Dynamic Kinetic Asymmetric Transformations of Racemic Allenes by the [3+2] Annulation of Aryl Ketimines. *Angew. Chem., Int. Ed.* **2013**, *52*, 10630

87. Trost, B. M.; Fandrick, D. R.; Dinh, D. C., Dynamic Kinetic Asymmetric Allylic Alkylations of Allenes. *J. Am. Chem. Soc.* **2005**, *127*, 14186

88. Kawai, J.; Chikkade, P. K.; Shimizu, Y.; Kanai, M., In situ Catalytic Generation of Allylcopper Species for Asymmetric Allylation: Toward 1H-isochromene Skeletons. *Angew. Chem., Int. Ed. Engl.* **2013**, *52*, 7177

89. Houk, K. N.; Cheong, P. H.-Y., Computational Prediction of Small-molecule Catalysts. *Nature* **2008**, *455*, 309

90. Peng, Q.; Duarte, F.; Paton, R. S., Computing Organic Stereoselectivity - From Concepts to Quantitative Calculations and Predictions. *Chem. Soc. Rev.* **2016**, *45*, 6093

91. Houk, K. N.; Liu, F., Holy Grails for Computational Organic Chemistry and Biochemistry. *Acc. Chem. Rev.* **2017**, *50*, 539

92. Poree, C.; Schoenebeck, F., A Holy Grail in Chemistry: Computational Catalyst Design: Feasible or Fiction? *Acc. Chem. Rev.* **2017**, *50*, 605

93. Garegg, P. J.; Regberg, T.; Stawinski, J.; Stromberg, R., A Phosphorus Nuclear-Magnetic-Resonance Spectroscopic Study of the Conversion of Hydroxy-Groups into Iodo Groups in Carbohydrates Using the Iodine Triphenylphosphine Imidazole Reagent. *J. Chem. Soc., Perkin Trans. 2* **1987**, 271

94. Cariou, K.; Mainetti, E.; Fensterbank, L.; Malacria, M., Tandem $PtCl_2$ catalyzed-thermal [3,3] Rearrangements of Enyne Acetates. *Tetrahedron* **2004**, *60*, 9745

95. Zhang, L. M., Tandem Au-catalyzed 3,3-rearrangement-[2+2] Cycloadditions of Propargylic Esters: Expeditious Access to Highly Functionalized 2,3-indoline-fused Cyclobutanes. *J. Am. Chem. Soc.* **2005**, *127*, 16804

96. Miki, K.; Ohe, K.; Uemura, S., Ruthenium-catalyzed Cyclopropanation of Alkenes Using Propargylic Carboxylates as Precursors of Vinylcarbenoids. *J. Org. Chem.* **2003**, *68*, 8505

97. Voutchkova, A. M.; Appelhans, L. N.; Chianese, A. R.; Crabtree, R. H., Disubstituted Imidazolium-2-Carboxylates as Efficient Precursors to N-Heterocyclic Carbene Complexes of Rh, Ru, Ir, and Pd. *J. Am. Chem. Soc.* **2005**, *127*, 17624

98. Xie, J.-H.; Zhou, Q.-L., Chiral Diphosphine and Monodentate Phosphorus Ligands on a Spiro Scaffold for Transition-Metal-Catalyzed Asymmetric Reactions. *Acc. Chem. Rev.* **2008**, *41*, 581

99. Fan, B. M.; Xie, J. H.; Li, S.; Tu, Y. Q.; Zhou, Q. L., Rhodium-catalyzed Asymmetric Pauson-Khand Reaction Using Monophosphoramidite Ligand SIPHOS. *Adv. Synth. Catal.* **2005**, *347*, 759

100. Franke, R.; Selent, D.; Borner, A., Applied Hydroformylation. *Chem. Rev.* **2012**, *112*, 5675

101. Chikkali, S. H.; van der Vlugt, J. I.; Reek, J. N. H., Hybrid Diphosphorus Ligands in Rhodium Catalyzed asymmetric Hydroformylation. *Coord. Chem. Rev.* **2014**, *262*, 1

102. Agbossou, F.; Carpentier, J.-F.; Mortreux, A., Asymmetric Hydroformylation. *Chem. Rev.* **1995**, *95*, 2485

103. Lei, M.; Wang, Z. D.; Du, X. J.; Zhang, X.; Tang, Y. H., Asymmetric Hydroformylation Catalyzed by RhH(CO)(2)[(R,S)-Yanphos]: Mechanism and Origin of Enantioselectivity. *J. Phys. Chem. A* **2014**, *118*, 8960

104. Yan, Y. J.; Zhang, X. M., A Hybrid Phosphorus Ligand for Highly Enantioselective Asymmetric Hydroformylation. *J. Am. Chem. Soc.* **2006**, *128*, 7198

105. Vallianatou, K. A.; Kostas, I. D.; Holz, J.; Börner, A., Me-AnilaPhos: A New Chiral Phosphine–Phosphoramidite Ligand for a Highly Efficient Rh-catalyzed Asymmetric Olefin Hydrogenation. *Tetrahedron Lett.* **2006**, *47*, 7947

106. Bart van Oort, A.; Budzelaar, P. H. M.; Frijns, J. H. G.; Guy Orpen, A., Mono- and Bi-nuclear Molybdenum Complexes of 2,6-bis(diphenylphosphino)-N-methylaniline. *J. Organomet. Chem.* **1990**, *396*, 33

107. Mather, G. G.; Pidcock, A.; Rapsey, G. J. N., Correlation of Nuclear Magnetic Resonance Coupling Constants with Transition Metal-ligand Bond Lengths in Tertiary Phosphine complexes. *J. Chem. Soc., Dalton Trans.* **1973**, 2095

108. Scheffel, D. J.; Cole, A. R.; Jung, D. M.; Schiavelli, M. D., Mechanism of Hydrolysis of Allenyl Acetates. *J. Am. Chem. Soc.* **1980**, *102*, 267

109. Drinkel, E.; Briceño, A.; Dorta, R.; Dorta, R., Hemilabile P-Alkene Ligands in Chiral Rhodium and Copper Complexes: Catalytic Asymmetric 1,4 Additions to Enones. 2†,(1). *Organometallics* **2010**, *29*, 2503

110. Defieber, C.; Ariger, M. A.; Moriel, P.; Carreira, E. M., Iridium-catalyzed Synthesis of Primary Allylic Amines from Allylic Alcohols: Sulfamic Acid as Ammonia Equivalent. *Angew. Chem., Int. Ed. Engl.* **2007**, *46*, 3139

111. Mariz, R.; Briceno, A.; Dorta, R.; Dorta, R., Chiral Dibenzazepine-Based P-Alkene Ligands and Their Rhodium Complexes: Catalytic Asymmetric 1,4 Additions to Enones. *Organometallics* **2008**, *27*, 6605

112. Dorta, R.; Herrera, A.; Linden, A.; Heinemann, F.; Brachvogel, R.-C.; von Delius, M., Optimized Syntheses of Optically Pure P-Alkene Ligands: Crystal Structures of a Pair of P-Stereogenic Diastereomers. *Synthesis* **2016**, *48*, 1117

113. Ojima, I.; Vu, A. T.; Bonafoux, D., Science of Synthesis. Thieme Chemistry: **2001**; Vol. 1, p 532.

114. Burrows, L. C.; Jesikiewicz, L. T.; Lu, G.; Geib, S. J.; Liu, P.; Brummond, K. M., Computationally Guided Catalyst Design in the Type I Dynamic Kinetic Asymmetric Pauson-Khand Reaction of Allenyl Acetates. *J. Am. Chem. Soc.* **2017**, *139*, 15022

115. Hoye, T. R.; Eklov, B. M.; Ryba, T. D.; Voloshin, M.; Yao, L. J., No-D NMR (No-Deuterium proton NMR) Spectroscopy: A Simple yet Powerful Method for Analyzing Reaction and Reagent Solutions. *Org. Lett.* **2004**, *6*, 953

116. Wilhelm, E.; Battino, R., Thermodynamic Functions of the Solubilities of Gases in Liquids at 25°C. *Chem. Rev.* **1973**, *73*, 1

117. Diaz-Torres, R.; Alvarez, S., Coordinating Ability of Anions and Solvents Towards Transition Metals and Lanthanides. *Dalton Trans.* **2011**, *40*, 10742

118. Murray, P. M.; Bellany, F.; Benhamou, L.; Bucar, D. K.; Tabor, A. B.; Sheppard, T. D., The Application of Design of Experiments (DoE) Reaction Optimization and Solvent Selection in the Development of New Synthetic Chemistry. *Org. Biomol. Chem.* **2016**, *14*, 2373

119. Leardi, R., Experimental Design in Chemistry: A Tutorial. *Anal. Chim. Acta* **2009**, *652*, 161

120. Weissman, S. A.; Anderson, N. G., Design of Experiments (DoE) and Process Optimization. A Review of Recent Publications. *Org. Process Res. Dev.* **2015**, *19*, 1605

121. Mills, J. E., Design of Experiments in Pharmaceutical Process Research and Development. In Chemical Process Research, American Chemical Society: **2003**; Vol. 870, pp 87-109.

122. Stazi, F.; Palmisano, G.; Turconi, M.; Clini, S.; Santagostino, M., Accelerated Koenigs-Knorr Glucuronidation of a Deactivated Nitrophenol: Unveiling the Role of Polyamine Additive 1,1,4,7,10,10-hexamethyltriethylenetetramine through Design of Experiments. *J. Org. Chem.* **2004**, *69*, 1097

123. Garcia-Cabeza, A. L.; Marin-Barrios, R.; Moreno-Dorado, F. J.; Ortega, M. J.; Massanet, G. M.; Guerra, F. M., Allylic Oxidation of Alkenes Catalyzed by a Copper-Aluminum Mixed Oxide. *Org. Lett.* **2014**, *16*, 1598

124. Colleville, A. P.; Horan, R. A. J.; Olazabal, S.; Tomkinson, N. C. O., C-H Arylation of Heterocyclic N-Oxides Through in Situ Diazotisation Of Anilines without Added Promoters: A Green And Selective Coupling Process. *Org. Process Res. Dev.* **2016**, *20*, 1283

125. Caldwell, N.; Jamieson, C.; Simpson, I.; Watson, A. J. B., Development of a Sustainable Catalytic Ester Amidation Process. *ACS Sustainable Chem. Eng.* **2013**, *1*, 1339

126. Karaluka, V.; Lanigan, R. M.; Murray, P. M.; Badland, M.; Sheppard, T. D., $B(OCH_2CF_3)_3$-mediated Direct Amidation of Pharmaceutically Relevant Building Blocks in Cyclopentyl Methyl Ether. *Org. Biomol. Chem.* **2015**, *13*, 10888

127. Martinot, T. A.; Austad, B. C.; Côté, A.; Depew, K. M.; Genov, D.; Grenier, L.; Helble, J.; Lescarbeau, A.; Nair, S.; Trudeau, M.; White, P.; Yu, L.-C., A Design of Experiments Approach to a Robust Final Deprotection and Reactive Crystallization of IPI-926, A Novel Hedgehog Pathway Inhibitor. *Org. Process Res. Dev.* **2015**, *19*, 1693

128. King, S. M.; Buchwald, S. L., Development of a Method for the N-Arylation of Amino Acid Esters with Aryl Triflates. *Org. Lett.* **2016**, *18*, 4128

129. Atkinson, A. C., Optimum Experimental Design. In International Encyclopedia of Statistical Science, Lovric, M., Ed. Springer Berlin Heidelberg: Berlin, Heidelberg, **2011**; pp 1037-1039.

130. Eriksson, L., Design of Experiments: Principles and Applications. Umetrics Academy: **2000**.

131. Wells, S. M.; Brummond, K. M., Conditions for a Rh(I)-catalyzed [2+2+1] Cycloaddition Reaction with Methyl Substituted Allenes and Alkynes. *Tetrahedron Lett.* **2015**, *56*, 3546

132. Schmid, T. M.; Consiglio, G., Mechanistic and Stereochemical Aspects of the Asymmetric Cyclocarbonylation of 1,6-enynes with Rhodium Catalysts. *Chem. Commun.* **2004**, 2318

133. Using JMP 12.0, Inc., S. I., Ed. Cary, NC, **2015**; pp 285-306.

134. Kamijo, S.; Dudley, G. B., A Tandem Carbanion Addition/carbon-carbon Cond Cleavage Yields Alkynyl Ketones. *J. Am. Chem. Soc.* **2005**, *127*, 5028

135. Tummatorn, J.; Dudley, G. B., Generation of Medium-Ring Cycloalkynes by Ring Expansion of Vinylogous Acyl Triflates. *Org. Lett.* **2011**, *13*, 1572

136. Zhang, Y.; Di, Y.; He, H.; Li, S.; Lu, Y.; Gong, N.; Hao, X., Daphmalenines A and B: Two New Alkaloids with Unusual Skeletons from Daphniphyllum himalense. *Eur. J. Org. Chem.* **2011**, 4103

137. Xu, G.; Hou, A.-J.; Zheng, Y.-T.; Zhao, Y.; Li, X.-L.; Peng, L.-Y.; Zhao, Q.-S., Przewalskin B, a Novel Diterpenoid with an Unprecedented Skeleton from Salvia przewalskii Maxim. *Org. Lett.* **2006**, *9*, 291

138. Kajiro, H.; Mitamura, S.; Mori, A.; Hiyama, T., Scandium Trifluoromethanesulfonate-catalyzed Mild, Efficient, and Selective Cleavage of Acetates Bearing a Coordinative Group. *Tetrahedron Lett.* **1999**, *40*, 1689

139. Jin, T.; Himuro, M.; Yamamoto, Y., Triflic Acid Catalyzed Synthesis of Spirocycles via Acetylene Cations. *Angew. Chem., Int. Ed.* **2009**, *48*, 5893

140. Kajiro, H.; Mitamura, S.; Mori, A.; Hiyama, T., Scandium Trifluoromethanesulfonate-catalyzed Cleavage of Esters Bearing a Coordinative Group at a Vicinal Position. *Bull. Chem. Soc. Jpn.* **1999**, *72*, 1553

141. Ma, K.; Martin, B. S.; Yin, X.; Dai, M., Natural product syntheses via carbonylative cyclizations. *Nat. Prod. Rep.* **2018**, *Advance Article*

142. Lledó, A.; Verdaguer, X.; Riera, A., The Enantioselective Pauson-Khand Reaction. In The Pauson-Khand Reaction, John Wiley & Sons, Ltd: **2012**; pp 147-180.

143. Clark, J. S.; Xu, C., Total Synthesis of (−)-Nakadomarin A. *Angew. Chem., Int. Ed.* **2016**, *55*, 4332

144. Hiroi, K.; Watanabe, T.; Kawagishi, R.; Abe, I., Catalytic Use of Chiral Phosphine Ligands in Asymmetric Pauson–Khand Reactions. *Tetrahedron: Asymmetry* **2000**, *11*, 797

145. Gibson, S. E.; Stevenazzi, A., The Pauson-Khand Reaction: The Catalytic Age is Here! *Angew. Chem., Int. Ed.* **2003**, *42*, 1800

146. Boñaga, L. V. R.; Krafft, M. E., When the Pauson–Khand and Pauson–Khand Type Reactions go Awry: A Plethora of Unexpected Results. *Tetrahedron* **2004**, *60*, 9795

147. Choi, Y. H.; Kwak, J.; Jeong, N., Solvent Effects on the Asymmetric Pauson–Khand-type Reaction by Rhodium. *Tetrahedron Lett.* **2009**, *50*, 6068

148. Kim, D. E.; Choi, C.; Kim, I. S.; Jeulin, S.; Ratovelomanana-Vidal, V.; Genêt, J.-P.; Jeong, N., Electronic and Steric Effects of Atropisomeric Ligands SYNPHOS® and DIFLUORPHOS®vs. BINAPs in Rh(I)-Catalyzed Asymmetric Pauson–Khand Reaction. *Adv. Synth. Catal.* **2007**, *349*, 1999

149. Kim, D. E.; Park, S. H.; Choi, Y. H.; Lee, S. G.; Moon, D.; Seo, J.; Jeong, N., Internal chelation-guided Regio- and Stereoselective Pauson-Khand-type Reaction by Chiral Rhodium(I) Catalysis. *Chem. Asian J.* **2011**, *6*, 2009

150. Knowles, W. S., Asymmetric Hydrogenation. *Acc. Chem. Rev.* **1983**, *16*, 106

151. Wang, H.; Sawyer, J. R.; Evans, P. A.; Baik, M. H., Mechanistic Insight into the Diastereoselective Rhodium-catalyzed Pauson-Khand Reaction: Role of Coordination Number in Stereocontrol. *Angew. Chem., Int. Ed. Engl.* **2008**, *47*, 342

152. Shibata, T.; Toshida, N.; Takagi, K., Rhodium Complex-catalyzed Pauson-Khand-type Reaction with Aldehydes as a CO source. *J. Org. Chem.* **2002**, *67*, 7446

153. Kwong Fuk, Y.; Li Yue, M.; Lam Wai, H.; Qiu, L.; Lee Hang, W.; Yeung Chi, H.; Chan Kin, S.; Chan Albert, S. C., Rhodium-Catalyzed Asymmetric Aqueous Pauson–Khand-Type Reaction. *Chem. – Eur. J.* **2005**, *11*, 3872

154. Fan, B.; Li, S.; Xie, J.; Wang, L.; Tu, Y.; Zhou, Q., Rhodium Catalyzed Asymmetric Pauson-Khand Reaction using SDP Ligands. *Sci. China, Ser. B: Chem.* **2006**, *49*, 81

155. Kim, D. E.; Kim, I. S.; Ratovelomanana-Vidal, V.; Genêt, J.-P.; Jeong, N., Asymmetric Pauson−Khand-type Reaction Mediated by Rh(I) Catalyst at Ambient Temperature. *J. Org. Chem.* **2008**, *73*, 7985

156. Kim, D. E.; Ratovelomanana-Vidal, V.; Jeong, N., 2,2′-Bis[bis(3,5-di-tert-butyl-4-methoxyphenyl)phosphino]-6,6′-dimethoxy-1,1′-biphenyl in Intramolecular Rhodium(I)-Catalyzed Asymmetric Pauson-Khand-Type Reactions. *Adv. Synth. Catal.* **2010**, *352*, 2032

157. Cristóbal-Lecina, E.; Costantino, A. R.; Grabulosa, A.; Riera, A.; Verdaguer, X., Rhodium-Catalyzed Pauson–Khand Reaction Using a Small-Bite-Angle P-Stereogenic C1-Diphosphine Ligand. *Organometallics* **2015**, *34*, 4989

158. Jeong, N.; Sung, B. K.; Kim, J. S.; Park, S. B.; Seo, S. D.; Shin, J. Y.; In, K. Y.; Choi, Y. K., Pauson-Khand-type Reaction Mediated by Rh(I) Catalysts. *Pure Appl. Chem.* **2002**, *74*, 85

159. Luhring, P.; Schumpe, A., Gas Solubilities (H-2, He, N-2, Co, O-2, Ar, Co2) in Organic Liquids at 293.2-K. *J. Chem. Eng. Data.* **1989**, *34*, 250

160. Kim Dong, E.; Ratovelomanana-Vidal, V.; Jeong, N., 2,2′-Bis[bis(3,5-di-tert-butyl-4-methoxyphenyl)phosphino]-6,6′-dimethoxy-1,1′-biphenyl in Intramolecular Rhodium(I)-Catalyzed Asymmetric Pauson–Khand-Type Reactions. *Adv. Synth. Catal.* **2010**, *352*, 2032

161. Hicks, F. A.; Buchwald, S. L., An Intramolecular Titanium-Catalyzed Asymmetric Pauson−Khand Type Reaction. *J. Am. Chem. Soc.* **1999**, *121*, 7026

162. He, Y.; Wang, B.; Dukor, R. K.; Nafie, L. A., Determination of Absolute Configuration of Chiral Molecules Using Vibrational Optical Activity: A Review. *Appl. Spectrosc.* **2011**, *65*, 699

163. Bartberger Michael, D., VCD Spectroscopy for Organic Chemists, by Philip J. Stephens, Frank J. Devlin, and James R. Cheeseman. CRC Press: Boca Raton, FL. 2012. Chirality **2013**, 25 (10), 673-674.

164. Jimenez-Oses, G.; Vispe, E.; Roldan, M.; Rodriguez-Rodriguez, S.; Lopez-Ram-de-Viu, P.; Salvatella, L.; Mayoral, J. A.; Fraile, J. M., Stereochemical Outcome of Copper-catalyzed C-H Insertion Reactions. An Experimental and Theoretical Study. *J. Org. Chem.* **2013**, *78*, 5851

165. Debie, E.; De Gussem, E.; Dukor Rina, K.; Herrebout, W.; Nafie Laurence, A.; Bultinck, P., A Confidence Level Algorithm for the Determination of Absolute Configuration Using Vibrational Circular Dichroism or Raman Optical Activity. *ChemPhysChem* **2011**, *12*, 1542

166. van den Berg, M.; Minnaard Adriaan , J.; Haak Robert , M.; Leeman, M.; Schudde Ebe , P.; Meetsma, A.; Feringa Ben , L.; de Vries André , H. M.; Maljaars, C. E. P.; Willans Charlotte , E.; Hyett, D.; Boogers Jeroen , A. F.; Henderickx Hubertus , J. W.; de Vries Johannes , G., Monodentate Phosphoramidites: A Breakthrough in Rhodium-Catalysed Asymmetric Hydrogenation of Olefins. *Adv. Synth. Catal.* **2003**, *345*, 308

167. Jeong, N.; Genêt, J.-P.; Ratovelomanana-Vidal, V.; Kim, D.; Choi, C.; Kim, I.; Jeulin, S., The Electronic Effect of Ligands on Stereoselectivity in the Rhodium(I)-Catalyzed Asymmetric Pauson-Khand-Type Reaction under a Carbon Monoxide Atmosphere. *Synthesis* **2006**, 4053

168. Berrisford, D. J.; Bolm, C.; Sharpless, K. B., Ligand-Accelerated Catalysis. *Angew. Chem., Int. Ed. Engl.* **1995**, *34*, 1059

169. Tolman, C. A., Steric Effects of Phosphorus Ligands in Organometallic Chemistry and Homogeneous Catalysis. *Chem. Rev.* **1977**, *77*, 313

170. Guillaneux, D.; Zhao, S.-H.; Samuel, O.; Rainford, D.; Kagan, H. B., Nonlinear Effects in Asymmetric Catalysis. *J. Am. Chem. Soc.* **1994**, *116*, 9430

171. Satyanarayana, T.; Abraham, S.; Kagan Henri , B., Nonlinear Effects in Asymmetric Catalysis. *Angew. Chem. Int. Ed.* **2008,** *48*, 456.

172. Pearson, A. J.; Dubbert, R. A., Cyclocarbonylation of 1,6-Enynes Promoted by Iron Carbonyls. *Organometallics* **1994**, *13*, 1656